A STUDY OF THE THERMAL DEGRADATION OF FLEXIBLE TDI-BASED POLYURETHANE FOAMS

DEBORAH TODD

A thesis submitted to the Department of Pure and Applied Chemistry, University of Strathclyde, in part fulfilment of the requirements for the degree of Doctor of Philosophy

June 2012

DECLARATION

This thesis is the result of the author's original research. It has been composed by the author and has not been previously submitted for examination which has led to the award of a degree.

Signed Date

Acknowledgements

Firstly, I would like to thank my supervisor Dr. John Liggat for his continued help, support and guidance throughout the course of my PhD and beyond!

In addition, I would like to thank Dr. John Daly for the synthesis of the polyurethane foams used throughout this research and Jim Morrow for his general assistance and good banter over the past three years. Thanks must also go to Neil Hodgson for his excellent glassblowing skills, without which this work would not be possible.

Thanks also go to Dr. Graham Skinner for his help in teaching me how to take good quality photos with shining white backgrounds!

Thank you to the all of the students, past and present, in TG521 for making this experience such an enjoyable one. I couldn't have got through it without our regular "exciting lunches"!

I would like also to thank my family and friends for their continued support and advice over the many years of my education. Thanks to my mum and dad for all of the proof reading and putting up with my constant phone calls on the long commute home!

The final, huge thanks goes out to my fiancé Gordon for his continued love, support and advice throughout the last three and a half years. Thanks for having the patience to listen to my long stories about chemistry, even though you never asked! You'll never ask how my day was again! I couldn't have got through this without you and for that I dedicate this thesis to you.

That's all folks!

Abstract

A novel environmentally friendly fire retardant formulation for use in polyurethane foams has previously been developed at the University of Strathclyde; however, the fundamental chemistry relating to the fire retardancy of this foam was not well understood. The purpose of this research project was, therefore, to study the degradation behaviour of toluene diisocyanate (TDI)-based polyurethane foams in order to determine the mechanisms which occur and the effect that various fire retardants have on the degradation mechanisms.

The results have demonstrated that the degradation of TDI-based polyurethane foam is a complex process consisting of different mechanisms which yield an array of volatile products and complex char residues. Degradation of the urethane linkages has been shown to occur by two competing mechanisms. The first involves depolymerisation of the urethane bond to yield TDI and polyol, whilst the second involves dissociation of the urethane linkages *via* a six-membered ring transition state to yield diaminotoluene (DAT), CO_2 and alkene-terminated polyol chains. The results have shown that the dominant mechanism varies depending on the experimental conditions of the pyrolysis or degradation technique employed. Characterisation of the pyrolysis residues has demonstrated that complex aromatic chars are formed, with the structure dependent on the environment in which the pyrolysis is conducted.

The addition of fire retardants adds to this complexity, making the understanding of the degradation processes a more complicated task. Ammonium polyphosphate (APP) has been shown to be an effective fire retardant, altering the degradation mechanisms of the foam and promoting char formation. The addition of vermiculite into the foam has been shown to have little effect on the fire retardancy when used alone. Cloisite® 30B, on the other hand, has been shown to have a detrimental effect, altering the degradation of the polyol such that copious quantities of propanal are evolved. This leads to the foam burning more readily.

Contents

Abbreviations List

APP	ammonium polyphosphate
ATR	attenuated total reflectance
CP	cross polarisation
CPMAS	cross polarisation mangle angle spinning
DAT	diaminotoluene
DSC	differential scanning calorimetry
FID	free induction decay
FT	Fourier transform
MAS	magic angle spinning
MDA	methylene dianiline
MDI	methylene diphenyl diisocyanate
PEG	poly(ethylene glycol)
PEO	poly(ethylene oxide)
PPG	poly(propylene glycol)
PPO	poly(propylene oxide)
SEM	scanning electron microscopy
TDI	toluene diisocyanate
TOSS	total suppression of sidebands
TGA	thermogravimetric analysis
TVA	thermal volatilisation analysis

1 Introduction

1.1 An Introduction to Polyurethanes

1.1.1 Background

Polyurethanes are one of the most versatile classes of polymers, exhibiting a wide range of physical properties and applications, and as such they are ubiquitous in everyday life. A polyurethane is a polymer containing urethane links, as illustrated in Figure 1.1, formed by the exothermic polymerisation reaction of a diisocyanate with a diol.[1,2]

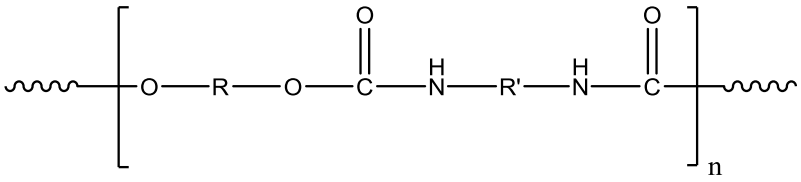

Figure 1.1: General structure of linear polyurethane

The pioneering work on polyurethanes was conducted by Bayer and his colleagues, with their discovery of the addition polymerisation reaction between diisocyanates and polyols occurring in 1937.[3,4,5] Their initial work was based on the reaction of diisocyanates with diamines which yielded polyureas, however, these materials did not possess the necessary properties required for them to be used commercially as plastics or fibres. It was following this work that the reaction of diisocyanates with simple glycols such as 1,4-butylene glycol was discovered, producing polyurethanes possessing properties which made them of great commercial interest as plastics and fibres.[1] In the years which followed, polyurethanes were developed into a variety of commercial products, with the development of elastomers and adhesives between 1945 and 1947 and rigid and flexible foams between 1947 and 1952.[1,2,6] Since these discoveries, the use and application of polyurethanes has become widespread.

1.1.2 Properties and Applications

The polymerisation reaction to produce polyurethane yields a solid material; however, a foamed material can also be produced by the formation of gas bubbles within the reaction mixture. During the polymerisation a polyol is employed which is a compound containing multiple hydroxyl groups. A broad range of polyols of different molecular weights and functionalities can be employed along with a more limited number of isocyanates,[7] each of which will impart different properties into the material. Linear polyurethanes are derived from diisocyanates and polyols containing two hydroxyl groups, with branched and cross-linked structures formed by increasing the functionality of the polyol. Polyurethanes, therefore, exist in a large variety of forms, including foams and elastomers, with such variety meaning that polyurethanes find applications in both industry and daily life, as illustrated in Table 1.1.[7,8]

Application	**Form of Polyurethane**	**Properties**
Soles of footwear	High density microcellular foam	Light and abrasion resistant
Furniture and upholstery	Flexible Foam	Soft but supportive with shape retention
Construction materials	Foam	Rigid with good thermal and sound insulation
Automobile interior components	Integral skin foam	Tough elastomeric material
Adhesives	Solid elastomer	Water resistant and weather proof

Table 1.1: Example applications of polyurethane

Foam-based materials find the most widespread use, forming approximately 56% of the total polyurethane market in 2000.[7] These materials are undoubtedly of great

commercial importance and this work will therefore focus primarily on this class of products.

1.2 Polyurethane Foams

1.2.1 Types of Foam

Polyurethane foams can be flexible or rigid materials depending on the nature of the starting materials employed. The three types of foam of greatest interest in industry are low- and high-density flexible foams and low-density rigid foams.

Flexible foams are composed of two distinct segments; a long, flexible polyol component known as the soft segment and a more rigid aromatic polyurethane or polyurea segment known as the hard block. The polyol segment, which imparts flexibility into the foam, forms a high percentage of the overall material. Flexible foams find uses in upholstery, mattresses and the automotive industry.[9] Low-density flexible foams have densities in the range of 10-80 kg m^{-3} and consist of polymer chains which are cross-linked to a small extent.[7] The foam produced has an open cell structure in which there is a path available for continuous air flow to occur. High-density flexible foams such as microcellular elastomers and moulded self-skinning foams have densities greater than 100 kg m^{-3}.[7] These types of foam can be both open and closed cell and are used in moulded components which possess a cellular core and a dense, decorative skin.

In contrast to flexible foams, low-density rigid foams consist of extensively cross-linked polymer chains which produce a foam with a closed cell structure. Rigidity is imparted into the material through use of branched polyols or isocyanates and the densities of such foams are in the range 28 to 50 kg m^{-3}.[7] Thin walls of polymer between the cells restrict the flow of air and liquids through the foam which leads to these materials having excellent thermal insulation properties; they are, therefore, employed in refrigerators and freezers.[10]

1.2.2 Materials Used in Polyurethane Foams

1.2.2.1 Polyols

A polyol is a compound containing two or more hydroxyl groups which reacts with an isocyanate to form a polyurethane. The nature of the polyol used, in particular the molecular weight and the functionality, significantly affects the final properties of the polyurethane formed. A wide range of polyols are available allowing a variety of different materials to be produced. In the manufacture of foams there are two key classes of polyol which are employed, namely polyether and polyester polyols.[7,11] Originally polyesters were predominantly used, however, it was later realised that polyether polyols were more suitable for use in the manufacture of flexible foams and these are now the most widely used type of polyol. Polyether polyols are easier to handle, less expensive and are more hydrolytically stable than their polyester counterparts.[2] In addition to this, they offer greater flexibility and viscosity to the resulting polymer.

The first polyether polyol designed principally for use in the manufacture of polyurethanes was a poly(oxatetramethylene) glycol derived from tetrahydrofuran.[2] Nowadays most polyether polyols used in polyurethane foams are derived from poly(propylene oxide) (PPO) and poly(ethylene oxide) (PEO), or co-polymers thereof.[7,11] The structures of PPO and PEO are presented in Figure 1.2 and Figure 1.3, respectively.

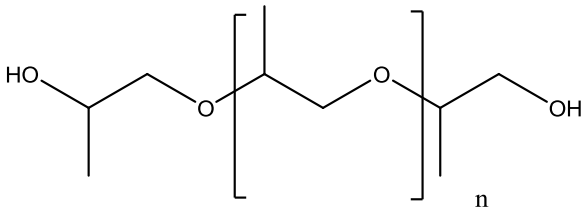

Figure 1.2: Poly(propylene) oxide

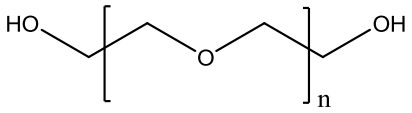

Figure 1.3: Poly(ethylene) oxide

Polyurethanes formed from PPO are hydrophobic with good resistance to hydrolysis, whilst those formed from PEO are hydrophilic and, as a result, are readily soluble in water with poor hydrolytic stability.[2] The use of PEO on its own is, therefore, very limited and most polyether polyols employed in the manufacture of flexible polyurethane foams are derived from either PPO alone or more commonly block co-polymers of PPO and PEO.

1.2.2.2 Isocyanates

An isocyanate is a compound containing the functional group –N=C=O and a functionality of two or more is required for the production of polyurethanes. Many of the isocyanates used in the production of polyurethanes are aromatic or cyclic in nature. For the production of foams the two isocyanates most commonly employed are methylene diphenyl diisocyanate (MDI) and toluene diisocyanate (TDI).[2,12]

MDI is generally used for the production of rigid foams and can exist in polymeric and monomeric forms, with the monomeric form most commonly used for polyurethane foam manufacture. Monomeric MDI is a mixture of 4,4- and 2,4- isomers,[7] the structures of which are shown in Figure 1.4.

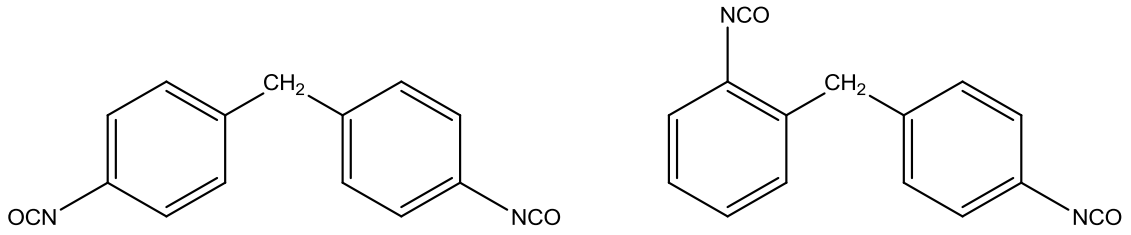

Figure 1.4: The structures of 4,4-MDI (left) and 2,4-MDI (right)

Polymeric MDI is a liquid mixture containing the monomeric MDI isomers as well as oligoisocyanates, the structure of which is shown in Figure 1.5.

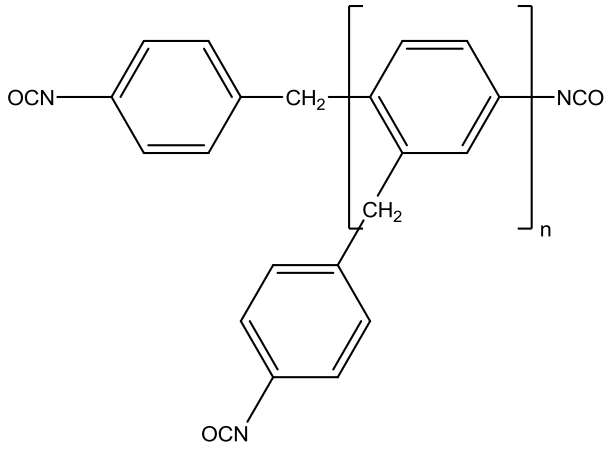

Figure 1.5: The structure of the oligoisocyanates found in polymeric MDI

TDI, on the other hand, is used extensively in the manufacture of flexible foams and consists of a mixture of 2,4- and 2,6-isomers, with an 80:20 ratio being most commonly encountered.[7] The structure of the 2,4- and 2,6-isomers of TDI are shown in Figure 1.6.

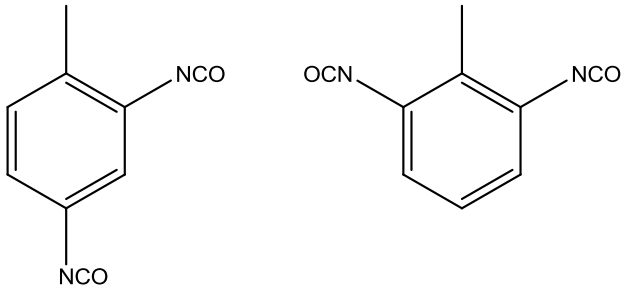

Figure 1.6: The structures of 2,4-TDI (left) and 2,6-TDI (right)

1.2.2.3 Blowing Agents

One of the most vital components for a polyurethane foam is the blowing agent, a substance which converts the polyurethane into a foamed structure by producing bubbles in the reaction mixture. Initially water was used as this reacts with isocyanates to yield a urea and carbon dioxide (CO_2), with the production of CO_2 causing bubbles to be formed in the reaction mixture.[7,13] As technology progressed chlorofluorocarbons (CFCs), which change from a liquid to a gas when heated, came into use as physical blowing agents. In particular trichlorofluoromethane (CFC-11) was the blowing agent of choice for a large number of foams due to its low molecular weight, low boiling

point, low toxicity and low thermal conductivity.[7,13,14] It was soon reported, however, that these compounds can have a negative impact on the environment, in particular through depletion of the ozone layer,[13,14] and these compounds are, therefore, now regarded as environmentally unacceptable. Following this discovery and the introduction of strict legislation on the use of CFCs, water once again became the blowing agent of choice for polyurethane foams.[6]

1.2.2.4 Catalysts

Catalysts are required for the production of polyurethane foams for two reasons: to catalyse and control the rate of reaction of the isocyanate with the polyol, and to catalyse and control the rate of the blowing reaction between the isocyanate and water.[7,15] Examples of catalysts which can be employed include tertiary amines, organometallics and carboxylic acid salts.[13] Amine catalysts are generally used for the blowing reaction whilst organometallic catalysts, on the other hand, are more commonly employed for the isocyanate-polyol reaction.[7] The most common organometallic catalysts are organotin compounds, although organomercury and organolead compounds also find use in some applications. The two main types of tin compound routinely employed as catalysts for polyurethane synthesis are tin II and tin IV compounds. Tin II compounds are primarily used in the manufacture of flexible foams, with the most common being stannous 2-ethylhexanoate, also known as stannous octoate.[14]

1.2.2.5 Surfactants

Surfactants are essential for the production of low density polyurethane foam, performing many key roles during the synthesis process.[7,13,14] They facilitate the mixing of any starting materials which may be incompatible and they are essential for stabilising the initial foam structure which forms before a self-supporting polymer network has formed. The surfactant lowers the surface tension of the small bubbles which form in the expanding foam mixture thereby stabilising them. In the absence of a surfactant these would coalesce into much larger, less stable bubbles. Surfactants can also help to

control the degree of cell opening within flexible foams. The majority of flexible polyurethane foams produced nowadays employ silicone-based surfactants.[14]

1.2.2.6 Cross-linking and Chain Extending Agents

Cross-linking agents and chain extenders are low molecular weight polyfunctional compounds which react with isocyanate groups to produce additional linkages within the polyurethane. Chain extenders are commonly used in the production of flexible foams and are typically difunctional glycols, amines or hydroxy amines which react with an isocyanate to produce an additional urethane or urea segment within the polymer chain.[7] Examples of chain extenders include ethylene glycol and diethylene glycol.[13]

Cross-linking agents, on the other hand, have a functionality greater than two and are used to increase the degree of cross-linking or branching within the polyurethane by the formation of additional urethane bonds.[7] These are most commonly used in the production of rigid foams and examples include glycerol and trimethylolpropane.[13]

1.2.2.7 Fillers

Fillers are solid materials insoluble in the foam which are used for a number of reasons, such as cost reduction, to increase the hardness or stiffness and to increase the thermal stability of the polyurethane.[7] Examples of fillers used in polyurethane foams are calcium carbonate, barium sulfate, and silica.[13]

1.2.2.8 Fire Retardants

Flexible polyurethane foams are easily ignited in air and burn relatively quickly.[13,14,16] Fire retardants are incorporated into foams in order to meet specific flammability and combustion test requirements. Examples of common fire retardants for flexible polyurethane foam are melamine, halogenated compounds and phosphorus compounds.[17,18] More recently, clays have been studied and tested for use as potential fire retardants in foams.[19,20] The flammability of polyurethane foams and the use of fire

retardants are of upmost importance for the successful application of these materials and will be discussed more extensively in Section 1.3.3.

1.2.3 Chemistry of Polyurethane Foam Synthesis

1.2.3.1 Primary Reactions

There are two key reactions which are of importance in the production of a polyurethane foam. The first is the exothermic reaction of a diisocyanate and a polyol to form a polyurethane,[2,7,21,] as illustrated in Figure 1.7, which is accelerated by use of a catalyst such as stannous octoate. This process is reversible at elevated temperatures with the specific temperature depending on the structures of the polyol and the diisocyanate.[7]

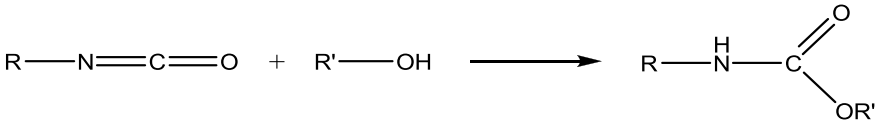

Figure 1.7: Primary reaction of an isocyanate with a hydroxyl group to form a urethane

The second important reaction is that of a diisocyanate with water to yield a substituted urea and CO_2,[7,21] which is used as the principal method of blowing in flexible polyurethane foams. The isocyanate first reacts with water to form a carbamic acid which decomposes into an amine and CO_2. The amine subsequently reacts with a second isocyanate group to form a substituted urea, as illustrated in Figure 1.8.[2]

Due to the water which is present in the formation of polyurethane foam the resulting foamed product is, therefore, not purely a polyurethane but is instead likely to be a mixture of polyurethane and polyurea segments.

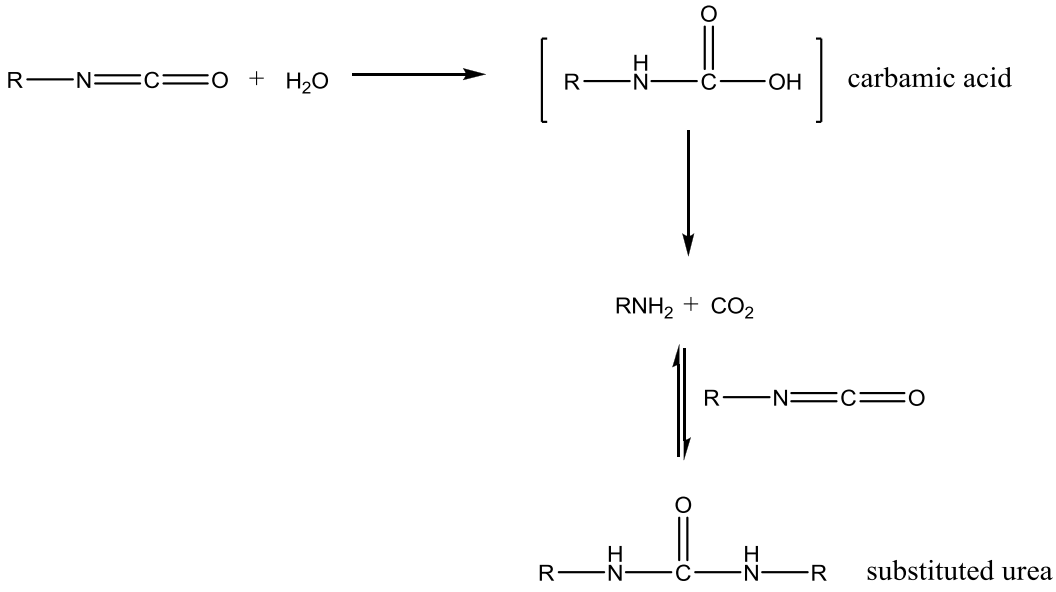

Figure 1.8: Primary reaction of an isocyanate with water to form a substituted urea

1.2.3.2 Secondary Reactions

During the synthesis of polyurethanes a number of secondary reactions can occur between isocyanates and other reactive groups, as well as reactions of isocyanates with themselves. Isocyanates can react with a urea or urethane linkage to form biuret and allophonate, respectively, as shown in Figure 1.9 and Figure 1.10.[2,21,22] These reactions increase the degree of cross-linking in the polyurethane.

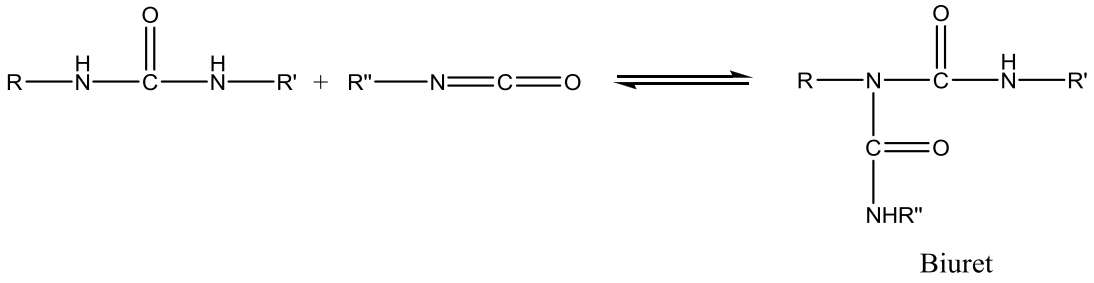

Figure 1.9: The formation of biuret

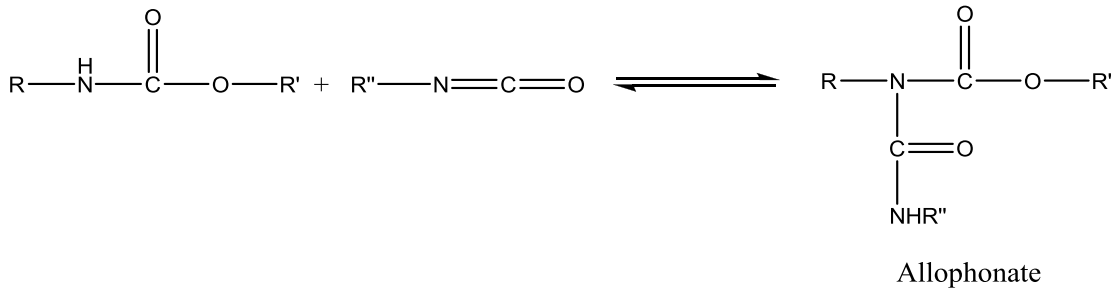

Figure 1.10: The formation of allophonate

A cycloaddition reaction can occur between two isocyanates to form a four-membered ring dimer known as uretidinedione, as shown in Figure 1.11.[2,21] This reaction is more prominent for MDI than for TDI.

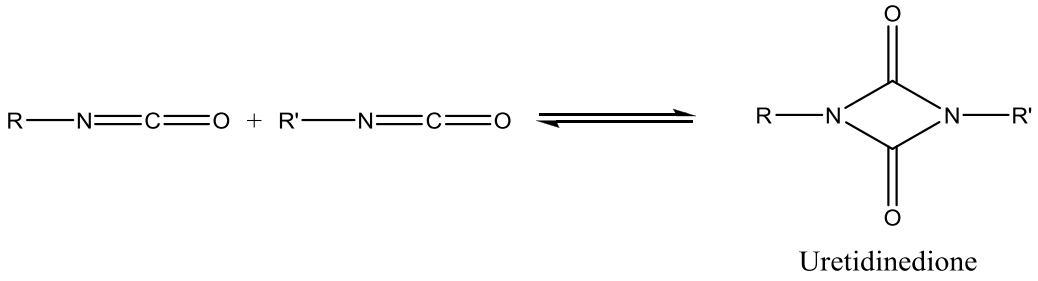

Figure 1.11: Formation of uretidinedione

At temperatures greater than 180^{o}C this reaction follows an alternative route with the result being the formation of carbodiimide, as shown in Figure 1.12.[2,7]

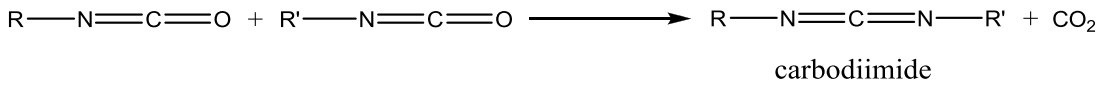

Figure 1.12: High temperature formation of carbodiimide

The final reaction of importance is the cyclisation reaction of three isocyanate molecules to form a six-membered ring compound known as isocyanurate, as illustrated in Figure 1.13.[2,21] Although this reaction can be undesirable, it can be used to introduce branching and cross-linking into the polymer and is commonly used in the production of rigid polyurethane foams.

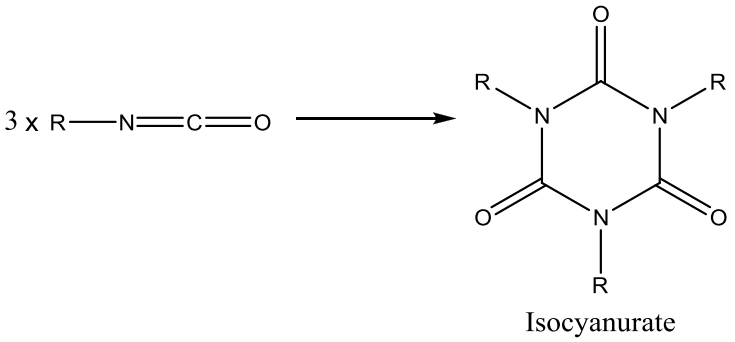

Figure 1.13: Formation of isocyanurate

With the above reactions in mind it is clear that polyurethane foams are complex materials containing not only urethane bonds but also urea linkages and secondary structures such as those possessing allophonate, biuret, isocyanurate and carbodiimide units.

1.3 Polyurethane Foams and the Fire Hazard

1.3.1 The Issue

As technology has advanced, polymers have been employed in place of conventional materials, such as wood and glass, and polymers now find vast use in today's society. These materials are not without their drawbacks however, a major of which is their flammability. Polymers are almost exclusively organic materials and like all organics they are flammable, more so than conventional materials, and they are therefore associated with an increased fire hazard.[23,24] The flammability of these materials is, however, not the only problem. The majority of deaths in fires are not normally a result of the flame or heat but are caused by inhalation of toxic gases and suffocation due to the smoke, [22,25] both of which arise due to degradation of polymeric materials within the fire. The fire hazard associated with these materials has caused concern over recent years and the polymer industry is being put under increasing pressure to produce materials which have increased fire retardancy. In order to do so, however, we must first understand the chemistry which occurs during the degradation of polymeric materials.

1.3.2 Polymer Combustion

Polymers themselves do not burn; it is the flammable volatile degradation products of these materials which do.[23] When subjected to sufficient heat a polymeric material will decompose releasing volatile products, many of which are flammable and will ignite when the temperature is high enough. If the heat evolved by the flame is sufficient to ensure that the decomposition rate of the polymer remains high enough to evolve a continuous stream of volatiles, then a self-sustaining combustion cycle will be established.[24]

The combustion of a polymer may be represented by the burning cycle shown in Figure 1.14.[23]

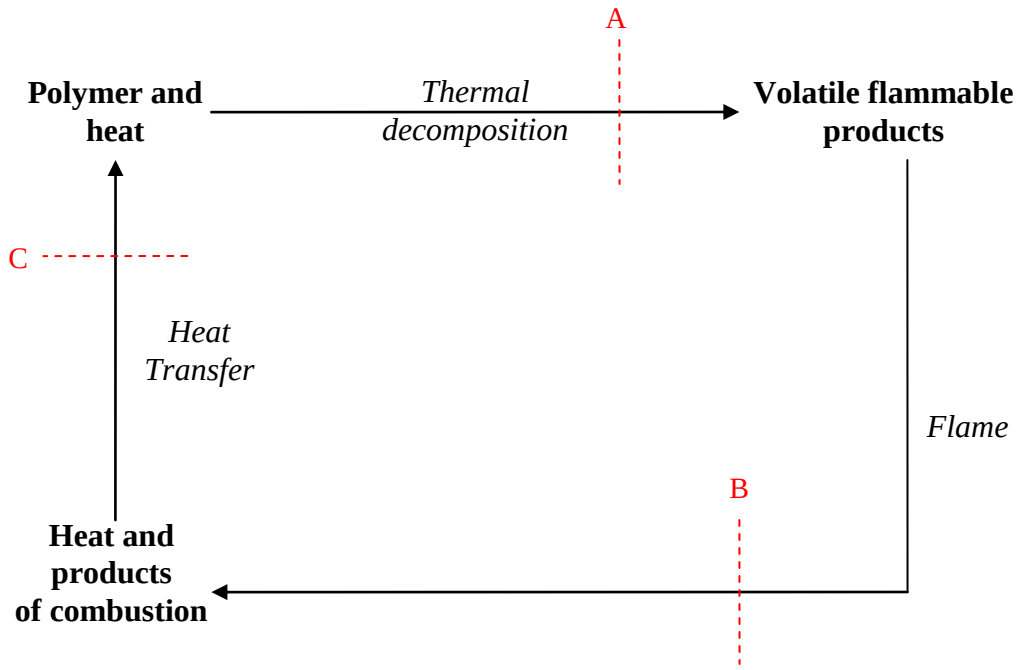

Figure 1.14: A model of the burning cycle of a polymer; see page 16 for reference to A, B and C.

The temperature of the polymer is raised by an external heat source and when sufficiently high will induce thermal decomposition of the material with subsequent evolution of volatile decomposition products. These are generally organic and flammable and will ignite in the presence of an external ignition source or by auto

ignition if the temperature is high enough.[24,25] These volatile degradation products are essentially the fuel which sustains the flame. Thermal feedback from the flame to the polymer causes further degradation and the cycle becomes self-sustaining.

For the burning cycle to continue, the heat must be sufficient to decompose the polymer, the temperature must be high enough to cause ignition of the volatile decomposition products and enough heat must be fed back to the polymer to maintain the cycle when the initial external heat source is removed. If these criteria are not met then burning will cease and the fire will extinguish.[23,24]

A polymer's behaviour during a fire is a result of various physical and chemical processes which occur in the condensed-phase.[24] Some polymers, as well as releasing volatile material, produce a carbonaceous solid residue as part of their degradation mechanism. These residues are rarely all carbon; however, they are referred to in the field of polymer degradation as chars. Char formation is one of the most important condensed-phase mechanisms for modifying the combustion process of a polymer as it protects the degrading polymer in a number of ways.[24,25] It acts as a barrier to heat flow thereby reducing the thermal feedback to the polymer and protecting the remaining polymer from further degradation. It also inhibits the diffusion of flammable gases into the flame and preserves the structural integrity of the polymer. The level of protection which a char provides is strongly dependent on its physical and chemical structure and the temperature at which it begins to form. A char will clearly be of little use if it forms after the temperature at which significant degradation of the polymer has occurred. The importance of the char structure on its efficiency can be illustrated by considering an ideal and a non-ideal char as shown in Figure 1.15.

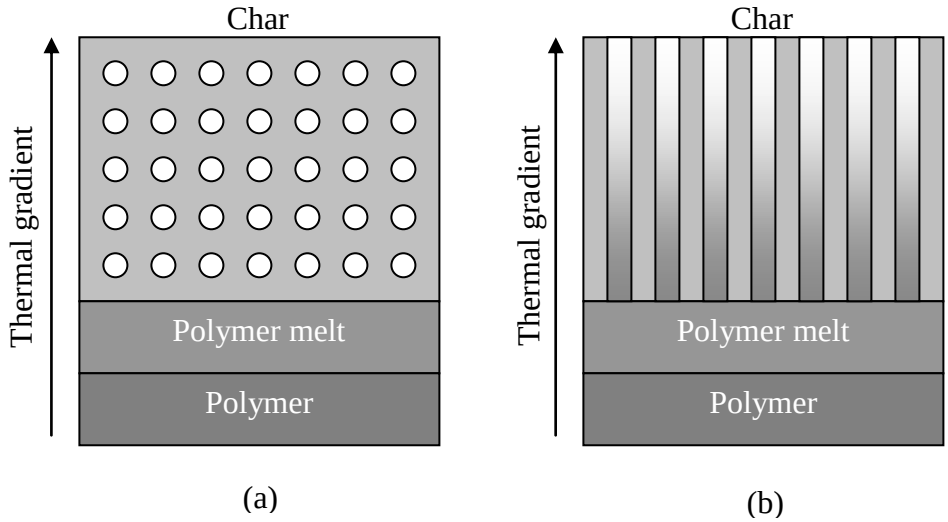

Figure 1.15: Illustration of (a) an ideal char and (b) a non-ideal char[24]

An ideal char is a structure consisting of closed cells or pores which contain gas pockets. The bubbles of gas are encapsulated within the polymer melt and upon solidification a honeycombed structure is formed. In the ideal char the flow of molten polymer or flammable gases into the flame is prevented by the closed cell structure. Furthermore, this form of char sufficiently insulates the remaining polymer or melt, thereby keeping it below its degradation temperature. The non-ideal char, on the other hand, has channels instead of closed cells and the result is that flammable gases can flow into the flame and molten polymer can migrate through the channels in the char by capillary action into regions of higher temperature where further decomposition of the material can occur. This type of char also has poor thermal insulation compared to the ideal char.[24] For a char to be efficient, therefore, it must not only form at a suitable temperature but it must also possess a structure as close to that of the ideal char as possible. It should be noted that the illustration in Figure 1.15 is not to scale. In a carbonaceous material, such as char, a large number of pores will be present with various sizes on a nanometer scale (micro-, meso- and macro-pores)[26] which results in the material having a high surface area.

1.3.3 Fire Retardants

The major issues associated with the combustion of polymers, in particular polyurethane foams, are the ease of flammability and the toxic nature of the degradation products evolved. Polyurethane foams are widely used in household furnishings and are easily ignited in air, with low density foams burning quickly due to the large surface area present. These foams can evolve vast quantities of harmful gases such as carbon monoxide and hydrogen cyanide during a fire. These are serious issues which are continually trying to be overcome and one way in which this is tackled is through the use of fire retardants.

1.3.3.1 Aims

The aim of a fire retardant is to increase the fire resistance of a material by reducing its ease of flammability, as well as reducing the toxicity of the volatile degradation products evolved.[24] This can be done by limiting the degradation which occurs or by changing the process of degradation to a more favourable one, for example, by which more carbonaceous char is formed.

Fire retardants act to break the burning cycle at one or more of the points labelled A, B and C in Figure 1.14, which can be done by:[23]

- Modifying the degradation mechanism of the polymer (A)
- Quenching or extinguishing the flame (B)
- Reducing the thermal feedback from the flame to the decomposing polymer (C)

There are several chemical and physical activities which a fire retardant can perform in order to achieve these actions which include:[13,24]

- Modifying the degradation process so that the flammable and volatile products evolved are reduced in favour of the formation of less flammable species

- Reducing the heat evolved to below that required to sustain the burning cycle, for example, by filling with heat-sink compounds which decompose endothermically thus acting as heat absorbers
- Introducing into the polymer compounds which evolve efficient flame inhibitors when heated
- Isolating the flame from the air supply
- Reducing the thermal feedback to the polymer by using a heat-sink compound or by formation of a protective barrier by inducing carbonaceous char formation
- Incorporating into the polymer materials which decompose to incombustible gases, such as water and CO_2, thereby diluting the fuel for the flame

Most flame retardant systems currently in use exhibit more than one of these features. For a fire retardant to be effective it must be stable at the temperatures at which the polymer is processed, it must be compatible with the polymer and it should not adversely affect the properties of the material or interfere with any other additives.[27]

1.3.3.2 Mechanisms and Modes of Action of Fire Retardants

The primary mechanisms of fire retardants can be divided into two main types, namely gas-phase and condensed-phase mechanisms.

1.3.3.2.1 Gas-phase Mechanisms

In a gas-phase mechanism the quantity of combustible material present and the nature of the decomposition products are not altered, however the heat released by the combustion process is reduced usually by dilution of the flammable volatiles feeding the flame with non-flammable volatiles.[28] This reduces the thermal feedback to the polymer and the degradation of the polymer becomes retarded. The fire retardant species must volatilise and reach the flame in a gaseous form in order to exert its effect or alternatively it must decompose, releasing the active component into the gas-phase.

A fire retardant acting in the gas-phase exerts its main activity by interfering with the combustion process of the polymer. When thermally decomposed, polymers produce species which can react with atmospheric oxygen to produce the H_2-O_2 scheme which propagates fuel combustion by the chain branching reactions shown in Equation 1.1 and Equation 1.2.[23,27,28]

$$H^{\bullet} + O_2 \rightarrow {}^{\bullet}OH + O^{-} \qquad \textbf{Equation 1.1}$$

$$O^{-} + H_2 \rightarrow {}^{\bullet}OH + H^{\bullet} \qquad \textbf{Equation 1.2}$$

The exothermic reaction which provides the majority of the energy required to sustain the flame is that of carbon monoxide (CO) with a hydroxyl radical as shown in Equation 1.3.[23,27,28]

$$^{\bullet}OH + CO \rightarrow CO_2 + H^{\bullet} \qquad \textbf{Equation 1.3}$$

In order to reduce the rate of combustion the chain branching reactions shown in Equation 1.1 and Equation 1.2 must be inhibited or altered. Halogen-based fire retardants are believed to operate in such a way, the mechanism of which will be discussed in more detail in Section 1.3.3.4.1.

1.3.3.2.2 Condensed-phase Mechanisms

A fire retardant acting *via* a condensed-phase mechanism alters the degradation pathway of the polymer and reduces the level of flammable volatile products evolved, often by formation of a carbonaceous char. It is proposed that the condensed-phase mechanism involves a chemical interaction between the fire retardant and the polymer at a temperature below that of the polymer's decomposition.[28] Two main modes of condensed-phase action which have been established for a number of polymers are dehydration and cross-linking, both of which lead to char formation.

Dehydration mechanisms have been shown to operate for some phosphorus-containing fire retardants. The effect of phosphorus on the fire retardance of different polymers varies and has been related to the susceptibility of the polymer to dehydrate and form char. For example, cellulosic materials which are reasonably easily dehydrated require

much lower levels of phosphorus fire retardant than polyolefin materials, as materials which do not contain hydroxyl groups interact with phosphorus slowly.[29]

Cross-linking has been shown to promote char formation in polymeric materials and in many cases reduces the flammability of the polymer. Cross-linking stabilises a polymer structure by the formation of strong covalent linkages between polymer chains which will need to be broken before decomposition of the polymer can begin. Cross-linking may also lead to an increase in the viscosity of the polymer melt thereby retarding the flow of combustible decomposition products into the flame.[28]

1.3.3.3 Additives and Reactives

Fire retardants can be incorporated into a polymer either as an additive or as a reactive. An additive is a compound which is mechanically mixed with the polymer, whereas a reactive is chemically bound within the polymer structure.[23,30] For example, phosphorus compounds can be used as reactive fire retardants in polyurethanes in the form of a phosphorus-containing diol or polyol which reacts with isocyanate to form a phosphorus-containing polyurethane.[16] As reactive fire retardants are bound within the polymer they are not lost by leaching from the polymer or by evaporation, a common problem with many additive fire retardants. Furthermore, they will be instantly available to protect the polymer during a fire as their liberation from the polymer will occur at the same time as the polymer begins to decompose.[23] Additives, on the other hand, are more problematic as their properties must be carefully matched with the polymer so that they decompose or volatilise at the temperature at which they are required to protect the polymer during a fire situation. The main disadvantage of a reactive fire retardant, however, is that the chemical stability or physical properties of the polymer are more likely to be altered than when an additive is employed. Reactives are, therefore, most commonly employed in rigid polyurethane foams where they are more easily incorporated into the highly cross-linked material without significantly affecting the properties.[13]

1.3.3.4 Common Fire Retardants and Their Modes of Action

The six elements most commonly used in fire retardants are chlorine, bromine, phosphorus, antimony, aluminium and boron.[23,30] Nitrogen compounds, such as melamine, are also employed in some polymer systems.[30] A particular fire retardant may exhibit multiple modes of action and it is, therefore, not possible to associate an element with one specific mechanism. Understanding the mechanisms of fire retardants requires knowledge of the degradation mechanism of the fire retardant and the material in which it is employed, as the mechanism of a fire retardant can depend on the polymer in which it is employed. It is generally the case, however, that phosphorus is strongly associated with changes in the degradation chemistry of the polymer, halogens and antimony are associated with flame quenching reactions and aluminium and boron inhibit heat flow.[23] The most widely used classes of fire retardants and their proposed modes of action are discussed in more detail in the sections which follow.

1.3.3.4.1 Halogens

It is generally accepted that halogenated fire retardants perform most of their fire retardant activity in the gas-phase by inhibiting the chain branching combustion reactions shown in equations 1.1 and 1.2,[23,28] and by diluting the gaseous decomposition products in the flame with non-flammable halogen-containing species.[18,31] When a halogen-containing compound (MX) decomposes it releases a halogen radical ($X^{\bullet}$) as shown in Equation 1.4.[28]

$$MX \rightarrow M^{\bullet} + X^{\bullet} \qquad \textbf{Equation 1.4}$$

The halogen radical then reacts with the polymer or fuel by abstracting a hydrogen radical to produce hydrogen halide as shown in Equation 1.5.[28]

$$RH + X^{\bullet} \rightarrow HX + R^{\bullet} \qquad \textbf{Equation 1.5}$$

If the fire retardant contains hydrogen then the hydrogen halide is formed directly, as illustrated in Equation 1.6.[28]

$$MX \rightarrow HX + M^{\bullet} \qquad \textbf{Equation 1.6}$$

Hydrogen halide is believed to be the active component which inhibits the chain branching combustion reactions as shown in Equation 1.7 and Equation 1.8.[27,28]

$$H^{\bullet} + HX \rightarrow H_2 + X^{\bullet} \qquad \textbf{Equation 1.7}$$

$$^{\bullet}OH + HX \rightarrow H_2O + X^{\bullet} \qquad \textbf{Equation 1.8}$$

The halogen radical formed is relatively unreactive, reacting slowly with the components of the combustion process to regenerate hydrogen halide. Commonly used halogen fire retardants include ammonium bromide (NH_4Br), ammonium chloride (NH_4Cl) and brominated biphenyl compounds.[23,32]

Chlorine fire retardants have been shown to be more effective when used in conjunction with metal oxides such as antimony oxide,[23,27] which is discussed in more detail in Section 1.3.3.4.5. Bromine is more effective than chlorine as a fire retardant element when employed as both an additive and a reactive, as the H-Br bond is more labile and undergoes the radical reactions in Equations 1.7 and 1.8 more readily.[28] Its compounds are, however, more expensive and are less resistant to thermolysis and photolysis which can cause issues during processing.[23]

As well as having an effect in the gas-phase, halogen compounds also exhibit some condensed-phase activity through the evolution of heavy halogen-containing gases which protect the condensed-phase by inhibiting the access of oxygen and heat transfer.[13,30] Furthermore, the abstraction of hydrogen from the polymer to form hydrogen halide can lead to unsaturation which can in turn lead to char formation.[30]

1.3.3.4.2 Phosphorus

Phosphorus fire retardants, in particular inorganic phosphates such as ammonium polyphosphate (APP), have been used for many years in the protection of cellulosic

materials such as wood and cotton.[23] Following the success of such compounds, organic phosphorus compounds have become widely used. Phosphorus fire retardants have been shown to exhibit multiple modes of action including flame inhibition and char promotion.[28] It is, however, generally accepted that phosphorus compounds exert most of their fire retardant activity in the condensed-phase.[13,16,30]

The role of phosphorus fire retardants has been studied in some detail and has been shown to involve degradation of the phosphorus compound to yield phosphoric acids.[18,23,33] The fire retardant activity of the phosphorus is likely, therefore, to be associated with the influence of these acids on the thermal degradation reactions of the polymer. In some cases it is proposed that the presence of acid promotes the formation of a carbonaceous char by dehydration of the polymer, whilst in other cases the formation of a glassy coating of phosphoric acid is considered to be a flame inhibiting process.[13,28]

The effect of phosphorus on the degradation of cellulosic materials has been extensively studied and a suitable mechanism of activity proposed.[23,27,33] The phosphoric acid formed from decomposition of the phosphorus fire retardant esterifies the hydroxyl groups of the cellulose with release of water. The cellulose phosphate then decomposes to produce stable conjugated unsaturated structures which are proposed to be precursors for char formation. In this case the phosphorus has exhibited multiple modes of action: as a char promoter, by reducing the level of fuel and by evolving non-combustible species such as water. A similar mode of action has been proposed for polyurethane materials, which will be discussed in more detail in Section 1.6.1.1.

In some cases phosphorus has been shown to inhibit smouldering by forming a physical barrier in the form of a polyphosphoric acid coating.[13] Phosphoric acids have also been shown to have an effect on the fire retardance by encouraging flow of the molten polymer from the flame zone. This is proposed to be due to acid-catalysed thermal decomposition of the polymer melt which reduces the viscosity and increases the flow of

the molten polymer.[28] It has also been shown that volatile phosphorus compounds can have an effective flame inhibiting effect. For example, triphenyl phosphate decomposes into small species such as P_2, PO, PO_2 and HPO_2 which inhibit the chain branching reaction shown in Equation 1.1, thereby quenching the flame.[28] This is a similar effect to that exhibited by halogen-based fire retardants.

A synergistic effect between phosphorus and halogen additives has been shown with the formation of phosphorus trihalides, pentahalides and oxyhalides.[13,30] The production of such heavy incombustible gases can aid in the quenching of the flame.

1.3.3.4.3 Melamine

Melamine, the structure of which is presented in Figure 1.16, is a nitrogen-containing fire retardant widely used in flexible polyurethane foams. It is regarded as being environmentally friendly as it contains only elements which are already present within the polyurethane.

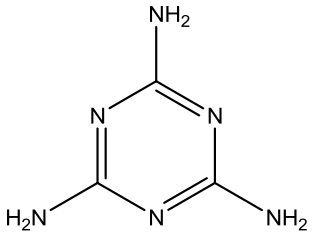

Figure 1.16: The structure of melamine

The mode of action of melamine is complex as it displays a number of mechanisms which may contribute to its effectiveness.[34] On heating, melamine is known to undergo progressive condensation reactions with elimination of ammonia to form polymeric products known as melam, melem and melon, as illustrated in Figure 1.17.[35,36]

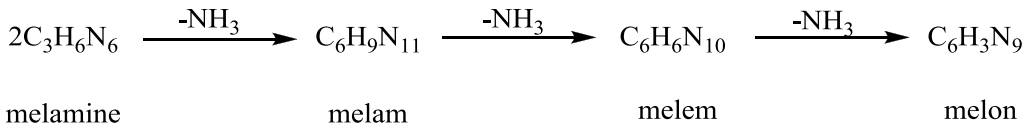

Figure 1.17: The decomposition of melamine into polymeric products

These reactions are endothermic, therefore, melamine exhibits a heat sink effect, as well as evolving inert nitrogen-containing gases which dilute the fuel. It has been proposed that melamine may also exhibit free radical scavenging properties and more recently solid-state NMR studies have suggested a condensed-phase action *via* the promotion of char formation.[37] Melamine can be used alone or in conjunction with other fire retardants and it is known to have a synergistic effect with phosphorus compounds.[28]

1.3.3.4.4 Aluminium

Aluminium was one of the earliest fire retarding elements employed, used in the form of alum for protecting cellulosic materials, and alumina trihydrate ($Al_2O_3.3H_2O$) is the most common aluminium fire retardant used nowadays.[23] It is only active in its hydrated form which suggests that the presence of water is a major factor in its mode of action. It decomposes endothermically between 230°C and 330°C to release the water[23,28] which mixes with the volatile polymer degradation products thereby diluting them and extinguishing the flame. The endothermic nature of the reaction is also part of the mode of action as this helps to reduce the temperature of the degrading polymer. Furthermore, once the water has been released a layer of Al_2O_3 ash remains on the surface of the polymer, forming a refractory layer which can act as a heat barrier thereby reducing the thermal feedback to the material.[30] The temperature range at which this material has its effect encompasses the degradation temperatures of a variety of polymeric materials thus making it a useful fire retardant for many applications.[18]

1.3.3.4.5 Antimony

Antimony compounds have been used for years as fire retardants in textiles, with their use in polyurethanes first described in the 1960s.[13] The most widely used compound is antimony trioxide, Sb_2O_3, which has been employed in flexible polyurethane foams. This compound has little activity by itself but has a synergistic effect with halogenated fire retardants.[23,27,30] When the two are employed together it is assumed that an antimony-halogen compound, most likely an antimony oxyhalide, is formed and this exerts the fire retardant activity.[28] If a polymer is able to liberate hydrogen halide during

its degradation, *e.g*. poly(vinyl chloride), then Sb_2O_3 can be employed on its own with that polymer.

Considering Sb_2O_3 with a chlorine-containing compound, antimony oxychloride (SbOCl) will be formed when these react. SbOCl subsequently decomposes into Sb_2O_3 and $SbCl_3$ in three steps between 245°C and 565°C, as illustrated in Equation 1.9, Equation 1.10 and Equation 1.11.[23]

$$5SbOCl \rightarrow Sb_4O_5Cl_2 + SbCl_3 \qquad \textbf{Equation 1.9}$$

$$4Sb_4O_5Cl_2 \rightarrow 5Sb_3O_4Cl + SbCl_3 \qquad \textbf{Equation 1.10}$$

$$3Sb_3O_4Cl \rightarrow 4Sb_2O_3 + SbCl_3 \qquad \textbf{Equation 1.11}$$

It is proposed that $SbCl_3$ is the active agent which functions primarily in the gas-phase by reacting directly with the chain propagating radicals to form HX, as shown in Equation 1.12, Equation 1.13 and Equation 1.14.[23,27]

$$SbX_3 + H^{\bullet} \rightarrow SbX_2 + HX \qquad \textbf{Equation 1.12}$$

$$SbX_2 + H^{\bullet} \rightarrow SbX + HX \qquad \textbf{Equation 1.13}$$

$$SbX + H^{\bullet} \rightarrow Sb + HX \qquad \textbf{Equation 1.14}$$

The efficiency of the antimony-halogen synergism is increased by the fact that the active SbX_3 species are liberated over a wide temperature range which corresponds with the degradation temperatures of a wide range of polymers.

1.3.3.4.6 Boron

In the 19th century borax ($Na_2B_2O_7.10H_2O$) and boric acid were important fire retardant additives for the protection of textiles such as cotton and wool.[23,28] The formation of a protective inorganic coating on the fibres is proposed to be the principal mode of action for such applications. Boric acid undergoes a two step decomposition, as shown in

Equation 1.15, forming metaboric acid followed by boric oxide.[38] Boric acid inhibits non-flaming surface combustion in the charred material, known as afterglow.

$$2H_3BO_3 \rightarrow 2HBO_2 \rightarrow B_2O_3 \qquad \textbf{Equation 1.15}$$

Borax, on the other hand, dissolves in its water of crystallisation when heated. The water is then evaporated and the material which remains melts to a clear, mobile liquid.[28] Borax is a more efficient fire retardant than boric acid, however, it is common for mixtures of borax and boric acid to be used as combining their complementary functions leads to more effective fire retardance.[38]

1.3.3.5 Nanocomposites

Nanocomposites constitute a relatively new development in the area of flame retardancy being of great interest due to their potential to show superior properties over conventional fire retardants. The benefits include increased thermal stability, enhanced gas barrier properties and improved mechanical properties.[39,40] Polymers incorporating layered silicate clays are the most common group of nanocomposite materials employed.[41] These were first reported by Blumstein in 1961;[42] however, the technology began to be more widely exploited in the 1990s.[43] Layered silicate clays have chemically stable siloxane surfaces, high surface areas and high aspect ratios and hence are most widely used.[43] There are two particular characteristics of layered silicate clays which allow them to be employed in the formulation of nanocomposites. First, the silicate nanolayers can be exfoliated into individual layers which maximises the contacts between the clay and the polymer. Second, their surface chemistry can be modified through ion-exchange reactions with organic and inorganic species.[40,41]

Montmorillonite is a smectite clay which is a common choice for nanocomposites due to its small particle size, high swelling capacity and high aspect ratio. Its structure consists of a sheet of octahedral aluminium oxide, AlO_6, sandwiched between two layers of tetrahedral silicon oxide, SiO_4, to form a platelet structure.[39,40,43] The platelets are

structured into ordered stacks known as tactoids, with regular spacing between each platelet. Isomorphic substitution of the aluminium within the layers with cations such as iron, magnesium or lithium generates negative charges at the platelet surface which are usually counterbalanced with sodium or potassium cations. These can then be exchanged with organic cations, such as alkylammonium species, converting the hydrophilic silicate surface into an organophilic surface, in turn, making it more compatible with polymers.[39,40]

When a polymer is mixed with a clay there are three types of nanocomposite structures which can be formed, as illustrated in Figure 1.18.[43]

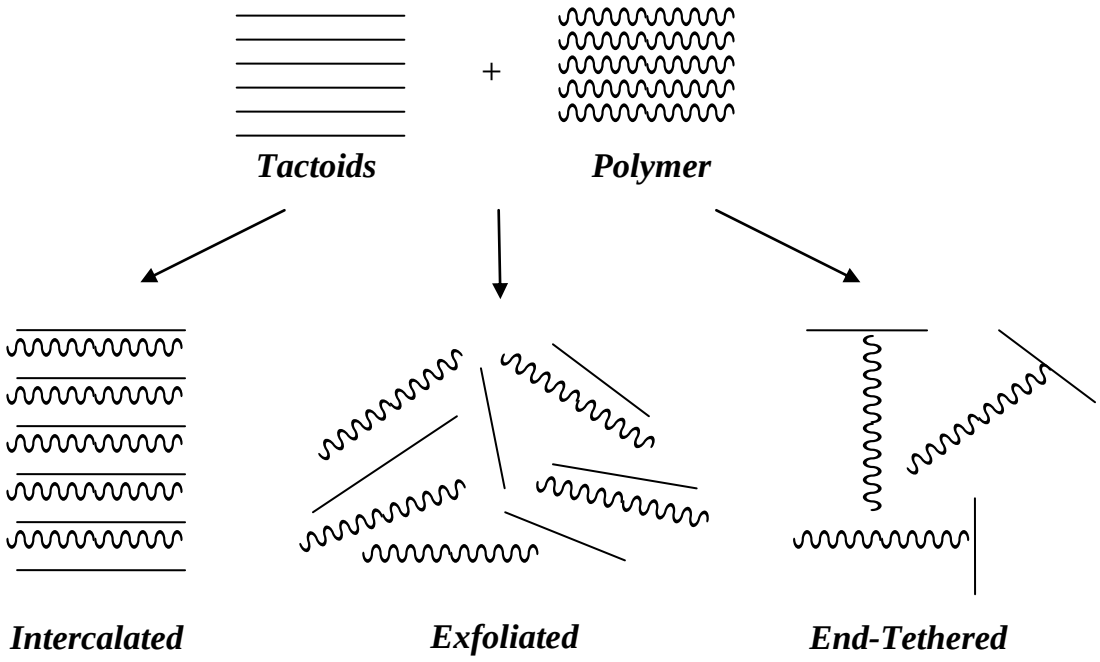

Figure 1.18: The three nanocomposites structures that can be formed

In an intercalated structure the polymer is sandwiched between the clay platelets but the stacks of platelets remain in tactoids. In exfoliated systems the platelets are completely separated from each other and are dispersed throughout the polymer matrix. With end-tethered structures the whole tactoid or a single platelet is attached at the end of a polymer chain. In the majority of polymer nanocomposites two or more of these

structures will be present.[39,40] Exfoliated nanocomposites show greater homogeneity than the other structures and tend to exhibit superior properties.[43]

Polymer-clay nanocomposites were first created using nylon 6 and were optimised by the research group at the Toyota Motor Company.[39,40,44] It was observed that exfoliation of layered silicates in nylon 6 greatly improved the thermal, mechanical and barrier properties of the polymer.[43] Following this discovery the technology has been extended to other polymer systems and a considerable number of papers have been published on polymer nanocomposites.[40] The large filler surface area of nanocomposites should, in principle, lead to good barrier properties and elevated melt viscosity; such properties are believed to be important in the mode of action of nanocomposites in fire retardant formulations. It has been recognised, however, that nanoclays often work best in conjunction with other fire retardants.[43]

1.4 Polymer Degradation

1.4.1 Introduction

As mentioned previously, advances in polymer technology has led to these materials replacing traditional materials such as glass and metal in a variety of applications. The major disadvantage of these materials over their conventional counterparts is that they are more liable to degradation and when this occurs they often produce harmful materials. Degradation usually involves physical and chemical modifications of a polymer by its environment, which is detrimental to the performance of the polymer. Types of degradation include thermal, thermo-oxidative, photo-degradation and biological degradation. For this study only thermal and thermo-oxidative degradation are relevant and will be discussed in more detail.

1.4.2 Thermal Degradation

When subjected to excess heat, polymers decompose by a process known as thermal degradation which is a major limiting factor in the application of polymers. Various

types of degradation processes can be thermally induced within a polymeric material but according to Grassie and Scott[45] these can be divided into two main classes, namely depolymerisation and substituent reactions.

1.4.2.1 Depolymerisation Reactions

This class of thermal degradation can proceed *via* a radical or non-radical mechanism and is characterised by scission of the main polymer backbone yielding products which are similar to the parent polymer in the sense that the monomer units are still distinguishable.

1.4.2.1.1 Radical Depolymerisation

One of the simplest examples of a radical depolymerisation reaction is that of poly(methyl methacrylate) (PMMA) which degrades *via* a radical chain reaction to produce the original monomers as its degradation products, as illustrated in Figure 1.19.[45,46]

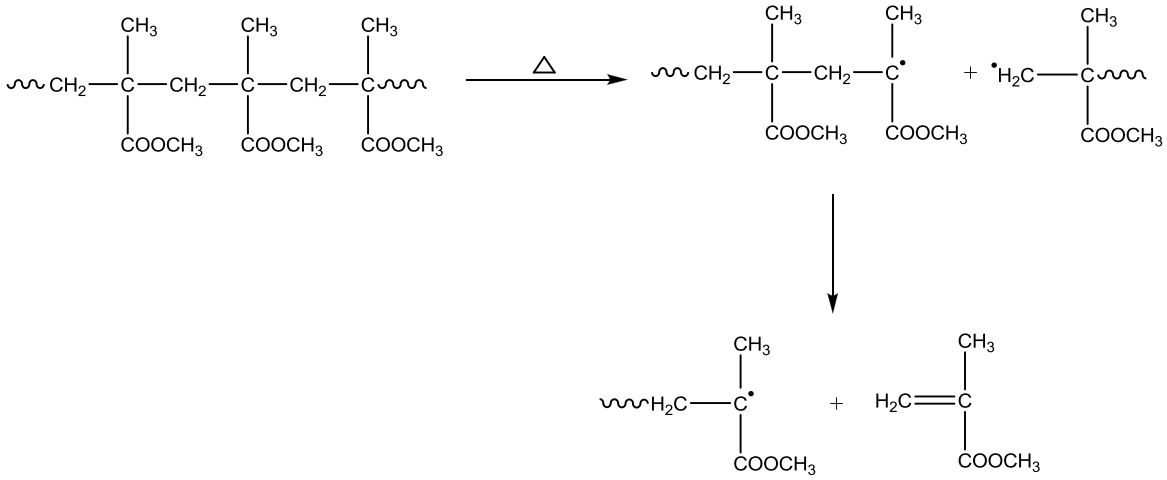

Figure 1.19: Radical depolymerisation of PMMA

Random scission of the polymer backbone occurs yielding radical species which depropagate in a reaction which is the reverse of the propagation reaction which forms PMMA. Termination then occurs by combination of two radical species or when the depropagation reaction reaches the end of the polymer chain**.** This type of reaction can

essentially be thought of as an 'unzipping' of the polymer chain along its backbone to yield the monomers from which the polymer was polymerised.

A polymer degrading by a radical depolymerisation reaction can be considered to follow the general mechanism outlined below, where *n* is the chain length of the starting polymer, M_i, M_j etc. represent 'dead' polymer molecules, and $M_i^\bullet$, $M_j^\bullet$, etc. represent long chain radicals *i*, *j*, etc. monomer units in length.[45]

Random initiation: $M_n \rightarrow M_j^\bullet + M_{n-j}^\bullet$

Terminal initiation: $M_n \rightarrow M_{n-1}^\bullet + M^\bullet$

Depropagation: $M_i^\bullet \rightarrow M_{i-1}^\bullet + M$

Intramolecular transfer and scission: $M_i^\bullet \rightarrow M_{i-z}^\bullet + M_z$

Intermolecular transfer: $M_i^\bullet + M_n \rightarrow M_i + M_n^\bullet$

Scission: $M_n^\bullet \rightarrow M_j + M_{n-j}^\bullet$

Termination: $M_i^\bullet + M_j^\bullet \rightarrow M_i + M_j \text{ or } M_{i+j}$

1.4.2.1.2 Non-radical Depolymerisation

There are many depolymerisation reactions, including those of polyesters and polyurethanes, which do not occur *via* a radical mechanism. In these types of reactions chain scission often occurs at a functional group linkage in a reaction which is the reverse of the polymerisation reaction. For example, in polyurethanes depolymerisation occurs *via* a non-radical scission of the urethane linkage, which can be considered to be a depolycondensation reaction, as illustrated in Figure 1.20.[45] The degradation mechanisms of polyurethanes are discussed in more detail in Section 1.5.

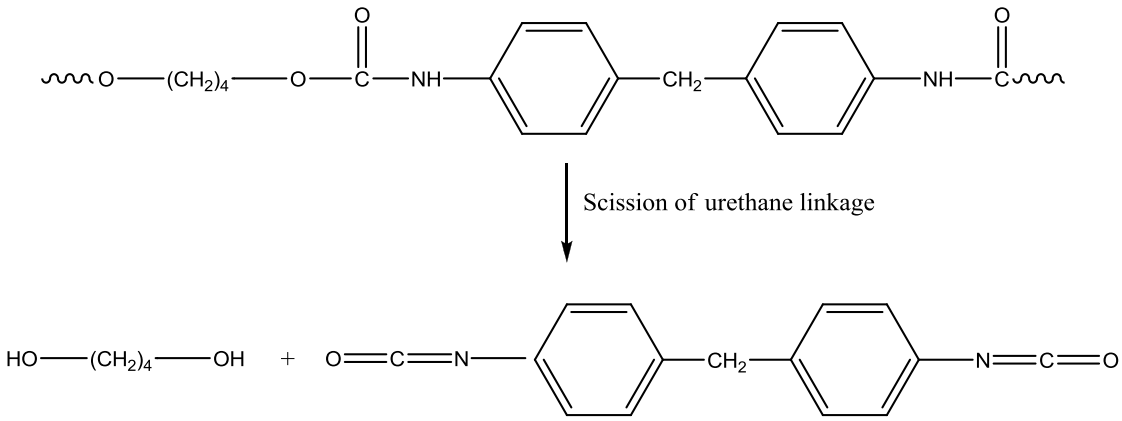

Figure 1.20: Non-radical depolymerisation of a polyurethane

1.4.2.2 Substituent Reactions

In this class of thermal degradation the substituent groups on the polymer backbone are involved which alters the chemical nature of the repeating unit. In contrast to depolymerisation reactions, any volatile products evolved will be unlike the monomers. The first type of substituent reaction which can occur is elimination, for example PVC degrades *via* elimination of hydrochloric acid from the polymer backbone, shown in Figure 1.21.[45]

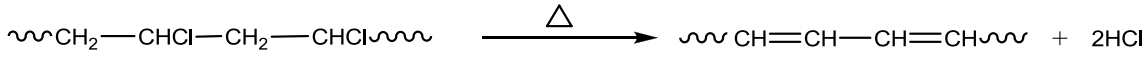

Figure 1.21: Degradation of PVC *via* elimination of HCl

The second type of substituent reaction which can occur is cyclisation, which commonly occurs between substituents which are adjacent in polymer chains, generally with elimination of a small molecule. For example, poly(methacrylic acid) eliminates water upon cyclisation as shown in Figure 1.22.[45]

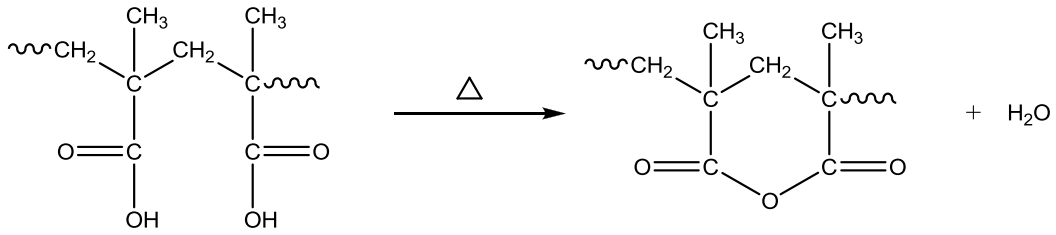

Figure 1.22: Degradation of poly(methacrylic acid) *via* cyclisation

1.4.3 Thermo-oxidative Degradation

Thermal degradation in the presence of oxygen usually occurs at a lower temperature and a faster rate than in the absence of oxygen.[47] The oxidation of polymers is an auto-catalytic process, *i.e*. the rate is slow initially but gradually accelerates as the reaction proceeds. The oxidation of polymers proceeds *via* a free radical chain mechanism and, like other radical mechanisms, consists of three steps (initiation, propagation and termination). The overall mechanism for thermo-oxidative degradation follows the general mechanism outlined below.[47,48,49]

Initiation: $RH \rightarrow R^{\bullet} + H^{\bullet}$

Propagation: $R^{\bullet} + O_2 \rightarrow ROO^{\bullet}$

$ROO^{\bullet} + RH \rightarrow ROOH + R^{\bullet}$

Termination: $2R^{\bullet} \rightarrow R - R$

$R^{\bullet} + ROO^{\bullet} \rightarrow ROOR$

$2ROO^{\bullet} \rightarrow ROOR + O_2$

The initiation step involves the production of polymer radicals, most likely by a thermal, mechanical or photochemical route. Oxygen subsequently reacts with these radicals *via* a chain reaction mechanism involving the consumption of one molecule oxygen and the formation of hydroperoxides. Finally, termination occurs *via* the combination of two

radicals with the reaction which occurs depending on the concentration of oxygen and the structure of the hydrocarbon being oxidised.

The rate of oxidation is initially slow, however, as the reaction proceeds the hydroperoxide concentration increases and decomposition of this species by a bimolecular or unimolecular mechanism occurs, as shown in the reactions below.

Bimolecular Decomposition: $2ROOH \xrightarrow{\Delta} RO^{\bullet} + H_2O + ROO^{\bullet}$

Unimolecular Decomposition: $ROOH \xrightarrow{h\nu} RO^{\bullet} + {}^{\bullet}OH$

The hydroxyl and alkoxy radicals can then abstract a hydrogen radical from the polymer chain to form new alkyl radicals which subsequently react with oxygen in the propagation step. The decomposition of the hydroperoxide, therefore, becomes the predominant initiation step. As the oxidation reaction proceeds the concentration of hydroperoxide increases, leading to an increased rate of initiation and a greater rate of oxidation. The reaction, therefore, becomes auto-catalytic in nature. The ease of thermo-oxidation of a polymer is largely determined by its structure; a polymer possessing labile C-H bonds will be more susceptible to thermo-oxidation than those which do not contain labile C-H bonds.

1.5 Degradation of Polyurethane

1.5.1 Introduction

Polyurethanes are one of the most versatile classes of polymers which find vast use in today's society; however a major drawback of these materials is their ease of flammability and the toxic nature of the gases which are evolved. The behaviour of a polymer in a fire is closely associated with its degradation behaviour and, as a result, much research has been conducted to study the thermal stability and degradation of polyurethane materials. The chemistry occurring during the degradation and the effect

of fire retardants on this process must be fully understood if fire retardant systems are to be effectively employed.

As has been established in the preceding sections, polyurethanes are complicated materials which can contain a variety of functional groups and exist in a number of different forms. The thermal degradation of polyurethanes is, therefore, unsurprisingly complex; it depends on the structure or form of the material making it strongly dependent on the type of polyol and polyisocyanate used to synthesise the polyurethane. The presence of additives can also significantly affect the degradation processes which occur.

It must be noted that degradation studies conducted in a laboratory and those occurring in a real fire situation may be significantly different; the results from such studies must, therefore, be used with caution. Laboratory based studies can, however, give insights into the degradation mechanisms which operate and the effect that fire retardants have on these mechanisms.

A number of studies have been published on the thermal degradation behaviour of polyurethane materials; however, the literature concerning the degradation of such foams is limited. The majority of studies have been concerned with elastomers and model compounds usually containing only one functional group, such as a urethane bond. Consequently, the results and conclusions from such studies may not be representative of the degradation of polyurethanes as a whole, as other groups such as urea, biuret and allophonate may be present.

1.5.2 Thermal Stability of the Major Linkages

Degradation of a complex material like polyurethane can be expected to begin at the thermally weakest linkage within the polymer chain. Polyurethanes can contain up to six types of major linkages which undergo thermal degradation at different temperatures: urethane, urea, biuret, allophonate, ether and ester. Biuret and allophonate groups are

the thermally weakest of the major linkages, undergoing thermal degradation in the temperature range 110°C to 170°C.[50,51] The next most thermally stable group is the urethane link, which is reported to begin degradation around 170°C, with the process becoming more intense at 200°C.[51] The urea group is the next most thermally stable followed finally by the ester and ether groups within the polyol moiety of the polyurethane. Rigid foams often contain a high proportion of isocyanurate linkages and these are reported to be stable up to 270°C,[50,51] more stable than any of the nitrogen-containing linkages and possibly more so than the ether and ester groups.

The literature concerning the thermal degradation of each of these linkages, as well as any secondary degradation reactions which may occur, is reviewed in detail in the sections which follow.

1.5.3 Thermal Degradation of Polyurethane

1.5.3.1 Primary Degradation Processes

1.5.3.1.1 The Urethane Linkage

If biuret and allophonate groups are absent then the urethane linkage will be the first to undergo thermal degradation. It has been reported that degradation of the urethane linkage in polyurethanes, based on most of the common isocyanates and polyols, begins in the region 150-200°C, reaching a maximum rate at 200-250°C.[50] A radical mechanism had been proposed for the thermal degradation of the urethane linkage,[50] however it is now generally accepted that degradation occurs by one or more of the following three reactions:[50,52,53,54]

1) Depolymerisation of the urethane group which yields the original isocyanate and polyol monomers, as shown in Figure 1.23

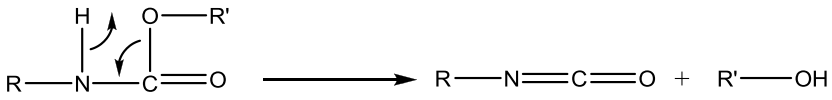

Figure 1.23: Reaction 1 - Depolymerisation of a urethane linkage

2) Dissociation of the urethane group, *via* a six-membered ring transition state, to form a primary amine, an olefin and CO_2, as shown in Figure 1.24

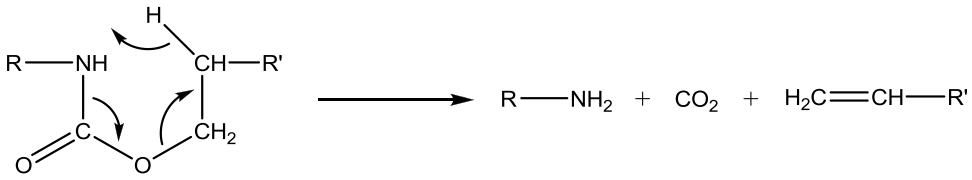

Figure 1.24: Reaction 2 - Dissociation of a urethane linkage *via* a six-membered ring transition state

3) Dissociation of the urethane group, *via* a four-membered ring transition state, to form a secondary amine and CO_2, as shown in Figure 1.25

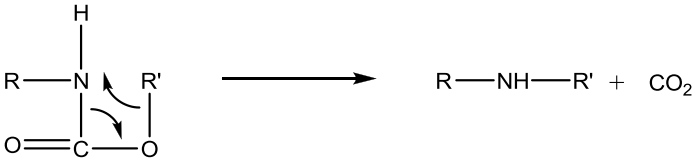

Figure 1.25: Reaction 3 - Dissociation of a urethane linkage *via* a four-membered ring transition state

It has been reported by many authors[50-52,54,55] that the depolymerisation reaction shown in Figure 1.23 is the predominant degradation reaction for the urethane linkage. If depolymerisation occurs the diisocyanate will be the major volatile species which can be evolved, however, this species can also undergo secondary decomposition reactions. This process would leave a residue containing almost exclusively regenerated polyol. If, on the other hand, the diisocyanate cannot volatilise it will become trapped within the pyrolysis zone and the reverse of reaction 1 can occur, *i.e.* the polyol and isocyanate can

recombine to reform the urethane bond, and an equilibrium would therefore become established. It has been reported in this situation that reaction 2, which is slower but irreversible, would become the more favoured reaction[50,51] and the major degradation products evolved would be an amine and CO_2. In this case the residue would resemble the polyol but with an unsaturated end group. It has also been reported that degradation *via* reaction 2 can become predominant if the alcohol or polyol employed has a β-hydrogen.[56,57] There have, however, been very few reports of reaction 3 occurring to any great extent.

A number of studies dealing with simple urethanes have been conducted in order to better understand the degradation of this type of bond. Dyer and Newborn[58] investigated the thermal degradation of a series of biscarbamates in which the isocyanate employed was 4,4-MDI and the alcohols were 1-butanol, 2,2-dimethyl-1-propanol and benzyl alcohol. When held isothermally at 300°C in an inert atmosphere all of the samples evolved CO_2, the parent alcohol and in some cases its dehydration products, with a non-volatile residue remaining at the end of the analysis. The presence of the parent alcohol confirms that in these systems the urethane bond degraded primarily *via* a depolymerisation reaction to yield the alcohol and MDI. CO_2 was proposed to have arisen from further reaction of the regenerated MDI to form carbodiimide structures. The presence of CO_2 could also be explained by degradation of the urethane bond *via* a six-membered ring transition state as shown in Figure 1.24, however, only the polyurethane derived from 1-butanol would undergo this mechanism as it is the only alcohol employed in this study which contains a β-hydrogen. It is, therefore, more likely that the CO_2 does arise from reaction of the MDI to form carbodiimide structures.

Dyer and Wright[56] studied the thermal degradation of alkyl *N*-phenyl carbamates of general formula $C_6H_5NHCOOR$, and found that the nature of the R group determined the route by which the urethane link degraded. Ethyl carbanilate ($R=C_2H_5$) yielded ethanol and phenyl isocyanate indicating that the urethane bond degraded primarily by a depolymerisation reaction. A similar mechanism was shown to operate for benzyl

carbanilate ($R=CH_2C_6H_5$). α-Methylbenzyl carbanilate ($R=CH(CH_3)C_6H_5$), on the other hand, yielded CO_2, styrene, aniline and α-methylbenzylaniline. The presence of CO_2, amines and olefin compounds is in contrast to the results observed for ethyl and benzyl carbanilate and suggests that degradation of the urethane bond in α-methylbenzyl carbanilate occurs *via* a six-membered transition state.

Thorne[54] observed that degradation of the urethane linkage by reaction 2 to produce an amine, CO_2 and olefin was the predominant route for thermal degradation of a series of *t*-alkyl *N*-arylcarbamates.

Ravey and Pearce[50] studied the primary thermal degradation stage of a flexible polyurethane foam based on TDI and a polyether polyol. Analysis of the pyrolysis residue by infrared (IR) spectroscopy revealed it to be identical to the source polyol with additional weak absorbances at 1750-1500 cm^{-1} attributed to residual urethane, urea and possibly isocyanurate groups. The nitrogen content of the volatiles evolved during the degradation was consistent with that of TDI, however TDI was only observed as a degradation product if the pyrolysis was conducted in such a way that the evolved volatiles were removed rapidly from the system. Under confined conditions TDI was not observed. Ravey and Pearce, therefore, proposed that degradation of the urethane linkage occurred *via* both a depolymerisation reaction and a six-membered ring transition state, but that the depolymerisation reaction occurs at a faster rate. If the volatiles are removed quickly from the system then the regenerated TDI escapes and is observed as the major volatile degradation product with the residue consisting of regenerated polyol. If, on the other hand, the pyrolysis is performed in a confined system then it is proposed that the TDI remains in the pyrolysis zone and recombines with the polyol; in this situation reaction 2 dominates and the main volatiles observed are diaminotoluene (DAT) and CO_2.

This proposal was confirmed by work conducted by Erickson[59] who observed that samples of rigid polyurethane foam released TDI when thermally degraded in an

unconfined environment; however, under confined conditions DAT and CO_2 were the primary products. Erickson observed similar results for an MDI-based foam with aniline, 4-methylaniline and CO_2 observed in place of MDI in a confined environment. It was also observed that when the degradation was conducted in an unconfined environment lower levels of isocyanate were observed compared to the TDI-based foam. This is due to the differences in volatility of the isocyanates used. MDI is less volatile than TDI, therefore, even in an unconfined system it remains in the pyrolysis zone for a greater period of time and the competing degradation reaction to form amine and CO_2 becomes more prevalent.

The results from these studies clearly demonstrate that the degradation mechanism of a polyurethane is dependent not only on the chemical structure of the material, but also on the experimental conditions of the pyrolysis employed. This reinforces the issue that results from laboratory based degradation studies must be used with caution and are not necessarily representative of a real fire situation.

Grassie and Zulfiqar[52,60] studied the thermal degradation of a polyurethane derived from 1,4-butanediol and MDI by means of Thermal Volatilisation Analysis (TVA), a form of evolved gas analysis which will be described in full detail in Section 2.2. The results showed that evolution of volatile degradation products began at 240°C reaching a maximum rate at 308°C. These observations were supported by results from Thermogravimetric Analysis (TGA) and Differential Scanning Calorimetry (DSC). A significant "cold-ring fraction" consisting of materials of high molar mass which are not volatile at room temperature was obtained. The liquid phase of the cold-ring fraction was identified as 1,4-butanediol and the solid phase as MDI. Above 250°C carbon monoxide (CO), CO_2, butadiene, tetrahydrofuran (THF), dihydrofuran (DHF) and water were evolved as a result of secondary reactions of 1,4-butanediol and MDI which will be discussed in more detail in Section 1.5.3.2. It was confirmed that these products were not due to degradation of the urethane linkage by reactions 2 or 3. Grassie and Zulfiqar, therefore, demonstrated that the urethane bond in the polyurethane under study degraded

primarily by a depolymerisation reaction to yield the isocyanate and diol monomers, as shown in Figure 1.26.

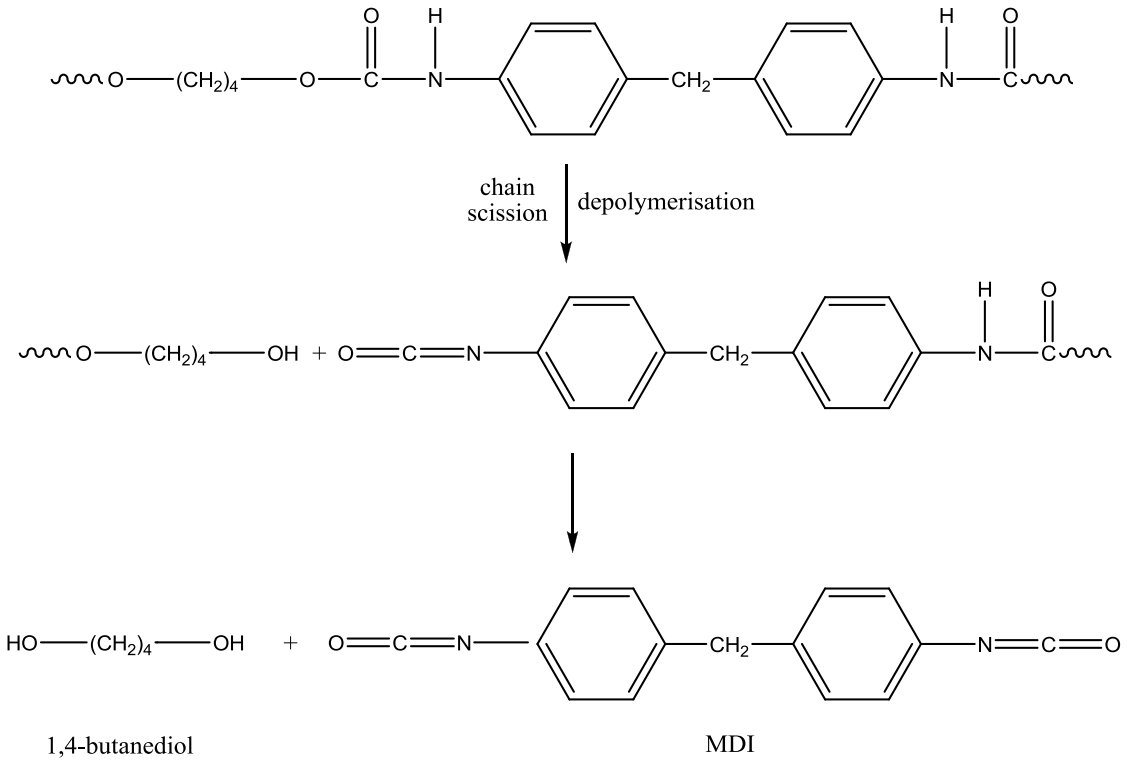

Figure 1.26: Thermal degradation of the urethane bond in an MDI/butanediol polyurethane, as proposed by Grassie and Zulfiqar

Grassie and Mendoza[61,62] studied the thermal degradation of polyurethanes prepared from MDI and poly(ethylene) glycol (PEG) and observed a two step degradation process. TVA results revealed that more volatiles were evolved in the second degradation step and when compared with the TGA results this suggests that in the first degradation step a large proportion of high molar mass products not volatile at room temperature are formed. A significant cold-ring fraction should, therefore, be observed. TGA results showed that mass loss occurred at a faster rate under vacuum than under nitrogen demonstrating that the primary volatile degradation products are able to diffuse more easily from the degrading polymer under vacuum, thereby decreasing the level of secondary reactions which can take place.

The volatile products of degradation were identified as ethylene, formaldehyde, ethylene oxide, acetaldehyde, ethoxy- and methoxyacetaldehyde, water, ethylene glycol and higher molar mass carbonyl and ester compounds. The cold-ring fraction, which constituted approximately 20% of the original polymer, comprised a liquid and solid fraction; the liquid was identified as PEG whilst the solid exhibited bands in its IR spectrum corresponding to MDI, polyurethane fragments, and urea groups.

The presence of MDI in the cold-ring fraction indicated that degradation of the urethane linkage by a depolymerisation reaction was the primary degradation step occurring in this polyurethane. It was suggested, however, that the presence of ethylene indicated that a second degradation mechanism was competing, proposed to be dissociation of the urethane linkage *via* a six-membered ring transition state to yield an alkene terminated PEG chain, a primary amine and CO_2. Thermal degradation of the alkene terminated PEG chain then occurs to yield ethylene and an aldehyde terminated PEG chain, whilst the primary amine reacts with the isocyanate groups in MDI to form the urea groups which were observed in the solid cold-ring fraction. This sequence of reactions is illustrated in Figure 1.27.

Similar results were observed by Zhang *et al*.[53] for the thermal degradation of a TDI-based polyurethane by pyrolysis-GC-MS. A high level of TDI was recovered suggesting that degradation of the urethane linkage occurred primarily by a depolymerisation reaction. DAT and CO_2, however, were also observed suggesting a competing degradation reaction *via* a six-membered ring transition state.

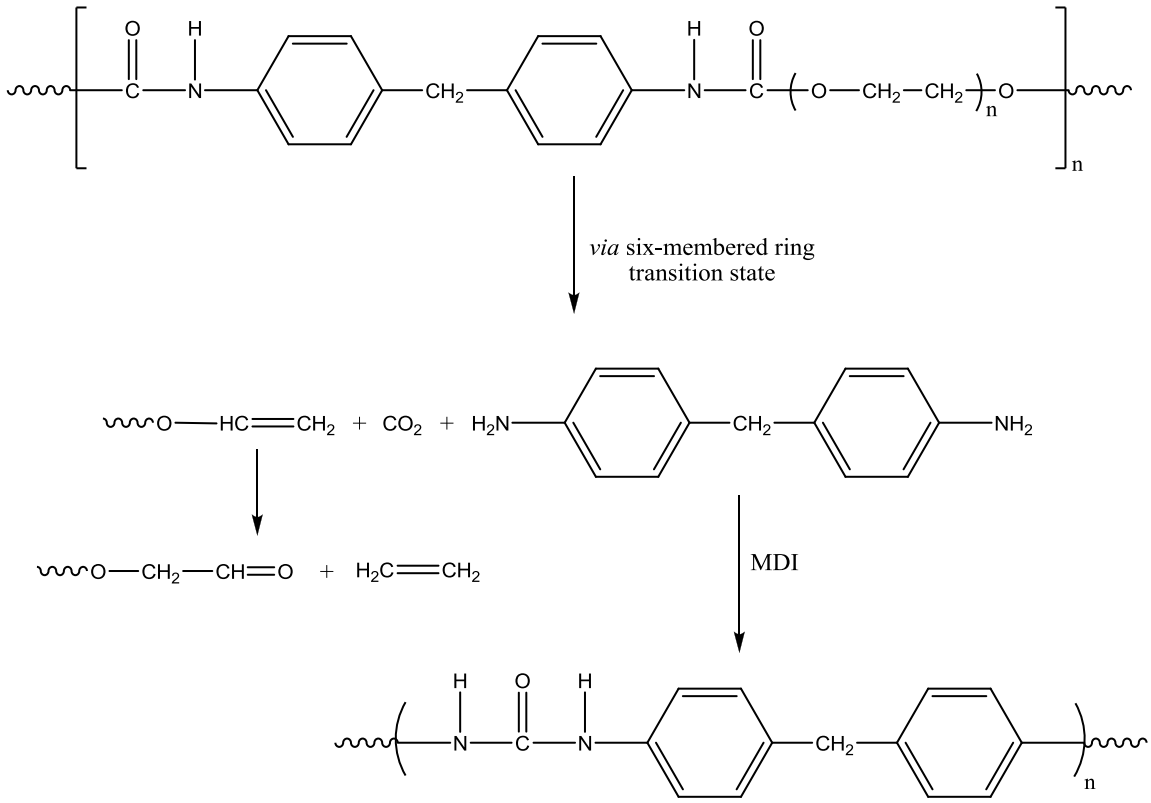

Figure 1.27: Thermal degradation of polyurethane *via* a six-membered ring transition state, followed by secondary reactions

Fan and Chien[63] studied the pyrolysis of segmented thermoplastic polyurethanes in which the soft domains were PPO or a polyacetal derived from butyraldehyde and diethylene glycol, and the hard domains were introduced by reacting the soft domains with MDI which had been chain extended with *N,N'*-bis(2-hydroxyethylphthalamide), pentanediol or butanediol. Pyrolysis of the polyurethanes containing PPO, MDI and *N,N'*-bis(2-hydroxyethylphthalamide) yielded three products which arise from the degradation of the urethane linkage: CO_2, 4,4'-methylenedianiline (MDA), which is the primary amine derived from MDI, and *N,N'*-divinylterephthalamide, shown in Figure 1.28, which is derived from the chain extender.

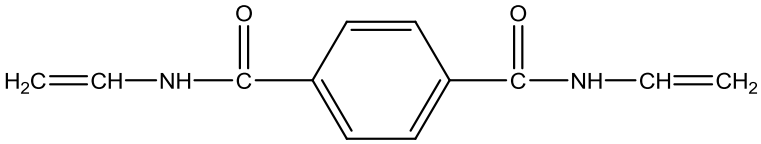

Figure 1.28: The structure of *N,N'*-divinylterephthalamide

The presence of a primary amine, CO_2 and unsaturated chain ends suggests that the urethane linkage within this material degraded by dissociation *via* a six-membered ring transition state as shown in Figure 1.29.

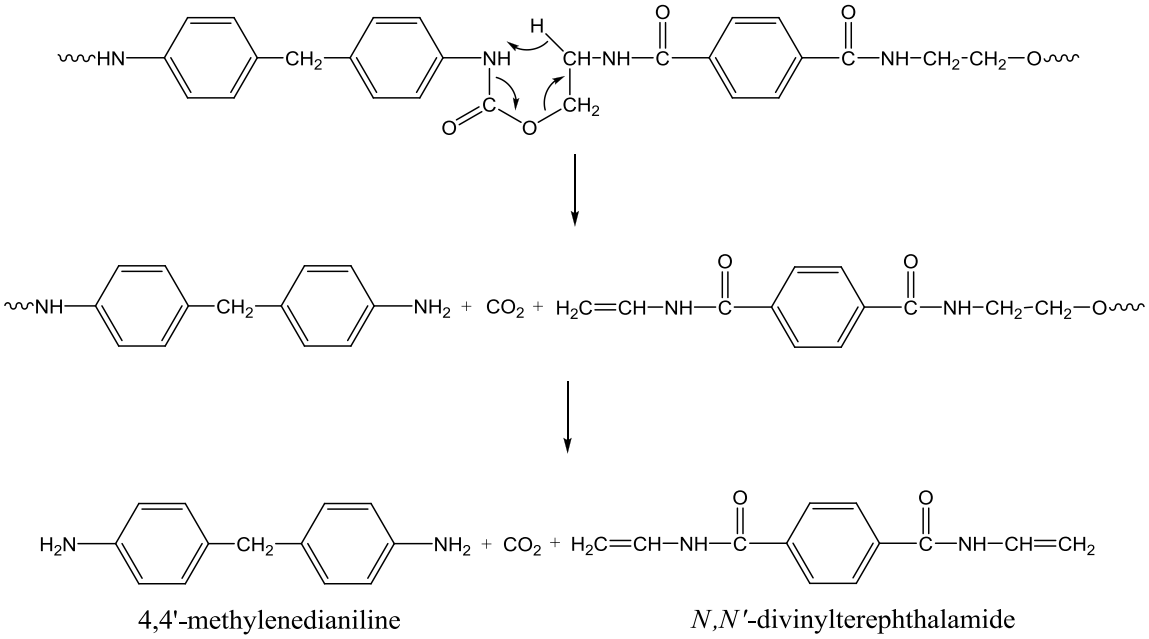

Figure 1.29: Proposed degradation mechanism for the polyurethane *via* a six-membered ring transition state

In contrast to these results the polyurethane containing pentanediol as the chain extender in place of *N,N'*-bis(2-hydroxyethylphthalamide) degraded *via* a depolymerisation reaction to yield MDI, pentanediol and PPO, which then undergoes further degradation which will be discussed in Section 1.5.3.2.1.

Finally, Fan and Chien studied two polyurethanes in which PPO was replaced by a polyacetal with one using *N,N'*-bis(2-hydroxyethylphthalamide) as the chain extender

and the other using butanediol.[63] In the material incorporating *N,N'*-bis(2-hydroxyethylphthalamide) the urethane linkages once again degraded by dissociation *via* a six-membered ring transition state to yield CO_2, MDA and *N,N'*-divinylterephthalamide. The polyurethane incorporating butanediol, on the other hand, yielded butanediol, THF, MDA and CO_2. The regeneration of butanediol confirms that degradation of the urethane linkage occurred by a depolymerisation reaction. Two possible mechanisms were proposed for the formation of THF. The first involved a back-biting type reaction in which THF is formed from a radical chain end, as shown in Figure 1.30. This mechanism is plausible as reactions of this type are not uncommon in the field of polymer degradation.[64]

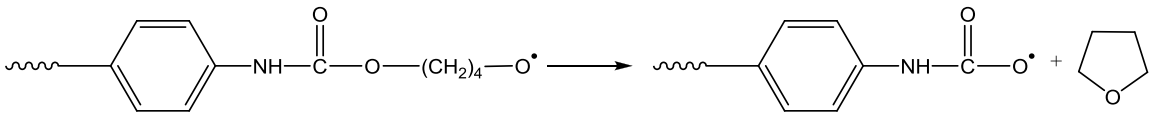

Figure 1.30: Formation of THF by a back-biting type reaction

The second mechanism involved an intramolecular rearrangement reaction of the hard segment to produce THF, CO_2, CO and an amine radical terminated chain, as shown in Figure 1.31. It was suggested that a hydrogen radical then combines with the amine radical to form MDA. This mechanism does not, however, seem plausible. It appears to involve the movement of an electron pair from the oxygen atom to a carbon atom which would be followed by heterolytic bond cleavage, yet one of the final products contains a radical which must have resulted from a homolytic bond cleavage. A mechanism containing both heterolytic and homolytic bond scissions seems unlikely to occur. The revised mechanism presented in Figure 1.31 seems more plausible and would result in the formation of the key products which were observed.

Literature mechanism

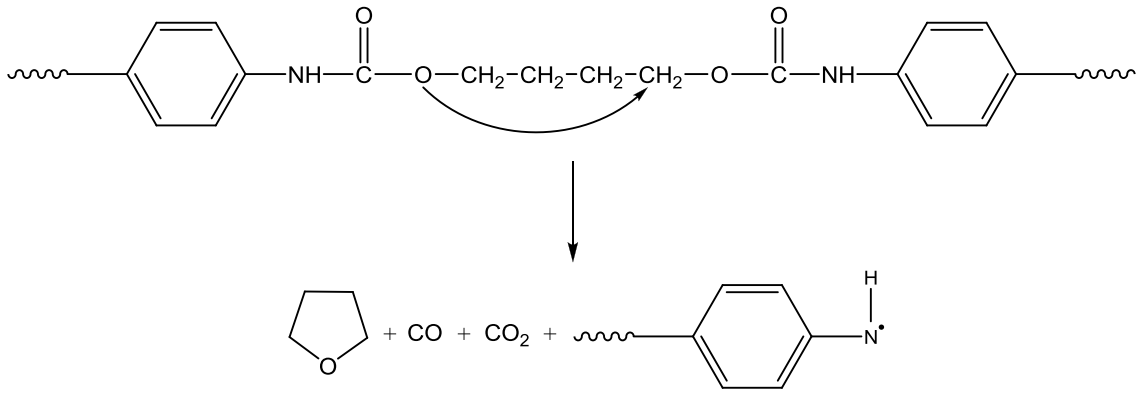

Revised mechanism

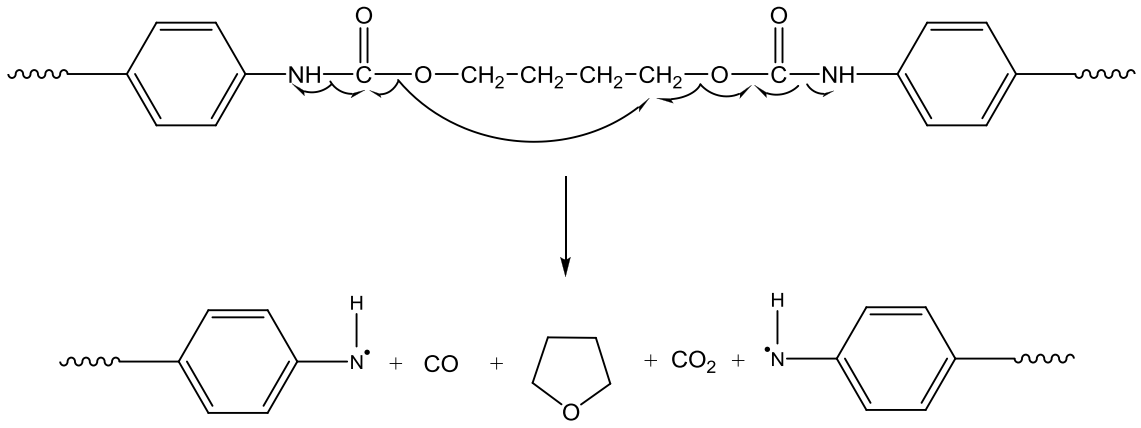

Figure 1.31: Formation of THF *via* an intramolecular rearrangement (literature mechanism) and the more plausible revised mechanism

In contrast to these mechanisms, it has been suggested by Grassie and Zulfiqar[52] that THF simply arises from the dehydration of butanediol. It is, therefore, possible that THF is formed by a combination of dehydration of the butanediol and the backbiting mechanism shown in Figure 1.30. Fan and Chien did not consider the possibility that two competing mechanisms of degradation of the urethane bond could be occurring, the first by a depolymerisation reaction to yield butanediol and MDI, and the second by a six-membered ring transition state to form MDA and CO_2 which would be in agreement with the work conducted by Grassie and Mendoza.[61,62]

The literature, therefore, demonstrates that whilst a depolymerisation reaction to yield the isocyanate and polyol monomers is the predominant thermal degradation route for many polyurethanes, dissociation *via* a six-membered ring transition state to yield an amine, an olefin and CO_2 can be the major mechanism in some cases. There is very little evidence in the literature for a mechanism similar to that in Figure 1.25 occurring. The mechanism of degradation has been shown to be dependent on the experimental conditions employed for the pyrolysis[50] and the component materials; the work by Fan and Chien[63] in particular showed that changing the chain extender drastically alters the degradation mechanism which operates.

1.5.3.1.2 The Urea Linkage

The urea linkage has been shown to dissociate reversibly upon heating to yield the isocyanate and amine precursors,[65,66] as shown in Figure 1.32, in a reaction which parallels the depolymerisation of the urethane bond.

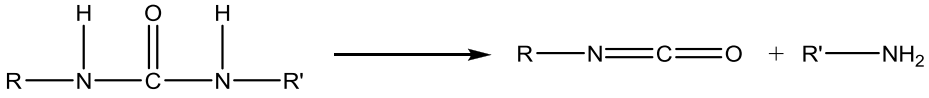

Figure 1.32: Thermal degradation of a urea linkage by dissociation

This degradation route was confirmed by Ravey and Pearce[50] who showed that in a flexible TDI-based polyurethane foam containing a high proportion of urea groups, the urea linkages dissociated into DAT and TDI. They also suggested that amino-isocyanato toluene, shown in Figure 1.33, could be produced by the dissociation reaction.

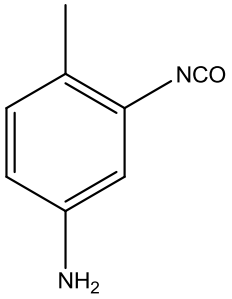

Figure 1.33: The structure of amino-isocyanato toluene

The presence of a base or an acid has been shown by Mukaiyama *et al*.[65,67] to accelerate the dissociation of urea linkages.

1.5.3.1.3 Biuret and Allophonate Linkages

If present, the biuret and allophonate linkages in a polyurethane will undergo thermal degradation *via* a dissociation reaction to yield the monomers from which they were formed as shown in Figure 1.34 and Figure 1.35.[50,51]

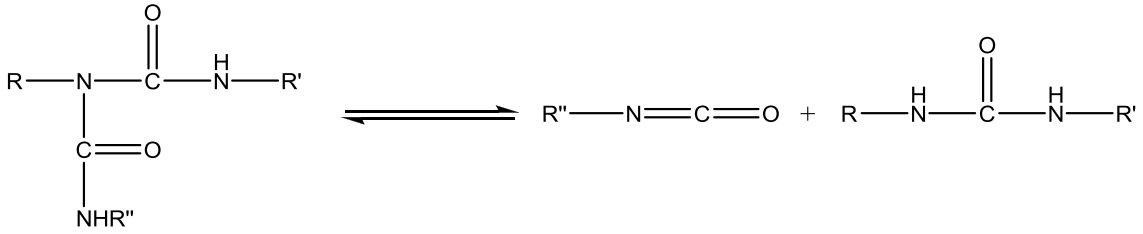

Figure 1.34: Thermal dissociation of a biuret linkage to form isocyanate and a urea

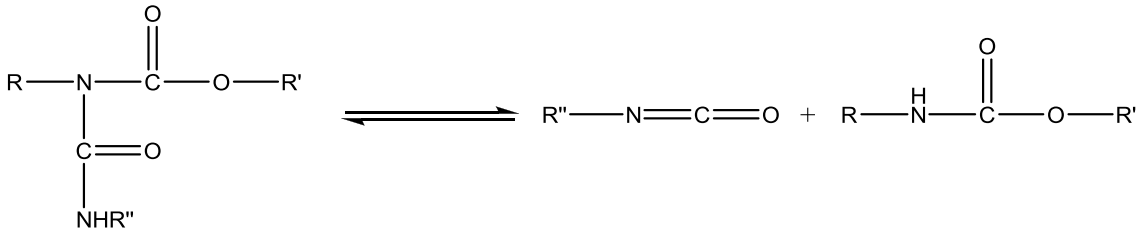

Figure 1.35: Thermal dissociation of an allophonate linkage to form isocyanate and a urethane

The urea and urethane groups will then undergo thermal degradation by the mechanisms described previously.

1.5.3.2 Secondary Degradation Processes

The first stage of degradation of polyurethanes corresponds to degradation of the urethane, urea, biuret and allophonate linkages which results in the formation of the primary decomposition products. Depending on the conditions of the degradation, these products can then undergo a number of secondary degradation processes which are outlined in the sections which follow.

1.5.3.2.1 Degradation of the Polyol Component

When degradation of a polyurethane occurs by a depolymerisation reaction the polyol component of the material is regenerated and will undergo thermal degradation to produce secondary degradation products. Degradation of most of the common polyols employed will begin in the region 250-320°C.[51] Polyether polyols are most commonly employed in the production of flexible polyurethane foams and PEO and PPO are of particular interest in this work.

- *Poly(ethylene oxide)*

The thermal degradation of PEO was studied by Madorsky and Straus[68,69] using a vacuum pyrolysis technique with product identification *via* mass spectrometry. The major degradation products observed were formaldehyde, ethanol, ethylene oxide and water, as well as twenty saturated and unsaturated products consisting of alcohols, acids, aldehydes, ketones, ethers and esters. In addition, lower levels of hydrogen, methane, CO and higher molar mass species not volatile at room temperature were observed.

Grassie and Mendoza[70] studied the thermal degradation of PEGs with approximate molecular weights of 1000 and 1500. TVA results revealed that evolution of volatile material occurred in a single step from 325°C to 410°C with a maximum rate at 366°C. The volatiles were identified as ethane, methane, CO, formaldehyde, ethylene oxide, propane, butane, acetaldehyde, methoxyacetaldehyde, ethoxyacetaldehyde, water, ethylene glycol and a number of low molecular weight hydroxyl, carboxyl, carbonyl and

ether compounds. In addition, a viscous yellow cold-ring fraction was obtained which was shown using IR spectroscopy to contain hydroxyl, carbonyl and ether groups, suggesting chain fragments incorporating terminal carbonyl and hydroxyl groups.

Cameron *et al.*[71] studied the thermal degradation of PEO with a molecular weight of 5,000,000. At 330°C the molecular weight was observed to decrease dramatically which is indicative of a degradation mechanism involving random scission of the bonds in the polymer backbone. TGA results showed a one step degradation process beginning at 350°C with a maximum rate at 415°C. TVA revealed that the evolution of volatiles occurred in a single step between 300 and 500°C, with the products being similar to those observed by Grassie and Mendoza.[70]

Following the results from these studies it was proposed that degradation of PEO or PEG involves random homolytic scission of the C-O and C-C bonds along the polymer backbone, as shown by points A and B in Figure 1.36.

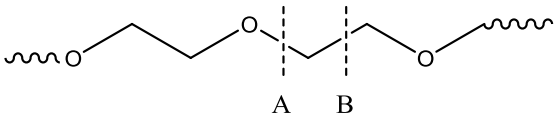

Figure 1.36: Points of scission in poly(ethylene oxide)

The radicals formed by scission at point A can then depolymerise as shown in Figure 1.37 to Figure 1.39[70,71] to form ethene, formaldehyde and acetaldehyde which will be in thermal equilibrium with ethylene oxide at the degradation temperatures (300 to 500°C).

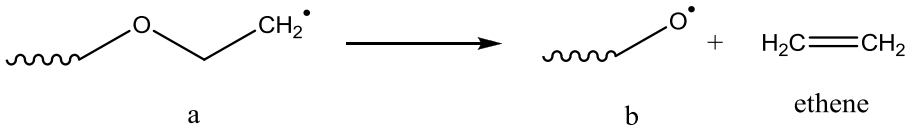

Figure 1.37: Formation of ethene from scission at point A

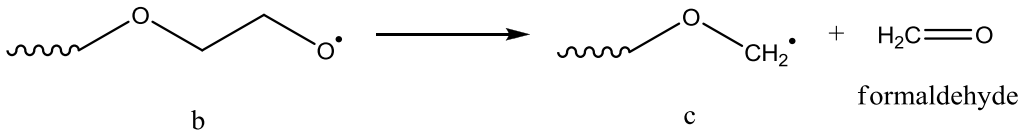

Figure 1.38: Formation of formaldehyde from scission at point A

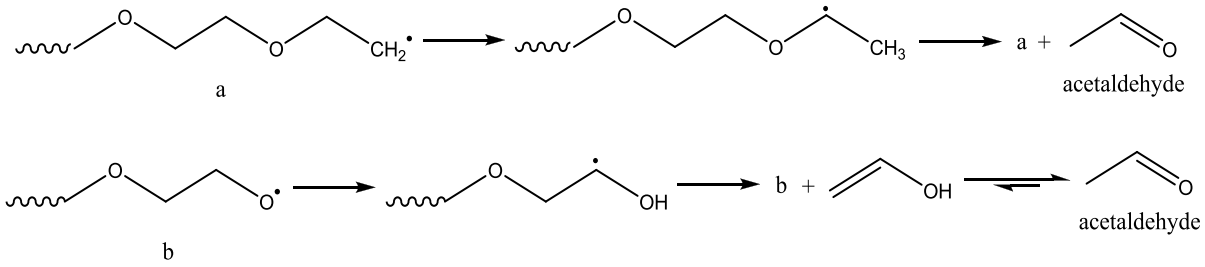

Figure 1.39: Formation of acetaldehyde and ethylene oxide from scission at point A

The radical formed from scission at point B will also form formaldehyde and ethylene oxide as shown in Figure 1.40.

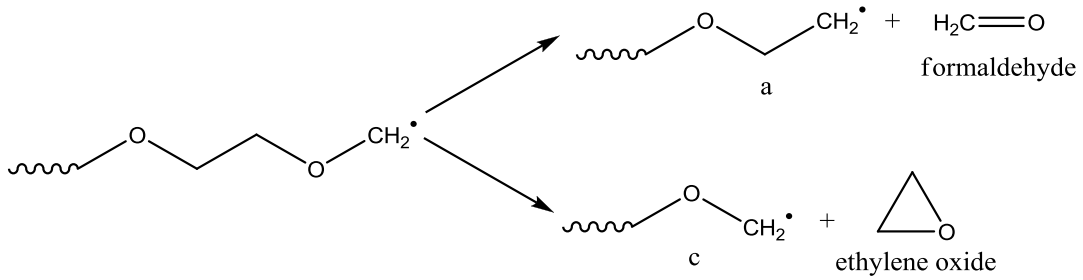

Figure 1.40: Formation of degradation products by radical scission at point B

Termination of radicals a and b can also occur by a disproportionation reaction which would result in unsaturated and hydroxyl chain ends, as shown in Figure 1.41.

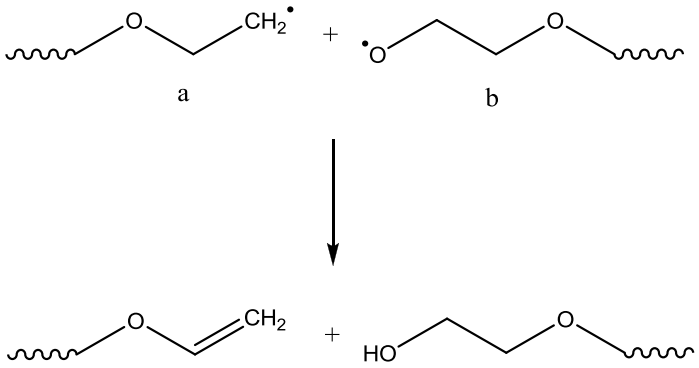

Figure 1.41: Formation of unsaturated and hydroxyl chain ends

It is proposed that methoxyacetaldehyde, ethoxyacetaldehyde and hydrocarbon are formed from radical a by the mechanism shown in Figure 1.42.

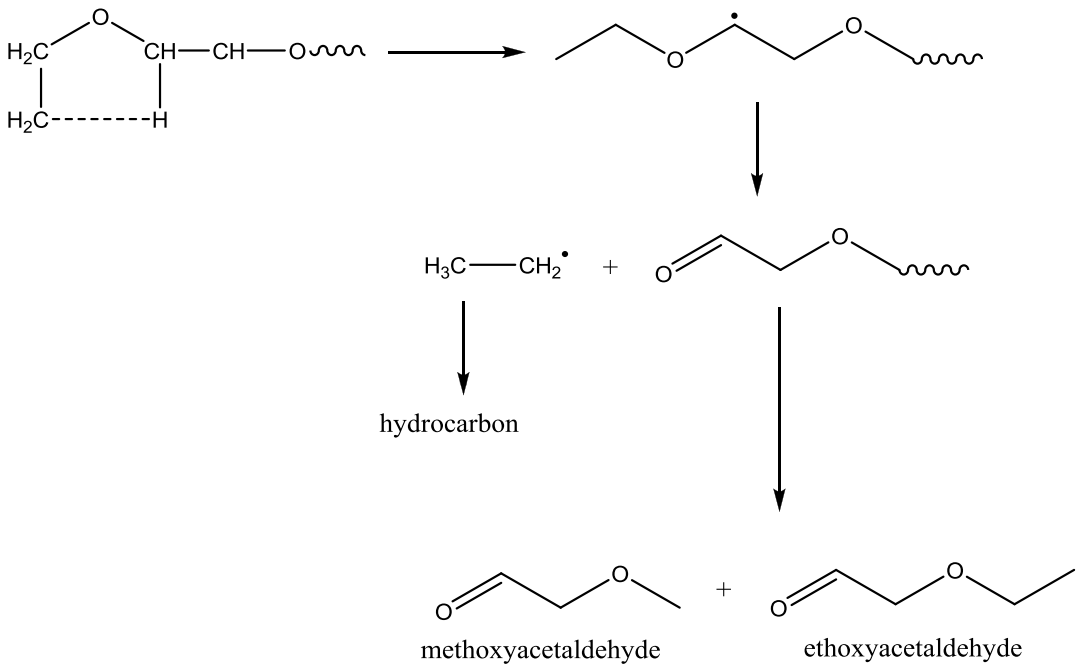

Figure 1.42: The formation of methoxyacetaldehyde, ethoxyacetaldehyde and hydrocarbon

Grassie and Mendoza[70] proposed that methane, ethane, propane and butane can be formed from hydrogen abstraction and combination of methyl and ethyl radicals. It is proposed that ethylene glycol and water are formed during reactions of the chain ends.

The reaction of two hydroxyl end groups to form an ether linkage would eliminate water, whilst ethylene glycol would be formed by scission of a C-O bond adjacent to a hydroxyl chain end followed by hydrogen abstraction, as shown in Figure 1.43.

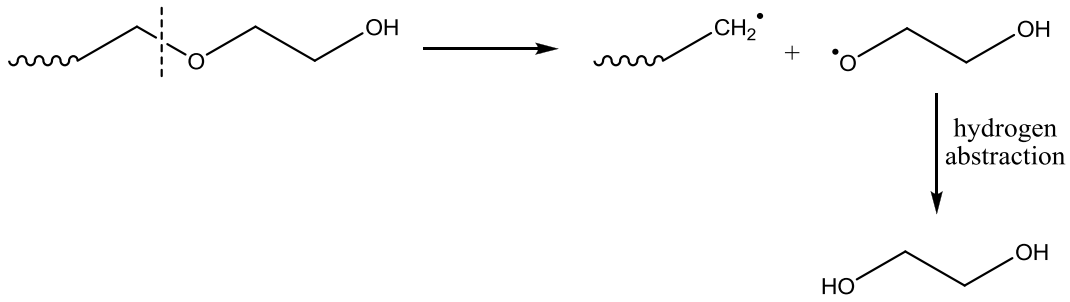

Figure 1.43: Formation of ethylene glycol

In summary, the thermal degradation of PEO has been shown to proceed *via* random homolytic scission of the C-O and C-C bonds to yield hydrocarbons, CO, formaldehyde, ethylene oxide, acetaldehyde, methoxy- and ethoxyacetaldehyde, water and ethylene glycol, as well as higher molar mass fragments.

- *Poly(propylene oxide)*

Fan and Chien[63] studied the pyrolysis of PPO and identified seventeen main products including hydrocarbons, CO, ethene, water, propene, formaldehyde, acetaldehyde, propylene oxide, acetone, propanal, isopropyl alcohol, and other hydroxyl terminated structures.

Costa *et al.*[72] studied the thermal degradation of PPO by means of TGA and TVA and found that it degraded in one step between 300°C and 400°C. The identification of the key volatiles showed species consistent with those indentified by Fan and Chien.[63]

Uyar and Hacaloğlu[73] reported that PPO undergoes significant thermal degradation above 350°C which is consistent with results obtained by Benbow and Cullis.[33] The

degradation products indentified by Uyar and Hacaloğlu were similar to those observed by Fan and Chien[63] and Costa *et al*.[72]

Following these studies it was proposed that the thermal degradation of PPO proceeds *via* random scission of the C-C and C-O bonds in the polymer backbone, as shown by points A, B and C in Figure 1.44.

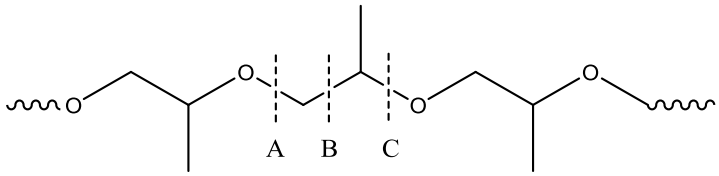

Figure 1.44: Points of scission in PPO

Scission at these points leads to the formation of the six radicals shown in Figure 1.45.[63,72]

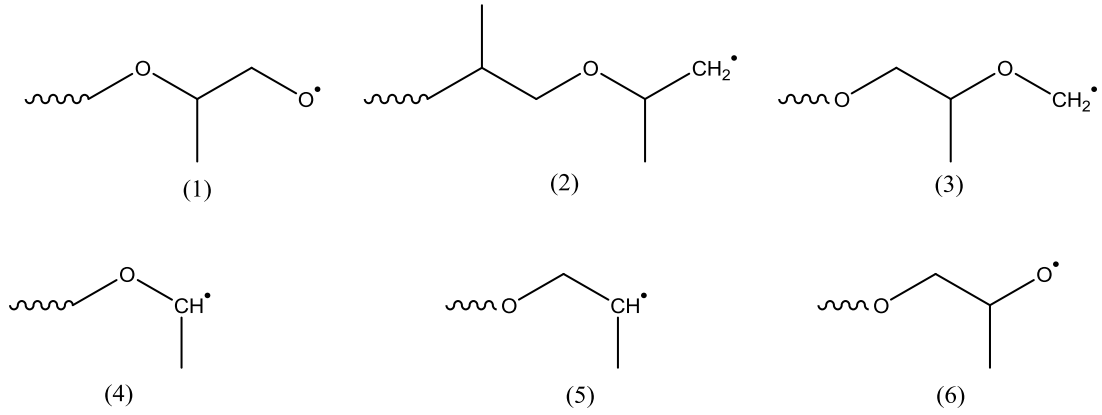

Figure 1.45: The six radicals formed by the scission of poly(propylene) oxide at points A, B and C

It is proposed that rearrangement of these radicals then occurs by the reactions shown in Figure 1.46 to Figure 1.51 leading to the formation of the major volatile products which were observed. In the following figures hydrogen or methyl shifts occur from the carbon labelled with a circle to the atom(s) labelled with a square.

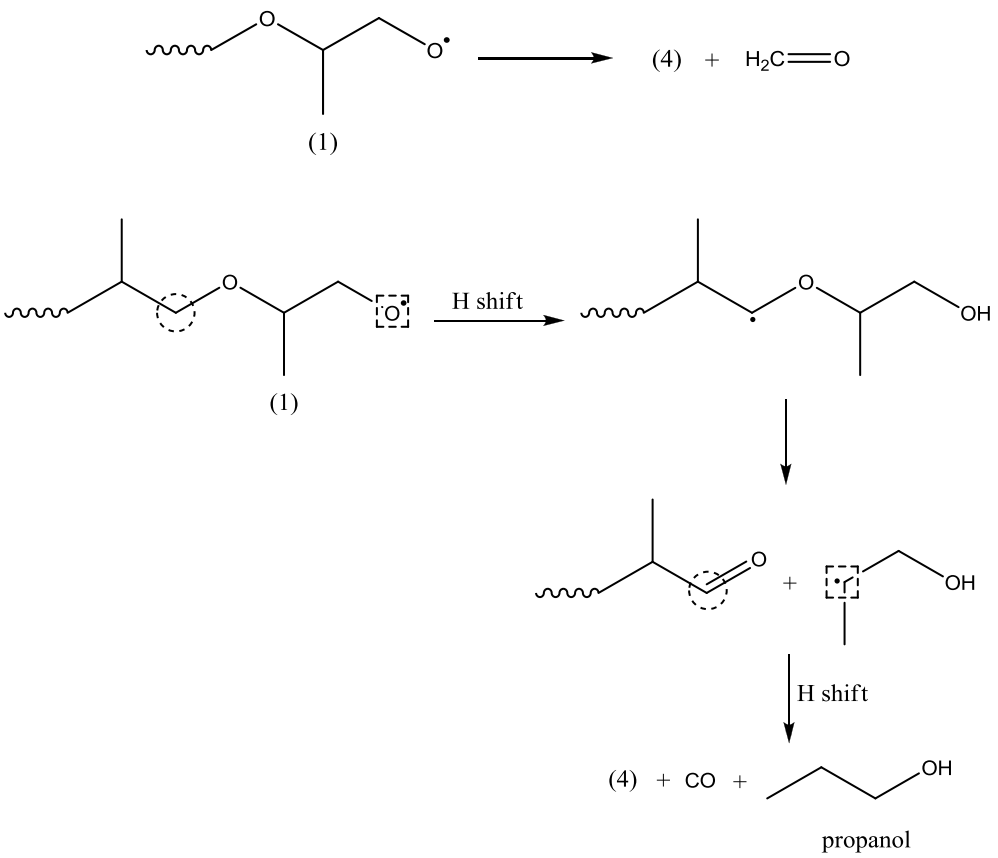

Figure 1.46: Rearrangement reactions of radical (1)

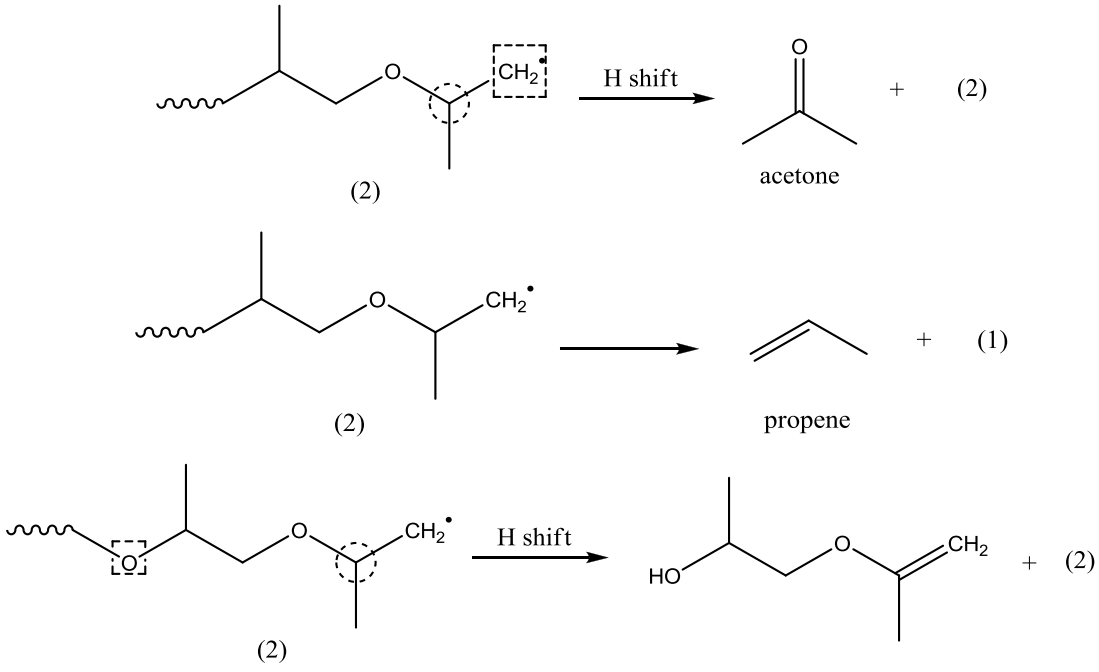

Figure 1.47: Rearrangement reactions of radical (2)

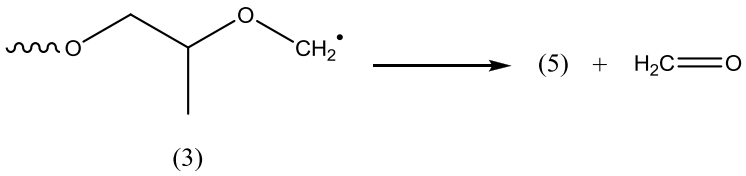

Figure 1.48: Rearrangement reaction of radical (3)

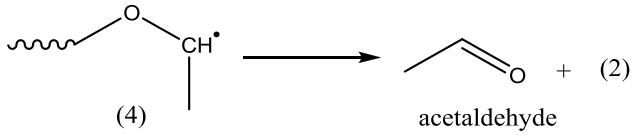

Figure 1.49: Rearrangement reaction of radical (4)

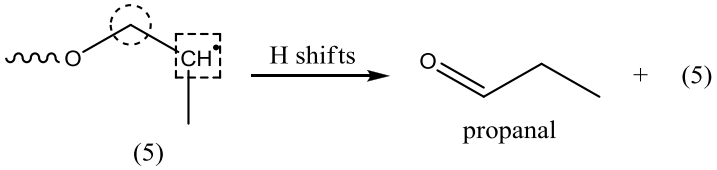

Figure 1.50: Rearrangement reaction of radical (5)

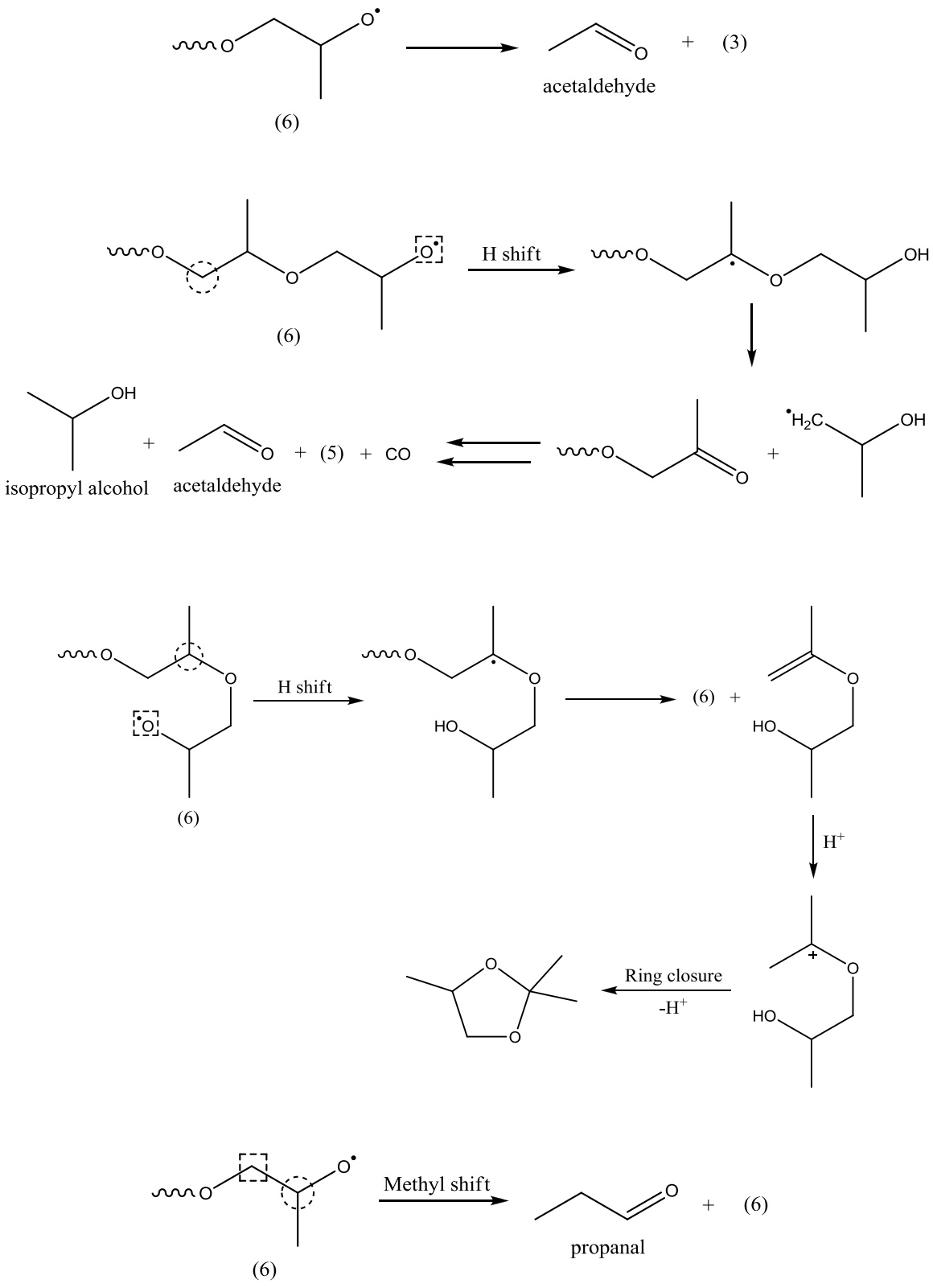

Figure 1.51: Rearrangement reactions of radical (6)

Fan and Chien[63] also proposed that scission of methyl groups from the polymer backbone leads to the formation of methane and ethene, both of which were observed as minor products. Costa *et al.*, on the other hand, suggested that these products are formed by the mechanisms shown in Figure 1.52.[72] Abstraction of a hydrogen atom from acetaldehyde and propanal leads to the formation of unstable radicals which decompose to form methyl and ethyl radicals, respectively; these will subsequently form methane and ethene.

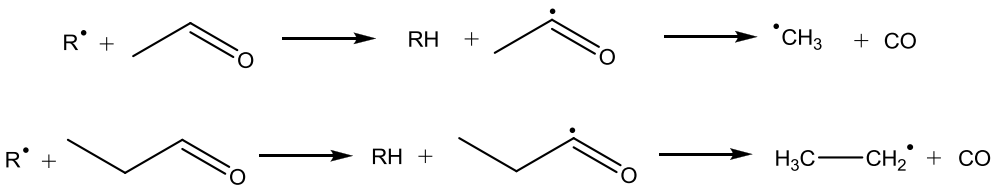

Figure 1.52: Formation of methyl and ethyl radicals from acetaldehyde and propanal

1.5.3.2.2 Degradation of the Isocyanate Component

Marks and Metcalfe[74] studied the stepwise degradation of aromatic diisocyanates, such as MDI and TDI, to aromatic nitriles and additional degradation products. The major degradation products of MDI were identified as *p*-toluene isocyanate, phenyl isocyanate, benzonitrile, acetonitrile, hydrogen cyanide, benzene, toluene, and low molar mass alkenes. Phenyl isocyanate was the major degradation product observed from the pyrolysis of TDI. It was proposed that a major step in the thermal degradation of an aromatic diisocyanate such as MDI involves scission of the aryl-CH_2 bond to yield a mono-isocyanate, as shown in Figure 1.53.

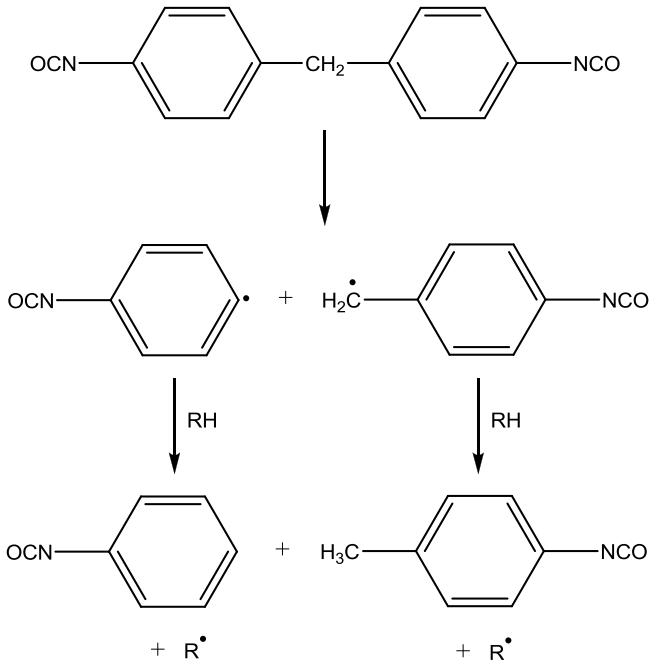

Figure 1.53: Thermal degradation of MDI to yield phenyl isocyanate and p-toluene isocyanate

The pyrolysis of *p*-toluene isocyanate was then studied as this was the major degradation product of MDI and was predicted to be an intermediate for the formation of a number of other degradation products which were observed. The results revealed that the most dominant degradation product was benzonitrile, with high concentrations of phenyl isocyanate, toluene, *p*-methylbenzonitrile, benzene and diphenyl also observed. Marks and Metcalfe proposed a mechanism for the formation of benzonitrile from *p*-toluene isocyanate which involves attack of a radical on the isocyanate group to form a short lived three membered ring intermediate which then eliminates an alkoxy radical, as shown in Figure 1.54.

Phenyl isocyanate, toluene and benzene can be formed by the radical reactions shown in Figure 1.55, whilst it is proposed that diphenyl can be formed by either recombination of two benzene radicals or by a radical displacement reaction, as shown in Figure 1.56.

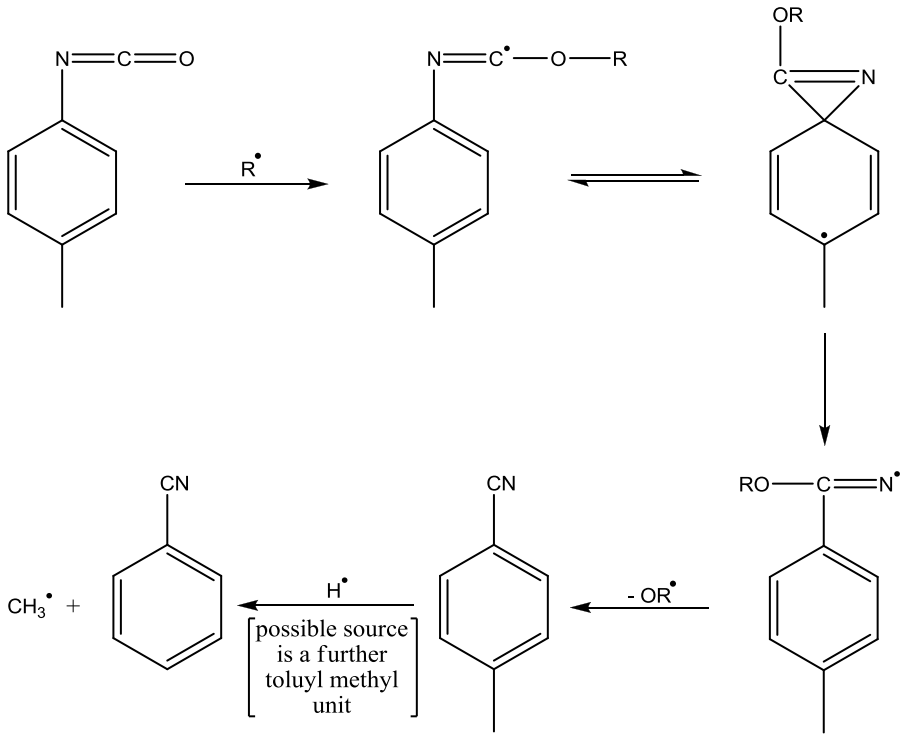

Figure 1.54: Proposed mechanism for the formation of benzonitrile from *p*-toluene isocyanate

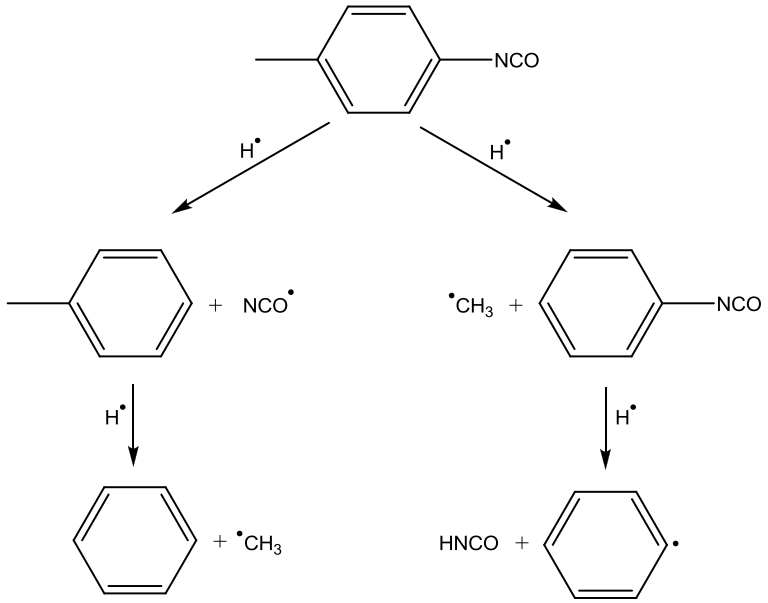

Figure 1.55: Formation of toluene, benzene and phenyl isocyanate

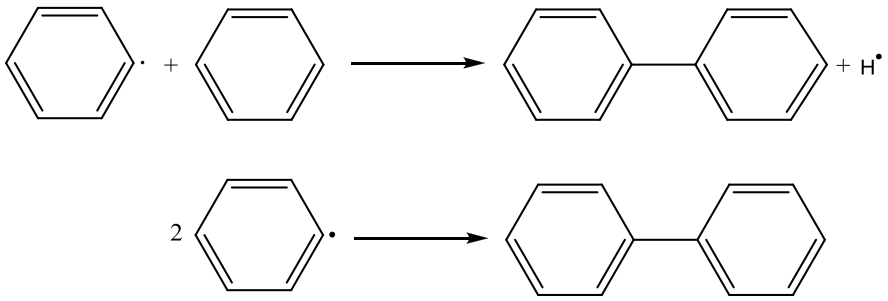

Figure 1.56: Possible mechanisms for the formation of diphenyl

Matuschek[75] studied the thermal degradation of MDI and also found *p*-toluene isocyanate to be a major degradation product, as well as aniline, methylaniline, toluene and phenyl isocyanate.

1.5.3.2.3 Formation of Carbodiimide and Urea

In the study by Dyer and Newborn[58] on the thermal degradation of biscarbamates, the samples incorporating 1-butanol and 2,2-dimethyl-1-propanol yielded large quantities of CO_2 and residues which were polymeric solids insoluble in common solvents and thermally stable at 300°C. Analysis by IR spectroscopy showed peaks which are characteristic of carbodiimide. Dyer and Newborn proposed that the MDI evolved from depolymerisation of the urethane bond undergoes a self condensation reaction to produce a polymeric carbodiimide, as shown in Figure 1.57. It was also proposed that once formed, the carbodiimide can then react with the regenerated alcohol to yield an amine, CO_2 and olefin.

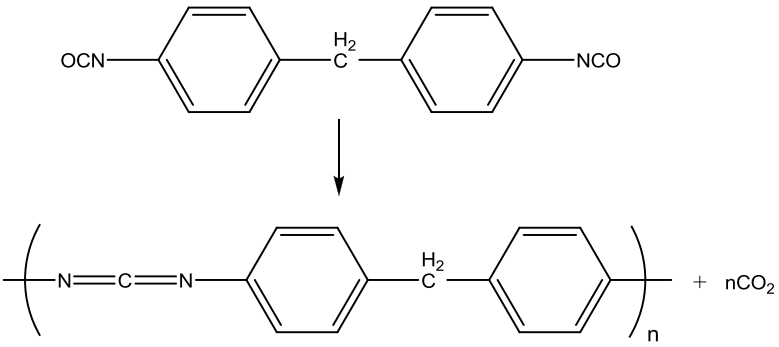

Figure 1.57: Formation of a polymeric carbodiimide from MDI

During the pyrolysis study of MDI conducted by Marks and Metcalfe[74] a large quantity of black residue was formed which was insoluble in most common solvents. Analysis of this residue by IR spectroscopy revealed peaks due to C=N and N=C=N structures and results from elemental analysis were similar to those predicted for a carbodiimide dimer formed from MDI. These results suggest that the formation of a carbodiimide dimer, shown in Figure 1.58, has occurred during the pyrolysis of MDI.

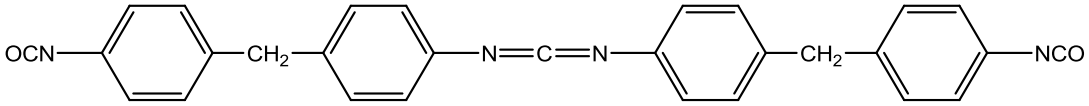

Figure 1.58: The carbodiimide dimer formed during the pyrolysis of MDI

During the thermal degradation of polyurethanes prepared from MDI and low molar mass PEGs, Grassie and Mendoza[61] obtained a residue which was identified by IR spectroscopy as primarily polycarbodiimide. Peaks associated with carbodiimide dimers and trimers, shown in Figure 1.59, were also observed. Carbodiimide structures were also identified in the pyrolysis residues obtained by Grassie and Zulfiqar[52] and Ravey and Pearce.[50]

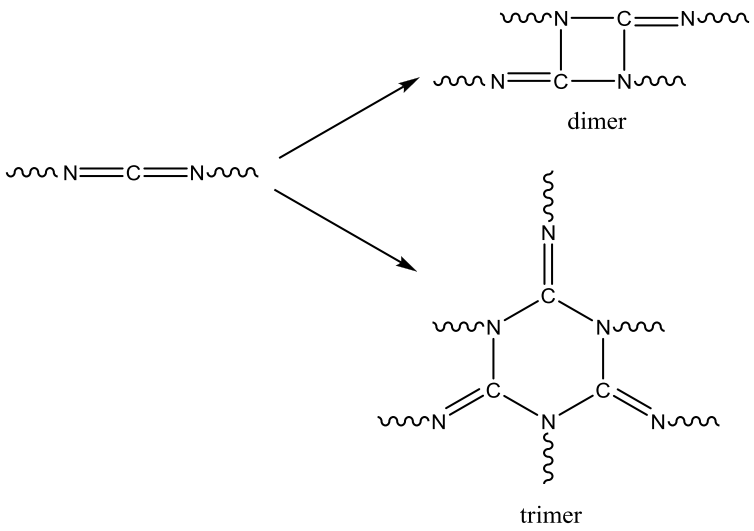

Figure 1.59: Formation of carbodiimide dimers and trimers

As was explained in Section 1.5.3.1.2, thermal degradation of a urea linkage yields an amine and isocyanate. According to Mukaiyama and co-workers[65,67] these cannot co-exist as they will react instantaneously to reform urea. Ravey and Pearce[50] proposed that they will recombine in the vapour phase to form polyurea in the form of an aerosol, explaining the presence of a yellow aerosol during their pyrolysis study. Wooley[76] also observed a yellow aerosol and proposed that this was due to polymerisation of the isocyanate which explained the poor recovery of TDI in this study. However, it seems more likely, given the results of Ravey and Pearce, that this was in fact polyurea. Ravey and Pearce also proposed that a cyclic urea trimer could be formed from amino-isocyanato toluene, as shown in Figure 1.60.[50]

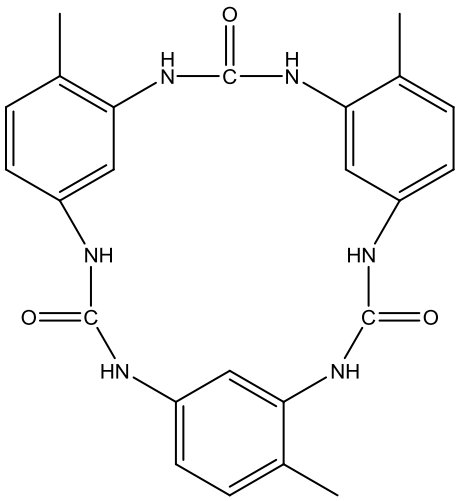

Figure 1.60: The cyclic urea trimer proposed by Ravey and Pearce

1.5.4 Thermo-oxidative Degradation

1.5.4.1 Thermo-oxidative Degradation of Polyurethane

The stability of polyurethanes under an oxidative environment is of great importance to polymer scientists as under most applications the material will be exposed to air for prolonged periods of time. In particular, the thermo-oxidative behaviour of polyurethane foams is of significance when considering the fire behaviour of these materials, as the polymer will be exposed to both high temperatures and oxygen during the course of a fire.

The thermo-oxidation of polyurethanes follows the general scheme outlined in Section 1.4.3. Initially free radicals $(R^{\bullet})$ are produced which subsequently react with molecular oxygen to form peroxy radicals $(ROO^{\bullet})$. The peroxy radicals abstract hydrogen from the polyurethane chain resulting in the formation of hydroperoxides $(ROOH)$ which then undergo thermal decomposition to yield more radicals which can further react with the polyurethane chain. This sequence of events leads to discolouration of the material and a loss in the physical properties.[77]

The soft segments in polyurethane are reported to be more susceptible to oxidative degradation than the hard segments,[77] making the products of thermo-oxidative degradation strongly dependant on the nature of the polyol employed. In some cases[33,78] it has even been reported that the presence of oxygen does not influence the primary degradation step of the polyurethane, *i.e.* depolymerisation of the urethane linkages to yield diisocyanate and polyol. Benbow and Cullis[33] observed that the first stage of degradation of TDI-based polyurethane foams under air, attributed to loss of isocyanate fragments, occurred at the same temperature as under an inert atmosphere. These results were later corroborated by Bilbao *et al*.[78] Furthermore, polyurethanes based on polyether polyols have been shown to be more susceptible to oxidative degradation than their polyester counterparts.[77,79,80]

Wlodarczak[81] studied the thermo-oxidative degradation of a polyurethane foam from 200°C to 700°C by means of pyrolysis-GC-MS. The major volatile degradation products which were identified included CO, CO_2, methanol, C1-C4 aliphatic hydrocarbons, acetonitrile, acrylonitrile and HCN. Isothermal experiments conducted at intervals of 100°C revealed that the concentrations of HCN, hydrocarbons and CO_2 increased with increasing temperature, whilst the methanol, acetonitrile and acrylonitrile concentrations peaked at 500°C.

Jellinek and Dunkle[82] studied the thermo-oxidative degradation of a number of polyurethanes synthesised from a variety of polyols and isocyanates. They proposed that for all polyurethanes a thermo-oxidative mechanism can be postulated based on the original mechanism proposed by Boland and Gee,[48] involving the formation of hydroperoxides which then degrade *via* radical chain reactions leading to deterioration of the polyurethane. The thermo-oxidative mechanism proposed by Jellinek and Dunkle is presented in Figure 1.61, where HRNH represents a typical polyurethane.

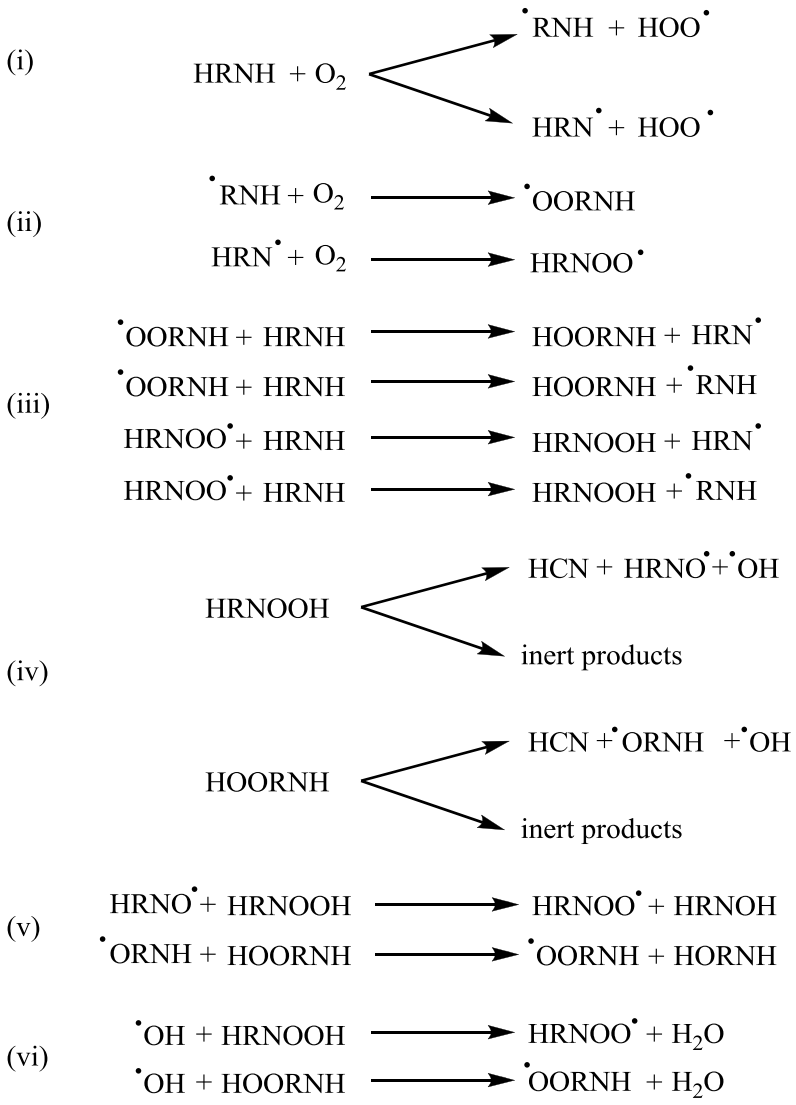

Figure 1.61: Mechanism of thermo-oxidative degradation of a polyurethane as proposed by Jellinek and Dunkle[82]

1.5.4.2 Thermo-oxidative Degradation of the Isocyanate Component

Servay *et al.*[83] studied the degradation of an MDI-based polyurethane following thermal ageing in air for 77 days at 150°C. As polyester polyols are more resistant to oxidation than their polyether counterparts, a polyester polyol was employed in order to better study the role of the hard segment during the thermo-oxidative degradation of the polyurethane. The products arising from the thermo-oxidative degradation of the hard

segments were monitored by solid-state NMR and ATR-IR spectroscopy. Solid-state NMR results revealed a number of changes in the material which were attributed to oxidation of the central methylene unit in the MDI segment to a keto unit which results in the formation of a benzophenone derivative, represented in Figure 1.62. The intensity of the new signal arising from the keto group was much lower than that of the urethane groups suggesting that approximately half of the methylene groups within the MDI segments had been oxidised.

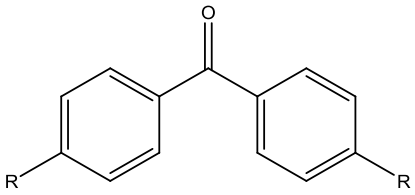

Figure 1.62: Structure of the benzophenone derivative resulting from oxidisation of the central methylene unit in the MDI segment

The IR spectroscopy results revealed a new signal in the aged sample at 1645 cm^{-1}, which again can be attributed to a keto group within the MDI unit. Comparison of this signal with the IR spectrum of benzophenone confirmed the proposal that the central methylene unit in the MDI had been oxidised to a benzophenone derivative.

Finally, the degraded polyurethane sample was hydrolysed in alkaline solution resulting in cleavage of the urethane bonds within the hard segment and formation of aromatic diamines. These were subsequently extracted and analysed by GC-MS. A small quantity of the non-oxidised product 4,4'-methylenedianiline (MDA) was identified as well as a significant quantity of 4,4'-diaminobenzophenone, the structures of which are shown in Figure 1.63.

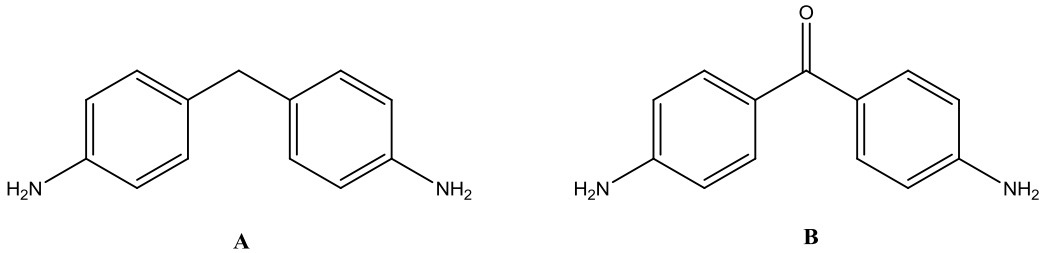

Figure 1.63: The structure of 4,4'-methylenedianiline (A) and 4,4'-diaminobenzophenone (B)

The formation of 4,4'-diaminobenzophenone by hydrolytic cleavage of the urethane linkages within the aged polyurethane confirms that oxidation of the central methylene unit within the MDI segment had occurred. The presence of MDA, however, confirms that not all of the MDI units within the aged polyurethane had been oxidised.

Following their results, Servay *et al*. proposed the mechanism shown in Figure 1.64 for the oxidation of the MDI unit.[83]

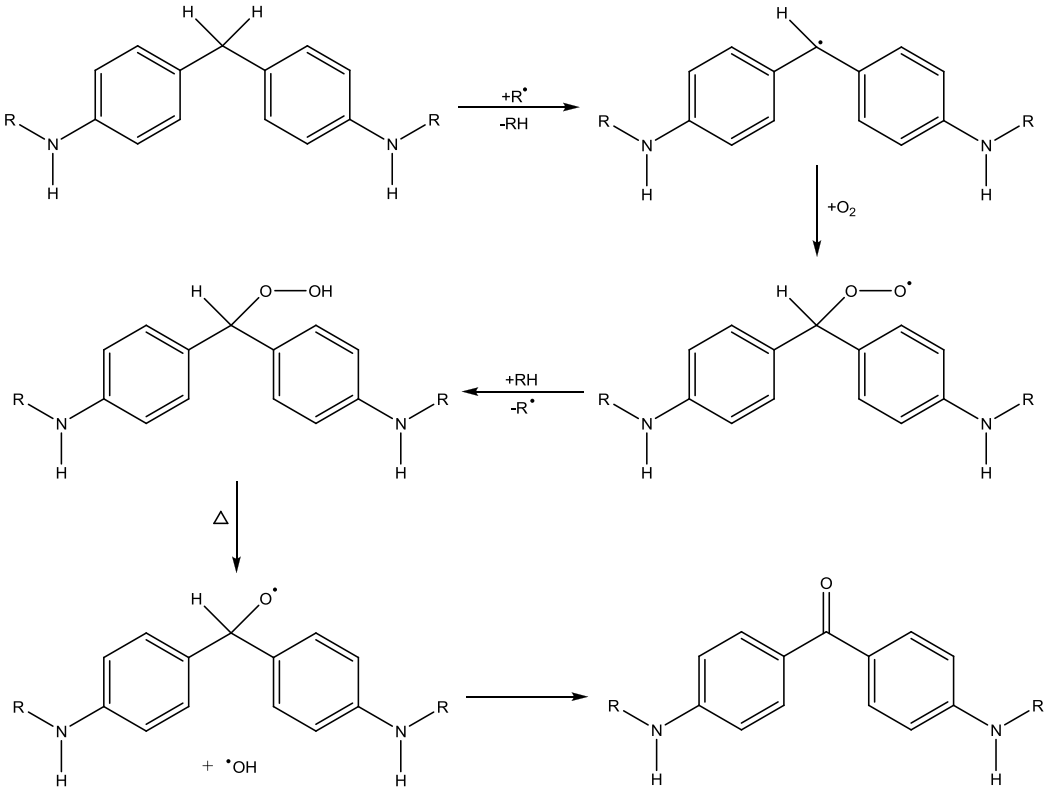

Figure 1.64: Proposed mechanism for the thermo-oxidative degradation of the MDI unit of the hard segment of a polyurethane

Khatua and Hsieh,[80] on the other hand, proposed a different mechanism for oxidation of the hard segment of polyurethanes synthesised from aromatic isocyanates. They proposed that formation of a conjugated structure occurs by abstraction of H atoms from the isocyanate segment of the polyurethane followed by electronic rearrangement, as

shown in Figure 1.65. The introduction of conjugation into the polymer leads to discoloration of the polyurethane.

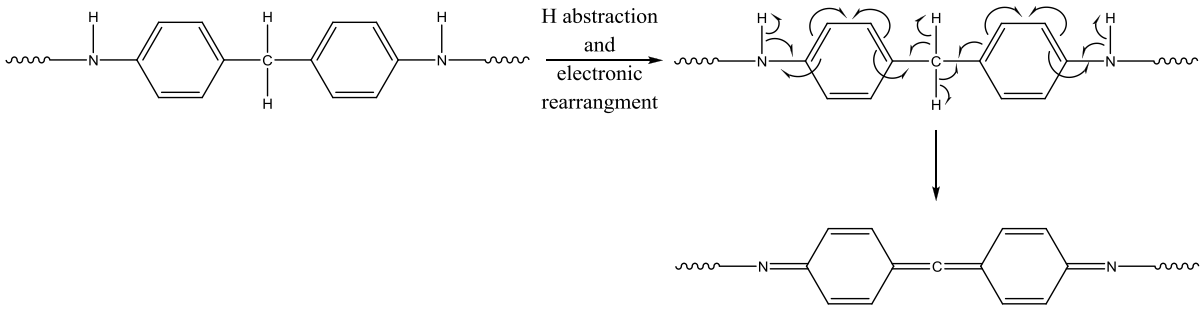

Figure 1.65: Formation of a conjugated structure by hydrogen abstraction and electronic rearrangement

1.5.4.3 Thermo-oxidative Degradation of the Polyol Segment

The soft segments in polyurethane are reported to be more susceptible to oxidative degradation than the hard segments,[77] making the products of thermo-oxidative degradation strongly dependant mainly on the nature of the polyol employed. The foams studied in this work are synthesised from polyether polyols, therefore, only this class of polyol will be discussed further. Polyurethanes based on polyether polyols have been shown to be more susceptible to oxidative degradation than their polyester counterparts, with oxidation being initiated at the α-position of the ether bridge.[77,80] This is then followed by a radical chain reaction which proceeds *via* formation of a hydroperoxide.[77] The two polyols of most importance in this work are poly(ethylene oxide) and poly(propylene oxide) and the thermo-oxidative degradation of these polymers is discussed in the sections which follow.

- *Poly(ethylene oxide)*

The thermo-oxidative degradation of PEO at 150°C was investigated by Yang *et al.*[84] by means of NMR spectroscopy. Additional peaks appeared in the spectra of the degraded sample corresponding to formate esters and hydroxyl end groups, with the former being generated in greater quantities as the degradation time was increased. The presence of a significant level of formate end groups suggests that thermo-oxidative degradation of

PEO had occurred principally by an oxidative scission mechanism and Yang *et al*. proposed the mechanism presented in Figure 1.66.[84] Initially a hydroperoxide is formed by reaction of PEO with oxygen; the resulting compound then undergoes chain scission to yield formate and hemiacetal end groups.

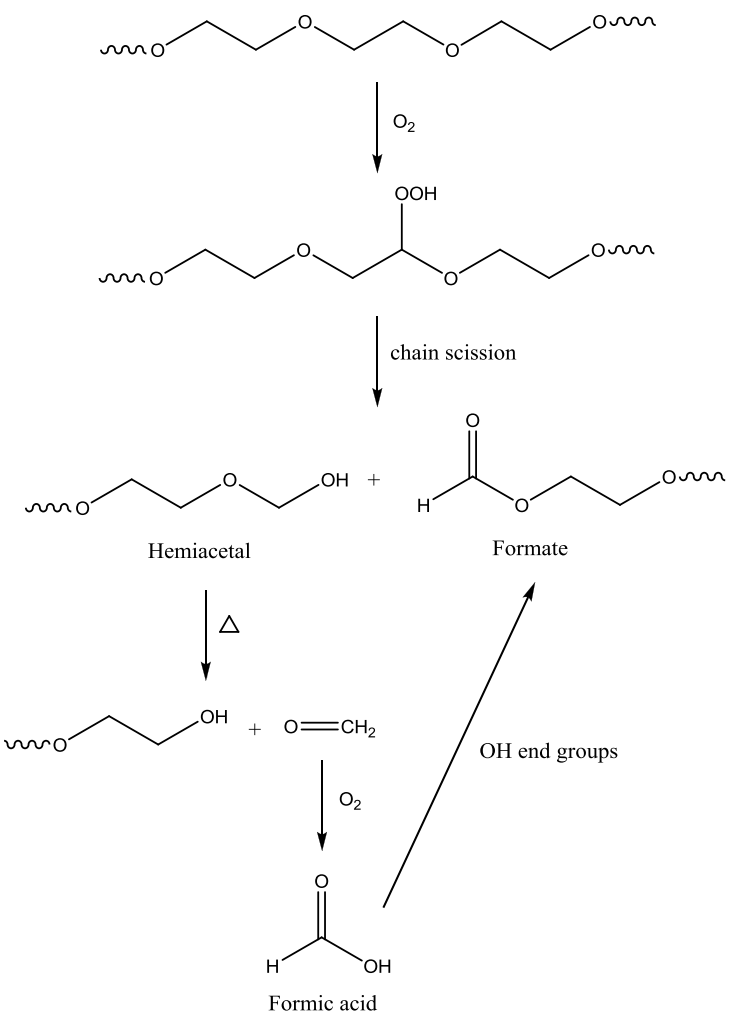

Figure 1.66: Proposed mechanism for thermo-oxidative degradation of PEO which yields formate esters[84]

The intensity of the peaks in the NMR spectra corresponding to hemiacetal were significantly lower than those of the other end groups, therefore, it was proposed that the hemiacetal groups thermally decompose yielding formaldehyde and a hydroxyl end group. The formaldehyde was then proposed to undergo oxidation to formic acid which

subsequently reacts with the hydroxyl end groups yielding formate esters, which explains the formation of larger quantities of formate ester end groups compared to hydroxyl end groups.

Costa *et al*.[85] studied the thermo-oxidative degradation of PEO by means of TGA with the volatile degradation products (collected in a U-trap cooled to -80°C) being analysed by GC-FTIR. A mass loss of 50% was observed by 300°C when PEO was heated in air; however, the same mass loss was not observed until 400°C under an inert environment, suggesting that the degradation of PEO is sensitive to the presence of oxygen. The most abundant volatile degradation products identified during the degradation in air were acetaldehyde, methanol and CO_2, with low levels of 1,4-dioxane and esters also observed.

Costa *et al*. proposed that the thermo-oxidative degradation of PEO is dominated by the initial formation of hydroperoxides which then degrade yielding alkoxy and hydroxy radicals. The former then undergo chain scissions and further reactions resulting in the formation of aldehydes, esters, formates and hemiacetals, as displayed in Figure 1.67.[85] The FTIR spectrum of the residue remaining after degradation in air revealed the presence of high levels of formate end groups but only low levels of other esters, and no peaks corresponding to aldehyde terminated chain ends. This suggests that scission of the C-C bond of the alkoxy radical (point B in Figure 1.67) is the most predominant degradation route whilst scission of the C-O bond (Point A in Figure 1.67) does not occur to any great extent.

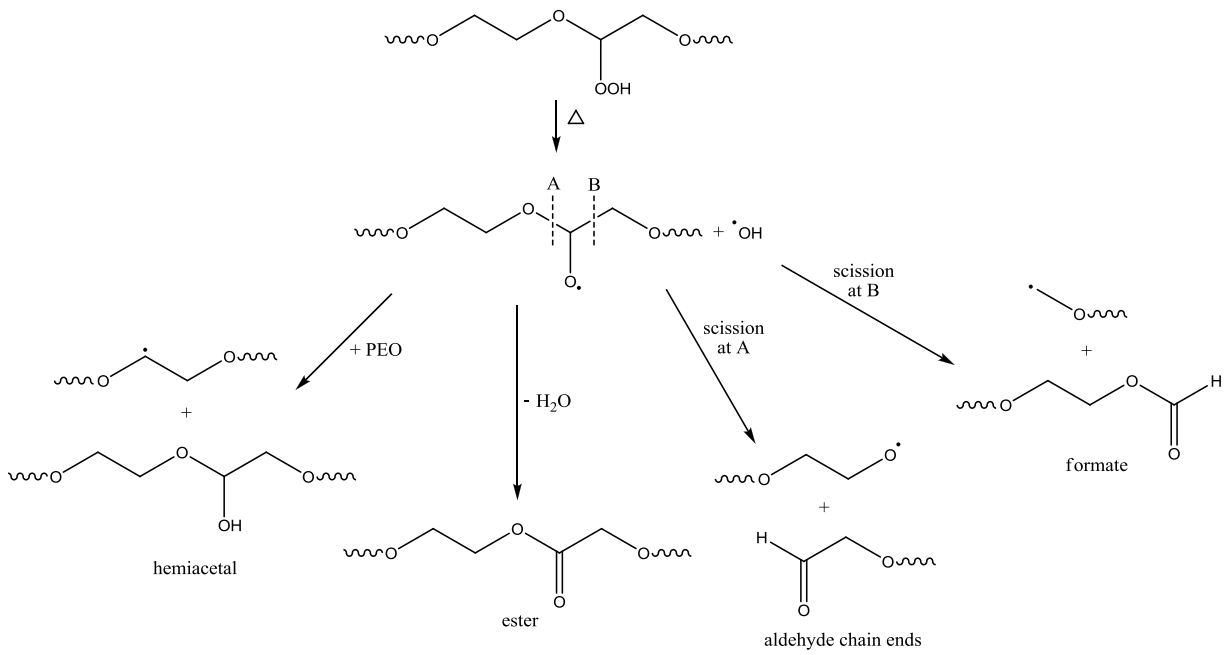

Figure 1.67: Proposed mechanism for the degradation of hydroperoxides formed during the thermo-oxidative degradation of PEO[85]

Costa *et al*. proposed that the formation of acetaldehyde, methanol, CO_2 and esters could be explained by the mechanism shown in Figure 1.68, which involves further reaction of the formate and radical formed through scission at point B in the initial stages of the thermo-oxidative degradation (Figure 1.67).[85]

Methanol was observed in large quantities by Costa *et al*. during the thermo-oxidative degradation of PEO[85] and the only step in Figure 1.68 which leads to the formation of methanol (scission at point B) also leads to the formation of aldehyde terminated chain ends. Formation of large quantities of methanol *via* this route would, therefore, also result in a significant level of aldehydes. There were, however, no peaks corresponding to aldehydes in the FTIR spectrum of the oxidised polymer. Costa *et al*., therefore, proposed that methanol was also formed by oxidation of some of the acetaldehyde produced during the thermo-oxidative degradation of PEO.[85]

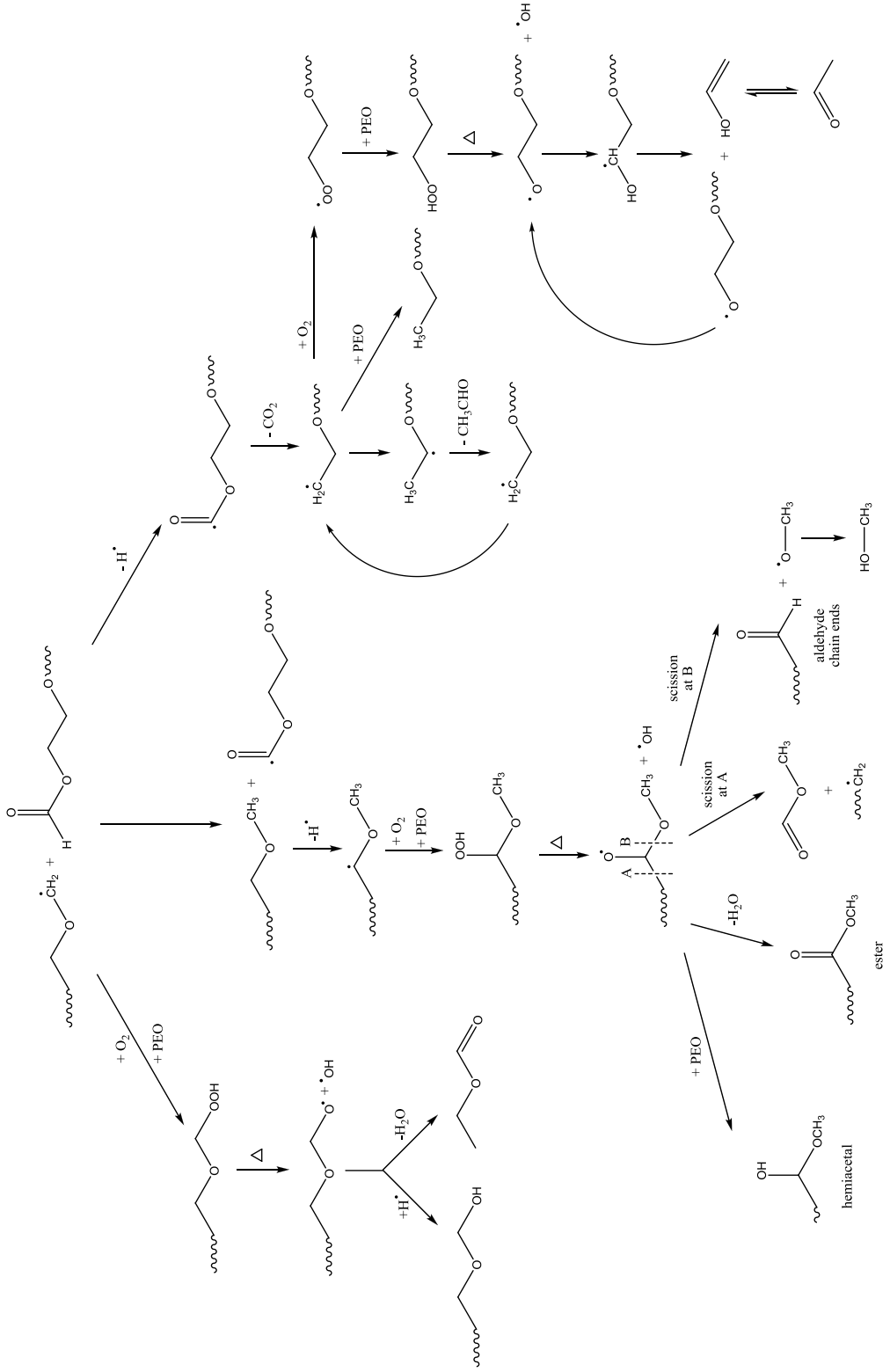

Figure 1.68: Proposed mechanism for the formation of secondary degradation products during the thermo-oxidative degradation of PEO[85]

1,4-Dioxane, which was observed at low levels, was proposed to have formed through the cyclisation reactions shown in Figure 1.69.

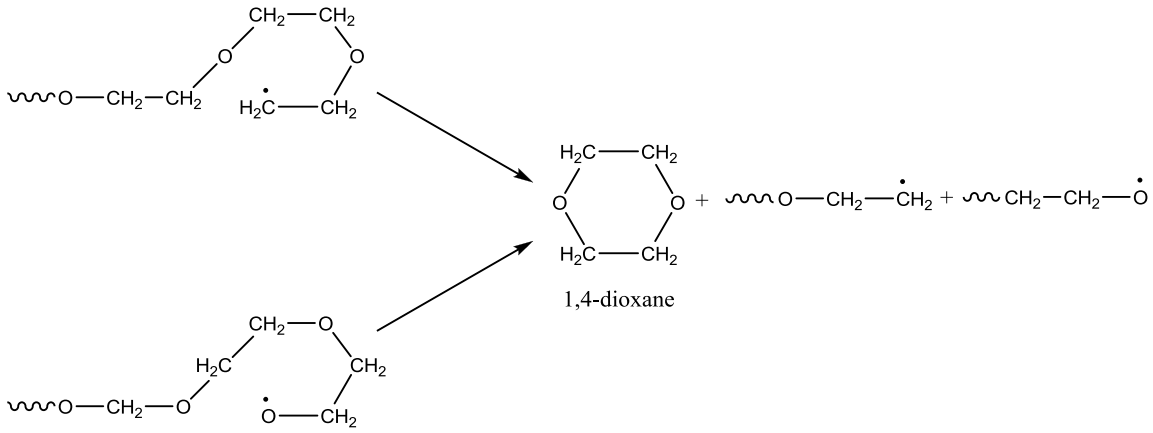

Figure 1.69: Proposed mechanism for the formation of 1,4-dioxane during the degradation of PEO[85]

Han *et al*.[86] studied the thermo-oxidative degradation of PEG with an average molecular weight of 6000 and also found that formic esters were produced as the main degradation products. It was proposed that PEG reacts with oxygen in the first step to yield an α-hydroperoxide which subsequently decomposes by a radical mechanism. These radicals then yield formic esters as a major thermo-oxidative degradation product.

Glastrup[87] also identified formic esters as major products in the thermo-oxidative degradation of tetraethylene glycol (TEG), a model compound for PEG. This compound contains hydroxyl end groups, two vicinal ether groups and one central ether group and was, therefore, expected to undergo the same degradation reactions as PEG.[87] Glastrup proposed that oxidation of the hydroxyl end group occurs producing formic acid which then reacts with TEG to yield formic acid esters.

Throughout the literature, therefore, there is agreement that formates are one of the major degradation products produced during the thermo-oxidative degradation of PEO, however, the mechanism by which they are formed continues to be the subject of some debate.

- *Poly(propylene oxide)*

The thermo-oxidative degradation of PPO at 150°C was investigated by Yang *et al.*[84] by means of NMR spectroscopy. Peaks corresponding to formate esters and acetate esters were identified in the spectrum of PPO after thermo-oxidative degradation, with primary and secondary hydroxyl end groups also present in the degraded sample. Yang *et al*. proposed that hydroperoxides are formed on the carbons of the PPO backbone which then undergo scission reactions to yield formate and acetate ester end groups as well as hemiacetals, as illustrated in Figure 1.70.[84]

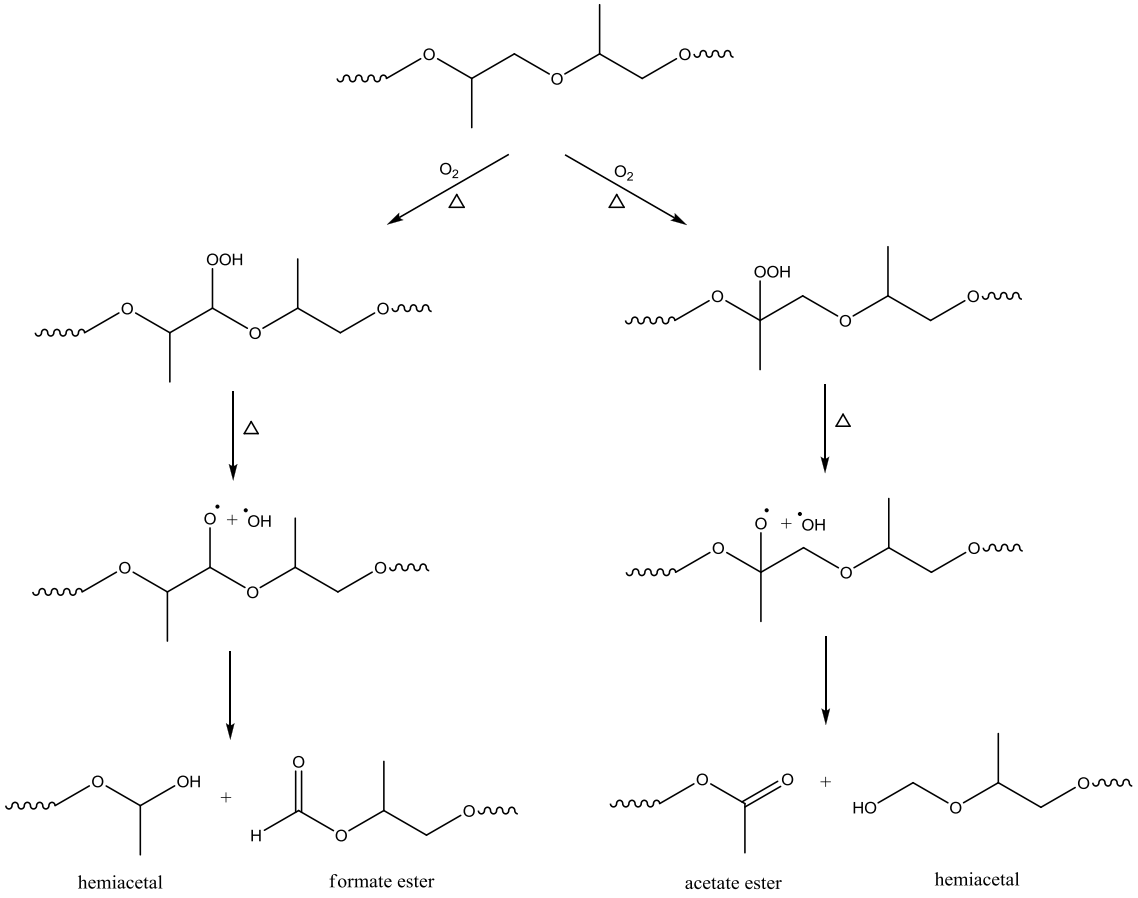

Figure 1.70: Proposed mechanism for the formation of formate and acetate esters during the thermo-oxidative degradation of PPO[84]

The hemiacetals groups are then proposed to undergo decomposition to yield primary and secondary hydroxyl end groups, formaldehyde and acetaldehyde. Formaldehyde

and acetaldehyde could then be oxidised to formic acid and acetic acid, which would in turn react with hydroxyl end groups to yield more formic and acetate esters.[84]

Costa *et al*.[88] studied the thermo-oxidative degradation of PPO by means of TGA with the volatile degradation products (collected in a U-trap cooled to -100°C) being analysed by GC-FTIR. The major degradation products which were identified were CO_2, formaldehyde, methanol, acetaldehyde, propanal, acetone and water. When investigating the thermal degradation of PPO in an inert atmosphere, unsaturated hydrocarbons, including ethene and propene, were formed.[72] These were, however, absent during the thermo-oxidative degradation. Costa *et al*. proposed that whilst both tertiary and secondary hydroperoxides form during the thermo-oxidative degradation of PPO, the formation of secondary hydroperoxides is preferential.[88] Decomposition of the secondary hydroperoxides into alkoxy and hydroxy radicals, followed by further reaction of these species, leads to the formation of the major degradation products which were observed. Presented in Figure 1.71 are the possible reactions which can occur following the decomposition of the secondary hydroperoxide. As was the case for PEO, methanol is proposed to have been formed by oxidation of some of the acetaldehyde produced during the thermo-oxidative degradation of PPO.[88]

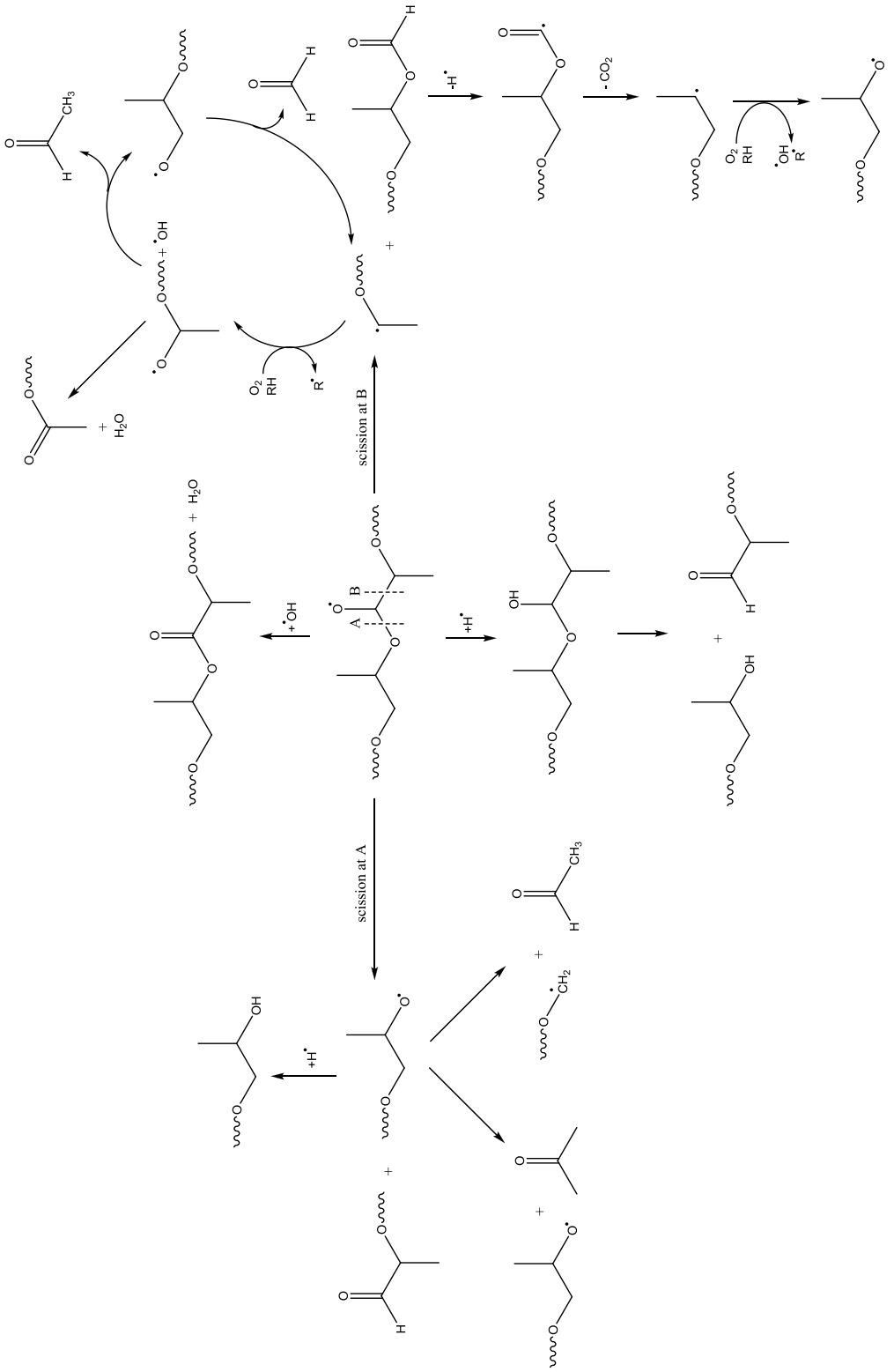

Figure 1.71: Proposed degradation mechanisms for the secondary hydroperoxide formed during the thermo-oxidative degradation of PPO[88]

1.6 Degradation of Polyurethanes in the Presence of Fire Retardants

1.6.1 Additive Fire Retardants

1.6.1.1 Phosphorus-based Fire Retardants

1.6.1.1.1 Ammonium Polyphosphate

It has been established by Camino *et al*.,[89] by means of TVA, that the thermal degradation of APP occurs in three steps between 200˚C and 400°C. In the first step, which begins near 230°C, ammonia is eliminated from the ONH_4 groups creating acidic hydroxyl groups which subsequently condense to form a crosslinked structure known as an ultraphosphate, shown in Figure 1.72. The second step involves thermal degradation of the ultraphosphate to yield a highly cross-linked polyphosphoric acid, ammonia, water and phosphate fragments. Finally, above 370°C the polyphosphoric acid decomposes to yield phosphate fragments which will accumulate in the cold-ring fraction during TVA.

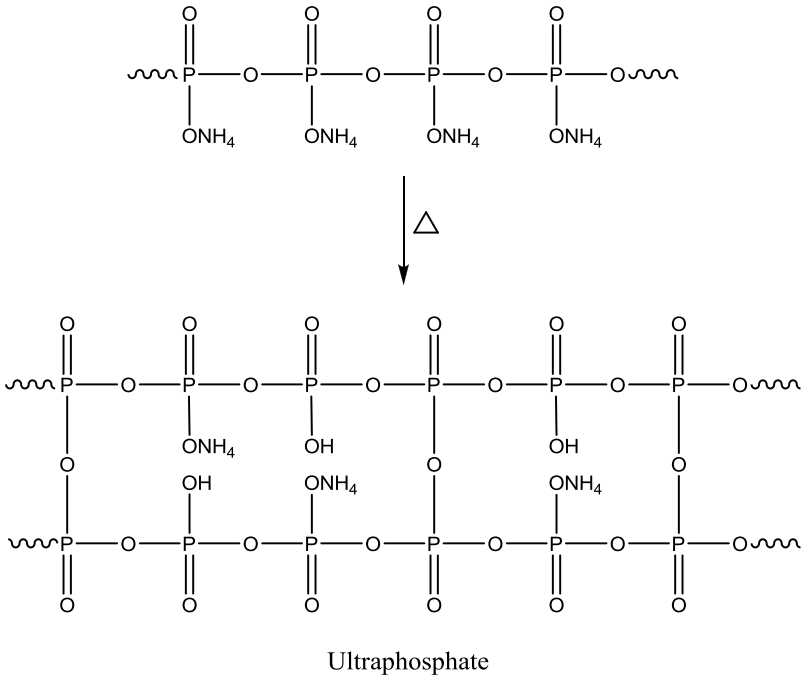

Figure 1.72: Degradation of APP to form an ultraphosphate

Grassie and Mendoza studied the effect of APP on the thermal degradation of a polyurethane based on MDI and PEGs of low molecular weights.[90] TVA results revealed that APP has a profound effect on the thermal degradation with significantly different products observed in the presence of the fire retardant. Volatile products observed included CO_2, ammonia, 1,4-dioxane, water, and aromatic amines including aniline and *N*-ethylaniline. In addition, a cold-ring fraction comprising 25% of the original sample was obtained which was shown to contain phosphorus and amines, although definitive identification of the species present was not possible. A large quantity of residue was also obtained which suggests that cross-linked structures have formed during the degradation, with analysis of this residue showing the presence of amines. It appears, therefore, that the presence of APP has promoted the production of amine compounds during the degradation of the polyurethane.

The presence of both MDI and the secondary amine *N*-ethylaniline suggests that degradation of the urethane linkage occurs by both a depolycondensation reaction and by a four-membered ring transition state mechanism, respectively. The depolycondensation reaction of the urethane is acid-catalysed by the acidic hydroxyl groups which arise from degradation of APP to form ultraphosphate, as shown in Figure 1.73.

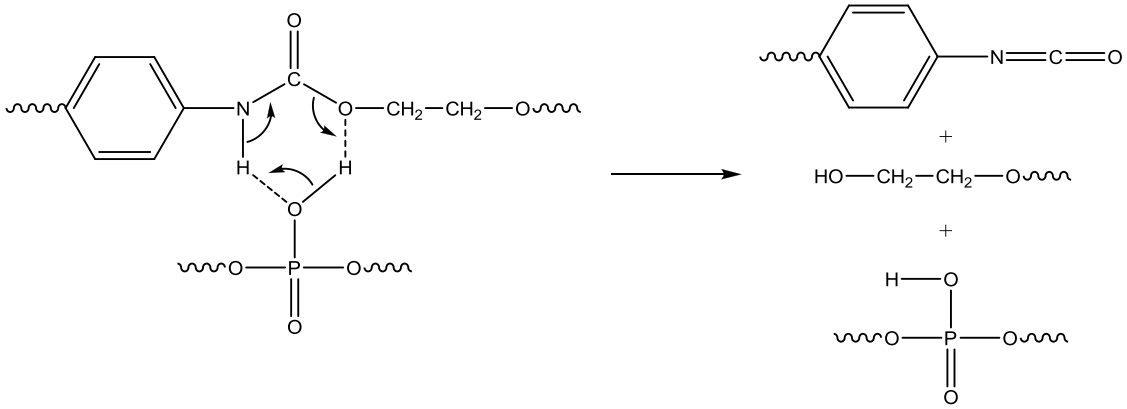

Figure 1.73: Acid-catalysed depolymerisation of the urethane linkage

In the presence of the acidic hydroxyl groups the regenerated PEG undergoes an acid-catalysed dehydration reaction to form 1,4-dioxane and water, as shown in Figure 1.74.[91] It is also possible that an alcoholysis reaction of the polyphosphate could occur to produce esters, resulting in a network of cross-linked polyether and polyphosphate chains. This network would then degrade yielding phosphate fragments, phosphoric acid and an alkene, which subsequently liberates acetaldehyde. Alkenes and acetaldehyde were not observed as degradation products suggesting that either this reaction does not occur or that once formed the phosphate esters volatilise and accumulate in the cold-ring before any further degradation can take place.

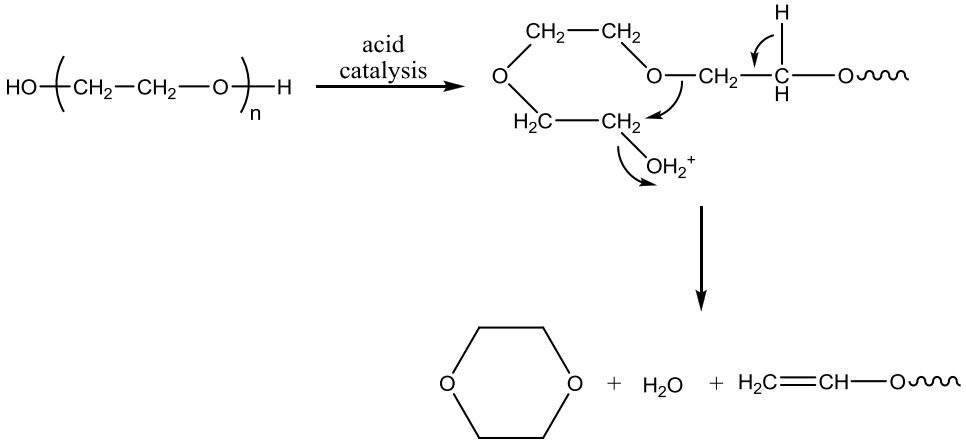

Figure 1.74: Acid-catalysed dehydration of PEG

The presence of acid groups during the degradation alters the route in which the secondary products are formed. In the pure polyurethane, thermal degradation yielded a residue rich in polycarbodiimide,[61] however this was not observed in the presence of APP. It was proposed that carbodiimide may have formed but subsequently reacts with other degradation products. Alternatively, instead of reacting to form carbodiimide the isocyanate groups could have reacted with water or acidic hydroxyl groups on the phosphate.

The effect of APP on polyurethanes prepared from MDI and high molecular weight PEGs was also studied[62] and it was observed that APP alters the degradation of these polyurethanes in a similar way as for those containing low molecular weight PEGs. The main difference was the presence of acetaldehyde and ethene which were proposed to have been formed from degradation of the urethane linkage *via* the six-membered ring transition state shown previously in Figure 1.24.

The mechanism for the degradation of polyurethane in the presence of APP as proposed by Grassie and Mendoza is shown in Figure 1.75.[62,90]

Duquesne *et al*.[92,93] also observed that the thermal degradation of polyurethane begins at a lower temperature in the presence of APP, due to acid catalysis of the depolycondensation reaction, and that a large quantity of residue is obtained. TGA studies under air and nitrogen revealed that the presence of oxygen leads to the formation of a carbonaceous char which is stable in the temperature range 350-530°C. ^{13}C and ^{31}P NMR analysis of the chars, in combination with FTIR spectroscopy, reveals that APP reacts with polyurethane and forms a phosphocarbonaceous char containing P-O-C bridges.[92]

It is proposed that the mode of action of APP in polyurethanes is associated primarily with condensed-phase processes and is similar to its activity in cellulosic materials, involving degradation to yield phosphoric acids which promote the formation of an insulating char. This explains the presence of large quantities of residue obtained when APP is present. This could occur by the reaction of the polyurethane with the degradation products of APP or the ultraphosphate could form a glass-like coating on the polymer thereby protecting it from heat and inhibiting the diffusion of combustible gases.

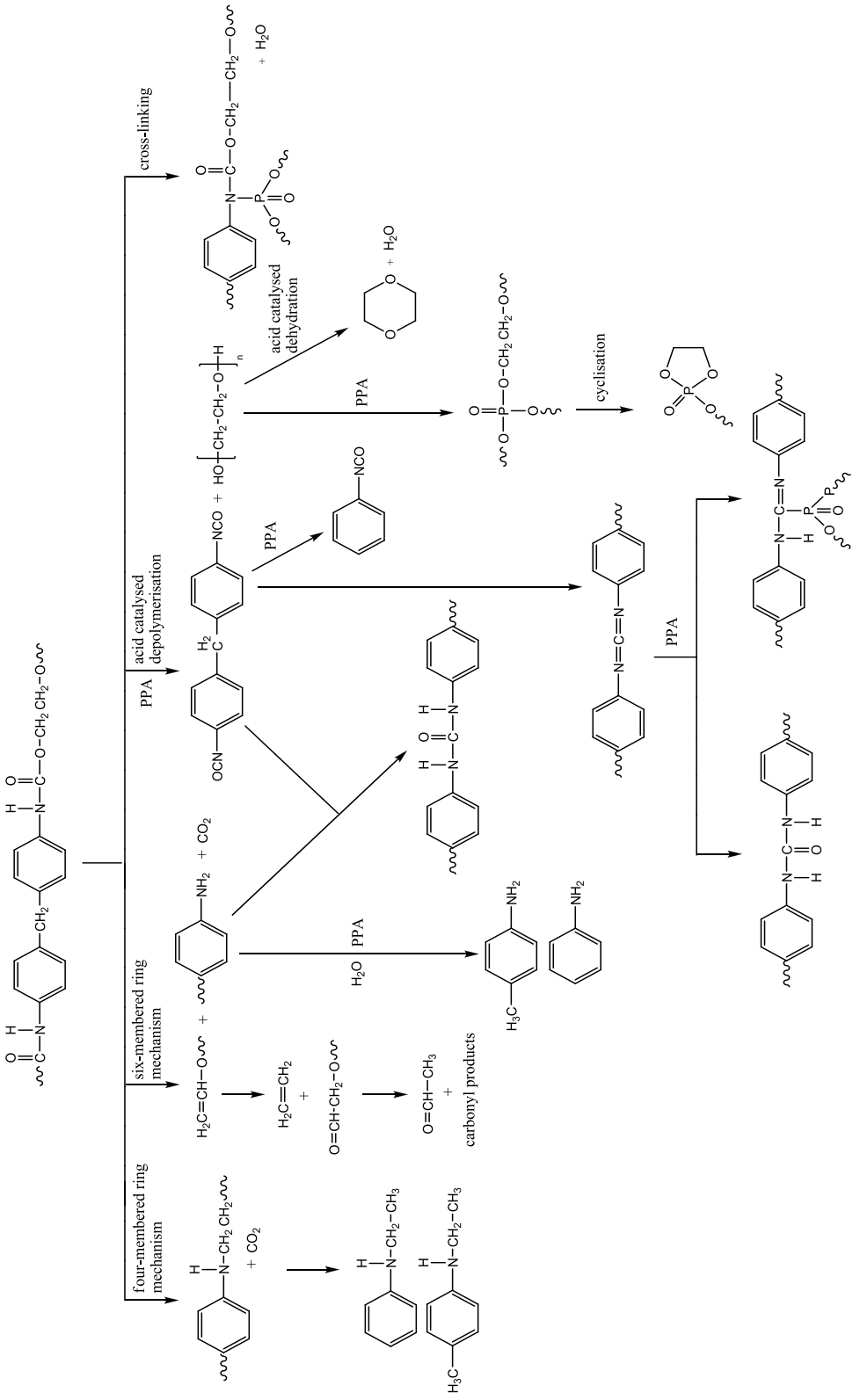

Figure 1.75: Proposed mechanism for the degradation of polyurethane in the presence of APP

1.6.1.1.2 Organic Phosphorus Fire Retardants

The thermal degradation of a TDI-based polyurethane foam containing the fire retardant tetrakis(2-chloroethyl)ethylenediphosphate was studied by Ohrbach and Kettrup.[94] A two stage degradation process was observed by TGA with the first step with a maximum degradation rate at 230°C corresponding to degradation of the fire retardant, and the second step with a maximum degradation rate at 294°C corresponding to degradation of the polyurethane. It is proposed that tetrakis(2-chloroethyl)ethylenediphosphate begins to decompose at 147°C to yield vinyl chloride, HCl and phosphorus acids which then act as char promoters. Batt and Appleyard[36] proposed that the fire retardant also acts in the gas-phase as the HCl released interferes with the radical reactions in the flame, as was described in Section 1.3.3.4.1.

Matuschek[75] studied the thermal degradation of polyurethane foams incorporating four different organic phosphoric ester fire retardants: tris(β-chloroisopropyl)-phosphate (TCPP), tris-(β,β'-dichloroisopropyl)-phosphate (TDCP), tris(β-chloroethyl)-phosphate (TCEP) and diethyl-*N*,*N*-bis-(2-hydroxyethyl)-aminomethylphosphonate (DAMP). The results demonstrated that degradation of the foams was very complex with those containing TCPP and TCEP degrading in five steps and those containing TDCP and DAMP degrading in four steps. Differences were observed in the nature of the degradation products for each foam in the region 200-220°C due to degradation of the fire retardants and following this all the degradation products were similar for each foam, arising from degradation of the polyol and isocyanate segments. Matuschek proposed that the phosphoric esters degrade to form acidic structures which exert their activity primarily in the condensed-phase by promoting char formation.

1.6.1.1.3 Phosphazenes

Phosphazenes have been studied as possible fire retardants as they contain phosphorus and nitrogen and therefore are expected to exhibit synergism. Wang *et al.*[95] studied the thermal degradation of a polyurethane incorporating poly(bispropoxyphosphazene) as a fire retardant. TGA results demonstrated that thermal degradation of the polyurethane

occurred at a lower temperature in the presence of the phosphazene and an increased level of char was obtained. As the level of phosphazene was increased, the onset degradation temperature decreased further and the two stages of the degradation process became more pronounced. The nature of the degradation products was also observed to be altered with THF produced in large quantities. IR spectroscopy was employed to monitor the condensed-phase pyrolysis products of the polyurethane and it was observed that in the presence of the phosphazene bands corresponding to P-O-P groups appeared, suggesting that phosphoric acids are formed during degradation of the fire retardant. It was proposed that the presence of acids accelerates the degradation of the polyurethane and leads to dehydration of the 1,4-butanediol chain extender to form THF.

1.6.1.1.4 Phosphoric Acid

Phosphoric acid is released during the degradation of a large number of phosphorus-based fire retardants and has been proposed to be the active species in these materials. Ravey and Pearce,[96] therefore, studied the effect of phosphoric acid on the flammability and thermal degradation of flexible polyurethane foams in order to establish if this is an active fire retardant. The results demonstrated that the presence of a layer of phosphoric acid on the foam surface reduced the flammability of the foam, with a linear relationship established between acid content and quantity of foam consumed. TGA results, however, showed decreased thermal stability of the foam in the presence of phosphoric acid, indicating that a reaction occurs between the acid and the polyurethane. The foam studied by Ravey and Pearce contains cross-links and it is proposed that the presence of phosphoric acid leads to these cross-links being broken.

1.6.1.2 Melamine

Batt and Appleyard[36] studied the thermal degradation and fire performance of polyurethane foams containing melamine and found that it had a beneficial effect on the fire performance. TGA results showed no evidence of an increased char yield and it was concluded that the degradation mechanism of the polyurethane foam was essentially unaltered in the presence of melamine. The primary mode of action of melamine was,

therefore, proposed to involve an endothermic heat sink effect as well as dilution of the combustible vapours with less flammable gases.

Price *et al*.[97] also studied the effect of melamine on the thermal degradation of polyurethane foam by TGA and pyrolysis-GC-MS. The base foam and the melamine foam degraded in two steps with similar onset degradation temperatures but in the first step the temperature at which the maximum rate occurred was lower in the melamine foam. The ammonia evolved during degradation of the melamine itself was proposed to accelerate the degradation of urea and urethane linkages within the polyurethane as has been shown by Mukaiyama and co-workers.[65,67] Pyrolysis-GC-MS revealed that the levels of 2,4- and 2,6-TDI released during the degradation of the foam were significantly reduced in the presence of melamine. Reaction of the amine groups in the melamine with the isocyanate group of the TDI is proposed to occur which leads to the formation of a polyurea.

Dick *et al*.[98] studied the thermal degradation of a polyurethane foam containing 10% melamine by means of TGA, DSC and pyrolysis under a nitrogen atmosphere. It was found that the onset of degradation was lower in the melamine foam compared to a base foam and it was proposed that this was due to volatilisation of melamine from the foam. No increase in char yield was observed for the foam containing melamine which is in agreement with the work of Batt and Appleyard.[36] Solid-state ^{13}C NMR analysis was performed on the chars obtained during the pyrolysis and revealed no significant structural differences between the char of the melamine and base foams. Elemental analysis of the chars, however, revealed a higher nitrogen content for the char from the melamine foam which suggests that small amounts of melamine-based structures were incorporated into the char.[98] High temperature *in situ* ^{1}H NMR experiments also revealed that the presence of melamine significantly lowered the temperature at which char formation begun. The work of Dick *et al*., therefore, demonstrates that melamine does exhibit some activity in the condensed-phase.

It has been recognised that melamine is most effective as a fire retardant for polyurethane foams when it is used in conjunction with other additives such as phosphorus-halogen fire retardants.[18,99]

1.6.1.3 Nanocomposites

Polyurethane nanocomposites incorporating various types of clay have been successfully prepared by various authors and have been shown to have superior properties to conventional polyurethanes.[39,40,100,101,102] Saha *et al.*[19] demonstrated by TGA that polyurethane foams containing organically modified montmorillonite had increased thermal stability suggesting that incorporation of a nanoclay has a stabilising effect on the thermal degradation of the foam. Kumari *et al.*[103] reported similar results for a hyperbranched polyurethane coating containing organically modified montmorillonite. Chen *et al.*[104] studied polyurethane nanocomposites incorporating sepiolite, a fibrous clay with silanol groups at the surface, and observed increased thermal stability and char residues in the presence of the clay. It is proposed that the silanol groups of the clay react with isocyanate groups creating crosslinks between the clay and the polyurethane. This in turn renders the polyurethane more thermally stable.

It has been recognised that nanoclays often work best in conjunction with other fire retardants. Modesti *et al.*[20] studied the potential synergistic effect of layered silicates and a phosphorus-based fire retardant, aluminium phosphinate, in polyurethane foams. TGA results revealed a 10% increase in the onset degradation temperature for the foams containing the nanoclays. In the foams containing both the nanoclay and the fire retardant the level of char obtained was much higher than with the fire retardant alone, which suggests some synergistic effect between the clay and fire retardant. Like most phosphorus fire retardants, aluminium phosphinate degrades to form acids which catalyse dehydration reactions leading to the formation of char. For the nanoclay a physical effect is prominent with the clay particles acting as an inert filler, promoting the formation of a compact barrier layer on the foam. This retards the escape of volatiles from the foam thereby delaying the onset temperature of degradation. When examining

the fire behaviour of the foams, however, no synergistic effect between the nanoclay and aluminium phosphinate was observed. A phosphonium modified montmorillonite was, on the other hand, shown to have synergy with aluminium phosphinate as a foam containing both materials had improved fire resistance and a higher onset temperature of degradation.

In contrast to these reports, Song *et al.*[105] observed decreased thermal stability with increased char residue in the presence of organically modified montmorillonite. It was proposed that this was due to the presence of acidic groups on the clay surface which acid-catalyse the depolymerisation reaction of the polyurethane whilst also promoting char formation. This effect is similar to that shown for phosphorus-based fire retardants such as APP. Acidic groups on the clay arise from degradation of the organic modifier *via* a Hofmann elimination, which results in the formation of an amine, an olefin and Brønsted acid sites on the clay surface.[39,106,107]

1.6.2 Reactive Fire Retardants

As was mentioned in Section 1.3.3.3, reactive fire retardants are incorporated into the structure of the polymer backbone and are beneficial as they are not lost by leaching and their liberation coincides with the degradation of the polymer.

1.6.2.1 Phosphorus-containing Diols and Polyols

The degradation of a series of polyurethanes incorporating a phosphorus-containing polyol, poly(butylene phenylphosphonate), was studied by Grassie and Mackerron.[108,109] TGA results demonstrated that the presence of phosphorus had a detrimental effect on the thermal stability of the polyurethane. This was confirmed by TVA which revealed that volatile products were evolved at significantly lower temperatures with increasing levels of phosphorus. This was proposed to be due to degradation of the phosphorus-containing segments leading to the formation of phosphonic acid structures which induce acid-catalysed degradation of the urethane linkage. As the phosphorus content was increased, amines and pyrrolidine compounds were evolved in increasing levels and

the level of carbodiimide decreased, suggesting that the formation of this compound or its secondary reactions are altered by the presence of phosphorus. It was proposed that a competition is established between self condensation of the isocyanate to form carbodiimide and reaction of the isocyanate with an amine to form urea.

Wang *et al*.[110] also studied the incorporation of a phosphorus-containing polyol into the polyurethane chain and demonstrated that the presence of phosphorus lowers the thermal stability of the polyurethanes. It was proposed that this is due to the presence of P-O-C bonds which are more susceptible to scission at lower temperatures than the urethane bond. More char is, however, observed which is proposed to be due to cross-linking occurring after initial scission of the P-O-C bonds has occurred.

Polyurethane systems incorporating phosphorus-containing diols at different levels have been studied by many workers[111,112,113,114] with similar results obtained in all cases. As the phosphorus level in the polyurethane backbone was increased, the thermal stability of the materials decreased and increased levels of residue were obtained.

It is, therefore, clear from these studies that whilst the introduction of a phosphorus-containing polyol or diol into a polyurethane lowers the thermal stability, it in turn promotes the formation of a thermally stable insulating char thus imparting increased fire resistance into the material.

1.6.2.2 Phosphorus-containing Isocyanates

Liu *et al*.[115] synthesised polyurethanes containing phosphorus by reacting phosphorus-containing isocyanates with a variety of polyols. The phosphorus-containing polyurethanes were observed to be less thermally stable than the base polyurethane as a result of the susceptibility of the phosphorus segment to thermal scission. However, higher char yields were obtained which demonstrates that the presence of phosphorus leads to improved fire resistance by promoting the formation of a thermally stable protective char.

1.6.2.3 Phosphazenes

Yuan *et al.*[116] studied the effect of a novel reactive fire retardant consisting of an aromatic phosphate-containing cyclotriphosphazene on the thermal stability of a TDI-based polyurethane. TGA results demonstrated that the presence of the phosphazene within the polyurethane increased the thermal stability. This is in contrast to the majority of the results reported in the literature for phosphorus-based fire retardants and is attributed to the high level of rigid aromatic groups within the fire retardant. Analysis of the residue during the degradation process by IR spectroscopy revealed the presence of phosphoric acids which suggests that the mode of action of this fire retardant may involve a condensed-phase mechanism.

1.7 Aims

Our laboratory at the University of Strathclyde has experience unique within UK academia of the synthesis of high quality polyurethane foams based on commercial formulations, and has for some time been researching the development of novel environmentally friendly fire retardant formulations for use in polyurethane foams. Prior to the start of this research project, our laboratory succeeded in developing a multi-component fire retardant package which rendered a TDI-based foam more fire retardant than commercially available alternatives. The chemistry behind this, however, was not well understood. This research project was, therefore, conceived to study the degradation behaviour of this fire retardant foam with the aim to better understand the chemistry which occurs. A number of studies have been published on the thermal degradation behaviour of polyurethanes, however, the literature concerning the degradation of foams, in particular those based on TDI, is limited. This project, therefore, aimed to expand on the limited knowledge of the processes which occur during the thermal and thermo-oxidative degradation of TDI-based polyurethane foams, and to study the effects that the fire retardants in the Strathclyde patented formulation have on the degradation chemistry.

An initial study aimed to investigate the thermal degradation of a standard TDI-based foam by means of Differential Scanning Calorimetry (DSC), Thermogravimetric Analysis (TGA) and Thermal Volatilisation Analysis (TVA). DSC and TGA allow the thermal behaviour of the material to be studied under oxidative and non-oxidative environments and provide a general overview of the thermal behaviour of the material. TVA, on the other hand, allows characterisation of the volatile products which are evolved from the material as it undergoes thermal degradation and has not been previously used to study TDI-based foams. It was envisaged, therefore, that by using these three complementary techniques detailed information would be gained with regards to the chemistry which occurs and this would allow degradation mechanisms to be proposed.

The condensed-phase behaviour of the material was also probed by means of pyrolysis studies under non-oxidative and oxidative environments, with characterisation of the char residues by solid-state ^{13}C NMR spectroscopy. Char formation is one of the most important condensed-phase mechanisms for modifying the combustion process of a polymer and by studying the structure of the chars formed during degradation information can be gained with regards to the condensed-phase behaviour of the polyurethane.

Following this, foams containing different fire retardants, some of which are part of the Strathclyde patented formulation, were studied in a similar manner with the aim of investigating the effects that these fire retardants have on the thermal degradation of the polyurethane. A small scale analogue of the legislative standard 'Crib 5' fire test was also performed on the foams to examine the effect which the fire retardants have on the flammability of the polyurethane foam. The fire retardants studied were APP and two nanoclays, namely Cloisite® 30B and vermiculite. APP and vermiculite were chosen as these form part of the Strathclyde patented formulation, whilst Cloisite® 30B was chosen as this had been previously shown to have an interesting but as yet unexplained effect on the flammability of the polyurethane foam.

1.8 References

[1] J. H. Saunders and K. C. Frisch, *Polyurethanes Chemistry and Technology: Part I. Chemistry*, Interscience Publishers, New York, 1962, Ch. I, p. 2

[2] G. Woods, *Flexible Polyurethane Foams: Chemistry and Technology*, Applied Science Publishers Ltd, Essex, 1982, Ch. 1, p. 1

[3] O. Bayer, W. Siefken, H. Rinke, L. Orthner and H. Schild, A Process for the Production of Polyurethanes and Polyureas, German Patent No. DRP 728981

[4] K. N. Edwards, *Urethane Chemistry and Application*, American Chemical Society, Washington D.C., 1981, p. 3

[5] J. M. Buist, *Developments in Polyurethane-1*, Applied Science Publishers Ltd, Essex, 1978, Ch. 1, p. 1

[6] Z. Wirpsza, *Polyurethanes: Chemistry, Technology and Applications*, Ellis Horwood, Chichester, 1993, Ch.1, p. 1

[7] D. Randall and S. Lee, *The Polyurethanes Book*, John Wiley and Sons Ltd, Everberg, 2002, Ch. 2, p. 9

[8] K. N. Edwards, *Urethane Chemistry and Application*, American Chemical Society, Washington D.C., 1981, Ch.1, p. 9

[9] J. H. Saunders and K. C. Frisch, *Polyurethanes Chemistry and Technology: Part II. Technology*, Interscience Publishers, New York, 1964, Ch. VII, p. 159

[10] J. H. Saunders and K. C. Frisch, *Polyurethanes Chemistry and Technology: Part II. Technology*, Interscience Publishers, New York, 1964, Ch. VIII, p. 268

[11] J. H. Saunders and K. C. Frisch, *Polyurethanes Chemistry and Technology: Part I. Chemistry*, Interscience Publishers, New York, 1962, Ch. II, p. 32

[12] J. M. Buist, *Developments in Polyurethane-1*, Applied Science Publishers Ltd, Essex, 1978, Ch. 2, p. 9

[13] G. Woods, *Flexible Polyurethane Foams: Chemistry and Technology*, Applied Science Publishers Ltd, Essex, 1982, Ch. 2, p. 47

[14] J. M. Buist, *Developments in Polyurethane-1*, Applied Science Publishers Ltd, Essex, 1978, Ch. 4, p. 77

[15] J. H. Saunders and K. C. Frisch, *Polyurethanes Chemistry and Technology: Part I. Chemistry*, Interscience Publishers, New York, 1962, Ch. V, p. 219

[16] W. C. Kuryla and A. J. Papa, *Flame Retardancy of Polymeric Materials*, volume 3, Marcel Dekker Inc., New York, 1975, Ch. 1, p. 1

[17] J. W. Lyons, *The Chemistry and Uses of Fire Retardants*, Wiley Interscience, New York, 1970, Ch. 8, p. 345

[18] H. Singh and A. K. Jain, *J. Appl. Polym. Sci.*, 2009, **111**, 1115

[19] M. C. Saha, M. E. Kabir and S. Jeelani, *Mater. Sci. Eng. A*, 2008, **479**, 213

[20] M. Modesti, A. Lorenzetti, S. Besco, D. Hrelja, S. Semenzato, R. Bertani and R. A. Michelin, *Polym. Degrad. Stabil.*, 2008, **93**, 2166

[21] J. H. Saunders and K. C. Frisch, *Polyurethanes Chemistry and Technology: Part I. Chemistry*, Interscience Publishers, New York, 1962, Ch. III, p. 63

[22] K. N. Edwards, *Urethane Chemistry and Application*, American Chemical Society, Washington D.C., 1981, Ch. 11, p. 127

[23] N. Grassie and G. Scott, *Polymer Degradation and Stabilisation*, Cambridge University Press, Cambridge, 1985, Ch. 6, p. 170

[24] A. R. Horrocks and D. Price, *Fire Retardant Materials*, Woodhead Publishing Ltd, Cambridge, 2001, Ch. 1, p. 1

[25] C. J. Hilado, *Flammability Handbook for Plastics*, Technomic Publishing Company Inc., Lancaster, 1990, Ch. 2, p. 37

[26] M. Inagaki, *New Carbon Materials*, 2009, **24**, 193

[27] G. Camino and L. Costa, *Polym. Degrad. Stabil.*, 1988, **20**, 271

[28] A. R. Horrocks and D. Price, *Fire Retardant Materials*, Woodhead Publishing Ltd, Cambridge, 2001, Ch. 2, p. 31

[29] J. W. Lyons, *The Chemistry and Uses of Fire Retardants*, Wiley Interscience, New York, 1970, Ch. 7, p. 281

[30] C. J. Hilado, *Flammability Handbook for Plastics*, Technomic Publishing Company Inc., Lancaster, 1990, Ch. 5, p. 167

[31] G. Dixon-Lewis, *Combust. Flame.*, 1979, **36**, 1

[32] W. C. Kuryla and A. J. Papa, *Flame Retardancy of Polymeric Materials*, volume 1, Marcel Dekker Inc., New York, 1973, Ch. 1, p. 1

[33] A. W. Benbow and C. F. Cullis, *Combust. Flame.*, 1975, **24**, 217

[34] A. R. Horrocks and D. Price, *Fire Retardant Materials*, Woodhead Publishing Ltd, Cambridge, 2001, Ch. 3, p. 69

[35] L. Costa and G. Camino, *J. Therm. Anal.*, 1988, **34**, 423

[36] A. M. Batt and P. Appleyard, *J. Fire Sci.*, 1989, **7**, 338

[37] C. Denecker, J. J. Liggat and C. E. Snape, *J. Appl. Polym. Sci.*, 2006, **100**, 3024

[38] W. C. Kuryla and A. J. Papa, *Flame Retardancy of Polymeric Materials*, volume 1, Marcel Dekker Inc., New York, 1973, Ch. 2, p. 133

[39] B. Chen, J. R. G. Evans, H. C. Greenwell, P. Boulet, P. V. Coveney, A. A. Bowden and A. Whiting, *Chem. Soc. Rev.*, 2008, **37**, 568

[40] M. Alexandre and P. Dubois, *Mat. Sci. Eng. R*, 2000, **28**, 1

[41] T. J. Pinnavaia and G. W. Beall, *Polymer-clay Nanocomposites*, John Wiley and Sons Ltd, Chichester 2000, Ch. 1, p. 1

[42] A. Blumstein, *I. Bull. Chem. Soc. Fr.*, 1961, 899

[43] A. R. Horrocks and D. Price, *Fire Retardant Materials*, Woodhead Publishing Ltd, Cambridge, 2001, Ch. 6, p. 204

[44] T. J. Pinnavaia and G. W. Beall, *Polymer-clay Nanocomposites*, John Wiley and Sons Ltd, Chichester 2000, Ch. 5, p. 97

[45] N. Grassie and G. Scott, *Polymer Degradation and Stabilisation*, Cambridge University Press, Cambridge, 1985, Ch. 2, p. 17

[46] N. Grassie, *Developments in Polymer Degradation-1*, Applied Science Publishers, London, 1977, p. 47

[47] N. Grassie and G. Scott, *Polymer Degradation and Stabilisation*, Cambridge University Press, Cambridge, 1985, Ch. 4, p. 86

[48] J. L. Boland and G. Gee, *Trans. Faraday Soc.*, 1949, **42**, 236

[49] G. Scott, *Atmospheric Oxidation and Antioxidants I*, Elsevier, Amsterdam, 1993, Ch. 2, p. 45

[50] M. Ravey and E. M. Pearce, *J. Appl. Poly. Sci.*, 1997, **63**, 47

[51] L. Shufen, J. Zhi, Y. Kaijun, Y. Shuqin and W. K. Chow, *J. Polymer-Plastics Technology and Engineering*, 2006, **45**, 95

[52] N. Grassie and M. Zulfiqar, *J. Polym. Sci. Pol. Chem.*, 1978, **16**, 1563

[53] Y. Zhang, Z. Xia, H. Huang and H. Chen, *Polym. Test.*, 2009, **28**, 264

[54] M. P. Thorne, *Can. J. Chem.*, 1967, **45**, 2537

[55] N. Grassie, M. Zulfiqar and M. I. Guy, *J. Poly. Sci. Pol. Chem.*, 1980, **18**, 265

[56] E. Dyer and G. C. Wright, *J. Am. Chem. Soc.*, 1959, **81**, 2138

[57] A. F. McKay and G. R. Vavasour, *Can. J. Chem.*, 1953, **31**, 688

[58] E. Dyer and G. E. Newborn Jr., *J. Am. Chem. Soc.*, 1958, **80**, 5495

[59] K. L. Erickson, *J. Therm. Anal. Calorim.*, 2007, **89**, 427

[60] N. Grassie and M. Zulfiqar, *Developments in Polymer Stabilisation 1*, Applied Science Publishers, London, 1979, Ch. 6, p. 197

[61] N. Grassie and A. P. Mendoza, *Polym. Degrad. Stabil.*, 1985, **10**, 267

[62] N. Grassie and A. P. Mendoza, *Polym. Degrad. Stabil.*, 1985, **11**, 359

[63] J. Fan and J. C. W. Chien, *Polym. Degrad. Stabil.*, 1985, **12**, 43

[64] J. P. Lewicki, J. J. Liggat, R. Pethrick, M. Patel and I. Rhoney, *Polym. Degrad. Stabil.*, 2008, **93**, 158

[65] T. Mukaiyama and M. Iwanami, *J. Am. Chem. Soc.*, 1957, **79**, 73

[66] T. Hoshino, T. Mukaiyama and H. Hoshino, *J. Am. Chem. Soc.*, 1952, **74**, 3097

[67] T. Mukaiyama and Y. Hoshino, *J. Am. Chem. Soc.*, 1956, **78**, 1946

[68] S. L. Madorsky and S. Straus, *J. Polym. Sci.*, 1959, **36**, 183

[69] S. L. Madorsky, *Polymer Reviews Volume 7: Thermal Degradation of Organic Polymers*, Interscience Publishers, New York, Ch. 11, p. 228

[70] N. Grassie and A. P. Mendoza, *Polym. Degrad. Stabil.*, 1984, **9**, 155

[71] G. G. Cameron, M. D. Ingram, M. Y. Qureshi, H. M. Gearing, L. Costa and G. Camino, *Eur. Polym. J.*, 1989, **25**, 779

[72] L. Costa, G. Camino, M. P. Luda, G. G. Cameron and M. Y. Qureshi, *Polym. Degrad. Stabil.*, 1995, **48**, 325

[73] T. Uyar and J. Hacaloğlu, *J. Anal. Appl. Pyrol.*, 2002, **64**, 379

[74] S. T. Marks and E. Metcalfe, *Combust. Flame*, 1996, **107**, 260

[75] G. Matuschek, *Thermochim. Acta*, 1995, **263**, 59

[76] W. D. Wooley, *Brit. Polym. J.*, 1972, **4**, 27

[77] D. K. Chattopadhyay and D. C. Webster, *Prog. Polym. Sci.*, 2009, **34**, 1068

[78] R. Bilbao, J. F. Mastral, J. Ceamanos and M. E. Aldea, *J. Anal. Appl. Pyrol.*, 1996, **37**, 69

[79] Z. Wirpsza, *Polyurethanes: Chemistry, Technology and Applications*, Ellis Horwood, Chichester, 1993, Ch. 4, p. 121

[80] S. Khatua and Y. Hsieh, *J. Polym. Sci. Pol. Chem.*, 1997, **35**, 3263

[81] D. Wlodarczak, *J. Appl. Polym. Sci.*, 1988, **36**, 377

[82] H. H. G. Jellinek and S. R. Dunkle, *J. Polym. Sci. Pol. Chem.*, 1983, **21**, 487

[83] T. Servay, R. Voelkel, H. Schmiedberger and S. Lehman, *Polymer*, 2000, **41**, 5247

[84] L. Yang, F. Heatley, T. G. Blease and R. I. G. Thompson, *Eur. Polym. J.*, 1996, **32**, 535

[85] L. Costa, A. M. Gad and G. Camino, *Macromolecules*, 1992, **25**, 5512

[86] S. Han, C. Kim and D. Kwon, *Polymer*, 1997, **38**, 317

[87] J. Glastrup, *Polym. Degrad. Stabil.*, 1996, **52**, 217

[88] L. Costa, G. Camino, M. P. Luda, G. G. Cameron and M. Y. Qureshi, *Polym. Degrad. Stabil.*, 1996, **53**, 301

[89] G. Camino, N. Grassie and I. C. McNeill, *J. Poly. Sci. Chem. Ed.*, 1978, **16**, 95

[90] N. Grassie and A. P. Mendoza, *Polym. Degrad. Stabil.*, 1985, **11**, 145

[91] N. Grassie and A. P. Mendoza, *Polym. Degrad. Stabil.*, 1985, **10**, 43

[92] S. Duquesne, M. Le Bras, S. Bourbigot, R. Delobel, G. Camino, B. Eling, C. Lindsay, T. Roels and H. Vezin, *J. Appl. Polym. Sci.*, 2001, **82**, 3262

[93] S. Duquesne, R. Delobel, M. Le Bras and G. Camino, *Polym. Degrad. Stabil.*, 2002, **77**, 333

[94] K. H. Ohrbach and A. Kettrup, *Polym. Degrad. Stabil.*, 1985, **13**, 99

[95] P. Wang, W. Chiu, L. Chen, B. Denq, T. Don and Y. Chiu, *Polym. Degrad. Stabil.*, 1999, **66**, 307

[96] M. Ravey and E. M. Pearce, *J. Appl. Polym. Sci.*, 1999, **74**, 1317

[97] D. Price, Y. Liu, G. J. Milnes, R. Hull, B. K. Kandola and A. R. Horrocks, *Fire Mater.*, 2002, **26**, 201

[98] C. Dick, C. Denecker, J. J. Liggat, M. H. Mohammed, C. E. Snape, G. Selley, C. Lindsay, B. Eling and P. Chaffanjon, *Polym. Int.*, 2000, **49**, 1177

[99] H. Singh, A. K. Jain and T. P. Sharma, *J. Appl. Poly. Sci.*, 2008, **109**, 2718

[100] S. Semenzato, A. Lorenzetti, M. Modesti, E. Ugel, D. Hrelja, S. Besco, R. A. Michelin, A. Sassi, G. Facchin, F. Zorzi and R. Bertani, *Appl. Clay. Sci.*, 2009, **44**, 35

[101] J. Xong, Z. Zheng, H. Jiang, S. Ye and X. Wang, *Compos. Part A-Appl. S.*, 2007, **38**, 132

[102] Y. H. Kim, S. J. Choi, J. M. Kim, M. S. Han and W. N. Kim, *Macromol. Res.*, 2007, **15**, 676

[103] S. Kumari, A. K. Mishra, A. V. R. Krishna and K. V. S. N. Raju, *Prog. Org. Coat.*, 2007, **60**, 54

[104] H. Chen, M. Zheng, H. Sun and Q. Jia, *Mater. Sci. Eng. A*, 2007, **445**, 725

[105] L. Song, Y. Hu, Y. Tang, R. Zhang, Z. Chen and W. Fan, *Polym. Degrad. Stabil.*, 2005, **87**, 111

[106] M. Kracalik, J. Mikesova, R. Puffr, J. Baldrian, R. Thomann and C. Friedrich, *Polym. Bull.*, 2007, **58**, 313

[107] X. Xu, Y. Ding, Z. Qian, F. Wang, B. Wen, H. Zhou, S. Zhang and M. Yang, *Polym. Degrad. Stabil.*, 2009, **94**, 113

[108] N. Grassie and D. H. Mackerron, *Polym. Degrad. Stabil.*, 1983, **5**, 43

[109] N. Grassie and D. H. Mackerron, *Polym. Degrad. Stabil.*, 1983, **5**, 89

[110] T. Wang, Y. Cho and P. Kuo, *J. Appl. Poly. Sci.*, 2001, **82**, 343

[111] B. Youssef, B. Mortaigne, M. Soulard and J. M. Saiter, *J. Therm. Anal. Calorim.*, 2007, **90**, 489

[112] W. El Khatib, B. Youssef, C. Bunel and B. Mortaigne, *Polym. Int.*, 2003, **52**, 146

[113] M. Lin, W. Tsen, Y. Shu and F. Chuang, *J. Appl. Poly. Sci.*, 2001, **79**, 881

[114] T. C. Chang, Y. S. Shiu, H. B. Chen and S. Y. Ho, *Polym. Degrad. Stabil.*, 1995, **47**, 375

[115] Y. Liu, G. Hsiue, C. Lan and Y. Chiu, *J. Polym. Sci. A: Polym. Chem.*, 1997, **35**, 1769

[116] C. Yuan, S. Y. Chen, C. H. Tsai, Y. S. Chiu and Y. W. Chen-Yang, *Poly. Advan. Technol.*, 2005, **16**, 393

2 Instrumental Techniques

2.1 Introduction

As will be demonstrated in the following chapters, the thermal and thermo-oxidative degradation of polymers, in particular polyurethanes, is a complex process which results in the formation of a variety of degradation products. Some of these products will be volatile only at the degradation temperatures employed, whilst others will be volatile at room temperature but condensable at liquid nitrogen temperatures. In addition to this, changes may occur within the condensed-phase which do not lead to the evolution of volatile material. When considering the fire behaviour of a polymer, the condensed-phase chemistry is of great importance and a number of fire retardants are believed to exhibit action in the condensed-phase. Char formation, in particular, is one of the most important condensed-phase mechanisms for modifying the combustion process of a polymer and by studying the structure of the chars formed during the degradation of polyurethane foams information can be gained with regards to the condensed-phase behaviour of the polyurethane. With such an array of degradation products formed it is, therefore, beneficial to employ a number of complementary techniques to study the degradation behaviour of polyurethane foams as this will allow as much information as possible to be obtained.

This chapter describes the different analysis techniques employed throughout this research. Thermogravimetric Analysis (TGA) and Differential Scanning Calorimetry (DSC) are two complementary thermal analysis techniques widely used for studying the thermal stability of polymers, and these have been employed in this work. The major technique used to study the thermal degradation behaviour, however, was Thermal Volatilisation Analysis (TVA) as this was the most versatile available method and allowed degradation products of all natures to be studied. Solid-state ^{13}C NMR was also employed in this work to study the structure of the chars formed during the degradation of the polyurethane foams.

2.2 Thermal Volatilisation Analysis

2.2.1 Background

Thermal Volatilisation Analysis (TVA) is a form of evolved gas analysis which relies on accurate pressure monitoring, cryogenic collection and subsequent separation and characterisation of the volatile species evolved from a sample undergoing a heating regime. TVA is not a commonly employed technique; however, in the last decade it has been re-developed by Liggat and co-workers in the Polymer Degradation Group at the University of Strathclyde and is now a routinely employed thermal analysis technique within this laboratory.

TVA was originally developed in the 1960s by McNeill and co-workers at the University of Glasgow as a tool for studying materials, predominantly polymers, which degrade when heated under vacuum releasing volatile products.[1] At the time the technique was popular and was commonly employed to study the thermal degradation behaviour of polymeric materials.[1,2,3] Several modifications were made to the technique in the years which followed, with the most valuable being the introduction of sub-ambient differential distillation,[4] which allows the thermal degradation of a material to be monitored as a function of pressure in conjunction with the cryogenic collection and subsequent separation and identification of the volatile products being evolved.

Although a versatile and useful technique, TVA was never developed as a commercial product and was no longer used following the retiral of McNeill at the University of Glasgow. The technique has since been re-developed and updated and now finds wide use in the analysis of the thermal degradation behaviour of polymeric materials, although due to its versatility it can be used for many other applications. The theory and instrumental set-up of the current TVA system in use at the University of Strathclyde will be discussed in detail in the sections which follow.

2.2.2 Theory

The technique of TVA is based upon the measurement of the pressure of volatile species evolved from a sample as a function of time and temperature as it undergoes a heating regime under vacuum. The volatiles are collected in a cryogenic trap and subsequently separated and characterised. The principle behind the TVA system is the same today as it was when it was originally developed by McNeill but with some significant enhancements. The updated system in use now consists of a continuously pumped, high vacuum system with a series of cryogenic traps with sensitive pressure monitoring.

The material under study is placed in a sample tube connected in series to a primary liquid nitrogen cooled trap and a number of parallel secondary cold traps. The entire system is continuously pumped to a vacuum of approximately $1x10^{-4}$ Torr. The sample is heated at a linear rate to a predetermined maximum temperature using a programmable tube furnace, during which time degradation of the material occurs. As the volatile degradation products are evolved they are collected in the primary cold trap which is situated some distance from the sample. When this occurs the pressure within the system rises due to the time taken for the products to distil from the hot zone to the cold trap. Two linear Pirani gauges placed at the entrance and exit to the primary cold trap monitor and record this pressure change as a function of time and temperature. The first Pirani gauge measures the total volatiles which are evolved from the sample, whilst the second Pirani gauge measures those volatiles which do not condense in the cold trap.

At the end of this stage of the analysis there are two categories of products which are present; involatile residue and volatile degradation products. The residue can be removed, if possible, and dissolved in a suitable solvent for analysis by GC-MS, NMR and FTIR spectroscopy, whilst insoluble material can be analysed by FTIR spectroscopy. The volatile degradation products can be divided into three classes: the "cold-ring" fraction, the condensable fraction and the non-condensable fraction.

The cold-ring fraction consists of high-boiling products with a molar mass of approximately 200 to 1000 g mol^{-1},[5] which are volatile at the degradation temperatures but condense under vacuum at ambient temperatures. These materials collect at the top of the sample tube in a region which is cooled by a cold-ring water jacket which ensures that these materials condense uniformly in one area and do not contaminate the rest of the apparatus. The cold-ring fraction can be removed from the tube by swabbing with cotton wool soaked in a suitable solvent or by scraping with a spatula if it consists of solid material.

The condensable fraction consists of the lower boiling point materials which are volatile at room temperature but condense under vacuum at liquid nitrogen temperatures. These materials are, therefore, collected in the primary cold trap. This fraction consists of materials from ethene up to molar masses of approximately 200 g mol^{-1}.

The non-condensable fraction consists of small molecules such as hydrogen, methane, and CO which are volatile even at -196°C. These materials pass through all the cold traps and are monitored by means of an online mass spectrometer positioned after the primary cold trap.

The second stage of TVA involves separation of the condensable fraction collected in the primary cold trap by means of sub-ambient differential distillation. In this technique there are four secondary liquid nitrogen cooled traps in parallel limbs positioned after the primary cold trap, with non-linear Pirani gauges positioned at the exit of these traps. The primary cold trap is gradually heated to ambient temperature during which time the degradation products will evaporate at specific temperatures. Pressure changes will occur as each of the products are distilled from the primary cold trap into the secondary traps and these pressure changes are measured by the linear Pirani gauge at the exit of the primary cold trap. The products can be separated according to their volatility into four separate fractions which can be subsequently analysed and characterised. This is

achieved through use of online mass spectrometry (MS), GC-MS, and gas-phase FTIR spectroscopy.

2.2.3 Instrumental Set-up

The instrument used throughout this work was built in-house based on the apparatus described by McNeill *et al.*[1] and a schematic diagram of the apparatus is shown in Figure 2.1. The apparatus consists of a glass sample tube with a flat base positioned in a Carbolite tube furnace which can be used to heat the sample isothermally or programmed to heat the sample at a linear heating rate. The temperature of the furnace is measured by means of a K-type thermocouple positioned on the outside base of the tube. Internal tube temperature calibrations have been carried out in order to determine the actual sample temperatures; this will be described in more detail in Chapter 3. The system is pumped to a vacuum of approximately $1x10^{-4}$ Torr by means of an Edwards two stage rotary pump and oil diffusion pump system.

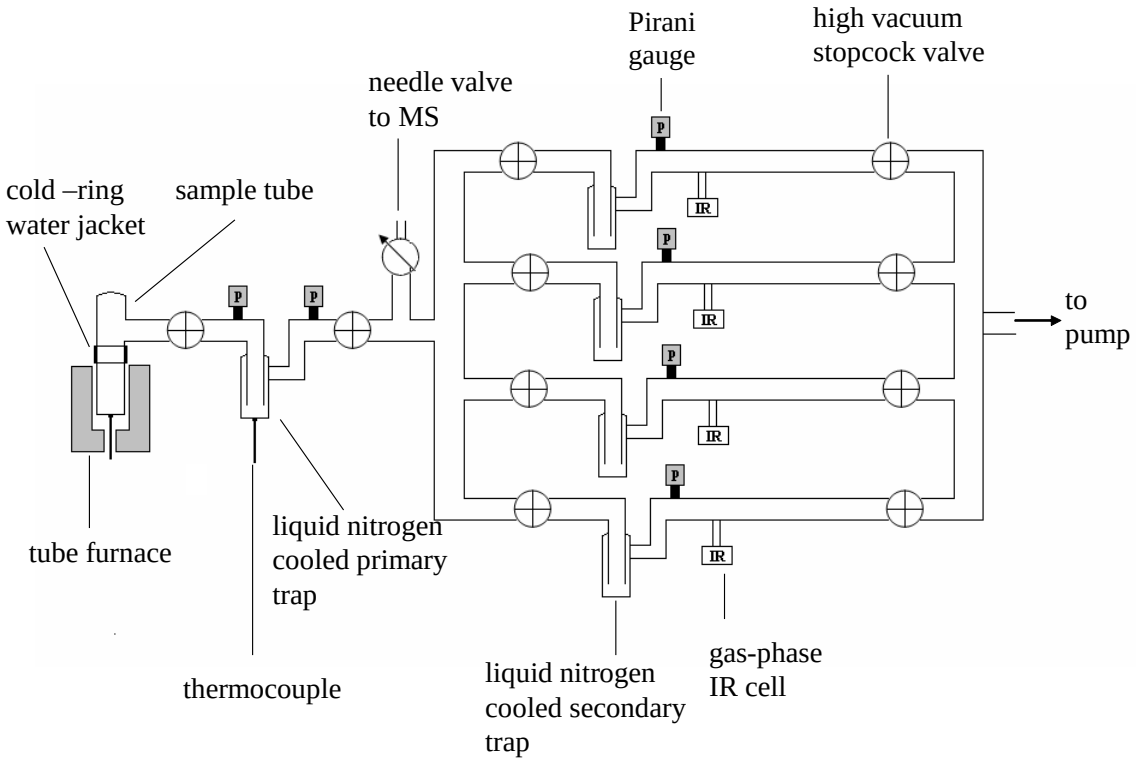

Figure 2.1: Schematic diagram of the TVA apparatus used at the University of Strathclyde

The primary cold trap is a glass tube of a double u-tube design positioned within a steel can packed with polymer beads which act as a thermal insulator. A K-type thermocouple positioned within the steel can records the temperature of the cold trap. For the first stage of the analysis this assembly is immersed in a Dewar filled with liquid nitrogen to allow cryogenic collection of the evolved volatiles. The liquid nitrogen is then removed for the second stage of analysis to allow the cold trap to gradually heat to ambient temperature. A 1-300 amu quadrupole mass spectrometer continually samples the stream of volatiles at the exit of the primary cold trap. This allows analysis and identification of the non-condensable materials as they pass through the trap in the first stage of the analysis and the condensable volatiles as they are separated during the differential distillation.

Gas-phase FTIR and GC-MS analyses are also performed on the four fractions of condensable volatiles which are collected in the secondary cold traps. This is achieved by isolating the limb in which the volatiles are collected and cooling a cold finger on a gas-phase collection cell with liquid nitrogen whilst allowing the secondary cold trap to heat to ambient temperature. There are two types of gas-phase collection cells which are employed as shown in Figure 2.2. The standard cell allows gas-phase FTIR analysis of the condensable volatiles. The second type of cell allows FTIR analysis to be obtained and then the volatiles are extracted into a suitable solvent in the side arm and subsequently analysed by GC-MS or NMR. This type of cell is reserved for the final fraction which contains higher molar mass volatiles.

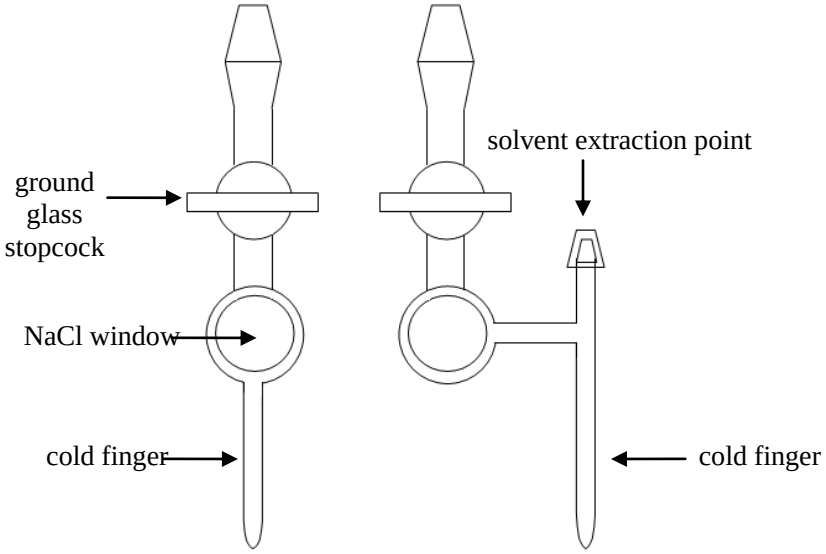

Figure 2.2: The two types of gas-phase collection cell employed: standard IR cell (left) and IR cell with side arm for extraction of higher molar mass volatiles (right)

2.3 Nuclear Magnetic Resonance Spectroscopy

2.3.1 Introduction

Nuclear magnetic resonance (NMR) spectroscopy is a valuable tool for the analysis and characterisation of polymers, both in solution and in the solid-state. NMR spectroscopy involves the study of molecular structure by the measurement of the absorption or emission of electromagnetic radiation from nuclei which are in a strong magnetic field.[6] The energy levels in the nuclei, which are split by the magnetic field, are influenced by the environment in which they are situated. The NMR spectrum, therefore, yields information regarding the chemical nature of the interacting atoms. The nuclei which are most widely studied by NMR spectroscopy are ^{1}H and ^{13}C.

2.3.2 Basic NMR Theory

2.3.2.1 Nuclear Spin and the Magnetic Moment

The phenomenon of NMR occurs because magnetic nuclei possess intrinsic angular momentum, also known as spin, which is characterised by the angular momentum vector

(I).The magnitude of this is related to the nuclear spin quantum number (*I*) and Planck's constant (*h*) as shown in Equation 2.1.[7]

$$\mathrm{I} = \frac{h}{2\pi}\left[I(I+1)\right]^{1/2} \qquad \textbf{Equation 2.1}$$

I is related to the mass number and atomic number and can have either integral or half-integral values (0, ½, 1,...).[8] When both the atomic number and mass number are even, for example in ^{12}C, then *I* is equal to zero and the nucleus is non-magnetic.[9] As a result, nuclei which have zero spin cannot be monitored by NMR spectroscopy. ^{1}H and ^{13}C, which are the most widely studied nuclei, have I = ½ and are NMR-active. The magnetic spin quantum number, m_I, can be used to express the intrinsic angular momentum and its component in a given direction. m_I can have values –I, -I+1,…, I-1, I,[8] *i.e.* for a nucleus with I = 3/2 m_I has values -3/2, -1/2, 1/2 , 3/2. There are, therefore, 2*I*+1 possible spin states of a nucleus.

A nucleus with angular momentum also has an associated magnetic moment (μ). This can be described by a parameter known as the magnetogyric ratio (γ), which is related to the magnetic moment and the angular momentum as shown in Equation 2.2.[10] The strength of the signal and, therefore, the sensitivity of the NMR experiment are related to the magnitude of the magnetic moment (μ).[11]

$$\gamma = 2\pi\mu / Ih \qquad \textbf{Equation 2.2}$$

2.3.2.2 The Nucleus in a Magnetic Field

In the absence of a magnetic field the magnetic moments will be oriented randomly and the 2*I*+1 spin states of the nucleus will be degenerate. When placed in a magnetic field, however, the magnetic moments interact and become aligned with the field. When this occurs there are 2*I*+1 possible spin orientations which can be adopted, with each one positioned at a particular angle (θ) with respect to the direction of the applied field.[12] When placed in the field the magnetic moments, therefore, undergo precession about the

direction of the applied field. This is known as Larmor precession and is illustrated in Figure 2.3.

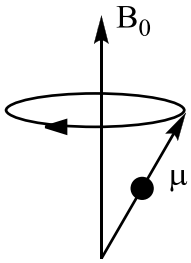

Figure 2.3: The precession of a magnetic moment in a magnetic field, known as the Larmor precession[10]

The frequency of the Larmor precession, ω_0, is given by Equation 2.3 where B_0 is the strength of the applied magnetic field and γ is the magnetogyric ratio as defined previously.[10]

$$\omega_0 = \gamma B_0 \qquad \textbf{Equation 2.3}$$

When the spins are aligned in the magnetic field they can be oriented with or against the direction of the applied field. The spin states are non-degenerate and, according to the Boltzmann distribution, one of the states will be slightly more populated than the other.[10] As a result the sample acquires a small magnetic moment of its own in the B_0 direction. When a sample is analysed by NMR spectroscopy a large number of nuclei will be present and it is the net magnetisation (M_0) which is monitored as illustrated in Figure 2.4.

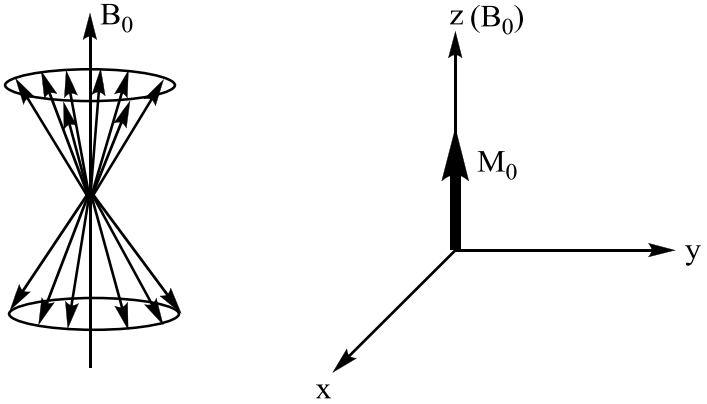

Figure 2.4: The magnetism induced by the application of an external field (B_o), showing the random distribution of the spins (left) and the net magnetisation (right)[10]

2.3.2.3 The Chemical Shift

When a nucleus is placed in a magnetic field the electron cloud surrounding the nucleus moves in such a way as to induce a secondary field which is opposed to the applied magnetic field.[7] The result is that the nucleus is shielded from the external magnetic field by its electrons and experiences an effective field (B_{eff}) which is defined in Equation 2.4, where B_i is the induced magnetic field.[13]

$$B_{eff} = B_0 - B_i \qquad \textbf{Equation 2.4}$$

The nucleus, therefore, resonates with a characteristic frequency which is also termed the chemical shift and this is determined by Equation 2.5.[13,14] σ is called the shielding constant and is dependent on the chemical environment of the nucleus.

$$\nu = \frac{\gamma(1-\sigma)B_0}{2\pi} \qquad \textbf{Equation 2.5}$$

The more shielded the nucleus is, therefore, the lower the observed frequency or chemical shift.

2.3.2.4 The Radio Frequency Magnetic Field

The equilibrium state of the NMR-active nuclei cannot be monitored directly; instead the system must be perturbed from equilibrium and this is achieved by applying a second radio frequency (RF) oscillating magnetic field (B_1) perpendicular to B_0. This is applied as a pulse of duration t_p, which is commonly a few μs. B_1 is applied by means of an RF current which is passed through a coil wound perpendicular to B_0, *i.e.* in the x-direction.[15] If B_1 has a frequency close to the Larmor frequency then the spins will be affected by this second field and will begin to precess around the effective field, B_{eff}. The effect that an RF pulse has on a particular spin system depends on the length of the pulse, the frequency and phase of the pulse, and the strength of the applied magnetic field B_1.[10]

In order to better understand and visualise the effects of RF pulses on the magnetisation the rotating reference frame is employed in which the labels x′, y′ and z′ are used to represent the axes.[9] In the rotating frame the x′ and y′ axes rotate around the z′-axis at the frequency at which the nuclear spins are precessing, *i.e.* the Larmor frequency. In this situation B_1, which is applied along the x′-axis, appears stationary. The result of applying B_1 is to tip the magnetisation of the sample from the z′-axis through an angle θ, known as the tip angle, which can be calculated by Equation 2.6.[15]

$$\theta = \gamma B_1 t_p \qquad \textbf{Equation 2.6}$$

The result of the RF pulse is that sample magnetisation (M) is rotated from its original position (M_0) into the x′y′-plane. This is known as transverse magnetisation and is detected by means of a receiver coil whose axis lies in the x′y′-plane.[7] The duration of the pulse determines the degree to which M is rotated and commonly t_p is chosen so that θ=90°. This is known as a $90°_x$ pulse and the result is that M is rotated onto the y'-axis.[10] Continued application of B_1 results in 180° rotation of M such that it lies in the –z direction, known as a $180°_x$ pulse.[10] When this occurs the transverse magnetisation will no longer be observed and no signal will be detected. The effects of the $90°_x$ and $180°_x$ RF pulses on the sample magnetisation are illustrated in Figure 2.5.

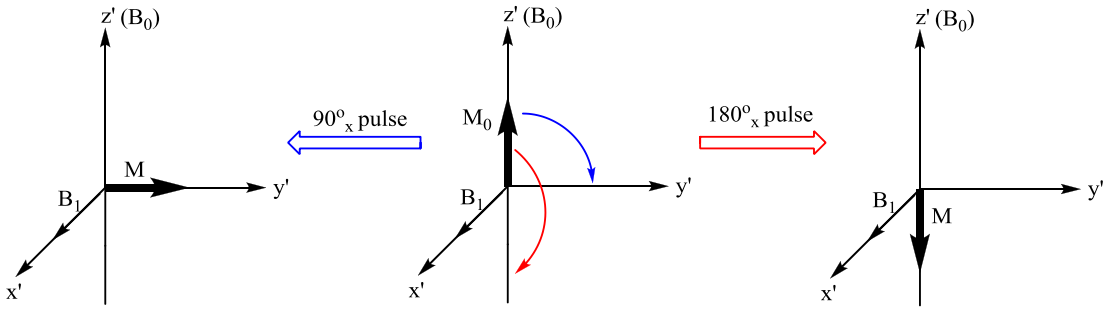

Figure 2.5: Effect of the $90°_x$ and $180°_x$ RF pulses on the sample magnetisation

2.3.2.5 Relaxation Processes

The application of B_1 perturbs the spins from their equilibrium state and when B_1 is switched off the sample must return to its equilibrium position on the z′-axis by releasing the excess energy which it has gained from the pulsing.[10] This is known as relaxation and the rate at which this occurs can provide important information about the system under study. Two different types of relaxation are of importance in NMR spectroscopy: longitudinal and transverse.

Longitudinal relaxation is more commonly referred to as the spin-lattice relaxation and is characterised by the spin-lattice relaxation time (T_1). This relaxation process involves transfer of the excess energy from the spins to the surroundings or lattice resulting in relaxation along the z′-axis.[7] T_1 is the time required for the sample magnetism to be restored to its initial position (M_0) along the z′-axis. Spin-lattice relaxation is not instantaneous; it is essentially an exponential decay process[9] and would require infinite time for complete recovery of the magnetism to occur. A time of $5xT_1$, however, corresponds to the time taken for 99% of the equilibrium magnetisation to be resorted and is accepted as the time taken for the equilibrium of the spins to be re-established.[16] This is commonly used as the time required between pulses, known as the recycle delay time, to ensure that saturation of the signal does not occur.[7]

The transverse relaxation is also termed the spin-spin relaxation and is characterised by the spin-spin relaxation time (T_2). This process involves loss of the magnetisation in the x′y′-plane by interactions between neighbouring spins and is also an exponential decay process.[11] In this type of relaxation the individual magnetic moments lose their phase coherence and return to a random arrangement around the z′-axis. This is, therefore, not a true energy transfer process but can be thought of as the loss of coherence of the magnetisation vector in the x′y′-plane.[7] T_2 is often much shorter than T_1, particularly in solid samples.[17] The spin-spin relaxation time determines the resolution in an NMR experiment as this is inversely related to the linewidth.[10] Long relaxation times,

therefore, lead to narrow linewidths and good resolution, whilst short relaxation times lead to broad linewidths and poor resolution.

By monitoring a system's return to equilibrium and the relaxation times a great deal of information can, therefore, be gained about the system under study.

2.3.2.6 Free Induction Decay and the Fourier Transform

The signal which is observed during a pulsed NMR experiment is a time-domain signal which consists of a sinusoidal wave which decays with time as a result of spin-spin relaxation.[18] This is known as the free induction decay (FID) and is illustrated in Figure 2.6.

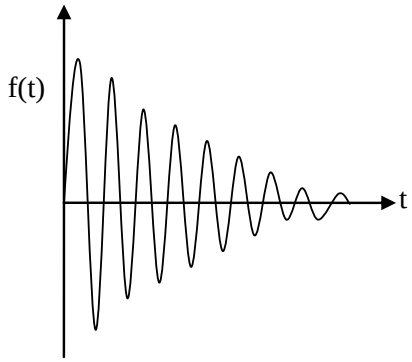

Figure 2.6: An illustration of the FID

The FID is difficult to interpret, therefore, it is more useful to view this signal as a function of frequency and this is achieved by use of the Fourier Transform (FT). This is a mathematical procedure used to convert the time domain signal from the FID into a plot of peaks as a function of frequency.[18] As the FT is a linear transform the amplitude of the waves contained in the FID are related to the intensities of the peaks in the frequency domain.[10] In many systems there will be a number of components which decay exponentially as a result of spin-spin relaxation and each will have a specific amplitude, frequency and value of T_2 in the FID which is obtained. After FT has been performed each component will correspond to a peak in the NMR spectrum at a particular frequency with a specific amplitude and linewidth.[10]

2.3.2.7 Coupling

Coupling can occur between NMR-active nuclei due to interaction of the spins and this can be used to gain information regarding the local environment of the nuclei. There are two types of coupling which are important, namely dipolar coupling and spin-spin or scalar coupling.

Dipolar coupling is a type of interaction between the nuclei that occurs "through space" affecting the lineshapes and relaxation times of the system.[10] In solution, there is a high degree of molecular motion and the dipolar interactions are averaged out. High resolution spectra are obtained as a result. In the solid-state, however, the molecular motion is more restricted and the dipolar couplings are not averaged out and the couplings can often be larger than the chemical shift range.[17] The problem of dipolar coupling in the solid-state will be discussed in more detail in section 2.3.3.

The spin-spin coupling is an interaction which occurs through the bonds between the nuclei and electrons and causes the resonances to be split into multiple peaks.[10] The strength of the magnetic field has no effect on the spin-spin couplings; however, they are strongly affected by the type of nuclei involved, the chemical structure and the bond length. The number of peaks into which a resonance is split by spin-spin coupling depends on the number of coupled spins and can give rise to important information regarding the number of NMR active nuclei in close proximity.

The ability to detect the NMR signals of nuclei within a sample is dependent upon both the natural abundance of the NMR-active nuclei and the magnetogyric ratio[10] with protons being the most sensitive nuclei. Carbon nuclei have a much lower sensitivity, however, as technology has progressed the NMR instruments have become more sensitive and carbon nuclei can now be routinely observed.

2.3.3 Solid-state NMR

2.3.3.1 Introduction

NMR studies in the solid-state are of great interest to the polymer scientist owing to the fact that the majority of polymers are employed in the solid-state and a number of polymers are insoluble in most common solvents. In some cases the NMR properties in the solid-state can be correlated with the macroscopic properties of the material.[10] Furthermore, solid-state NMR is a useful tool to the polymer scientist as it a non-destructive technique.

In solid polymers the motion of the molecules is restricted by the proximity of neighbouring polymer chains and this means that the interactions which cause line broadening are not averaged as they are in solution.[10] The NMR spectra of solid samples are, therefore, fundamentally different to those obtained in solution and acquiring high resolution spectra is more complicated. There are three main factors which contribute to line broadening and poor resolution in the NMR of solid samples:[19]

1. Dipolar couplings
2. Chemical shift anisotropy
3. Long relaxation times

2.3.3.2 Dipolar Couplings

One of the major contributions to line broadening in solid-state ^{13}C NMR is the dipolar interaction which occurs between the ^{1}H and ^{13}C nuclear spins. This coupling gives rise to a local magnetic field at the ^{13}C nucleus (B_{loc}) which can be defined by Equation 2.7.[20]

$$B_{loc} = \pm \mu_H r^{-3} \left(3\cos^2 \theta - 1\right) \qquad \textbf{Equation 2.7}$$

μ_H is the magnetic moment of ^1H, r is the internuclear distance between the ^{13}C and ^1H which are coupled and θ is the angle between the applied magnetic field (B_0) and the internuclear vector. The ± sign is present as the spins which generate the B_{loc} can be oriented with or against the applied field.[20] The geometric term is averaged out in solution by rapid molecular motion of the molecules.

In the solid-state, however, molecular motion is restricted and the dipolar couplings can often be larger than the chemical shift range.[17] When this occurs broad, unresolved lines are obtained which are the sum of all of the dipolar couplings[10] and to obtain a high resolution spectrum these dipolar couplings must be removed or suppressed. This is most commonly achieved through the use of a technique known as dipolar decoupling. In this technique one of the proton spins is irradiated with a high power RF field at the ^1H Larmor frequency which results in rapid transitions between the two spin states of the proton. With sufficiently high power irradiation these transitions will occur so rapidly that the ^{13}C nucleus coupled to the proton is no longer able to distinguish between the two orientations of the proton and it sees only the average of the orientations.[21] When this occurs the dipolar coupling between the ^1H and ^{13}C nuclei disappears. For dipolar decoupling to be successful the magnitude of the irradiation must exceed that of the dipolar coupling.[10]

2.3.3.3 Chemical Shift Anisotropy

The second factor which causes problems in the NMR of solid samples is the chemical shift anisotropy. The chemical shift occurs as a result of the nucleus being shielded from the magnetic field by its electrons. Chemical shifts are dependent upon the magnetic environment which surrounds the nuclei and the local magnetic field around a nucleus is given by Equation 2.3.[10]

$$B_{loc} = B_0(1-\sigma) \qquad \textbf{Equation 2.8}$$

σ is composed of three principal components, σ_{11}, σ_{22}, and σ_{33}. In solution NMR the rapid molecular motion causes the chemical shift anisotropy to be averaged and the value observed is the isotropic value (σ_{iso}) which is defined in Equation 2.9.[10]

$$\sigma_{iso} = \frac{1}{3}(\sigma_{11} + \sigma_{22} + \sigma_{33}) \qquad \textbf{Equation 2.9}$$

In the solid-state, however, the molecular motion is more limited and groups of molecules may have different but fixed orientations with respect to the applied field.[19] In this case the chemical shift anisotropy is not averaged and this leads to line broadening and poor resolution.[10] The chemical shift anisotropy lineshapes can contain useful information concerning the polymer system; however, it is often the case that the lineshape is almost as large as the chemical shift range and the peaks overlap. In order to obtain a high resolution spectrum the lineshape must be collapsed into a single sharp peak and the most commonly employed technique for achieving this is magic angle spinning, which will be described in more detail in section 2.3.3.5.

2.3.3.4 Long Relaxation Times

The third problem associated with the NMR of solids is that the nuclei such as ^{13}C possess long spin-lattice relaxation times. Once excited, it is necessary for the nuclei to relax to equilibrium, therefore, a considerable amount of time is needed for an FID to be acquired which will have a good signal to noise ratio when converted by FT.[19] The problem of long relaxation times can be overcome by the use of cross polarisation which will be discussed in more detail in section 2.3.3.6.

2.3.3.5 Magic Angle Spinning

The chemical shift is dependent upon the orientation of the molecule relative to B_0. A change in the chemical shift can, therefore, be induced by anything which causes a change in the molecular orientation. If a solid sample is rapidly rotated about an axis which is positioned at an angle β with respect to B_0 then the molecular orientations and,

therefore, the chemical shifts become time dependent and the time average of σ under such conditions is given by Equation 2.10.[10,22]

$$\sigma = \frac{1}{2}\sin^2\beta(\sigma_{11}+\sigma_{22}+\sigma_{33}) + \frac{1}{2}(3\cos^2\beta - 1) \qquad \textbf{Equation 2.10}$$

When β=54.7°, $\sin^2\beta$ is equal to 2/3 and the first term in Equation 2.10 becomes equal to $1/3(\sigma_{11}+ \sigma_{22}+ \sigma_{33)}$.[10] This is the isotropic chemical shift value defined previously in Equation 2.9. The $3\cos^2\beta$ -1 term, on the other hand, equals zero at this value of β and the second term in Equation 2.10, therefore, equals zero.[10] Spinning the sample at such an angle, therefore, reduces the anisotropic component to zero and σ becomes equal to the isotropic value which is observed in solution. β=54.7° is known as the magic angle and the technique of spinning the sample rapidly at this angle is known as magic angle spinning (MAS). Presented in Figure 2.7 is an illustration showing the arrangement for MAS. The effect of spinning the sample at the magic angle is analogous to the effects of rapid molecular motion in solution and a high resolution spectrum can be obtained.[10]

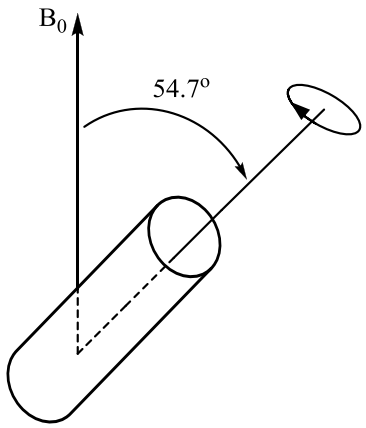

Figure 2.7: The arrangement for MAS. The sample container is positioned at an angle of 54.7° to the applied magnetic field and is rotated rapidly.

The maximum spinning speed which can be achieved in MAS depends on the probe type and the rotor diameter, and it is often the case that the chemical shift anisotropy pattern is larger than the highest available spinning speed. If this occurs then the lineshape gets

split into a series of sharp peaks known as spinning sidebands, with the separation between these bands corresponding to the spinning speed.[23] These spinning sidebands can be problematic if they overlap with the peaks of interest in the spectrum; however, they change their position with spinning frequency and the spinning speed can be altered to ensure that these bands do not obscure the sample peaks. Alternatively, the sidebands can be removed completely by using a spectral editing method known as the total suppression of sidebands (TOSS).[10,20] This involves the application of a sequence of 180° RF pulses at carefully determined time delays during the sample rotation which causes the magnetisation vectors to align in a way which causes destructive interference between the sidebands.[24]

2.3.3.6 Cross-polarisation

The sensitivity of a number of the NMR-active nuclei, including carbon, is low in the solid-state. This is due to both the intrinsic low sensitivity of the nuclei and the fact that spin-lattice relaxation times are very long in solids as the molecular motion is restricted.[10] These problems can be overcome by the use of a technique known as cross polarisation (CP) which increases the sensitivity of the dilute spins (^{13}C) by utilising the spins' interactions with the more abundant spins (^{1}H).[21] The overall result of CP is that the magnetisation is transferred from the abundant spins to the dilute spins. The increase in sensitivity which occurs during CP arises as the population difference between the two spin states of the ^{13}C nuclei is increased and the delay time required between successive FIDs is shortened.[21]

Initially the abundant spin system, *i.e.* ^{1}H, is put into a low temperature state. This is achieved by applying a 90° RF pulse in the ^{1}H channel which rotates the magnetisation from the z′-axis onto the y′-axis in the rotating frame.[21] The phase of the pulse is then changed by 90° so that its vector now lies parallel with the spins. This means that the magnetisation becomes spin-locked in the rotating frame and will precess around the y′-axis at an angular frequency, ω_{1H}, which is defined in Equation 2.11.[20]

$$\omega_{1H} = \gamma_H B_{1H} \qquad \textbf{Equation 2.11}$$

The results of this stage of the procedure is that the magnetisation for the abundant ^{1}H spin system is precessing around the y′-axis with a spin temperature which is lower than the lattice temperature.

At the same time as the spin-locking field is employed in the ^{1}H channel, the ^{13}C nuclei are subjected to a continuous RF field which forces them to precess in the rotating frame at an angular frequency, ω_{1C}, as defined in Equation 2.12.[20]

$$\omega_{1C} = \gamma_C B_{1C} \qquad \textbf{Equation 2.12}$$

The result of this is that there is an oscillating component of the ^{1}H magnetisation at a frequency of ω_{1H} at the ^{13}C nuclei and vice versa. If the angular frequencies are adjusted so that they are equal (*i.e.*, $\omega_{1C} = \omega_{1H}$) then an exchange of energy can occur between the two spin systems by a spin flip or relaxation mechanism.[21] Adjustment of the precession frequencies in the rotating frame so that they match is called the Hartmann-Hann condition and is defined by Equation 2.13.[21,23]

$$\gamma_C B_{1C} = \gamma_H B_{1H} \qquad \textbf{Equation 2.13}$$

When the spins are allowed to come into contact with each other then heat will flow from the ^{13}C system (which is at a spin temperature lower than the lattice temperature) to the ^{1}H system and this causes a drop in spin temperature of the ^{13}C system. Essentially the population difference between the two spin states of the ^{13}C nuclei has increased, which in turn increases the sensitivity.[21] Good thermal contact between the spin systems also leads to less time being required for the ^{13}C nuclei to relax back to their equilibrium state. This means that more FIDs can be acquired resulting in a better signal to noise ratio.[23]

Once the spins have been in contact for the desired time the ^{13}C field RF field is switched off and the FID of the ^{13}C nuclei is then acquired. The spin-lock is maintained in the ^{1}H channel which means that the protons are decoupled from the carbon nuclei.[20]

To summarise the technique of CP, a 90° RF pulse is applied in the ^{1}H channel followed by spin-locking of the ^{1}H magnetisation in the y′-direction in the rotating frame. At the same time, the dilute ^{13}C spins are subjected to an RF field and the precession frequencies of the two spin systems are adjusted to match the Hartmann-Hann condition. The systems are then kept in thermal contact for a period (known as the contact time)[19] which allows an exchange of energy to occur between the ^{1}H and ^{13}C nuclei. Following this the FID of the ^{13}C nuclei is acquired. The pulse sequence required for CP is illustrated in Figure 2.8.

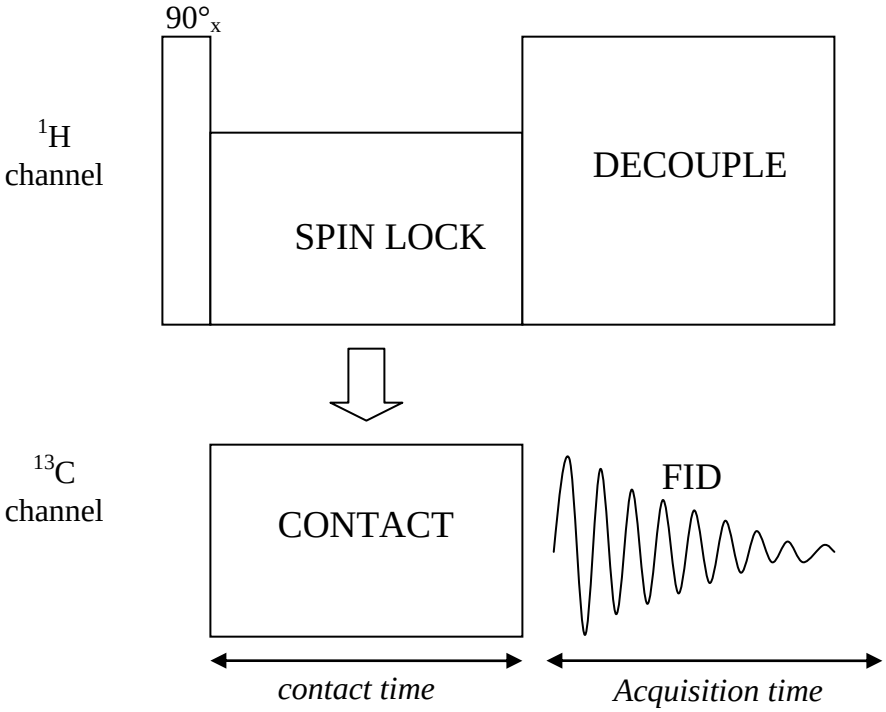

Figure 2.8: Illustration of the pulse sequence used for a CP experiment

A key feature of the CP experiment when applied to a polymers is that the time it takes for the magnetisation to build up and subsequently relax in the dilute spin system is strongly dependent on the dynamics of the polymer system.[23] The magnetisation will

build up quickly in a crystalline or rigid phase and will decay slowly. A more mobile phase will take longer to build up the magnetisation. The contact time can, therefore, be adjusted to allow the enhancement of one signal over another. The use of both short and long contact times will allow both the rigid and mobile phases to be examined. CP is, therefore, an important method for distinguishing between the different phases in polymer samples. An example of this is presented in Figure 2.9.

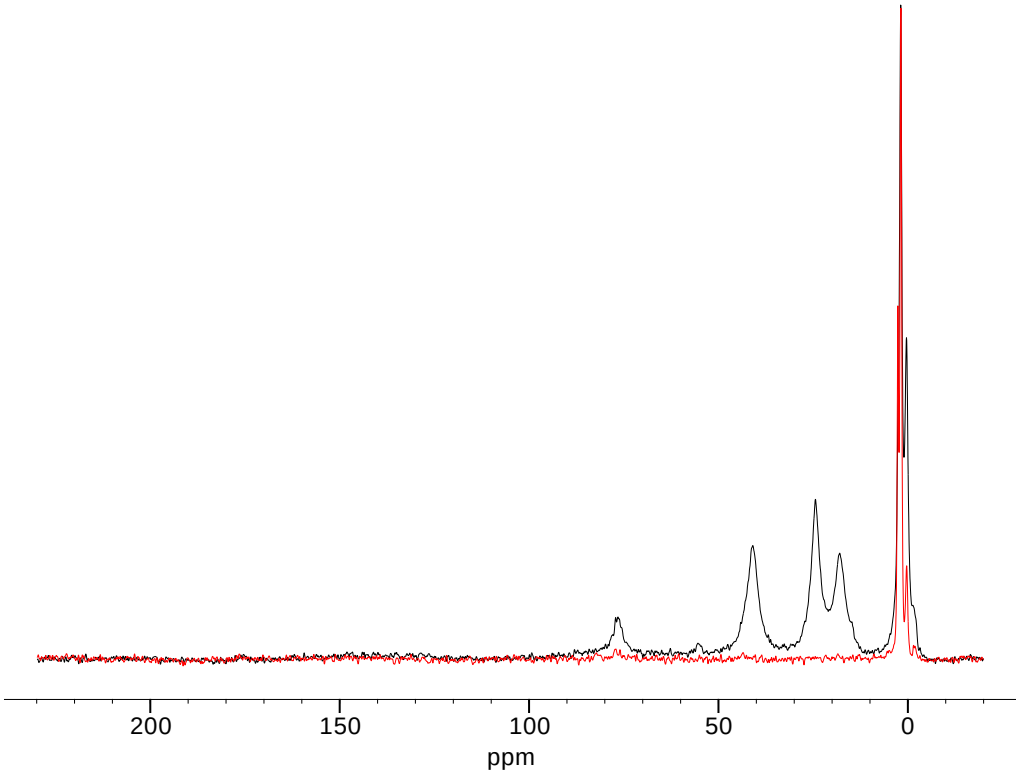

Figure 2.9: Solid-state ^{13}C NMR spectrum of a vinyl carborane-siloxane network copolymer with contact times of 0.5 ms (black line) and 10 ms (red line)[25]

The system under study is a carborane-siloxane network which had been synthesised by reacting a vinyl carborane with a silane branched poly(dimethylsiloxane) (PDMS).[25] Solid-state ^{13}C NMR was employed to determine if all of the free vinyl groups on the carborane had been incorporated into the system. Two contact times were used to probe the different phases of the system. The shorter contact time (0.5 ms), which probes the more rigid components of the material, revealed the presence of carbon atoms from the carborane, CH_2 groups adjacent to carborane and CH_2 from reacted vinyl groups. When

a longer contact time (10 ms) was used the peaks corresponding to CH_2 groups from the vinyl carborane component disappeared which confirms that all the vinyl carborane has been successfully bound into the polymer network.

2.3.3.7 Dipolar Dephasing

This technique, commonly used is in conjunction with CP in solid-state ^{13}C NMR experiments, simplifies the NMR spectrum by removing the signals which originate from any nuclei directly attached to a proton. The technique of dipolar dephasing relies on the fact that the dipolar interaction between the ^{13}C and ^{1}H nuclei has a $1/r^3$ dependence with r being the distance between the ^{13}C and ^{1}H nuclei.[26] The dipolar coupling is, therefore, greater for carbons which are directly bonded to protons compared to non-protonated carbons which couple with protons attached to neighbouring carbon atoms. This allows us to discriminate between protonated and non-protonated carbons by modification of the NMR experiment. The dipolar dephasing experiment works by introducing a time delay, without dipolar decoupling, between the cross polarisation and the acquisition of the spectrum.[20] During this time delay, known as the dephasing period, the signals originating from species which are strongly dipolar coupled to a proton will decay (diphase) faster than the signals originating from species which have weak proton coupling. If the length of the dephasing period is selected carefully then complete suppression of the signal originating from species with attached hydrogens can be achieved. For ^{13}C dipolar dephasing a dephasing delay of 40 to 50 μs is usually sufficient to achieve the required level of discrimination between protonated and non-protonated carbons.[27] The decoupling field is then switched on and the remaining FID signal acquired. The resulting spectrum should, therefore, only contain signals from species with no attached protons. This technique, however, rarely suppresses methyl signals as these species have a high degree of molecular motion and rapid rotation of these groups suppresses their C-H dipolar coupling even in the solid-state.[20] The pulse sequence required for dipolar dephasing with CP is illustrated in Figure 2.10.

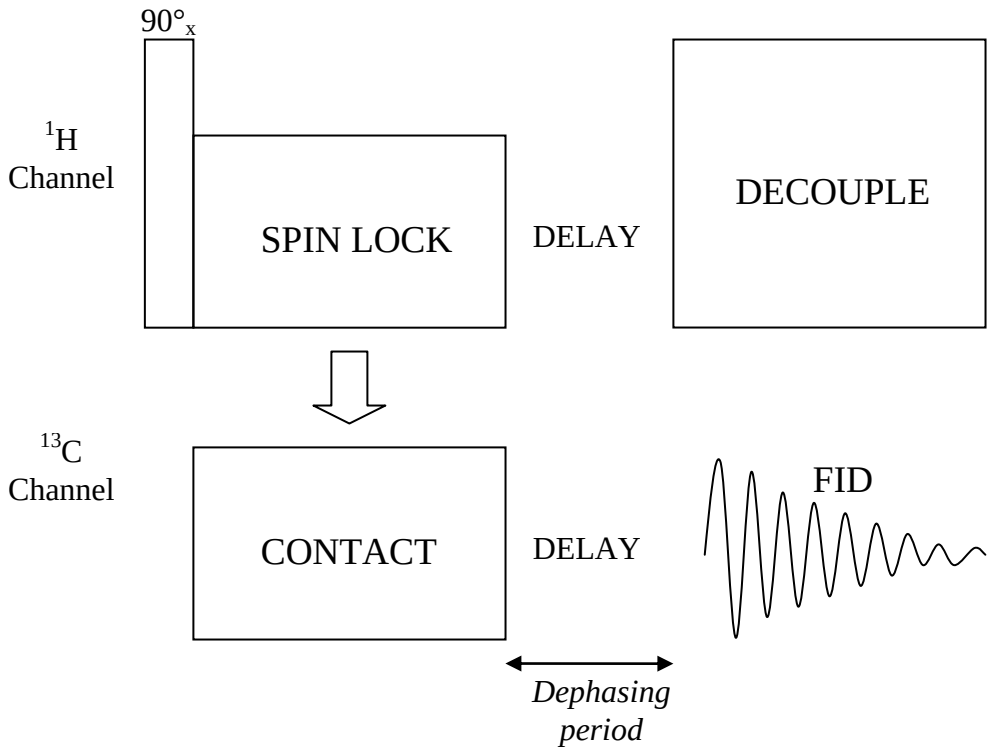

Figure 2.10: Illustration of the pulse sequence used for dipolar dephasing when combined with CP

2.4 Thermogravimetric Analysis

2.4.1 Theory

Thermogravimetric Analysis (TGA) is a technique in which the mass change of a material is measured as a function of temperature as it is subjected to a controlled heating programme.[28,29] This is achieved by means of a sensitive microbalance positioned within a furnace. The mass loss can be then be attributed to processes in which volatile species are evolved such as thermal degradation, thermo-oxidative degradation and dehydration. Processes which do not evolve volatile species cannot be monitored by TGA. The technique can be conducted under a variety of conditions such as high pressure and vacuum and in a variety of oxidising, reducing and inert atmospheres.[30]

2.4.2 Instrumental Set-up

The mass loss characteristics of a sample have a strong dependence on the experimental conditions employed; therefore, the instrumental set-up and parameters are crucial as are the sample mass and shape.[30] The TGA apparatus consists of an inert sample crucible, commonly made of platinum, attached to a microbalance and surrounded by a furnace. A number of arrangements of this apparatus are available with each differing in the positioning of the furnace relative to the microbalance.[28] The instrument employed in this research has the furnace positioned below the microbalance as illustrated in Figure 2.11. Measurement of the actual sample temperature is problematic due to the sensitive nature of the microbalance[30] and in this case the sample temperature is measured by means of a thermocouple placed in close proximity to the sample crucible.

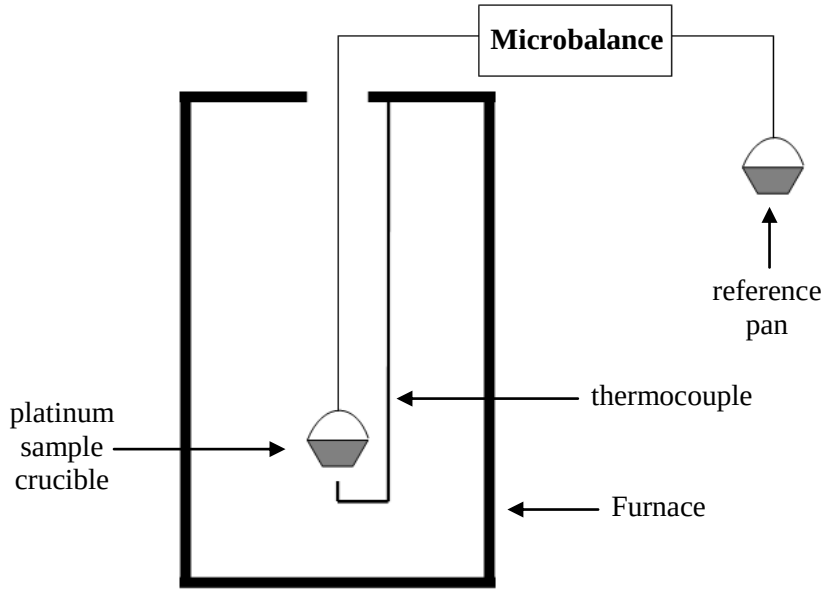

Figure 2.11: Set-up of the TGA apparatus

As the sample is heated from ambient temperature to a predetermined maximum temperature the mass of the sample changes as volatiles are evolved due to processes such as degradation occurring. The sensitive microbalance records these mass changes as a function of temperature. TGA results are usually plotted as percentage mass versus temperature or time, with the resulting thermogram being sigmoidal in shape. An

example thermogram for a simple one stage mass loss process is illustrated in Figure 2.12.

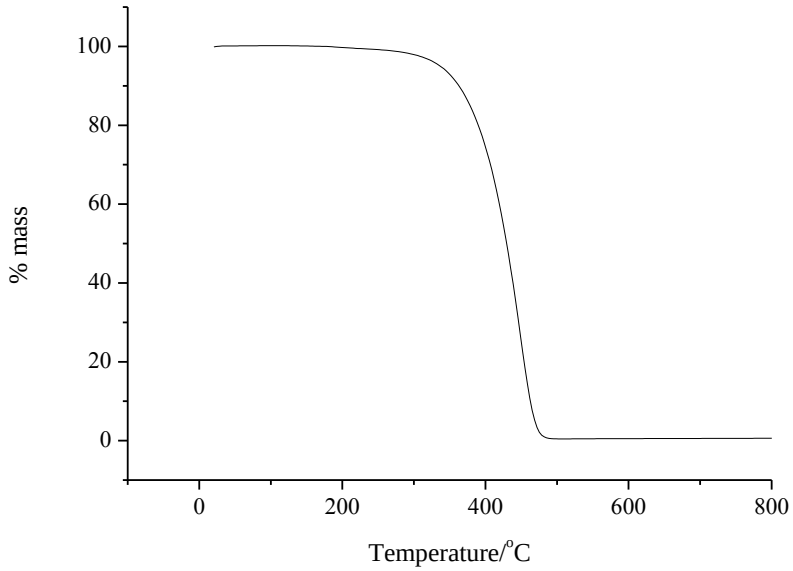

Figure 2.12: An example TGA thermogram

Alternatively, results can be presented as a derivative of the original curve to give rate of mass loss against time (dm/dt) or against temperature (dm/dT) which is then plotted against temperature or time. This is known as Derivative Thermogravimetry (DTG) and gives a plot in which the peak maxima illustrate the temperature at which maximum rate of weight loss is occurring. This is of use if there are overlapping reactions occurring during the analysis, as each will be plotted as distinct peaks. Figure 2.13 shows an example DTG curve which is the derivative of the curve in Figure 2.12.

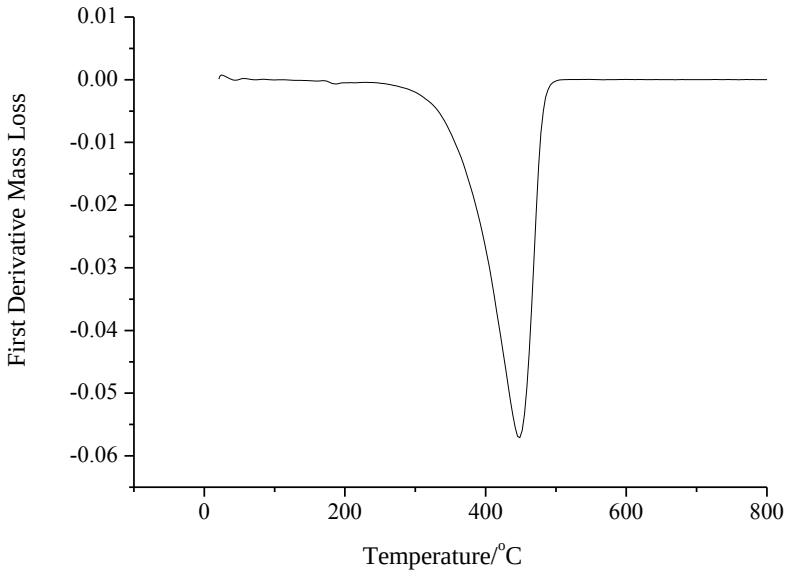

Figure 2.13: An example DTG curve

2.5 Differential Scanning Calorimetry

2.5.1 Introduction

Differential Scanning Calorimetry (DSC) is a technique which measures the thermal properties of a sample as it is being heated or cooled. The changes in temperature and heat flow of a material over a specific temperature range with a set heating or cooling rate are recorded as a function of time and temperature, and are compared to an inert reference sample.[31] This allows quantitative and qualitative information to be gained with regards to both the chemical and physical transformations which occur within the material in both inert and oxidative atmospheres. This technique allows the study of thermal transitions such as the glass transition temperature (T_g), melting (T_m), crystallisation (T_c) and degradation.

2.5.2 Theory

There are two types of DSC instruments which can be employed: heat-flux and power-compensated. The instrument used in this research is a heat-flux DSC therefore only this type will be discussed in more detail. A heat-flux DSC instrument contains a sample and a reference pan positioned in a single furnace thereby allowing both pans to

be subjected to the same controlled atmosphere and temperature programme.[32] The heat-flux DSC cell is illustrated in Figure 2.14.

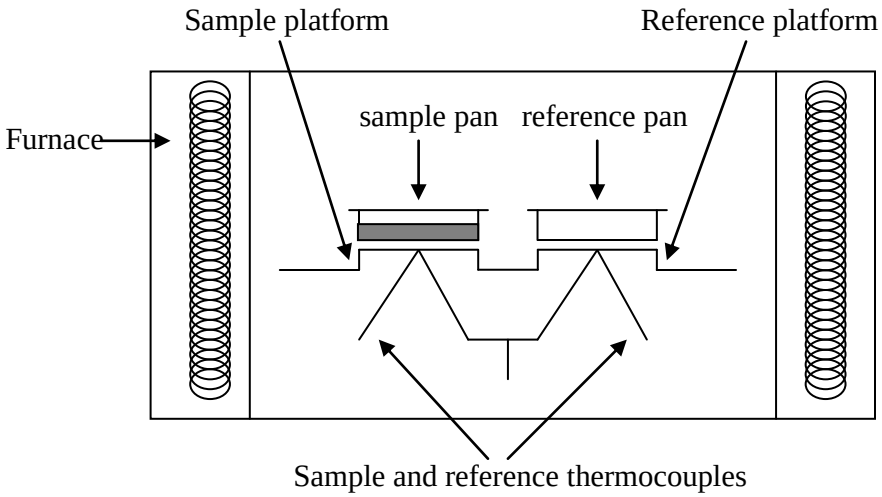

Figure 2.14: The heat-flux DSC cell

The sample pan containing the material to be analysed and the empty reference pan are placed on raised platforms through which the heat is transferred. The temperature difference between the sample and the inert reference (ΔT) is measured by thermocouples attached to the base of the sample and reference platforms as a function of temperature or time as the sample is subjected to a controlled temperature programme. The difference in temperature is proportional to the change in heat-flux, which is the energy input per unit time.[31] During a phase change in the sample this heat-flux will be altered as the material emits or absorbs heat. During an endothermic transition, such as melting, the temperature recorded at the sample platform is lower than that of the reference and ΔT is negative.[29] During an exothermic transition, on the other hand, ΔT is positive. ΔT is then converted to heat capacity by the instrument software using equation 2.1 where q is the heating rate employed, C_p is the heat capacity and K is a calibration factor.[33]

$$\Delta T = q\frac{C_p}{K} \qquad \textbf{Equation 2.14}$$

The results from DSC analysis are displayed as a thermogram which shows heat flow versus temperature. Shown in Figure 2.15 is an illustration of a DSC thermogram showing some of the major processes which can be observed. Endothermic transitions appear as downwards peaks whilst exothermic transitions appear as upwards peaks.

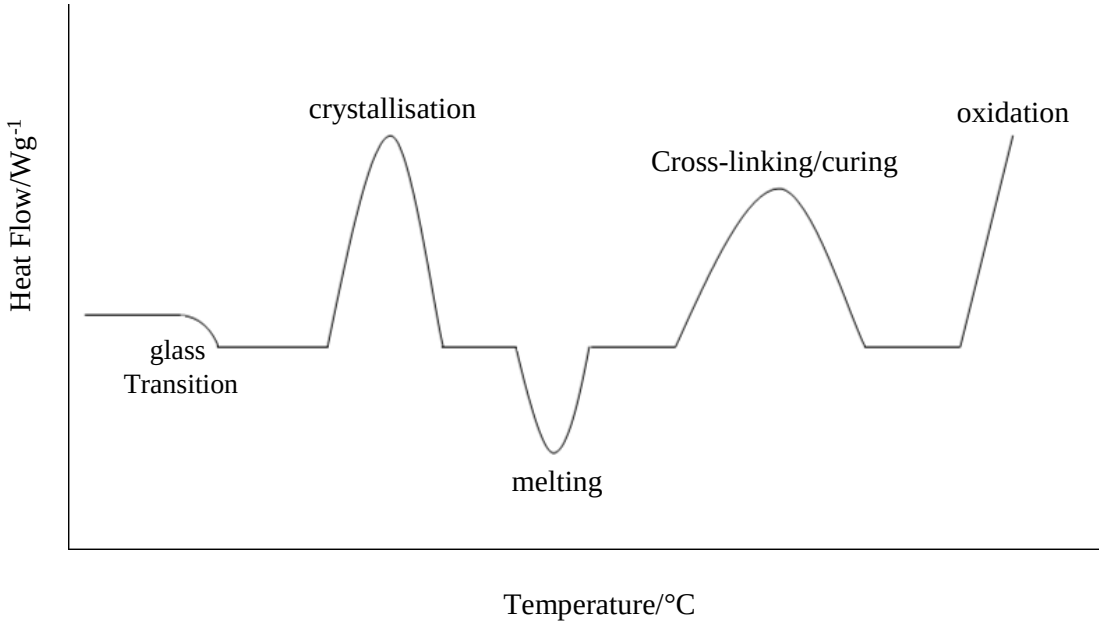

Figure 2.15: Illustration of a DSC thermogram

2.6 References

[1] I. C. McNeill, *Eur. Poly. J.*, 1967, **3**, 409

[2] I. C. McNeill, L. Ackerman, S. N. Gupta, M. Zulfiqar and S. Zulfiqar, *J. Polym. Sci. A: Polym. Chem.*, 1977, **15**, 2381

[3] I. C. McNeill, *Developments in Polymer Degradation-1*, Applied Science Publishers, London, 1977, p. 43

[4] W. J. McGill, *Developments in Polymer Degradation-5*, Applied Science Publishers, London, 1977, p. 1

[5] X. Guo, B. Huang, T. Dyakonov, Y. Chen, L. Padron, T. Vickstrom, J. Kuhn, J. Hodkiewicz and W. T. K. Stevenson, *Appl. Spectrosc.*, 1999, **53**, 1403

[6] R. S. Macomber, *A Complete Introduction to Modern NMR Spectroscopy*, John Wiley and Sons, New York, 1998, Ch.1, p. 1

[7] D. Campbell, R. A. Pethrick and J. R. White, *Polymer Characterisation: Physical Techniques*, Stanley Thornes Publishers Ltd., Cheltenham, 2000, Ch. 6, p. 108

[8] R. J. Abraham, J. Fisher and P. Loftus, *Introduction to NMR Spectroscopy*, John Wiley and Sons, Chichester, 1988, Ch. 1, p. 1

[9] R. S. Macomber, *A Complete Introduction to Modern NMR Spectroscopy*, John Wiley and Sons, New York, 1998, Ch.2, p. 6

[10] P. A. Mirau, *A Practical Guide To Understanding the NMR of Polymers*, John Wiley and Sons, 2005, Ch.1, p. 1

[11] W. Kemp, *Organic Spectroscopy*, Macmillan Education Ltd., London, 1991, Ch. 3, p. 101

[12] J. W. Akitt, *NMR and Chemistry: An Introduction to Modern NMR Spectroscopy*, Chapman and Hall, London, 1992, Ch. 1, p. 1

[13] R. S. Macomber, *A Complete Introduction to Modern NMR Spectroscopy*, John Wiley and Sons, New York, 1998, Ch.6, p. 68

[14] J. W. Akitt, *NMR and Chemistry: An Introduction to Modern NMR Spectroscopy*, Chapman and Hall, London, 1992, Ch.2, p. 17

[15] J. K. M. Sanders and B. K. Hunter, *Modern NMR Spectroscopy: A Guide for Chemists*, Oxford University Press, Oxford, 1993, Ch. 1, p. 10

[16] J. Keeler, *Understanding NMR Spectroscopy*, John Wiley and Sons, Chichester, 2010, Ch. 9, p. 241

[17] R. S. Macomber, *A Complete Introduction to Modern NMR Spectroscopy*, John Wiley and Sons, New York, 1998, Ch.15, p. 283

[18] J. W. Akitt, *NMR and Chemistry: An Introduction to Modern NMR Spectroscopy*, Chapman and Hall, London, 1992, Ch. 5, p. 99

[19] R. J. Abraham, J. Fisher and P. Loftus, *Introduction to NMR Spectroscopy*, John Wiley and Sons, Chichester, 1988, Ch. 8, p. 240

[20] J. K. M. Sanders and B. K. Hunter, *Modern NMR Spectroscopy: A Guide for Chemists*, Oxford University Press, Oxford, 1993, Ch. 9, p. 260

[21] E. O. Stejskal and J. D. Memory, *High Resolution NMR in the Solid State*, Oxford University Press, New York, 1994, Ch. 2, p. 61

[22] E. O. Stejskal and J. D. Memory, *High Resolution NMR in the Solid State*, Oxford University Press, New York, 1994, Ch. 4, p. 109

[23] P. A. Mirau, *A Practical Guide To Understanding the NMR of Polymers*, John Wiley and Sons, 2005, Ch.2, p. 104

[24] http://www.dur.ac.uk/resources/SSNMR/three82.pdf, 31st March 2012

[25] A. Apedaile, 2nd Year PhD Report, *Development of Siloxane Elastomers Incorporating Nanoscale Modifiers*, University of Strathclyde, Glasgow, 2009

[26] S. J. Opella and M. H. Frey, *J. Am. Chem. Soc.*, 1979, **101**, 5854

[27] http://www.dur.ac.uk/resources/SSNMR/three81.pdf, 31st March 2012

[28] P. J. Haines, *Principles of Thermal Analysis and Calorimetry*, RSC, Cambridge, 2002, Ch. 2, p. 10

[29] D. Campbell, R. A. Pethrick and J. R. White, *Polymer Characterisation: Physical Techniques*, Stanley Thornes Ltd, Cheltenham, 2000, Ch. 12, p. 362

[30] T. Hatakeyama and F. X. Quinn, *Thermal Analysis: Fundamentals and Applications to Polymer Science*, John Wiley and Sons, Chichester, 1999, Ch. 4, p. 45

[31] T. Hatakeyama and F. X. Quinn, *Thermal Analysis: Fundamentals and Applications to Polymer Science*, John Wiley and Sons, Chichester, 1999, Ch. 2, p. 5

[32] P. J. Haines, *Principles of Thermal Analysis and Calorimetry*, RSC, Cambridge, 2002, Ch. 3, p. 55

[33] S. R. Sandler, W. Karo, J. Bonesteel and E. M. Pearce, *Polymer Synthesis and Characterisation: A Laboratory Manual*, Academic Press, California, 1998, Ch. 16, p. 120

3 Experimental

3.1 Materials

Flexible polyurethane foams were synthesised specifically for this investigation in the University of Strathclyde by Dr. John Daly following a patented standard formulation.[1] The isocyanate employed was TDI (80:20 mixture of the 2,4- and 2,6-isomers) and the polyol was Alcupol F-5611, a polyether polyol composed of PPG chains tipped with PEG. Water was employed as the blowing agent and the catalysts employed were dimethylethanolamine (DMEA), triethylenediamine (Dabco 33LV) and stannous octoate (Kosmos 29). A silicone-based surfactant (L620LV) was also employed. Four different foams were synthesised and analysed throughout this research:

- Foam without fire retardant (standard)
- Foam containing 13.35% ammonium polyphosphate (APP)
- Foam containing 1.94% vermiculite
- Foam containing 1.94% Cloisite® 30B

Vermiculite and Cloisite® 30B are nanoclays, therefore, the foams which contain these materials are classed as clay-nanocomposite foams. Vermiculite is an unmodified clay mineral whilst Cloisite® 30B is a montmorillonite clay which has been organically modified with the methyl, tallow, bis-2-hydroxyethyl, quaternary ammonium salt shown in Figure 3.1, where T represents tallow (~65% C18; ~30% C16; ~5% C14).

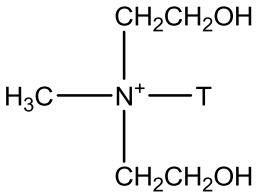

Figure 3.1: The organic modifier in Cloisite® 30B

3.2 TVA

3.2.1 Instrument

The TVA instrument used throughout this research was designed and built in-house based on the apparatus and techniques described in Section 2.2.

3.2.2 Tube Calibrations

During a TVA experiment the temperature of the furnace is monitored by means of a thermocouple positioned on the outside base of the glass sample tube. Due to the insulating effect of the borosilicate glass a temperature differential will exist between the outside and inside surfaces of the tube. The sample temperature will, therefore, be lower than that measured by the external thermocouple. Sample temperatures could be measured directly during each analysis by means of a permanent thermocouple positioned within the tube; however, this is problematic as it introduces the risk of sample contamination and air leaks. Instead the internal tube base temperature is obtained to give a temperature calibration curve. This is achieved by permanently fixing a K-type thermocouple into a modified tube head as shown in Figure 3.2.

The head is attached to the sample tube ensuring that the thermocouple positioned inside the tube is in contact with the base of the tube in a central position. The system is then pumped to a high vacuum and the tube is heated at 10°C min^{-1} to the desired temperature, this was 550°C for a degradation run but varied for the isothermal runs. Measurements from both the external and internal thermocouples are recorded throughout to produce a calibration curve similar to that shown in Figure 3.3. This is repeated for each tube employed and using the calibration curves the internal tube base temperature can be obtained for any furnace temperature during a TVA experiment. Throughout this report all TVA curves will be presented as furnace temperature versus pressure, with the furnace temperature being that measured by the thermocouple on the external base of the tube. By using the calibration curves the furnace temperatures will be converted to sample temperatures which will be reported in an accompanying table.

The error for the temperatures measurements for the TVA system, which takes into account both sample reproducibility and the tube calibrations, has been calculated as ±3°C.

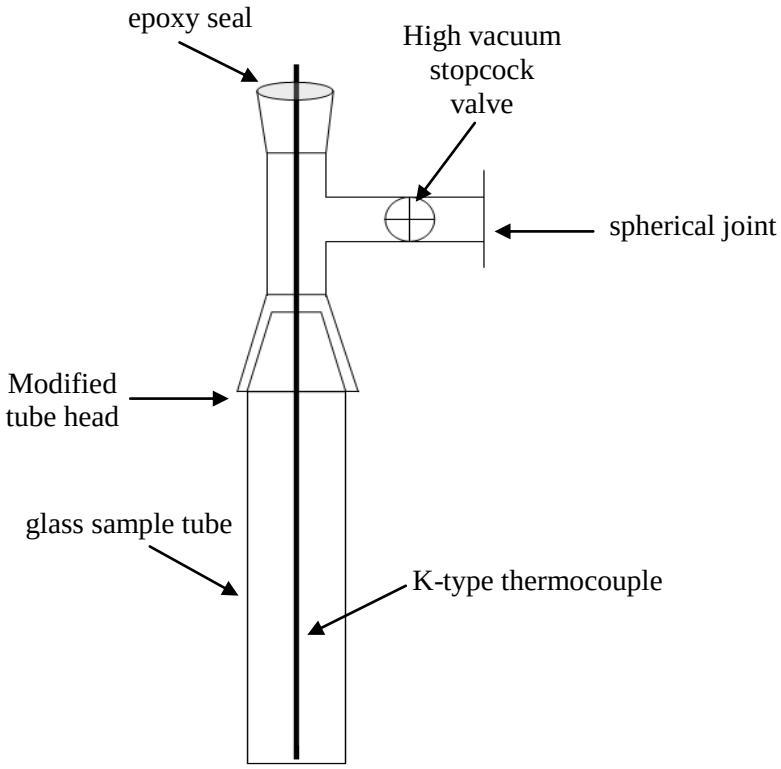

Figure 3.2: Illustration of the modified tube head used for the internal tube temperature calibrations

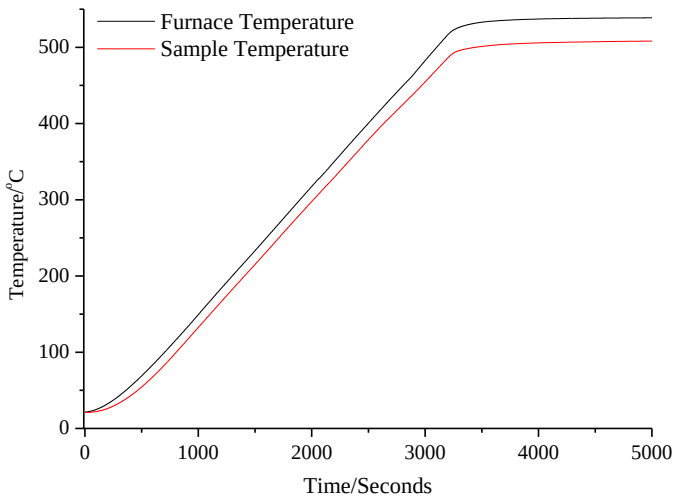

Figure 3.3: Example tube calibration curve

3.2.3 Sample Preparation

All samples were prepared in the same manner with the sample mass kept as constant as possible. In order to keep the results as reproducible as possible foam samples were prepared as single square pieces of foam. The standard sample size used for a degradation run was approximately 25 mg, however, in order to obtain better GC-MS and FTIR analysis repeat runs were performed using 100 mg samples. The reproducibility with these larger sample sizes is poorer, therefore, only the TVA curves for the 25 mg samples will be presented.

3.2.3.1 Degradation and Sub-ambient Differential Distillation

Samples were pumped to vacuum on the TVA system overnight before being analysed the following day. This was done in order to reduce the background level of water and CO_2 within the system and to ensure that any air trapped within the foam sample had been removed. All samples were heated to 550°C at a rate of 10°C min^{-1} and held isothermally at 550°C for 10 minutes with continual cryogenic collection of the evolved volatiles. Sub-ambient differential distillation was then performed on the collected volatiles by allowing the primary cold trap to heat to ambient temperature. The separated volatiles were subsequently analysed by a combination of MS, FTIR spectroscopy and GC-MS as described in the following sections.

3.2.3.2 Isothermal Studies

In order to further probe the degradation chemistry of the polyurethane foams, isothermal TVA experiments were conducted in which the sample was heated to a specific temperature and held at this temperature for a set period of time. For these studies the temperatures employed were 250, 300, 350 and 400°C. 50 mg samples were heated to the chosen temperature and held isothermally for 30 minutes with continual cryogenic collection of the evolved volatiles, followed by sub-ambient differential distillation of the collected volatiles.

3.2.3.3 MS

MS analysis was carried out by means of an online 1-300 amu Hiden single quadrupole RGA mass spectrometer operating in continual scan mode.

3.2.3.4 FTIR Spectroscopy

All FTIR analyses were carried out using a Perkin Elmer Spectrum 100 FTIR Spectrometer in transmission mode. The cold-ring fractions were removed from the sample tube and dissolved in chloroform before being cast onto sodium chloride discs for analysis. Low-boiling volatile species were analysed in the gas-phase using the gas-phase collection cells described in section 2.2.3.

3.2.3.5 GC-MS

All GC-MS analyses were carried out using a Finnigan ThermoQuest capillary column trace GC and Finnigan Polaris Quadrupole Mass Spectrometer which scanned an m/z range of 30 to 650. The GC column was programmed with a temperature ramp from 40 to 320^{o}C at a rate of 20^{o}C min^{-1}, with a helium carrier gas. Cold-ring fractions were removed from the sample tube and dissolved in chloroform, whilst the higher molar mass products were collected for GC-MS analysis by means of the collection cell described in section 2.2.3.

3.2.4 Reproducibility Tests

The thermal analysis of foams can be problematic due to their low densities and non-uniformity. This can lead to problems with the reproducibility of the results obtained. In order to test the reproducibility of the TVA technique three repeat runs were conducted with 25 mg samples of the standard foam. Shown in Figure 3.4 and Figure 3.5 are the degradation profiles and sub-ambient differential distillation traces, respectively.

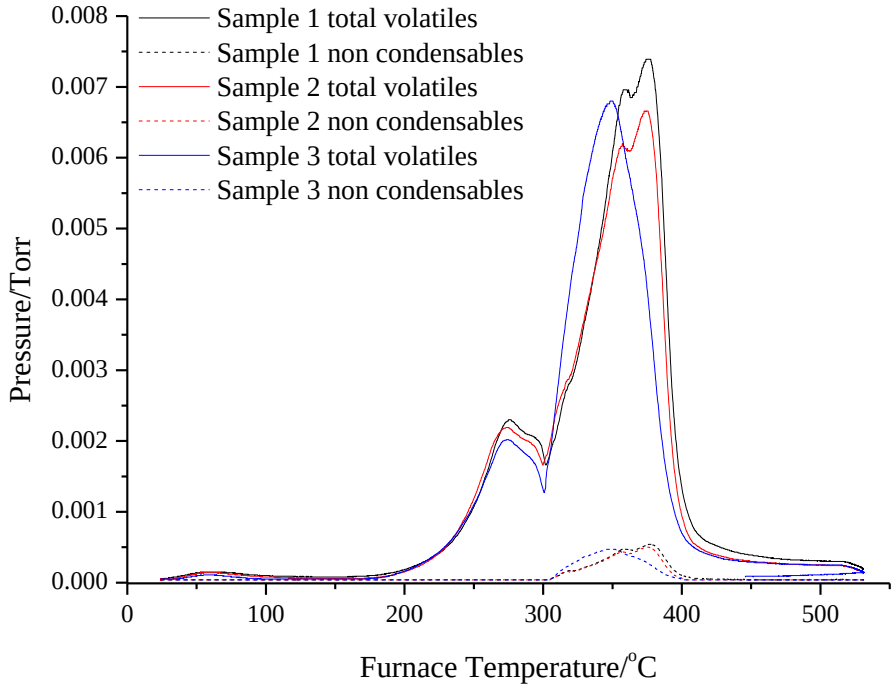

Figure 3.4: TVA degradation traces showing the rate of volatiles evolution as a function of pressure vs. furnace temperature for three samples of polyurethane foam

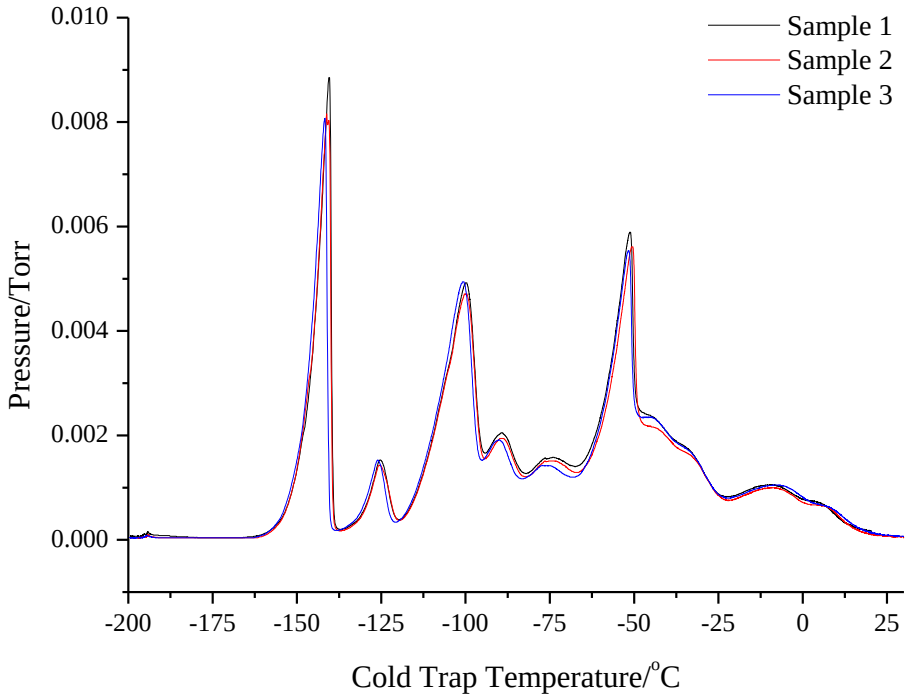

Figure 3.5: Sub-ambient differential distillation trace for the three samples of polyurethane foam

It can be observed from Figure 3.4 that the initial degradation process produces a highly reproducible peak whilst the second process is more variable. This variation is likely to be due to physical changes within the foam as it degrades which can affect the diffusion of volatiles from the foam. The reproducibility of the sub-ambient differential distillation, on the other hand, is excellent with the levels of each volatile component being almost identical between samples. It can, therefore, be concluded that this technique yields reproducible results for the analysis of foams.

3.3 TGA

3.3.1 Instrument

The TGA instrument employed throughout this work was a Perkin Elmer TGA7.

3.3.2 Sample Preparation

All samples were prepared in the same manner with cylinders of foam being cut to shape to fit in the sample crucible. The dimensions of the foam cylinders were kept the same in each case but due to the differing densities of the foams this lead to the sample masses varying in the range 3-5 mg. This is one of the difficulties associated with working with foam materials and it is considered that in this case it is more representative to compare samples with similar dimensions rather than similar masses.

3.3.3 Experimental Procedure

Before analysis the system was purged with a flow of 30 mL min^{-1} of the gas being employed during the analysis. Helium and air were employed in order to investigate non-oxidative and oxidative thermal degradation, respectively. The system was heated to 50°C and held isothermally for 5 minutes. Following this the sample was heated at a rate of 10°C min^{-1} from 50°C to 800°C where it was held isothermally for 5 minutes.

Throughout this investigation the temperature at which significant mass loss occurs will be reported, this is taken as the temperature at which the material has lost 5% of its original mass.

3.4 DSC

3.4.1 Instrument

The heat-flux DSC instrument employed throughout this research was a TA Instruments DSC Q1000 with an autosampler and a RC90 refrigerated cooling unit which has a base temperature of -90°C.

3.4.2 Sample Preparation

The analysis of foam samples by DSC is problematic as their cellular nature leads to air becoming trapped within the foam and their low density means that only a small mass of foam can be analysed. Previous work within this research group has found ~1.5 mg and ~0.75 mg to be the optimum sample mass for analysis of polyurethane foam under nitrogen and air respectively.[2] In order to keep the DSC results as reproducible as possible the samples were prepared as single pieces of foam. All sample masses were kept within the following ranges in order to be as close to the optimum mass as possible:

- Samples for non-oxidative degradation: 1.4-1.6 mg
- Samples for oxidative degradation: 0.7-0.8 mg

The samples were analysed in aluminium hermetic pans with the lids pierced four times to allow volatile degradation products to diffuse out of the sample. In order to avoid compression of the foam the lids were secured by lightly crimping the sides of the pan.

3.4.3 Experimental Procedure

Samples were analysed together with a reference sample consisting of an empty aluminium hermetic pan and lid. A flow rate of 60 mL min^{-1} of the selected gas was employed. For the analysis under an air (oxidative) atmosphere the sample was held isothermally at 30°C for five minutes, this time was increased to thirty minutes for the samples analysed under a nitrogen (inert) atmosphere to ensure that all the air trapped within the foam had been flushed out with nitrogen prior to the sample being heated.

The samples were then heated to 550°C at a rate of 10°C min^{-1}. All samples were analysed in triplicate, however, three sets of data will only be presented for the standard foam. For all other foams the data which best represents the three analyses will be presented. Any temperatures quoted from the DSC results will be reported as the mean value obtained from the three repeats ± the standard deviation. For each DSC thermogram the results will be on the same vertical scale but the curves will be separated for clarity.

3.5 Pyrolysis

3.5.1 Instrument

Char residues were prepared using a pyrolysis rig which had been designed and constructed for this purpose. The equipment comprised of a block heater in which pyrex sample tubes were positioned. Each tube was fitted with a specially designed head which allowed a gas stream to be passed over the sample and the volatile degradation products to be vented from the tubes. The gas stream was introduced by means of a custom built pyrolysis rig which allowed four tubes to be connected simultaneously. The volatiles from the tubes were vented into dreschel bottle which were attached to the outlet of the tube heads. Presented in Figure 3.6 is a simplified schematic of this equipment.

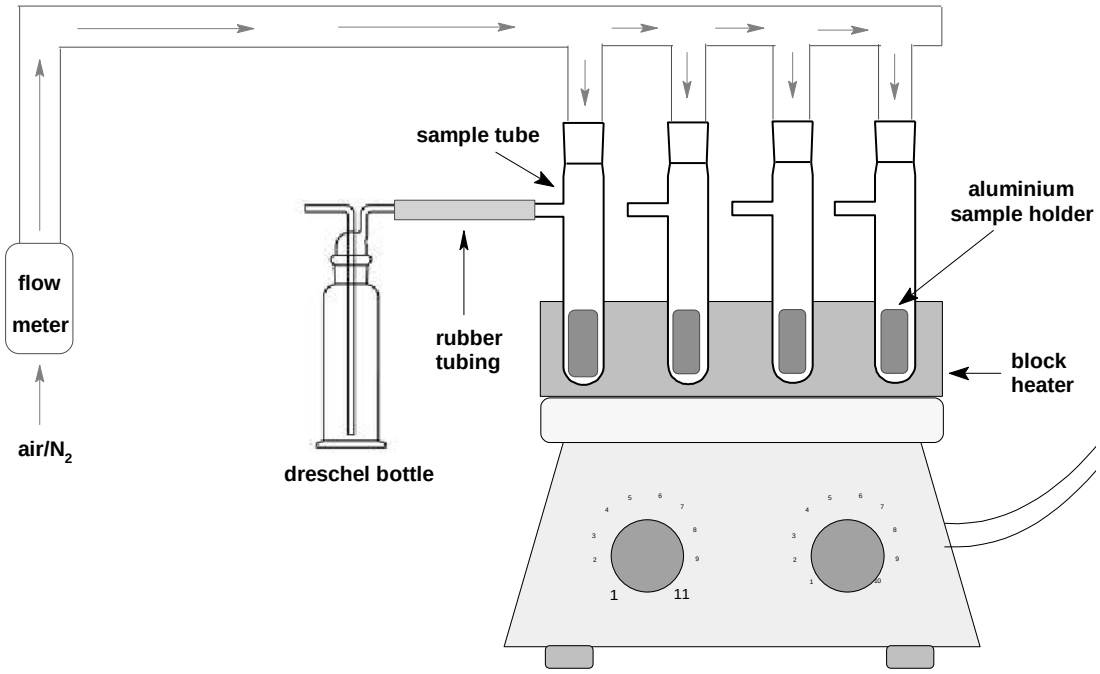

Figure 3.6: Schematic of the pyrolysis rig

3.5.2 Sample Preparation

Aluminium sample holders were made by wrapping a square section of foil around the end of a test tube to create a cylinder shape. This was done to allow easy removal of the sample from the tubes after the pyrolysis, allowing post-pyrolysis analysis to be carried out. Cylinders of foam with masses in the range 200-300 mg were then cut and placed inside the foil sample holders. Samples of this size were used in order to generate enough char to allow characterisation of the residue by solid-state ^{13}C NMR.

3.5.3 Experimental Procedure

Each foam was pyrolysed at four different temperatures under nitrogen, air and 3% oxygen in nitrogen. The pyrolysis temperatures employed were the same as those used for the isothermal TVA experiments, *i.e.* 250, 300, 350 and 400°C. At each pyrolysis temperature four samples of the same foam were degraded in order to ensure reproducibility of the results and to ensure that an adequate level of residue was generated to allow solid-state ^{13}C NMR analysis. Each pyrolysis run followed the same general experimental procedure as outlined below:

1) The aluminium sample holders and foam samples were weighed and the combined mass recorded before being inserted into the sample tubes.
2) The tubes were placed into the block heater and the tube heads connected to the pyrolysis rig by means of screw-top connectors and rubber tubing.
3) The gas of choice was then fed into the pyrolysis rig at a rate of 160 ml min^{-1}, allowing a gas flow of 40 ml min^{-1} to reach each of the four sample tubes. The system was purged with the gas for 15 minutes before the pyrolysis was started.
4) The samples were heated to the desired pyrolysis temperature at a rate of 10°C min^{-1} and held isothermally at the pyrolysis temperature for 30 minutes.
5) Following the isothermal hold period the tubes were removed from the block heater and allowed to cool before the aluminium sample holders were removed and weighed. This allowed the percentage mass loss for each sample to be calculated.
6) The "cold-ring" type material which formed at the top of the tubes was then removed and dissolved in chloroform before being analysed by FTIR spectroscopy and GC-MS.

3.5.4 Analysis of the Residue

The residues which remained in the aluminium sample holder were comprised of a chloroform soluble component and a chloroform insoluble component, which will be referred to throughout this work as tar and char, respectively. In order to separate these components the residues were removed from the foil, placed in a small jar containing chloroform and this solution was subsequently filtered through pre-weighed Whatman® filter tubes with a 1 μm pore size. Pre-weighed vials were placed below the filter tubes to collect the soluble tar components whilst the chars remained in the filter tubes. The tars and chars were then left to dry to ensure that all solvent had evaporated before the vials and filer tubes were weighed; this allowed the quantities of tar and char to be calculated as a percentage of the total residue collected at each pyrolysis temperature. Following this the tars were analysed by FTIR spectroscopy whilst the chars were analysed by solid-state ^{13}C NMR, FTIR spectroscopy and elemental analysis.

3.6 Solid-state ^{13}C NMR

All solid-state ^{13}C NMR spectroscopy was conducted by the Solid-state NMR Service at Durham University. The samples were analysed as received using a Varian VNMRS spectrometer operating at 100.56 MHz for ^{13}C using cross-polarisation with magic angle spinning (CPMAS). A 6 mm magic-angle spinning probe was employed with a spin rate of 6.8 kHz. For each sample two spectra were recorded, the first was recorded using the TOSS technique to remove any spinning sidebands from the spectra and the second was recorded using dipolar dephasing with no sideband suppression.

3.7 FTIR Spectroscopy

FTIR analysis of any cold-ring fractions, tars or TVA gas-phase fractions were carried out using a Perkin Elmer Spectrum 100 FTIR Spectrometer in transmission mode.

FTIR analysis of the solid pyrolysis chars was achieved by use of an A2 Technology ML FTIR with a diamond ATR cell (now an Agilent 5500a FTIR with diamond ATR cell). The spectra obtained from ATR-FTIR experiments are traditionally plotted as absorbance versus wavelengths, however, for the purposes of this work these have been converted to % transmittance so that all the FTIR spectra are of the same format. Presented in Figure 3.7 is an ATR-IR spectrum of a standard polyurethane foam plotted as absorbance and as % transmittance, which illustrates that there is no loss of information when plotting the spectrum as % transmittance instead of absorbance.

Presented in Table 3.1 is a list of common functional groups and characteristic bands typically encountered during the FTIR analysis of polyurethanes and their degradation products. This table has been used during this work for the identification of the polyurethane samples and their degradation products.

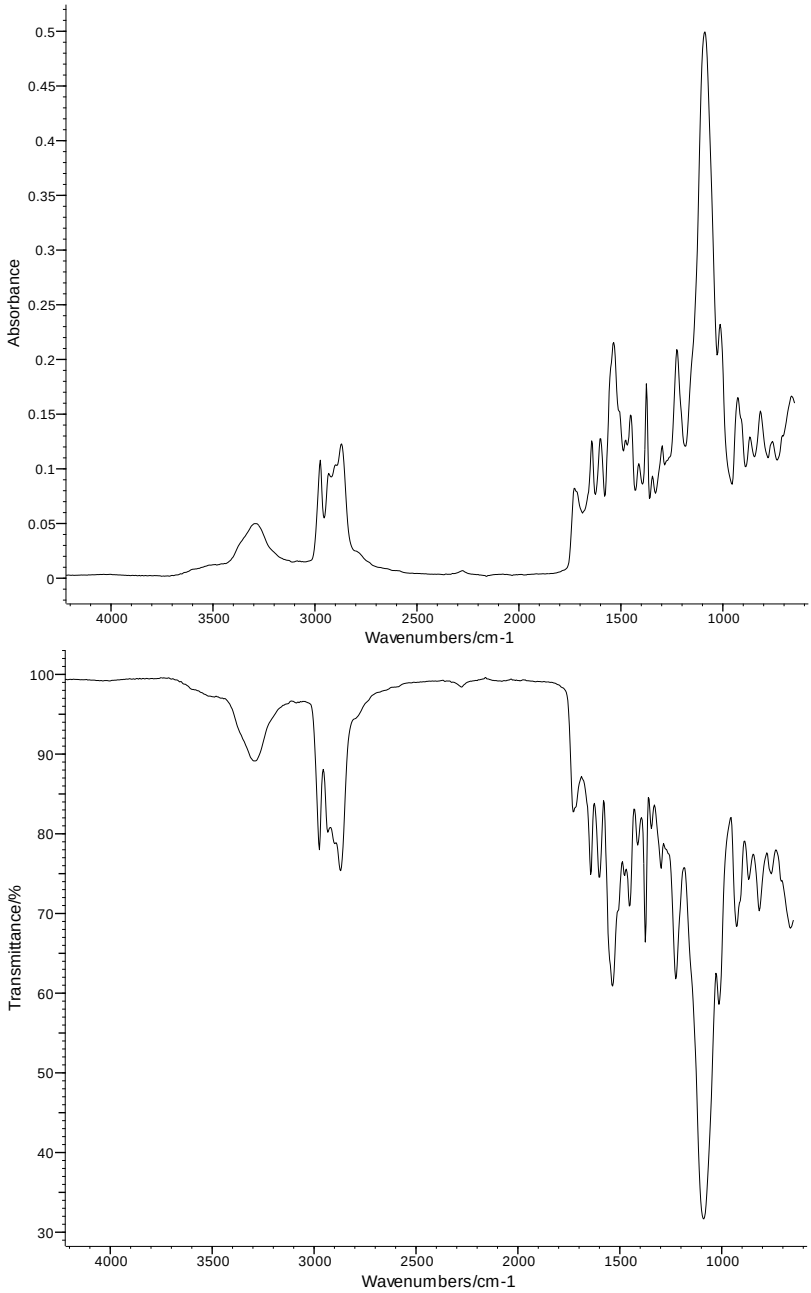

Figure 3.7: ATR IR spectra of polyurethane foam plotted as absorbance (top) and % transmittance (bottom)

Functional Group/Compound	Formula	Band(s) (cm^{-1})	Vibration
Urethane	RNHCOOR	1740-1690 1200-1400	C=O stretching C-N stretching
Urea	RNHCONHR	1660 1200-1400	C=O stretching C-N stretching
Isocyanate	RN=C=O	2275-2250	N=C=O stretching
Aromatic groups	Ar-H	3040-3010 ~1600, ~1580, ~1500	C-H stretching C=C skeletal stretching
Alcohol (polyol)	R-OH	3600-3200 1410-1260	O-H stretching O-H bending
Alkyl Ether (polyol)	R-O-R	1150-1070	C-O-C stretch
Aliphatic groups	$-CH_3$ or $-CH_2-$ R_3-CH	2960-2850 1470-1430 2890-2880	C-H Stretching C-H deformations C-H stretching
Alkene	$R_2C=CR_2$	1680-1620 3095-3010 995-790	C=C stretching C-H stretching C-H out of plane deformations
Ketone	R-CO-R Ar-CO-R	1725-1705 1700-1680	C=O stretching C=O stretching
Aldehyde	R-CHO Ar-CHO	1740-1720 1715-1695	C=O stretching C=O stretching
Carbodiimide	RN=C=NR	2155-2130	C=N stretching
Amine	RNHR, RNH_2, ArNHR, $ArNH_2$	3500-3300 1650-1560 1200-1400	N-H stretching N-H bending C-N stretching

Table 3.1: Correlation table for the typical FTIR bands observed for polyurethanes and their degradation products[3,4]

3.8 SEM

All SEM work reported in this thesis was kindly carried out by Mr. Jim Morrow using a Cambridge Instruments Stereoscan90 instrument. Samples of foam were cut to the appropriate size before being coated with a gold/palladium alloy using a Polaron SC500A sputter coater. This was carried out at a current of 20 mA for 2 minutes.

Samples were then viewed at different levels of magnification, with the magnification employed being displayed at the upper left corner of the SEM images.

3.9 Elemental Analysis

All elemental analyses were carried out at the University of Strathclyde using the microanalysis service. C, H and N analysis was performed on each sample.

3.10 Mini-crib Fire Tests

The mini-crib fire test performed in this investigation has been designed based on the British Standard 5852 crib-5 test[5] which is used to test the flammability of upholstered seating when exposed to a flaming ignition source.

3.10.1 Sample Preparation

Foam samples were cut into squares with dimensions 10 x 10 x 2 cm which were then desiccated permanently at 40°C to ensure the samples had similar moisture contents before the fire test was performed.

3.10.2 Experimental Procedure

Two 12 x 12 cm squares of wire gauze were joined together at one edge and their mass recorded. Two 10 x 10 cm squares of foam were then pinned together using upholstery pins to form a "chair" and placed onto the wire gauze. The mass of the foam and gauze was then recorded and a piece of cotton wool pinned onto the foam chair. This assembly was then positioned on top of metal back and base plates positioned on a wooden block. An illustration of this assembly is shown in Figure 3.8. To start the test 0.5 g of propan-2-ol was poured onto the cotton wool and lit. The foam was then left to burn and once the fire had extinguished the assembly was weighed and the mass loss of the foam during the fire calculated.

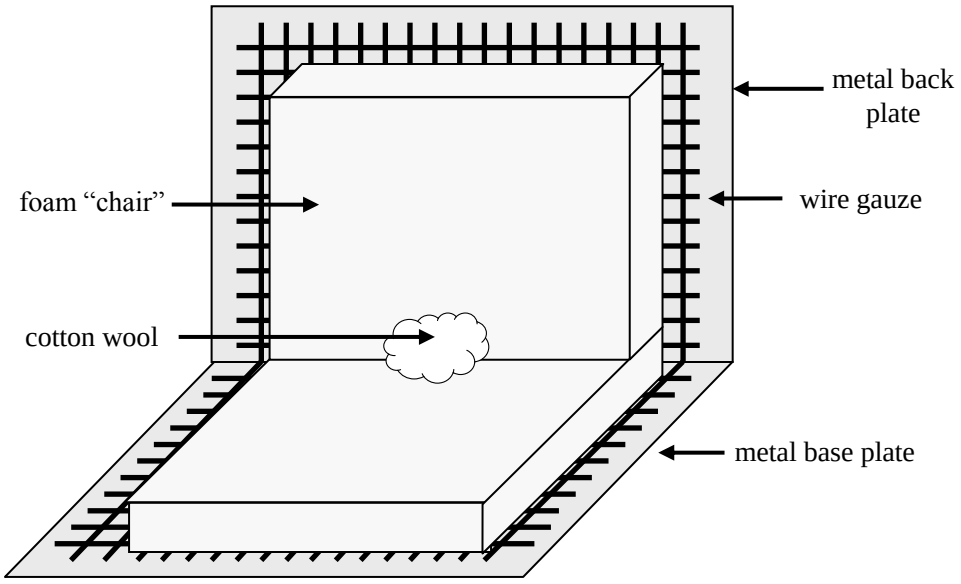

Figure 3.8: Set-up for the mini-crib fire test

3.11 References

[1] J. H. Daly, J. J. Liggat, L. McCulloch and R. A. Pethrick, Fire Retarded Flexible Foam, UK Patent Application PCT/WO2009/007715

[2] F. McCormack, MSci Thesis, *The Effects of Ageing on the Stability of Polyurethane Foams*, University of Strathclyde, Glasgow, 2008

[3] W. Kemp, *Organic Spectroscopy*, Macmillan Education Ltd., London, 1991, Ch. 2, p. 19

[4] D. H. Williams and I. Fleming, in *Spectroscopic Methods in Organic Chemistry Fifth Edition*, The McGraw-Hill Publishing Company, 1995, Ch. 2, p. 28

[5] British Standards Institution, BS 5852:1990, *Methods of test for the assessment of the ignitability of upholstered seating by smouldering and flaming ignition sources*, 1990

4 Study on the Standard Foam

A comprehensive study was conducted on the standard polyurethane foam in order to fully understand the thermal and thermo-oxidative behaviour of this type of polyurethane, and to determine the degradation processes which occur in this material. The standard foam was synthesised from TDI and a polyether polyol containing PPG units tipped with PEG and contained no fire retardant additives.

Initially, the overall degradation behaviour of this material was examined by means of TGA, DSC and TVA. TGA and DSC analysis were performed in order to study the thermal behaviour of the material in both oxidative and inert atmospheres, whilst TVA was employed to fully characterise the volatile products evolved during the degradation of this material, allowing possible mechanisms of degradation to be proposed. Following this, the degradation behaviour of the material was investigated in more detail by means of isothermal TVA experiments and pyrolysis studies. The isothermal TVA studies allowed characterisation of the volatile products being evolved during different stages of the degradation, whilst the pyrolysis studies allowed characterisation of the condensed-phase behaviour which had occurred in inert and oxidative environments.

4.1 Overview of the Degradation Behaviour

4.1.1 DSC

Presented in Figure 4.1 are the results from the DSC analysis of the standard foam samples under air. The results show two main exothermic peaks which indicate that a two stage degradation process is occurring for the standard foam. The initial degradation process results in a highly reproducible peak which exhibits a peak maximum at 272 ± 2°C, and is proposed to involve degradation of the urethane linkages by one of the mechanisms discussed in section 1.5.3.1.1. The second degradation step occurs between 285°C and 360°C and is proposed to be associated with secondary

degradation processes, such as thermo-oxidative degradation of the polyol. It is clear from Figure 4.1 that the second peak exhibits more variation than the first degradation step and this is proposed to be a result of the physical structure of the foam collapsing as the material degrades, thereby affecting the diffusion of oxygen into the foam. As the foam will not always collapse in the same manner the level of oxygen present in the second degradation step will vary between samples, therefore, the peak arising from this second degradation step will exhibit greater variability than the primary degradation step.

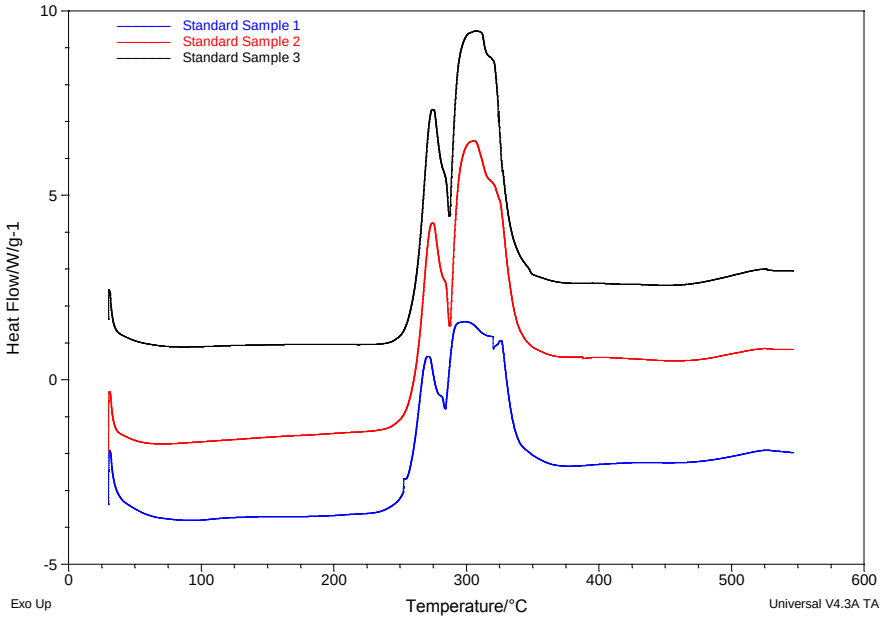

Figure 4.1: DSC curves for the standard foam analysed in air

The results from the DSC analysis of the standard foam under nitrogen are presented in Figure 4.2 and it is clear that the degradation under nitrogen exhibits better reproducibility compared to the analyses performed under air. The presence of two distinct endothermic peaks indicates that a two stage thermal degradation process is occurring under nitrogen for the standard foam. The first peak, with a peak maximum at 295 ± 2°C, is again attributed to thermal degradation of the urethane linkages within the foam. The second process, with a peak maximum at 380 ± 1°C, is likely to correspond to secondary degradation reactions such as thermal degradation of the polyol component. The peak maxima for the degradation under nitrogen occur at significantly

higher temperatures than those observed under air which suggests that thermo-oxidative degradation occurs at a lower temperature than thermal degradation. This is expected as the presence of oxygen is known to accelerate the thermal degradation process.[1]

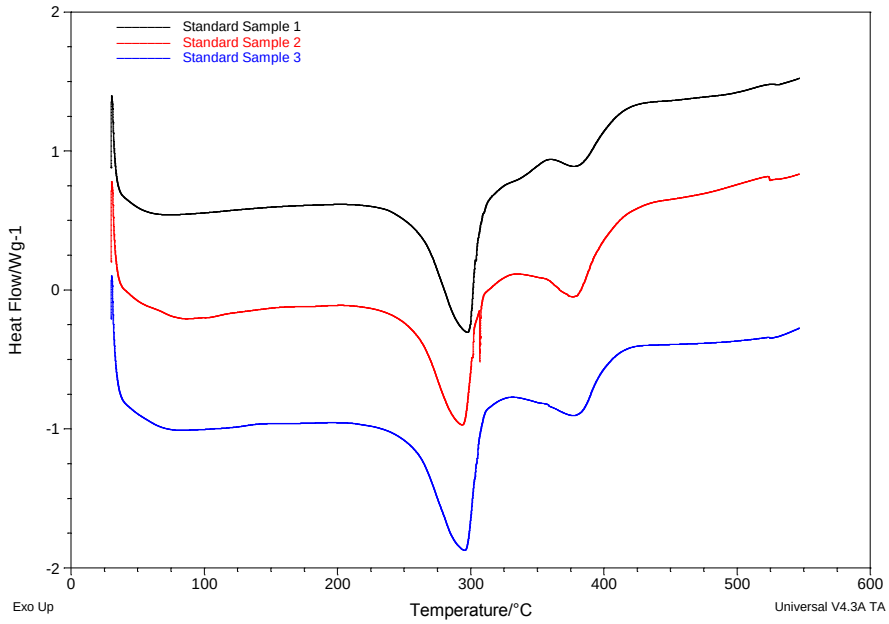

Figure 4.2: DSC curves for the standard foam analysed in N_2

4.1.2 TGA

Shown in Figure 4.3 are the thermogravimetry (TGA) and differential thermogravimetry (DTG) curves for the standard foam analysed in air. Significant mass loss is evident from 260°C and continues through two stages until approximately 380°C, after which a slow continual mass loss occurs until 800°C. A negligible residue remains at the end of the analysis. The presence of a two step mass loss process suggests that thermo-oxidative degradation of this material occurs *via* a two step mechanism, which is in agreement with the results obtained from the DSC analyses. The first degradation step has a maximum rate of mass loss at 294°C and is attributed to degradation of the urethane linkages by one of the three main mechanisms discussed in section 1.5.3.1.1. The second step, which is proposed to involve secondary degradation processes, has a maximum rate of mass loss at 330°C and exhibits a greater mass loss than the first step. It can be observed that the first mass loss step produces a sharp well defined peak whilst the second step is much broader which indicates a more gradual mass loss. This is in

correlation with the results obtained for the DSC analyses and is again likely to be a result of diffusion effects as the foam structure collapses during degradation. Not only will diffusion of oxygen into the foam be affected, but diffusion of the volatile degradation products out of the foam will be retarded by the collapse of the foam structure.

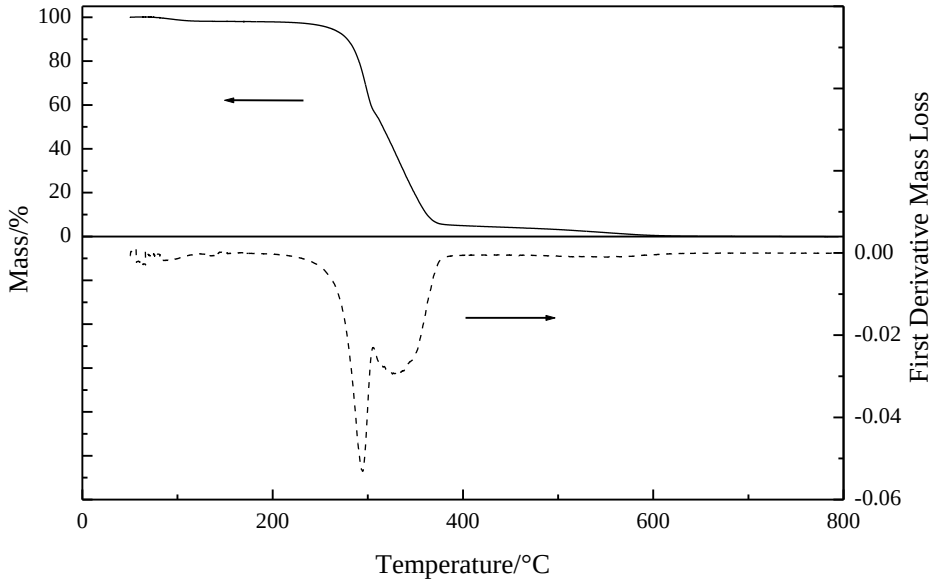

Figure 4.3: TGA (solid line) and DTG (dashed line) results for the standard foam analysed in air

Presented in Figure 4.4 are the TGA and DTG curves for the standard foam analysed under helium. As was the case for the thermo-oxidative degradation, a two stage mass loss is observed which suggests that a two step degradation mechanism also operates under an inert atmosphere. Significant mass loss is evident from 260°C and continues until approximately 410°C, after which a slow continual mass loss occurs until 800°C. Once again a negligible residue remains at the end of the analysis. The first degradation step has a maximum rate of mass loss at 290°C and can once again be attributed to degradation of the urethane linkages. The second step, which involves secondary degradation processes, has a maximum rate of mass loss at 370°C. As was the case for the analysis under air, the mass loss observed for the secondary degradation processes is greater than for the first degradation step.

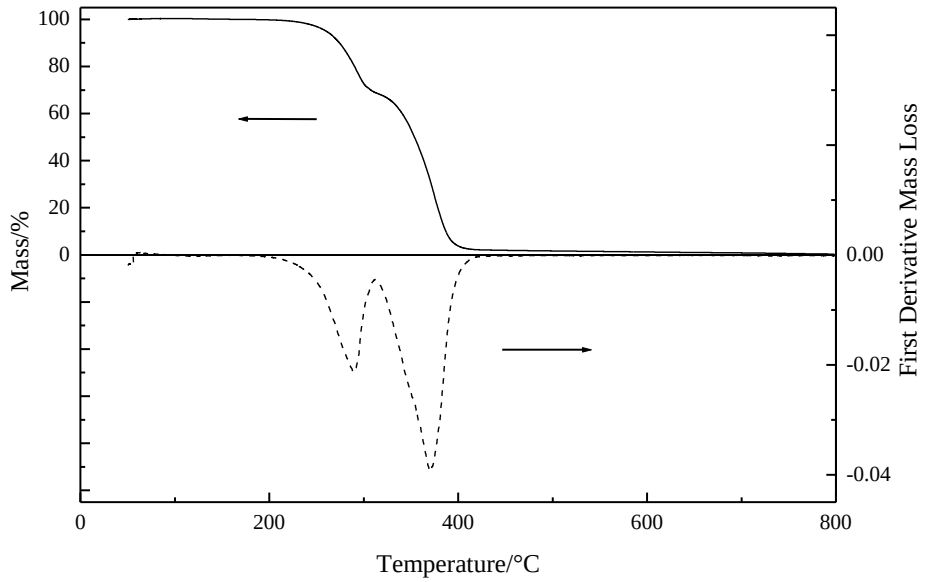

Figure 4.4: TGA (solid line) and DTG (dashed line) results for the standard foam analysed in He

The TGA results reveal that the onset of significant mass loss and the peak maxima temperatures for the primary degradation step do not differ significantly between inert and oxidative environments, which is consistent with reports within the literature that the presence of oxygen does not significantly influence the primary degradation process of polyurethane.[2,3] The secondary degradation step, on the other hand, which is proposed to involve degradation of the polyol segments, occurs at a lower temperature in an oxidative atmosphere. This demonstrates that the secondary degradation reactions are altered in the presence of oxygen which is once more in agreement with the literature in which it is reported that that the polyol segments are more susceptible to oxidative degradation than the hard segments.[4]

4.1.3 TVA

4.1.3.1 Dynamic TVA Study

- ***Degradation Profile***

The TVA degradation profile for the standard foam, which shows the rate of volatiles evolution as a function of furnace temperature, is presented in Figure 4.5. The black line

represents all of the material which is volatile at room temperature (total volatiles) and the red line represents the permanent gases which pass through the cold trap (non-condensables).

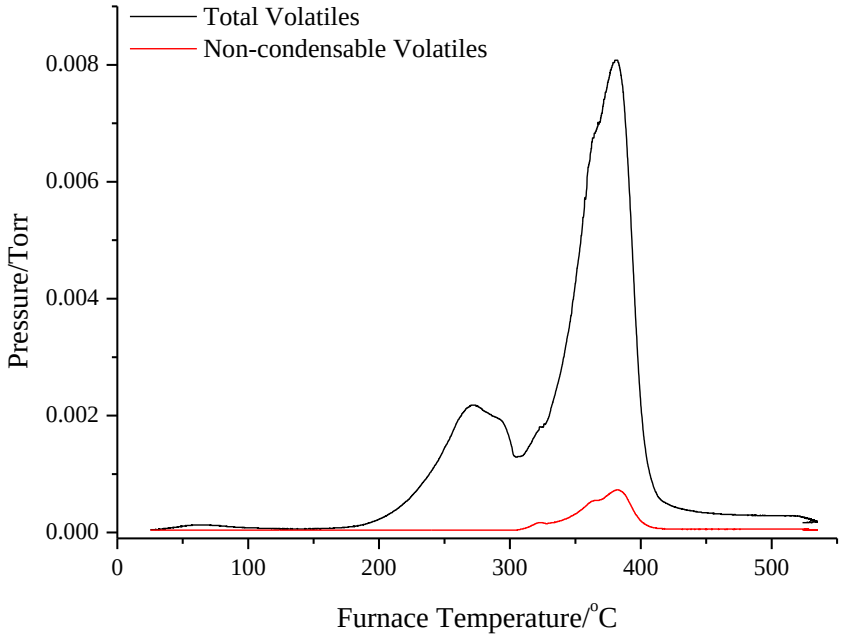

Figure 4.5: TVA degradation profile for the standard foam

Presented in Table 4.1 are the furnace temperatures for the major events which occur during the thermal degradation of the standard foam (obtained from Figure 4.5) with the corresponding sample temperatures which have been derived from the tube calibrations.

Event	**Furnace Temperature/°C**	**Sample Temperature/°C**
Onset of Volatile Evolution	~180	~145
Peak 1 maximum rate of volatile evolution	272	241
Peak 2 maximum rate of volatile evolution	381	351
End of volatile evolution	~430	~400

Table 4.1: Furnace temperatures and corresponding sample temperatures for the key events occurring during thermal degradation of the standard foam

Two peaks are observed in the TVA degradation profile which confirms the presence of a two stage degradation process; this is in correlation with the DSC and TGA results. The temperatures at which these two peaks occur in the TVA profile, however, differ from those obtained from the TGA and DSC analysis under inert atmospheres. In TVA the sample is heated under vacuum and the degradation proceeds at a lower temperature as volatilisation of the degradation products is facilitated under vacuum. Evolution of volatile material commences at approximately 145°C with a maximum rate of evolution observed at 241°C and 351°C for the primary and secondary degradation steps, respectively. The evolution of volatile material is complete by approximately 400°C.

It can be observed from Figure 4.5 that the first degradation step evolves a smaller quantity of volatile material than the second step; this is in agreement with the TGA results in which a greater mass loss was observed for the second degradation stage compared to the first. It is proposed that the first peak in the TVA profile arises due to volatile products, such as CO_2, which result from degradation of the urethane bonds within the foam by one of the mechanisms described in section 1.5.3.1.1. The second step will then involve secondary degradation reactions, primarily thermal degradation of the polyol component of the foam if this has been regenerated during degradation of the urethane linkages.

Finally, it can be observed from Figure 4.5 that small quantities of non-condensable volatiles were evolved during the thermal degradation of the standard foam. These were identified by online MS and the mass spectrum, presented in Figure 4.6, illustrates that the non-condensable volatiles consist of a mixture of CO, methane and hydrogen. These volatiles are only present during the second degradation step and must, therefore, be associated with the secondary degradation reactions, most likely degradation of the polyol component of the foam.

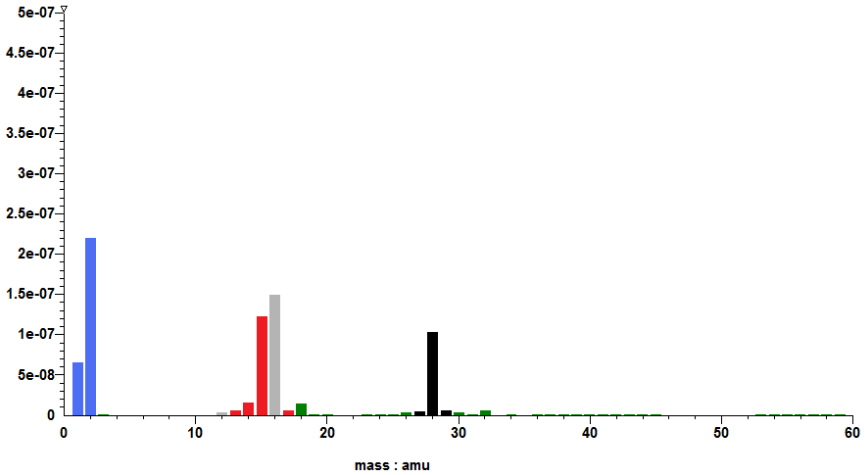

Figure 4.6: Mass spectrum of the non-condensable volatiles observed during the TVA of the standard foam confirming the presence of CO (black), methane (red) and hydrogen (blue). Grey peaks are common to both methane and CO.

- ***Cold-ring Fraction Analysis***

During the thermal degradation of the standard foam a pale yellow, liquid cold-ring fraction was collected. Analysis of this material by FTIR spectroscopy yielded the spectrum shown in Figure 4.7.

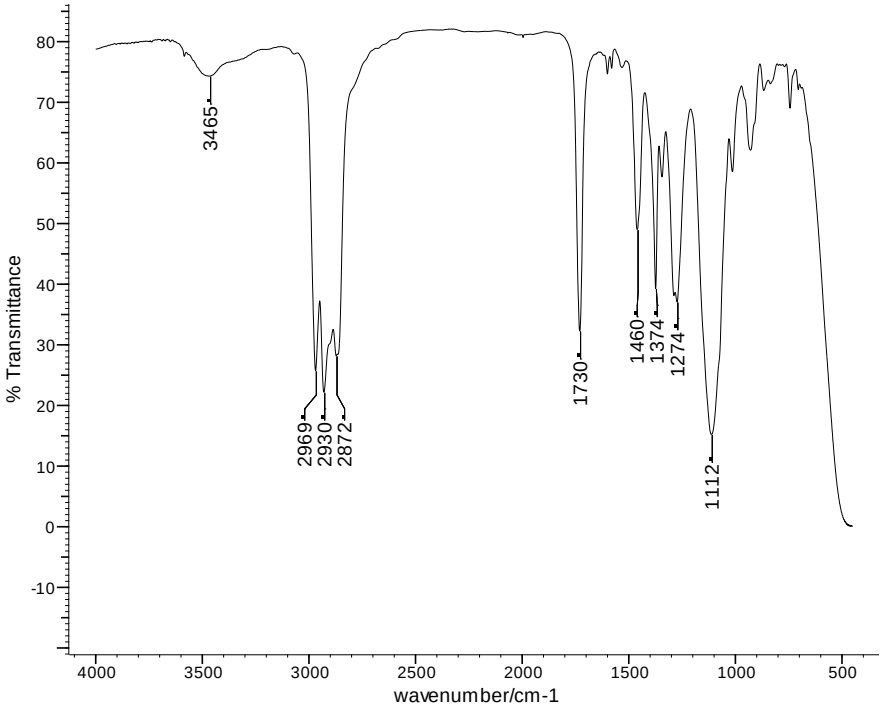

Figure 4.7: FTIR spectrum of the cold-ring fraction collected from the standard foam

The majority of the peaks are associated with structures which resemble the polyether polyol component of the foam. It is proposed that these species are most likely to be high molar mass chain fragments which have resulted from the breakdown of the polyol chains in the second degradation step. The peak at 1730 cm^{-1} could correspond to carbonyl-containing polyol fragments; however, it could also correspond to carbonyl groups within residual urethane linkages which may be present in the cold-ring fraction.

GC-MS analysis was also conducted on the cold-ring fraction and the resultant total-ion chromatogram is presented in Figure 4.8.

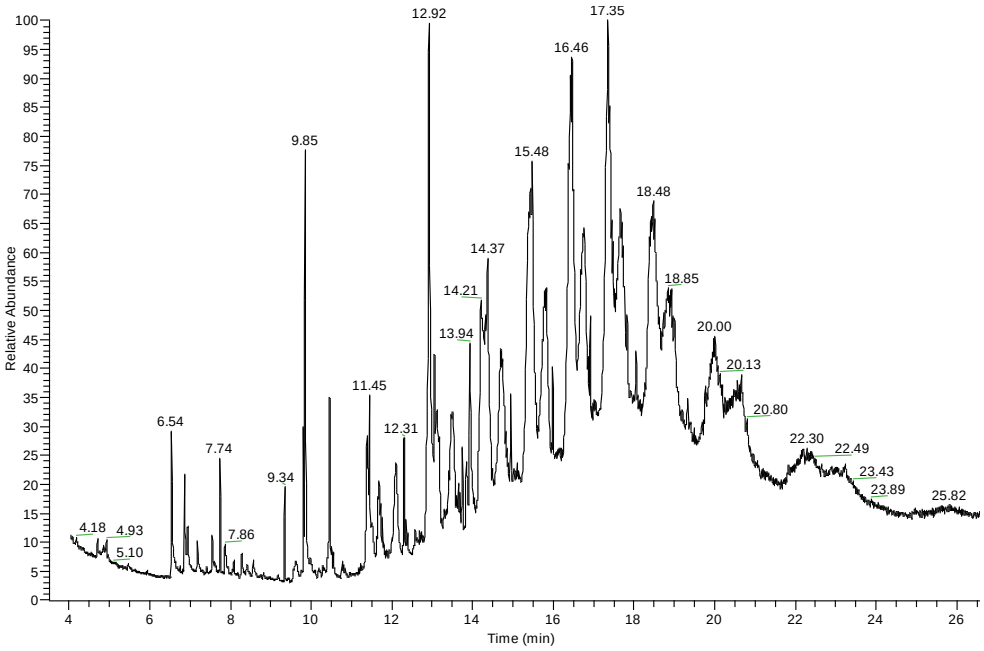

Figure 4.8: GC-MS total-ion chromatogram for the cold-ring fraction collected from the standard foam

Several of the main peaks in the chromatogram are due to siloxane breakdown products from the stationary phase within the GC column. The peaks at a retention time of 9.80 and 9.85 minutes have been positively identified as 2,6- and 2,4-TDI, respectively. The series of peaks from 10.50 minutes to 20 minutes can be attributed to high molar mass polyol chain fragments, many of which have common m/z fragments of 101, 87, 73, 59, 45, 43 and 41. Due to the large number of possible products which could be derived

from the random chain scission of the polyol backbone, complete identification of these species was not possible.

The results from the combined FTIR and GC-MS analyses, therefore, demonstrate that that the cold-ring fraction collected from the standard foam is composed of TDI and high molar mass fragments derived from the polyether polyol chain. The presence of TDI within the cold-ring fraction confirms that degradation of the urethane bonds within the foam has occurred *via* a depolymerisation reaction to yield the isocyanate and regenerated polyol. The regenerated polyol is then proposed to degrade in the second step *via* random radical chain scission to yield the high molar mass chain fragments which are observed. This is consistent with the results reported by Ravey and Pearce[5] and Erickson[6] who identified regenerated TDI and polyol when foams were degraded in an environment in which the volatiles were removed from the system. Grassie and co-workers[7,8,9] also observed isocyanate as a degradation product when polyurethanes were analysed by means of TVA.

- ***Condensable Fraction: Sub-ambient Differential Distillation and Characterisation***

The condensable fraction collected in the primary cold trap was separated by sub-ambient differential distillation into three fractions which were subsequently analysed by FTIR spectroscopy and GC-MS. The sub-ambient differential distillation trace presented in Figure 4.9 provides a qualitative indication of the volatile degradation products which are evolved. The temperature ranges of the three fractions collected and the identity of each of the products are presented in Table 4.2.

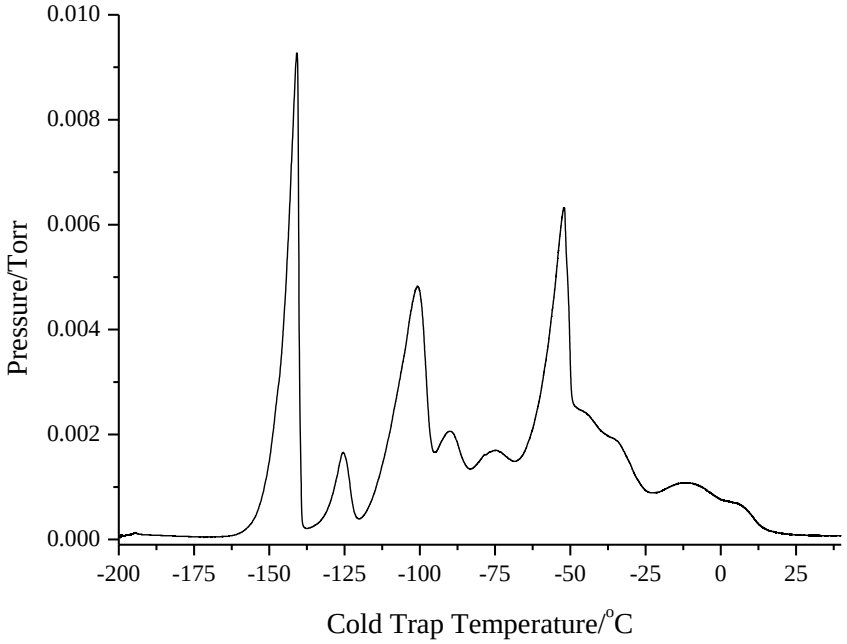

Figure 4.9: Sub-ambient differential distillation trace for the condensable fraction collected from the standard foam

Fraction	Temperature Range	Peak	Product Identification
1	-196°C to -120°C	1	Propene and CO_2
		2	Formaldehyde
2	-120°C to -65°C	3	Acetaldehyde
		4	C_3H_6O compound
3	-65°C to 30°C	5	High molar mass polyol fragments
		6	Water and high molar mass polyol fragments

Table 4.2: Sub-ambient differential distillations fractions collected from the standard foam

The first fraction of compounds evolved during the sub-ambient differential distillation consisted of propene and CO_2 which co-evolve to give a single peak, followed by formaldehyde. Identification of this initial fraction of volatiles has been achieved by MS (Figure 4.10 and Figure 4.11) and FTIR spectroscopy (Figure 4.12). The corresponding peak identifications for the FTIR spectrum are displayed in Table 4.3.

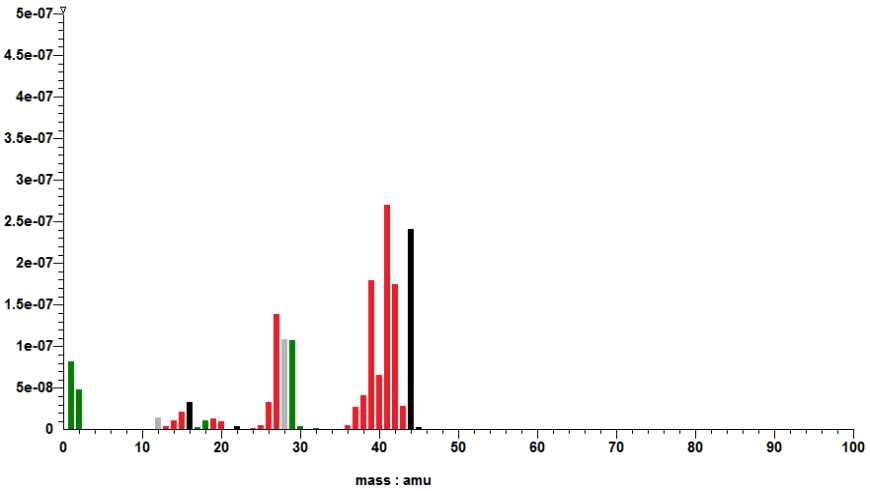

Figure 4.10: Mass spectrum of CO_2 (black) and propene (red), grey peaks are common to both products.

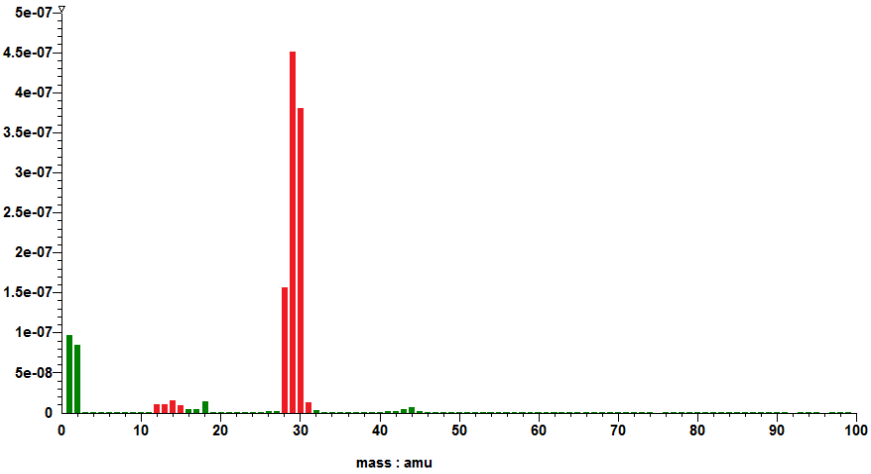

Figure 4.11: Mass spectrum of formaldehyde

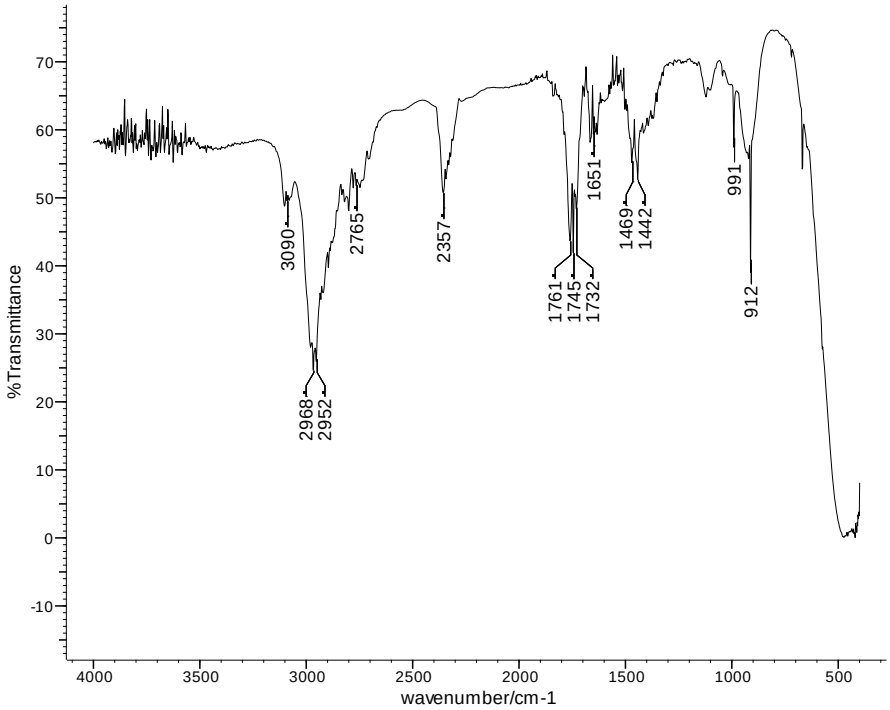

Figure 4.12: FTIR spectrum for fraction 1 collected from the standard foam

Compound	**Peak Wavenumbers/cm^{-1}**
Propene	3090, 2968, 2952, 1651, 1469, 1442, 991, 912
CO_2	2357
Formaldehyde	2765, 1761, 1745, 1732

Table 4.3: Peak assignments for the FTIR spectrum of fraction 1 from the standard foam

The second fraction of volatiles collected during the sub-ambient differential distillation consisted of acetaldehyde and a mixture of C_3H_6O isomers. Again identification has been achieved by MS (Figure 4.13 and Figure 4.14) and FTIR spectroscopy (Figure 4.15).

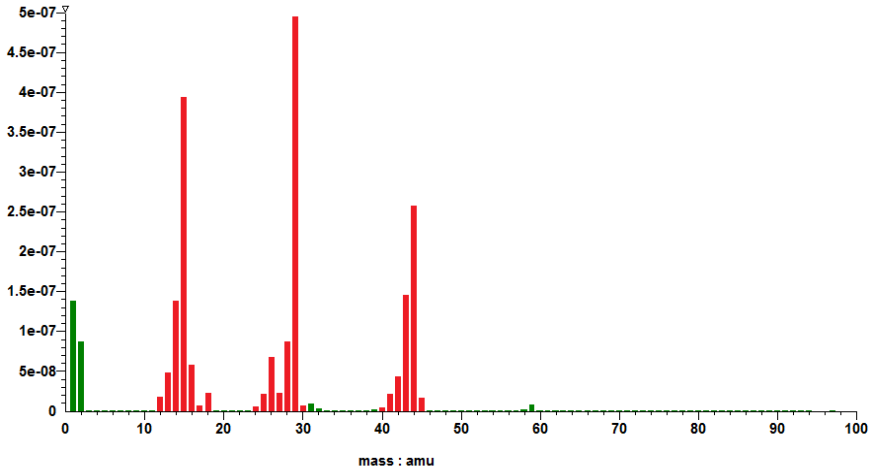

Figure 4.13: Mass spectrum of acetaldehyde

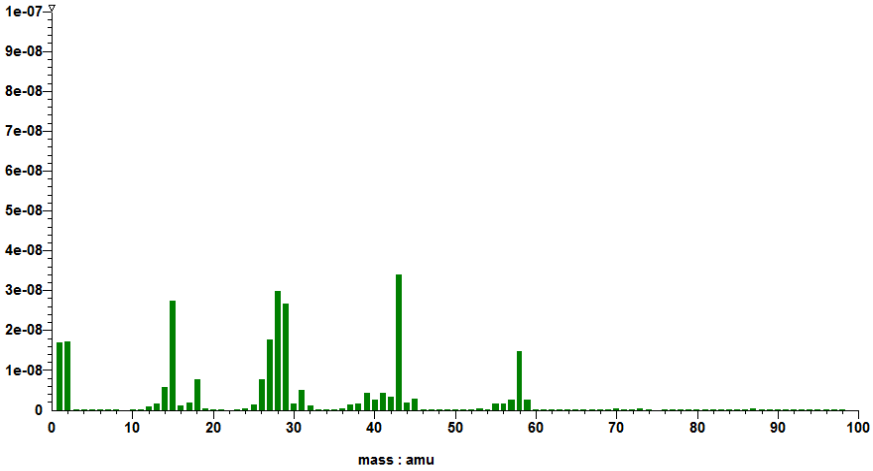

Figure 4.14: Mass spectrum of peak 4 comprised of a mixture of C_3H_6O isomers

The mass spectrum presented in Figure 4.14 has peaks common to a number of polyol-derived species with formula C_3H_6O including propanal, propylene oxide and acetone. It is likely, therefore, that a mixture of these isomers is present. Acetaldehyde is the most dominant species in this fraction; therefore the FTIR spectrum in Figure 4.15 closely resembles that of acetaldehyde.

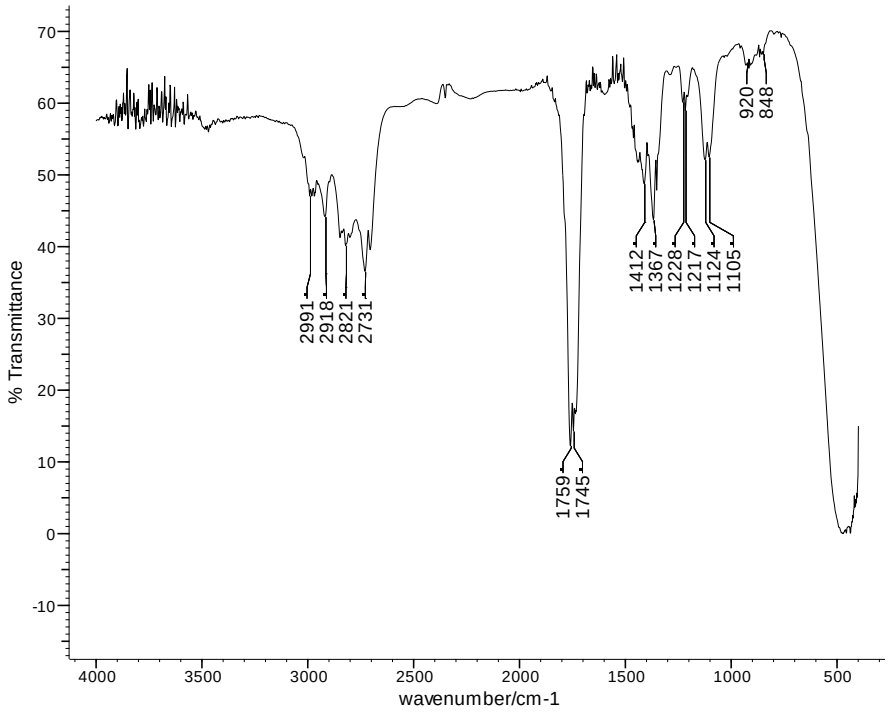

Figure 4.15: FTIR spectrum for fraction 2 collected from the standard foam

The final fraction of volatiles collected from the standard foam consisted of water and higher molar mass species. The mass spectrum for the water peak is presented in Figure 4.16. There are additional peaks present in this spectrum which do not arise from the water and this indicates that co-elution of some high molar mass species has occurred with the water.

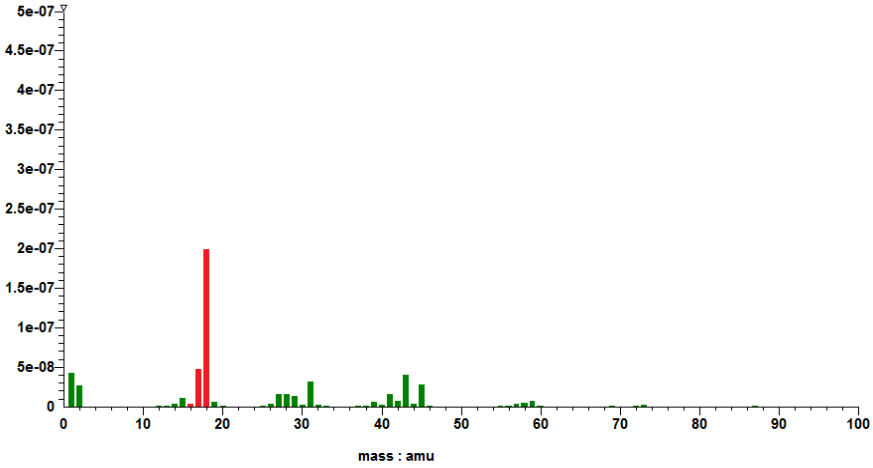

Figure 4.16: Mass spectrum of water

The mass spectrum of the high molar mass species was complex and was indicative of a number of different species co-eluting. The FTIR spectrum for this fraction of volatiles is presented in Figure 4.17. The majority of the peaks are associated with hydroxyl and carbonyl-containing polyol fragments which will have resulted from thermal degradation of the polyol chains.

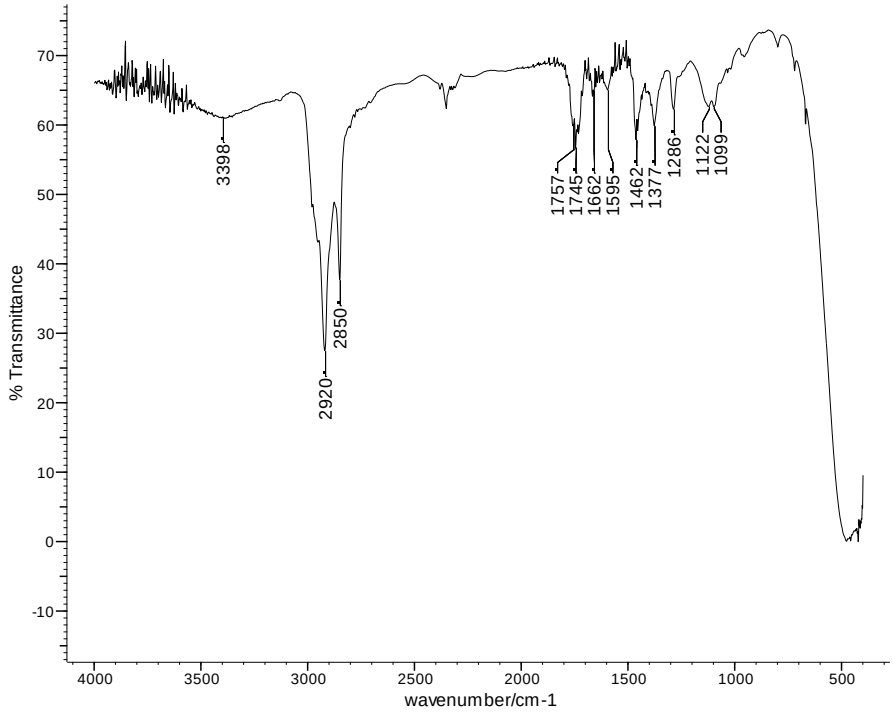

Figure 4.17: FTIR spectrum for fraction 3 collected from the standard foam

GC-MS analysis was also conducted on the third fraction of volatiles and the resultant total-ion chromatogram is presented in Figure 4.18. Several of the main peaks in the chromatogram are due to siloxane breakdown products from the stationary phase within the GC column. The other major peaks in the GC chromatogram correspond to polyol fragments which contain hydroxyl, alkene and carbonyl groups. Complete identification of these species was, however, not possible due to the large number of possible fragments which could result from degradation of the polyol chain by random radical chain scission.

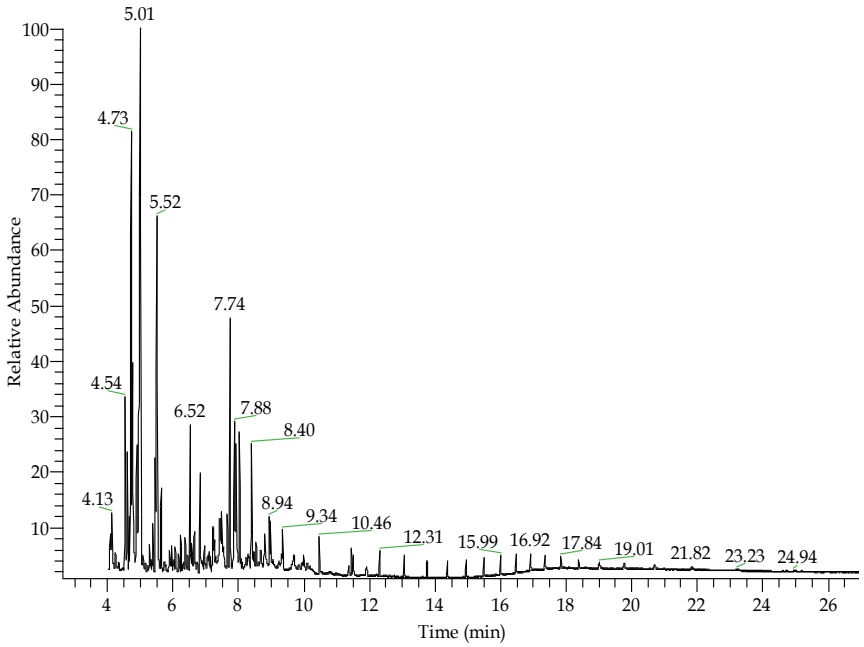

Figure 4.18: GC-MS total-ion chromatogram for fraction 3 from the standard foam

The results from the differential distillation and characterisation of the condensable volatiles, therefore, demonstrate that the major condensable degradation products evolved from the polyurethane foam are propene, CO_2, formaldehyde, acetaldehyde, C_3H_6O isomers (*e.g.* propanal, propylene oxide, acetone) and polyol chain fragments of various structures. All of these products, except for CO_2, are likely to arise from degradation of the polyol component of the foam. CO_2 could arise from degradation of the urethane linkages *via* a six-membered ring transition state or a four-membered ring transition state similar to those shown in Figure 1.24 and Figure 1.25, respectively. CO_2 could also be present as a degradation product if the TDI evolved during the degradation of the urethane linkages undergoes a self-condensation reaction to form carbodiimide.

4.1.3.2 Isothermal TVA Study

In order to further probe the degradation chemistry of the standard foam, isothermal TVA experiments were conducted at 250, 300, 350 and 400°C. These temperatures were chosen to represent the temperature range within which significant degradation of the polymer occurs and to correlate with the pyrolysis studies which will be discussed in

Section 4.2. The full characterisation data for the isothermal TVA studies can be found in Appendix 1.

- ***Isothermal TVA Profiles***

Presented in Figure 4.19 are the TVA curves for the isothermal degradation studies for the standard foam, showing the rate of volatiles evolution as a function of time and furnace temperature. In each case the sample has been heated dynamically at 10°C min^{-1} to the desired temperature after which the sample is held isothermally for 30 minutes.

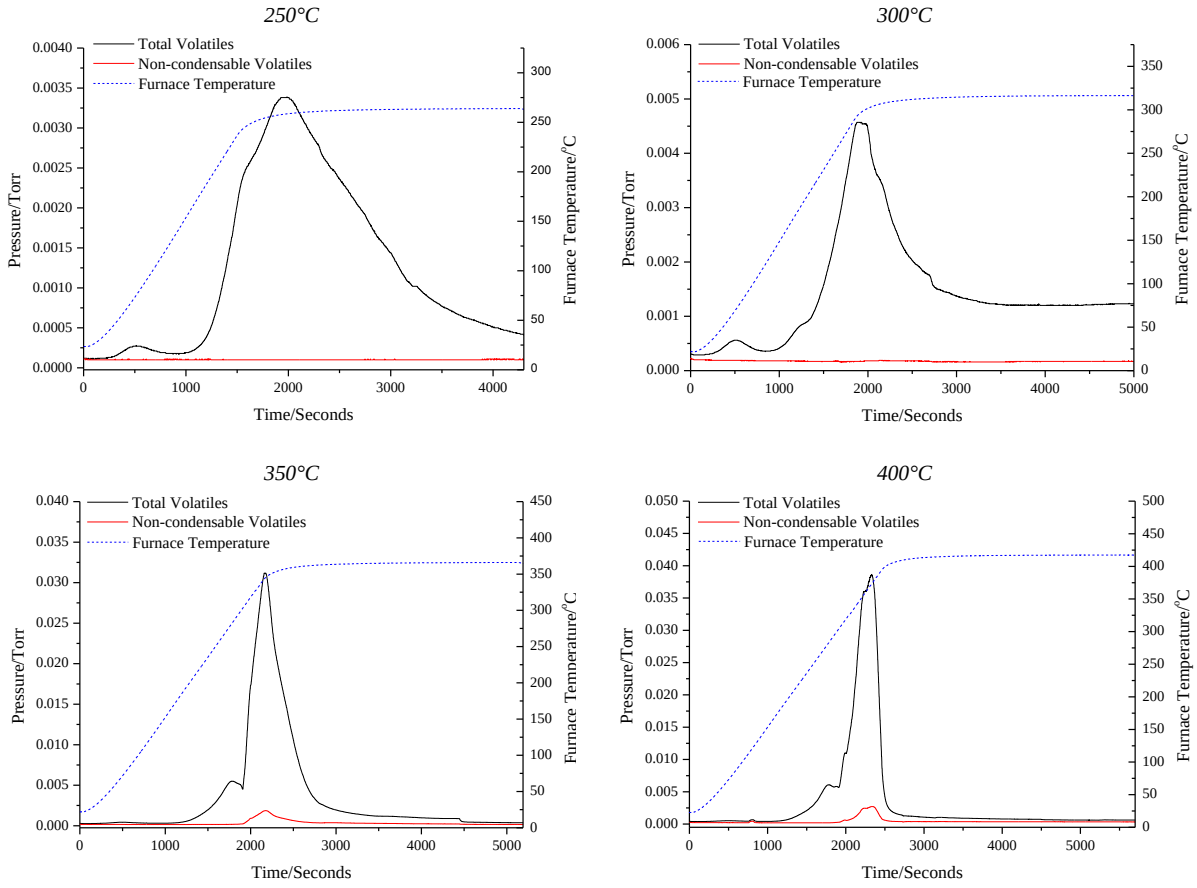

Figure 4.19: Isothermal TVA curves for the standard foam at 250, 300, 350 and 400°C

The TVA profile at 250°C shows only one peak corresponding to the evolution of a low level of degradation products that are volatile at ambient temperature. At this temperature these are most probably the degradation products associated with the primary degradation step of the polyurethane, *i.e.* the degradation of the urethane

linkages. The volatiles may, however, also be associated with the degradation of the polyol component of the foam, if it begins to occur at this temperature. By 300°C there is still only one major peak observed in the TVA profile which indicates that the secondary degradation reactions have not reached their maximum rate at this temperature. There were no non-condensable volatiles detected at 250°C and 300°C which confirms that the degradation reactions which yield CO, methane and hydrogen are not significant at these lower temperatures.

By 350°C a significantly greater level of volatiles are evolved and the second degradation step is now evident. Furthermore, a peak corresponding to the evolution of non-condensable volatiles (methane, CO and hydrogen) is now observed. This indicates that at temperatures between 300 and 350°C degradation of the polyol component of the foam has become significant and the reactions which yield non-condensable material have occurred. This is in agreement with TVA studies conducted by Grassie and Mendoza,[10] Costa *et al.*[11] and Cameron *et al.*[12] which revealed that the thermal degradation of polyether polyols occurs between 300°C and 500°C, depending on the structure of the polyol. The TVA profile at 400°C shows little difference to that at 350°C.

- ***Cold-ring Fraction Analysis***

At 250°C a small amount of white, cloudy cold-ring fraction was observed. This was swabbed with chloroform and analysed by FTIR spectroscopy and GC-MS, however, due to the small amount of cold-ring fraction present the spectra were weak and showed no major peaks of interest. At 300°C the amount of cold-ring fraction collected was still small; however, the FTIR and GC-MS spectra showed peaks corresponding to TDI and polyol-based degradation products.

By 350°C the cold-ring fraction was more significant and was identified as consisting of TDI and polyol-based degradation products, with similar results obtained for that at 400°C. These results reveal that volatilisation of polyol-based degradation products

occurs as low as 300°C, which in turn indicates that degradation of the polyol also begins to occur at this temperature.

- ***Residue Analysis***

During the isothermal degradation of the standard foam it was observed that the foam structure collapsed into a clear liquid which was recovered from the base of the TVA tube following the degradations at 250, 300 and 350°C. These liquid residues were soluble in chloroform and were expected to primarily consist of polyol or polyol-based material which had been regenerated during the thermal degradation of the standard foam. There was no residue remaining at 400°C which indicates that the foam has degraded completely by this temperature. Presented in Figure 4.20 is the FTIR spectrum of the residue collected from the standard foam at 250°C.

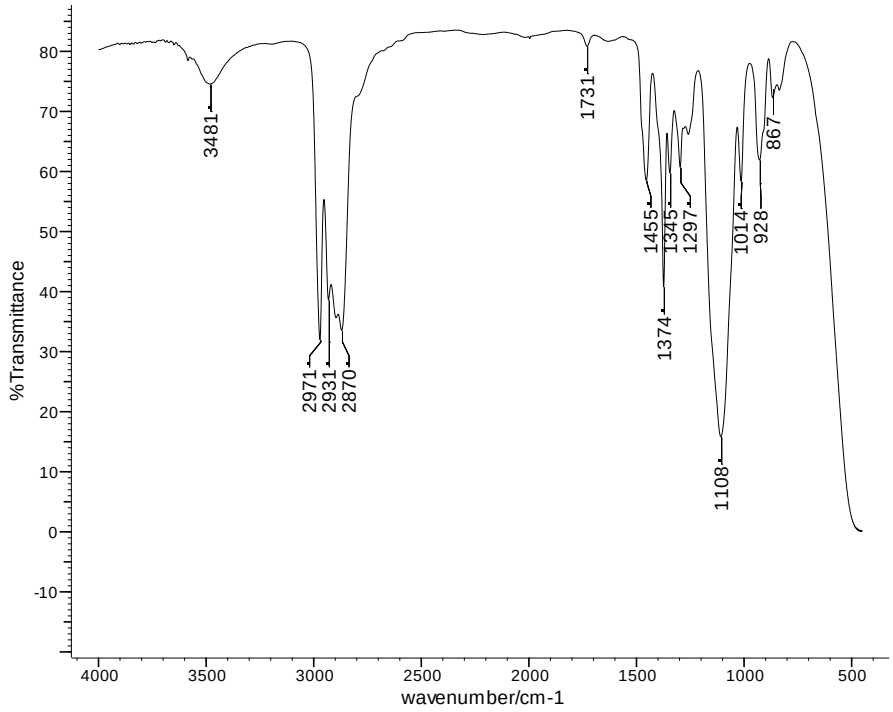

Figure 4.20: FTIR spectrum of the residue collected from the standard foam following the isothermal TVA at 250°C

The majority of the peaks are associated with structures which resemble the polyether polyol component of the foam, as was expected to be the case. Comparison of the FTIR

spectrum with that of the neat polyol (Figure 4.21) confirms that the residue consists of regenerated polyol. The spectrum of the residue is identical to that of the polyol expect for the additional small peak corresponding to carbonyl groups at 1731 cm^{-1}, which indicates the presence of residual urethane linkages within the residue at 250°C.

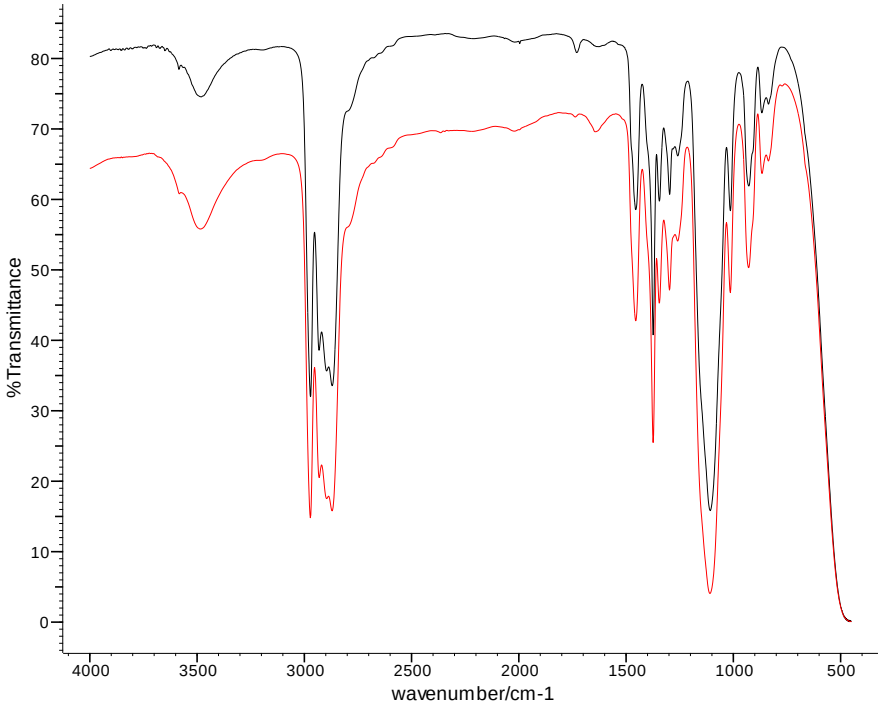

Figure 4.21: Comparison of the FTIR spectra for the residue collected from the standard foam following the TVA isothermal at 250°C (black) and the neat polyol (red)

The residues at 300°C and 350°C are identical to that at 250°C, consisting of polyol regenerated during the primary degradation step. Carbonyl groups are still present within the residue at 350°C as indicated by the peak at 1729 cm^{-1}; however, by this temperature it is expected that all of the urethane linkages within the residue will have fully degraded. It is, therefore, proposed that the residue now consists of degraded polyol which contains carbonyl groups within its structure.

These results are in correlation with those presented by Ravey and Pearce[5] which showed that during the primary degradation step of polyurethane the residue obtained

was identical to the source polyol with small additional peaks corresponding to residual urethane linkages within the residue.

NMR spectroscopy was also performed on the residues obtained from the standard foam. Presented in Figure 4.22 is a comparison of the ^{1}H NMR spectra for the residue recovered following the isothermal TVA at 250°C and the neat polyol.

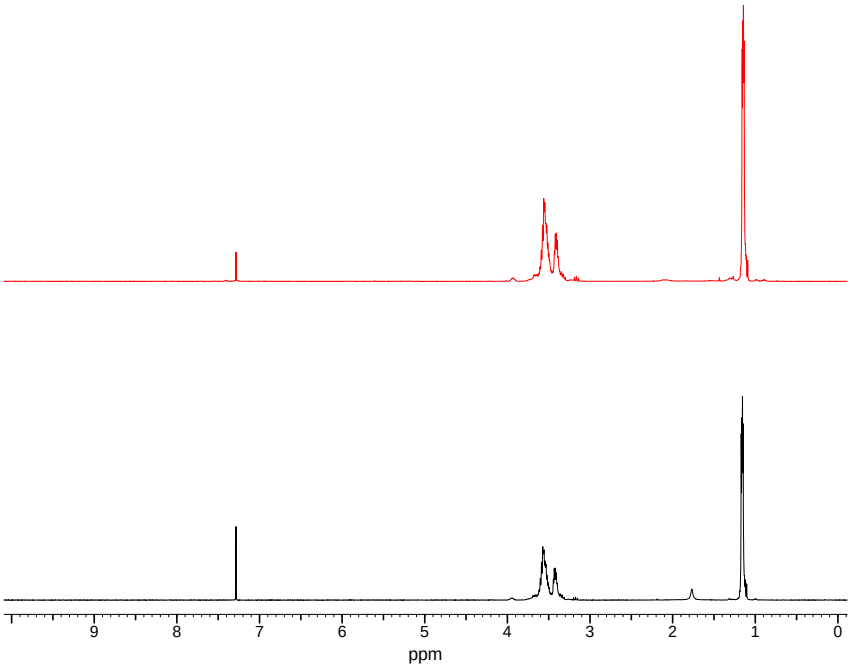

Figure 4.22: Comparison of the ^{1}H MR spectra for the residue at 250°C (black) and the neat polyol (red)

It can be observed that the spectrum for the residue at 250°C is almost identical to that of the neat polyol. The signal at 1.1 ppm can be assigned to the polyol methyl groups, the signals between 3 and 3.7 ppm to the CH and CH_2 groups within the polyol and the small peak at 3.9 ppm to the hydroxyl groups. The additional peak at 1.8 ppm in the spectrum of the residue is believed to result from low levels of water present within the residue. The NMR data, therefore, confirms that the residue consists of regenerated polyol. The NMR spectra for the residues at 300°C and 350°C were identical to the spectrum at 250°C.

- ***Condensable Fraction: Sub-ambient Differential Distillation and Characterisation***

The condensable fractions collected during each isothermal experiment were separated by sub-ambient differential distillation into four fractions which were subsequently analysed by FTIR spectroscopy, online MS and GC-MS. The sub-ambient differential distillation traces, presented in Figure 4.23, provide a qualitative indication of the volatile degradation products evolved at the different degradation temperatures. The temperature ranges of the fractions collected and the identity of the products within each fraction are presented in Table 4.4.

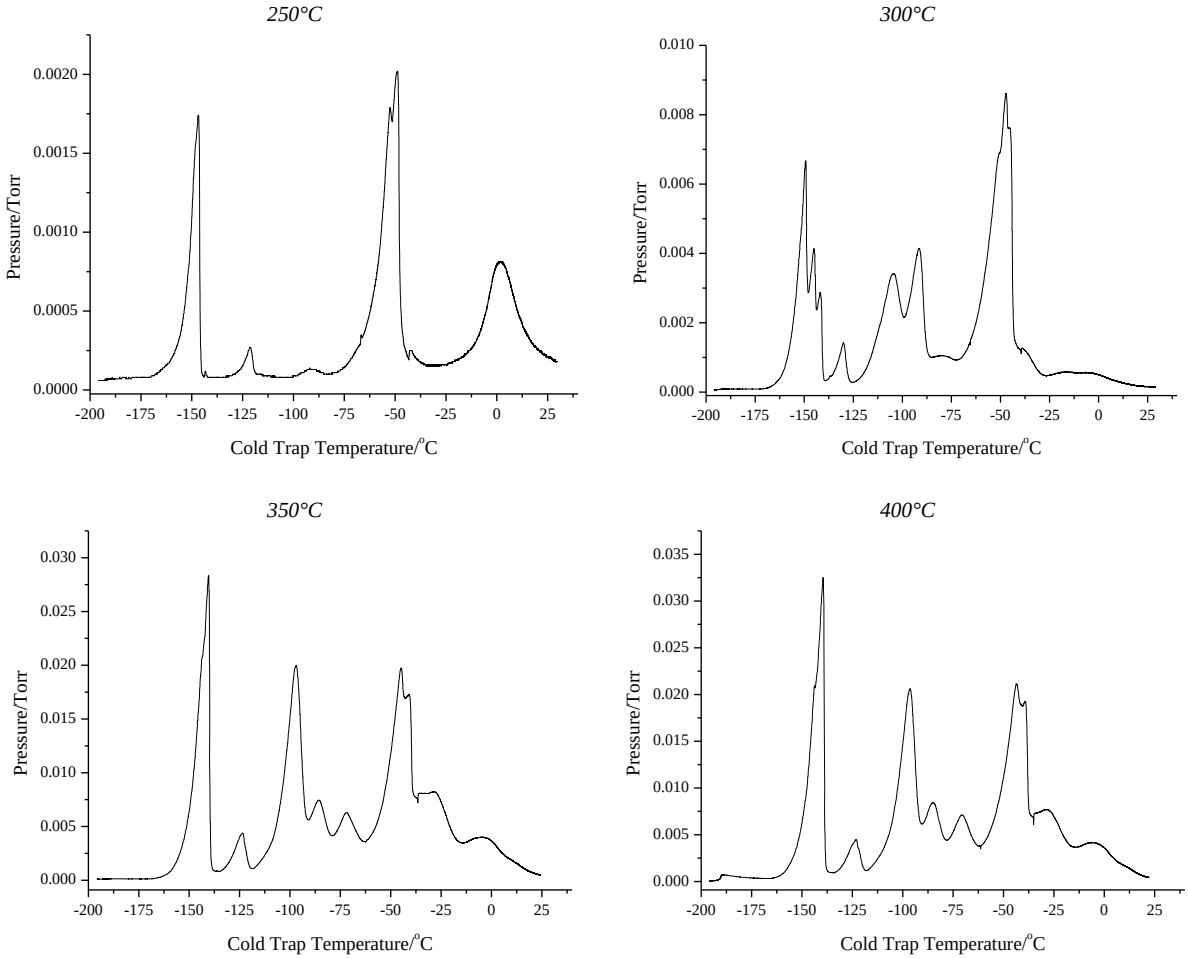

Figure 4.23: Sub-ambient differential distillation trace for the condensable fractions collected from the isothermal TVA studies on the standard foam

Fraction Temperature Range	**Product Identification**			
	250°C	**300°C**	**350°C**	**400°C**
-196°C to -140°C	CO_2	Propene, CO_2	Propene, CO_2	Propene, CO_2
-140°C to -60°C	Acetaldehyde, C_3H_6O isomers	Formaldehyde, acetaldehyde, C_3H_6O isomers	Formaldehyde, acetaldehyde, C_3H_6O isomers	Formaldehyde, acetaldehyde, C_3H_6O isomers
-60° to -40°C	Water	Water	Water and high molar mass polyol fragments	Water and high molar mass polyol fragments
-40°C to 25°C	High molar mass polyol fragments, TDI	High molar mass polyol fragments, TDI	High molar mass polyol fragments	High molar mass polyol fragments

Table 4.4: Sub-ambient differential distillations fractions collected from the isothermal TVA studies

It can be observed from Figure 4.23 that as the isothermal degradation temperature is increased greater quantities of condensable volatiles are evolved, and the product distribution becomes increasingly more complex. At 250°C the main products observed are CO_2, water and higher molar mass species including TDI. Low levels of acetaldehyde and C_3H_6O isomers are also observed at this temperature. This is the temperature at which degradation of the urethane linkages is proposed to occur, therefore, the presence of CO_2 and TDI indicate that there are two competing degradation mechanisms occurring for the urethane linkages within the standard foam. The presence of acetaldehyde and C_3H_6O isomers at this temperature is surprising; indicating that degradation of the polyol has begun to occur at 250°C. These volatiles are, however, only observed at a low level which suggests that the polyol degradation has not yet become significant.

By 300°C the sub-ambient differential distillation trace is more complex, with additional degradation products such as formaldehyde and propene now being observed. At 350°C the level of condensable volatiles evolved is significantly greater than at the lower temperatures which is indicative of significant polyol degradation occurring. This is in

agreement with the TVA profile presented previously in which the secondary degradation peak was evident at 350°C. There is no difference in the products distribution at 350°C and 400°C which indicates that no new degradation reactions which yield volatile material occur at 400°C.

4.1.4 Summary and Proposed Mechanisms of Degradation

The results from the TVA, TGA and DSC analysis show that the standard foam undergoes a two stage degradation process under both oxidative and inert atmospheres. The first stage can be attributed to degradation of the urethane linkages whilst the second stage is associated with secondary degradation reactions. Thermal degradation under nitrogen and helium occurs over the temperature range 260-400°C, whilst under vacuum the degradation occurs at a lower temperature as volatilisation of the degradation products is facilitated under vacuum. The TGA results revealed that the temperature at which the primary degradation step occurs is not significantly altered in an oxidative environment, however, the secondary degradation processes do occur at lower temperatures. This indicates that the secondary degradation reactions, such as degradation of the polyol, are altered in the presence of oxygen.

The dynamic TVA results revealed that both isomers of TDI were present in the cold-ring fraction which confirms that degradation of the urethane linkage within the foam occurs primarily *via* a depolymerisation reaction to yield the original monomers, as illustrated in Figure 4.24.

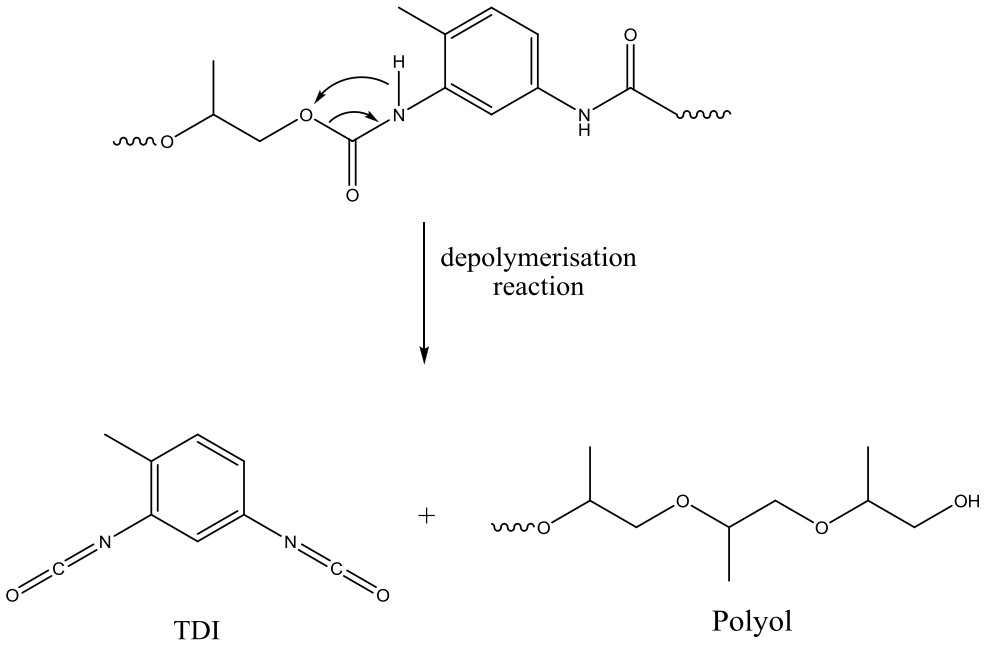

Figure 4.24: Degradation of the urethane linkage by a depolymerisation reaction

The presence of CO_2, however, suggests that a second mechanism may be operating. CO_2 could arise from degradation of the urethane linkage *via* either a six-membered ring transition state or a four-membered ring transition state similar to those shown in Figure 1.24 and Figure 1.25, respectively. Both of these mechanisms lead to the formation of amines, however, no amines were identified during the analysis. It is likely that if these amines are produced they will react in the vapour phase with the regenerated TDI to form a polyurea as was observed by Ravey and Pearce.[5] A pale white waxy solid which was insoluble in most common solvents was recovered during the analysis of the standard foam and the FTIR spectrum of this material, presented in Figure 4.25, confirms that it is a polyurea. The peak at 1634 cm^{-1} corresponds to carbonyl stretching and the peak at 1544 cm^{-1} corresponds to N-H stretching. The structure of this compound will be mainly aromatic but the peaks expected at 3000 cm^{-1} are obscured by the broad N-H peak at 3329 cm^{1}. However, the aromatic skeletal ring vibrations can be observed at 1594 cm^{-1}. The small peak at 2272 cm^{-1} suggests some residual isocyanate groups are also present.

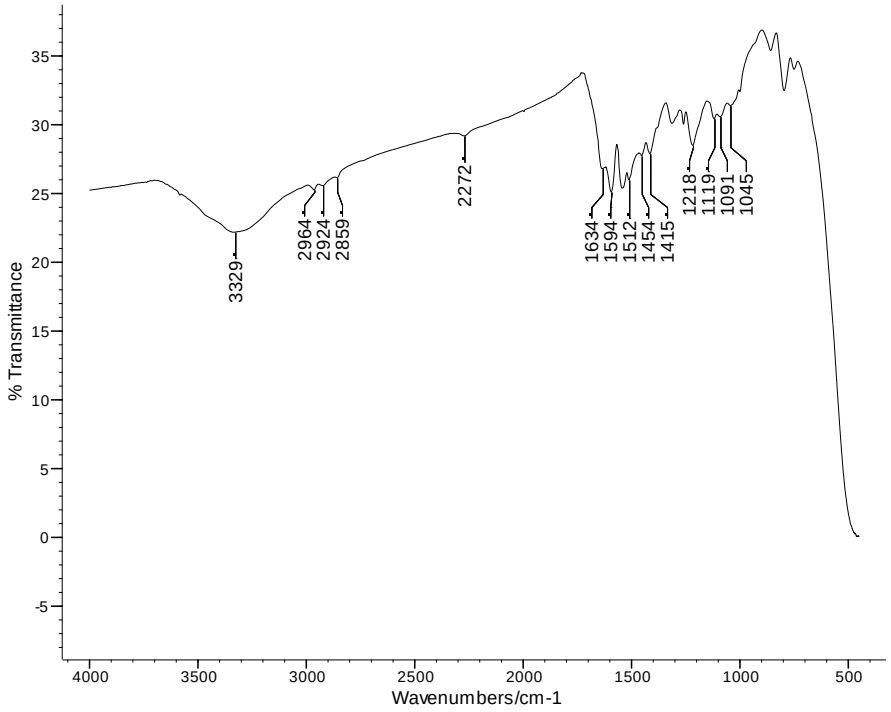

Figure 4.25: FTIR spectrum of the insoluble solid recovered from the standard foam

The presence of polyurea, therefore, confirms that amines were evolved during the degradation of this foam and this, in conjunction with the presence of CO_2, confirms that the urethane linkage degrades *via* both a depolymerisation reaction to yield TDI and polyol and a dissociation reaction to yield diaminotoluene (DAT), CO_2 and an alkene terminated polyol chain, as shown in Figure 4.26.

CO_2 could also be present as a degradation product if the TDI which is evolved during degradation of the urethane linkages undergoes a self-condensation reaction to form carbodiimide. This reaction has been widely reported during the thermal degradation of MDI-based polyurethanes[7,8,13,14] with insoluble residues being recovered as a result. There was no evidence of carbodiimide formation during the TVA of the standard foam; therefore, it is unlikely that carbodiimide formation is the source of the CO_2. The absence of carbodiimide during the TVA of the standard foam is proposed to be a result of the greater volatility of the TDI under vacuum compared to the MDI. TDI has a lower molar mass than MDI and volatilisation into the cold-ring fraction will occur more

readily. The self-condensation reaction is, therefore, less likely to occur during the degradation of a TDI-based foam.

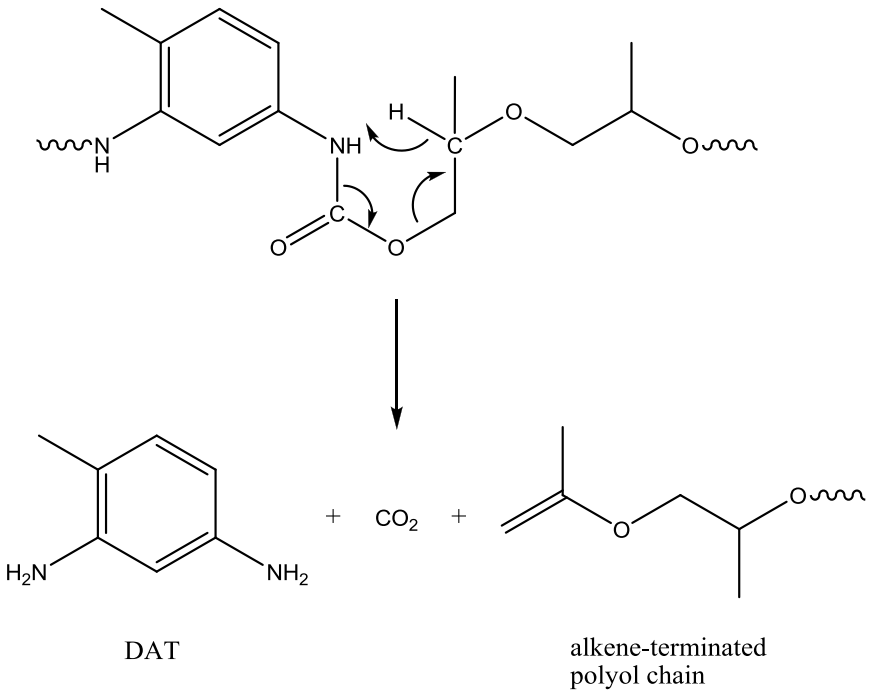

Figure 4.26: Dissociation of the urethane linkage *via* a six-membered ring transition state to yield DAT, CO_2 and an alkene-terminated polyol chain

The second degradation step can be attributed to secondary degradation reactions, in particular degradation of the polyol or alkene-terminated polyol chain which was regenerated during the primary degradation processes. The major condensable degradation products identified by TVA were propene, CO_2, formaldehyde, acetaldehyde, C_3H_6O isomers (*e.g.* propanal, propylene oxide, acetone) and polyol chain fragments of various structures. These products all arise from degradation of the polyol component of the foam, except for CO_2 which arises in the first degradation step as explained above. It is proposed that degradation of the polyol occurs by random radical chain scission of the C-C and C-O bonds in the polymer backbone at the points shown in Figure 4.27 to yield the major condensable products. Degradation of the polyol component also leads to the formation of the non-condensable volatiles (methane, CO and hydrogen) which were observed during the TVA of the standard foam.

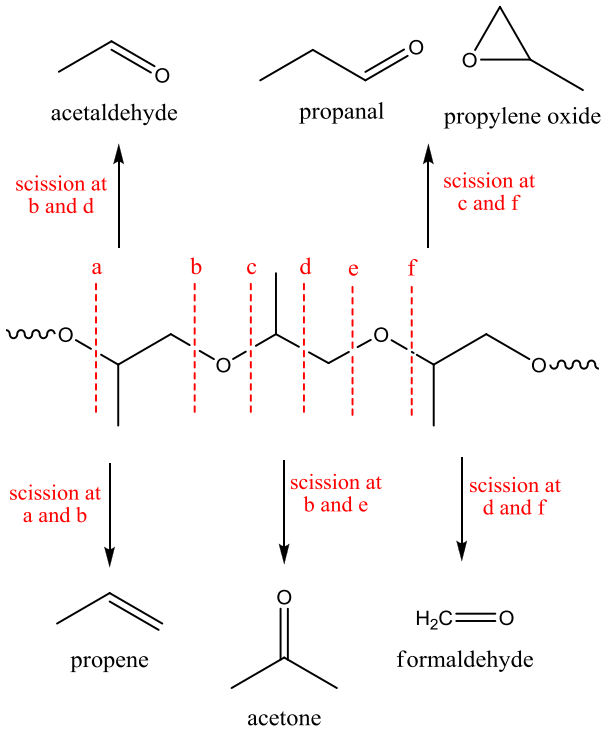

Figure 4.27: Points of scission in the polyol chain which form the major condensable products

The results from the isothermal TVA studies provide further insight into the degradation processes occurring within the standard foam. The presence of TDI and a polyol residue at 250°C confirms that degradation of the urethane linkages occurs *via* a depolymerisation. The presence of CO_2 at this temperature, however, indicates that the urethane linkages also degrade by dissociation *via* the six-membered ring or four-membered ring transition states, which were discussed in Section 1.5.3.1.1. There are, however, very few reports in the literature concerning the four-membered ring transition state occurring to any great extent. It is, therefore, most likely that the CO_2 arises from degradation of the urethane linkages *via* the six-membered ring transition state. This mechanism would lead to collapse of the foam to a liquid residue consisting of alkene-terminated polyol chains. Analysis of the residues recovered from the standard foam, however, showed no peaks corresponding to C=C groups within the residue. It is, therefore, proposed that degradation of the urethane linkages *via* a depolymerisation reaction to yield TDI and polyol is the predominant reaction which occurs for the

standard foam, which is in agreement with a number of studies published previously on the thermal degradation of polyurethane.[7,15,16] The second, competing mechanism is proposed to be less significant for this particular polyurethane system.

In addition to providing further information regarding the mechanism of degradation of the urethane linkages, the isothermal TVA studies also revealed more information regarding the degradation of the polyol component of the foam. The TVA profiles revealed that the second pressure peak, corresponding to the evolution of volatiles from thermal degradation of the polyol, and the non-condensable volatiles were not evident until temperatures above 300°C. The cold-ring fractions, on the other hand, showed the presence of high molar mass polyol species at 300°C and characterisation of the condensable volatiles revealed low levels of polyol-derived volatiles such as acetaldehyde and formaldehyde at 250°C and 300°C. Considering these results together it is, therefore, proposed that degradation of the polyol component of the foam under vacuum begins at temperatures as low as 250°C but does not yield a significant level of volatile material until temperatures higher than 300°C. The TVA degradation profile of the neat polyol (see Appendix 1) confirms this, with the evolution of volatile material commencing at ~240°C but not reaching a maximum rate until 350°C.

4.2 Pyrolysis Studies

Pyrolysis studies were conducted on the standard foam in order to further probe the degradation behaviour of the polyurethane under both oxidative and non-oxidative environments. Similar to the TVA experiments, a wealth of information can be gained from pyrolysis studies including mass loss data and characterisation of cold-ring fractions and residues. The pyrolysis studies, however, differ from the TVA experiments in that the degradation is not conducted under vacuum, which could be deemed more representative of a fire situation. Furthermore, different gases can be employed during the pyrolysis allowing the degradation to be studied under a variety of environments. Finally, the pyrolysis studies allow the use of significantly larger samples which leads to the generation of greater quantities of char material, allowing

characterisation of this material to be achieved. Char formation is one of the most important condensed-phase mechanisms for modifying the combustion process of a polymer and by studying the structure of the chars formed during the degradation information can be gained with regards to the condensed-phase behaviour of the polyurethane. The pyrolysis of the standard foam was studied under three different environments: nitrogen, air and 3% oxygen in nitrogen. The full characterisation data for the pyrolysis studies can be found in Appendix 1.

4.2.1 Pyrolysis under Nitrogen

4.2.1.1 Mass Loss Data and Observations

Presented in Table 4.5 are the residues obtained, calculated as a percentage of the original sample mass, after pyrolysis of the standard foam under a nitrogen environment. The quantities of residue obtained are the averages which have been calculated from the four repeat analyses.

Pyrolysis Temperature/°C	**Residue/Mass%**
250	98
300	75
350	39
400	15

Table 4.5: Residues obtained for the standard foam after pyrolysis under nitrogen

A plot of the quantity of residue obtained as a function of the pyrolysis temperature is presented in Figure 4.28. It can be observed that as the pyrolysis temperature is increased the mass loss increases and the quantity of residue decreases. This is indicative of degradation occurring to a greater extent at the higher temperatures which leads to larger quantities of volatile material being evolved.

Very little mass loss occurs at 250°C which indicates that only a small quantity of volatile material has been evolved at this temperature. There was no visible discolouration or degradation of the foam at this temperature and extraction of the

sample with chloroform did not yield any tarry material. This is the temperature at which the urethane bonds within the material are reported to begin to degrade; however, these results suggest that a significant level of scission has not occurred at this temperature. This is in correlation with the results from the TGA and DSC analysis which showed that degradation of the standard foam in an inert environment did not become significant until temperatures greater than 250°C.

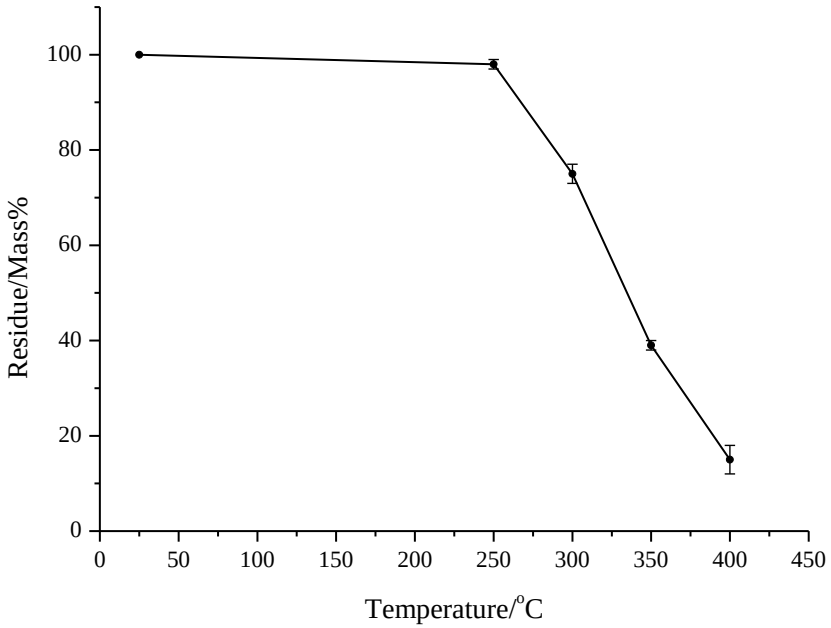

Figure 4.28: Residue obtained vs. pyrolysis temperature for the standard foam under nitrogen

As the pyrolysis temperature was increased the foam became darker in colour and by 400°C the foam appeared black and highly charred, indicating that significant degradation of the polyurethane had occurred. This correlates with the mass loss data which shows that by 400°C 85% of the foam has been converted into volatile material.

4.2.1.2 Cold-ring Fraction Analysis

During the pyrolysis a "cold-ring" type fraction consisting of high molar mass material which had volatilised from the sample was deposited at the top of the sample tubes. This was removed by swabbing with chloroform and analysed by FTIR spectroscopy and GC-MS. As was mentioned above, during the pyrolysis at 250°C very little mass

loss had occurred. There was, therefore, little cold-ring in the tube at this temperature and the GC-MS and FTIR spectroscopy analysis showed no significant peaks of interest. At all other temperatures a cold-ring fraction was deposited which consisted of two components: a white wax-like insoluble residue and a yellow/orange chloroform soluble residue. The FTIR spectrum of the white insoluble component of the cold-ring fractions was similar to that obtained during the TVA study, showing peaks consistent with a polyurea structure. This indicates that amines were also evolved during the pyrolysis of the standard foam.

Presented in Figure 4.29 is the FTIR spectrum of the yellow/orange chloroform soluble component of the cold-ring fraction collected from the standard foam after pyrolysis at 300°C.

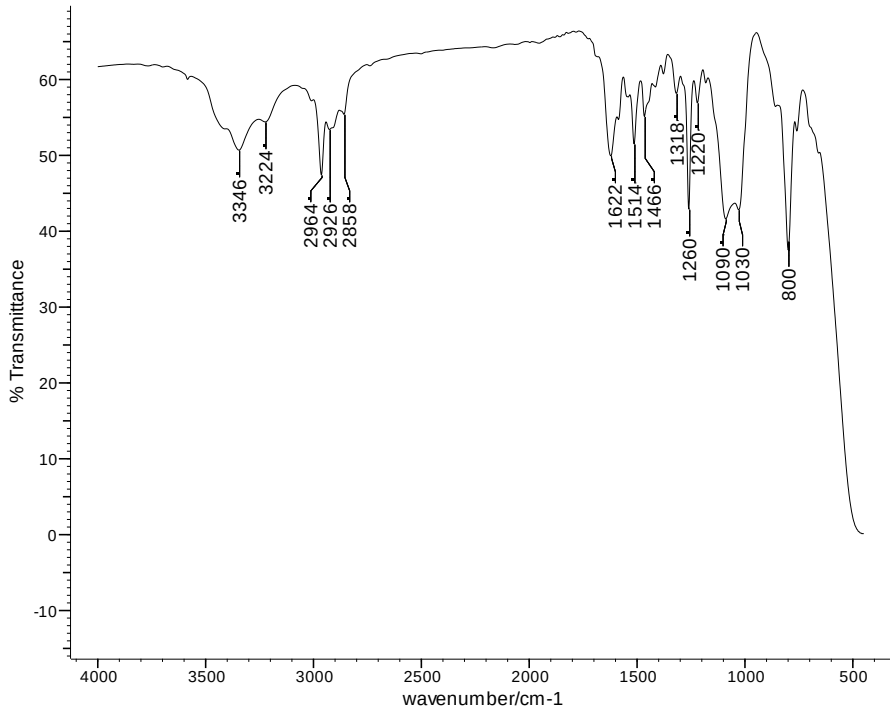

Figure 4.29: FTIR spectrum of the cold-ring fraction obtained from the standard foam after pyrolysis under nitrogen at 300°C

The FTIR spectrum shows peaks corresponding to ether-containing fragments and aromatic amines. The aromatic amine peaks suggest that DAT may be produced during

the pyrolysis of the standard foam and the ether-containing fragments are likely to be higher molar mass fragments produced from degradation of the polyol component of the foam.

By 400°C the FTIR spectrum of the cold-ring fraction, presented in Figure 4.30, has a number of peaks which correspond to structures resembling the polyol component of the foam. In addition, the peak at 1727 cm^{-1} indicates the presence of carbonyl-containing compounds within the cold-ring. It is, therefore, proposed that by 400°C the cold-ring fraction is composed mainly of high molar mass polyol fragments, some of which contain carbonyl groups within their structure.

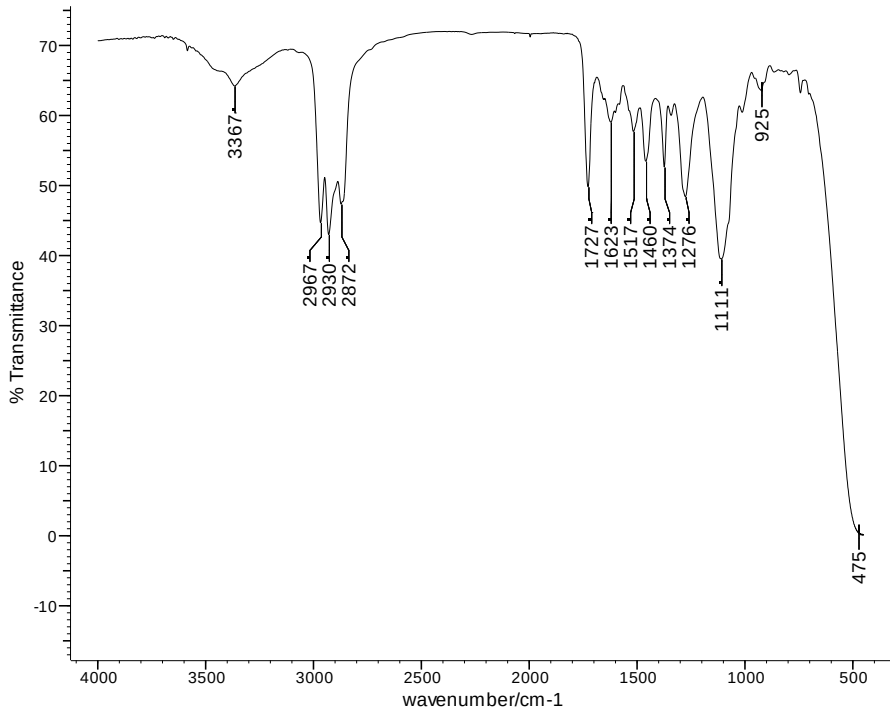

Figure 4.30: FTIR spectrum of the cold-ring fraction collected from the standard foam after pyrolysis under nitrogen at 400°C

GC-MS analysis was also conducted on the chloroform soluble cold-ring fractions collected from the standard foam and complex chromatograms were obtained. Presented in Figure 4.31 is an example total-ion chromatogram for the standard foam which is representative of the cold-ring fractions collected. The large peak at a retention time of

10.33 minutes has been positively identified as DAT, whilst smaller peaks at 9.70 minutes and 9.74 minutes have been identified as 2,6-TDI and 2,4-TDI, respectively. The remainder of the peaks correspond in the most part to high molar mass polyol chain fragments sharing common m/z fragments. Due to the large number of possible products which could be derived from the polyol chain complete identification of these species was not possible. There were also a small number of peaks which could not be definitively identified but library searches suggest nitrogen-containing aromatic compounds.

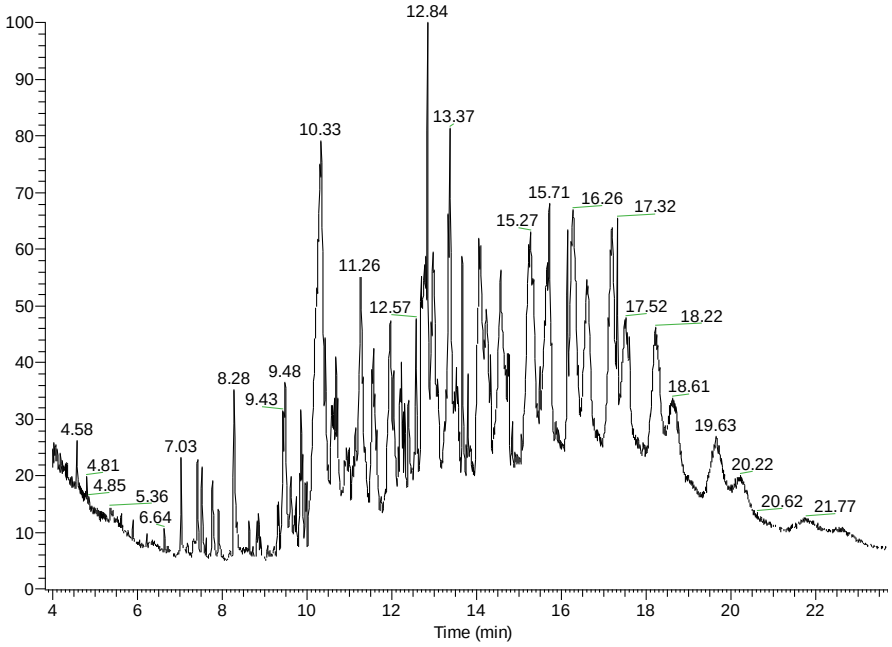

Figure 4.31: GC-MS total-ion chromatogram for the cold-ring fraction collected from the standard foam after pyrolysis under nitrogen at 350°C

The presence of polyurea and DAT within the cold-ring fractions is significant as this gives further insight into the thermal degradation mechanisms of the standard foam. As has been discussed previously the urethane linkages can degrade *via* a depolymerisation reaction to yield isocyanate and polyol, or *via* six-membered or four-membered ring transition states to yield primary or secondary amines. It has been reported in many cases that the depolymerisation reaction is the predominant degradation mechanism,[7,15,16] however, it has been shown that if the diisocyanate cannot volatilise

from the system it will become trapped within the pyrolysis zone and the polyol and isocyanate can recombine to reform the urethane bond.[5,16] In this situation the slower, irreversible reaction *via* a six-membered ring transition state becomes favoured and a primary amine would be produced.

The TVA studies revealed the predominant degradation mechanism of the urethane linkages within the standard foam to be depolymerisation to yield isocyanate and polyol. The TVA technique operates under a vacuum of approximately 10^{-4} Torr and the volatiles are pumped from the degrading polymer system. The pyrolysis studies, on the other hand, are conducted at atmospheric pressure (760 Torr); therefore, degradation of the sample in the pyrolysis system occurs at pressures which are seven orders of magnitude higher compared to the TVA system. Degradation in the pyrolysis system is, therefore, a higher pressure, more confined situation and this will have an effect on the reactions which occur. Under vacuum it is proposed that degradation of the urethane linkages *via* the depolymerisation reaction occurs at a faster rate than the cyclic mechanism. When the depolymerisation reaction occurs to yield the monomers the high vacuum facilitates the volatilisation of the TDI into the cold-ring fraction. Loss of TDI from the degrading polymer system drives the equilibrium in the forward direction and makes it less likely for the TDI and polyol to recombine in the reverse reaction.

In the pyrolysis experiments at atmospheric pressure DAT is observed as a major degradation product and it is proposed that the higher pressure, more confined situation changes the balance of the depolymerisation-polymerisation equilibrium such that the reverse reaction (recombination of the polyol and TDI) occurs to a greater extent than was the case under vacuum. In this situation the six-membered ring transition state mechanism, which is irreversible, then begins to dominate to yield the DAT, CO_2 and alkene terminated polyol chains. The higher pressure conditions, therefore, appear to have a significant effect on the mechanism by which the urethane linkages degrade, causing the usually slower, irreversible six-membered ring transition state reaction to become the predominant mechanism. This is in agreement with the work of Ravey and

Pearce[5] and Erickson[6] who found that TDI-based foams yielded isocyanate when thermally degraded in an unconfined environment, however, under confined conditions DAT was released in larger amounts. Ravey and Pearce also proposed that the DAT can react in the vapour phase with any isocyanate released to form a polyurea aerosol.[5] It is, therefore, proposed that a similar reaction occurs in this system to yield the white polyurea residue observed in the cold-ring fraction.

4.2.1.3 Residue Analysis

The residues which remained in the aluminium sample holder were comprised of a chloroform soluble component (tar) and an insoluble component (char). These components were separated as described in section 3.5.4 to allow for further analysis. The tar was analysed by FTIR spectroscopy, whilst the char was characterised by elemental analysis, solid-state ^{13}C NMR and FTIR spectroscopy. No discolouration was present in the residue obtained after pyrolysis at 250°C and extraction of this sample with chloroform did not yield any tar. The residues at all other temperatures yielded both tar and char.

4.2.1.3.1 Quantification of the Tar and Char

Presented in Table 4.6 are the quantities of char and tar, calculated as a percentage of the total residue collected, for the standard foam after pyrolysis under nitrogen.

Temperature/°C	**Tar/% of residue**	**Char/% of residue**
250	0	100
300	82	18
350	71	29
400	40	60

Table 4.6: Quantities of tar and char obtained as a percentage of the residue collected

At 250°C there was no tar collected and the residue consisted entirely of insoluble material. This was not unexpected as the previous results have shown that very little degradation had occurred at this low a temperature. It can be observed that the sample pyrolysed at 300°C produced significantly more tar than char, and as the pyrolysis

temperature was increased the level of tar within the residue began to decrease as the foam became more charred in nature. The tar is comprised of the chloroform soluble components of the residue and is expected to primarily contain regenerated polyol or polyol-based material. The level of tar was, therefore, expected to decrease as the pyrolysis temperature increased due to degradation and volatilisation of the polyol component.

4.2.1.3.2 Analysis of the Tar

Presented in Figure 4.32 is the FTIR spectrum for the tar obtained from the standard foam at 300°C.

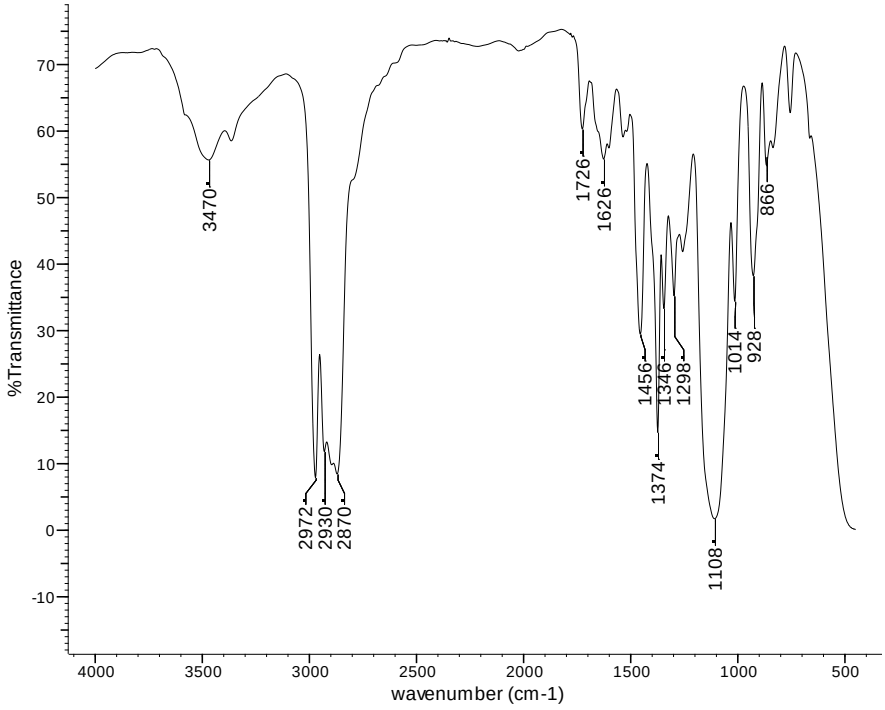

Figure 4.32: FTIR spectrum of the tar extracted from the standard foam after pyrolysis at 300°C under nitrogen

The majority of the peaks are associated with structures which resemble the polyether polyol component of the foam; this is confirmed by comparison with the FTIR spectrum of the polyol as shown in Figure 4.33. The spectra are almost identical; however, there are peaks in the FTIR spectrum of the tar which are not present in the polyol spectrum. In particular, the peaks at 1626 cm^{-1} and 928 cm^{-1} indicate that unsaturation is present

whilst the peak at 1726 cm^{-1} indicates the presence of carbonyl groups within the tar. This suggests that the tar does not simply consist of regenerated polyol but instead consists of polyol which has degraded to some extent. This is confirmed by the appearance of the tar which is brown in colour whereas the undegraded polyol is colourless. The carbonyl groups could be present due to degradation of the polyol; however, they could also be carbonyl groups within urethane linkages which would suggest that some residual urethane links are present within the tar at 300°C.

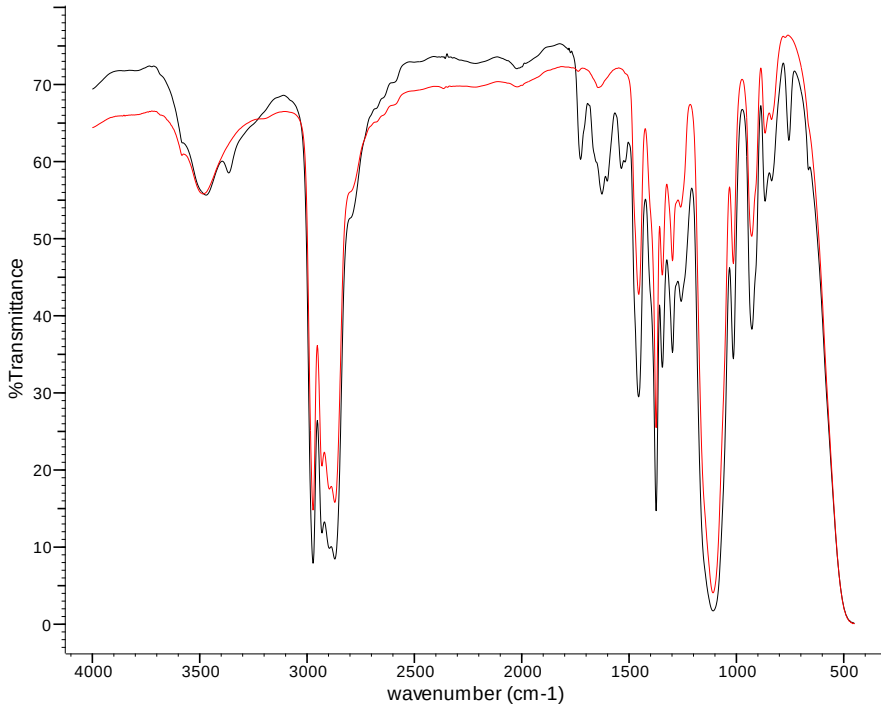

Figure 4.33: Comparison of the FTIR spectrum of the tar from the standard foam after pyrolysis under nitrogen at 300°C (black) and Alcupol F-5611 (red)

The presence of C=C peaks is significant as this gives further insight into the mechanisms by which the urethane linkages are degrading. As was discussed previously, degradation of the urethane linkage by a six-membered ring mechanism would yield an amine as the major degradation product instead of the isocyanate. If this was the case, then the residue which remained would resemble the polyol but with an unsaturated end group. The presence of unsaturation within the tar, therefore, supports the earlier proposal that under confined pyrolysis conditions the standard foam is undergoing thermal degradation primarily *via* a six-membered ring transition state to

yield DAT, CO_2 and alkene terminated polyol chains. This is once again in contrast to the results obtained when the foam was degraded under the less confined conditions of TVA.

The FTIR spectra of the tars collected from the standard foam at 350°C and 400°C showed no major differences compared to that at 300°C which indicates that although the quantity of tar decreases as the temperature is increased, the structure remains similar.

4.2.1.3.3 Analysis of the Char

Presented in Figure 4.34 are photographs of the chars collected from the pyrolysis of the standard foam under nitrogen.

Figure 4.34: Photographs of the chars collected from the standard foam after pyrolysis under nitrogen

At 250°C the standard foam showed no significant difference in its in appearance compared to the virgin foam, however, by 300°C the foam is light brown in colour and

has begun to lose its foamed structure, which indicates that the urethane bonds have begun to degrade at this temperature. At 350°C and 400°C the chars have completely lost their foamed structure and are dark brown/black in colour, which is indicative of significant degradation occurring at these temperatures.

Characterisation of these chars was achieved by means of solid-state ^{13}C NMR, FTIR spectroscopy and elemental analysis.

- *Solid-state ^{13}C NMR*

Presented in Figure 4.35 is the ^{13}C CPMAS TOSS spectrum for the virgin foam.

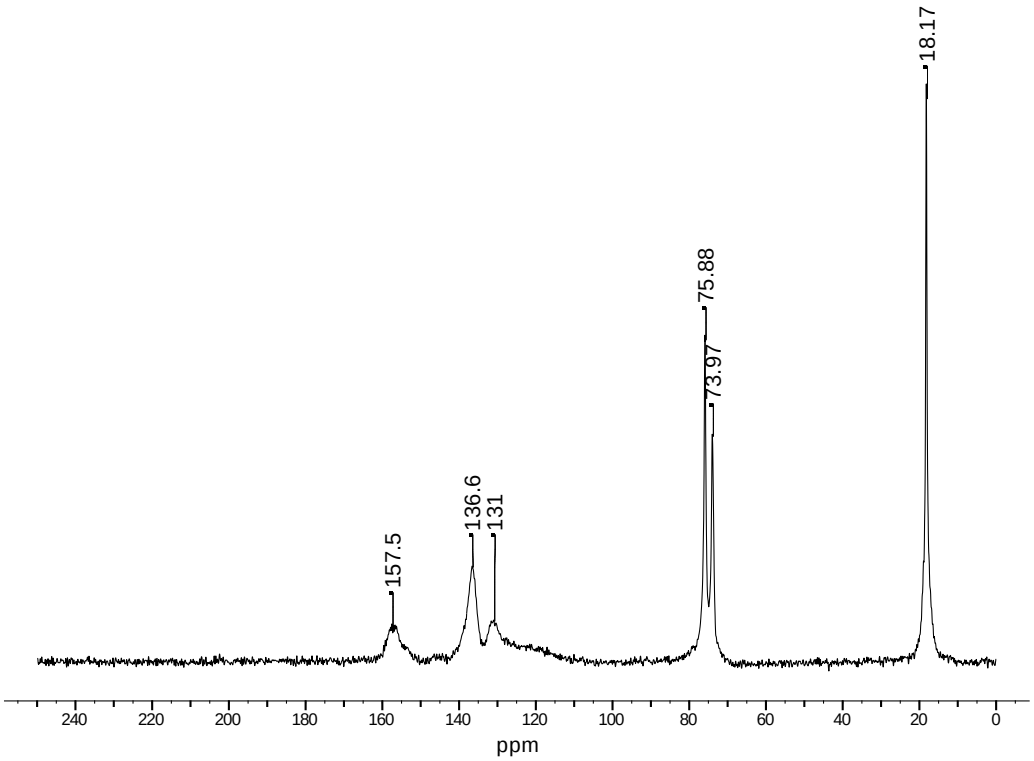

Figure 4.35: ^{13}C CPMAS TOSS spectrum of the virgin standard foam

The signals between 110 and 160 ppm arise from the aromatic and urethane carbons and are broad, which is typical of a rigid or hard component in a polymeric material. The narrower signals between 70 and 80 ppm are indicative of a soft component which has more molecular mobility; therefore, these peaks can be assigned to the aliphatic carbons within the polyol component of the polyurethane. The signal at 18.2 ppm arises from

methyl carbons and appears as a composite peak as there are two sources of methyl group: the methyl groups within the poly(propylene glycol) segments of the polyol and the methyl groups of the TDI component.

Presented in Figure 4.36 is the ^{13}C CPMAS dipolar dephased spectrum for the virgin foam. Dipolar dephasing is employed as it suppresses the signals originating from protonated carbons, therefore, it can provide further information regarding the structure of any chars which form. In this spectrum the label * is used to denote the spinning sidebands as it was recorded without suppression of sidebands.

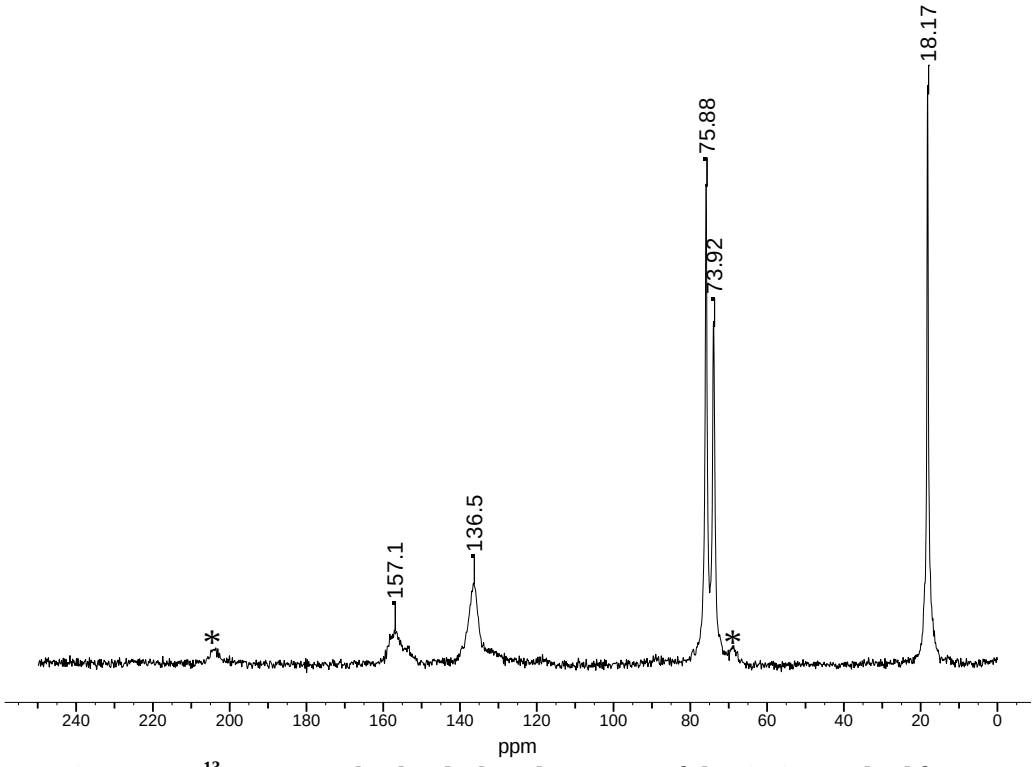

Figure 4.36: ^{13}C CPMAS dipolar dephased spectrum of the virgin standard foam

All of the signals detected in the TOSS spectrum remain after dipolar dephasing apart from the signal at 131 ppm. This arises from the protonated aromatic carbons of the TDI component within the foam and is, therefore, suppressed by the dipolar dephasing. The signals at 157.1 and 136.5 ppm remain as these correspond to the unprotonated urethane carbons and the quaternary aromatic carbons, respectively. This technique does not, however, suppress species with a high degree of molecular mobility and, as a

consequence, the peak corresponding to the methyl carbons at 18.2 ppm is retained. The peaks arising from the protonated polyol carbons at 73.9 and 75.9 ppm are also retained which confirms that this component has a high degree of mobility.

Presented in Figure 4.37 are the ^{13}C CPMAS TOSS spectra for the virgin foam and the chars obtained from the standard foam after pyrolysis at 250, 300, 350 and 400°C.

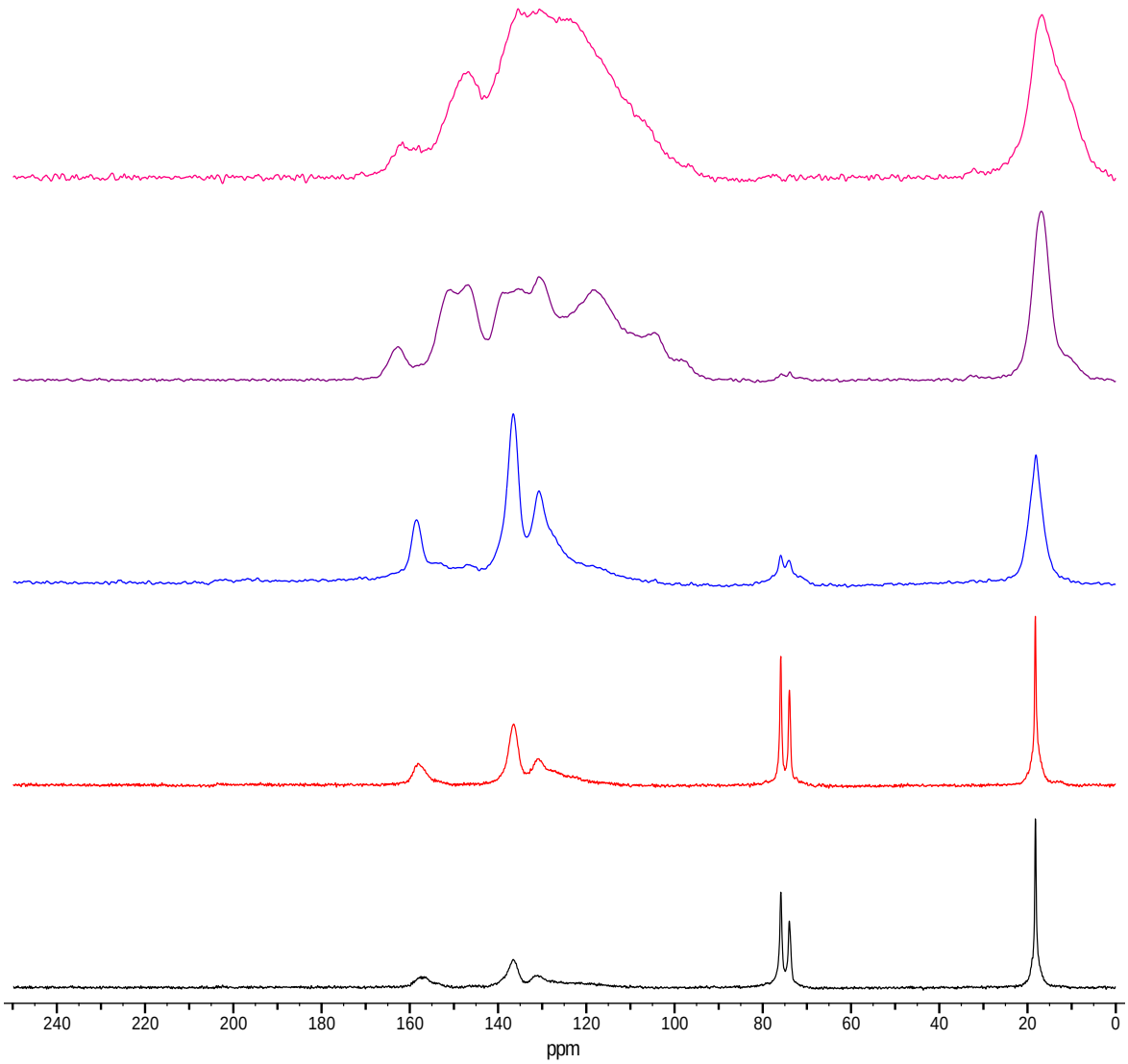

Figure 4.37: Comparison of the ^{13}C CPMAS TOSS spectra of the virgin standard foam (black) with the chars obtained after pyrolysis under nitrogen at 250°C (red), 300°C (blue), 350°C (purple) and 400°C (pink)

The spectrum at 250°C is similar to the virgin foam with all the original signals still being present. This confirms that no significant degradation of the polyurethane has occurred at this temperature and that a significant number of urethane linkages are still present within the foam. By 300°C the polyol signal is significantly reduced which suggests that significant degradation of the urethane linkages has occurred by this temperature. This correlates well with the results from the tar analysis which revealed that a large quantity of polyol-based tar had been produced at 300°C. As the level of polyol present has decreased significantly at this temperature, the peak at 18 ppm will be expected to now be largely due to the methyl groups of the TDI component. The broadness of this peak suggests that this is the case as a broader peak indicates a methyl group with more restricted mobility.

The spectrum of the char at 350°C is considerably different to those at the lower temperatures and indicates a change in the structure of the char at this temperature. The polyol signal has almost disappeared by this temperature and there is a significant change in the high chemical shift region of the spectrum. There are several peaks now observed between 110 to 170 ppm which indicates a number of aromatic carbons in different chemical environments, suggesting that the char has a complex aromatic structure at this temperature. Furthermore, the signal from the methyl group has become broader suggesting more restricted mobility of this component.

By 400°C no polyol peaks are observed in the char, the methyl signal is even broader still and the peaks in the high chemical shift region are poorly resolved. This suggests that by this temperature the foam which remains is highly charred, as is evident in the photographs presented in Figure 4.34, and that this char consists entirely of aromatic structures which are complex in nature.

Displayed in Figure 4.38 are the ^{13}C CPMAS dipolar dephased spectra for the virgin foam and the chars obtained from the standard foam after pyrolysis at 250, 300, 350 and 400°C.

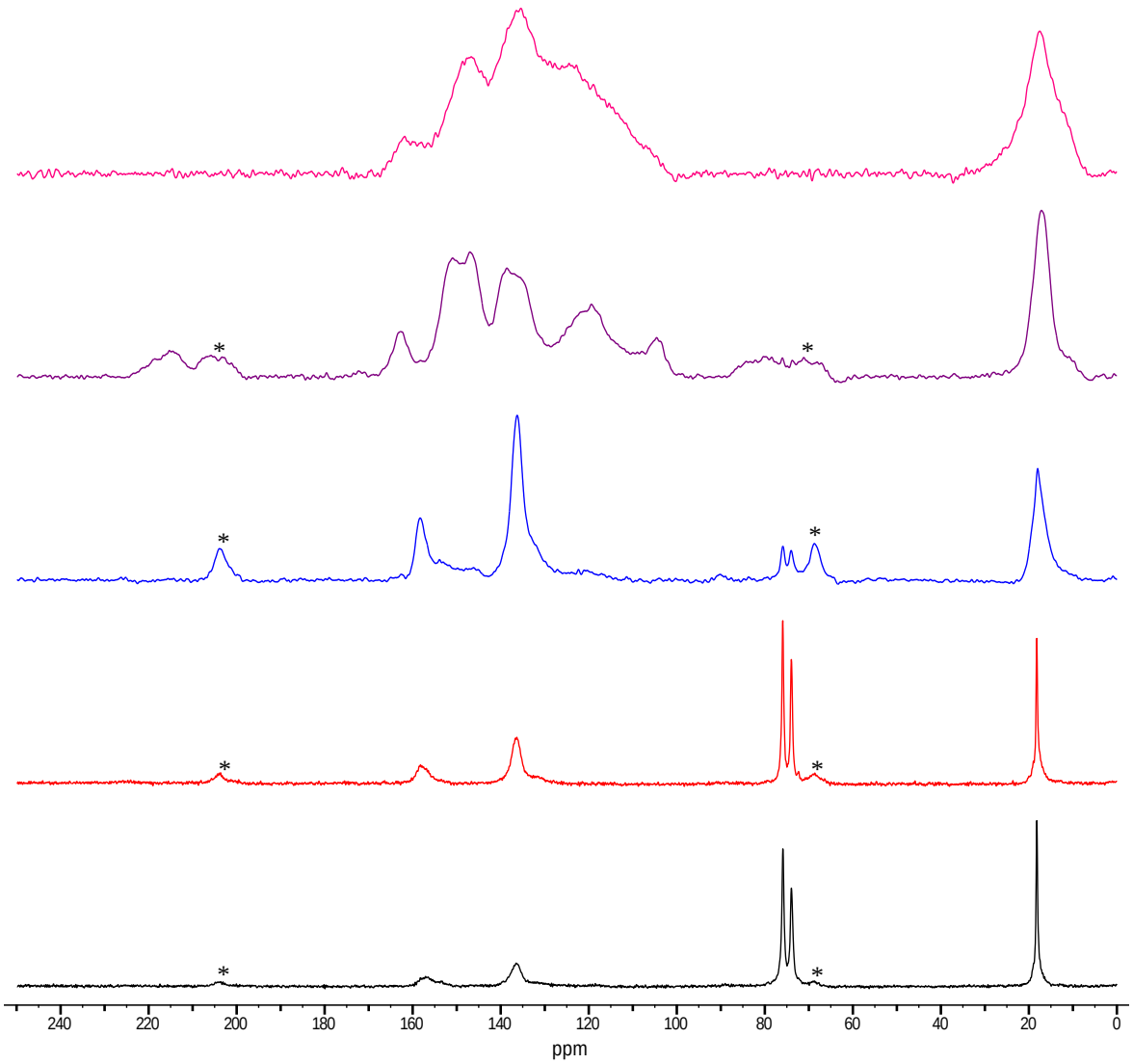

Figure 4.38: Comparison of the ^{13}C CPMAS dipolar dephased spectra of the virgin standard foam (black) with the chars obtained after pyrolysis under nitrogen at 250°C (red), 300°C (blue), 350°C (purple) and 400°C (pink)

The spectra at 250°C and 300°C exhibit the same characteristics as the TOSS spectra, showing loss of polyol with retention of the aromatic species within the char. The high chemical shift region of the dipolar dephased spectrum at 350°C is similar to that of the TOSS spectrum at this temperature, which indicates that the majority of the carbons contributing to the signal are unprotonated. This is also the case for the spectra at 400°C and this confirms that the char generated at the higher temperatures is aromatic and that a considerable quantity of this is unprotonated. This suggests that a significant amount

of ring fusion has occurred at the higher temperatures generating a complex char structure which consists of a number of aromatic species.

- *FTIR Spectroscopy*

Presented in Figure 4.39 is the complex FTIR spectrum of the virgin standard foam.

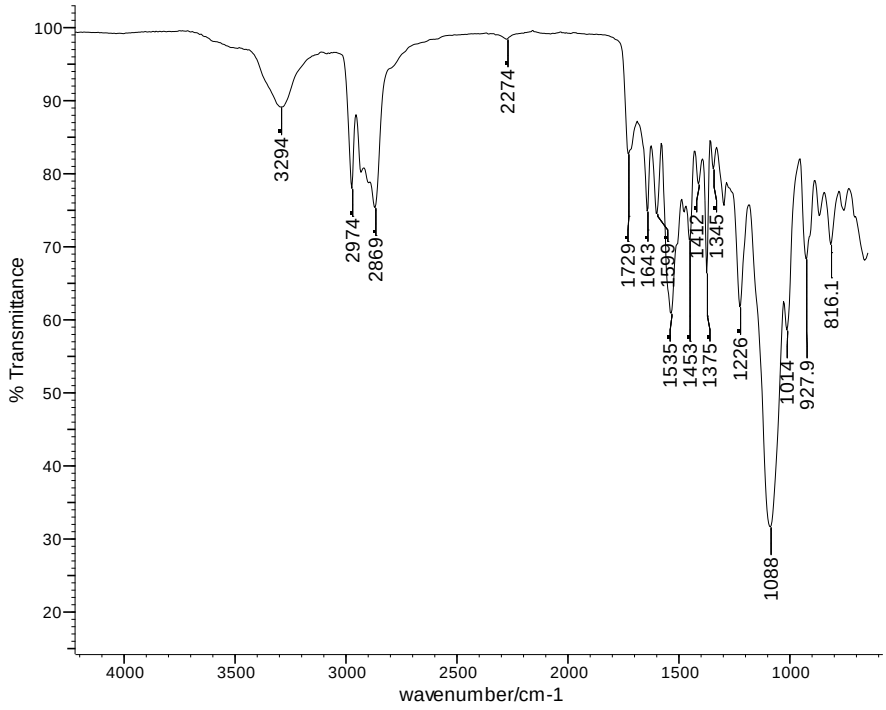

Figure 4.39: FTIR spectrum of the virgin foam

Comparison of this spectrum with the polyol (Figure 4.40) reveals that the majority of the peaks in the spectrum arise from the polyol component of the foam; however, there are additional peaks of importance. The peaks at 1729 and 1226 cm^{-1} are due to the urethane linkages, whilst the peaks between 1500 and 1650 cm^{-1} correspond to the aromatic segments of the foam. The peak at 3294 cm^{-1} is likely due to the N-H stretching of the urethane linkages and any urea linkages which may be present. The small peak at 2274 cm^{-1} suggests the presence of a small quantity of unreacted isocyanate groups within the foam.

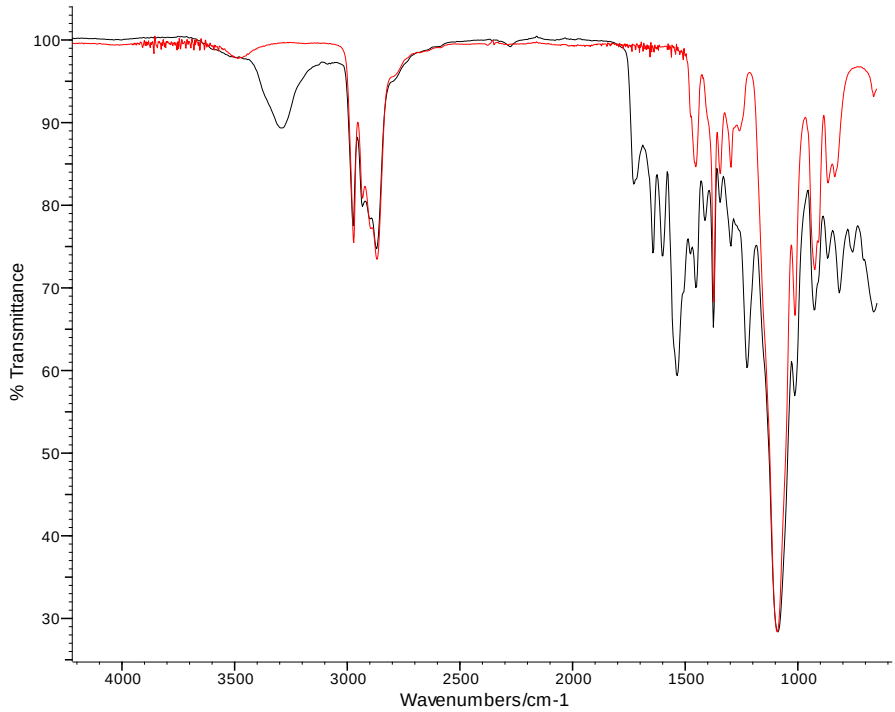

Figure 4.40: Comparison of the FTIR spectrum of the virgin foam (black) with the polyol (red)

Presented in Figure 4.41 are the FTIR spectra for the virgin foam and the chars obtained from the standard foam after pyrolysis under nitrogen at 250, 300, 350 and 400°C. The spectrum at 250°C is similar to the virgin foam with the only difference being the absence of the peak at 2274 cm^{-1} corresponding to residual isocyanates groups, which indicates that unreacted isocyanates groups are no longer present at 250°C. The peaks corresponding to the urethane linkages are still present which suggests that a significant number of urethane linkages remain in the foam at this temperature. These results are in correlation with the solid-state ^{13}C NMR results and confirm that there has been no significant degradation of the polyurethane at 250°C. By 300°C the urethane carbonyl peak at 1729 cm^{-1} is small and the polyol peaks are no longer as dominant in the spectrum. This indicates that significant degradation of the urethane linkages has occurred by this temperature, which is in agreement with the results presented previously.

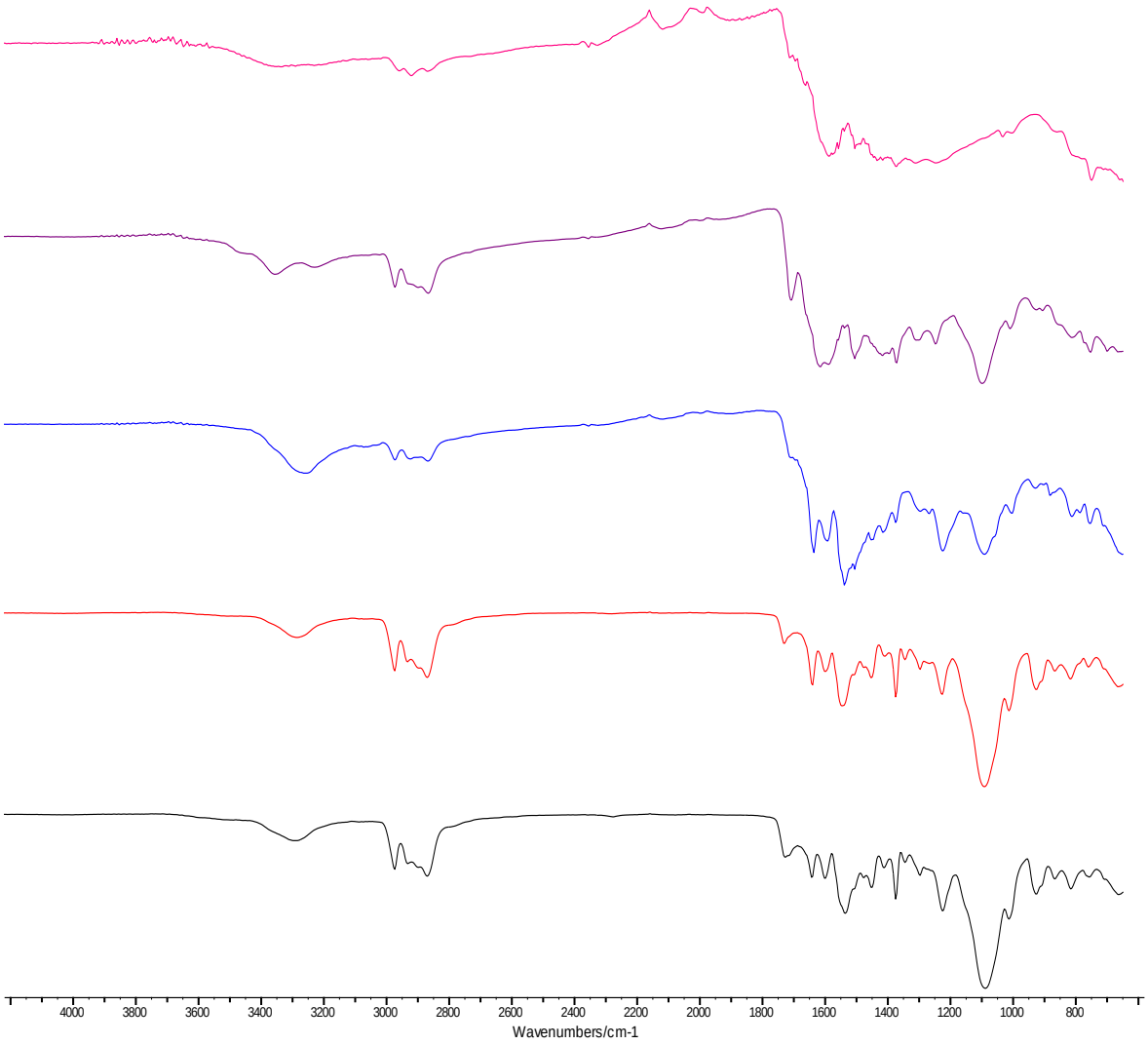

Figure 4.41: Comparison of the FTIR spectra of the virgin standard foam (black) with the chars obtained after pyrolysis under nitrogen at 250°C (red), 300°C (blue), 350°C (purple) and 400°C (pink)

At 350°C there are still weak polyol peaks present, as was the case in the solid-state NMR, and a new carbonyl peak is now present at 1710 cm^{-1}. This suggests that any polyol remaining in the char has now begun to degrade yielding carbonyl-containing structures. There is now much less of a signal present from the hydroxyl groups of the polyol component of the foam and a second peak around 3350 cm^{-1} can now be observed, which suggests the presence of aromatic amines within the char. The previous results suggested that DAT is a major degradation product arising from the pyrolysis of

the standard foam; therefore, it could be the case that this undergoes secondary reactions and is incorporated into the char at 350°C.

By 400°C the foam is highly charred and the FTIR spectrum is unstructured and difficult to interpret, which confirms that the char is carbonaceous in nature.

- *Elemental Analysis*

The virgin foam and the pyrolysis chars were submitted for elemental analysis to determine the quantities of carbon, hydrogen and nitrogen present which may provide further information regarding the structure of the chars obtained. The results from the elemental analysis are reported in Table 4.7.

Deg Temp/°C	**%C**	**%H**	**%N**	**C/H**	**C/N**
Virgin	61.7	9.1	5.3	6.8	11.6
250	61.9	9.2	5.0	6.7	12.4
300	64.0	6.6	13.4	9.7	4.8
350	64.8	6.2	14.7	10.4	4.4
400	69.4	4.8	12.3	14.4	5.6

Table 4.7: Elemental analysis results for the virgin standard foam and the pyrolysis chars

In order to illustrate more clearly the changes occurring in the chars the ratio of each element with respect to the percentage carbon has been calculated and these are presented as a function of the pyrolysis temperature in Figure 4.42. At 250°C the C:H and C:N ratios are not significantly different to those of the virgin foam indicating that very little degradation has occurred at this temperature. This is in agreement with the data presented thus far. The C:H ratio is then observed to significantly increase between 250°C and 300°C which suggests loss of polyol has occurred. This is again in agreement with the previous results which demonstrated that by 300°C significant degradation of the urethane linkages has occurred to yield a polyol-based tar and an aromatic char. Between 350°C and 400°C the C:H ratio significantly increases once again which correlates well with the solid-state ^{13}C NMR results which suggests that at

these higher temperatures significant ring fusion of the aromatics occurs to yield a complex, highly unprotonated carbonaceous char.

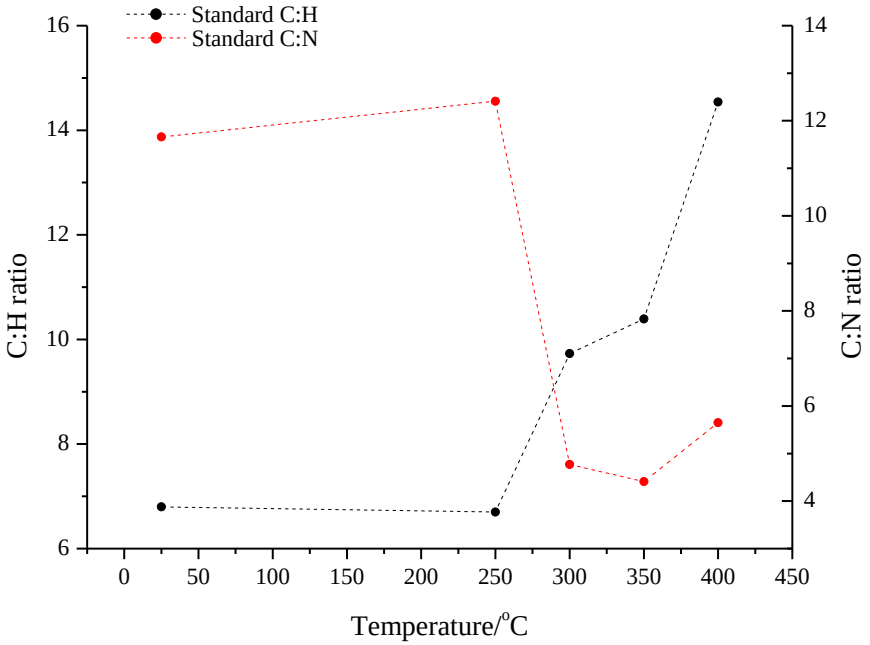

Figure 4.42: C:H and C:N ratios for the pyrolysis chars from the standard foam as a function of temperature

The C:N ratio, on the other hand, decreases between 250°C and 350°C which indicates that as the polyol is lost from the system, a large proportion of the nitrogen from the urethane linkages remains within the char. This is in agreement with the FTIR results which showed the presence of aromatic amine species within the char at 350°C. This suggests that in the confined environment of the pyrolysis the nitrogen-containing species (*e.g.* TDI and DAT) undergo secondary reactions and, as a result, a large proportion of the nitrogen-containing species become incorporated into the char. Calculation of the quantity of nitrogen in the char as a percentage of the nitrogen present in the virgin foam reveals that approximately 22% of the original nitrogen present in the foam remains within the char after pyrolysis at 400°C. The quantity of original carbon remaining, on the other hand, is 11%. This indicates that the nitrogen-containing species are preferentially retained within the char as the polyol is lost from the system. This is

expected as the char has been shown to be mostly aromatic in nature, with the aromatic units within the foam deriving from the isocyanate.

4.2.1.4 Summary

The results from pyrolysis of the standard foam under nitrogen are interesting and provide an insight into the mechanisms of degradation of the polyurethane, in particular in the condensed-phase.

After pyrolysis at 250°C no discolouration of the standard foam had occurred and only a small mass loss was observed. Furthermore, no tar was obtained at this temperature and solid-state ^{13}C NMR spectroscopy, FTIR spectroscopy and elemental analysis results revealed no significant change in the structure of the char residue. It is, therefore, proposed that little degradation has occurred during the pyrolysis of the standard foam at 250°C under nitrogen.

As the pyrolysis temperature was increased the foam was observed to degrade and the product profile indicates that this is a complex process. Both TDI and DAT were identified in the cold-ring fractions at 300°C and above which indicates that the urethane linkages are degrading by two competing degradation mechanisms. Degradation of the urethane linkage by a depolymerisation reaction to yield TDI and polyol is proposed to occur initially; however, as the pyrolysis is conducted under higher pressure, more confined conditions the diisocyanate becomes trapped within the pyrolysis zone and reacts with the polyol to reform the urethane bond. Under these conditions it is proposed that degradation of the urethane linkages *via* a six-membered ring transition state becomes the predominant reaction to form DAT, CO_2 and alkene terminated polyol chains. This proposal is supported by the identification of C=C bonds in the FTIR spectrum of the tars at 300°C above and polyurea within the cold-ring fraction, which indicates the presence of amines within the system.

Solid-state ^{13}C NMR spectroscopy of the chars indicates that at temperatures above 300°C ring fusion of the aromatic components within the foam occurs and this leads to a carbonaceous char which has a complex aromatic structure. In addition, elemental analysis results revealed that a significant quantity of nitrogen is present within the higher temperature chars which confirms that the char is composed of nitrogen containing aromatic structures. It is proposed that under the confined conditions of the pyrolysis the aromatic nitrogen-containing species, such as TDI and DAT, undergo secondary reactions and ring fusion to yield a complex char structure.

4.2.2 Pyrolysis under Air

4.2.2.1 Mass Loss Data and Observations

The residues obtained, calculated as a percentage of the original sample mass, after pyrolysis of the standard foam under air are presented in Table 4.8. The quantities of residue obtained are the averages which have been calculated from the four repeat analyses. Presented in Figure 4.43 is a plot of the quantity of residue obtained as a function of the pyrolysis temperature.

Pyrolysis Temperature/°C	**Residue/Mass%**
250	95
300	47
350	27
400	18

Table 4.8: Mass losses and residues for the standard foam after pyrolysis under air

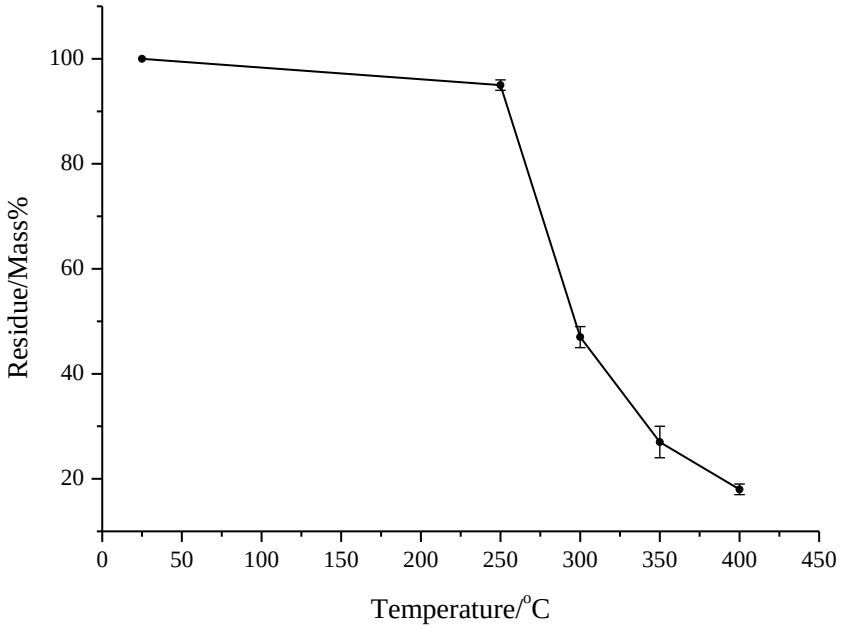

Figure 4.43: Residue obtained vs. pyrolysis temperature for the standard foam under air

An increase in mass loss and decrease in the quantity of residue is observed as the pyrolysis temperature increases. Again this is indicative of increased levels of degradation at the higher temperatures, which leads to larger quantities of volatile material being evolved. At 250°C discolouration of the foam had occurred, indicating that degradation had occurred to some extent at this temperature but the corresponding mass loss is relatively small. This suggests that degradation of the urethane linkages within the foam has occurred; however, the products formed during the degradation have not volatilised to any great extent or undergone secondary reactions to produce volatile degradation products. As the pyrolysis temperature was increased the extent of degradation will have increased and it can be observed from Figure 4.43 that the greatest mass loss occurred between 250°C and 300°C. This indicates that significant quantities of volatile degradation products have been evolved from the sample in this temperature range, and it is proposed that this occurs as a result of thermo-oxidative degradation of the polyol component of the foam.

Presented in Figure 4.44 is a comparison of the quantities of residue obtained from pyrolysis of the standard foam under nitrogen and air.

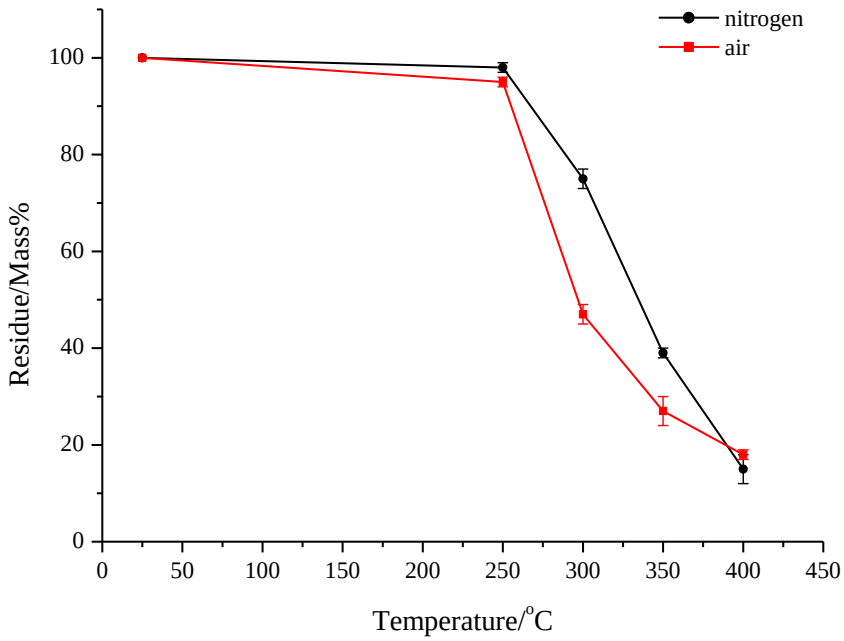

Figure 4.44: Comparison of the residues obtained for the standard foam under nitrogen and air

It is clear that there are no significant differences in the mass losses under air or nitrogen at 250°C, however, above this temperature the mass loss is clearly accelerated in air. It has been reported that the presence of oxygen does not significantly influence the primary degradation step of the polyurethane[2,3] and the results presented in Figure 4.44 suggest that this is indeed the case for the standard foam. This is in correlation with the TGA results presented previously. It has also been reported that the soft segments of the polyurethane, *i.e.* the polyol chains, are more susceptible to oxidative degradation than the hard segments.[4] It is, therefore, proposed that above 250°C thermo-oxidative degradation of the polyol segments within the foam occurs, producing a large quantity of volatile degradation products. Thermo-oxidative degradation of the polyol is expected to occur at lower temperatures than thermal degradation[1], therefore, increased mass loss is observed at lower temperatures relative to the degradation under nitrogen. This is in correlation with a number of studies published on the degradation of polyurethanes.[17,18,19]

4.2.2.2 Cold-ring Fraction Analysis

In contrast to the pyrolysis under nitrogen, a yellow cold-ring fraction was obtained at all temperatures during the pyrolysis under air, although only a small quantity was present at 250°C. This indicates that degradation of the polyurethane is accelerated in the presence of oxygen which correlates with the mass loss data and observations discussed previously. In addition, white polyurea residue was not observed during the pyrolysis under air.

The FTIR spectrum of the cold-ring fraction collected at 250°C is presented in Figure 4.45. The FTIR spectrum of the cold-ring fraction at 250°C indicates the presence of structures containing ether, carbonyl and hydroxyl groups. These are, therefore, likely to be higher molar mass fragments produced from the thermo-oxidative degradation of the polyol component of the foam.

GC-MS analysis was also conducted on the cold-ring fraction at 250°C and a complex chromatogram was obtained which is presented in Figure 4.46. The peaks of interest in the chromatogram correspond in the most part to high molar mass polyol chain fragments which share common m/z fragments. Due to the large number of possible products which could be derived from the polyol chain complete identification of these species is not possible, however, the library searches suggest the presence of cyclic species derived from the polyol such as dioxane-type structures. At this temperature TDI and DAT were not identified in the cold-ring fraction.

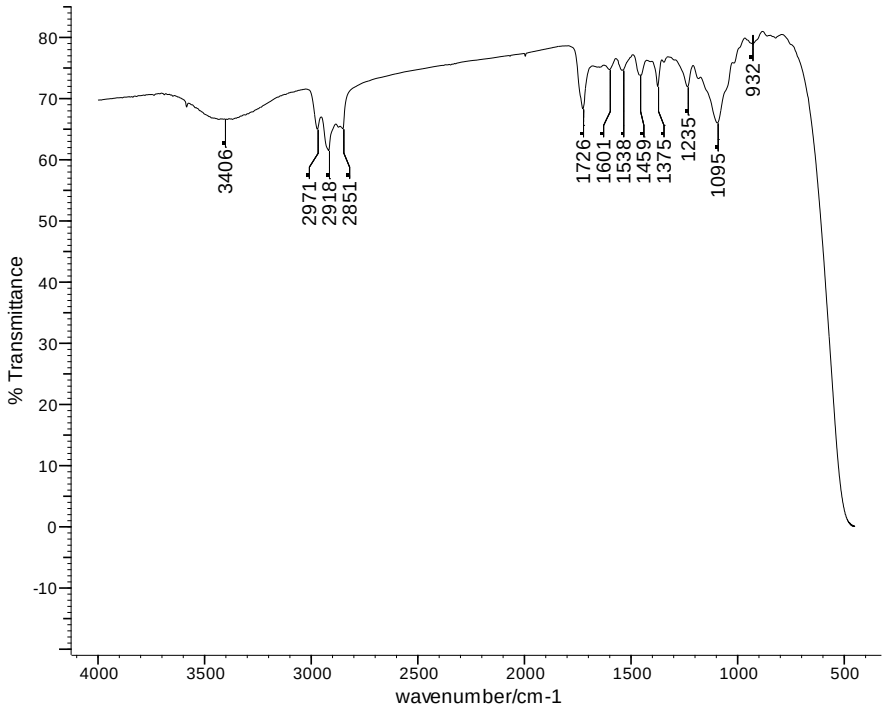

Figure 4.45: FTIR spectrum of the cold-ring fraction collected from the standard foam after pyrolysis under air at 250°C

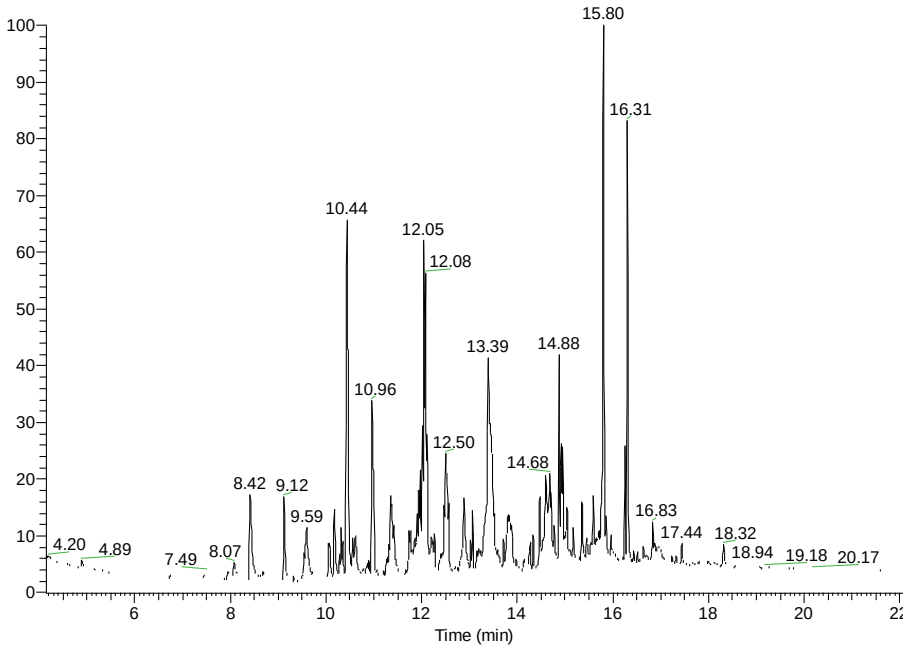

Figure 4.46: GC-MS total-ion chromatogram for the cold-ring fraction collected from the standard foam after pyrolysis under air at 250°C

The GC-MS and FTIR spectroscopy results, therefore, indicate that the cold-ring fraction at 250°C consists primarily of polyol fragments. This confirms that at 250°C thermo-oxidative degradation of the polyol component has occurred to some extent; however, this is not likely to have reached its maximum rate at this temperature as the mass loss observed is only 5%. These results also confirm that thermo-oxidative degradation of the polyol occurs at a lower temperature than thermal degradation, as there was no polyol-based cold-ring fraction collected at 250°C during the pyrolysis under nitrogen.

The cold-ring fractions collected at 300, 350 and 400°C were similar to that collected at 250°C, consisting primarily of high molar mass polyol fragments. TDI and DAT were not identified in any of these cold-ring fractions.

Analysis of the cold-ring fractions, therefore, indicates that thermo-oxidative degradation of the polyol component of the foam occurs at temperatures as low as 250°C and yields higher molar mass polyol fragments. The absence of the white polyurea residue which was observed during the pyrolysis of the foam under nitrogen suggests that amines, in particular DAT, are not released during the degradation of this foam. DAT arises from degradation of the urethane linkage *via* a six-membered ring transition state; however, this mechanism is proposed to be predominant only under confined conditions when the TDI and polyol released from the depolymerisation reaction become trapped in the pyrolysis zone and recombine. The results presented so far, however, demonstrate that under an oxidative environment the polyol undergoes degradation at a much lower temperature than in an inert atmosphere. It could, therefore, be the case that the polyol is not trapped within the pyrolysis zone for any length of time and so the polyol and TDI do not recombine. It could also be the case that the polyol gets oxidised and is, therefore, not available to recombine with the TDI. In both of these cases the six-membered ring mechanism would not occur to any great extent which would explain the lack of polyurea residue during the pyrolysis under air.

The GC-MS analysis revealed that TDI was also absent from the cold-ring fractions and it is likely that this undergoes secondary degradation reactions under an oxidative environment. This would again prevent recombination of the polyol and the TDI.

4.2.2.3 Residue Analysis

The residues obtained from the pyrolysis under air yielded both tar and char at all temperatures. This is in contrast to the pyrolysis under nitrogen which yielded no tar at 250°C and confirms that degradation of the polyurethane is altered in the presence of oxygen. The tars were analysed by FTIR spectroscopy, whilst the chars were characterised by elemental analysis, solid-state ^{13}C NMR and FTIR spectroscopy.

4.2.2.3.1 Quantification of the Tar and Char

Presented in Table 4.9 are the quantities of tar and char, as a percentage of the total residue, collected from the standard foam after pyrolysis under air. It can be observed that the sample at 250°C produced a significant quantity of tar which confirms that degradation of the polyurethane has begun to occur at this temperature. As was mentioned previously, it has been reported that the soft segments of the polyurethane are more susceptible to oxidative degradation than the hard segments.[4] It is, therefore, likely that the tar at 250°C originates from thermo-oxidative scission of the soft segments within the polyurethane. The corresponding mass loss at this temperature was, however, relatively small and only a small quantity of cold-ring fraction was obtained. This indicates that whilst scission of the polyol chains to yield tar has occurred, the tar has not begun to degrade significantly to yield volatile material at this temperature.

Temperature/°C	**Tar/% of residue**	**Char/% of residue**
250	36	64
300	16	84
350	14	86
400	1	99

Table 4.9: Quantities of tar and char obtained as a percentage of the total residue collected

As the pyrolysis temperature was increased, the level of tar within the residue decreased as the foam became more charred in nature, which is likely to be a result of thermo-oxidative degradation of the tar at the higher temperatures. The foam consisted almost entirely of char by 400°C. Comparison of the percentages of tar and char in the residues obtained from the pyrolyses under nitrogen and air reveals that the residues under air are more charred in nature at all temperatures, which indicates that the presence of oxygen has altered the degradation of the foam leading to char being formed at lower temperatures. Comparison of the quantities of char as a percentage of the original mass of foam, presented in Table 4.10, confirms that the oxidative environment leads to a significantly increased level of char.

Temperature/°C	**Char/% of original sample under nitrogen**	**Char/% of original sample under air**
250	100	61
300	14	40
350	12	25
400	9	18

Table 4.10: Quantities of char obtained as a percentage of the original sample for the pyrolysis under nitrogen and air

4.2.2.3.2 Analysis of the Tar

Presented in Figure 4.47 is the FTIR spectrum for the tar obtained from the standard foam at 250°C. As was the case for the tars collected under nitrogen, the majority of the peaks are associated with structures which resemble the polyether polyol component of the foam; this is confirmed by comparison with the FTIR spectrum of the polyol as shown in Figure 4.48.

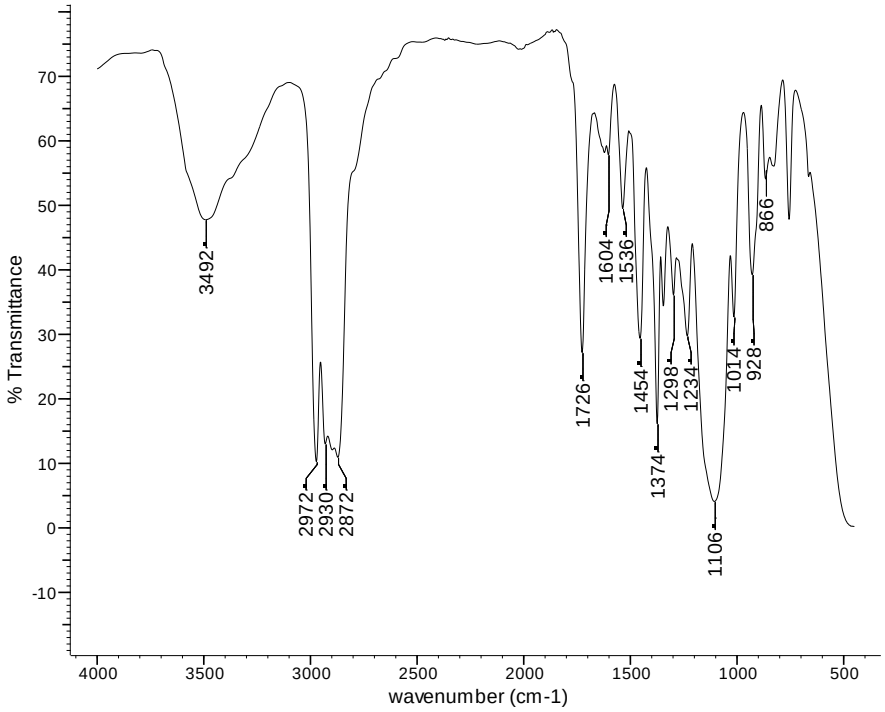

Figure 4.47: FTIR spectrum of the tar extracted from the standard foam after pyrolysis at 250°C under air

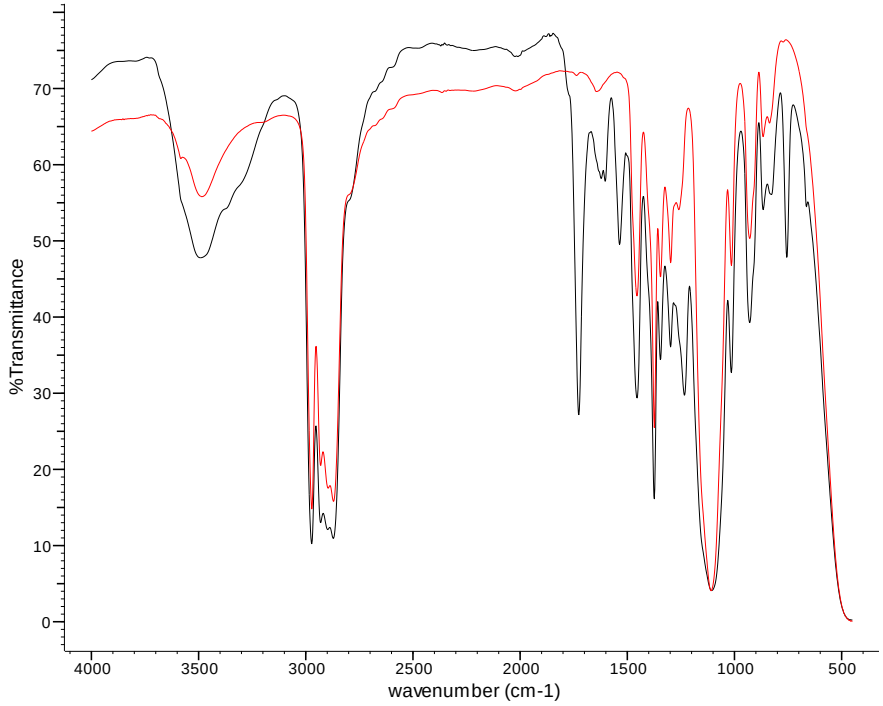

Figure 4.48: Comparison of the FTIR spectrum of the tar from the standard foam after pyrolysis under air at 250°C (black) and Alcupol F-5611 (red)

The spectra are almost identical; however, there are additional peaks in the FTIR spectrum of the tar. The peaks at 1536 and 756 cm^{-1} are present as a result of residual solvent within the tar. The major difference, however, is the peak at 1726 cm^{-1} which indicates the presence of carbonyl groups within the tar. The carbonyl groups could be a result of thermo-oxidative degradation of the polyol or they could be due to residual urethane bonds present within the tar. The presence of a large quantity of polyol-based tar at 250°C, which was absent during the pyrolysis under nitrogen, confirms that degradation of the soft segments of the foam occurs at a lower temperature in the presence of oxygen.

At 300°C and 350°C the peaks at 1726 and 1234 cm^{-1} became progressively smaller indicating either loss of the residual urethane linkages or loss of a carbonyl-containing polyol fragment due to further thermo-oxidative degradation of the tar. At these temperatures the FTIR spectra indicate that the tars consist mostly of regenerated polyol. By 400°C very little tar remains and the FTIR spectrum is weak, suggesting significant thermo-oxidative degradation of the polyol has occurred by this temperature.

4.2.2.3.3 Analysis of the Char

Presented in Figure 4.49 are photographs of the chars collected from the standard foam after pyrolysis under air, which were significantly different to those obtained under nitrogen. The char obtained at 250°C under air resembled the char at 300°C under nitrogen, being brown in colour and having lost some of the foamed structure. By 300°C under air the char was already blackened and powdery, having lost all of its original foamed structure. The chars at 350°C and 400°C were similar in appearance. These observations suggest that the presence of oxygen has accelerated or altered the degradation processes occurring in the foam and is in agreement with the results presented so far. Characterisation of the chars was achieved by means of solid-state ^{13}C NMR, FTIR spectroscopy and elemental analysis.

Figure 4.49: Photographs of the chars collected from the standard foam after pyrolysis under air

- *Solid-state ^{13}C NMR*

Presented in Figure 4.50 are the ^{13}C CPMAS TOSS spectra for the virgin foam and the chars obtained from the standard foam after pyrolysis at 250, 300, 350 and 400°C under air. The peak assignments for the virgin foam are the same as those discussed previously. The spectrum at 250°C is similar to the virgin foam with all the original signals still being present; however, there is a decrease in the intensity of the polyol peaks at 73.9 and 75.9 ppm relative to the aromatic peaks between 110 and 170 ppm. The methyl peak at 18.2 ppm is also broader at this temperature which indicates that less of a signal is present from the more mobile methyl groups of the polyol. This indicates that a significant quantity of the polyol component has been lost from the char at 250°C, which is in agreement with the results from the tar analysis which revealed that a large quantity of polyol-based tar was extracted at this temperature. When compared to the spectrum at 250°C under nitrogen, this confirms that the presence of oxygen has caused scission of the soft segments of the foam at this temperature.

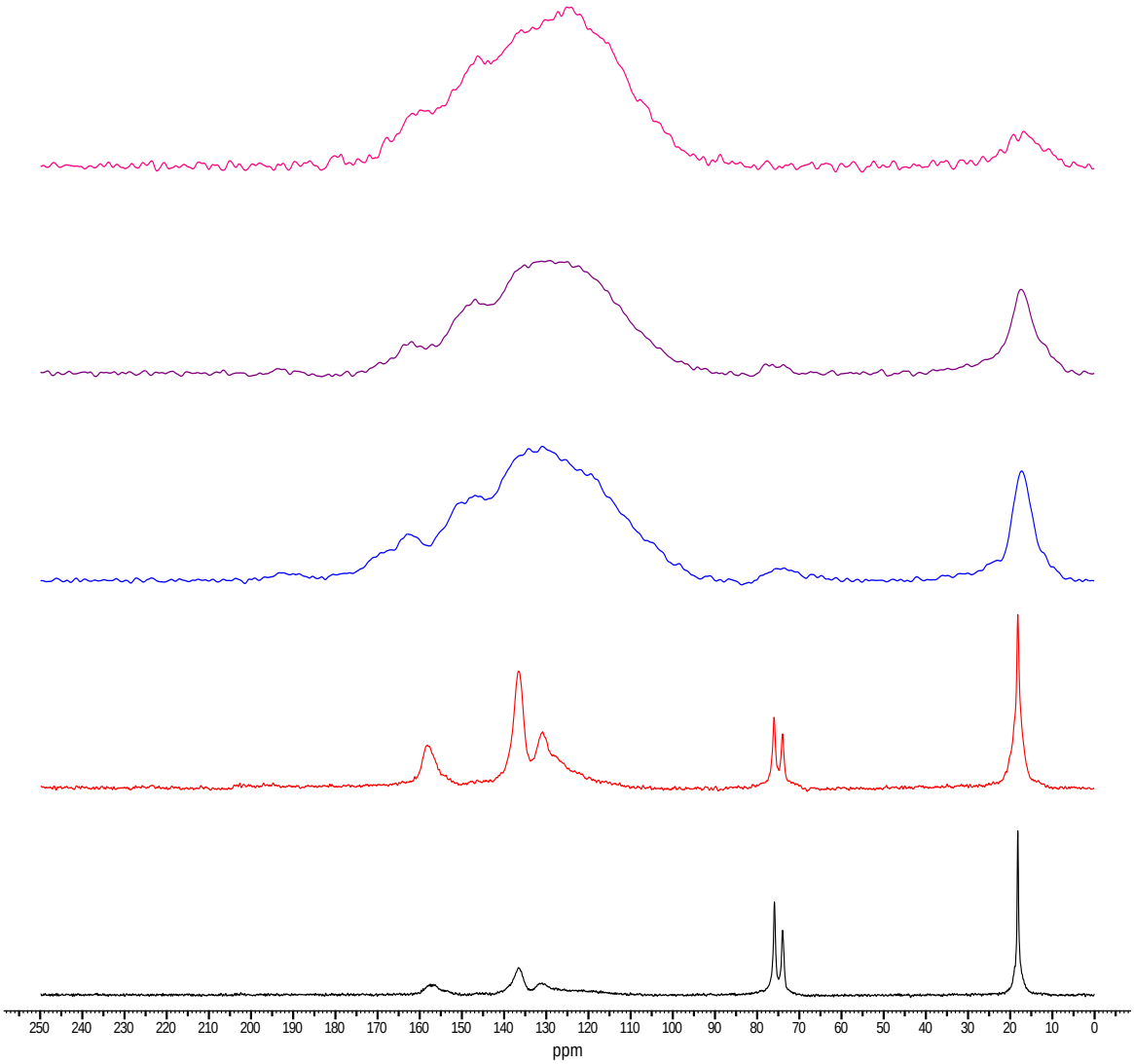

Figure 4.50: Comparison of the ^{13}C CPMAS TOSS spectra of the virgin standard foam (black) with the chars obtained after pyrolysis under air at 250°C (red), 300°C (blue), 350°C (purple) and 400°C (pink)

The spectrum of the char at 300°C is considerably different to that at 250°C and indicates a change in the structure of the char at this temperature. Almost complete loss of the polyol is observed at this temperature and the broad signal at 18.2 ppm, which indicates a methyl group with more restricted mobility, is now almost entirely due to the methyl groups of the TDI component. Furthermore, the peak corresponding to the carbons of the urethane linkages at 157.5 ppm is absent which indicates that no urethane

bonds remain. Once again this demonstrates that the degradation of the foam is altered in the presence of oxygen as urethane bonds were still observed in the NMR spectrum of the char obtained at 300°C under nitrogen. The spectrum under air also shows a significant change in the high chemical shift region of the spectrum compared to the 250°C spectrum. There appears to be a number of signals between 110 and 170 ppm which are poorly resolved; this suggests the foam is highly charred by this temperature and that the char consists of complex aromatic structures. This is in stark contrast to the char obtained under nitrogen at this temperature and demonstrates that the degradation under air is significantly accelerated compared to the degradation under nitrogen.

The spectrum for the char at 350°C shows little difference to that at 300°C, indicating that the structure does not alter significantly between these temperatures. By 400°C, however, the high chemical shift region of the spectrum is even less resolved and the methyl signal at ~18 ppm is almost completely lost. Under nitrogen at this temperature, however, a large methyl peak was still observed. This may suggest that at the higher temperatures under air, rather than remaining as a pendant group on the aromatic system, the carbon of the methyl group gets incorporated into the aromatic structures during the ring fusion reactions. Alternatively, under an oxidative environment the aromatic components of the char may undergo reactions which lead to loss of the methyl group. Servay *et al*.[20] reported that the central methylene group in MDI undergoes oxidative reactions; therefore, it could be the case that the methyl groups in TDI undergo similar oxidative reactions at the higher temperatures. It could also be the case that scission of the methyl group causes this to be lost as methane.

The ^{13}C CPMAS dipolar dephased spectra for the virgin foam and the chars obtained under air are presented in Figure 4.51.

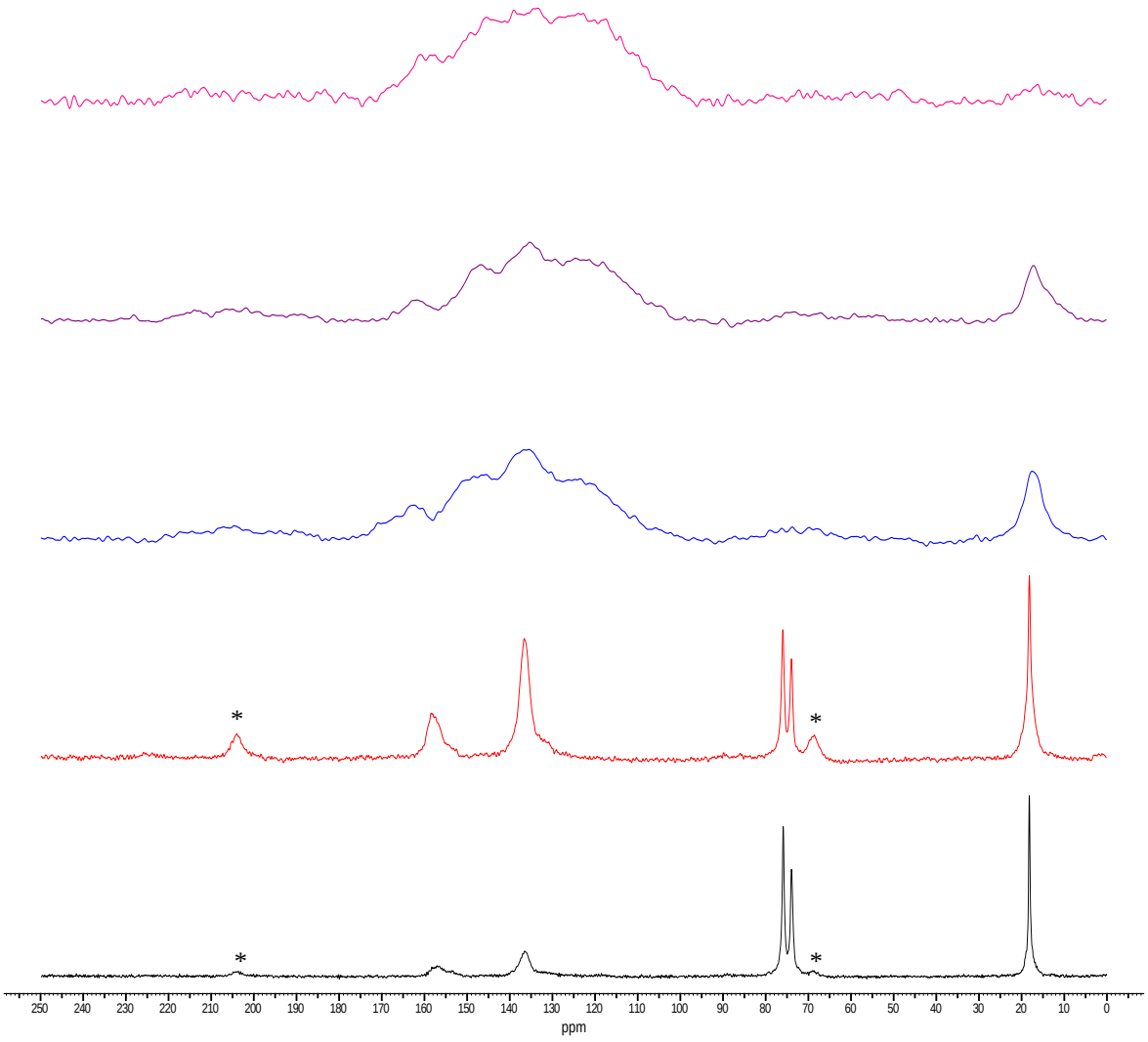

Figure 4.51: Comparison of the ^{13}C CPMAS dipolar dephased spectra of the virgin standard foam (black) with the chars obtained after pyrolysis under air at 250°C (red), 300°C (blue), 350°C (purple) and 400°C (pink)

The dipolar dephased spectra do not show significant differences to the TOSS spectra which indicates that the majority of carbons contributing to the signal from 300°C onwards are unprotonated. This confirms that the char generated at these temperatures is aromatic and unprotonated, suggesting that a significant amount of ring fusion has occurred to generate a highly complex char structure consisting of aromatic species.

- *FTIR Spectroscopy*

Presented in Figure 4.52 are the FTIR spectra for the virgin foam and the chars obtained from the standard foam after pyrolysis under air at 250, 300, 350 and 400°C.

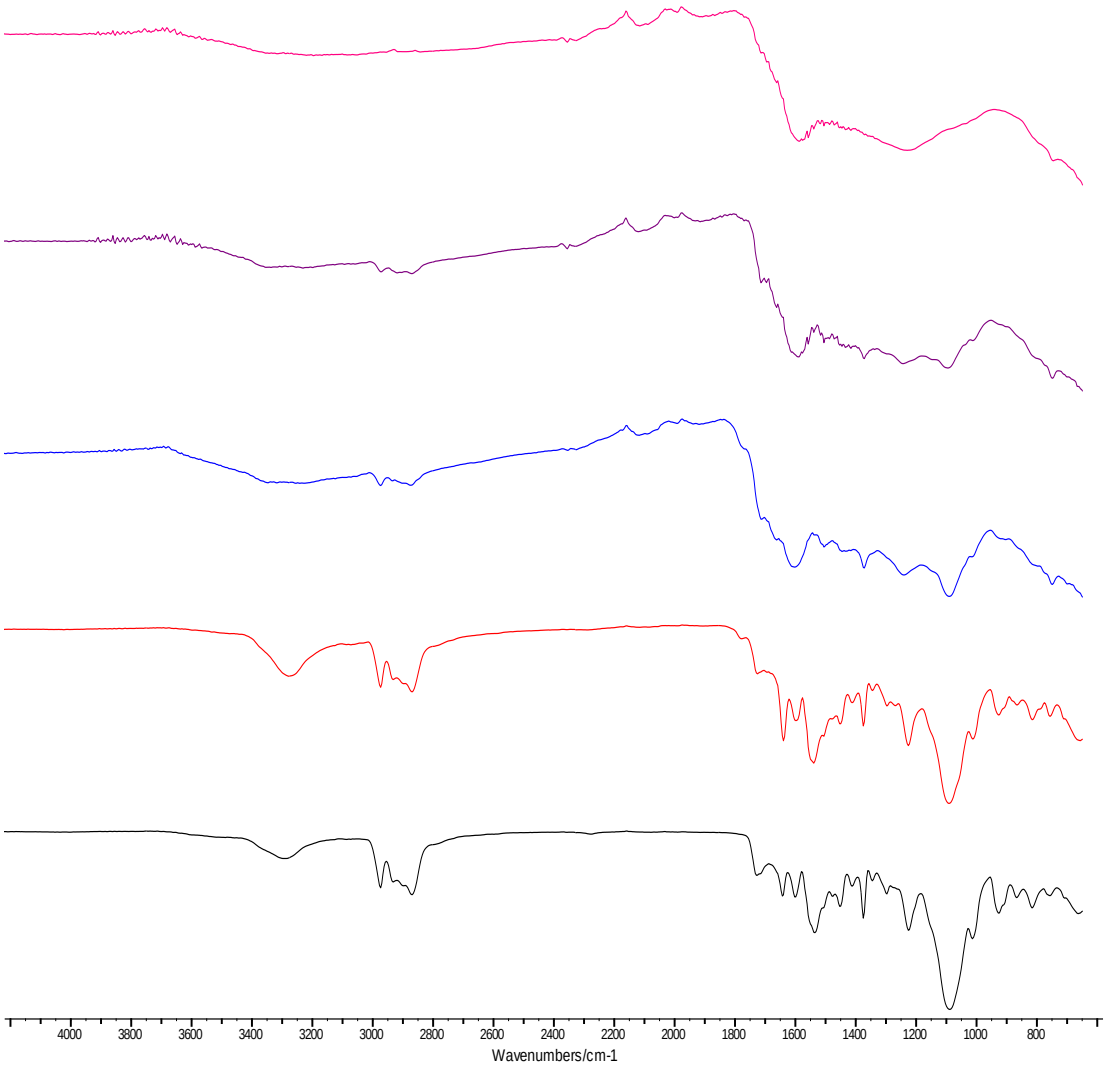

Figure 4.52: Comparison of the FTIR spectra of the virgin standard foam (black) with the chars obtained after pyrolysis under air at 250°C (red), 300°C (blue), 350°C (purple) and 400°C (pink)

The spectrum at 250°C is similar to the virgin foam with the peaks corresponding to the urethane linkages still present, which indicates that significant degradation of the urethane linkages has not occurred at this temperature. By 300°C the FTIR is weak and difficult to interpret. This indicates that the foam is already highly charred and

carbonaceous by this temperature and is in correlation with the previous results. The urethane carbonyl peak at 1729 cm^{-1} is significantly reduced which indicates that significant degradation of the urethane linkages has occurred by 300°C. The spectrum at 300°C under air closely resembles that at 400°C under nitrogen which once again indicates that the degradation of the polyurethane foam is accelerated in the presence of oxygen. The spectra for the chars at 350°C and 400°C are weaker still, indicating further charring of the foam at these temperatures. No further information could be gained from these spectra due to the charred nature of these samples.

- *Elemental Analysis*

The virgin foam and the chars from the pyrolysis under air were submitted for elemental analysis to determine the percentages of carbon, hydrogen and nitrogen which were present as this may provide more information regarding the structure of the chars. The results are presented in Table 4.11.

Deg Temp/°C	**%C**	**%H**	**%N**	**C/H**	**C/N**
Virgin	61.7	9.1	5.3	6.8	11.6
250	62.2	7.4	8.7	8.4	7.1
300	60.3	4.2	11.4	14.4	5.3
350	67.4	4.7	10.5	14.3	6.4
400	65.2	3.0	13.6	21.7	4.8

Table 4.11: Elemental analysis results for the virgin standard foam and the pyrolysis chars under air

The ratio of each element with respect to the percentage carbon has been calculated in order to more clearly illustrate the changes occurring in the chars and is presented in Figure 4.53 as a function of the pyrolysis temperature.

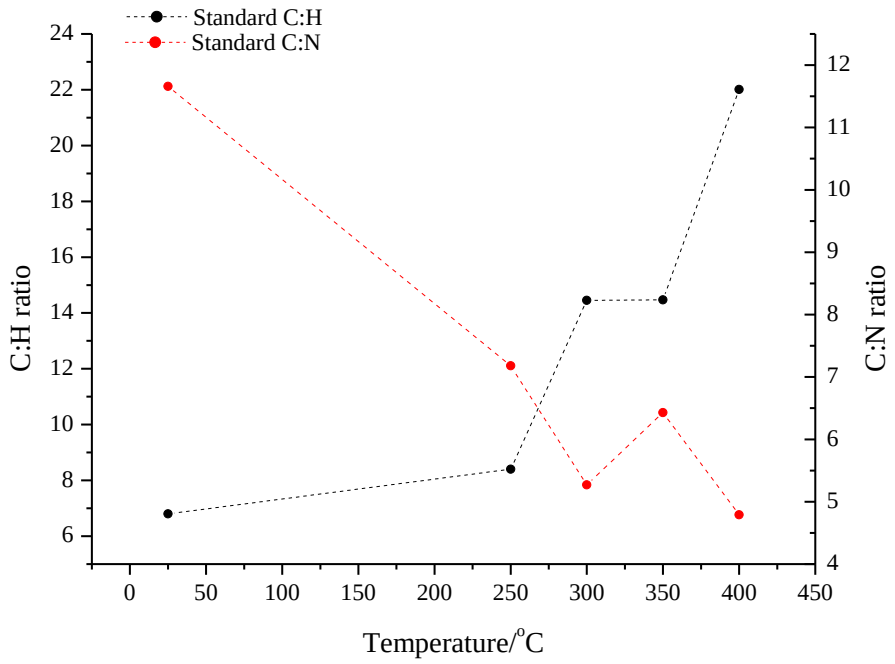

Figure 4.53: C:H and C:N ratios for the pyrolysis chars from the standard foam under air as a function of temperature

At 250°C the C:H ratio increases relevant to the virgin foam which indicates that loss of polyol has occurred. This is in agreement with the data presented previously which indicated that thermo-oxidative degradation of the soft segments had occurred by this temperature, with the extraction of a large quantity of polyol-based tar and a decrease in the intensity of the polyol signals within the solid-state NMR ^{13}C. This is, however, in contrast to the results obtained under nitrogen which showed no significant differences between the C:H ratios of the virgin foam and the char at 250°C, which again confirms that the degradation of the soft segments is altered in the presence of oxygen.

The C:H ratio then increases even more significantly between 250°C and 300°C which indicates further loss of the polyol at this temperature. This is in correlation with the solid-state ^{13}C NMR results which showed almost complete loss of polyol by 300°C. Between 350°C and 400°C the C:H ratio increases once again which suggests loss of a hydrogen rich component between these temperatures. Almost complete loss of the methyl group was observed in the solid-state ^{13}C NMR at 400°C and one suggestion for

this occurrence was loss of the methyl group in the form of methane. This would explain the increase in the C:H ratio at 400°C.

The C:N ratio, on the other hand, decreases significantly at 250°C compared to the virgin foam, and again between 250°C and 300°C. This indicates that a large quantity of the nitrogen-containing components of the foam remain within the char when the polyol-based tar is lost from the system. As was the case under nitrogen, this suggests that under the confined conditions of the pyrolysis the nitrogen-containing species, such as TDI, may undergo secondary reactions which lead to a large proportion of nitrogen remaining within the char. The C:N ratio then increases at 350°C which is indicative of loss of nitrogen compounds from the char at this temperature. Finally, the C:N ratio decreases again at 400°C which indicates that the remaining nitrogen stays within the char whilst a carbon-containing component is lost. This could again be explained by loss of methyl groups in the form of methane and is in agreement with the C:H data.

4.2.2.4 Summary

The results from pyrolysis of the standard foam under air demonstrate that degradation of the polyurethane occurs at a lower temperature than under nitrogen and that the chemistry occurring in the condensed-phase is different.

After pyrolysis at 250°C the foam was discoloured and a large quantity of tar was extracted which was shown to be highly polyol-based. Solid-state ^{13}C NMR and elemental analysis confirmed that a significant level of polyol had been lost from the char at this temperature. FTIR spectroscopy and GC-MS analysis of the cold-ring fraction at this temperature revealed that the polyol had begun to undergo thermo-oxidative degradation to yield high molar mass polyol fragments, including cyclic species. The mass loss observed at this temperature, however, was small which indicates that degradation of the polyol had not reached a maximum rate at this temperature.

The solid-state ^{13}C NMR and FTIR spectroscopy results at 300°C revealed that almost complete loss of the polyol from the char had occurred by this temperature and few urethane linkages remained with the char. At this temperature the overall mass loss from the foam had reached almost 50% and it is proposed that significant thermo-oxidative degradation of the polyol had occurred by this temperature yielding volatile degradation products. The foam was also observed to be highly charred at this temperature and the solid-state ^{13}C NMR results revealed that the char consists of complex aromatic structures. The NMR spectrum at 400°C revealed that the methyl signal was almost completely lost by this temperature and, in combination with the elemental analysis results, it is proposed that at the higher temperatures under air the methyl groups are lost in the form of methane.

Finally, analysis of the cold-ring fractions revealed a number of interesting points. The white polyurea residue observed during the pyrolysis of the foam under nitrogen was absent during the pyrolysis under air and this suggested that amines, in particular DAT, were not released during the degradation of this foam. The GC-MS analysis confirmed that DAT was not present in any of the cold-ring fractions. DAT arises from degradation of the urethane linkage *via* a six-membered ring mechanism which is proposed to be the predominant reaction under confined conditions when the TDI and polyol released from the depolymerisation reaction become trapped and recombine. The results, however, demonstrated that under an oxidative environment the polyol undergoes degradation at a much lower temperature than in an inert atmosphere. It was, therefore, proposed that the polyol does not reside within the pyrolysis zone for as long and so cannot recombine with the TDI. Alternatively, the polyol may undergo oxidative degradation which prevents it from recombining with the TDI. The six-membered ring mechanism, therefore, would not occur to any great extent, which would explain the lack of polyurea residue during the pyrolysis under air.

The GC-MS analysis, however, also revealed that TDI was absent from all of the cold-ring fractions. It may, therefore, also be the case that the TDI undergoes oxidative

degradation reactions which thereby prevent it from recombining with the polyol. The solid-state ^{13}C NMR results revealed that by 300°C the foam is highly charred and aromatic which indicates that aromatic components have already been incorporated into the char at this temperature. This, therefore, suggests that the TDI does undergo secondary reactions under air and explains the absence of this compound in the cold-ring fractions.

These results are in stark contrast to those obtained under nitrogen and clearly demonstrate that oxygen alters the degradation of the polyurethane, leading to char being formed at a lower temperature. The solid-state ^{13}C NMR results also indicate that the chars obtained under air may be structurally different to those obtained under nitrogen, particularly at the higher temperatures.

4.2.3 Pyrolysis under 3% Oxygen in Nitrogen

Following the pyrolysis studies under nitrogen and air, a study was carried out under a 3% oxygen in nitrogen environment. A low oxygen environment is deemed to be more representative of a fire situation where depletion of the oxygen can occur quickly. The aim of this pyrolysis study was, therefore, to determine if degradation of the standard foam in a low oxygen environment resembles the degradation under air or nitrogen, *i.e.* is thermal or thermo-oxidative degradation the dominant process in this situation. If thermo-oxidative degradation is the only process occurring then the results would be expected to match those presented for the pyrolysis under air. On the other hand, if the effect of the oxygen was not significant then the results would match the pyrolysis under nitrogen. Finally, it could be the case that both thermal and thermo-oxidative processes occur, in which case the degradation behaviour would lie somewhere between the two extremes.

4.2.3.1 Mass Loss Data and Observations

Presented in Figure 4.54 is a comparison of the quantities of residue obtained from the pyrolysis of the standard foam under nitrogen, air and 3% oxygen in nitrogen. There is very little difference in the mass losses at 250°C under all three environments. As was the case during the pyrolysis under air, the foam was discoloured following the pyrolysis at 250°C under 3% oxygen in nitrogen. As the pyrolysis temperature is increased it can be observed that the mass loss in 3% oxygen in nitrogen resembles the mass loss in air more closely than that under nitrogen, although the mass loss under the low oxygen environment is not as large. The mass loss data, therefore, suggests that thermo-oxidative degradation is more dominant when the standard foam is pyrolysed in a low oxygen environment.

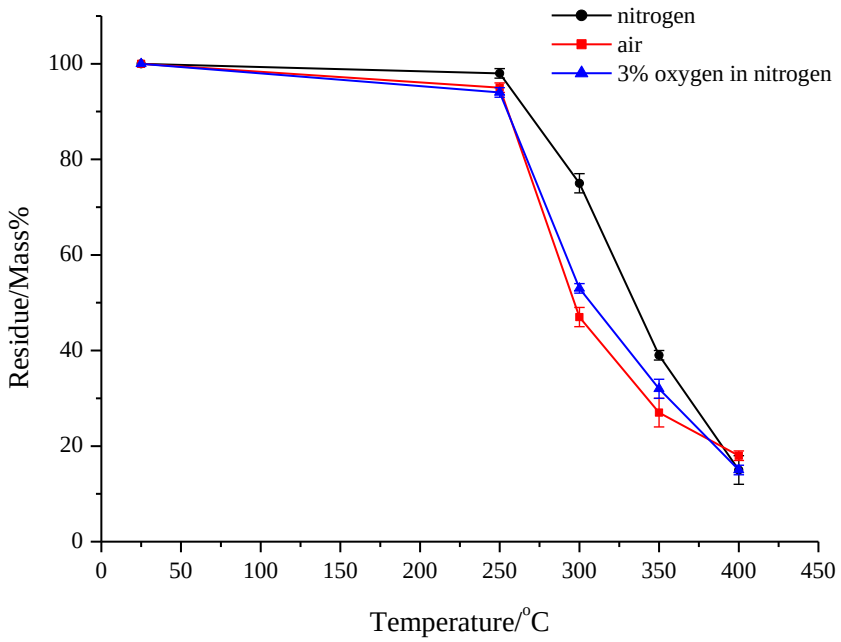

Figure 4.54: Residue obtained vs. pyrolysis temperature for the standard foam under nitrogen, air and 3% oxygen in nitrogen

4.2.3.2 Cold-ring Fraction Analysis

A cold-ring fraction was obtained at all temperatures during the pyrolysis under 3% oxygen in nitrogen, although there was only a small amount present at 250°C. This indicates that degradation of the polyurethane has begun to occur as low as 250°C and is consistent with thermo-oxidative degradation being dominant. Presented in Figure 4.55

is the FTIR spectrum of the cold-ring fraction collected at 250°C. This indicates the presence of structures containing ether, carbonyl and hydroxyl groups which may arise from thermo-oxidative degradation of the polyol component of the foam.

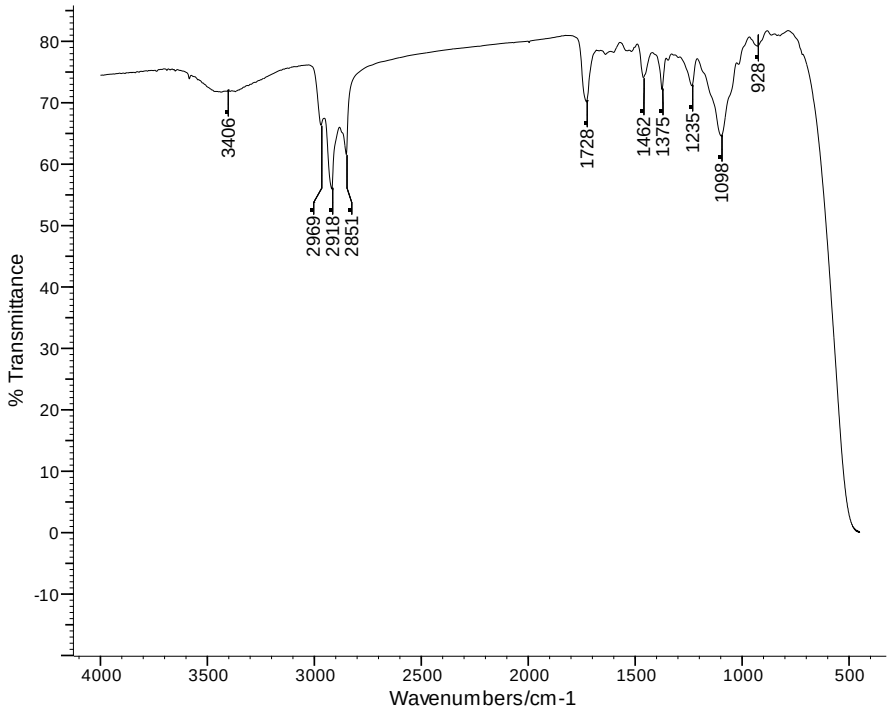

Figure 4.55: FTIR spectrum of the cold-ring fraction collected from the standard foam after pyrolysis at 250°C under 3% oxygen in nitrogen

Presented in Figure 4.56 is a comparison of this spectrum with that of the cold-ring fraction collected under air at 250°C. It is clear from this comparison that the cold-ring fraction from the 3% oxygen in nitrogen pyrolysis is identical to that from the pyrolysis under air, which confirms that the degradation at this temperature is dominated by thermo-oxidative degradation mechanisms.

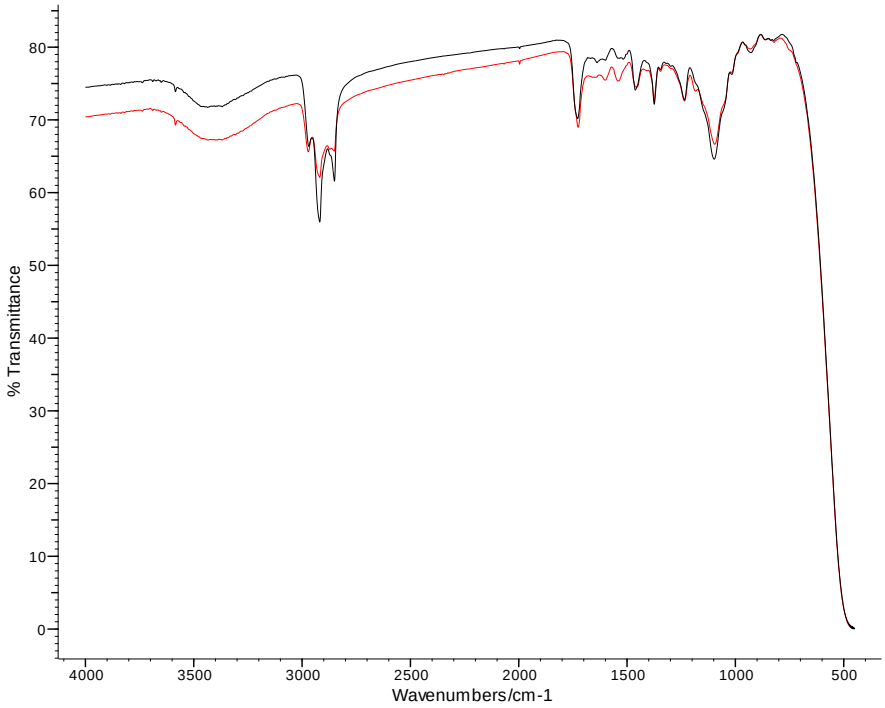

Figure 4.56: Comparison of the FTIR spectrum of the cold-ring fraction collected from the standard foam after pyrolysis at 250°C under 3% oxygen in nitrogen (black) and air (red)

The FTIR spectra of the cold-ring fractions collected at 300, 350 and 400°C were similar to that of the cold-ring fraction collected at 250°C, and similar to the cold-ring fractions collected from the pyrolysis under air. The GC-MS analysis also showed similarities between the cold-ring fractions collected under 3% oxygen in nitrogen and air, revealing the presence of high molar mass polyol chain fragments but no TDI or DAT.

The cold-ring fraction results, therefore, indicate that degradation of the standard foam under 3% oxygen in nitrogen is dominated by thermo-oxidative degradation which yields a cold-ring fraction consisting primarily of high molar mass polyol fragments. As was the case for the pyrolysis under air, the absence of DAT within the cold-ring fraction suggests that the six-membered ring mechanism does not occur to any great extent under a 3% oxygen in nitrogen environment. The TDI generated from depolymerisation of the urethane linkages is likely to undergo secondary degradation reactions which thereby prevent its recombination with the polyol and lead to its absence in the cold-ring fractions.

4.2.3.3 Residue Analysis

The residues obtained from the pyrolysis under 3% oxygen in nitrogen yielded tar and char at all temperatures. This once again suggests that the pyrolysis under a low oxygen environment is dominated by oxidative degradation reactions as there was no tar collected from the standard foam under nitrogen at 250°C. Analysis of the tars was achieved by FTIR spectroscopy, whilst the chars were characterised by solid-state ^{13}C NMR spectroscopy, FTIR spectroscopy and elemental analysis.

4.2.3.3.1 Quantification of the Tar and Char

Presented in Figure 4.57 are comparisons of the quantities of tar and char collected from the standard foam after pyrolysis under nitrogen, air and 3% oxygen in nitrogen.

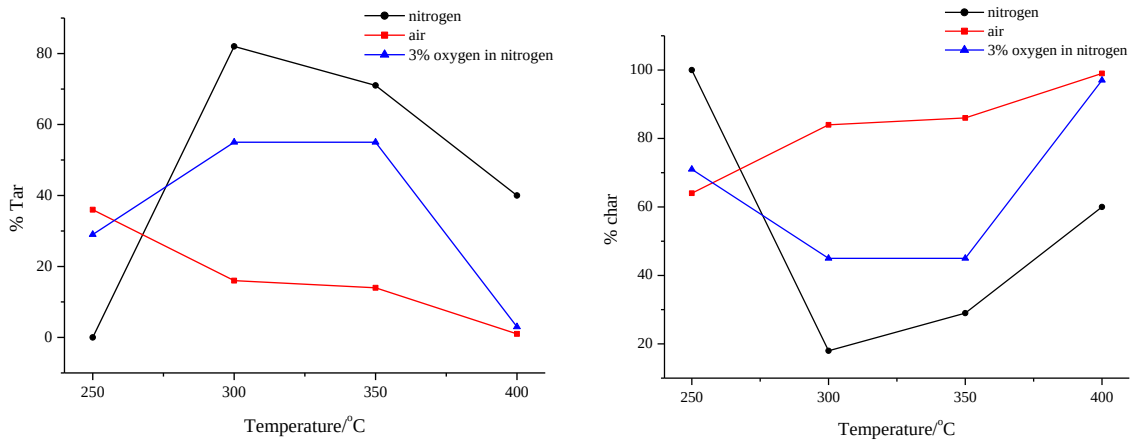

Figure 4.57: Comparisons of the quantities of tar and char collected from the standard foam after pyrolysis under nitrogen, air and 3% oxygen in nitrogen

It can be observed that the quantities of tar and char collected from the standard foam after pyrolysis under 3% oxygen in nitrogen lie between the values for nitrogen and air. At 250°C the quantities for 3% oxygen in nitrogen are close to those for the pyrolysis in air which suggests that at this temperature degradation of the standard foam under a low oxygen environment is similar to the degradation under air. As a result, thermo-oxidative degradation of the polyol has occurred to yield a significant quantity of tar. At temperatures above 250°C, however, the trend follows that of the pyrolysis under nitrogen and at 300°C and 350°C the values lie closer to those under nitrogen. At these

temperatures, lower levels of char are present from the pyrolysis under 3% oxygen in nitrogen than from the air pyrolysis, which indicates that the foam has not charred as readily in the low oxygen environment. This confirms that the degradation behaviour is not simply oxidative, but shows both oxidative and non-oxidative characteristics. This is important as it demonstrates that degradation of polyurethane foam during a fire is a very complex process, and that if the oxygen concentration is low both thermal and thermo-oxidative degradation mechanisms can be occurring.

By 400°C the quantities of tar and char under 3% oxygen in nitrogen are once again similar to the quantities collected under air, indicating that oxidative degradation becomes dominant once more at the higher temperatures.

4.2.3.3.2 Analysis of the Tar

Presented in Figure 4.58 is the FTIR spectrum of the tar collected from the standard foam after pyrolysis under 3% oxygen in nitrogen at 250°C. As was the case for the pyrolysis under nitrogen and air, the majority of the peaks are associated with the polyol component of the foam. The peak at 1729 cm^{-1} indicates the presence of carbonyl groups within the tar which arise as a result of thermo-oxidative degradation of the polyol component of the foam or from residual urethane linkages within the tar.

By 350°C the carbonyl peak at 1729 cm^{-1} is no longer present which suggests that degradation of the residual urethane linkages or volatilisation of a carbonyl-containing polyol fragment from the tar has occurred. By 400°C very little tar remains which indicates that significant degradation of the polyol has occurred by this temperature.

The FTIR spectra of the tars collected from the pyrolysis under 3% oxygen in nitrogen resemble those from the pyrolysis under air, which again suggests that thermo-oxidative degradation may be the more dominant process under the low oxygen environment.

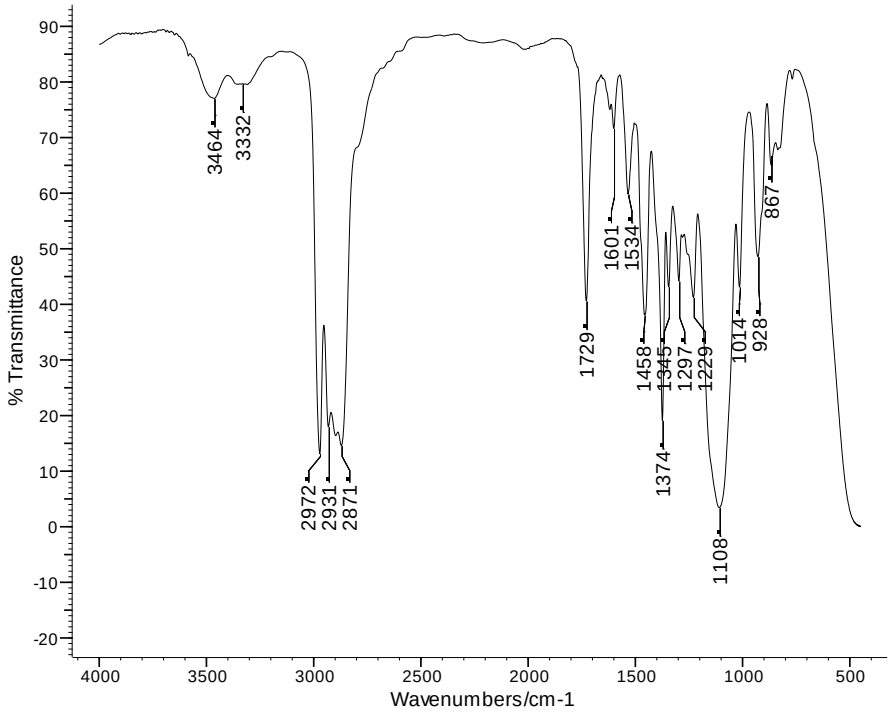

Figure 4.58: FTIR spectrum of the tar collected from the standard foam after pyrolysis at 250°C under 3% oxygen in nitrogen

4.2.3.3.3 Analysis of the Char

Presented in Figure 4.59 are photographs of the chars collected from the standard foam after pyrolysis under 3% oxygen in nitrogen. The char obtained at 250°C shows a significantly greater level of discolouration than the char under nitrogen which indicates that thermo-oxidative degradation of the standard foam has occurred at 250°C. The discolouration, however, is not as severe as in the char obtained under air. This indicates that thermo-oxidative degradation of the foam has occurred, but to a lesser extent than under air, and once again indicates that degradation of the standard foam under a low oxygen environment is complex. At 300°C the chars are similar to those obtained under air, having become black and lost their foamed structure.

Figure 4.59: Photographs of the chars collected under 3% oxygen in nitrogen

Characterisation of the chars was achieved by solid-state ^{13}C NMR spectroscopy, FTIR spectroscopy and elemental analysis.

- *Solid-state ^{13}C NMR*

Presented in Figure 4.60 are the ^{13}C CPMAS TOSS spectra for the virgin foam and the chars obtained from the standard foam after pyrolysis under 3% oxygen in nitrogen. The peak assignments for the virgin foam are the same as those discussed previously. At 250°C there is a decrease in the intensity of the polyol peaks at 75.9 and 73.8 ppm relative to the aromatic peaks which indicates that scission of the soft segments has begun to occur at this temperature. The reduction in polyol signal is, however, not as significant as it was at 250°C under air which suggests that scission of the polyol has not occurred to the same extent under 3% oxygen in nitrogen.

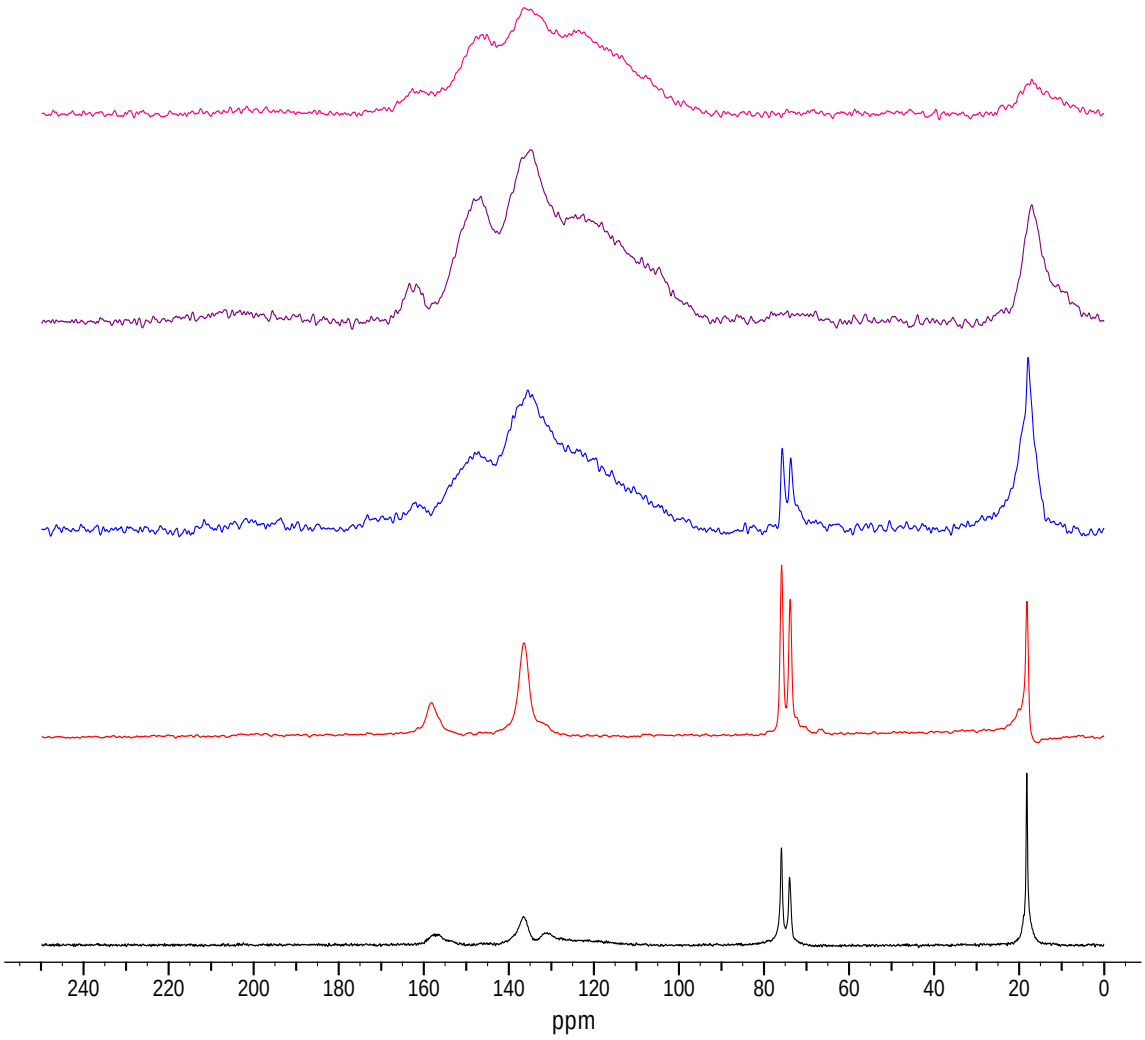

Figure 4.60: Comparison of the ^{13}C CPMAS TOSS spectra of the virgin standard foam (black) with the chars obtained after the pyrolysis under 3% oxygen in nitrogen at 250°C (red), 300°C (blue), 350°C (purple) and 400°C (pink)

The spectrum of the char at 300°C is significantly different to that at 250°C, showing a number of poorly resolved peaks between 100 and 170 ppm which indicates that the foam is highly charred at this temperature. This in contrast to the char obtained under nitrogen which still displayed well resolved peaks for the urethane linkages and aromatic carbons at this temperature. This indicates that under 3% oxygen in nitrogen the foam is in a more charred state than under a non-oxidative environment, which confirms that thermo-oxidative degradation of the foam is significant. Once again, however, the

spectrum at 300°C is not identical to that under air as polyol peaks can still be observed in the 3% oxygen in nitrogen spectrum. This indicates that there is some polyol retained within the char at 300°C as was the case for the pyrolysis under nitrogen. The spectra of the chars at 350°C and 400°C are similar to those under air.

These results, therefore, indicate that under a low oxygen environment the foam begins to char at lower temperatures than under a non-oxidative environment, however, the charring is not in as advanced a state as under air. This again confirms that the degradation of the standard foam under 3% oxygen in nitrogen is not simply an oxidative process.

- *FTIR Spectroscopy*

Presented in Figure 4.61 are the FTIR spectra for the virgin standard foam and the chars collected after pyrolysis under 3% oxygen in nitrogen at 250, 300, 350 and 400°C. The peak assignments for the virgin foam are the same as discussed previously. The spectra are similar to those obtained from the pyrolysis under air, although there are some differences observed. The spectrum at 250°C shows similarities to the virgin foam, with the presence of the carbonyl peak at 1729 cm^{-1} indicating that there are still a number of urethane linkages present within the foam at this temperature By 300°C the foam is significantly more charred and the spectrum appears more distorted. Loss of the urethane carbonyl is evident at this temperature; however, the polyol ether peak remains relatively strong at this temperature. This indicates that there is some polyol remaining within the char at this temperature and is in contrast with the results obtained under air which showed a more distorted spectrum and a weaker polyol signal. The spectra for the chars at 350°C and 400°C are more distorted as a result of the char being more carbonaceous at these temperatures.

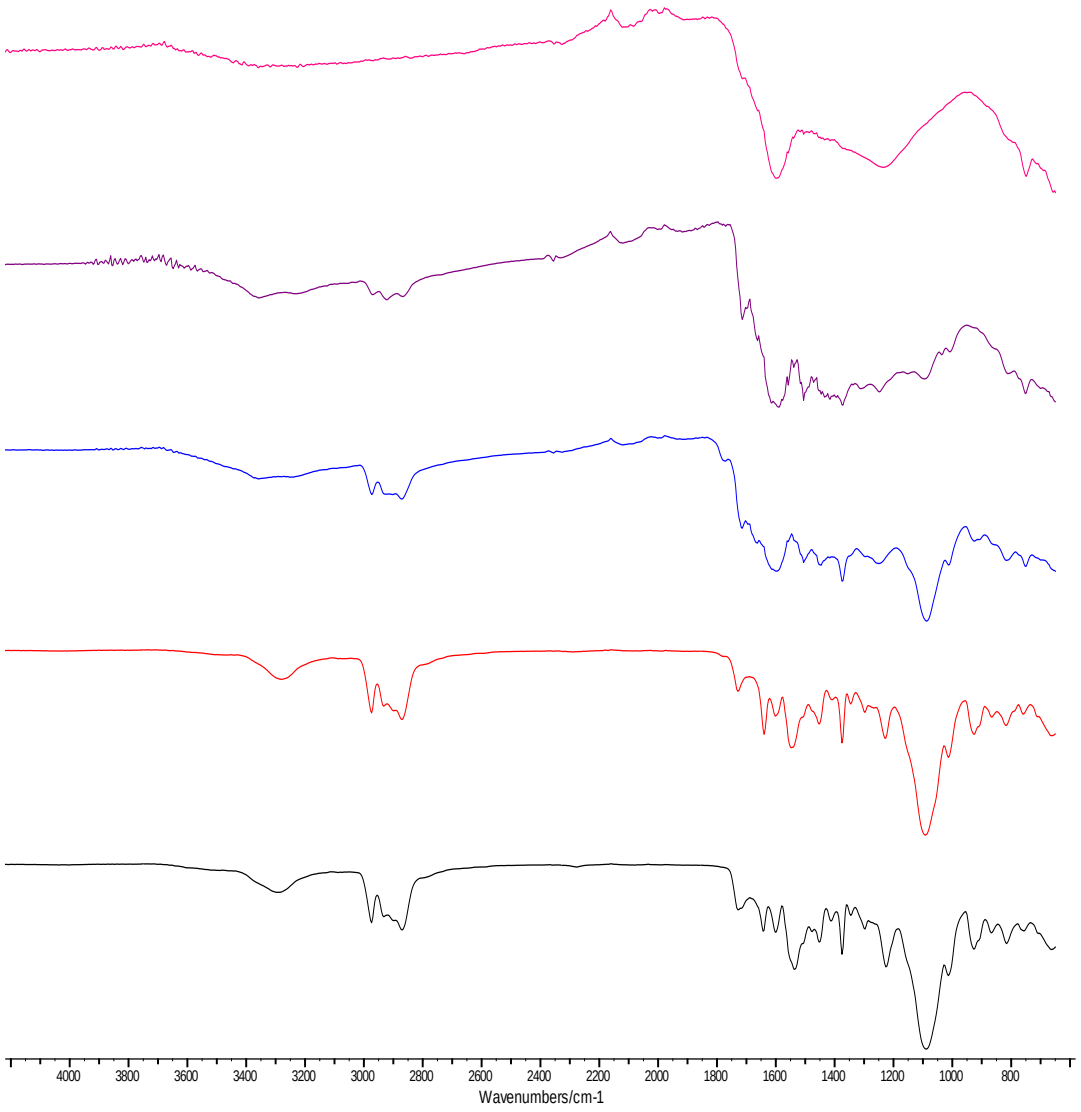

Figure 4.61: Comparison of the FTIR spectra of the virgin standard foam (black) with the chars obtained after pyrolysis under 3% oxygen in nitrogen at 250°C (red), 300°C (blue), 350°C (purple) and 400°C (pink)

These results, therefore, once again demonstrate that under the low oxygen environment thermo-oxidative degradation is more dominant, leading to charring of the foam at lower temperatures than under a non-oxidative environment. There are, however, differences observed between the pyrolysis under air and 3% oxygen in nitrogen which indicates that the degradation is not simply oxidative in nature but also shows some non-oxidative characteristics.

- *Elemental Analysis*

The chars obtained under 3% oxygen in nitrogen were submitted for elemental analysis to determine the percentages of carbon, hydrogen and nitrogen which were present. The ratio of each element with respect to the percentage carbon was then calculated in order to illustrate more clearly the changes occurring in the chars. These results are compared in Figure 4.62 with the results obtained from the pyrolysis under nitrogen and air.

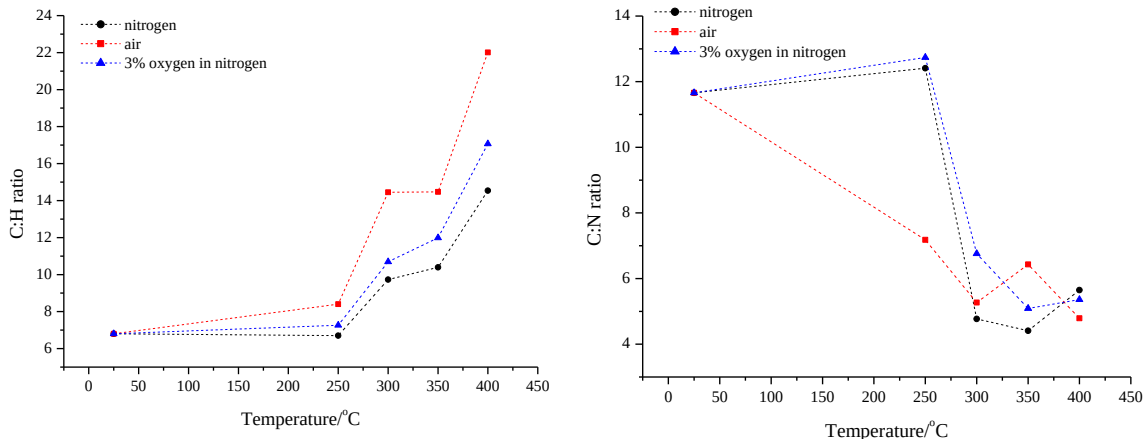

Figure 4.62: Comparison of the C:H and C:N ratios for the pyrolysis chars obtained from the standard foam under nitrogen, air and 3% oxygen in nitrogen

Under all three environments the C:H ratio increases as the pyrolysis temperature increases. This is indicative of loss of polyol from the char at the lower temperatures and ring fusion of the aromatics at the higher temperatures which yields a complex, highly unprotonated carbonaceous char. It can also be observed that the C:H ratio for the chars obtained under 3% oxygen in nitrogen lie between the values for those under nitrogen and air. This confirms that degradation of the standard foam under a low oxygen environment is not a fully thermo-oxidative process and there must be a degree of thermal degradation occurring too.

The C:N ratio shows a more similar trend to the chars obtained under nitrogen, indicating that as the polyol is lost from the system a large quantity of the nitrogen in the foam gets incorporated into the char. At 350°C under air the C:N ratio was observed to increase before decreasing again at 400°C. This was, however, not observed for the

chars obtained under 3% oxygen in nitrogen which once again indicates that thermo-oxidative degradation is not the only process occurring under 3% oxygen in nitrogen.

4.2.3.4 Summary

The aim of the pyrolysis under 3% oxygen in nitrogen was to determine if degradation of the standard foam in a low oxygen environment resembles thermal or thermo-oxidative degradation, as this will indicate which process dominates. The results are interesting and reveal that degradation in a low oxygen environment is a complex process, with the degradation behaviour lying somewhere between that observed under nitrogen and air.

There was little difference in the mass losses between the three environments at 250°C, however, the foam had discoloured at this temperature under 3% oxygen in nitrogen, a large quantity of polyol-based tar was extracted and a small level of cold-ring fraction was obtained. These results were similar to those under air but in contrast to the results under nitrogen, which indicates that thermo-oxidative degradation of the polyurethane is dominant at 250°C.

At temperatures above 250°C the mass losses more closely resembled those observed under air. The quantities of tar and char, however, were between those obtained under nitrogen and air and this was also the case for the elemental analysis results. This suggests that the degradation behaviour is not simply oxidative but is complex and likely involves both thermal and thermo-oxidative degradation processes.

The chars obtained under 3% oxygen in nitrogen showed levels of discolouration between those observed for the chars generated under air and nitrogen. Analysis of the chars by solid-state ^{13}C NMR and FTIR spectroscopy revealed that the foam was in a more charred state at the lower temperatures than the chars obtained from the pyrolysis under nitrogen at equivalent temperatures. The foam was, however, charred to a lesser extent than during the pyrolysis under air.

The results from the 3% oxygen in nitrogen pyrolysis, therefore, reveal that degradation of the standard foam in a low oxygen environment is complex, with both thermal and thermo-oxidative processes likely to occur. This is important and must be considered when developing new fire retardants systems for use within polyurethane foams, as any fire retardant must be able to work under both inert and oxidative conditions.

4.3 Conclusions

The results presented in this chapter have demonstrated that the thermal and thermo-oxidative degradation of a standard TDI-based polyurethane foam are complex processes which consist of different competing mechanisms which yield an array of volatile and involatile degradation products, as well as complex residues consisting of tar and char material. The results have also demonstrated that the degradation mechanisms of polyurethane are dependent on the experimental conditions of the pyrolysis or degradation technique being employed.

Under an inert environment the foam is observed to undergo a two step thermal degradation mechanism in which the initial step corresponds to degradation of the urethane linkages and the second step consists of secondary degradation processes. Thermal degradation under nitrogen and helium occurs over the temperature range 260°C to 400°C, whilst under vacuum the degradation occurs at lower temperatures as volatilisation of the degradation products is facilitated.

Results from the TVA studies revealed that degradation of the urethane linkages under vacuum occurs by two competing mechanisms. The first mechanism, proposed to be the predominant mechanism, involves simple depolymerisation of the urethane bond to yield TDI and polyol. A second, competing mechanism is proposed to occur which involves dissociation of the urethane linkages to yield DAT, CO_2 and alkene-terminated polyol chains. The amines are then proposed to react in the vapour phase with the regenerated TDI to yield polyurea. The secondary degradation processes observed by TVA, TGA and DSC can be attributed primarily to degradation of the polyol which was regenerated

in the first degradation step. Isothermal TVA studies revealed that this occurs as low as 250°C under vacuum but does not become significant until temperatures greater than 300°C. Degradation of the polyol is proposed to occur by random radical chain scission to yield propene, formaldehyde, acetaldehyde, C_3H_6O isomers and high molar mass polyol chain fragments of various structures.

Pyrolysis studies under nitrogen also revealed the presence of two competing degradation mechanisms for the urethane linkages, however, in this study DAT was observed as a major degradation product. It is proposed that degradation of the urethane linkages occurs *via* a depolymerisation reaction to yield TDI and polyol, however, under the higher pressure, more confined conditions of the pyrolysis the isocyanate cannot volatilise from the system as readily as under vacuum and so recombines with the polyol to reform the urethane bond. Degradation of the urethane linkages *via* a six-membered ring transition state then becomes the predominant reaction. Thermal degradation of the polyol-based tar then occurs to yield volatile degradation products and high molar mass fragments. Analysis of the char residues reveals that at the higher temperatures a complex aromatic carbonaceous char is formed.

Pyrolysis studies under air revealed that degradation of the polyurethane occurs at a lower temperature than under nitrogen and that the chemistry occurring in the condensed-phase is different. The foam was observed to be highly charred by 300°C which confirms that the presence of oxygen alters or accelerates the charring reactions of the foam. During this pyrolysis study neither TDI nor DAT were observed as major degradation products and there are a number of proposed reasons for this. The polyol is observed to undergo thermo-oxidative degradation at much lower temperatures than thermal degradation and so the polyol will not reside within the pyrolysis zone for as long and so cannot recombine with the TDI. Alternatively the polyol may undergo oxidative degradation reactions which prevent it from recombining with the TDI. In both these cases the six-membered ring transition state would not be dominant and as such DAT would not be evolved. The absence of TDI was proposed to be a result of this

species undergoing oxidative degradation reactions which lead to it being incorporated into the char.

Finally, degradation in a low oxygen environment was shown to be a complex process, with the degradation behaviour lying between that of thermal and thermo-oxidative degradation. The foam begins to degrade and becomes more charred at lower temperatures than under nitrogen, however this is not as extreme as when the foam is pyrolysed under air. It is, therefore, proposed that both thermal and thermo-oxidative degradation occurs when the foam is degraded in a low oxygen environment and this is important to understand when considering a fire situation and when developing new fire retardant systems. These results also reinforce the issue that results from laboratory based degradation studies must be used with caution and may not necessarily be representative of a fire situation. In most cases degradation studies will deal simply with the degradation under air and/or nitrogen, not in a low oxygen environment.

4.4 References

[1] N. Grassie and G. Scott, *Polymer Degradation and Stabilisation*, Cambridge University Press, Cambridge, 1985, Ch. 4, p. 86

[2] A. W. Benbow and C. F. Cullis, C*ombust. Flame.*, 1975, **24**, 217

[3] R. Bilbao, J. F. Mastral, J. Ceamanos, and M. E. Aldea, *J. Anal. Appl. Pyrol.*, 1996, **37**, 69

[4] D. K. Chattopadhyay and D. C. Webster, *Prog. Polym. Sci.*, 2009, **34**, 1068

[5] M. Ravey and E. M. Pearce, *J. Appl. Poly. Sci.*, 1997, **63**, 47

[6] K. L. Erickson, *J. Therm. Anal. Calorim.*, 2007, **89**, 427

[7] N. Grassie and M. Zulfiqar, *J. Polym. Sci. Pol. Chem.*, 1978, **16**, 1563

[8] N. Grassie and A. P. Mendoza, *Polym. Degrad. Stabil.*, 1985, **10**, 267

[9] N. Grassie and A. P. Mendoza, *Polym. Degrad. Stabil.*, 1985, **11**, 359

[10] N. Grassie and A. P. Mendoza, *Polym. Degrad. Stabil.*, 1984, **9**, 155

[11] L. Costa, G. Camino. M. P. Luda, G. G. Cameron and M. Y. Qureshi, *Polym. Degrad. Stabil.*, 1995, **48**, 325

[12] G. G. Cameron, M. D. Ingram, M. Y. Qureshi, H. M. Gearing, L. Costa and G. Camino, *Eur. Polym. J.*, 1989, **25**, 779

[13] E. Dyer and G. E. Newborn Jr., *J. Am. Chem. Soc.*, 1958, **80**, 5495

[14] S. T. Marks and E. Metcalfe, *Combust. Flame.*, 1996, **107**, 260

[15] M. P. Thorne, *Can. J. Chemistry.*, 1967, **45**, 2537

[16] L. Shufen, J. Zhi, Y. Kaijun, Y. Shuqin and W. K. Chow, *J. Polymer-Plastics Technology and Engineering*, 2006, **45**, 95

[17] T. C. Chang, W. S. Shen, Y. S. Chiu and S. Y. Ho, *Polym. Degrad. Stabil.*, 1995, **49**, 353

[18] L. Shufen, J. Zhi, Y. Kaijun, Y. Shuqin and W. K. Chow, *J. Polymer-Plastics Technology and Engineering*, 2006, **45**, 95

[19] L. Costa, G. Camino, M. P. Luda, G. G. Cameron and M. Y. Qureshi, *Polym. Degrad. Stabil.*, 1996, **53**, 301

[20] T. Servay, R. Voelkel, H. Schmiedberger and S. Lehman, *Polymer*, 2000, **41**, 5247

5 Study on the APP Foam

A comprehensive study was conducted on a TDI-based foam containing 13.35% APP in order to examine the effect that this conventional fire retardant has on the thermal and thermo-oxidative degradation behaviour of the polyurethane foam. Again the overall degradation behaviour was examined by means of TGA, DSC and TVA studies. A small scale mini-crib fire test was also performed on the APP foam to examine the fire behaviour of the polyurethane foam and the effect which the fire retardant has on the flammability of the foam. Finally, pyrolysis studies were employed to characterise the condensed-phase behaviour in inert and oxidative environments. Any additional data not presented within this chapter can be found in Appendix 2.

5.1 Overview of the Degradation and Fire Behaviour

5.1.1 DSC

Presented in Figure 5.1 are the DSC curves for the standard and APP foams analysed under an oxidative environment. The APP foam clearly shows differences in its thermo-oxidative behaviour compared to the standard foam which suggests that the fire retardant foam undergoes a different degradation process. The APP foam exhibits three main exothermic events which correspond to different degradation processes. The first exotherm, which occurs between 255°C to 290°C, is significantly reduced and appears to consist of two peaks which suggest two separate degradation processes are occurring in this temperature range. It is proposed that this step corresponds not only to degradation of the urethane linkages, but also to the initial degradation stage of the fire retardant. The reduction in the heat flow suggests that either the fire retardant is decomposing endothermically thereby exhibiting a heat-sink effect, or the degradation reactions occurring are different to those which occur for the standard foam. The DSC of APP on its own exhibits a small endotherm around 250°C which corresponds to the first degradation step of the fire retardant. This small endotherm does not, however,

equate to the significant reduction in heat flow which is observed in Figure 5.1. This indicates that the reduced heat flow is not as a result of APP acting as a heat-sink but instead must be as a result of the different degradation chemistry which is occurring in the presence of the APP.

The second and third exothermic peaks, which occur in the temperature range 290°C to 400°C, are proposed to correspond to further degradation of the APP fire retardant and the secondary degradation reactions of the polyurethane. The fact that these peaks are not fully resolved from one another suggests that the temperature ranges of these two degradation processes overlap. The thermo-oxidative degradation of the APP foam is, therefore, significantly different to that of the standard foam.

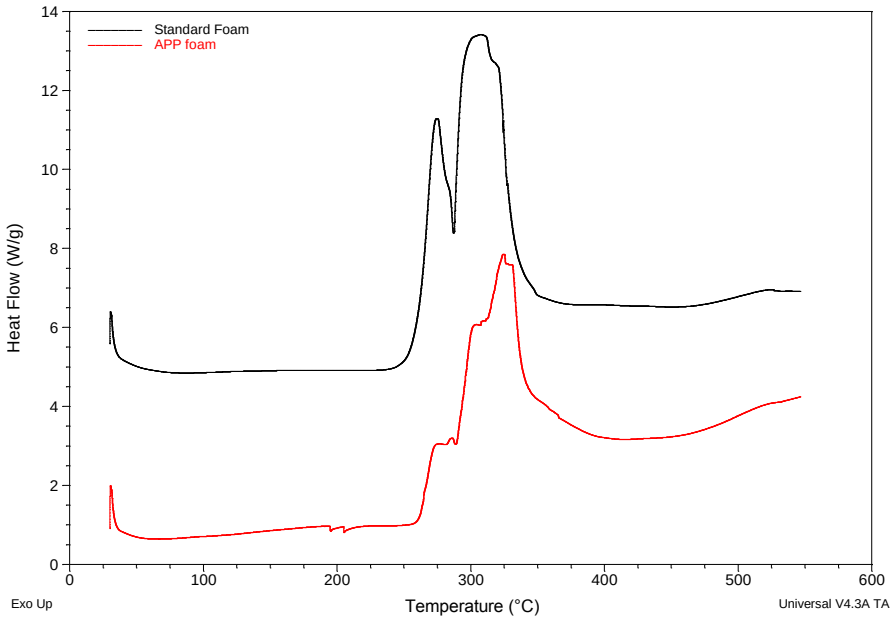

Figure 5.1: DSC curves for the standard foam and APP foam in air

The DSC curves for the analysis of the standard and APP foams under nitrogen are presented in Figure 5.2. The APP foam is similar to that of the standard foam, exhibiting two distinct endothermic peaks. Displayed in Table 5.1 are the temperatures of the peak maxima for the standard and APP foams analysed under nitrogen. The similarities in the temperatures for the first peak suggest that the primary degradation

step of the polyurethane, *i.e.* degradation of the urethane linkages, is not significantly altered in the presence of APP. The temperature of the second peak maxima, on the other hand, is slightly lower in the APP foam which suggests that the secondary degradation reactions, in particular degradation of the polyol component of the foams, are altered by the fire retardant.

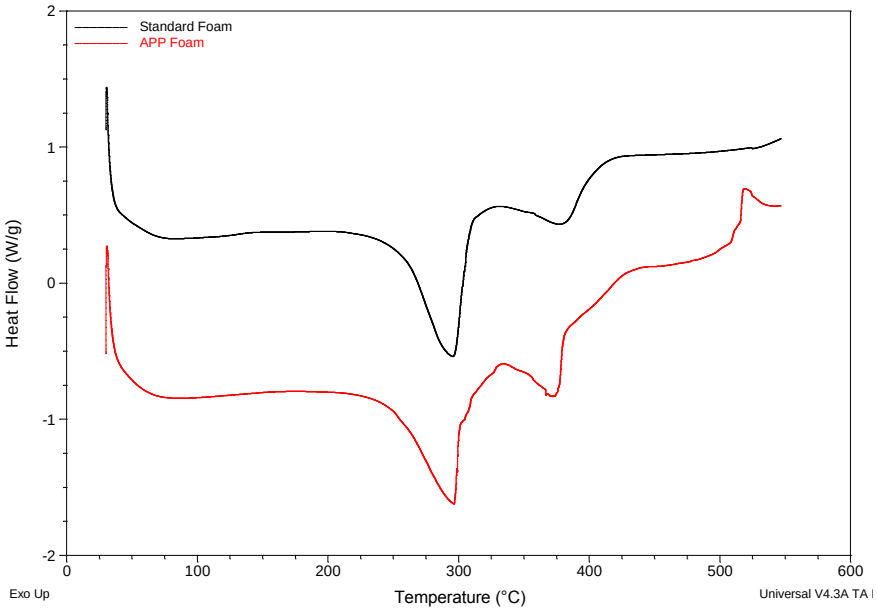

Figure 5.2: DSC curves for the standard and APP foams analysed in N_2

Type of Foam	**Peak 1 Maximum/°C**	**Peak 2 Maximum/°C**
Standard	295 ± 2	380 ± 1
APP	297 ± 1	374 ± 2

Table 5.1: Peak maxima for the standard and APP foams

5.1.2 TGA

The TGA and DTG curves for the standard and APP foams analysed in air are presented in Figure 5.3, with the temperatures at which significant mass loss occurs and the maximum temperatures of the DTG peaks displayed in Table 5.2. A two step degradation process is observed for the APP foam, however, there are differences

observed in the thermo-oxidative behaviour compared to that of the standard foam. Significant mass loss is evident at similar temperatures for both foams and the initial mass loss step for the APP occurs with a maximum rate of mass loss at the same temperature as for the standard foam. This suggests that the temperature at which the first degradation step of the polyurethane occurs is not significantly altered in the presence of APP under an oxidative environment. The APP foam, however, exhibits less mass loss in this first step than the standard foam which suggests that the mechanisms of degradation may be altered by the fire retardant.

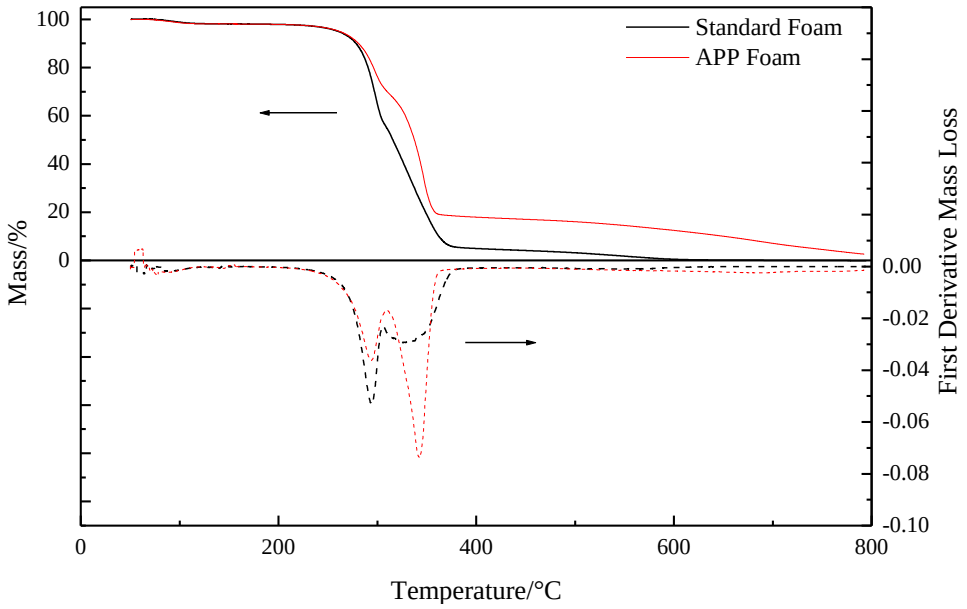

Figure 5.3: TGA (solid lines) and DTG (dashed lines) results for the standard and APP foam analysed in air

Type of Foam	Onset of Significant Mass Loss/°C	Peak 1 Maximum/°C	Peak 2 Maximum/°C
Standard	260	294	330
APP	261	294	343

Table 5.2: Onset temperatures and peak maxima for the standard and APP foams analysed in air

The maximum rate of mass loss for the second step occurs at a higher temperature in the APP foam which suggests that the fire retardant is altering the secondary degradation

mechanisms of the polyurethane foam. Finally, it can be observed from Figure 5.3 that the APP foam has a residue of approximately 20% remaining at 360°C before a slow continual mass loss occurs until 800°C resulting in a final residue of 3%. The standard foam, on the other hand, has significantly less residue remaining after the second mass loss step (approximately 6%) and has a negligible residue remaining at the end of the analysis. An increase in the level of char is expected as a proportion of the APP will remain in the solid-phase even at 800°C. The TGA of APP on its own under air shows that a residue of approximately 4% remains at 800°C, which equates to 0.5% of the 3% residue observed for the foam which contains 13.35% APP. This confirms that the observed increase in char yield for the APP foam is a result of the fire retardant promoting char formation, as has been reported in the literature.[1,2]

Presented in Figure 5.4 are the TGA and DTG curves for the standard and APP foams analysed in helium. The temperatures at which significant mass loss occurs and the maximum temperatures of the DTG peaks are displayed in Table 5.3.

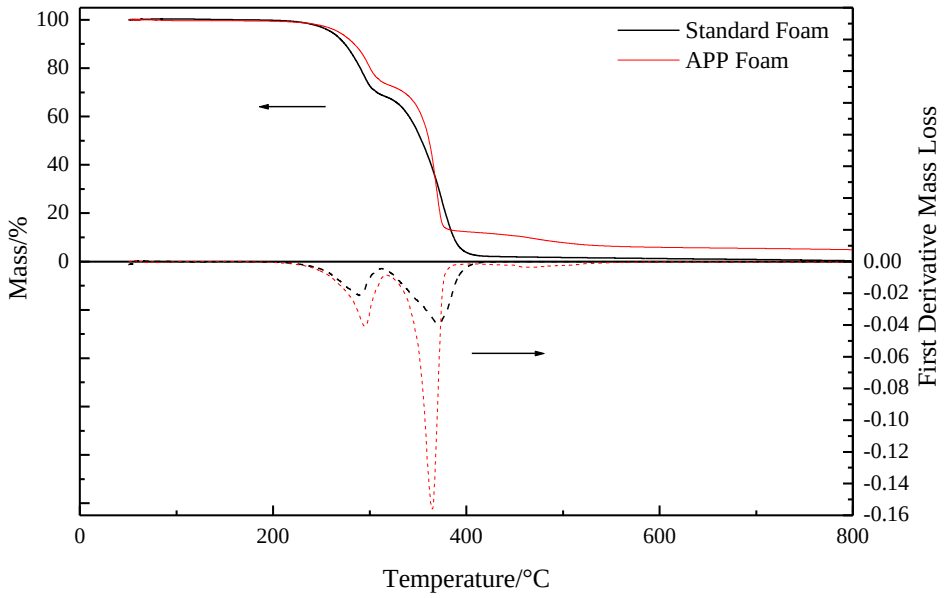

Figure 5.4: TGA (solid lines) and DTG (dashed lines) results for the standard and APP foams analysed in He

Type of Foam	**Onset of Significant Mass Loss/°C**	**Peak 1 Maximum/°C**	**Peak 2 Maximum/°C**
Standard	260	289	370
APP	268	295	365

Table 5.3: Onset temperatures and peak maxima for the standard and APP foams analysed in He

Once again it can be observed that the APP foam shows differences in its thermal degradation behaviour compared to that of the standard foam. A higher onset of significant mass loss is observed for the APP foam and the initial mass loss step occurs with a maximum rate of mass loss at higher temperatures. This suggests that the primary degradation step of the polyurethane foam may be altered in the presence of the fire retardant. The second degradation step, on the other hand, occurs with a maximum rate of mass loss at a lower temperature than for the standard foam. This suggests that the secondary degradation processes are accelerated in the presence of APP or are different to those which occur for the standard foam.

Finally, it can be observed from Figure 5.4 that the foam has a residue of approximately 13% remaining at 380°C before a slow continual mass loss occurs until 800°C resulting in a final residue of 5%. This is in contrast to the standard foam which has significantly less residue remaining after the second mass loss step (approximately 3%) and has a negligible residue remaining at the end of the analysis. The TGA of APP on its own under helium shows that again a residue of approximately 4% remains at 800°C, which equates to 0.5% of the 5% residue observed for the foam. Again this indicates that APP promotes the formation of char in this polyurethane foam.

The TGA results reveal that the char yields obtained from the APP foam differ significantly between the oxidative and inert environments. At the lower temperatures under air the quantity of char is larger than under nitrogen. This is in correlation with the results of Duquesne *et al.* who reported that the presence of oxygen during the

degradation of an APP-containing polyurethane leads to the formation of a carbonaceous char which is stable in the temperature range 350-530°C.[3,4]

5.1.3 TVA

5.1.3.1 Dynamic TVA Study

- ***Degradation Profile***

The TVA degradation profiles for the standard and APP foams showing the rate of volatiles evolution as a function of furnace temperature are presented in Figure 5.5. The sample temperatures for the major events which occur during the degradation of these foams are presented in Table 5.4.

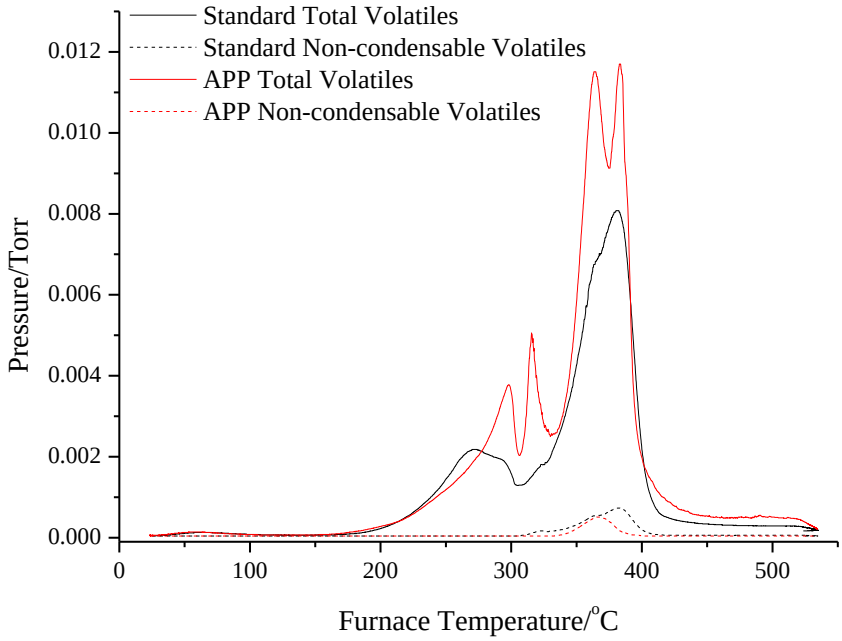

Figure 5.5: TVA degradation profiles for the standard and APP foams

Foam	Onset of Volatiles Evolution (°C)	Peak 1 Max. rate of volatiles evolution (°C)	Peak 2 Max. rate of volatiles evolution (°C)	Peak 3 Max. rate of volatiles evolution (°C)	Peak 4 Max. rate of volatiles evolution (°C)	End of volatiles evolution (°C)
Standard	~145	241	351	-	-	~400
APP	~135	268	285	334	352	~410

Table 5.4: Sample temperatures for the key events occurring during the degradation of the standard and APP foams

It can be clearly observed from Figure 5.5 that the APP foam exhibits a significantly different degradation profile to that of the standard foam. Evolution of volatile material occurs at a lower temperature for the APP foam which could be a result of degradation of the fire retardant commencing, or it could indicate that the fire retardant lowers the temperature at which the polyurethane begins to degrade. Grassie and Mendoza[5] and Duquesne *et al.*[4] proposed that the depolycondensation reaction of the urethane linkages is acid-catalysed by the acidic hydroxyl groups which arise from degradation of APP to form ultraphosphate. It could, therefore, be the case that the evolution of volatile material occurs at a lower temperature as a result of the degradation of the urethane linkages being catalysed by the acidic species produced as the fire retardant degrades.

It can be observed from Figure 5.5 that the volatile degradation products are evolved from the APP foam in four steps, each of which corresponds to a different degradation process. The first two degradation steps with maximum rates of volatiles evolution at 268°C and 285°C are likely to correspond to degradation of the urethane linkages within the foam, primarily by an acid-catalysed depolycondensation reaction, and degradation of the APP to form the ultraphosphate followed by degradation of this compound to yield polyphosphoric acid.[6] The third degradation process, which exhibits a maximum rate of volatiles evolution at 334°C, occurs with evolution of a low level of non-condensable volatiles. These volatiles were identified by online MS as primarily methane and CO, with traces of hydrogen also present. This third step can, therefore, be attributed to degradation of the polyol component of the foam as these non-condensable volatiles result from degradation reactions of the polyol. This occurs at a lower temperature than that of the standard foam which suggests that the degradation mechanisms which are operating are altered in the presence of APP. Finally, the fourth degradation step can be proposed to be due to the final degradation step of the APP in which the polyphosphoric acid decomposes to yield phosphate fragments.[6]

It is interesting to note that the TVA profile revealed the presence of four stages of volatiles evolution, whereas the TGA results only showed a two step mass loss profile.

It can be observed from the TVA profile that the first two steps are not completely resolved from each other, nor are the third and fourth steps, which indicates that the degradation steps for the APP foam are overlapping. Volatilisation of the degradation products is facilitated under vacuum; therefore, the presence of four overlapping steps is more evident in the TVA curves. During the TGA experiments, on the other hand, the degradation steps overlap to such an extent that only two mass loss steps are observed. This observation highlights the value of the TVA technique and the need to employ complementary analysis techniques when studying the degradation of polymers.

A significant residue remained at the base of the TVA tube following the analysis of the analysis of the APP foam; this was not observed during the degradation of the standard foam and suggests that APP promotes the charring reactions within the foam. Due to complications with removing the residue from the sample tube no further analysis was conducted on this material.

- ***Cold-ring Fraction Analysis***

During the analysis of the APP foam a significant yellow liquid cold-ring fraction was collected. The FTIR spectrum for this cold-ring fraction showed peaks similar to those for the cold-ring fraction collected from the standard foam (Figure 4.7). The GC-MS chromatogram also showed similar results to that of the standard foam with TDI being identified, as well as a series of high molar mass polyol chain fragments which arise from degradation of the polyol component of the foam. The presence of TDI in the cold-ring fraction confirms that the degradation mechanism of the urethane bonds within the polyurethane foam is not significantly affected by the APP. The depolymerisation reaction is, therefore, proposed to be the predominant reaction which occurs.

- ***Condensable Fraction: Sub-ambient Differential Distillation and Characterisation***

The condensable fraction collected from the APP foam was separated by sub-ambient differential distillation into three fractions which were subsequently analysed by FTIR spectroscopy and GC-MS. The sub-ambient differential distillation trace for the

standard and APP foams are presented in Figure 5.6. with the identifications for each of the peaks in the sub-ambient differential distillation trace presented in Table 5.5.

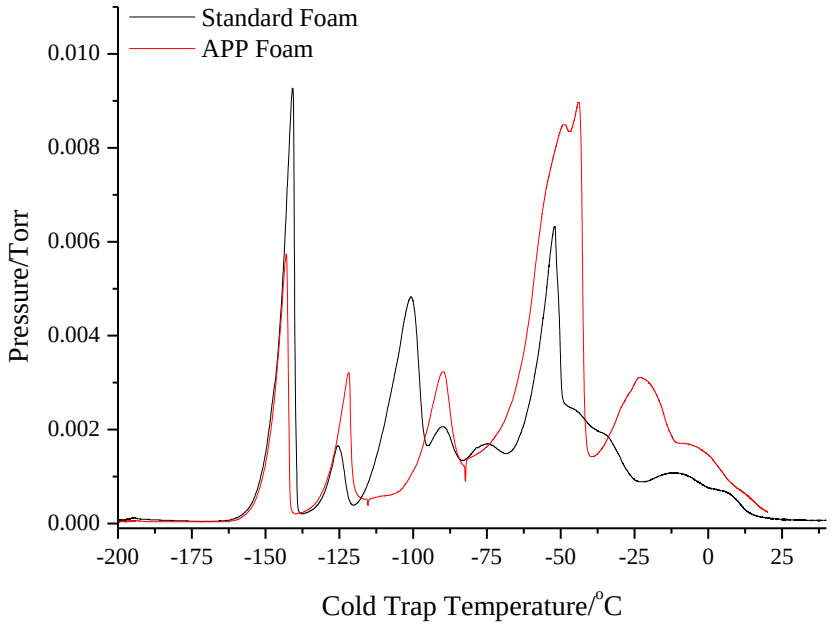

Figure 5.6: Sub-ambient differential distillation traces for the condensable fractions collected from the standard and APP foams

Peak	**Standard Foam**	**APP Foam**
1	Propene and CO_2	Propene and CO_2
2	Formaldehyde	Ammonia
3	Acetaldehyde	No peak 3 present for this foam
4	C_3H_6O compounds	Propanal
5	Higher molar mass polyol fragments	No peak 5 present for this foam
6	Water and higher molar mass polyol fragments	Water and higher molar mass polyol fragments
7	Higher molar mass polyol fragments	Higher molar mass polyol fragments including 2,5-dimethyl-1,4-dioxane

Table 5.5: Identifications for the peaks in the sub-ambient differential distillation traces of the standard and APP foams

It can be observed that the APP foam shows significant differences in both the nature and level of the degradation products evolved compared to the standard foam. Formaldehyde and acetaldehyde, which are two key degradation products evolved from the standard foam, are absent in the APP foam. Instead, ammonia and propanal are evolved and much larger quantities of water and higher molar mass species are observed.

Shown in Figure 5.7 is the mass spectrum of the second peak from the APP foam which confirms the presence of ammonia. Ammonia and water are evolved during the degradation of the APP foam as a result of degradation of the fire retardant.[6]

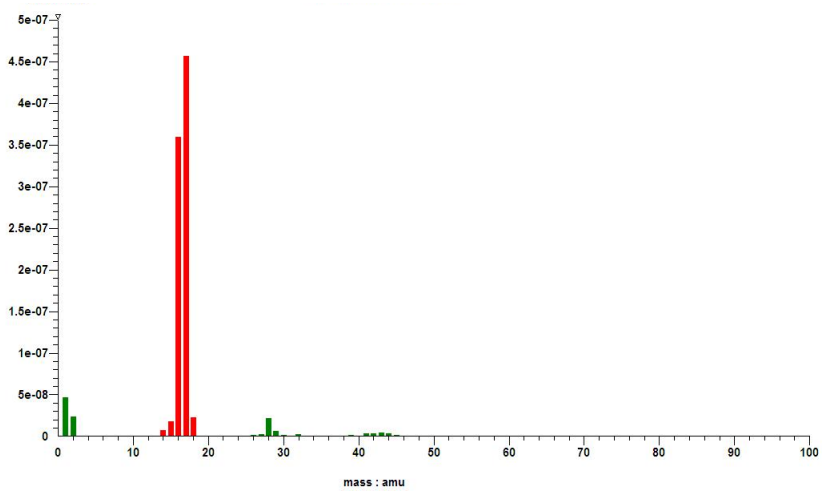

Figure 5.7: Mass spectrum of ammonia from the APP foam

A complex mixture of higher molar mass compounds was evolved from -40°C onwards; these are likely to consist of polyol fragments and phosphate fragments which arise from degradation of the APP. The GC-MS chromatogram for the final fraction collected from the APP revealed the presence of an additional compound not present in the standard foam. The compound was identified as 2,5-dimethyl-1,4-dioxane, the structure of which is shown in Figure 5.8.

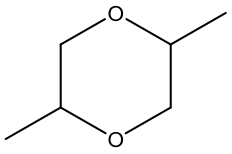

Figure 5.8: The structure of 2,5-dimethyl-1,4-dioxane

The fundamental differences which are observed in the sub-ambient differential distillation trace for the APP foam compared to the standard foam suggest that different degradation mechanisms are occurring for this foam.

5.1.3.2 Isothermal TVA Study

In order to gain further information regarding the overlapping degradation processes observed during the degradation of the APP foam, isothermal TVA experiments were conducted at 250, 300, 350 and 400°C.

- ***Isothermal TVA Profiles***

Presented in Figure 5.9 are the TVA curves for the isothermal degradation studies for the APP foam.

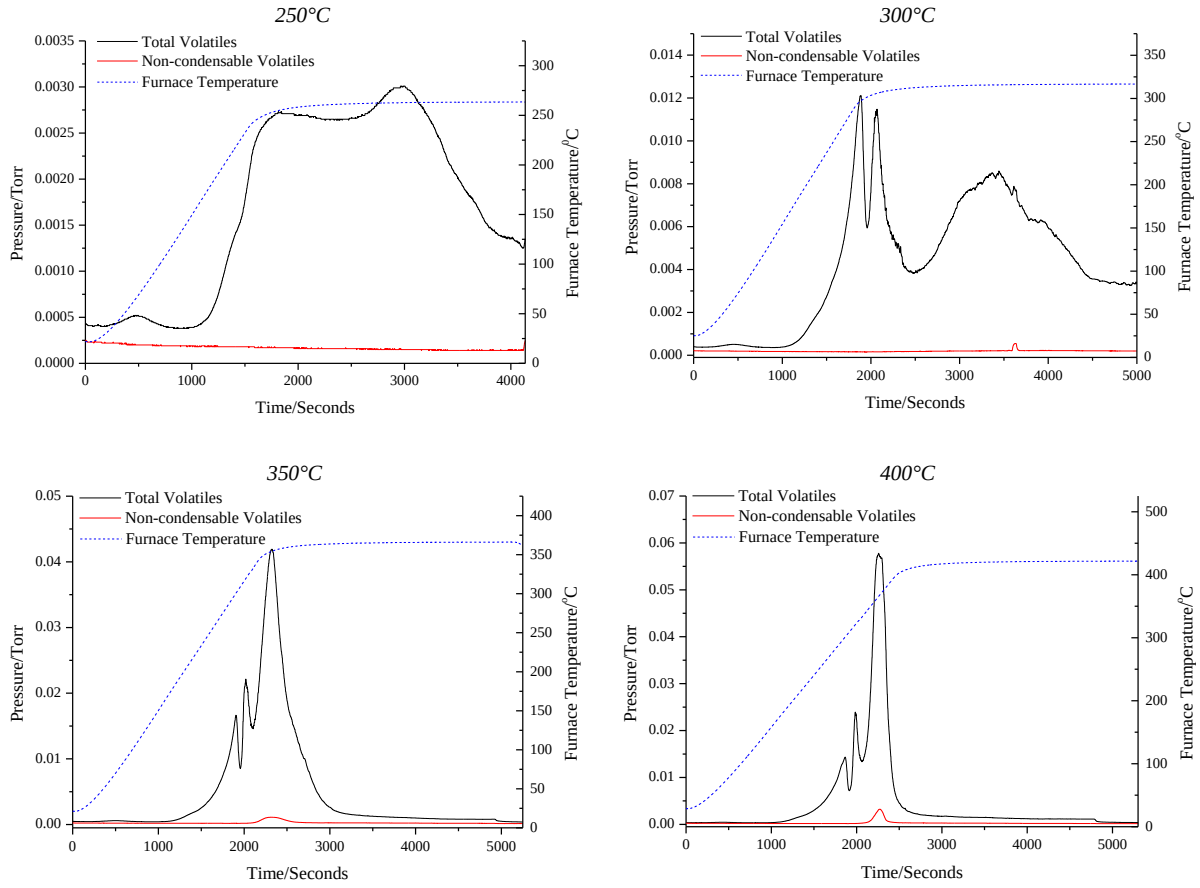

Figure 5.9: Isothermal TVA curves for the APP foam at 250, 300, 350 and 400°C

The TVA profile at 250°C shows the presence a broad peak corresponding to the evolution of a low level of volatile material at this temperature. These volatiles are most likely degradation products associated with the degradation of the urethane linkages and polyol component of the foam; however, the volatiles may also be associated with first degradation step of the APP fire retardant, *i.e.* degradation of the APP to form an ultraphosphate. If this was the case then ammonia and water would be observed. By 300°C the first two degradation steps are complete and the third step begins to occur during the isothermal hold. As was the case for the analysis of the standard foam, there were no significant non-condensable volatiles detected by 300°C which indicates that the degradation reactions of the polyol which yield CO, methane and hydrogen are not significant at lower temperatures.

By 350°C the third peak is essentially complete and a peak corresponding to the evolution of non-condensable volatiles (methane, CO and traces of hydrogen) is now observed. This indicates that at temperatures between 300°C and 350°C the degradation reactions of the polyol which yield non-condensable material have become significant. The TVA profile at 400°C shows little difference to that at 350°C. It is interesting to note that in the dynamic TVA experiment in which the sample was heated to 550°C there were two overlapping peaks observed between 300°C and 400°C, whilst in the isothermal runs there was only one peak observed. This suggests that in the isothermal experiments, where larger sample sizes are employed, the two peaks completely overlap and appear as one single peak. This is most likely a result of the greater thermal lag effects which will be encountered through use of significantly larger samples of foam.

- ***Cold-ring Fraction Analysis***

At 250°C a small amount of cold-ring fraction was recovered, however, the FTIR and GC-MS spectra of this fraction were weak and showed few peaks of interest. By 300°C the cold-ring fraction was more significant, with the FTIR and GC-MS spectra revealing the presence of TDI and polyol-based degradation products. This indicates that at 300°C degradation of the polyol component of the foam to yield high molar mass fragments has

become significant. Similar spectra were obtained for the cold-ring fractions collected at 350°C and 400°C.

- ***Residue Analysis***

During the isothermal degradation of the APP foam a clear liquid chloroform-soluble residue was recovered from the base of the TVA tube following the degradations at 250°C and 300°C. There was no liquid residue remaining at 350°C or 400°C which indicates that the polyol had degraded completely by 350°C. This is in contrast to the results for the standard foam which showed that a liquid residue was still present at 350°C. The absence of a liquid residue at 350°C for the APP foam could be due to degradation of the polyol being accelerated in the presence of the fire retardant or it could be the case that the APP causes the foam to char at lower temperatures and the remaining polyol gets incorporated into the char structure at 350°C. In either case these results, once again, highlight that the APP foam shows differences in its degradation compared to the standard foam.

The FTIR and ^{1}H NMR spectra of the residues collected from the APP foam were almost identical to those obtained from the standard foam and those of the neat polyol, demonstrating that the residues consist primarily of regenerated polyol. The FTIR spectrum of the residue at 250°C showed an additional small peak not observed in the polyol spectrum at 1731 cm^{-1}, which indicates the presence of residual urethane linkages within the residue. This carbonyl peak was less significant in the FTIR spectrum of the residue at 300°C, which indicates that further degradation of the urethane linkages has occurred by this temperature.

- ***Condensable Fraction: Sub-ambient Differential Distillation and Characterisation***

The condensable fractions collected during the isothermal TVA experiments were separated by sub-ambient differential distillation into four fractions which were then analysed by online MS, FTIR spectroscopy and GC-MS. Presented in Figure 5.10 are

the differential distillation traces which show the volatile degradation products which are evolved at each of the temperatures employed.

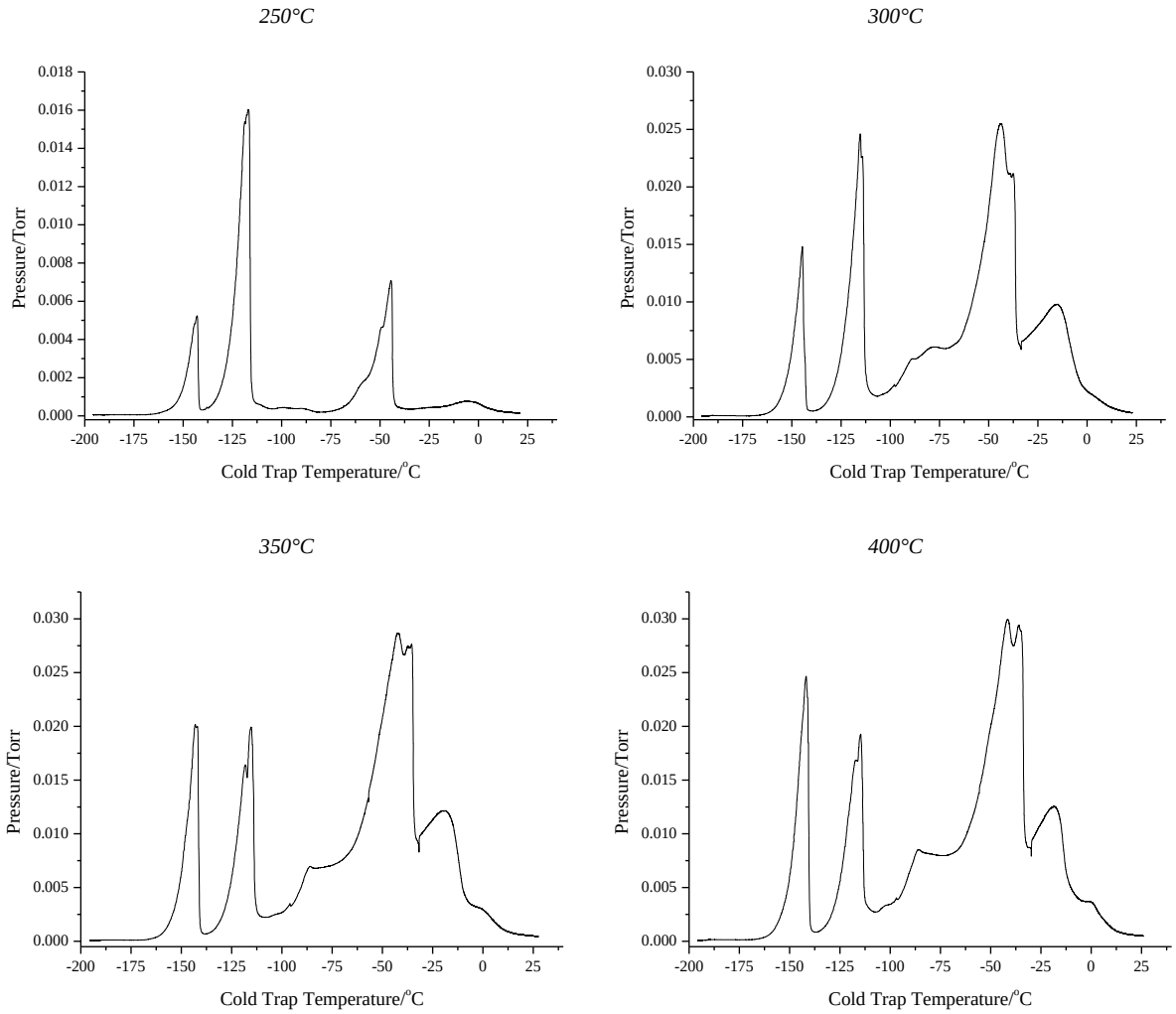

Figure 5.10: Differential distillation traces for the isothermal TVA studies on the APP foam

The temperature ranges of the fractions collected and the identity of each of the products within the fractions are presented in Table 5.6.

Fraction Temperature Range	**Product Identification**			
	250°C	**300°C**	**350°C**	**400°C**
-196°C to -140°C	CO_2	Propene, CO_2	Propene, CO_2	Propene, CO_2
-140°C to -60°C	Ammonia	Ammonia, propanal	Ammonia, propanal	Ammonia, propanal
-60° to -40°C	Water and high molar mass polyol fragments	Water and high molar polyol fragments	Water and high molar polyol fragments	Water and high molar polyol fragments
-40°C to 25°C	High molar mass polyol fragments	High molar mass polyol fragments	High molar mass polyol fragments	High molar mass polyol fragments

Table 5.6: Sub-ambient differential distillations fractions collected from the isothermal TVA studies

It can be observed from Figure 5.10 that as the degradation temperature is increased greater quantities of condensable volatiles are evolved, and the product distribution is altered. At 250°C three major peaks are observed which correspond to CO_2, ammonia and water. Low levels of higher molar mass species are also observed at this temperature. As was the case for the standard foam, the presence of CO_2 and TDI confirms that there are two competing degradation mechanisms occurring for the urethane linkages within the APP foam. The presence of ammonia and water at this temperature indicates that the fire retardant has begun to degrade to form ultraphosphate at 250°C.

By 300°C the trace is more complex, with propene, propanal and larger quantities of high molar mass polyol fragments now being observed which is indicative of significant polyol degradation occurring. There are no new products observed above 300°C, however, the level of some products does change, with the propene/CO_2 and propanal peaks increasing in size as further degradation of the polyol occurs.

5.1.4 Fire Tests

Presented in Figure 5.11 and Figure 5.12 are pictures taken at different stages throughout the mini-crib fire tests of the standard and APP foams, respectively.

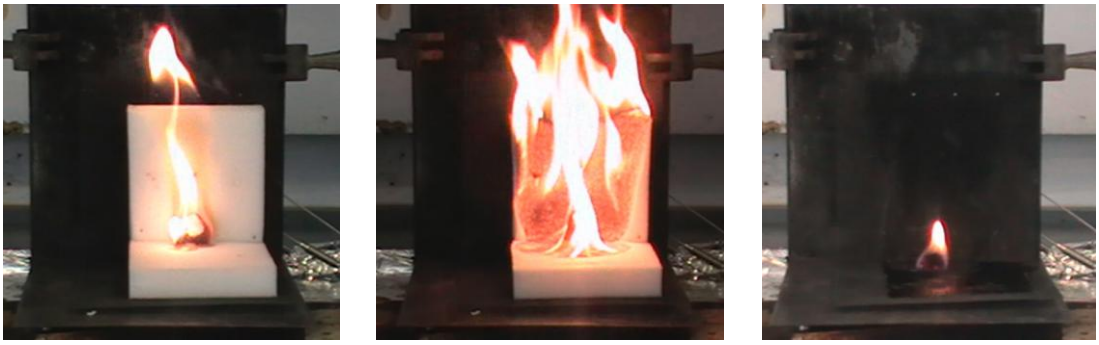

Beginning of Test ***After 30 seconds*** ***End of test***

Figure 5.11: Images from the mini-crib fire test on the standard foam

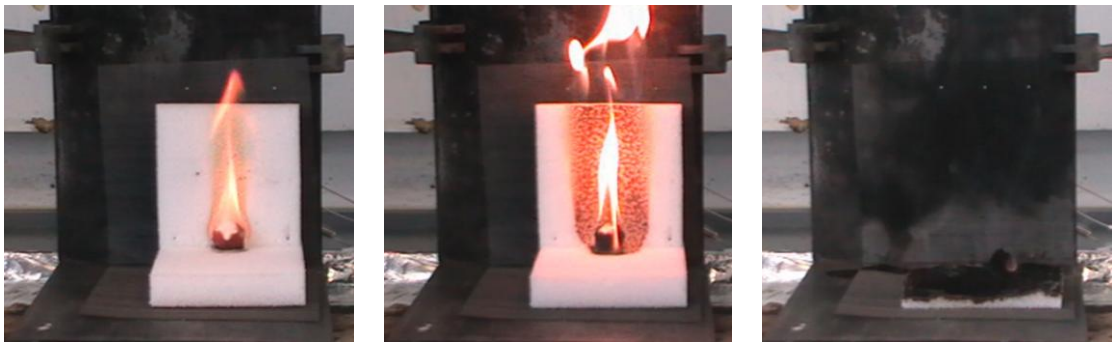

Beginning of Test ***After 30 seconds*** ***End of test***

Figure 5.12: Images from the mini-crib fire test of the APP foam

It can be observed from Figure 5.11 that once ignited the standard foam burned readily and did not self-extinguish the flame. This result is expected as non-fire retarded flexible polyurethane foams are reported to be easily ignited in air and burn rapidly once ignited.[1,7] The calculated mass loss for the foam once the flame had been extinguished was 86.4%. The APP foam, on the other hand, burned much more slowly than the standard foam and extinguished the flame before the entire foam was consumed. It can be observed from Figure 5.12 that a section of the APP foam which has a layer of protective black char on the surface remains at the end of the test. The calculated mass loss from the APP foam was 44.5%, almost half that of the standard foam.

The results from the fire tests, therefore, confirm that APP reduces the flammability of the foam through the formation of a protective char which leads to significantly smaller quantities of the material being consumed.

5.1.5 Summary and Proposed Mechanisms of Degradation

The results from the TVA, TGA and DSC analysis show that the APP foam undergoes a significantly different degradation mechanism to the standard foam. The DSC and TGA results revealed the presence of a two stage degradation process under a non-oxidative environment. The TVA results, on the other hand, revealed that degradation of the APP foam in fact occurs in four overlapping steps compared to the two step process which occurs for the standard foam. The additional degradation steps observed for the APP foam are proposed to correspond to degradation of the fire retardant.

Evolution of volatile material was also observed to occur at a lower temperature for the APP foam and it is proposed that degradation of the urethane linkages *via* a depolycondensation reaction is acid-catalysed by the acidic hydroxyl groups which arise from degradation of APP, as shown in Figure 5.13. This is in correlation with the work of Grassie and Mendoza which showed that APP caused the depolymerisation reaction for an MDI-based polyurethane to be acid-catalysed.[5]

The sub-ambient differential distillation trace revealed that the nature and distribution of the volatiles evolved from the APP foam was profoundly different to the standard foam, which confirms that the secondary degradation processes are altered in the presence of APP. It is possible that acid-catalysed degradation of the regenerated polyol could occur as was observed by Grassie and Mendoza.[5] This would result in the formation of 2,5-dimethyl-1,4-dioxane, water and an alkene-terminated polyol chain as shown in Figure 5.14. Acid hydrolysis of the alkene-terminated polyol chain would then yield propanal.

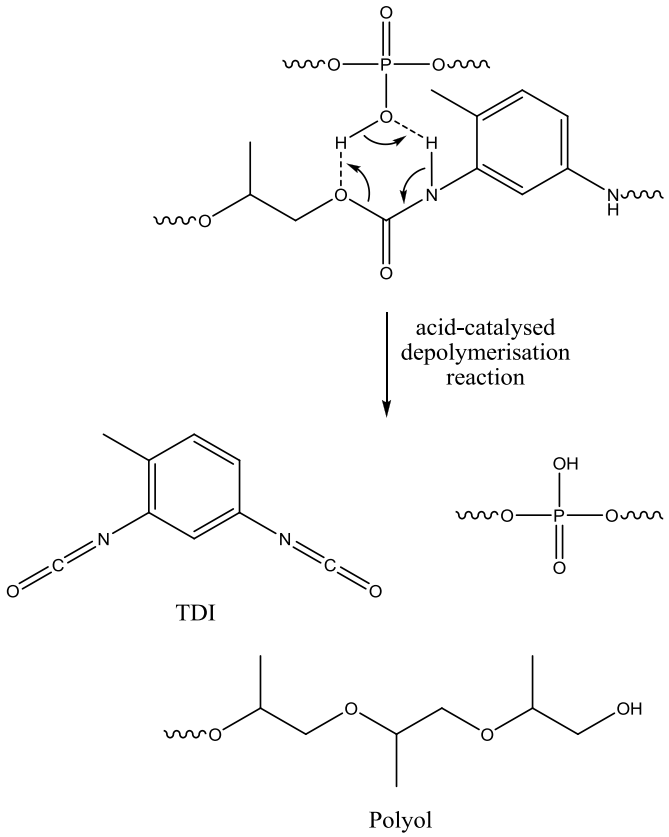

Figure 5.13: Acid-catalysed degradation of the urethane linkages

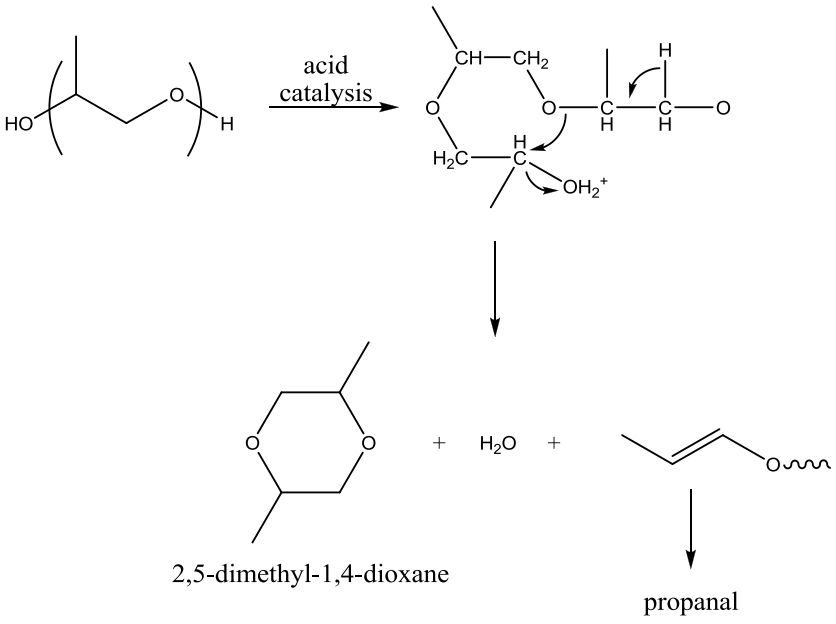

Figure 5.14: Acid-catalysed degradation of the polyol component

Grassie and Mendoza also proposed that a phosphorylation reaction could occur between the ultraphosphate and the polyol which would lead to phosphorus esters. Degradation of this network would then occur yielding phosphoric acid and an alkene terminated chain, as shown in Figure 5.15. This would once again generate propanal by acid hydrolysis.

Both of the mechanisms shown in Figure 5.14 and Figure 5.15 are plausible and explain the absence of acetaldehyde and formaldehyde and the presence of 2,5-dimethyl-1,4-dioxane and large quantities of propanal. The presence of acidic species during the degradation of the foam is believed to promote char formation and this is evident from the results of the mini-crib fire tests.

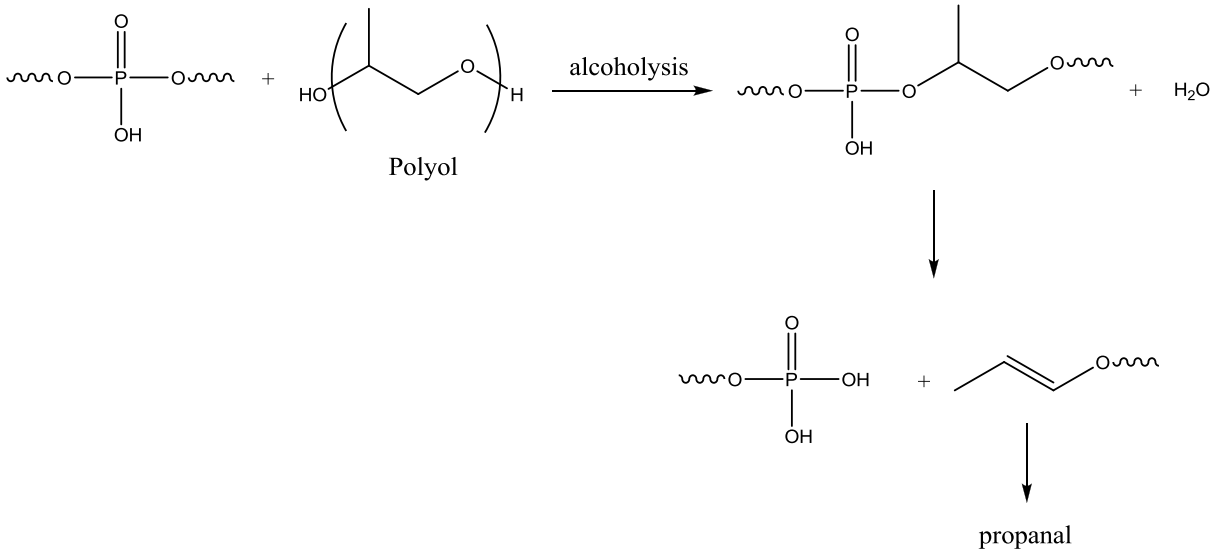

Figure 5.15: Phosphorylation of the polyol and subsequent degradation of the phosphorus esters

The results from the isothermal TVA studies provide further information regarding the degradation processes occurring within the APP foam. The presence of a polyol-based residue at 250°C and 300°C and TDI within the cold-ring fractions confirms that degradation of the urethane linkages within the APP foam occurs *via* a depolymerisation reaction. As was the case for the standard foam, CO_2 was identified as a degradation

product at 250°C which indicates that the urethane linkages in the APP foam also degrade by dissociation *via* the six-membered ring or four-membered ring transition states discussed in Section 1.5.3.1.1.

In addition to CO_2, water and ammonia were evolved from the APP foam in significant quantities at 250°C. This confirms that the APP fire retardant begins to degrade at this temperature to yield an ultraphosphate, with water and ammonia as the volatile degradation products. By 300°C the polyol is proposed to be undergoing significant degradation, with propene and propanal being observed as additional degradation products. At temperatures above 300°C no new degradation products were evolved, however, the levels of the volatile degradation products increases as the polyol undergoes further degradation.

In contrast to the standard foam, there were no liquid residues recovered from the APP foam at 350°C and 400°C. This suggests that degradation of the polyol in the presence of APP, which is proposed to occur *via* an acid-catalysed mechanism, is complete at lower temperatures than the random radical chain scission mechanism which occurs in the standard foam. It could also be the case, however, that APP causes the foam to char at lower temperatures and, as a result, any remaining polyol becomes incorporated into the char structure.

5.2 Pyrolysis Studies

Pyrolysis studies were conducted on the APP foam to further probe the degradation behaviour of the fire retardant polyurethane under both oxidative and non-oxidative environments. The pyrolysis studies allow the use of larger quantities of sample which allows chars to be generated and characterised. Char formation is one of the most important condensed-phase mechanisms for modifying the combustion process of a polymer and it has been proposed that the mode of action of APP in polyurethanes is associated primarily with condensed-phase processes, in particular with the promotion of

char formation.[2,8,9] The pyrolysis studies should, therefore, confirm if this is indeed the case.

The pyrolysis of the APP foam was studied under three different environments: nitrogen, air and 3% oxygen in nitrogen.

5.2.1 Pyrolysis under Nitrogen

5.2.1.1 Mass Loss Data and Observations

Presented in Table 5.7 are the residues obtained, calculated as a percentage of the original sample mass, after pyrolysis of the standard and APP foams under a nitrogen environment. The quantities of residue obtained are the averages which have been calculated over four repeat analyses. A plot of the quantity of residue obtained as a function of the pyrolysis temperature for both foams is presented in Figure 5.16.

Pyrolysis Temperature (°C)	**Standard Foam Residue/Mass%**	**APP Foam Residue/Mass%**
250	98	97
300	75	74
350	39	30
400	15	25

Table 5.7: Mass losses and residues for the standard and APP foams after pyrolysis under nitrogen

It can be observed from Table 5.7 and Figure 5.16 that the APP foam exhibits the same overall trend as the standard foam, with an increase in mass loss observed as the pyrolysis temperature is increased. This indicates that at the higher temperatures a greater level of degradation occurs, which results in greater quantities of volatile material being evolved.

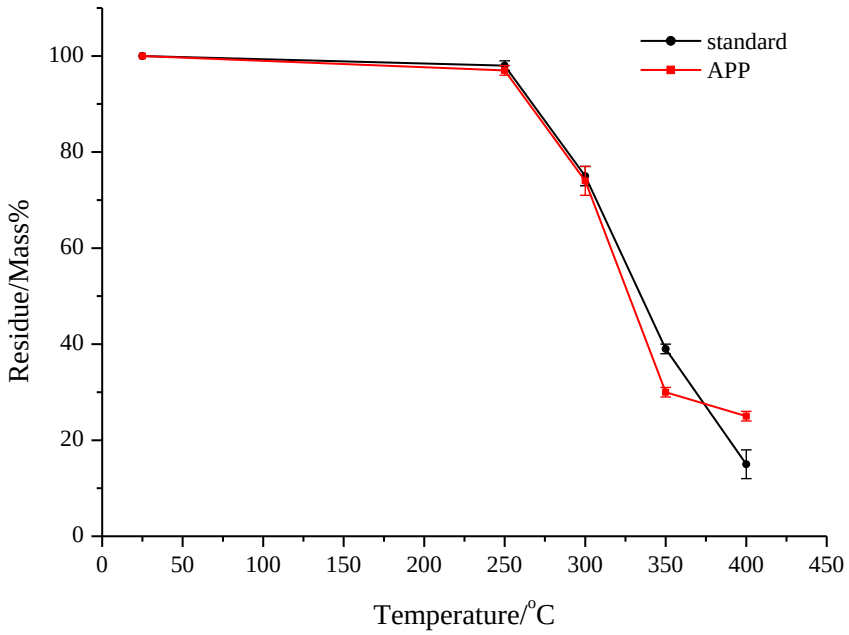

Figure 5.16: Residue obtained vs. pyrolysis temperature for the standard and APP foams under nitrogen

The mass loss trends observed for the APP and standard foams are similar to the TGA curves presented previously. At 250°C the APP foam shows a small mass loss similar to that of the standard foam which indicates that this fire retardant has not had a major effect at this temperature. There was no significant discolouration of the foam at this temperature and extraction of the sample with chloroform did not yield any tarry material. This suggests that significant degradation of the urethane linkages has not occurred at this temperature for the APP foam. This is in agreement with the DSC and TGA results which revealed that degradation of the APP foam becomes significant at temperatures above 250°C.

As the temperature was increased the foam quickly became darker in colour and by 350°C the foam was highly charred and black. This is in contrast to the standard foam which did not show this change in colour until 400°C, and indicates that APP promotes the formation of char at a lower temperature. At 350°C the APP foam shows increased mass loss compared to the standard foam. This is the temperature at which degradation of the polyol is significant; therefore, this indicates that APP may accelerate the

degradation of the polyol component of the foam. This is in agreement with the work of Grassie and Mendoza[5,10] and Duquesne *et* al.[3] which demonstrated that degradation of the polyol is catalysed by the acidic compounds resulting from the degradation of APP.

At 400°C the overall quantity of residue obtained is higher for the APP foam than for the standard foam which indicates that APP promotes the formation of char. This is not unexpected as phosphorus fire retardants are proposed to exert most of their fire retardant activity in the condensed-phase and APP has been shown to promote the formation of large quantities of residues in polyurethanes.[3,4,5]

5.2.1.2 Cold-ring Fraction Analysis

During the pyrolysis of the APP foam very little mass loss had occurred at 250°C and as a result there was no significant cold-ring fraction deposited in the tube at this temperature. At temperatures of 300°C and above a yellow/orange cold-ring fraction was present which was analysed by means of FTIR spectroscopy and GC-MS. The FTIR spectra of the cold-ring fractions showed similarities to those for the standard foam but with the peaks corresponding to N-H containing compounds being more intense. This indicates that the cold-ring fractions consist of high molar mass polyol fragments and amine-containing compounds. The -MS analysis confirms this; however, the nitrogen-containing species could not be positively identified. These results are in agreement with the work by Grassie and Mendoza[5] who also observed an increased level of amines present in their cold-ring fractions during the analysis of polyurethanes containing APP.

Furthermore, no TDI was identified in the cold-ring fractions from the APP foam. Two possible explanations for this are proposed. It could be the case that the TDI reacts with the hydroxyl groups of the ultraphosphate which is formed when the APP degrades, thereby resulting in the TDI remaining in the char instead of volatilising into the cold-ring fraction. Alternatively, the water released from the degradation of the APP could react with the TDI to yield amines.

5.2.1.3 Residue Analysis

The tars obtained from the APP residues were analysed by FTIR spectroscopy, whilst the chars were characterised by elemental analysis, FTIR and solid-state ^{13}C NMR spectroscopy. For the APP foam little discolouration was present in the residue obtained after pyrolysis at 250°C and extraction of this sample with chloroform did not yield any tar. The residues at all other temperatures yielded both tar and char.

5.2.1.3.1 Quantification of the Tar and Char

Presented in Table 5.8 are the quantities of char and tar, calculated as a percentage of the total residue collected, for the standard and APP foams after pyrolysis under nitrogen. For both foams at 250°C the residue consisted entirely of insoluble material which was not unexpected as the previous results suggested little degradation had occurred at this temperature. Plots of the quantities of tar and char as a function of pyrolysis temperature are displayed in Figure 5.17.

Foam	**Temperature/°C**	**Tar/% of residue**	**Char/% of residue**
Standard	300	82	18
	350	71	29
	400	40	60
APP	300	33	67
	350	17	83
	400	1	99

Table 5.8: Quantities of tar and char obtained as a percentage of the residue collected for the standard and APP foams

It can be observed that as the pyrolysis temperature increases the quantity of tar decreases for both the APP and standard foams as the foams become more charred in nature. This is expected as the tar consists primarily of polyol-based material which will degrade and volatilise at the higher temperatures. In contrast to the standard foam, the residues collected from the APP foam consist more of char than tar at all three temperatures. Furthermore, the residues from the APP foam contain significantly greater quantities of char than the standard foam. These results confirm that APP

exhibits condensed-phase activity in the polyurethane foam under study, promoting the formation of significant quantities of char. The formation of a protective char will lead to a reduction in the flammability of the foam, as was demonstrated by the mini-crib fire tests.

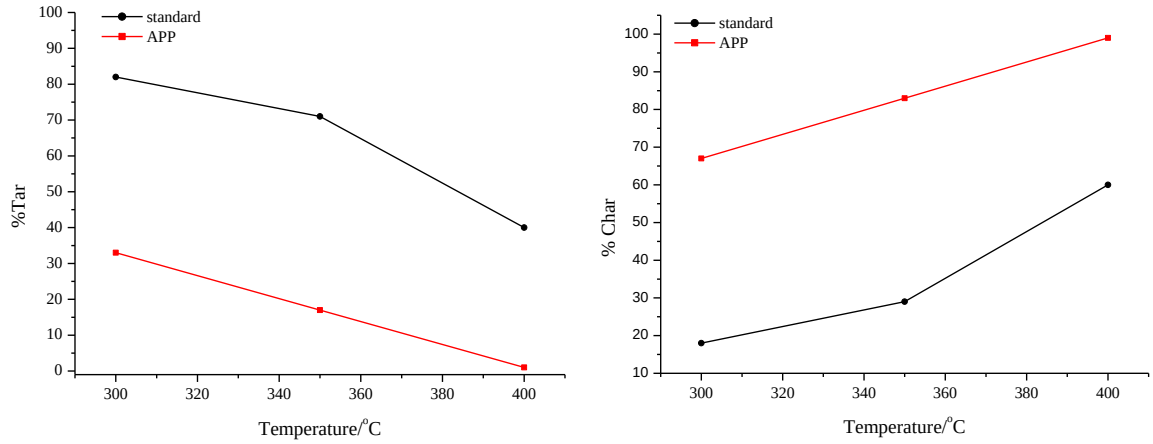

Figure 5.17: Comparison of the %tar and %char collected from the standard and APP foams after pyrolysis under nitrogen

5.2.1.3.2 Analysis of the Tar

Presented in Figure 5.18 is the FTIR spectrum for the tar obtained from the APP foam at 300°C. The spectrum of the tar is almost identical to that of the polyol but with additional peaks at 1710 cm^{-1} and 1648 cm^{-1}. The peak at 1710 cm^{-1} corresponds to carbonyl groups which may be present due to residual urethane linkages within the tar or from degradation of the polyol. The peak at 1648 cm^{-1} could correspond to the carbonyl stretch of a urea; alternatively it could correspond to the N-H stretching of an amine. The presence of amines within the tar correlates with the results from analysis of the cold-ring fractions, which indicated that increased levels of amines were evolved during the pyrolysis of the APP foam.

The FTIR spectra of the tar collected from the APP foam at 350°C was weak due to there being little tar present at this temperature, and no significant differences were observed in this spectrum compared to the spectrum at 300°C. This indicates that as the pyrolysis temperature increases, the structure of the tar remains similar but the quantity

of tar present decreases due to increased degradation and volatilisation of the polyol. By 400°C there was insufficient tar present to obtain a useful FTIR spectrum. This indicates that by this temperature almost all of the polyol-based tar has degraded or volatilised leaving only char in the residue.

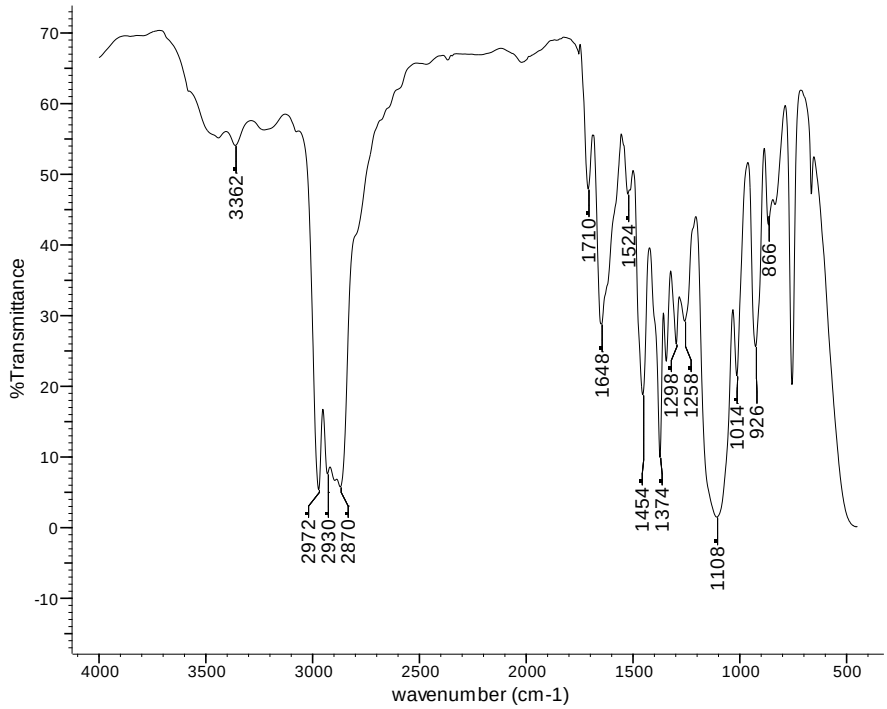

Figure 5.18: FTIR spectrum of the tar extracted from the APP foam after pyrolysis at 300°C under nitrogen

5.2.1.3.3 Analysis of the Char

Presented in Figure 5.19 are photographs of the chars collected from the pyrolysis of the APP foam under nitrogen. At 250°C the foam has begun to discolour which indicates that some degradation has begun to occur at this temperature. This is in contrast to the standard foam (Figure 4.34) which showed little discolouration at 250°C. By 300°C the char is brown in colour and has lost its foamed structure, which indicates that significant degradation of the urethane linkages has occurred by this temperature. By 350°C the foam is highly charred and black in colour.

Characterisation of these chars was achieved by means of solid-state ^{13}C NMR, FTIR spectroscopy and elemental analysis.

Figure 5.19: Photographs of the chars collected from the APP foam after pyrolysis under nitrogen

- *Solid-state ^{13}C NMR*

Presented in Figure 5.20 and Figure 5.21 are the ^{13}C CPMAS TOSS and dipolar dephased spectra, respectively, for the virgin APP foam. In the dipolar dephased spectrum the label * is again used to denote the spinning sidebands. APP is an inorganic fire retardant, therefore, no new peaks are observed in the ^{13}C spectrum of this foam compared to the standard foam (Figure 4.35). Once again the broad signals between 110 and 160 ppm arise from the hard segment (aromatic and urethane carbons) whilst the narrower signals between 70 and 80 ppm arise from the softer aliphatic polyol component. The composite peak at 18.2 ppm arises from the methyl groups within the polyol and the TDI component. In the dipolar dephased spectrum only the peak at 131 ppm arising from the protonated aromatic carbons of the TDI component within the foam is suppressed.

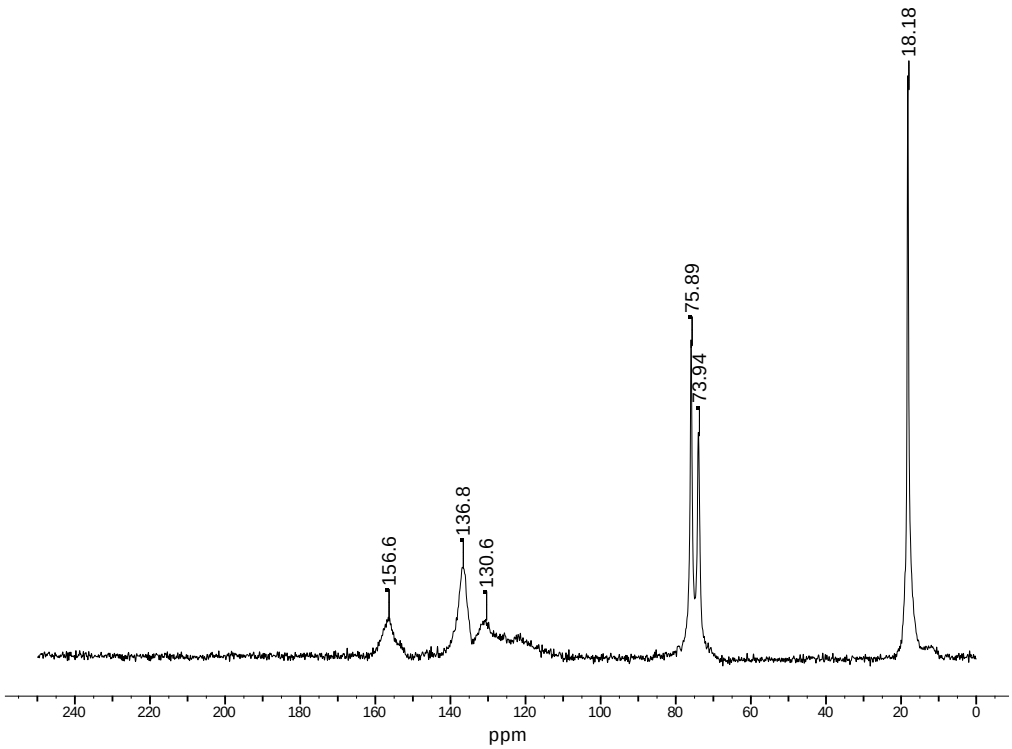

Figure 5.20: ^{13}C CPMAS TOSS spectrum of the virgin APP foam

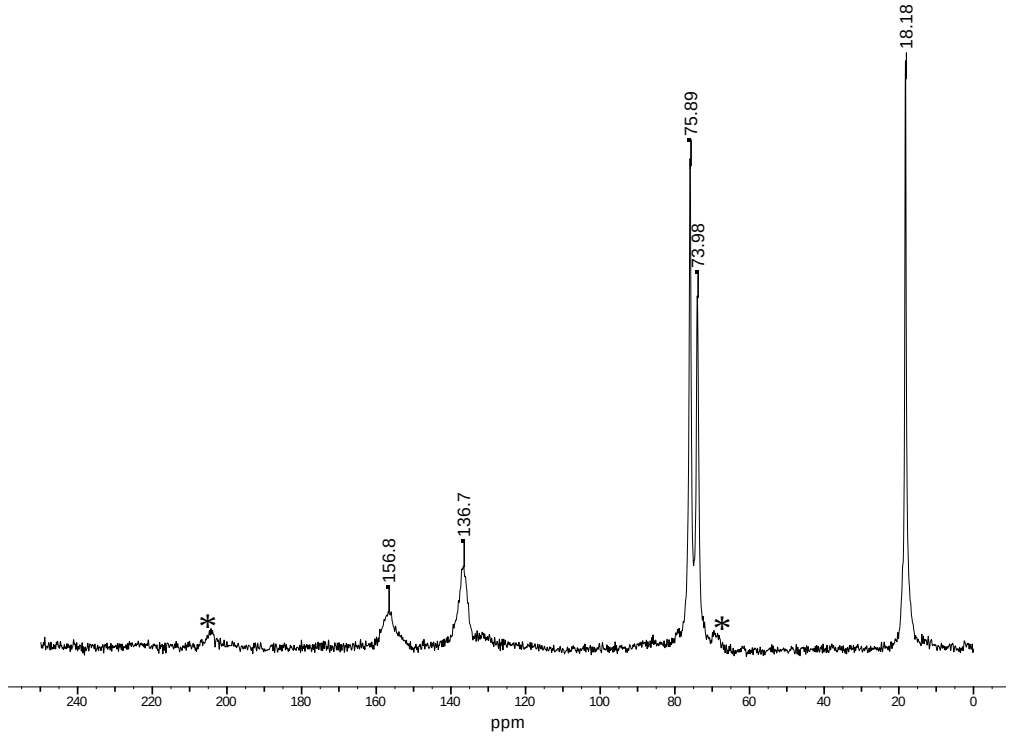

Figure 5.21: ^{13}C CPMAS dipolar dephased spectrum of the virgin APP foam

Presented in Figure 5.22 are the ^{13}C CPMAS TOSS spectra for the virgin APP foam and the chars obtained after pyrolysis at 250, 300, 350 and 400°C under nitrogen.

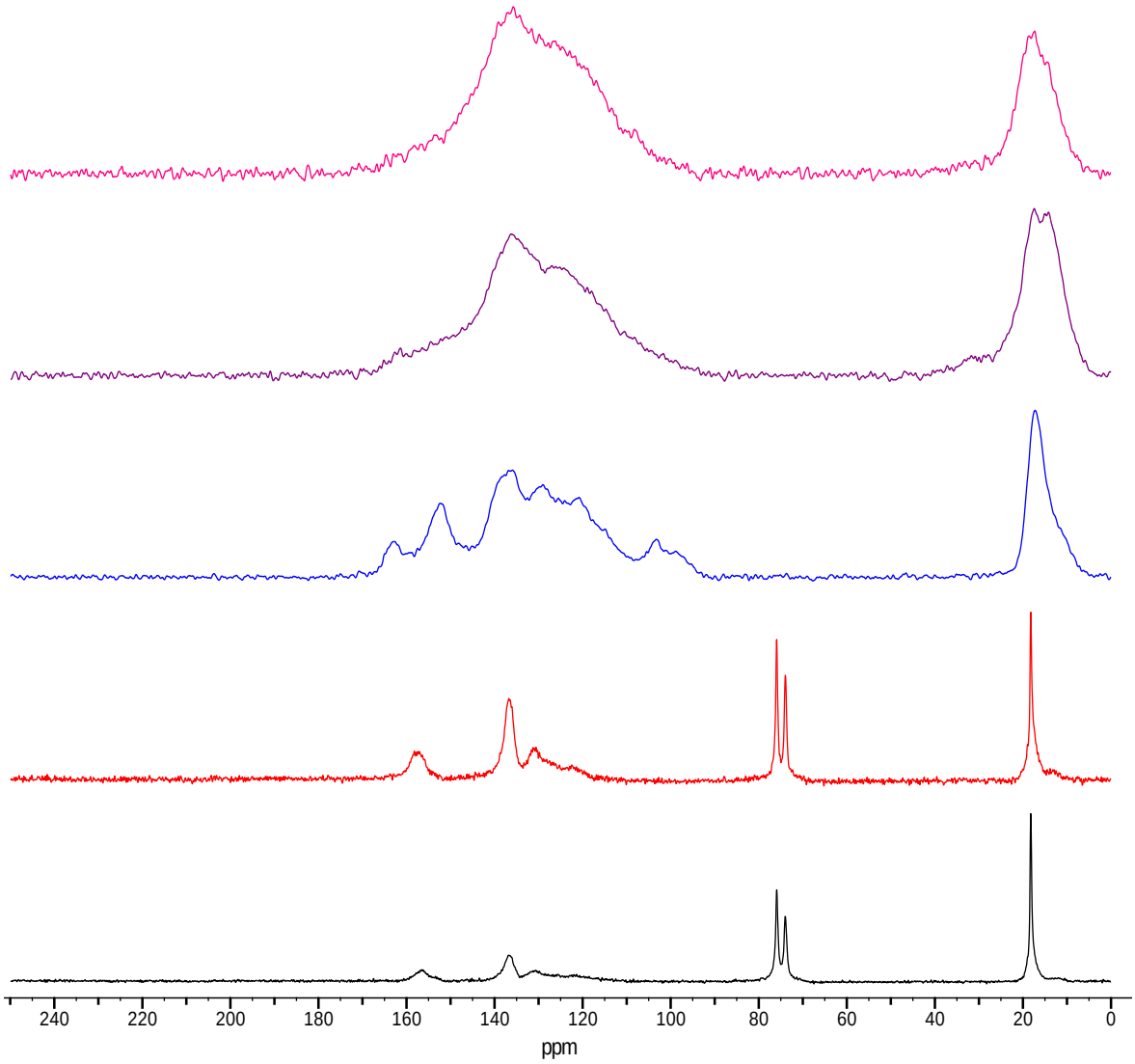

Figure 5.22: Comparison of the ^{13}C CPMAS TOSS spectra of the virgin APP foam (black) with the chars obtained after pyrolysis under nitrogen at 250°C (red), 300°C (blue), 350°C (purple) and 400°C (pink)

The spectrum at 250°C is similar to the virgin APP foam which indicates that no significant degradation of the polyurethane has occurred at this temperature. By 300°C, however, the spectrum is markedly different to that obtained from the char at 250°C, indicating a change in the structure of the char at this temperature. The polyol and

urethane signals have disappeared which indicates that complete degradation of the urethane linkages and volatilisation or degradation of the polyol has occurred by this temperature in the APP foam. This is in contrast to the results from the standard foam (Figure 4.37) which showed that polyol and urethane linkages remained within the char at 300°C. The absence of urethane linkages within the char at 300°C confirms that APP accelerates the degradation of the urethane linkages within the foam. This is again in agreement with the work of Grassie and Mendoza[5] and Duquesne *et al*.[4] Furthermore, several peaks are observed between 110 to 170 ppm which indicates a number of aromatic carbons in different chemical environments. This is similar to the spectrum at the higher temperatures for the standard foam and suggests that the char from the APP foam already has a complex aromatic structure at 300°C. These results, therefore, indicate that the APP foam is in a more advanced state of charring than the standard foam at 300°C, which confirms that APP promotes the formation of char at lower temperatures.

By 350°C the signals in the high chemical shift region are completely unresolved which again indicates that the APP foam is in a more advanced state of charring than the standard foam at this temperature, and a similar trend is observed for the spectrum at 400°C.

Displayed in Figure 5.23 are the ^{13}C CPMAS dipolar dephased spectra for the virgin APP foam and the chars obtained after pyrolysis at 250, 300, 350 and 400°C.

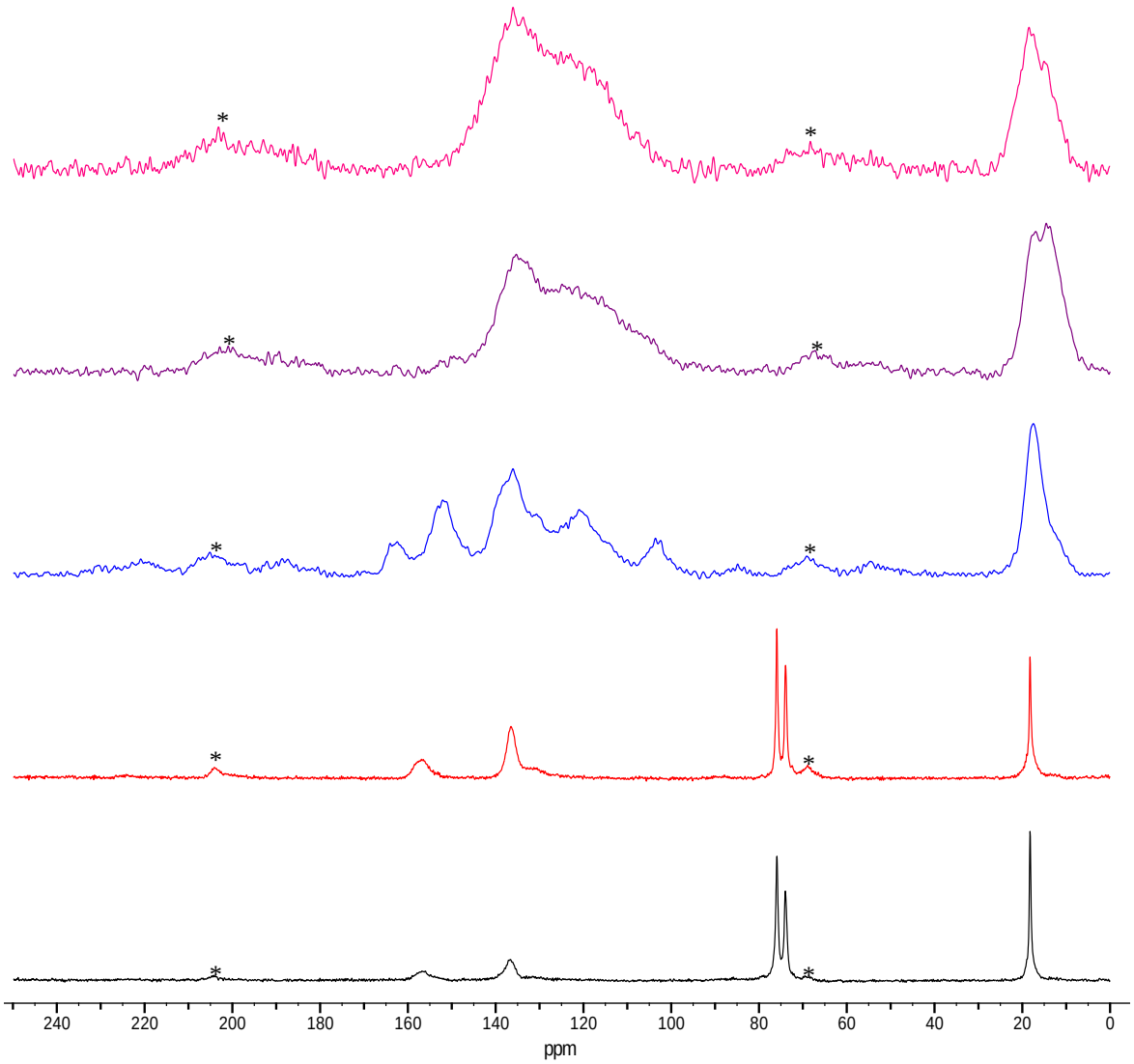

Figure 5.23: Comparison of the ^{13}C CPMAS dipolar dephased spectra of the virgin APP foam (black) with the chars obtained after pyrolysis under nitrogen at 250°C (red), 300°C (blue), 350°C (purple) and 400°C (pink)

The dipolar dephased spectra exhibit the same characteristics as the TOSS spectra, which indicates that the majority of the carbons contributing to the signal in the high chemical shift region of the spectra at 300°C and above are unprotonated. This confirms that the char generated at these temperatures is aromatic and highly unprotonated, and suggests that ring fusion has begun to occur as low as 300°C in the APP foam to generate a complex aromatic char. This behaviour was not observed until 350°C for the

standard foam which once more confirms that APP alters the degradation of the polyurethane and promotes the formation of char at a lower temperature.

- *FTIR Spectroscopy*

Presented in Figure 4.39 is the complex FTIR spectrum of the APP foam.

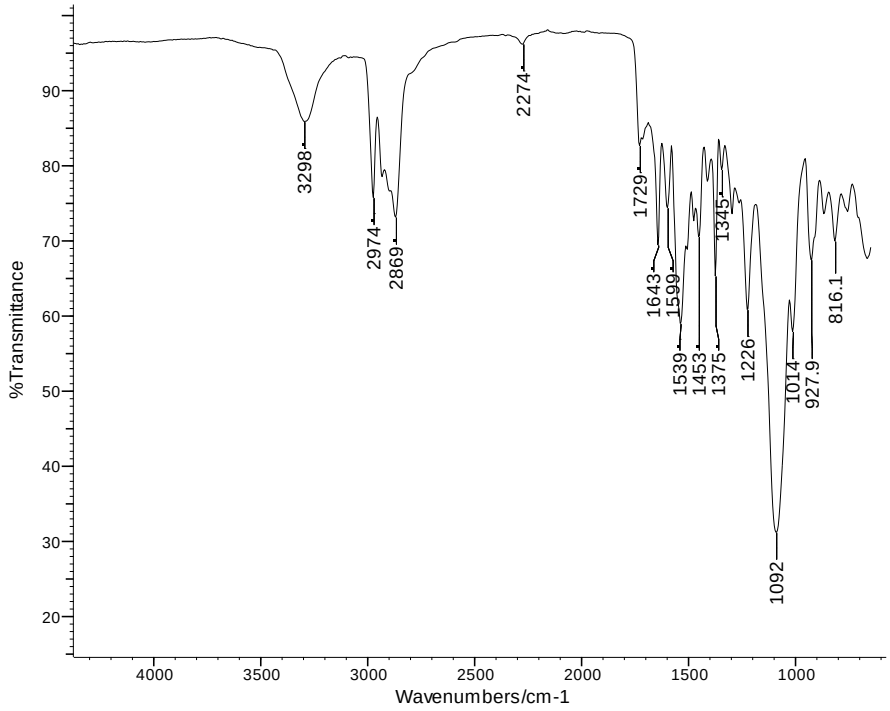

Figure 5.24: FTIR spectrum of the APP foam

As was the case for the standard foam, the majority of the peaks in the spectrum arise from the polyol component. The additional peaks at 1729 cm^{-1} and 1226 cm^{-1} correspond to the urethane linkages, the peaks between 1500 cm^{-1} and 1650 cm^{-1} to the aromatic units within the polyurethane and the peak at 2274 cm^{-1} to unreacted isocyanate groups within the foam. The peak at 3298 cm^{-1} most likely arises from the N-H groups within the urethane linkages or urea linkages which may be present within the foam.

Presented in are the FTIR spectra for the virgin APP foam and the chars obtained after pyrolysis under nitrogen at 250, 300, 350 and 400°C.

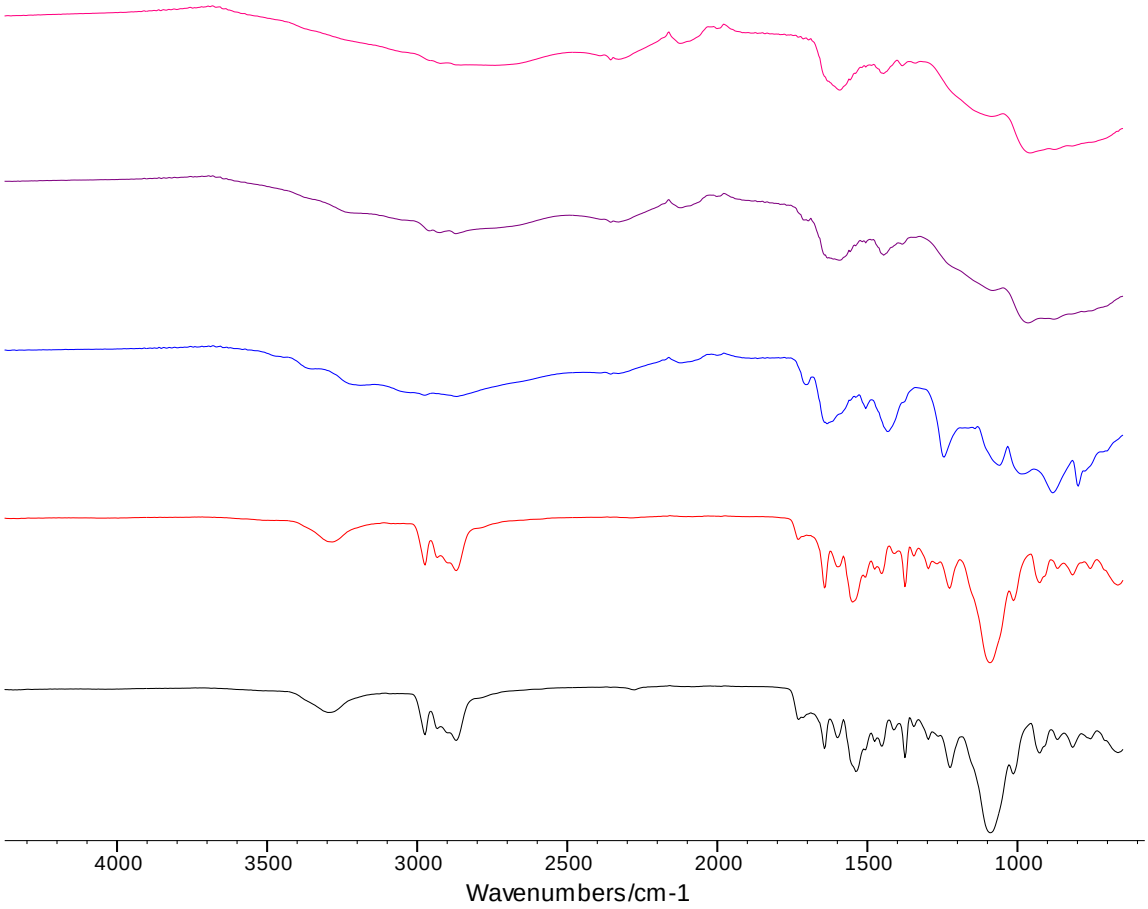

Figure 5.25: Comparison of the FTIR spectra of the virgin APP foam (black) with the chars obtained after pyrolysis under nitrogen at 250°C (red), 300°C (blue), 350°C (purple) and 400°C (pink)

The spectrum at 250°C is similar to that of the virgin foam, with the peaks corresponding to the urethane linkages still present. This indicates that no significant degradation of the APP foam has occurred at 250°C, which is in correlation with the previous data. There is a significant change in the spectrum at 300°C indicating a structural change in the char at this temperature, which is in agreement with the solid-state ^{13}C NMR results. The urethane peaks have disappeared and the polyol signals have diminished significantly. This confirms that significant degradation of the polyurethane has occurred at 300°C. This is once again in contrast to the results from the standard foam (Figure 4.41) which showed that some urethane linkages and polyol remained within the char at 300°C.

By 350°C the foam is highly charred and the FTIR spectrum is difficult to interpret, which confirms that the chars formed are highly carbonaceous. The spectrum of the APP char at 350°C resembles that of the standard foam at 400°C (Figure 4.41) which suggests the APP foam is in a more advanced state of charring than the standard foam at 350°C. These results, therefore, confirm that APP promotes the formation of char.

- *Elemental Analysis*

The virgin foam and pyrolysis chars collected from the APP foam were submitted for elemental analysis to determine the quantities of carbon, hydrogen and nitrogen present. The results from the elemental analysis for the standard and APP foams under nitrogen are reported in Table 5.9.

Foam	**Deg Temp/°C**	**%C**	**%H**	**%N**	**C/H**	**C/N**
Standard	*Virgin*	61.7	9.1	5.3	6.8	11.6
	250	61.9	9.2	5.0	6.7	12.4
	300	64.0	6.6	13.4	9.7	4.8
	350	64.8	6.2	14.7	10.4	4.4
	400	69.4	4.8	12.3	14.4	5.6
APP	*Virgin*	52.5	8.6	6.7	6.1	7.9
	250	52.6	7.8	6.2	6.7	8.5
	300	27.9	4.9	12.6	5.7	2.2
	350	36.9	5.2	7.5	7.1	4.9
	400	43.1	3.9	6.1	11.0	7.0

Table 5.9: Elemental analysis results for the virgin foam and the pyrolysis chars obtained under nitrogen for the standard and APP foams

In order to illustrate more clearly the changes occurring in the chars the C:H and C:N ratios have been calculated and are presented as a function of the pyrolysis temperature in Figure 5.26 and Figure 5.27, respectively.

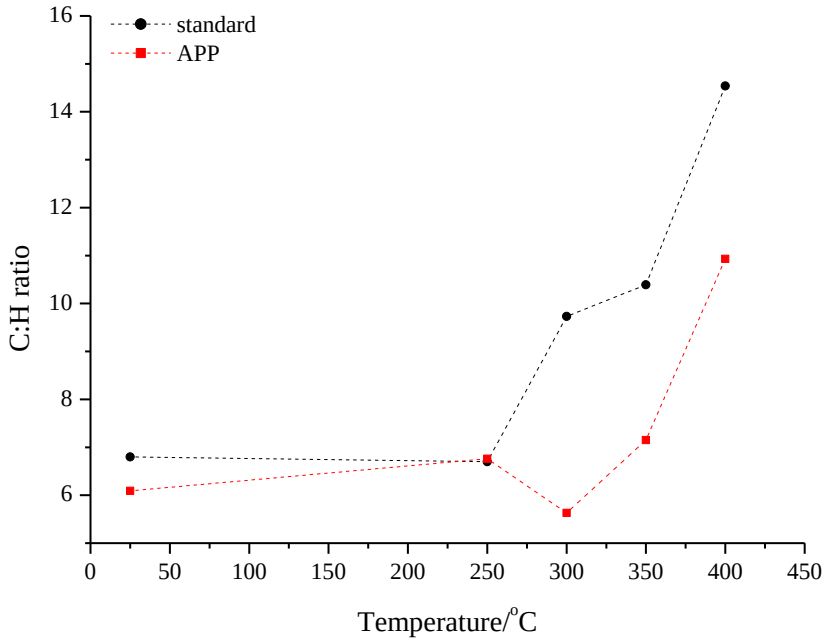

Figure 5.26: C:H ratio for the pyrolysis chars obtained from the standard and APP foams as a function of temperature

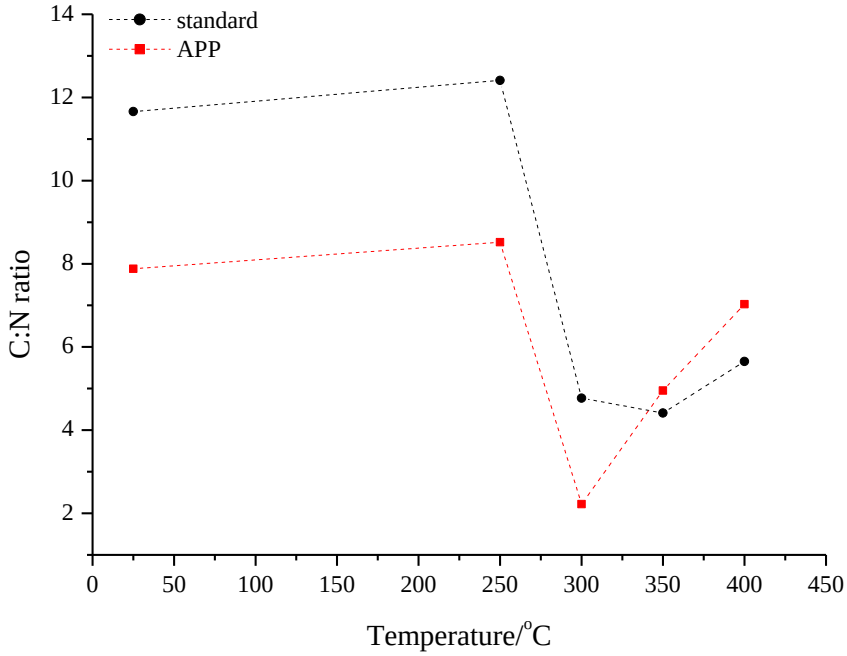

Figure 5.27: C:N ratio for the pyrolysis chars obtained from the standard and APP foams as a function of temperature

The initial C:H and C:N ratios are lower for the virgin APP foam compared to the standard foam due to the presence of the inorganic fire retardant within the foam. At 250°C the C:H and C:N ratios for the APP foam increase slightly which could be caused

by loss of small quantities of ammonia at this temperature as the APP begins to thermally degrade.

As the pyrolysis temperature increases the C:H and C:N ratios exhibit similar trends, initially decreasing at 300°C before decreasing at the higher temperatures which is in contrast to the results obtained for the standard foam. The solid-state ^{13}C NMR results revealed that at this temperature the char contains no residual polyol and the foam is in a more advance state of charring compared to the standard foam. The decrease in C:N ratio, therefore, indicates that as the polyol is lost from the system the APP remains resulting in a higher level of nitrogen being present within the char. The C:N ratio then increases above 300°C due to loss of nitrogen from the system as further degradation of the APP occurs. This could also be the reason for a decrease in the C:H ratio as the APP contains hydrogen but no carbon, therefore, if this component is retained in the char then the C:H ratio would also be expected to decrease.

5.2.1.4 Summary

The results from pyrolysis of the APP foam under nitrogen are interesting and reveal that APP significantly alters the condensed-phase behaviour of the foam. The APP foam does not appear to have a significant effect on the degradation of the foam at 250°C. Above this temperature, however, the mass loss increased compared to the standard foam which suggests that APP alters the degradation mechanisms of the polyurethane. Furthermore, the APP foam appeared charred and black in colour at lower temperatures than for the standard foam which indicates that APP promotes char formation at lower temperatures.

The solid-state ^{13}C NMR analysis revealed that by 300°C the char from the APP foam contained no polyol or urethane linkages, which is in contrast to the results for the standard foam. This confirms that the fire retardant accelerates the degradation of the urethane linkages within the foam. It is proposed that degradation of the urethane linkages *via* a depolycondensation reaction is acid-catalysed by the acidic hydroxyl

groups which arise from degradation of APP, as was previously proposed by Grassie and Mendoza during their work on MDI-based polyurethanes.[5]

The solid-state ^{13}C NMR and FTIR spectroscopy results also revealed that the APP foam was in a more advanced state of charring than the standard foam at 300°C and the residues from the APP foam were shown to consist primarily of char as opposed to tar. This confirms that APP promotes the formation of char at lower temperatures which is proposed to be due to the presence of phosphoric acids generated when APP degrades.[3,4] The solid-state ^{13}C NMR analysis revealed the structure of the chars at 300, 350 and 400°C to be aromatic and highly unprotonated, indicating that a significant degree of ring fusion has occurred during pyrolysis of the APP foam.

5.2.2 Pyrolysis under Air

Presented in Table 5.10 are the residues obtained, calculated as a percentage of the original sample mass, after pyrolysis of the standard and APP foams under air. The quantities of residues obtained are the averages which have been calculated from four repeat analyses. A plot of the quantity of residue obtained as a function of the pyrolysis temperature for both foams is presented in Figure 5.28.

Pyrolysis Temperature (°C)	**Standard Foam Residue/Mass%**	**APP Foam Residue/Mass%**
250	95	94
300	47	72
350	27	37
400	18	32

Table 5.10: Mass losses and residues for the standard and APP foams after pyrolysis under air

It can be observed that as the pyrolysis temperature is increased the mass loss increases and the quantity of residue decreases for both the standard and APP foams, indicating that increased degradation is occurring at the higher temperatures which results in an increase in the quantity of volatile material being evolved. Again the mass loss trends observed are similar to the TGA curves presented previously. At 250°C the APP foam

had discoloured which indicates that some degradation had occurred within this foam at this temperature, however, the corresponding mass loss is small. The mass loss at 250°C is similar to that of the standard foam which indicates that the fire retardant has not had a significant effect on the degradation of the polyurethane at this temperature.

As the pyrolysis temperature was increased from 250°C to 300°C, however, the foam became black in colour and the mass loss observed is significantly lower than for the standard foam. This trend continues at 350°C and 400°C and suggests that under an oxidative environment APP is promoting the formation of char which subsequently alters the degradation of the polyurethane.

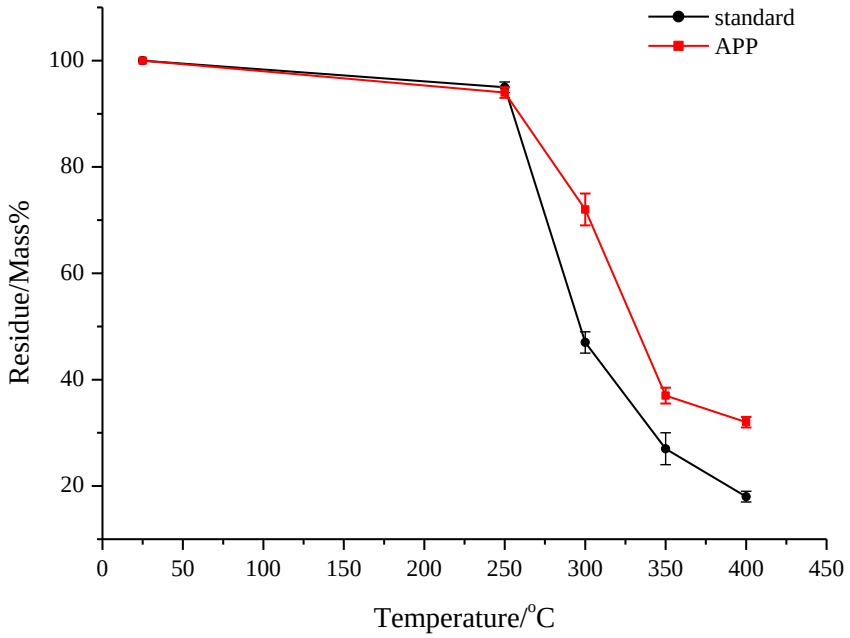

Figure 5.28: Residue obtained vs. pyrolysis temperature for the standard and APP foams under air

Presented in Figure 5.29 is a comparison of the quantities of residue obtained from pyrolysis of the APP foam under nitrogen and air. Similar mass losses are observed at the lower temperatures under air and nitrogen; however at the higher temperatures a larger quantity of residue is obtained under an oxidative environment. This indicates that APP exerts a similar effect at the lower temperatures regardless of the atmosphere in

which the pyrolysis is conducted. This is in agreement with results of Duquesne *et al.*[3] who demonstrated that the TGA of APP on its own and a polyurethane containing APP were similar under air and nitrogen at lower temperatures.

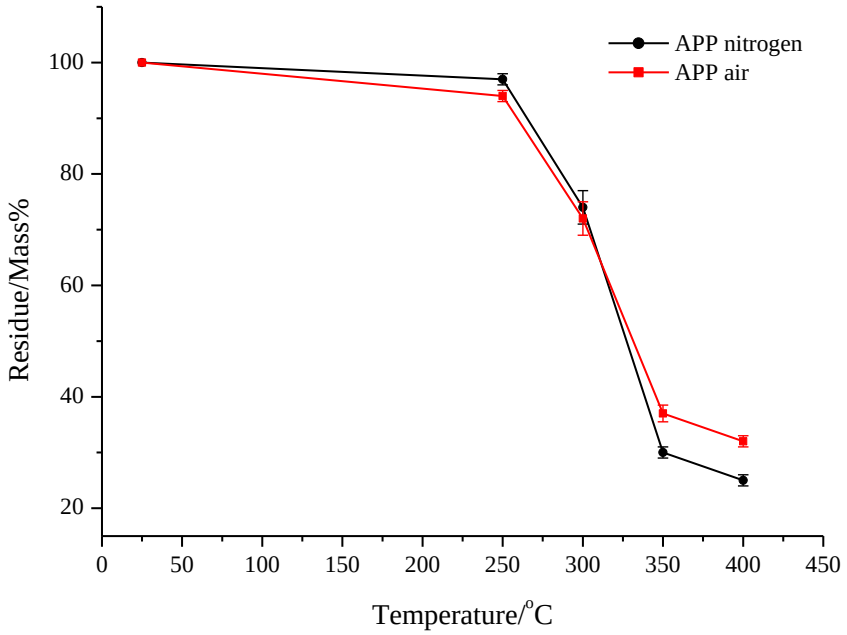

Figure 5.29: Comparison of the residues obtained for the APP foam under nitrogen and air

5.2.2.1 Cold-ring Fraction Analysis

Cold-ring fractions were obtained from the APP foam at all temperatures in the pyrolysis under air, although only a small quantity was present at 250°C and the FTIR and GC-MS spectra were weak. The analysis of the cold-ring fractions from the APP foam yielded similar results at all temperatures. The FTIR spectra showed similar peaks to the cold-ring fraction collected from the standard foam under air which indicates that the cold-ring fractions consist of high molar mass polyol fragments produced from the thermo-oxidative degradation of this component. The GC-MS analysis confirms this and also revealed the presence of nitrogen-containing compounds at 300°C. As was the case under nitrogen, TDI is absent from the cold-ring fractions and it is again proposed that the TDI reacts with the water or hydroxyl groups which result from the degradation of the APP to form an ultraphosphate.

Nitrogen-containing compounds were also identified during the pyrolysis of the APP foam under nitrogen and it is likely that these arise from secondary reactions of the TDI or DAT released when the urethane linkages degrade.

The FTIR spectra of the cold-ring fractions collected at 350°C and 400°C from the APP foam under air appeared weaker than those obtained under nitrogen. This is expected as less mass loss had occurred at these temperatures under air which indicates that less volatile material had been evolved during the thermo-oxidative degradation of the APP foam. This is likely to be a consequence of greater levels of char being formed during the oxidative pyrolysis, which will prevent the foam from degrading to yield more volatile material.

5.2.2.2 Residue Analysis

The residues obtained from the pyrolysis of the APP foam under air yielded both tar and char at all temperatures. This is in contrast to the pyrolysis under nitrogen which yielded no tar, even at 250°C, and indicates that degradation of the polyurethane has been altered in the presence of oxygen.

5.2.2.2.1 Quantification of the Tar and Char

Presented in Table 5.11 are the quantities of char and tar, calculated as a percentage of the total residue collected, for the standard and APP foams after pyrolysis under air. Plots of the quantities of tar and char as a function of pyrolysis temperature are displayed in Figure 5.30.

Foam	Temperature/°C	Tar/% of residue	Char/% of residue
Standard	250	36	64
	300	16	84
	350	14	86
	400	1	99
APP	250	47	53
	300	25	75
	350	3	97
	400	1	99

Table 5.11: Quantities of tar and char obtained as a percentage of the residue collected for the standard and APP foams

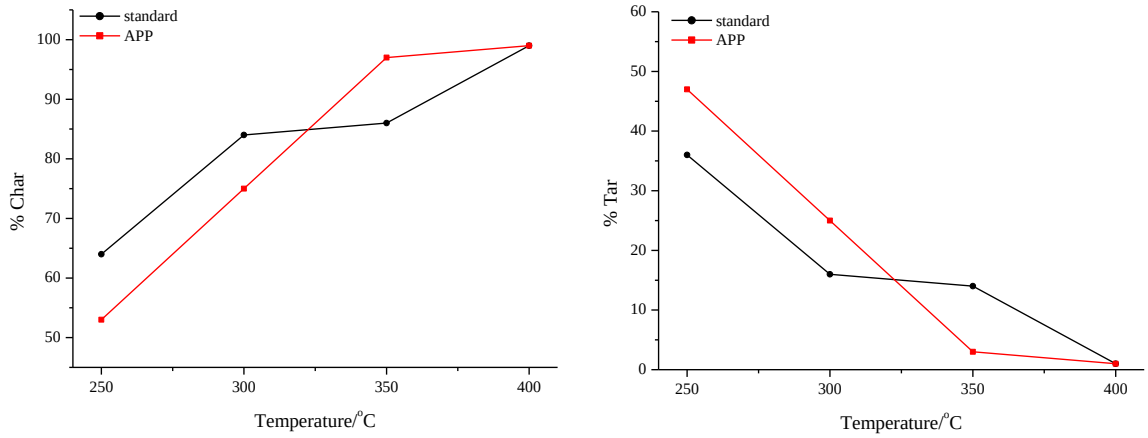

Figure 5.30: Comparison of the %tar and %char collected from the standard and APP foams after pyrolysis under air

It can be observed that a significant quantity of tar was produced at 250°C for the APP foam which confirms that degradation of the foam has begun at this temperature; however, the mass loss at this temperature was small and only a small quantity of volatile material was present as a cold-ring fraction. This suggests that degradation of the foam has begun at 250°C to yield polyol-based tar; however, degradation of the tar to yield volatile material has not yet become significant.

As was the case for the pyrolysis under nitrogen, the quantity of tar decreased as the pyrolysis temperature was increased due to the foam becoming more charred in nature. It is interesting to note, however, that at 250°C and 300°C the residues from the APP

foam contain a greater percentage of tar than the standard foam. This indicates that at the lower temperatures the APP foam has degraded to a greater extent to yield a larger quantity of polyol-based tar. This suggests that APP may accelerate the degradation of the urethane linkages or the thermo-oxidative degradation of the soft segments of the foam. At 350°C and 400°C, however, the APP foam is significantly more charred than the standard foam, which confirms that under an oxidative environment APP promotes the formation of char. This is in correlation with the TGA results shown previously. As was mentioned previously this will lead to a reduction in the flammability of the foam, as demonstrated by the mini-crib fire tests.

Comparison of the results obtained under nitrogen and air reveals that the residues generated in an oxidative environment are more charred than those generated under non-oxidative conditions. This indicates that the presence of oxygen has promoted the formation of larger quantities of char in the APP foam. Comparison of the quantities of char as a percentage of the original mass of foam, presented in Table 5.12, confirms that the oxidative environment does lead to an increased level of char.

Temperature/°C	**Char/% of original sample under nitrogen**	**Char/% of original sample under air**
250	100	50
300	48	55
350	25	36
400	25	32

Table 5.12: Quantities of char obtained as a percentage of the original sample for the pyrolysis of the APP foam under nitrogen and air

5.2.2.2.2 Analysis of the Tar

Presented in Figure 5.31 is the FTIR spectrum for the tar obtained from the APP foam at 250°C. This spectrum is similar to that of the standard foam at 250°C (Figure 4.47), with the majority of the peaks being associated with structures which resemble the

polyether polyol component of the foam. This indicates that the tar from the APP foam consists primarily of polyol-based material. The peak at 1732 cm^{-1} indicates the presence of carbonyl groups within the tar. As was the case for the standard foam, the carbonyl groups could result from thermo-oxidative degradation of the polyol or from residual urethane bonds present within the tar. The presence of a significant quantity of tar at 250°C, which was absent during the pyrolysis under nitrogen, confirms that degradation of the soft segments in the APP foam occurs at a lower temperature in an oxidative environment.

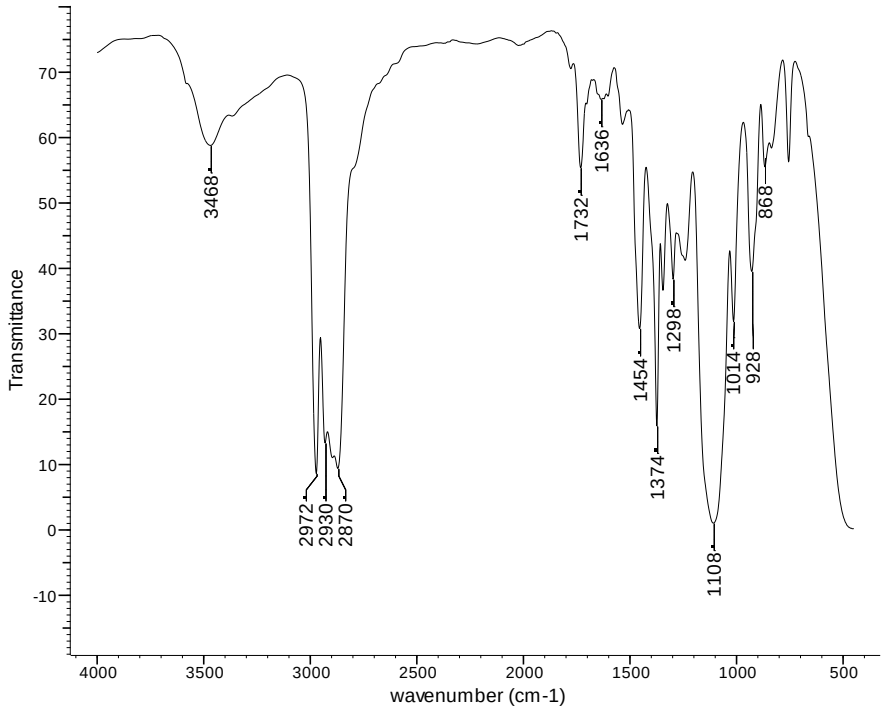

Figure 5.31: FTIR spectrum of the tar extracted from the APP foam after pyrolysis at 250°C under air

At 300°C the carbonyl peak diminishes, as was the case for the standard foam, which indicates either loss of a carbonyl-containing polyol fragment due to further thermo-oxidative degradation of the tar or degradation of the residual urethane linkages. By 350°C the FTIR spectrum is much weaker as there is little tar present at this temperature and by 400°C there was insufficient tar for an FTIR spectrum to be obtained. This indicates that by 350°C the majority of the tar has either undergone significant thermo-

oxidative degradation to yield volatile material or has been incorporated into the insoluble char component of the foam. There are no significant differences in the FTIR spectra of the tars collected under air and nitrogen which indicates that the tars are structurally similar under both environments.

5.2.2.2.3 Analysis of the Char

Presented in Figure 5.32 are photographs of the chars obtained from the APP foam after pyrolysis under air, which were significantly different to those obtained under nitrogen.

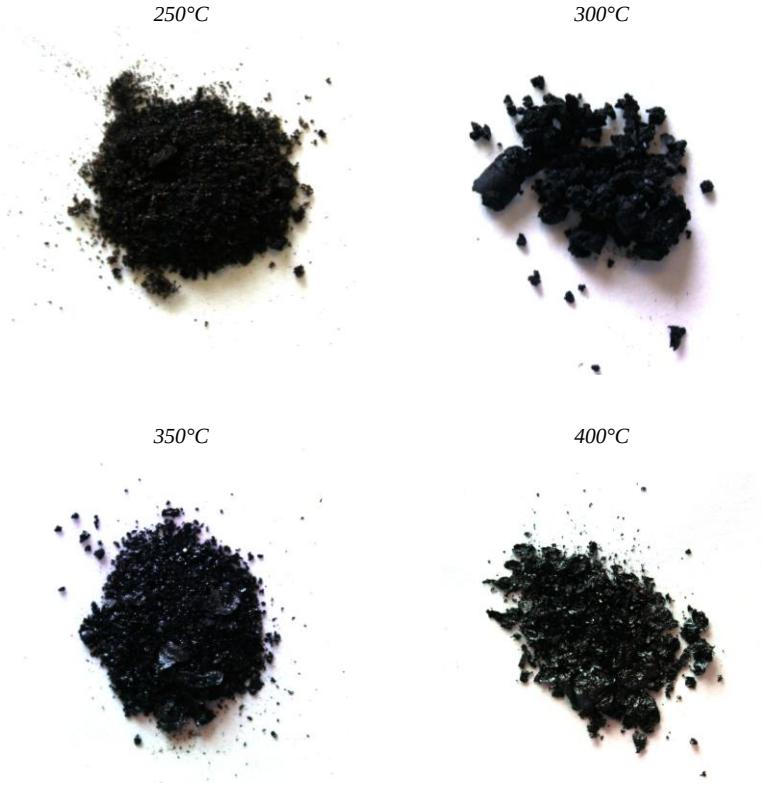

Figure 5.32: Photographs of the chars collected from the APP foam under air

It can be observed that at 250°C under air the APP is already significantly charred and black in colour, resembling the char obtained at 350°C under nitrogen. This indicates that under an oxidative environment the APP foam forms char at significantly lower temperatures. The chars at 300°C and above were similar in appearance. This suggests

that the presence of oxygen has accelerated or altered the degradation processes within the foam, leading to the foam charring at lower temperatures. Characterisation of these chars was achieved by means of solid-state ^{13}C NMR spectroscopy, FTIR spectroscopy and elemental analysis.

- *Solid-state ^{13}C NMR*

Presented in Figure 5.33 are the ^{13}C CPMAS TOSS spectra for the virgin APP foam and the chars obtained after pyrolysis at 250, 300, 350 and 400°C under air. The peak assignments for the virgin foam are the same as those discussed previously.

A significant decrease in the polyol signals at 73.9 ppm and 75.9 ppm and a broadening of the methyl signal at 18.2 ppm is observed for the char at 250°C. This indicates that some of the polyol component has been lost from the char at this temperature, which is in correlation with the previous results which showed that polyol-based tar was extracted from the APP foam at this temperature. The level of polyol present in the NMR spectrum at 250°C under air is lower than was present under nitrogen at the same temperature, which confirms that the presence of oxygen has led to scission of the soft segments of the foam at lower temperatures.

The spectrum obtained at 300°C is considerably different to that at 250°C and indicates a change in the structure of the char at this temperature. The high chemical shift region of the spectrum now consists of a broad band with no well defined peaks, which is indicative of the presence of several types of aromatic species. This is in contrast to the results under nitrogen at 300°C (Figure 5.22) where there were more defined peaks observed in this region and suggests that the foam is in a more advanced state of charring at 300°C under air. This demonstrates that the oxidative atmosphere has accelerated the degradation and charring processes within the foam.

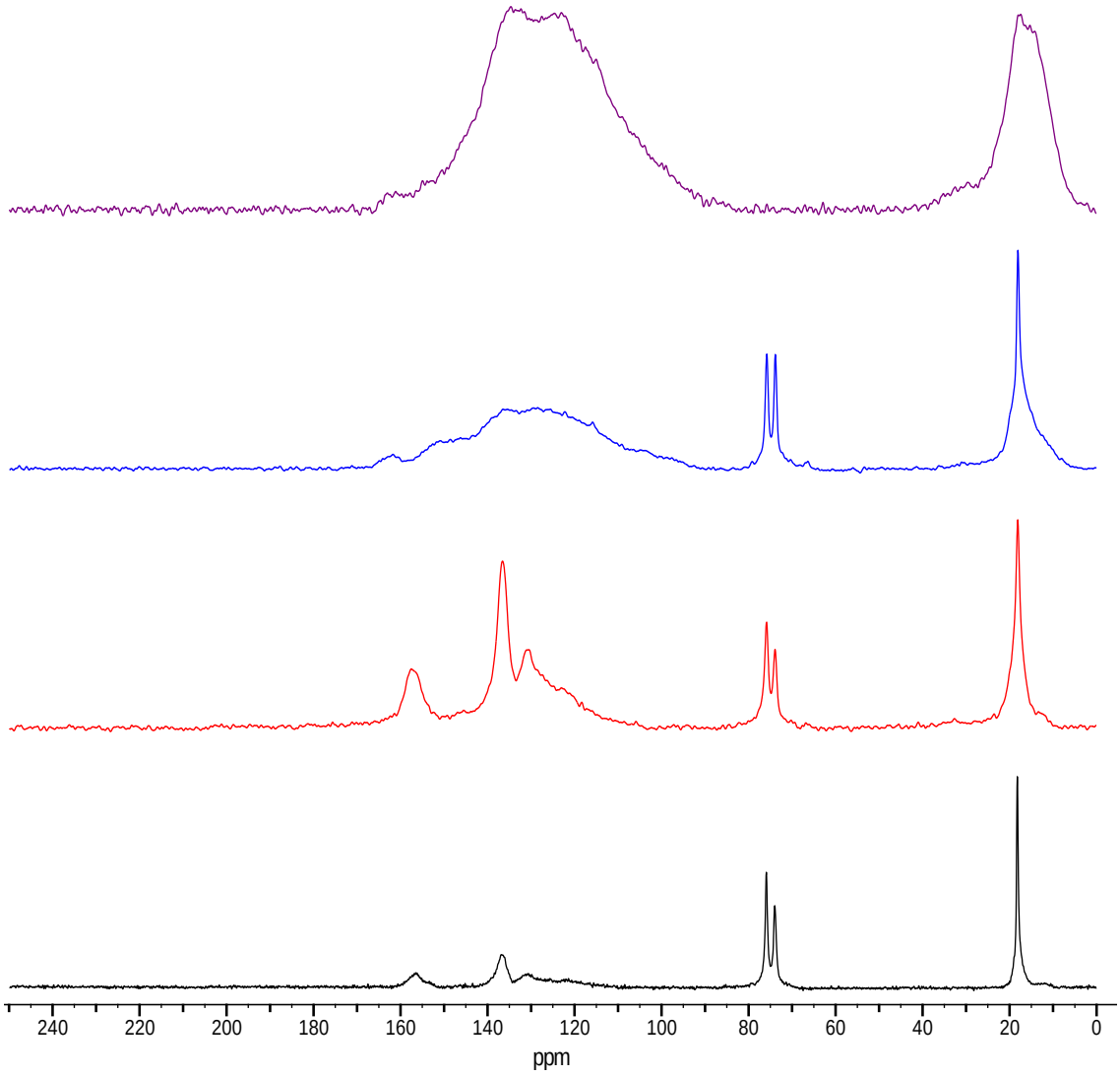

Figure 5.33: Comparison of the ^{13}C CPMAS TOSS spectra of the virgin APP foam (black) with the chars obtained after pyrolysis under air at 250°C (red), 300°C (blue) and 350°C (purple)

The most remarkable difference in the spectrum at 300°C under air, however, is the presence of the sharp signals at 73.9 ppm and 75.9 ppm which correspond to the polyol component of the foam. These peaks were absent in the pyrolysis under nitrogen and the pyrolysis of the standard foam at this temperature (Figure 4.37). The methyl signal at ~18 ppm is also much sharper in this spectrum which indicates that a large proportion of this signal arises due to the more mobile methyl groups of the polyol component. These results, therefore, suggest that a significant portion of the polyol component has

remained bound within the char of the APP foam at this temperature, which is in agreement with the mass loss data which revealed a decreased mass loss for the APP foam compared to the standard foam at this temperature. As there are no distinct peaks in the high chemical shift region corresponding to any residual urethane linkages it is proposed that the polyol or polyol-based material must have reacted with the APP under air causing it to become bound within the char at this temperature. As was discussed previously, a phosphorylation reaction can occur between the hydroxyl groups of the polyol and the ultraphosphate (see Figure 5.15) which would result in the polyol becoming bound within the char. Thermo-oxidative degradation of the polyol occurs under air and this will result in an increased level of hydroxyl end groups being present within the residue compared to the residue under nitrogen.[11] If more hydroxyl groups are present then more phosphorylation reactions can occur and this will result in polyol-based material becoming bound within the char under oxidative environments. This explains the presence of polyol peaks at 300°C and confirms that APP exhibits a significant condensed-phase activity in polyurethane foams.

By 350°C the foam is in an advanced state of charring as indicated by the broad, poorly defined peaks in the aromatic region of the spectrum, which suggest the presence of complex aromatic structures. There is no spectrum for the char obtained at 400°C as there were issues with the spinning of the sample; this occurs when a sample is conducting and indicates that the char from the APP foam at 400°C is highly graphitic. Duquesne *et al.*[3] also experienced problems obtaining a spectrum for their polyurethane/APP samples after heating at high temperatures and proposed that this was due to free radicals trapped within the aromatic carbonaceous structure of the char. An ESR study confirmed that this was the case and the signal was assigned to free radicals trapped within large polyaromatic structures within the char. A similar phenomenon could, therefore, be occurring for the APP foam pyrolysed at 400°C under air in this study.

The ^{13}C CPMAS dipolar dephased spectra for the APP foam, presented in Figure 5.34, do not show significant differences to the TOSS spectra. This indicates that the carbons contributing to the signals in the high chemical shift region at 300°C and 350°C are predominantly unprotonated, and suggests that a significant amount of ring fusion has occurred to generate a complex char structure consisting of several aromatic species.

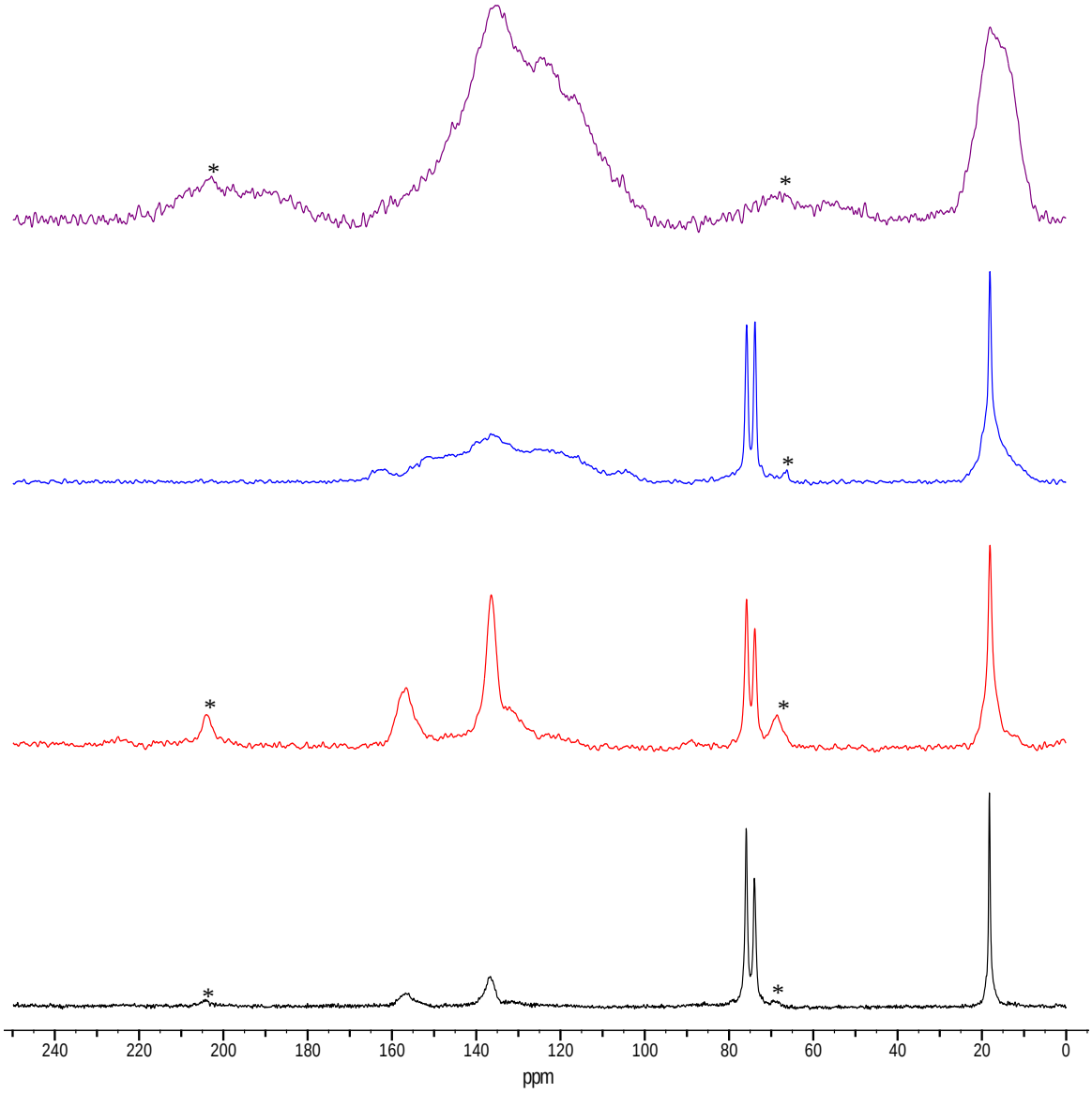

Figure 5.34: Comparison of the ^{13}C CPMAS dipolar dephased spectra of the virgin APP foam (black) with the chars obtained after pyrolysis under air at 250°C (red), 300°C (blue) and 350°C (purple)

- *FTIR Spectroscopy*

Presented in Figure 5.35 are the FTIR spectra for the virgin APP foam and the chars obtained after pyrolysis under air at 250, 300, 350 and 400°C.

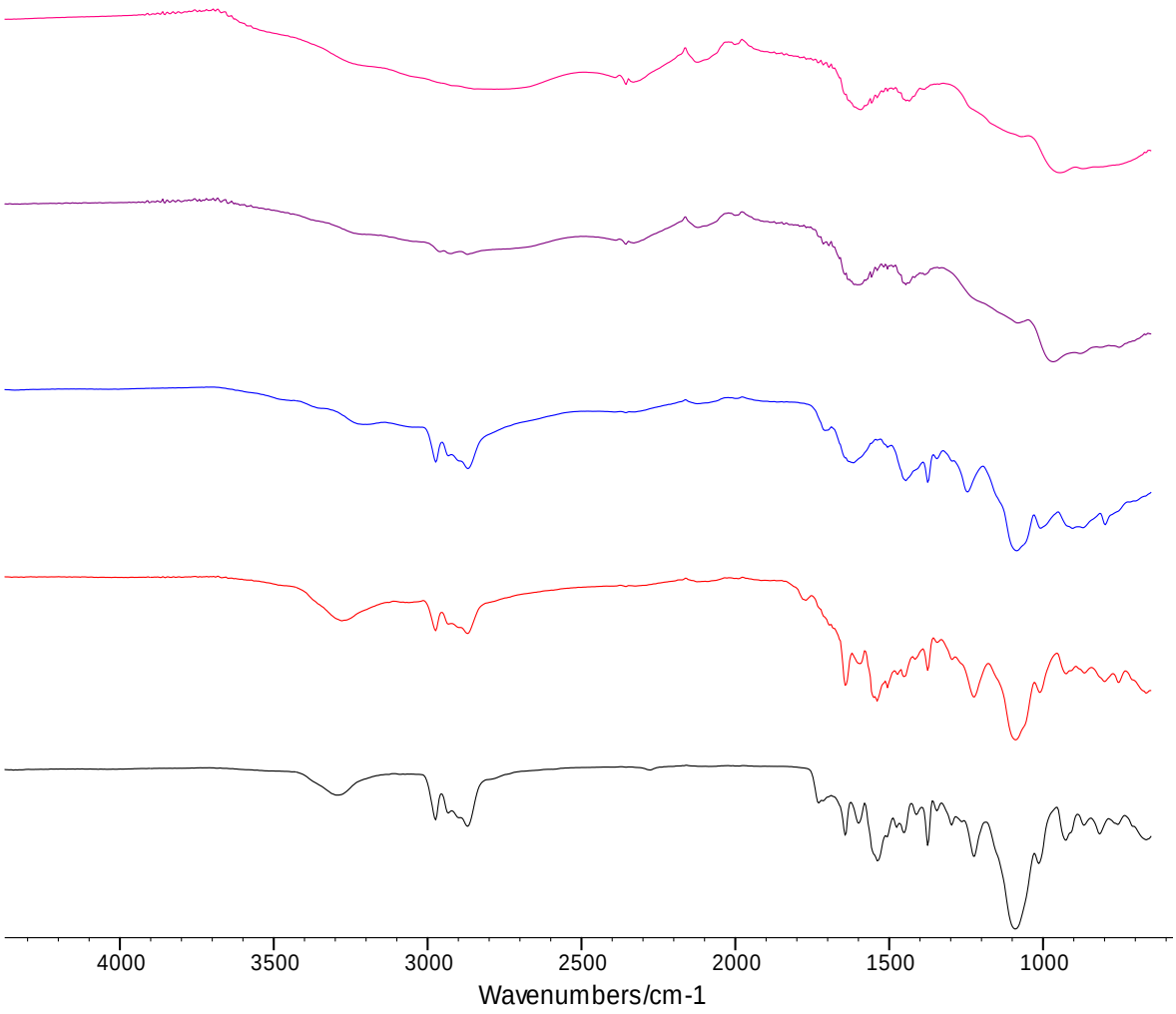

Figure 5.35: Comparisons of the FTIR spectra of the virgin APP foam (black) with the chars obtained after pyrolysis under air at 250°C (red), 300°C (blue), 350°C (purple) and 400°C (pink)

The spectrum at 250°C is similar to that of the virgin APP foam, although the carbonyl signal corresponding to the urethane linkages has now diminished significantly. This indicates that significant degradation of the urethane linkages within the APP foam has occurred at this temperature. By 300°C the foam is in a more advanced state of

charring. Polyol peaks can, however, still be observed within the FTIR spectrum at this temperature which is in agreement with the solid-state ^{13}C NMR results and confirms that polyol remains within the char obtained from the pyrolysis of the APP foam under air at 300°C. The spectra at 350°C and 400°C are weak and difficult to interpret, indicating that the foam is highly charred by these temperatures.

- *Elemental Analysis*

The virgin APP foam and the chars generated under air were submitted for elemental analysis to determine the percentages of carbon, hydrogen and nitrogen present. The results from the elemental analysis of the standard and APP foams are displayed in Table 5.13. The C:H and C:N ratios have also been calculated in order to more clearly illustrate the changes occurring in the chars and the results are presented in Figure 5.36 and Figure 5.37.

Foam	**Deg Temp/°C**	**%C**	**%H**	**%N**	**C/H**	**C/N**
Standard	*Virgin*	61.7	9.1	5.3	6.8	11.6
	250	62.2	7.4	8.7	8.4	7.1
	300	60.3	4.2	11.4	14.4	5.3
	350	67.4	4.7	10.5	14.3	6.4
	400	65.2	3.0	13.6	21.7	4.8
APP	*Virgin*	52.5	8.6	6.7	6.1	7.9
	250	46.9	6.1	10.2	7.7	4.6
	300	45.9	6.1	8.8	7.5	5.2
	350	43.1	4.6	7.7	9.4	5.6
	400	46.7	3.5	7.1	13.3	6.6

Table 5.13: Elemental analysis results for the standard and APP foams after pyrolysis under air

At 250°C the C:H ratio increases slightly and the C:N ratio decreases significantly which indicates loss of polyol from the system with retention of the nitrogen-containing components. This is in correlation with the previous results which showed a reduction in the intensity of the polyol peaks within the solid-state ^{13}C NMR and extraction of a large quantity of polyol-based tar. This is also in contrast to the results under nitrogen which did not show a significant decrease in the C:N ratio at this temperature. These

results once again confirm that degradation of the polyurethane is altered in the presence of oxygen.

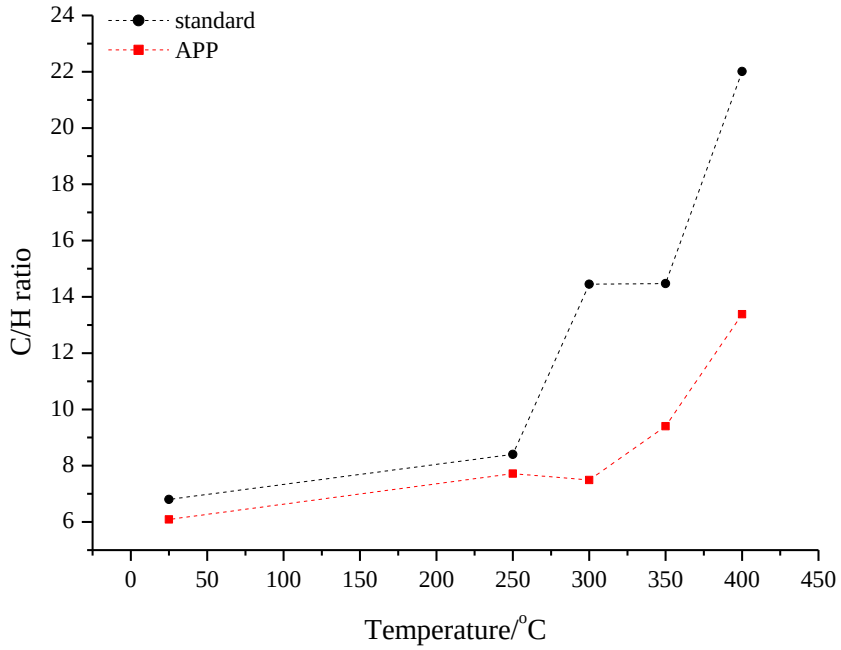

Figure 5.36: C:H ratios as a function of temperature for the pyrolysis chars obtained from the standard and APP foams under air

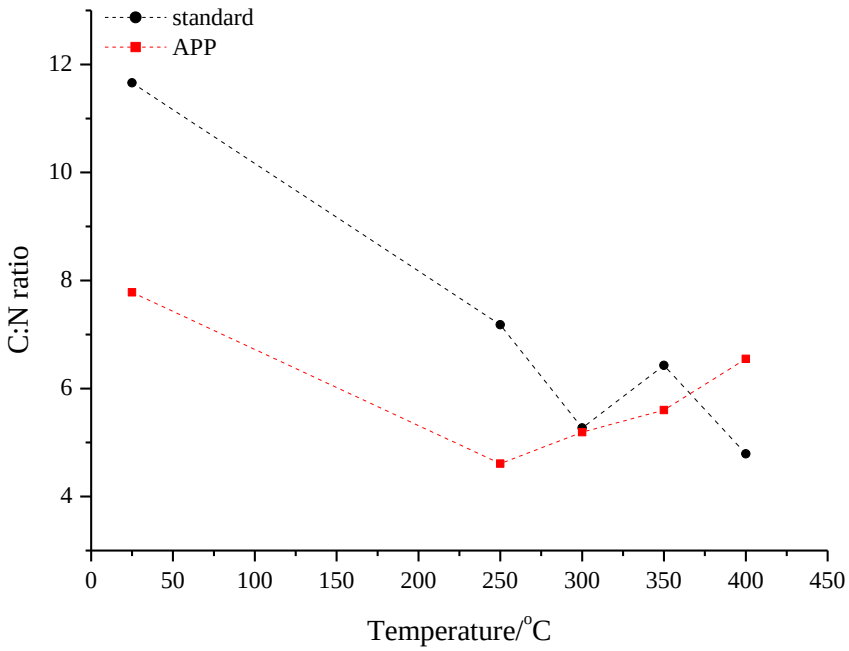

Figure 5.37: C:N ratios as a function of temperature for the pyrolysis chars obtained from the standard and APP foams under air

At 300°C there is little change in the C:H ratio which indicates that there is little loss of polyol from the char at this temperature. This is in agreement with the solid-state ^{13}C NMR results which revealed that the char generated under air at 300°C still contained a significant level of polyol. The C:N ratio, on the other hand, increases at 300°C which indicates volatilisation of nitrogen-containing species at this temperature. This is in correlation with the cold-ring fraction results which showed that nitrogen-containing products had volatilised from the APP foam into the cold-ring fraction at 300°C.

The ratios then both increase at 350°C and 400°C which indicates loss of hydrogen and nitrogen from the char. This could be explained by loss of ammonia from the fire retardant as it begins to degrade further and promote char formation.

5.2.2.3 Summary

The results from pyrolysis of the APP foam under air demonstrate that the degradation of the polyurethane occurs at a lower temperature than under nitrogen and the chemistry occurring in the condensed-phase is different. Significantly lower mass losses were observed at 300°C and above compared to the standard foam, which indicates that APP is exhibiting a condensed-phase action by promoting the formation of char. This was confirmed by the pictures of the chars obtained from the APP foam which showed that even at 250°C the foam was black and charred in appearance. Furthermore, comparisons of the char quantities revealed that under an oxidative environment the foams were more charred, which confirms that char formation is more significant under air.

The solid-state ^{13}C NMR results revealed that polyol remained within the char from the APP foam under air at higher temperatures than for the standard foam. It is proposed that the hydroxyl end groups resulting from thermo-oxidative degradation of the polyol react with the ultraphosphate formed from degradation of the APP, resulting in polyol-based material becoming bound within the char. By 400°C APP foam was in such an advanced state of charring that no solid-state ^{13}C NMR spectrum could be obtained.

This could be due to the presence of free radicals trapped within the aromatic carbonaceous structure of the char as was demonstrated by Duquesne *et al.* for a polyurethane/APP coating.[3]

5.2.3 Pyrolysis under 3% Oxygen in Nitrogen

Following the pyrolysis studies under nitrogen and air, a study was carried out under a 3% oxygen in nitrogen environment, which better represents a fire situation. The aim of this pyrolysis study was to determine if thermal or thermo-oxidative degradation is the dominant process in this situation. If thermo-oxidative degradation is the only process occurring then the results would be expected to match those presented for the pyrolysis under air. On the other hand, if the effect of the oxygen was not significant then the results would match the pyrolysis under nitrogen. Finally, if both thermal and thermo-oxidative processes occur, as was the case for the standard foam, then the degradation behaviour would lie somewhere between the two extremes.

5.2.3.1 Mass Loss Data and Observations

Presented in Figure 5.38 is a comparison of the quantities of residue obtained from the pyrolysis of the APP foam under nitrogen, air and 3% oxygen in nitrogen. There is very little difference in the mass losses at 250°C and 300°C under all three environments. At 250°C the foam was discoloured under 3% oxygen in nitrogen, as was the case for the pyrolysis under air. As the pyrolysis temperature was increased to 350°C it can be observed that the mass loss in 3% oxygen in nitrogen is identical to that under nitrogen, however, by 400°C the mass loss lies between the mass losses under nitrogen and air. These results demonstrate that at the low temperatures the atmosphere does not have a significant effect on the mass loss observed; however, at the higher temperatures the type of gas does become important. This indicates that the degradation behaviour of the APP foam under 3% oxygen in nitrogen is complex and most likely involves both thermal and thermo-oxidative mechanisms.

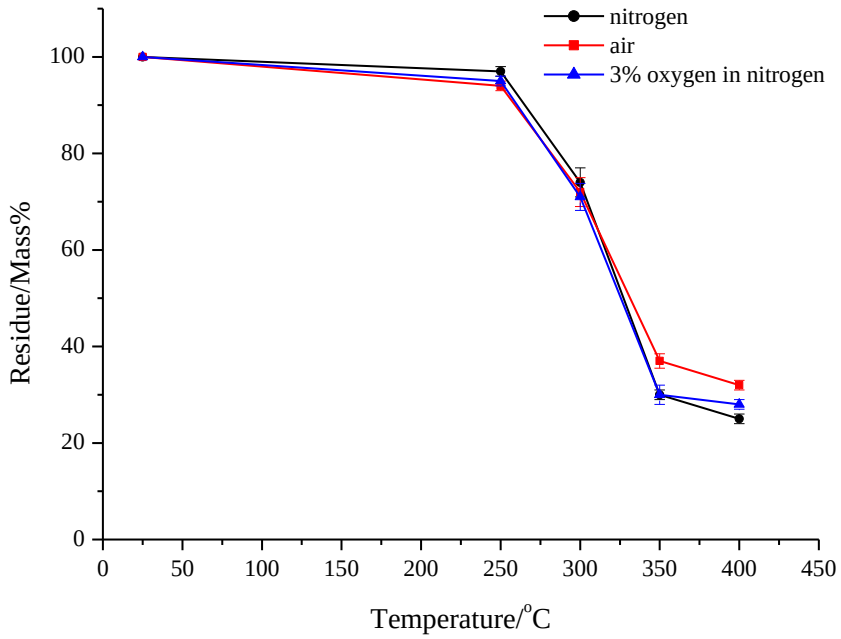

Figure 5.38: Residue obtained vs. pyrolysis temperature for the APP foam under nitrogen, air and 3% oxygen in nitrogen

5.2.3.2 Cold-ring Fraction Analysis

A cold-ring fraction was obtained at all temperatures during the pyrolysis of the APP foam under 3% oxygen in nitrogen, although there was only a small amount present at 250°C. This indicates that degradation of the APP foam has begun to occur as low as 250°C to yield volatile material. There was no cold-ring fraction collected from the APP foam after the pyrolysis at 250°C under nitrogen, therefore, the presence of a cold-ring fraction indicates that thermo-oxidative degradation is occurring at this temperature. The cold-ring fractions collected at 300°C and above were all similar, indicating the presence of polyol fragments and N-H containing compounds. These spectra were also similar to those obtained for the APP foam under nitrogen which indicates that thermal degradation has occurred to some extent under 3% oxygen in nitrogen.

These results, therefore, demonstrate that the degradation behaviour of the APP foam under 3% oxygen in nitrogen is complex and appears to involve both thermal and thermo-oxidative mechanisms.

5.2.3.3 Residue Analysis

The residues obtained from the pyrolysis of the APP foam under 3% oxygen in nitrogen yielded tar and char at all temperatures. There was no tar collected from the APP under nitrogen at 250°C which, once again, indicates that thermo-oxidative degradation of the polyurethane is occurring at 250°C. Analysis of the tars was achieved by FTIR spectroscopy, whilst the chars were characterised by solid-state ^{13}C NMR spectroscopy, FTIR spectroscopy and elemental analysis.

5.2.3.3.1 Quantification of the Tar and Char

Presented in Figure 5.39 are comparisons of the quantities of tar and char collected from the APP foam after pyrolysis under nitrogen, air and 3% oxygen in nitrogen.

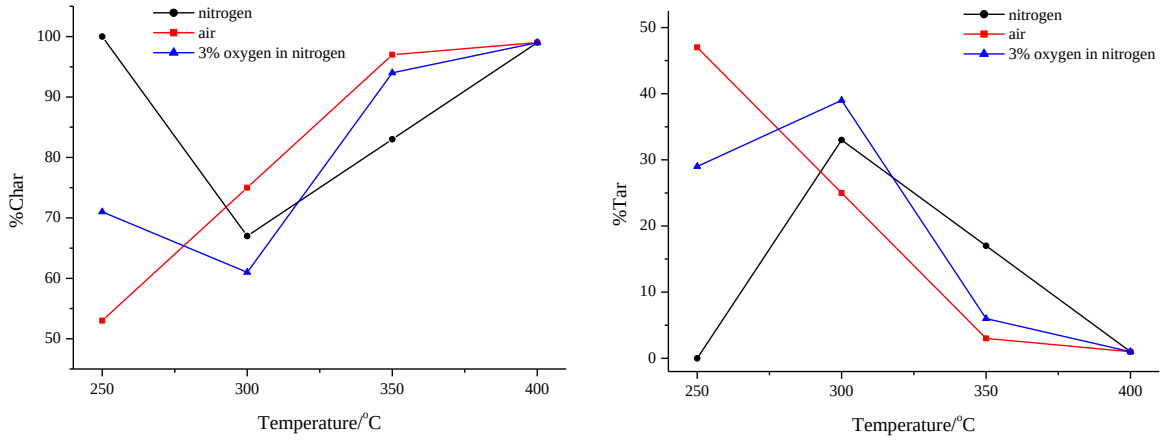

Figure 5.39: Comparisons of the quantities of tar and char collected from the APP foam after pyrolysis under nitrogen, air and 3% oxygen in nitrogen

It can be observed that the quantities of tar and char collected from the APP foam after pyrolysis under 3% oxygen in nitrogen lie between the values for nitrogen and air. At 250°C the values for 3% oxygen in nitrogen lie almost in the middle of those for nitrogen and air. At 300°C the level of char obtained is lower than under both nitrogen and air, whilst the level of tar collected is higher. This is clearly an anomaly as this value should lie between the two extremes. Unfortunately, due to time constraints and instrument failures this experiment could not be repeated. The overall trend in the data can, however, still be observed regardless of this. By 350°C the values for 3% oxygen

in nitrogen lie closer to those of air, although the foam is not as charred in the low oxygen environment. As was the case for the standard foam, this confirms that the degradation behaviour of the APP foam is not simply oxidative, but shows both oxidative and non-oxidative characteristics, with the oxidative environment promoting the formation of greater quantities of char. This is once again important as it demonstrates that degradation of fire retardant polyurethane foam during a fire is complex, and can involve both thermal and thermo-oxidative processes.

5.2.3.3.2 Analysis of the Tar

Presented in Figure 5.40 is the FTIR spectrum of the tar collected from the APP foam after pyrolysis under 3% oxygen in nitrogen at 250°C.

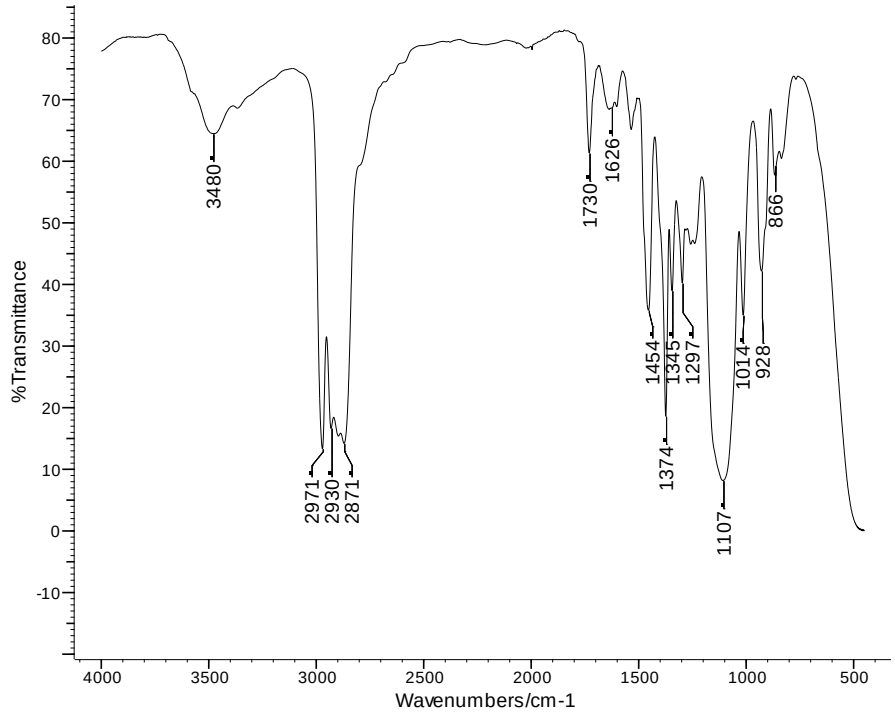

Figure 5.40: FTIR spectrum of the tar collected from the APP foam after pyrolysis at 250°C under 3% oxygen in nitrogen

The majority of the peaks in the FTIR spectrum are associated with the polyol component of the foam, which was also the case for the tars generated under nitrogen and air. The carbonyl peak at 1730 cm^{-1} indicates the presence of residual urethane

linkages within the tar or carbonyl-containing products arising from degradation of the polyol component of the foam. The presence of a polyol-based tar at 250°C under 3% oxygen in nitrogen confirms that thermo-oxidative degradation processes are occurring, as no tar was extracted from the pyrolysis under nitrogen.

By 300°C the carbonyl group is significantly diminished which indicates either degradation of the residual urethane linkages or loss of carbonyl-containing polyol fragments has occurred. By 400°C there was insufficient tar present to obtain a useful FTIR spectrum. The FTIR spectra of the tars are similar under all three environments which indicates that the structures of the tars do not vary significantly between the oxidative and non-oxidative pyrolyses.

5.2.3.3.3 Analysis of the Char

Presented in Figure 5.41 are photographs of the chars collected from the standard foam after pyrolysis under 3% oxygen in nitrogen. The char at 250°C shows a greater level of discolouration than the char obtained under nitrogen; however, the discolouration is not as severe as the char obtained under air. This indicates that thermo-oxidative degradation of the foam has occurred under 3% oxygen in nitrogen but not to as great an extent as under air. At 300°C the char is black and has lost its foamed structure, again resembling the oxidative char more than the non-oxidative char. There is little difference in the chars obtained at 350°C and 400°C. These observations once again demonstrate that degradation of the APP foam under a low oxygen environment is complex, most likely consisting of both oxidative and non-oxidative processes.

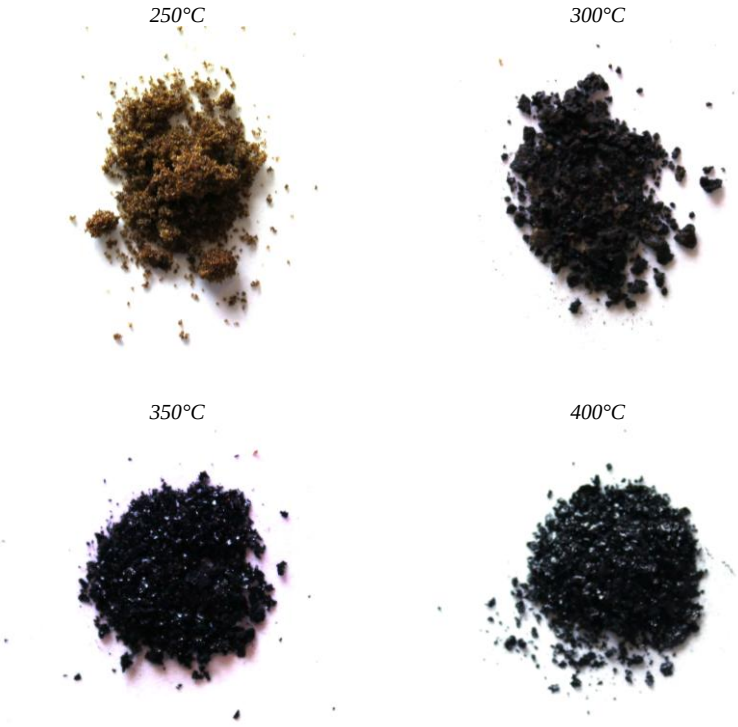

Figure 5.41: Photographs of the chars collected from the APP under 3% oxygen in nitrogen

Characterisation of the chars was achieved by solid-state ^{13}C NMR spectroscopy, FTIR spectroscopy and elemental analysis.

- *Solid-state ^{13}C NMR*

Presented in Figure 5.42 are the ^{13}C CPMAS TOSS spectra for the virgin APP foam and the chars obtained after pyrolysis under 3% oxygen in nitrogen. The peak assignments for the virgin foam are the same as those discussed previously. At 250°C there is a decrease in the intensity of the polyol signals which indicates that scission of the soft segments has begun to occur at this temperature. The loss of polyol-based material is, however, not as significant as it was at this temperature under air which suggests that the degradation has not occurred to the same extent under 3% oxygen in nitrogen.

By 300°C the foam is significantly charred which indicates that significant degradation of the APP foam has occurred by this temperature. The spectrum at 300°C is similar to that obtained under air except that polyol signals were still observed in the spectrum

under air. The spectrum at 300°C under nitrogen, on the other hand, showed no polyol peaks at this temperature but the peaks in the aromatic region were more resolved. The spectrum under 3% oxygen in nitrogen appears to be intermediate between these two extremes, showing loss of polyol but with more significant charring than under nitrogen. This once again demonstrates that degradation of the APP foam under a low oxygen environment is complex and involves both oxidative and non-oxidative processes.

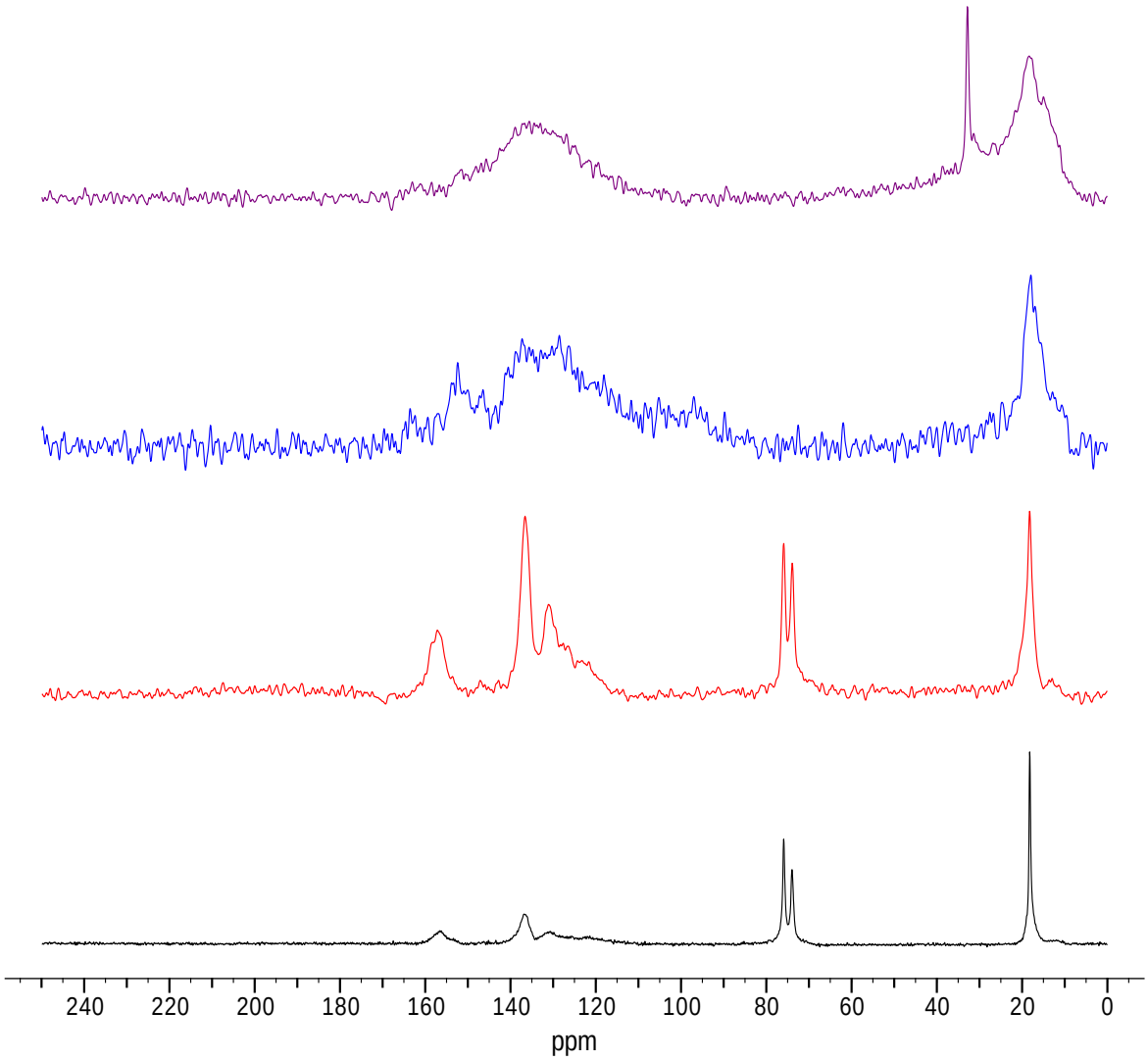

Figure 5.42: Comparison of the ^{13}C CPMAS TOSS spectra of the virgin APP foam (black) with the chars obtained after the pyrolysis under 3% oxygen in nitrogen at 250°C (red), 300°C (blue), 350°C (purple) and 400°C (pink)

The spectrum at 350°C is similar to the spectra under air and nitrogen; however, there is an additional sharp peak at 32.77 ppm in the spectrum under 3% oxygen in nitrogen. This is unusual as it has not been observed in any of the spectra before and it is proposed that this arises from contamination within the sample. As was the case for the pyrolysis under air, there is no spectrum for the char at 400°C as the graphitic nature of this sample caused problems with the spinning. This indicates that at 400°C thermo-oxidative degradation has been significant leading to the foam being in a highly advanced state of charring.

These results, therefore, indicate that under a low oxygen environment the foam begins to char at lower temperatures than under a non-oxidative environment, however, the degradation and charring is not as advanced as that under air until the higher temperatures. This again confirms that the degradation of the fire retardant foam under 3% oxygen in nitrogen is complex and is not simply an oxidative process.

- *FTIR Spectroscopy*

Presented in Figure 5.43 are the FTIR spectra for the virgin APP foam and the chars collected after pyrolysis under 3% oxygen in nitrogen at 250, 300, 350 and 400°C. The spectrum at 250°C is similar to that under air with the carbonyl peak at 1729 cm^{-1} significantly reduced, indicating that degradation of the urethane linkages has occurred at this temperature. By 300°C the foam is significantly charred and polyol peaks are no longer observed in this spectrum. This is in contrast to the results under air which showed that polyol peaks were still present in the char at this temperature. The spectra for the chars at 350°C and 400°C are similar, being significantly distorted as a result of the char being more carbonaceous at these temperatures.

These results, therefore, demonstrate that under the low oxygen environment degradation of the APP foam is complex, showing oxidative and non-oxidative characteristics.

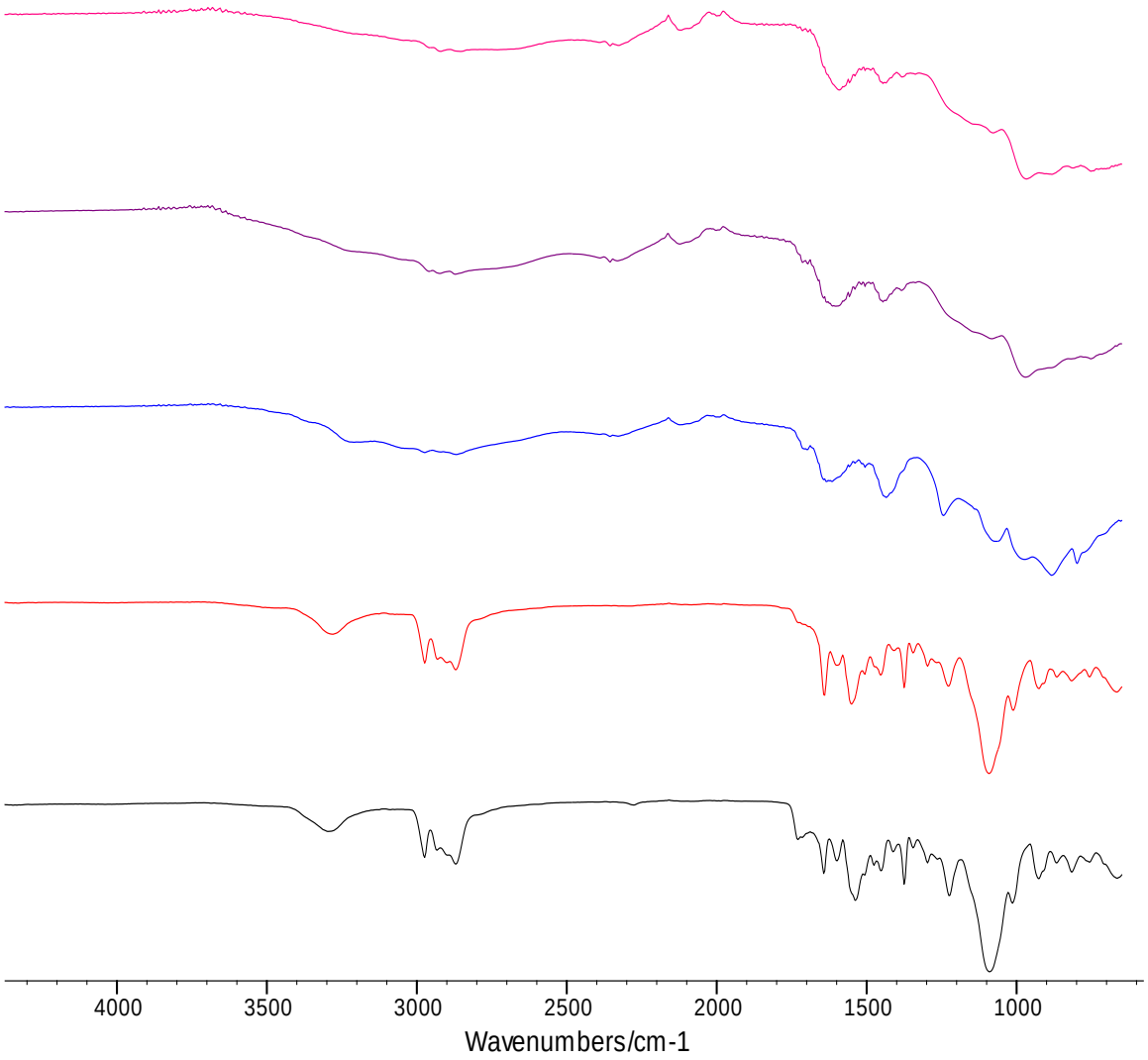

Figure 5.43: Comparison of the FTIR spectra of the virgin APP foam (black) with the chars obtained after pyrolysis under 3% oxygen in nitrogen at 250°C (red), 300°C (blue), 350°C (purple) and 400°C (pink)

- *Elemental Analysis*

The chars obtained from the APP foam under 3% oxygen in nitrogen were submitted for elemental analysis and the ratios of H and N with respect to the percentage carbon were calculated in order to illustrate more clearly the changes occurring in the chars. These results are compared in Figure 5.44 with the results obtained from the pyrolysis under nitrogen and air.

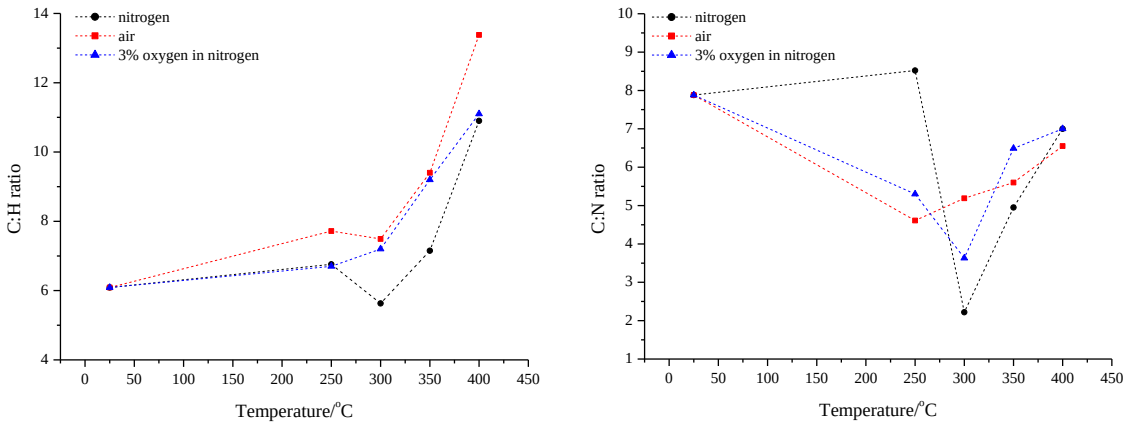

Figure 5.44: Comparison of the C:H and C:N ratios for the pyrolysis chars obtained from the APP foam under nitrogen, air and 3% oxygen in nitrogen

Under all three environments the overall trend observed for the C:H ratio is that it increases with increasing temperature, which is indicative of polyol being lost from the char at the lower temperatures and ring fusion of the aromatics to yield a complex carbonaceous char at the higher temperatures. It can also be observed that the C:H ratio for the chars obtained under 3% oxygen in nitrogen lie between the values for those under nitrogen and air, being closer to the nitrogen values at 250°C and 400°C but close to the air values at 300°C and 350°C.

The C:N ratios for the chars under 3% oxygen in nitrogen are again similar to the nitrogen values at some temperatures but the air values at other temperatures. The decrease in C:N ratio at 250°C indicates that polyol is lost from the system at this temperature, as was the case for the analysis under air. This is in agreement with the previous results which showed a significant quantity of tar was extracted at 250°C. The C:N ratio then follows a similar trend to that of the chars under nitrogen, decreasing at 300°C then increasing at higher temperatures as nitrogen is lost from the foam as further degradation of the APP and the polyurethane occurs.

These results once again confirm that degradation of the APP foam under a low oxygen environment is complex and shows characteristics of both oxidative and non-oxidative degradation.

5.2.3.4 Summary

The aim of the pyrolysis under 3% oxygen in nitrogen was to determine if degradation of the fire retardant APP foam in a low oxygen environment is dominated by thermal or thermo-oxidative degradation. The results are interesting, revealing that degradation of the APP foam in a low oxygen environment is complex and the degradation behaviour lies between that observed under nitrogen and air.

There was little difference observed in the mass losses between the three environments at 250°C, however, the foam pyrolysed under 3% oxygen in nitrogen had discoloured, a cold-ring fraction was obtained and a significant quantity of tar was extracted. These results were in contrast to the results obtained under nitrogen and indicate that thermo-oxidative degradation of the APP foam had occurred at 250°C. At 300°C the mass losses were again similar under all three environments which indicates that at the lower temperatures the atmosphere does not have a significant effect on the mass loss. At 350°C the mass loss resembled that under nitrogen, whilst at 400°C the mass loss was between the values for air and nitrogen. This suggests that the degradation behaviour is complex and is likely to involve both thermal and thermo-oxidative degradation processes.

The chars obtained from the APP foam under 3% oxygen in nitrogen showed levels of discolouration between those observed for the chars generated under air and nitrogen, which again suggests that the degradation behaviour lies between the two extremes. The solid-state ^{13}C NMR results revealed that the foam was more charred than under nitrogen, with problems obtaining a spectrum of the char at 400°C. This was the same problem which was encountered for the pyrolysis under air. The chars were, however, not identical to those under air.

Pyrolysis of the APP foam under 3% oxygen in nitrogen, therefore, reveals that the degradation is complex when there are low levels of oxygen present, with both thermal and thermo-oxidative processes proposed to be occurring. This information is important as it shows that fire retardants may behave differently depending on the environment in which they are being employed.

5.3 Conclusions

The results presented in this chapter have demonstrated that the degradation of a TDI-based polyurethane foam containing APP as a fire retardant is complex, consisting of a number of steps which yield an array of volatile products and residues which consist of tar and complex char.

Under an inert environment the APP foam degrades in four steps which overlap to some degree. The first two steps correspond to degradation of the urethane linkages within the foam and degradation of the APP to yield an ultraphosphate with evolution of ammonia and water. The last two steps correspond to secondary degradation reactions, such as degradation of the polyol, and further degradation of the APP.

TVA studies revealed that degradation of the urethane linkages under vacuum occurs by two competing mechanisms, as was the case for the standard foam. The predominant mechanism is proposed to be depolymerisation of the urethane bond to yield TDI and polyol, with the second mechanism involving dissociation of the urethane linkages to yield DAT, CO_2 and alkene-terminated polyol chains. Evolution of volatile material was also observed to occur at a lower temperature for the APP foam and it is proposed that degradation of the urethane linkages *via* a depolycondensation reaction is acid-catalysed by the acidic hydroxyl groups, which arise from degradation of the APP, as shown in Figure 5.45. The isothermal TVA studies revealed that degradation of the APP occurs as low as 250°C and degradation of the polyol becomes significant by 300°C.

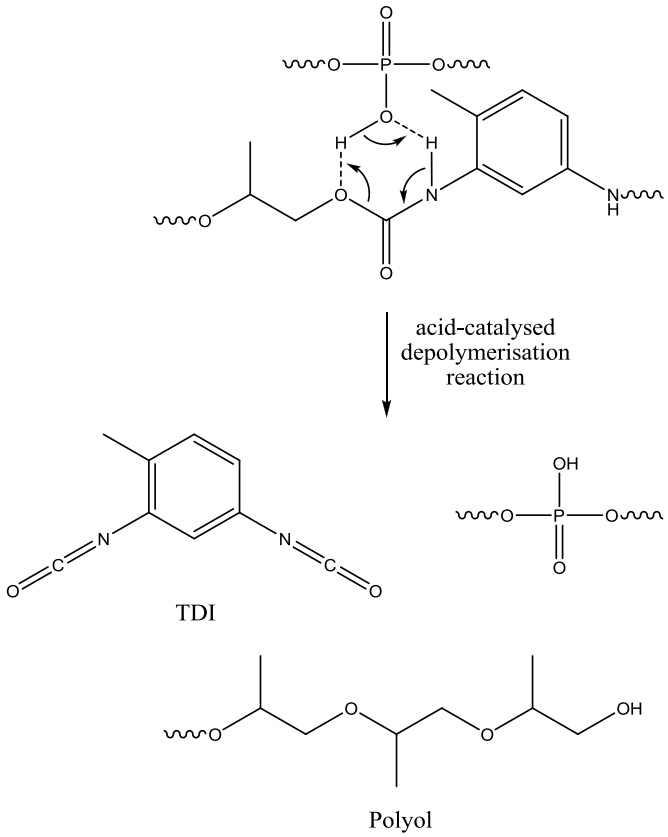

Figure 5.45: Acid-catalysed degradation of the urethane linkages

Furthermore, the TVA studies revealed that the volatile degradation products evolved from the polyurethane are altered in the presence of APP. The reason for this is believed to be the presence of acidic species which are generated from degradation of the APP. This leads to acid-catalysed degradation of the polyol, with propanal and 2,5-dimethyl-1,4-dioxane as the major volatile degradation products, as shown in Figure 5.46. This is in contrast to the standard foam which yielded additional volatile products including acetaldehyde and formaldehyde.

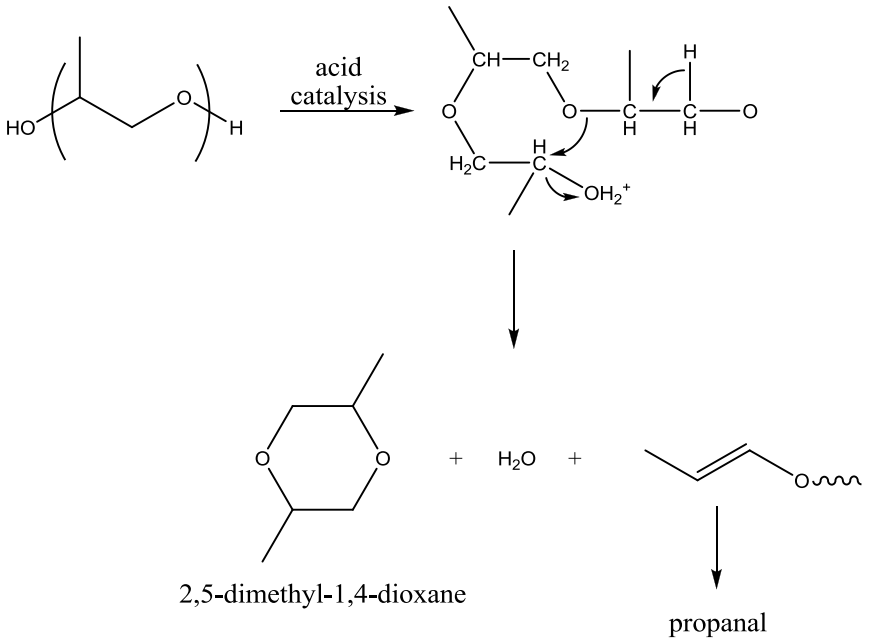

Figure 5.46: Acid-catalysed degradation of the polyol component

Alternatively, a phosphorylation reaction could occur between the ultraphosphate and the polyol, as shown in Figure 5.47, which would lead to phosphorus esters. Degradation of this network would then occur yielding phosphoric acid and an alkene terminated chain. This would once again generate propanal by acid hydrolysis.

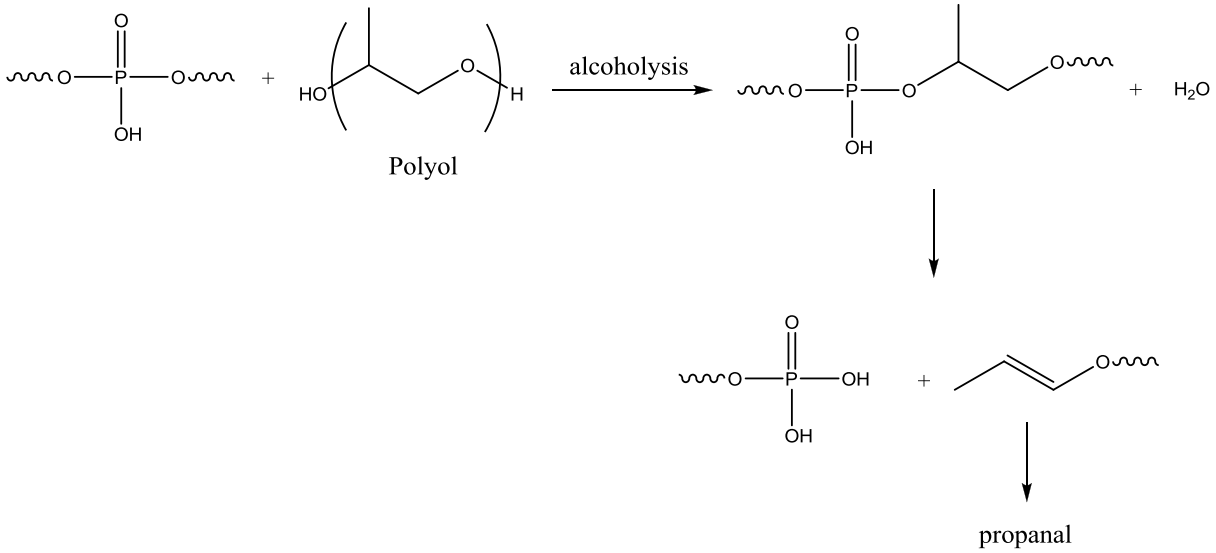

Figure 5.47: Phosphorylation of the polyol and subsequent degradation of the phosphorus esters

Pyrolysis studies under nitrogen revealed that APP exhibits a significant condensed-phase activity by promoting char formation in the polyurethane. Solid-state ^{13}C NMR studies demonstrated that the APP foam is in a significantly more advanced state of charring than the standard foam at 300°C, with the residues consisting primarily of complex aromatic carbonaceous char at this temperature. As the temperature was increased the foam became even more charred in nature, consisting entirely of char by 400°C.

Pyrolysis studies under air revealed that degradation and charring of the APP foam occurs at lower temperatures than under nitrogen. At temperatures of 300°C and above the mass loss was significantly lower under air than under nitrogen and the residues consisted of greater quantities of char. It is proposed that degradation of the polyol under an oxidative environment yields hydroxyl end groups which undergo phosphorylation reactions with the ultraphosphate formed when APP degrades. This results in polyol-based material becoming bound within the char. By 400°C under air the APP foam was so significantly charred that a solid-state ^{13}C NMR spectrum could not be obtained due to the graphitic nature of the sample. These results, therefore, indicate that under an oxidative environment APP promotes char formation at even lower temperatures than in a non-oxidative environment.

Finally, degradation in a low oxygen environment was shown to be complex, with the degradation behaviour showing characteristics of thermal and thermo-oxidative degradation. The foam discolours and becomes charred at lower temperatures than under nitrogen, however, this is not as extreme as when the foam is pyrolysed under air. It is, therefore, likely that both thermal and thermo-oxidative degradation processes occur in a low oxygen environment and this is important to understand when considering the performance of fire retardant materials in a fire situation.

Degradation of the polyurethane foam containing APP can, therefore, be summarised as consisting of the following key steps

- The APP fire retardant decomposes yielding water, ammonia and an ultraphosphate containing acidic hydroxyl groups

- The ultraphosphate acidic hydroxyl groups then catalyse the degradation of the urethane linkages *via* a depolymerisation reaction which yields TDI and polyol

- Acid-catalysed degradation of the polyol may occur which yields 2,5-dimethyl-1,4-dioxane, water, propanal and propene

- Phosphorylation of the regenerated polyol can also occur which yields phosphorus esters which then degrade to yield phosphoric acid, propanal and propene

- Under an oxidative environment the phosphorylation reaction becomes important, as the hydroxyl end groups produced as a result of thermo-oxidative degradation of the polyol react with the ultraphosphate resulting in polyol-based material becoming bound within the char

- The acidic species generated during the degradation of the APP promote the formation of char formation within the polyurethane foam

5.4 References

[1] G. Woods, *Flexible Polyurethane Foams: Chemistry and Technology*, Applied Science Publishers Ltd, Essex, 1982, Ch. 2, p. 47

[2] W. C. Kuryla and A. J. Papa, *Flame Retardancy of Polymeric Materials*, Volume 3, Marcel Dekker Inc., New York, 1975, Ch. 1, p. 1

[3] S. Duquesne, M. Le Bras, S. Bourbigot, R. Delobel, G. Camino, B. Eling, C. Lindsay, T. Roels and H. Vezin, *J. Appl. Polym. Sci.*, 2001, **82**, 3262

[4] S. Duquesne, R. Delobel, M. Le Bras and G. Camino, *Polym. Degrad. Stabil.*, 2002, **77**, 333

[5] N. Grassie and A. P. Mendoza, *Poly. Degrad. Stabil.*, 1985, **11**, 145

[6] G. Camino, N. Grassie and I. C. McNeill, *J. Polym. Sci. Chem. Ed.*, 1978, **16**, 95

[7] J. H. Saunders and K. C. Frisch, *Polyurethanes Chemistry and Technology: Part I. Chemistry*, Interscience Publishers, New York, 1962, Ch. II, p. 32

[8] A. R. Horrocks and D. Price, *Fire Retardant Materials*, Woodhead Publishing Ltd, Cambridge, 2001, Ch. 2, p. 31

[9] C. J. Hilado, *Flammability Handbook for Plastics*, Technomic Publishing Company Inc., Lancaster, 1990, Ch. 5, p. 167

[10] N. Grassie and A. P. Mendoza, *Polym. Degrad. Stabil.*, 1985, **11**, 359

[11] L. Yang, F. Heatley, T. G. Blease and R. I. G. Thompson, *Eur. Polym. J.*, 1996, **32**, 535

6 Study on the Nanocomposite Foams

Degradation studies were conducted on two TDI-based nanocomposite foams, one containing 1.94% vermiculite and one containing 1.94% Cloisite® 30B, in order to examine the effect that these nanoclays have on the degradation behaviour of the polyurethane. Nanocomposites are of great interest in the field of fire retardancy due to their potential to show superior properties over conventional fire retardants. In this study the overall degradation behaviour of the nanocomposite foams was examined by means of DSC, TGA and TVA studies, with a mini-crib fire test used to examine the effect that these clays have on the flammability of the foam. Any additional data not presented in this chapter can be found in Appendix 3.

6.1 Characterisation of the Nanocomposite Foams

When a polymer and clay are mixed to form a nanocomposite there are a number of structures which can be formed. The structure which is understood to impart superior properties into the polymer is the exfoliated nanocomposite,[1] in which the stacks of clay platelets are separated and dispersed throughout the polymer. Scanning Electron Microscopy (SEM) is a technique which can be employed to take images of polymer nanocomposites to determine if the clay is dispersed on a nanometre scale, which will confirm the formation of a nanocomposite, and if the platelets are dispersed throughout the polymer homogenously.

Presented in Figure 6.1 are SEM images of the Cloisite® 30B foam taken at increasing levels of magnification. It can be observed from these images that the Cloisite® 30B foam has an open cell structure as would be expected for a low density flexible foam. When compared to the SEM images of the standard foam (Figure 6.2), however, it is clear that the Cloisite® 30B foam is significantly more open celled in nature than the standard foam. This suggests that the clay has had an effect during the synthesis of the foam, leading to a more open cell structure being produced. This will allow the air and

volatiles to flow in and out of the foam more easily, which may have a detrimental effect on its fire behaviour. It can also be observed from the more magnified SEM images that the clay particles are dispersed throughout the structure of the foam, with many of the particles being nanometres in size. This confirms that a nanocomposite has been produced and suggests that exfoliation of the clay platelets has occurred; however, there are a number of larger particles which indicates that other nanocomposite structures, such as intercalated or end-tethered, are also present. This is not unexpected as in the majority of polymer nanocomposites two or more structures are present.[2,3]

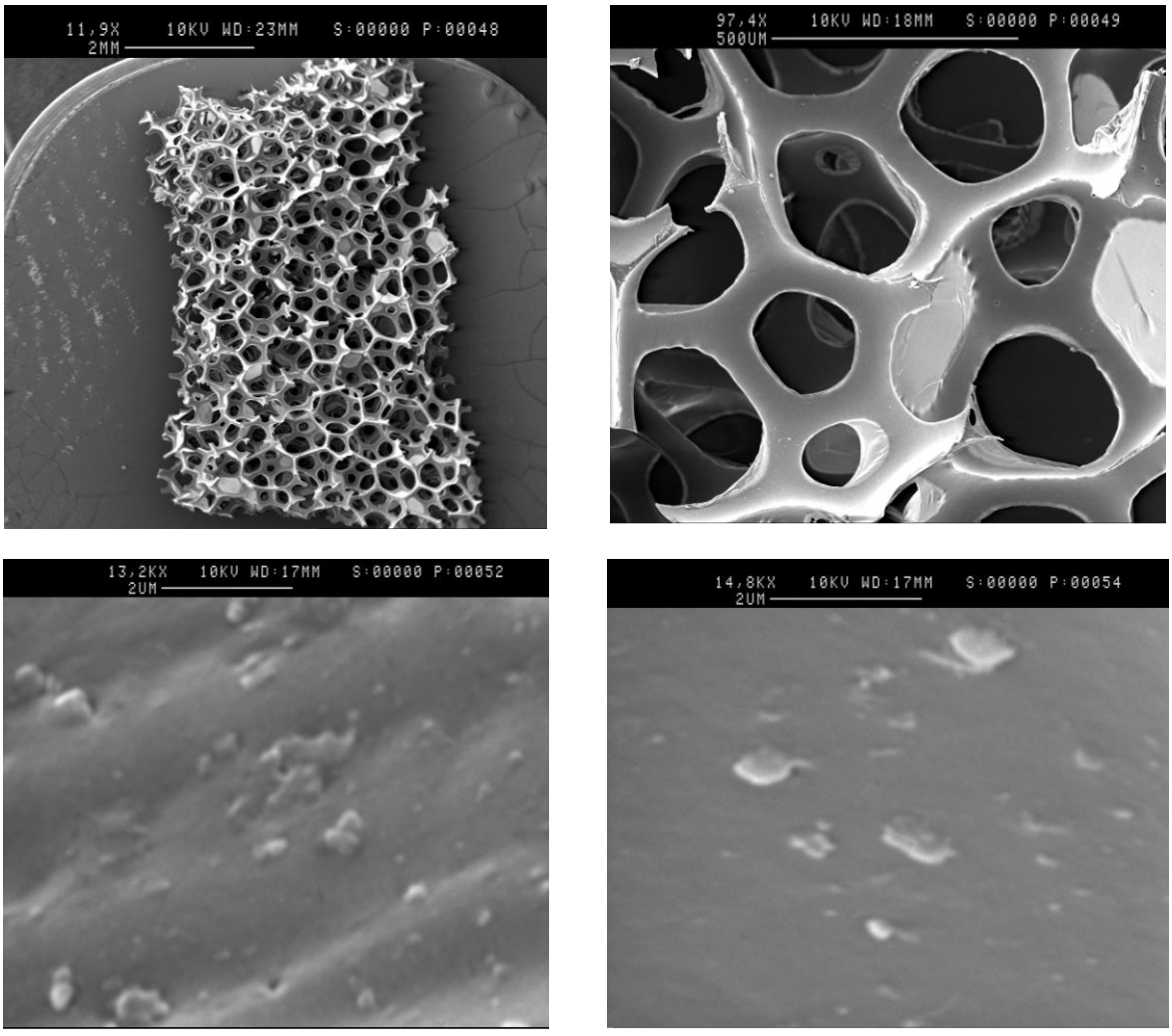

Figure 6.1: SEM images of the Cloisite® 30B foam (magnification and scale are displayed at the top of each image)

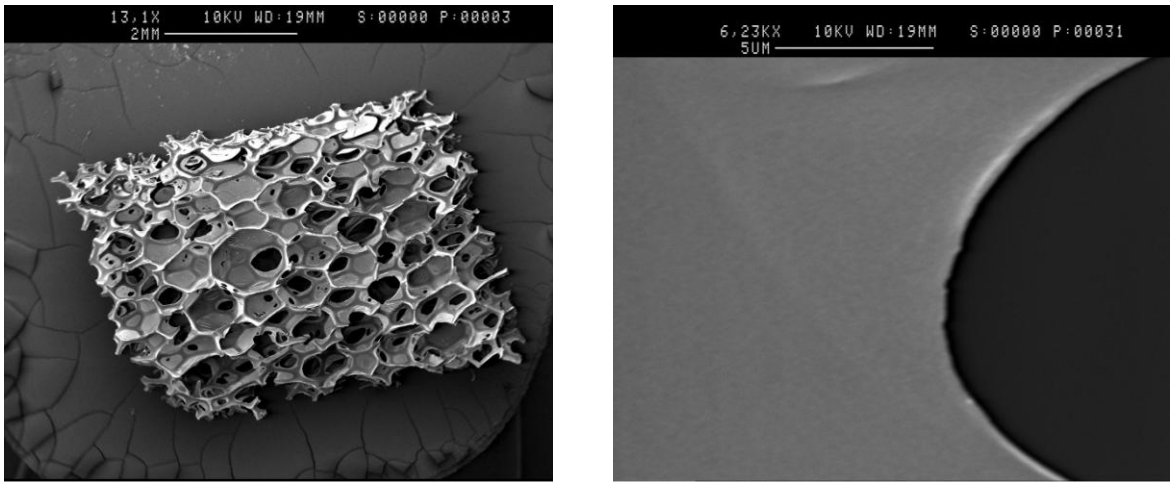

Figure 6.2: SEM images of the standard foam (magnification and scale are displayed at the top of each image)

Presented in Figure 6.3 are the SEM images of the vermiculite foam. It can be observed that the vermiculite foam is less open celled in nature than the Cloisite® 30B foam, appearing more similar in structure to the standard foam. The more magnified image shows that the clay particles are similar to those in the Cloisite® 30B, with some smaller, nanometre sized particles as well as larger ones.

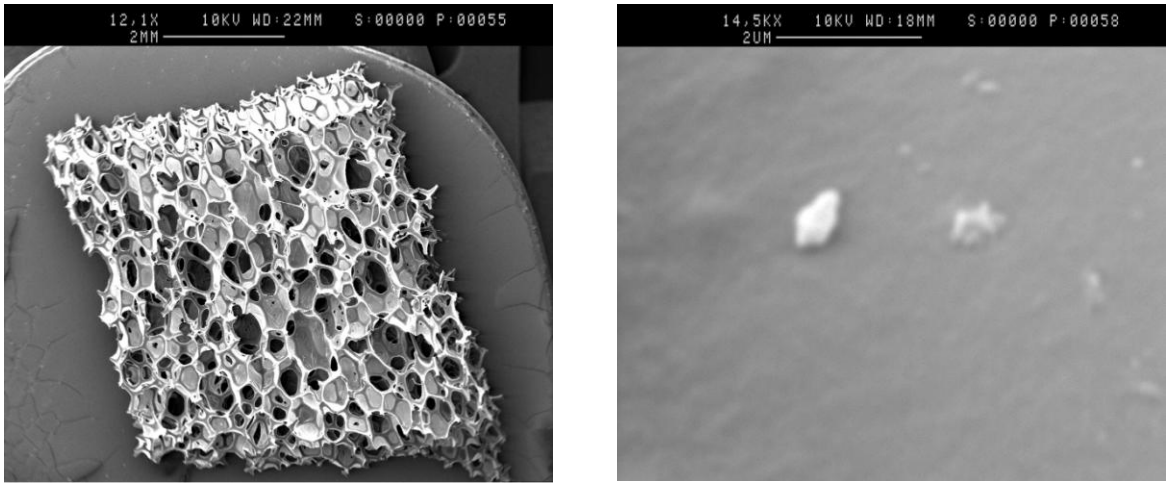

Figure 6.3: SEM images of the vermiculite foam (magnification and scale are displayed at the top of each image)

6.2 Overview of the Degradation and Fire Behaviour

6.2.1 DSC

Presented in Figure 6.4 are the DSC curves for the standard and nanocomposite foams under air.

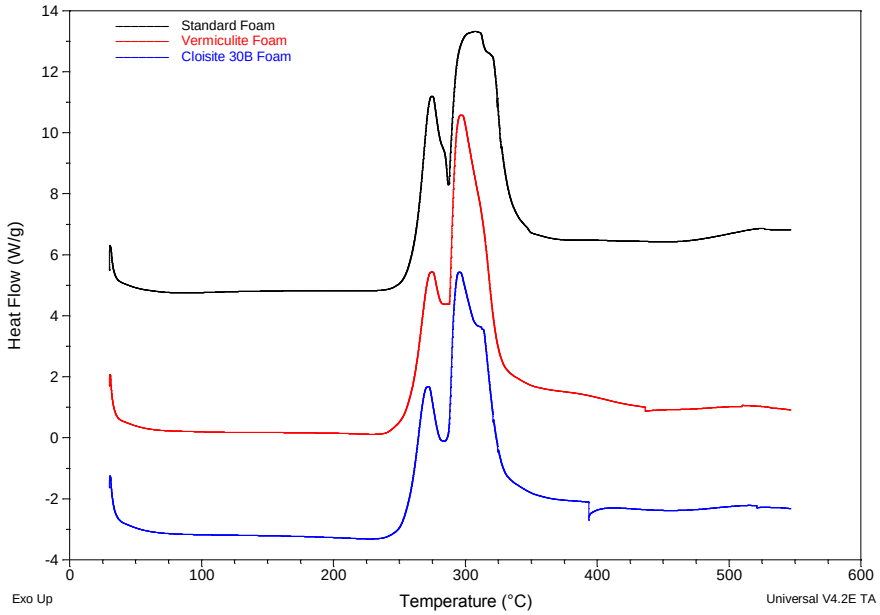

Figure 6.4: DSC curves for the standard and nanocomposite foams analysed in air

Both foams show two main exothermic peaks which correspond closely to those of the standard foam. The first degradation peak for the three foams is similar in shape and peak maximum (272 ± 2°C) which suggests that the initial degradation step in an oxidative environment is not significantly altered in the presence of the nanoclays. The second degradation step, on the other hand, shows some differences. The temperature range in which this second step occurs remains similar to that of the standard foam, however, a more reproducible peak is observed for the nanocomposite foams than for the standard foam. As was discussed in section 4.1.1, the variability exhibited by the second degradation step for the standard foam is due to foam collapse which affects the diffusion of air into the foam. The presence of the nanoclays, however, is expected to reinforce the cellular structure of the foam which will prevent the foam structure from

collapsing as readily. The diffusion of oxygen into the material will, therefore, not be affected to the same extent and the resultant peak in the DSC thermogram becomes sharper and more reproducible.

The DSC curves for the analysis of the nanocomposite foams under nitrogen are presented in Figure 6.5.

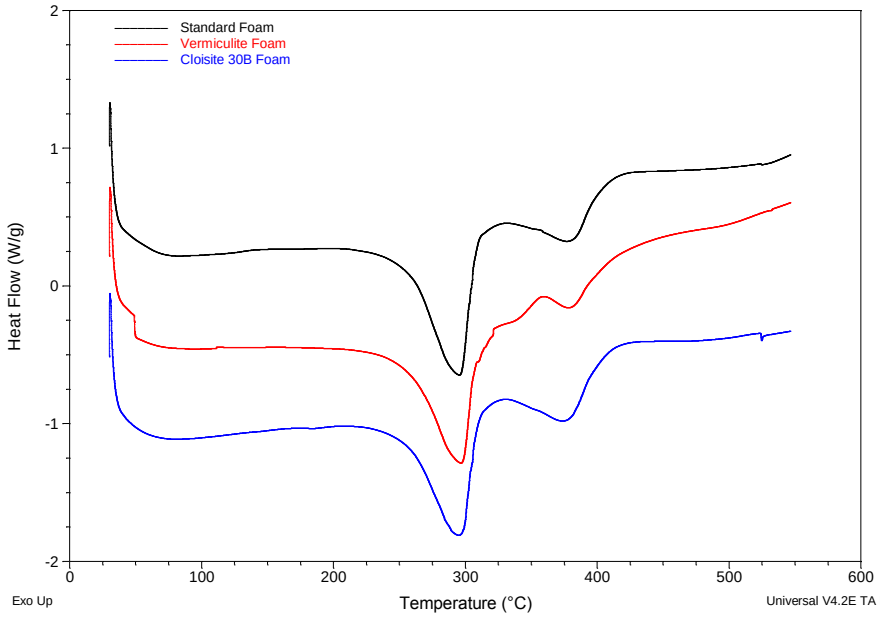

Figure 6.5: DSC curves for the standard and nanocomposite foams analysed in N_2

It can be observed that the curves for both the nanocomposite foams and the standard foam are very similar, showing two main endothermic peaks. This suggests that a two step thermal degradation process is still occurring in the presence of the nanoclay, with the first step corresponding primarily to degradation of the urethane linkages and the second to secondary degradation reactions. Displayed in Table 6.1 are the endothermic peak maxima for the standard and nanocomposite foams. The similarities in the peak maxima suggest that the nanocomposite foams undergo similar degradation reactions to the standard foam. Based on these results, therefore, it appears that the presence of the nanoclays within the polyurethane foam has not significantly altered the thermal degradation behaviour under an inert atmosphere.

Type of Foam	**Peak 1 Maximum/°C**	**Peak 2 Maximum/°C**
Standard	295 ± 2	380 ± 1
Vermiculite	294 ± 3	380 ± 2
Cloisite® 30B	296 ± 1	378 ± 1

Table 6.1: Peak maxima for the standard and nanocomposite foams

6.2.2 TGA

Presented in Figure 6.6 are the TGA and DTG curves for the standard and nanocomposite foams analysed in air. Shown in Table 6.2 are the temperatures at which significant mass loss occurs and the maximum temperatures of the DTG peaks for the nanocomposite and standard foams.

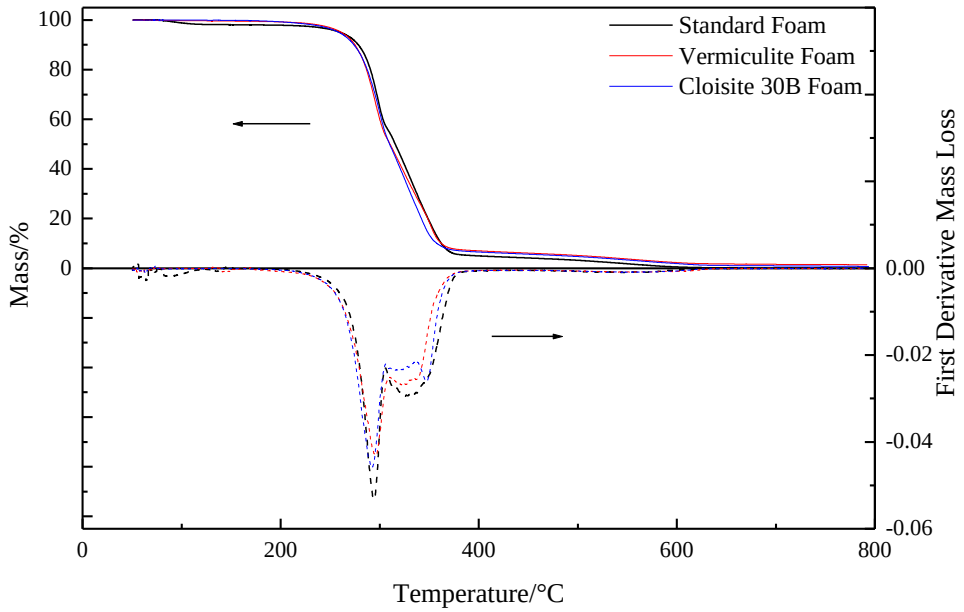

Figure 6.6: TGA and DTG results for the standard and nanocomposite foams analysed in air

The nanocomposite foams show similar thermal behaviour to the standard foam with two major mass loss steps observed. This suggests that the nanocomposite foams degrade *via* a two step mechanism as was the case for the standard foam. The temperatures at which the onset of significant mass loss and the first peak maximum occur are also similar in all cases which suggest that the primary degradation step is not

significantly altered in the presence of the nanoclays. The temperatures of the second mass loss stages are, however, lower for the nanocomposite foams which suggests the nanoclays may be altering the secondary degradation mechanisms of the polyurethane. Neither clay, however, appears to be exhibiting a significant barrier effect in the polyurethane foam, as if this was occurring then a delay in the evolution of volatile material would be expected to be observed.

Type of Foam	**Onset of Significant Mass Loss/°C**	**Peak 1 Maximum/°C**	**Peak 2 Maximum/°C**
Standard	260	294	330
Vermiculite	261	293	320
Cloisite® 30B	258	295	323

Table 6.2: Onset temperatures and peak maxima for the standard and nanocomposite foams analysed in air

The TGA and DTG curves for the standard and nanocomposite foams analysed in helium are presented in Figure 6.7.

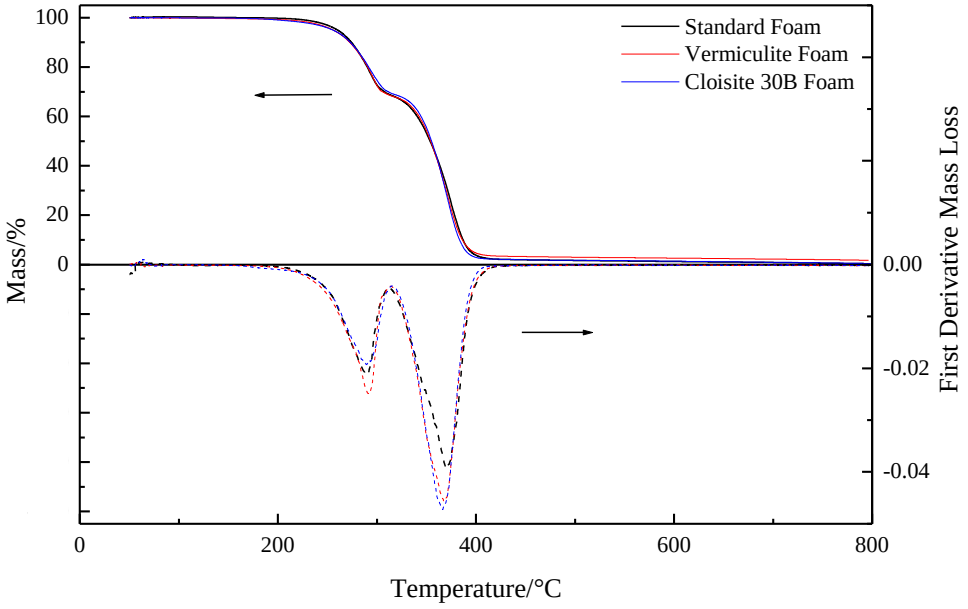

Figure 6.7: TGA and DTG results for the standard and nanocomposite foams analysed in He

The temperatures at which significant mass loss occurs and the maximum temperatures of the DTG peaks for each foam are displayed in Table 6.3.

Type of Foam	**Onset of Significant Mass Loss/°C**	**Peak 1 Maximum/°C**	**Peak 2 Maximum/°C**
Standard	260	289	370
Vermiculite	256	292	368
Cloisite® 30B	256	290	366

Table 6.3: Onset temperatures and peak maxima for the standard and nanocomposite foams analysed in He

It can be observed from Figure 6.7 that the TGA curves for the nanocomposite foams are almost identical and the temperatures shown in Table 6.3 are similar for all three foams. This suggests that the nanoclays have very little effect on the thermal degradation of the foam under an inert atmosphere.

The TGA results for the nanocomposite foams under both air and helium atmospheres demonstrate that, contrary to the reports in the literature,[2,4] the montmorillonite and vermiculite nanoclays do not increase the thermal stability of the polyurethane and do not exhibit a significant barrier effect.

6.2.3 TVA

- **Degradation Profile**

The TVA degradation profiles for the standard and nanocomposites foams are presented in Figure 6.8. The sample temperatures for the major events which occur during the degradation of these foams are presented in Table 6.4. Two major peaks are observed in the degradation profile for the nanocomposite foams which confirm that a two stage degradation process is operating, as was the case for the standard foam. Although evolution of volatile material commences at a slightly lower temperature for the vermiculite foam than for the standard foam, the temperature of the maximum rate of

evolution for the first degradation steps are identical. The maximum rate of evolution for the second degradation step, on the other hand, is lower for the vermiculite foam which suggests that the clay may be altering the secondary degradation reactions which are occurring. It can, however, be observed from Figure 6.8 that the level of volatiles evolved by these secondary processes is lowered in the presence of vermiculite. This suggests that although the degradation reactions may occur at slightly lower temperatures the vermiculite appears to reduce the level of volatile material evolved under vacuum. A low level of non-condensable volatiles were evolved from the vermiculite foam and were identified by online MS as a mixture of CO, methane and hydrogen.

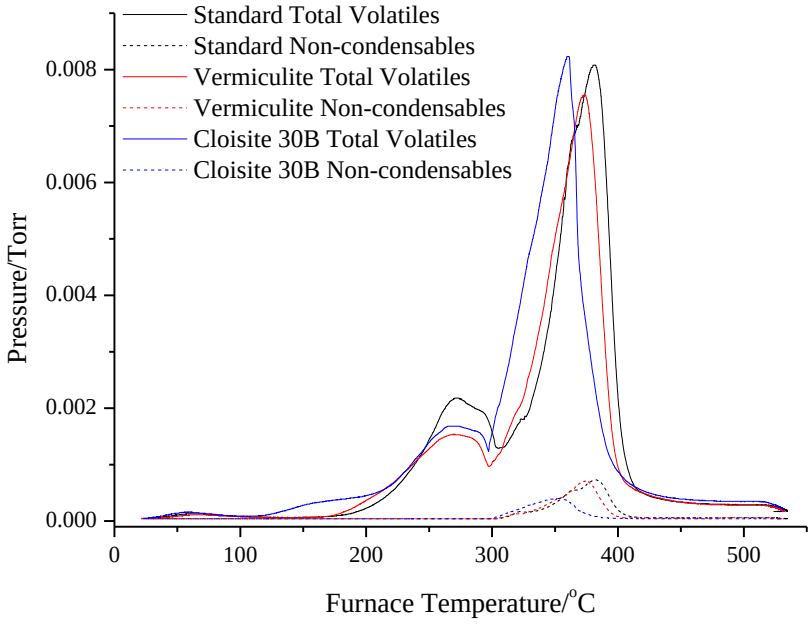

Figure 6.8: TVA degradation profiles for the standard and nanocomposite foams

Type of Foam	Onset of Volatiles Evolution/°C	Peak 1 Maximum rate of volatiles evolution/°C	Peak 2 Maximum rate of volatiles evolution/°C	End of volatiles evolution/°C
Standard	~145	241	351	~400
Vermiculite	~140	241	344	~400
Cloisite® 30B	~90	237	327	~395

Table 6.4: Sample temperatures for the key events occurring during degradation of the standard and nanocomposite foams

The foam containing Cloisite® 30B, on the other hand, shows more significant differences compared to the standard foam. Two major degradation processes are still observed, however, low levels of volatiles are evolved prior to the primary degradation step. This is most likely due to evolution of any moisture which may be present in the foam due to the presence of the clay. It can be observed from Table 6.4 that the temperature of the maximum rate of volatiles evolution for the first degradation step is slightly lower in the Cloisite® 30B foam, which suggests that the nanoclay may alter the initial degradation process. Furthermore, the maximum rate of volatiles evolution occurs at a significantly lower temperature for the second degradation step, which suggests that the secondary degradation processes which are occurring are altered in the presence of Cloisite® 30B. Finally, it can be observed that the non-condensable volatiles (methane, CO and hydrogen) are evolved from the Cloisite® 30B foam at lower temperatures than for the standard foam. These materials are produced from degradation of the polyol component of the foam; therefore, this confirms that Cloisite® 30B is altering the degradation processes which occur within the foam.

- ***Cold-ring Fraction Analysis***

During the analysis of the nanocomposite foams a yellow liquid cold-ring fraction was collected from both foams. The FTIR spectra of these fractions showed similar peaks to those from the cold-ring fraction collected from the standard foam (Figure 4.7). Similar results to those of the standard foam were also observed in the GC-MS total-ion chromatograms, with TDI and high molar mass polyol fragments being identified. The presence of TDI in the cold-ring fractions confirms that degradation of the urethane linkages *via* a depolymerisation reaction is the predominant reaction which occurs for the nanocomposite foams. This suggests that the nanoclays have not significantly altered the mechanisms by which the urethane bonds within the polyurethane foam degrade.

- ***Condensable Fraction: Sub-ambient Differential Distillation and Characterisation***

The condensable fractions collected from the nanocomposite foams were separated by sub-ambient differential distillation and subsequently analysed by FTIR spectroscopy and GC-MS. The sub-ambient differential distillation traces for the nanocomposite and standard foams are presented in Figure 6.9, with the identifications for each of the peaks presented in Table 6.5.

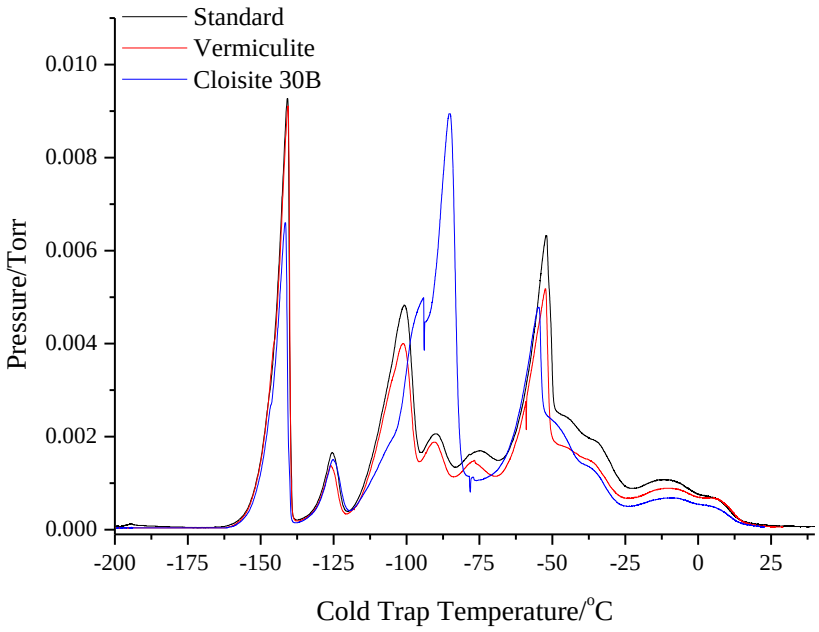

Figure 6.9: Sub-ambient differential distillation traces for the condensable fraction from the standard and nanocomposite foams

The vermiculite foam evolves the same volatile degradation products as the standard foam; however, it can be observed from Figure 6.9 that the levels of volatiles in peak 3 onwards are slightly lower in the vermiculite foam than in the standard foam. It can, therefore, be concluded that vermiculite does not affect the degradation reactions which occur within the foam but does slightly reduce the level of volatiles which are evolved. This may be achieved by the clay acting as a barrier to the diffusion of volatile degradation products from the foam or by the promotion of char formation.

Peak	Standard Foam	Vermiculite Foam	Cloisite 30B Foam
1	Propene and CO_2	Propene and CO_2	Propene and CO_2
2	Formaldehyde	Formaldehyde	Formaldehyde
3	Acetaldehyde	Acetaldehyde	Acetaldehyde
4	C_3H_6O compounds	C_3H_6O compounds	Propanal
5	High molar mass polyol fragments	High molar mass polyol fragments	No peak 5 present for this foam
6	Water and high molar mass polyol fragments	Water and high molar mass polyol fragments	Water and high molar mass polyol fragments including 2,5-dimethyl-1,4-dioxane

Table 6.5: Sub-ambient differential distillations fractions collected from the nanocomposite foams

The Cloisite® 30B foam, on the other hand, shows differences in both the nature and level of the degradation products evolved. It is clear from Figure 6.9 that whilst the standard foam evolved a mixture of C_3H_6O compounds, the Cloisite® 30B foam evolves copious quantities of propanal and some of the higher molar mass polyol fragments are absent from the Cloisite® 30B foam. In addition, 2,5-dimethyl-1,4-dioxane was identified from the GC-MS analysis of the final fraction. This species was also identified from the APP foam (chapter 5) and was proposed to arise from acid-catalysed degradation of the polyol. These results, therefore, confirm that the Cloisite® 30B nanoclay is altering the mechanisms by which the polyol segment of the foam degrades, and suggests that an acid-catalysed mechanism may be operating.

6.2.4 Fire Tests

Presented in Figure 6.10 and Figure 6.11 are pictures taken at different stages throughout the mini-crib fire tests of the nanocomposite foams. Both foams show similar behaviour to the standard foam (Figure 5.11) during the fire test, burning readily and not self-

extinguishing the flame. This suggests that neither clay significantly reduces the flammability of the material.

Beginning of Test ***After 30 seconds*** ***End of test***

Figure 6.10: Images from the mini-crib fire test of the vermiculite foam

Beginning of Test ***After 30 seconds*** ***End of test***

Figure 6.11: Images from the mini-crib fire test of the Cloisite® 30B foam

Shown in Table 6.6 are the calculated mass losses for the nanocomposite foams and the standard foam during the fire tests.

Type of Foam	**% Mass Loss**
Standard	86.4
Vermiculite	83.7
Cloisite® 30B	95.8

Table 6.6: Masses of foam lost during the mini-crib fire tests

Similar mass losses are observed for the vermiculite and standard foams which suggest that the vermiculite has not effectively reduced the flammability of the foam or promoted the formation of a protective layer of char. The Cloisite® 30B foam, on the other hand, shows much greater mass loss compared to the standard foam. This clay clearly has a detrimental effect on the fire behaviour of the foam, causing more material to be consumed during the fire test. The SEM images revealed that the Cloisite® 30B foam has a more open cell structure which will allow air and volatiles to flow in and out of the foam more easily. This would be expected to cause the foam to burn more readily and may be the reason why the Cloisite® 30B foam exhibits an increased mass loss compared to the standard foam.

6.2.5 Summary and Proposed Mechanisms of Degradation

The results from the TVA, TGA and DSC analysis revealed that the nanocomposite foams undergo a two stage degradation process, as was the case for the standard foam. The first degradation step is again attributed primarily to degradation of the urethane linkages, whilst the second stage is due to the secondary degradation reactions of the polyurethane. The DSC and TGA results did not reveal significant differences in the thermal degradation behaviour of the nanocomposite foams compared to the standard foam. The TVA results for the vermiculite foam revealed that although the degradation chemistry of the foam did not appear to be altered in the presence of the clay, the levels of volatiles which were evolved were reduced. It is proposed that the clay may exhibit a slight barrier effect which inhibits the diffusion of the volatiles from the foam. The mechanisms of degradation for the vermiculite foam are, however, proposed to be the same as that of the standard foam, described previously in section 4.1.4.

The TVA results for the Cloisite® 30B foam, on the other hand, revealed significant differences in the degradation chemistry. The maximum rate of volatiles evolution for the initial degradation step was observed at a lower temperature compared to the standard foam, which suggests that Cloisite® 30B may alter the degradation mechanism of the urethane linkages. It was also observed that the maximum rate of volatiles

evolution for the second degradation step occurs at a significantly lower temperature than for the standard foam; this suggests that the Cloisite® 30B alters the secondary degradation processes which are occurring. The sub-ambient differential distillation of the condensed volatiles confirmed this as a significantly greater level of propanal was evolved and a fraction of the higher molar mass species observed for the standard foam were absent. In addition, 2,5-dimethyl-1,4-dioxane, a species previously proposed to arise from acid-catalysed degradation of the polyol, was identified from this foam. These results, therefore, confirm that Cloisite® 30B alters the mechanism by which the polyol component of the foam thermally degrades. At this stage of the study, however, the reasons for this change in chemistry were not clear. The presence of 2,5-dimethyl-1,4-dioxane, which was observed during the degradation of the APP foam, suggests that an acid-catalysed mechanism may be operating for the Cloisite® 30B foam, in which case acidic species must be present at some stage during the degradation of this foam. It was, however, not known if these acids are associated with the natural montmorillonite clay itself or with the organic modifiers present in the Cloisite® 30B clay. A study was, therefore, conducted to examine the effect of unmodified montmorillonite (Cloisite® Na^+) and the organically modified montmorillonite (Cloisite® 30B) on the neat polyol in order to better understand the changes in degradation chemistry which occur when Cloisite® 30B is present.

6.3 Polyol-Cloisite® Clay Study

6.3.1 Samples

Two samples of Alcupol F-5611 (the polyol from which the foam is synthesised) were prepared, one containing 3% Cloisite® Na^+ and the other 3% Cloisite® 30B. These samples were analysed by TVA and compared to a sample of neat polyol containing no clay.

6.3.2 TVA

- ***Degradation Profile***

Presented in Figure 6.12 are the TVA degradation profiles for the polyol and Cloisite® samples, showing the rate of total volatiles evolution as a function of furnace temperature.

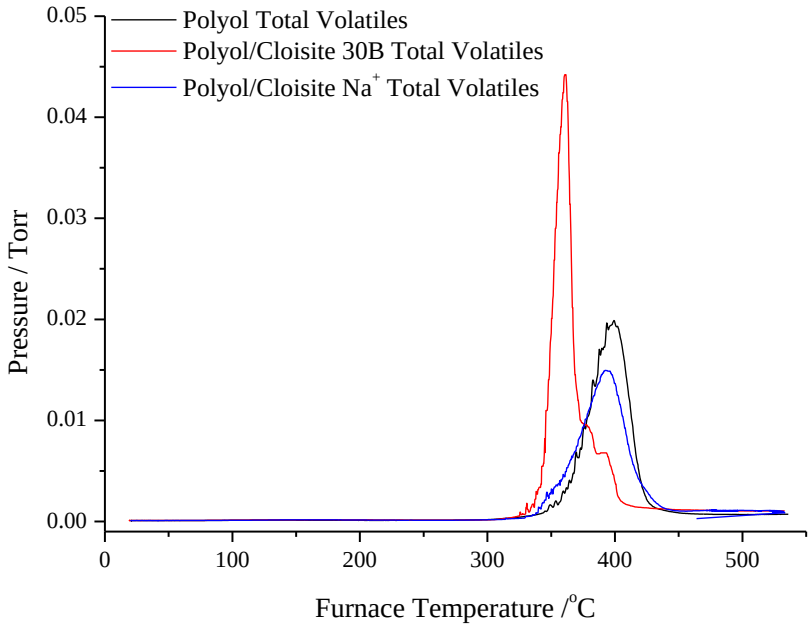

Figure 6.12: TVA degradation profile showing the level of total volatiles evolved for the polyol and Cloisite® samples

It can be observed that the degradation profile of the polyol sample containing Cloisite® 30B is significantly different compared to that of the polyol on its own. A larger, sharper peak is observed for the Cloisite® 30B sample and the maximum rate of volatiles evolution occurs around 40°C lower than for the neat polyol. The sample containing Cloisite Na^+, on the other hand, has a similar profile to that of the polyol. These results, therefore, suggest that degradation of the polyol is significantly altered in the presence of the organically modified Cloisite® 30B nanoclay but not the unmodified clay. The organic modifier present in this clay must, therefore, be inducing a change in degradation mechanism.

Presented in Figure 6.13 are the TVA degradation profiles showing rate of non-condensable volatiles evolution as a function of furnace temperature.

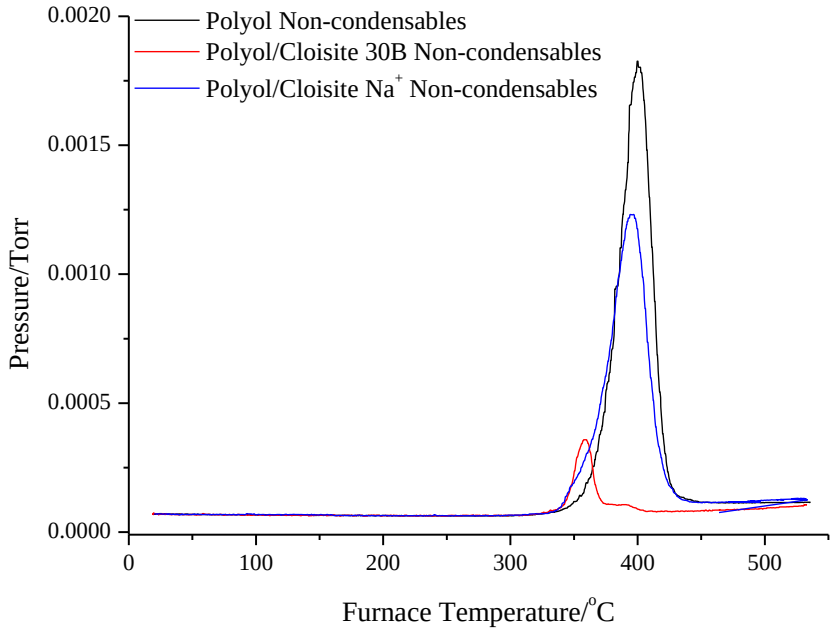

Figure 6.13: TVA degradation profile showing the level of non-condensable volatiles evolved for the polyol and Cloisite® samples

It can be observed from Figure 6.13 that the degradation profile for the non-condensable volatiles is also different for the Cloisite® 30B sample, with significantly lower levels being evolved. These materials result from random radical chain scission of the polyol as it undergoes thermal degradation. A reduction in the level of these compounds, therefore, indicates that a different polyol degradation mechanism is operating when Cloisite® 30B is present.

- ***Condensable Fraction: Sub-ambient Differential Distillation and Characterisation***

The condensable fractions collected from the polyol and Cloisite® samples were separated by sub-ambient differential distillation and the traces are presented in Figure 6.14. The identifications for each of the peaks in the sub-ambient differential distillation trace are presented in Table 6.7.

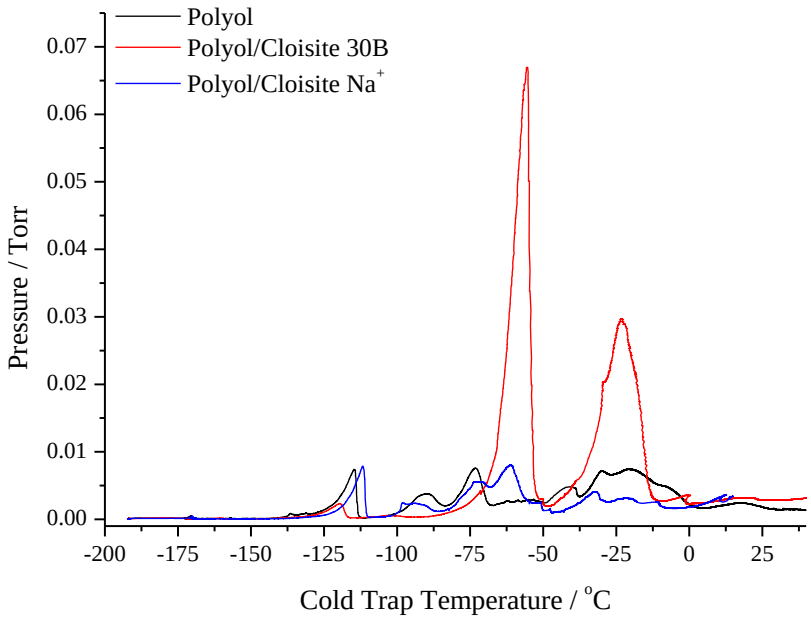

Figure 6.14: Sub-ambient differential distillation traces for the condensable fractions collected from the polyol/Cloisite® samples

Peak	**Polyol**	**Polyol/Cloisite® 30B**	**Polyol/Cloisite® Na^+**
1	Propene and CO_2	Propene and CO_2	Propene and CO_2
2	Formaldehyde	Not present	Formaldehyde
3	Acetaldehyde	Not present	Acetaldehyde
4	C_3H_6O isomers	Propanal	C_3H_6O isomers
5	High molar mass polyol fragments	Not present	Not present
6	Water and higher molar mass polyol fragments	Water and higher molar mass polyol fragments including 2,5-dimethyl-1,4-dioxane	Water and higher molar mass polyol fragments

Table 6.7: Identifications for the peaks in the sub-ambient differential distillation traces of the polyol/Cloisite® samples

It can be observed that the distribution and nature of the volatiles evolved from the Cloisite® 30B sample is significantly different to those from the Cloisite® Na^+ sample

and the polyol on its own. Formaldehyde and acetaldehyde are both absent whilst copious quantities of propanal are evolved. The FTIR spectrum and mass spectrum which confirm the presence of propanal are presented in Figure 6.15 and Figure 6.16. A large increase in the level of higher molar mass polyol fragments, which include 2,5-dimethyl-1,4-dioxane, is also observed for the polyol/Cloisite® 30B sample.

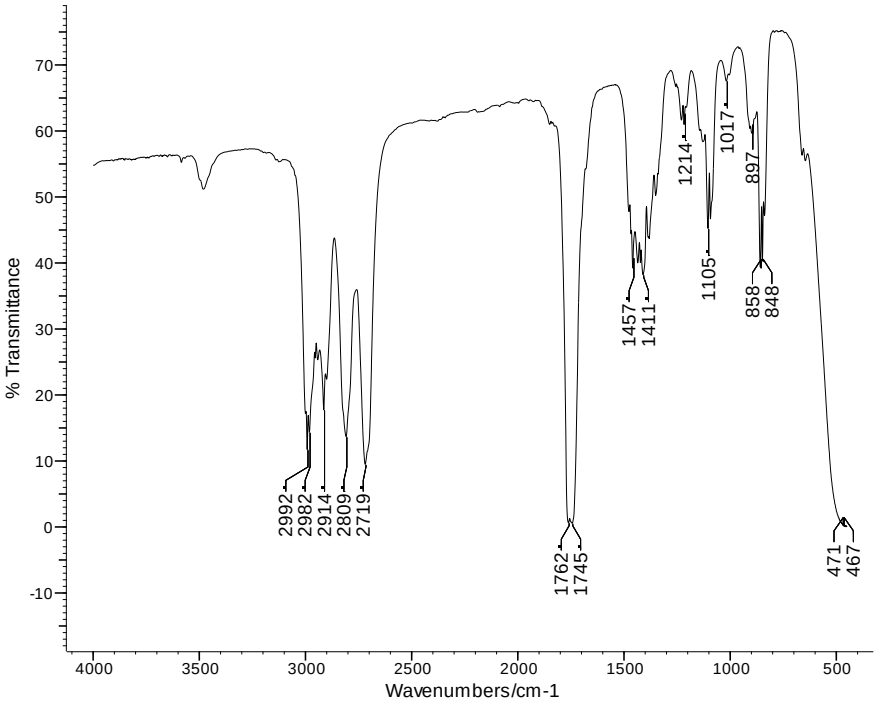

Figure 6.15: FTIR spectrum of propanal collected from the polyol/Cloisite® 30B sample

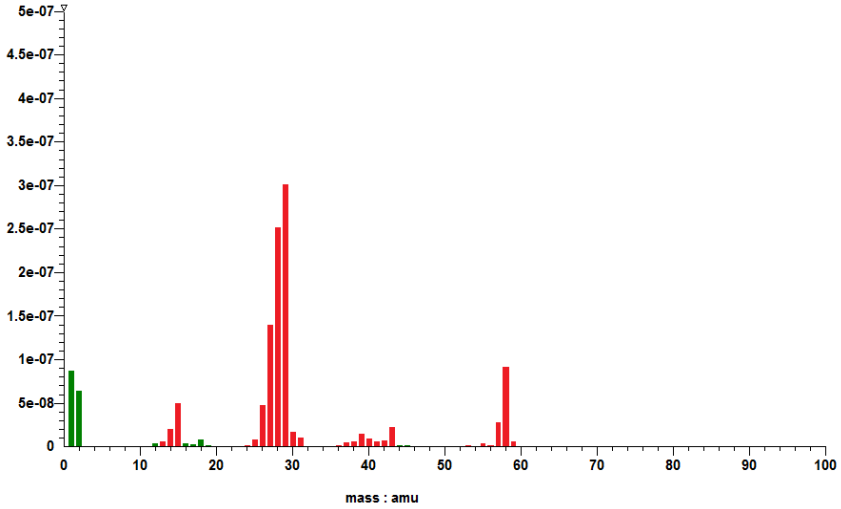

Figure 6.16: Mass spectrum of propanal collected from the polyol/Cloisite® 30B sample

These results, therefore, confirm that degradation of the polyol occurs by a different mechanism in the presence of the organically modified Cloisite® 30B clay but not in the presence of the unmodified Cloisite® Na^+ clay.

6.3.3 Proposed Mechanism of Degradation

It has previously been reported by many authors that organically modified montmorillonite nanoclays can have a detrimental effect on the degradation of different polymers.[5,6] It has been proposed in these cases that degradation of the polymer is catalysed by acidic groups which are present on the organically modified clay surface. In Cloisite® 30B, thermal degradation of the organic modifier occurs *via* a reaction known as the Hofmann elimination, which results in the formation of a tertiary amine, an alkene terminated tallow and Brønsted acid sites on the clay surface,[2,5] as illustrated in Figure 6.19.

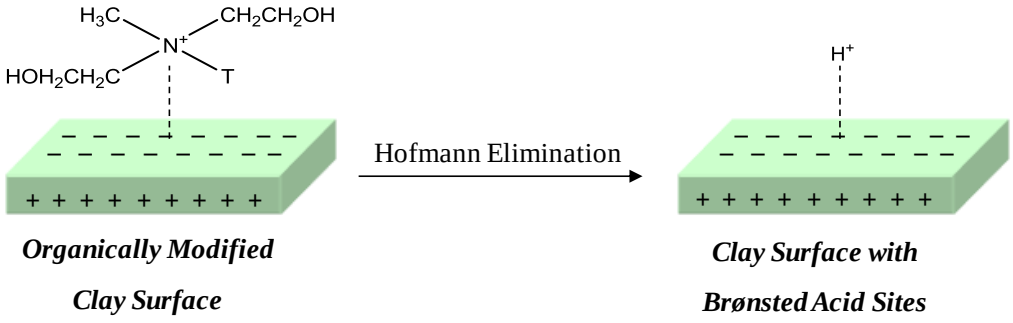

Figure 6.17: Degradation of the organic modifier to yield surface acid sites

It was, therefore, proposed that the acidic sites generated when thermal degradation of the modifier occurs are the cause of the significant changes in degradation chemistry which were observed in the TVA studies of the polyol/Cloisite® 30B sample and Cloisite® 30B polyurethane foam. An acid-catalysed degradation mechanism similar to that proposed for the APP foam could occur, as shown in Figure 6.18. This mechanism would explain the absence of acetaldehyde and formaldehyde, the formation of 2,5-dimethyl-1,4-dioxane and the large increase in propanal which is observed.

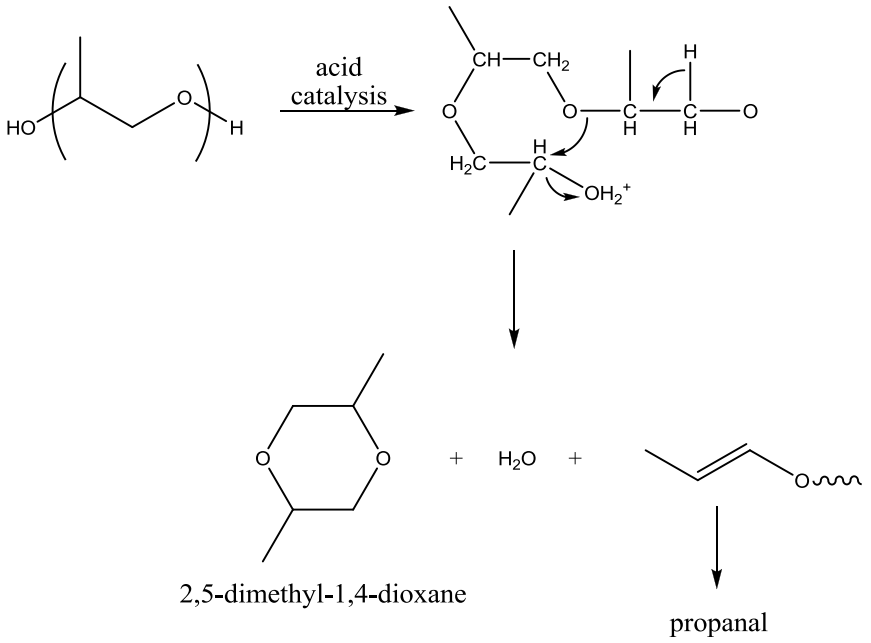

Figure 6.18: Acid-catalysed degradation of the polyol

It is also possible that acid-catalysed ether hydrolysis of the polyol occurs, and the proposed mechanism for this is presented in Figure 6.19. Protonation of the oxygen of the ether occurs followed by a methyl shift (Wagner-Meerwein rearrangement) which yields large quantities of propanal as the major volatile degradation product.

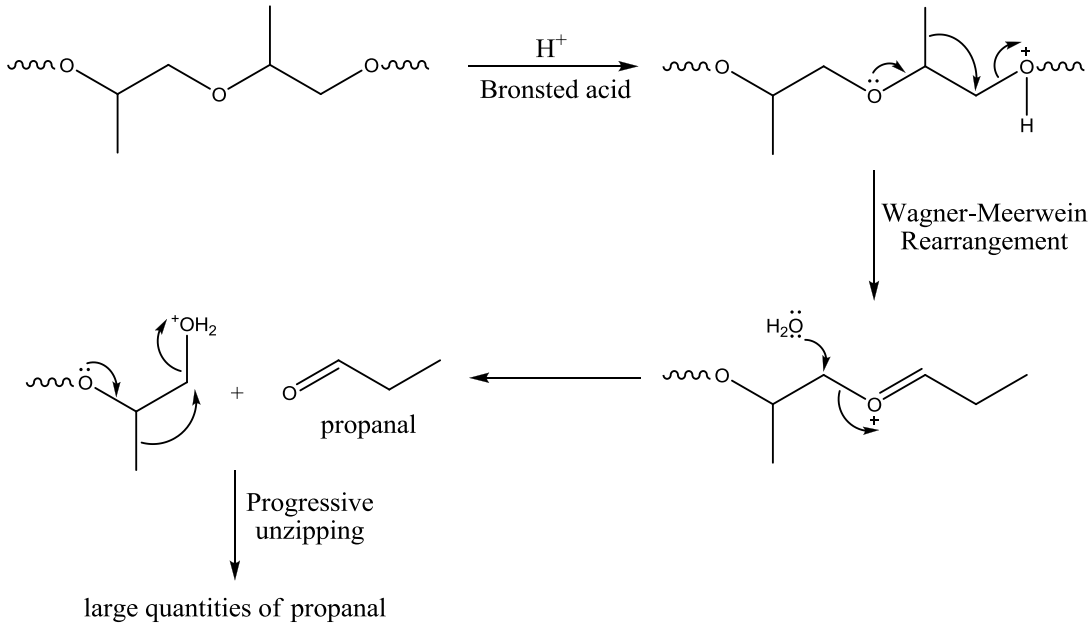

Figure 6.19: Proposed mechanism for acid-catalysed ether hydrolysis of the polyol

This mechanism would also explain the presence of copious quantities of propanal at the expense of the other polyol degradation products. With this mechanism, however, acetone would be expected to form as an alternative degradation product if the Wagner-Meerwein rearrangement occured by shift a hydrogen rather than a methyl group. The mechanism shown in Figure 6.18 is, therefore, more likely to be the major mechanism which occurs.

6.3.4 Repeat TVA Study

Throughout the course of this research project, the polyol/Cloisite® clay studies were repeated in order to ensure that the significant differences observed in the degradation chemistry were genuine and reproducible. Similar results were obtained for repeat analyses which were conducted using the same batches of clay. The following results were, however, obtained when a different batch of the unmodified Cloisite® Na^+ clay was used. For this repeat study a clay loading of 4% was used.

- ***Degradation Profile***

Presented in Figure 6.20 are the TVA degradation profiles for the new batches of polyol and Cloisite® samples, showing the rate of total volatiles evolution as a function of furnace temperature. It can be observed that the degradation profile of the polyol sample containing Cloisite® 30B is still significantly different compared to that of the polyol on its own and the Cloisite® Na^+ sample. As was the case with the original results for these samples, a larger, sharper peak is observed for the Cloisite® 30B sample and the maximum rate of volatiles evolution occurs at a lower temperature. For the sample which contains the new batch of Cloisite® Na^+ clay, a greater level of volatiles evolution compared to the neat polyol is observed. This is in contrast to the original results obtained and suggests that there is a difference in the degradation behaviour of the sample prepared using the new batch of Cloisite® Na^+.

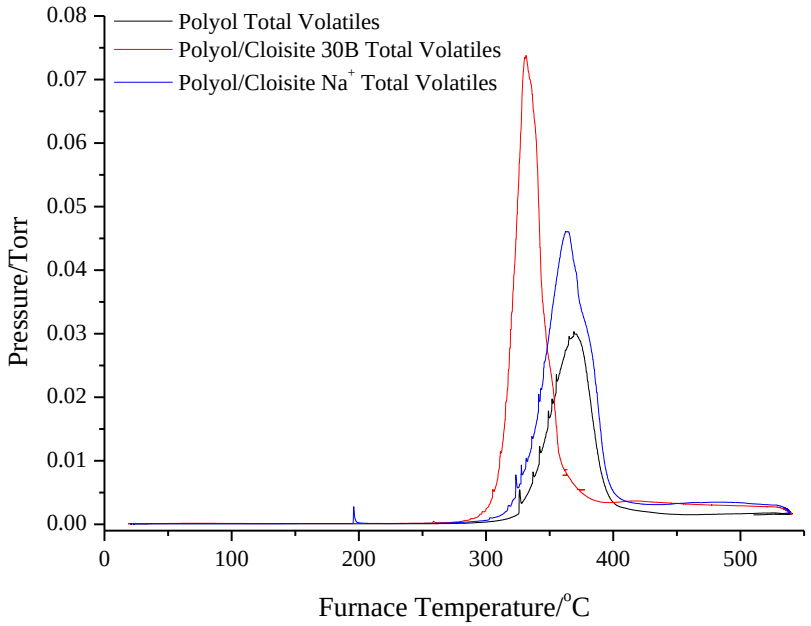

Figure 6.20: TVA degradation profile showing the level of total volatiles evolved for the new batches of polyol and Cloisite® samples

Presented in Figure 6.21 are the TVA degradation profiles for the new batch of samples showing the rate of non-condensable volatiles evolution as a function of furnace temperature. Again it can be observed that the degradation profile is different for the Cloisite® 30B sample, with significantly lower levels of non-condensable volatiles evolved. This once again indicates that a different polyol degradation mechanism is operating when Cloisite® 30B is present. For the sample containing the new batch of Cloisite® Na^+ clay, a reduction in the level of non-condensable volatiles evolution is observed compared to the original results. This once again indicates that there are differences in the degradation behaviour of the samples prepared using the different batches of Cloisite® Na^+ clay.

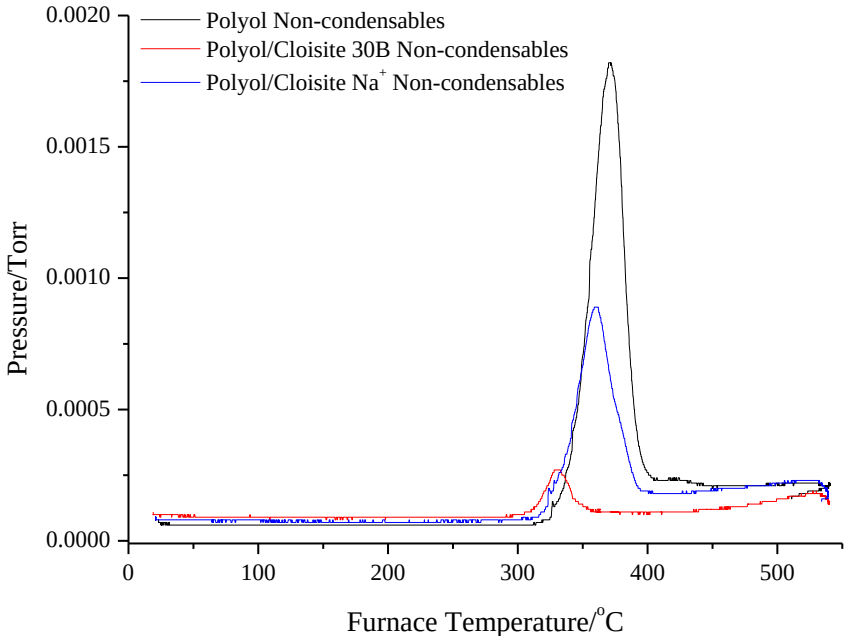

Figure 6.21: TVA degradation profile showing the level of non-condensable volatiles evolved for the new batches of polyol and Cloisite® samples

- ***Condensable Fraction: Sub-ambient Differential Distillation and Characterisation***

The condensable fractions collected from the new polyol and Cloisite® samples were separated by sub-ambient differential distillation and the traces are presented in Figure 6.22. The identifications for each of the peaks in the sub-ambient differential distillation traces are the same as presented previously. It can be observed from Figure 6.22 that the distribution and nature of the volatiles evolved from both the Cloisite® 30B and Cloisite® Na^+ samples are significantly different to those from the polyol on its own. Formaldehyde and acetaldehyde are absent from the polyol/Cloisite® 30B sample and reduced in the polyol/ Cloisite® Na^+ sample. Furthermore, copious quantities of propanal are evolved from both Cloisite® samples. These results indicate that degradation of the polyol occurs by a different mechanism in the presence of both the organically modified Cloisite® 30B clay and the unmodified Cloisite® Na^+. This is in contrast to the results obtained for the previous samples, which revealed that this difference was only observed for the organically modified Cloisite® clay.

As was explained previously, the difference in degradation behaviour which is observed in the presence of Cloisite® 30B is proposed to result from the presence of acidic sites which arise from thermal degradation of the modifier. These acidic species cause acid-catalysed degradation of the polyol to occur, which results in propanal being produced as the major volatile product. These results, however, suggest that the second batch of the unmodified clay also causes acid-catalysed degradation of the polyol. Unmodified montmorillonite can be naturally acidic, however, these result indicate that there can be significant batch to batch variability in the level of acidity. This highlights an important point which must be considered when employing clays for use in polymers, as the presence of acids within the clay can clearly affect the degradation mechanisms which occur and this may have a detrimental effect on the polymer.

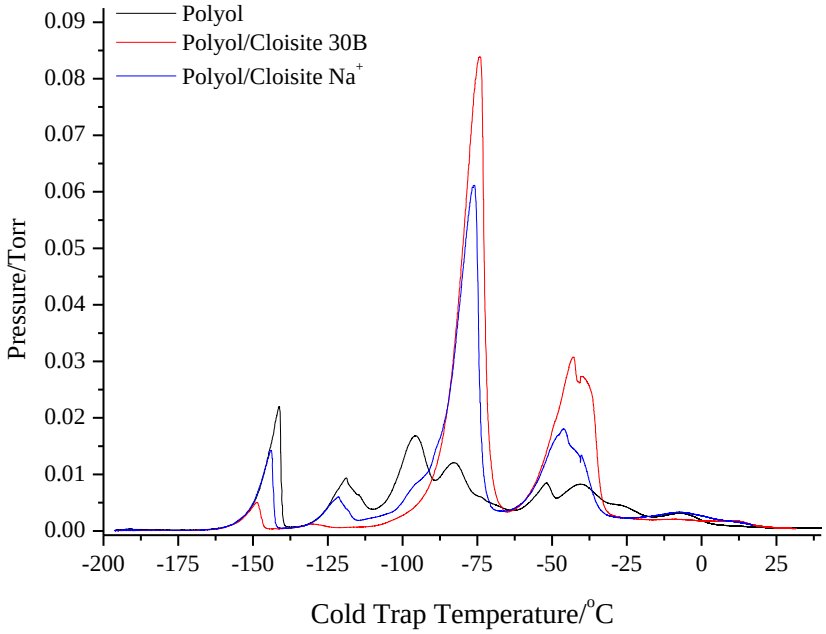

Figure 6.22: Sub-ambient differential distillation traces for the condensable fractions collected from the new batch of polyol/Cloisite® samples

6.4 Conclusions

The results presented in this chapter have demonstrated that the degradation of nanocomposite TDI-based polyurethane foams can be complex, with very different results obtained for the different clays which were employed.

The results from the TVA, TGA and DSC analysis of the vermiculite foam revealed the presence of a two stage degradation process similar to that of the standard foam. The DSC and TGA results did not reveal any significant difference in the thermal degradation behaviour of the vermiculite foam compared to the standard foam. The TVA results revealed that although the degradation chemistry of the foam did not appear to be altered in the presence of vermiculite, the levels of volatiles which were evolved were reduced. It is, therefore, possible that the clay exhibits a slight barrier effect which inhibits the diffusion of the volatiles from the foam. The mini-crib fire test results, however, revealed that there was little difference in the mass losses observed for the vermiculite and standard foams which indicates that vermiculite does not exhibit a significant fire retardant effect. This is not altogether unsurprising as it has been recognised that nanoclays work best when used in conjunction with other fire retardants.[1] With these results in mind, therefore, it is proposed that the mechanisms of degradation for the vermiculite foam are the same as those of the standard foam, described previously in section 4.1.4.

The DSC and TGA results did not reveal any significant differences in the thermal degradation behaviour of the Cloisite® 30B foam compared to the standard foam. The TVA results, however, revealed that the degradation chemistry of the polyurethane was significantly altered in the presence of Cloisite® 30B. This once again highlights the value of the TVA technique, as it allows characterisation of the degradation products which are evolved, not just the mass loss or thermal properties of the sample. For the Cloisite® 30B foam the maximum rate of volatiles evolution for the initial degradation step was observed at a lower temperature compared to the standard foam which suggests that the nanoclay alters the degradation mechanism of the urethane linkages. The maximum rate of volatiles evolution for the second degradation step was also observed to occur at a significantly lower temperature than for the standard foam which suggested that the Cloisite® 30B alters the secondary degradation processes which are occurring.

The sub-ambient differential distillation confirmed this, revealing that copious quantities of propanal were evolved and a fraction of the higher molar mass species observed for the standard foam were absent. In addition, 2,5-dimethyl-1,4-dioxane was identified as a degradation product from this foam. This species was also identified during the degradation of the APP foam (Chapter 5) and was proposed to arise from acid-catalysed degradation of the polyol. The TVA results, therefore, confirmed that Cloisite® 30B alters the mechanism by which the polyol component of the foam thermally degrade and suggested that an acid-catalysed mechanism is operating.

An initial study into the effect of the clay on the polyol component alone revealed that propanal was only evolved in large quantities in the presence of the organically modified clay and not the unmodified clay. Degradation of the organic modifier on the clay is proposed to occur *via* the Hofmann elimination which yields Brønsted acid sites on the clay surface. The acidic species are proposed to acid-catalyse the depolycondensation reaction of the foam and the degradation of the polyol, for which two mechanisms are proposed. The first involves protonation of the hydroxyl end groups of the polyol chains (Figure 6.23) as was previously proposed for the APP foam.

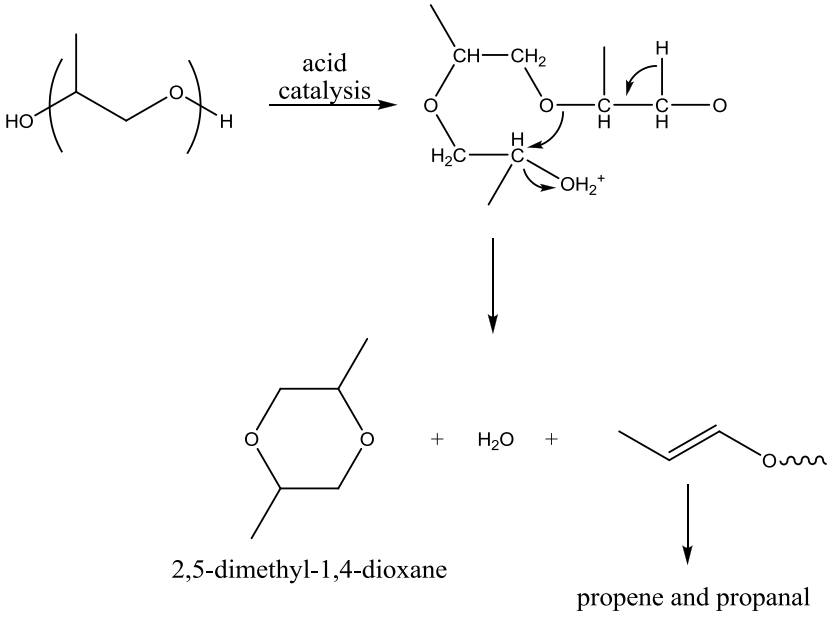

Figure 6.23: Acid-catalysed degradation of the polyol

This mechanism explains the absence of acetaldehyde and formaldehyde and the large increase in propanal which is observed. A second mechanism is also proposed which involves acid-catalysed ether hydrolysis of the polyol to yield propanal, as shown in Figure 6.24. This mechanism would also explain the presence of copious quantities of propanal at the expense of the other polyol degradation products; however, acetone could also be formed through this route if the Wagner-Meerwein rearrangement occurs by a hydrogen shift as opposed to a methyl shift. It is, therefore, more likely that the mechanism presented in Figure 6.23 is the major route to propanal formation.

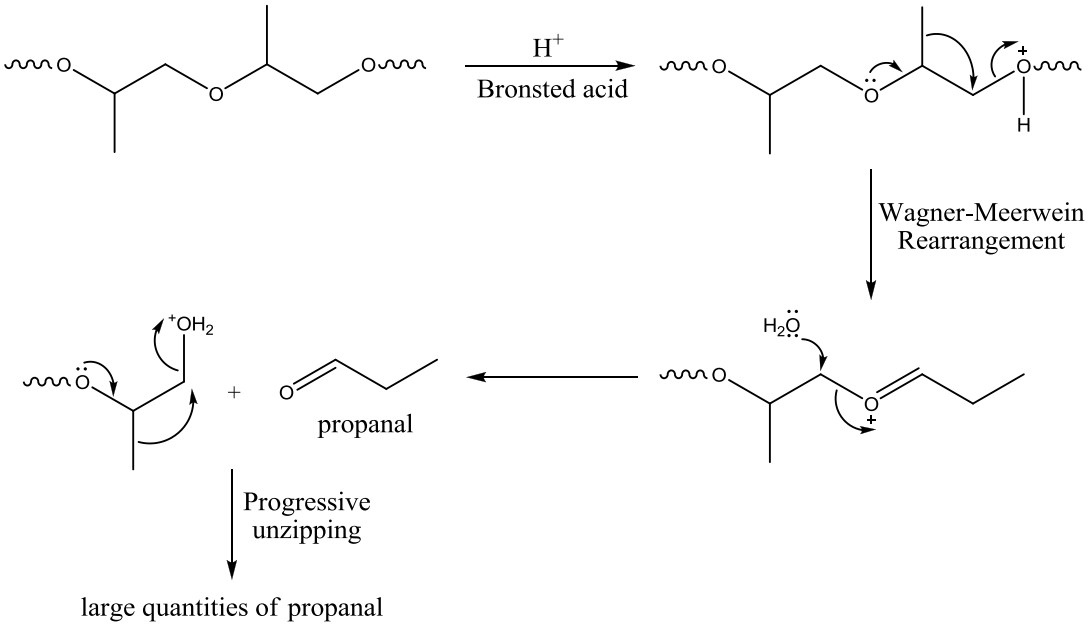

Figure 6.24: Proposed mechanism for acid-catalysed ether hydrolysis of the polyol

A second study using different batches of clay revealed that the degradation behaviour of the polyol was altered in the presence of the organically modified and unmodified montmorillonite clay, with large quantities of propanal evolved in both cases. These results were interesting as it suggests that the surface acidity of unmodified montmorillonite can vary significantly between different batches. This is an important point which needs to be considered when using such clays for the preparation of polymer nanocomposites as the presence of acidic species could affect the degradation and have a detrimental effect on the polymer.

Finally, the mini-crib fire tests revealed that the Cloisite® 30B foam burns to a greater extent than the standard foam as less residue remains at the end of the test. This result can be understood by considering the SEM and TVA results which were obtained. The SEM images revealed that the Cloisite® 30B foam has a more open cell structure which results in flow of air and volatiles in and out of the foam more easily, and the TVA results revealed that large quantities of propanal are evolved during the degradation of this foam. It is, therefore, proposed that the presence of such a large quantity of a flammable product, in combination with the more open cell structure of the foam, leads to the foam burning more readily.

What is clear from the results presented in this chapter is that, contrary to the reports within the literature,[2,4,] the nanoclays do not increase the thermal stability of the polyurethane foam and do not improve the fire performance of the material. It has, however, been reported in the literature that nanoclays often work best in conjunction with more conventional fire retardants.[1,7] This has been found to be the case at Strathclyde where the patented multi-component fire retardant system[8] which includes vermiculite has been shown to significantly reduce the flammability of TDI-based polyurethane foam.

6.5 References

[1] A. R. Horrocks and D. Price, *Fire Retardant Materials*, Woodhead Publishing Ltd, Cambridge, 2001, Ch. 6, p. 204

[2] B. Chen, J. R.G. Evans, H. C. Greenwell, P. Boulet, P. V. Coveney, A. A. Bowden and A. Whiting, *Chem. Soc. Rev.*, 2008, **37**, 568

[3] M. Alexandre and P. Dubois, *Mat. Sci. Eng. R*, 2000, **28**, 1

[4] M. C. Saha, M. E. Kabir and S. Jeelani, *Meter. Sci. Eng. A*, 2008, **479**, 213

[5] X. Xu, Y. Ding, Z. Qian, F. Wang, B. Wen, H. Zhou, S. Zhang and M. Yang, *Poly. Degrad. Stabil.*, 2009, **94**, 113

[6] M. Kracalik, J. Mikesova, R. Puffr, J. Baldrian, R. Thomann and C. Friedrich, *Polym. Bull.*, 2007, **58**, 313

[7] M. Modesti, A. Lorenzetti, S. Besco, D. Hrelja, S. Semenzato, R. Bertani and R. A. Michelin, *Polym. Degrad. Stabil.*, 2008, **93**, 2166

[8] J.J. Liggat, R. A. Pethrick, and I. Rhoney, Fire Retarded Flexible Nanocomposite Foams, International Patent Application PCT/GB2005/002600

7 Final Conclusions

The work carried out in this research project has demonstrated that the thermal and thermo-oxidative degradation of a TDI-based polyurethane foam is a complex process consisting of different competing mechanisms which yield an array of volatile products as well as complex char residues. The addition of fire retardants into the system adds to this complexity, making understanding the degradation processes which occur a more complicated task. This work has also demonstrated that the degradation mechanisms of polyurethane foam are dependent on the experimental conditions of the pyrolysis or degradation technique being employed, and highlights the need to employ complementary analysis techniques when studying the degradation of polymers.

The standard foam was observed to undergo a two step thermal degradation mechanism under an inert environment, in which the initial step corresponds to degradation of the urethane linkages and the second step consists of secondary degradation processes. Degradation of the urethane linkages is proposed to occur by two competing mechanisms. The first mechanism involves simple depolymerisation of the urethane bond to yield TDI and polyol, whilst the second mechanism involves dissociation of the urethane linkages *via* a six-membered ring transition state to yield DAT, CO_2 and alkene-terminated polyol chains. The results demonstrated that the depolymerisation reaction is the dominant mechanism under vacuum; however, under pyrolysis conditions the second mechanism involving the six-membered ring transition state becomes dominant. It is proposed that the pyrolysis conditions are more confined and, as a result, volatilisation of the TDI does not occur as readily and this recombines with the polyol to reform the urethane bond. Degradation of the urethane linkages *via* a six-membered ring transition state then becomes the predominant reaction.

The secondary degradation reactions are attributed primarily to degradation of the polyol or polyol-based tar which was regenerated in the first degradation step to yield volatile products. Isothermal TVA studies revealed that thermal degradation of the polyol occurs as low as 250°C but does not become significant until temperatures greater than 300°C. Degradation of the foam under air occurs at a lower temperature than under nitrogen as a result of thermo-oxidative degradation of the polyol occurring at lower temperatures than thermal degradation. Analysis of the char residues revealed that complex aromatic carbonaceous chars are formed under inert and oxidative conditions, with char being formed at lower temperatures under the oxidative environment.

Degradation of the standard foam under 3% oxygen in nitrogen was shown to be an even more complex process, with the degradation behaviour lying between that of thermal and thermo-oxidative degradation. It is, therefore, proposed that both thermal and thermo-oxidative degradation occurs when the foam is degraded in a low oxygen environment and this is important to understand when considering a fire situation and when developing new fire retardant systems. These results also highlight the issue that results from laboratory based degradation studies must be used with caution and may not necessarily be representative of a fire situation. In most cases degradation studies will deal simply with the degradation under air and/or nitrogen, however, these results show that studying the behaviour in a low oxygen environment is useful. It would also be useful to characterise the volatiles which are evolved under air and the low oxygen environment to see if these differ significantly from those identified under an inert atmosphere.

The results from the standard foam revealed some interesting points which should be considered in future when developing fire retardant polyurethane foams. First, the results have demonstrated that the process which yields the greatest quantity of volatile material is the degradation of the polyol component of the foam. These volatile polyol degradation products will provide the majority of the fuel which will sustain the flame in a fire situation. It can be envisaged, therefore, that a successful fire retardant for this

foam would exhibit part of its activity by modifying the degradation mechanism of the polyol so that the volatile products are reduced or replaced by less volatile species. Second, the pyrolysis results demonstrated that when the foam is pyrolysed under confined conditions the dominant mechanism becomes degradation *via* the six-membered ring transition state to yield DAT, amine and alkene-terminated polyol chains. If this mechanism could be prevented or retarded then this would help to increase the thermal stability of these materials and possibly improve their fire retardancy. One way in which this could possibly be achieved is through the use of a polyol which does not contain a β-hydrogen. This would prevent the six-membered ring mechanism from occurring and would alter the degradation behaviour of the polyurethane. How easy this would be to achieve, whilst maintaining the desirable properties of the flexible foam, remains to be seen. Finally, the fact that aromatic amines can be a major degradation product from polyurethane foams is of concern as these materials can pose a potential health hazard, being reported as potential carcinogens and mutagens. The majority of deaths in fires are not normally due to the flame or heat but are instead caused by inhalation of the toxic gases. Any material which increases the toxicity of the fumes is, therefore, undesirable. Preventing the degradation mechanism which yields aromatic amines, either by modification of the polyol or by addition of a suitable fire retardant, would clearly be beneficial.

Following the study on the standard foam, degradation of a foam containing APP was shown to consist of multiple overlapping steps which involve degradation of the polyurethane and the fire retardant. First, the APP decomposes yielding water, ammonia and an ultraphosphate containing acidic hydroxyl groups. These acidic hydroxyl groups then catalyse the degradation of the urethane linkages *via* the depolymerisation reaction which yields TDI and polyol. The second, competing mechanism involving dissociation of the urethane linkages to yield DAT, CO_2 and alkene-terminated polyol chains is also proposed to occur but to a much lesser extent. This is an important result as this fire retardant alters the degradation of the foam in such a way that the mechanism which yields aromatic amines is not as dominant. In terms of the fire behaviour of this

material, this will be beneficial as it removes the potential health implications associated with these species.

Acid-catalysed degradation of the polyol is then proposed to occur to yield volatile material which differs to that observed in the absence of APP. Phosphorylation of the regenerated polyol can also occur and this reaction is proposed to become important under an oxidative environment where the hydroxyl end groups produced as a result of thermo-oxidative degradation of the polyol react with the ultraphosphate resulting in polyol material becoming bound within the char. This demonstrates that APP is an effective fire retardant for this foam as it reacts with the polyol thereby altering its degradation mechanism and causing it to become bound into the char. As was mentioned previously, this will help to reduce the level of volatile material which is available to fuel and sustain the flame in a fire.

The pyrolysis studies revealed that APP exhibits a significant condensed-phase activity as the acidic species generated during the degradation of the APP promote char formation in the polyurethane foam. Solid-state ^{13}C NMR studies demonstrated that the APP foam is in a significantly more advanced state of charring than the standard foam at 300°C, with the residues consisting primarily of a complex aromatic carbonaceous char at this temperature. This was observed to occur at an even lower temperature under air. As was the case for the standard foam the pyrolysis under the low oxygen environment was shown to be complex, with the degradation behaviour showing characteristics of thermal and thermo-oxidative degradation. Again this is important to understand when considering the performance of fire retardant materials in a fire situation. The mini-crib fire tests demonstrated that APP is an effective fire retardant for the TDI-based polyurethane foam under study, as the foam self-extinguished during the test. Again, it would be useful to characterise the volatiles which are evolved under air and the low oxygen environment to see if these differ significantly from those under an inert environment.

Finally, two nanocomposite foams were studied and very different results were obtained. Vermiculite was shown to have little effect on the degradation mechanisms of the foam, with a two stage degradation process similar to that of the standard foam being observed. The results suggested that vermiculite reinforces structure of the foam as it degrades which limits the foam collapse and it may act as a physical barrier thereby reducing the level of volatiles evolved. The mini-crib fire tests results, however, revealed that vermiculite does not exhibit a significant fire retardant effect when used on its own. The work on the Strathclyde patented multi-component formulation, however, has found that when used in conjunction with conventional fire retardants, such as APP, vermiculite significantly reduces the flammability of TDI-based polyurethane foam. This confirms that nanoclays do work best when used in conjunction with other fire retardants.

The presence of Cloisite® 30B, on the other hand, significantly changes the degradation mechanisms of the foam. Initially, the DSC and TGA results did not reveal any significant differences in the thermal degradation behaviour of the Cloisite® 30B foam compared to the standard foam. The TVA results, however, revealed that the degradation chemistry of the polyurethane was significantly altered in the presence of Cloisite® 30B. This once again highlights the value of the TVA technique, as it allows characterisation of the degradation products which are evolved, not just the mass loss or thermal properties of the sample. This also shows the need to employ multiple analysis techniques when studying the degradation of polymers. Too often in the field of polymer degradation TGA is employed as the main technique and this research has shown that this technique does not always reveal the complete picture.

Copious quantities of propanal were evolved during the degradation of the Cloisite® 30B and it was proposed that acid-catalysed degradation of the polyol was occurring. An initial study into the effect of the clay on the polyol component alone revealed that propanal was only evolved in large quantities in the presence of the organically modified clay and not the unmodified clay. Degradation of the organic modifier on the clay is proposed to occur *via* the Hofmann elimination which yields Brønsted acid sites on the

clay surface. The acidic species are proposed to acid-catalyse the depolycondensation reaction of the foam and the degradation of the polyol, for which two mechanisms are proposed. The first involves protonation of the hydroxyl end groups of the polyol chains and the second involves acid-catalysed ether hydrolysis of the polyol which involves a Wagner-Meerwein rearrangement step. The first mechanism would explain the presence of copious quantities of propanal at the expense of the other polyol degradation products and is proposed to be the major mechanism which occurs.

A second study using different batches of clay revealed that the degradation behaviour of the polyol was altered in the presence of the organically modified and unmodified montmorillonite clay, with large quantities of propanal evolved in both cases. These results suggest that the surface acidity of unmodified montmorillonite can vary significantly between different batches. This is an important point which needs to be considered when using such clays for the preparation of polymer nanocomposites as the presence of acidic species could affect the degradation and have a detrimental effect on the polymer. It would be useful to study other organically modified montmorillonite clays and other types of clay to determine if these also have the same effect on the degradation of the polyol.

Finally, the mini-crib fire tests revealed that the Cloisite® 30B foam burns to a greater extent than the standard foam as less residue remains at the end of the test. It is proposed that the presence of large quantities of a flammable degradation product like propanal, in combination with the more open cell structure of the foam which was revealed by SEM images, leads to the foam burning more readily. This study is interesting as it reveals that the nanoclay, originally employed in the foam as a potential fire retardant, has in fact had a detrimental effect on the foam by altering the degradation mechanism of the polyol in such a way that more flammable species are evolved. This result was unexpected and highlights the need to fully study the degradation chemistry of any potential new fire retardant systems.

This research project has, therefore, shown that the degradation behaviour of polyurethane foams with and without fire retardants is complex, with the mechanisms dependant on the experimental conditions and degradation technique being employed. This demonstrates that complementary analysis techniques should be employed when studying the degradation of polymers. This research has shown that under certain conditions aromatic amines are formed which has implications in terms of the health hazards associated with these materials. It has also shown that an effective fire retardant for this particular polyurethane foam is one which alters the degradation chemistry of the polyol and promotes the formation of char. The results have also demonstrated that it is important when considering the behaviour of polyurethane foam in a fire that the degradation behaviour under a low-oxygen environment is studied as this may be more representative of a fire situation. The degradation behaviour in this environment has been shown to be complex, consisting of both thermal and thermo-oxidative mechanisms.

It has also been demonstrated throughout this research project that the structure of the chars generated from polyurethane foams can vary depending on the environment in which the foam is degraded and the nature of the fire retardants which are present. This information could have implications in the field of forensic fire investigation, in which research is being conducted to attempt to be able to differentiate between different types of char material collected from a fire. This work has demonstrated, therefore, that it could be possible to gain information regarding the nature of the fire and the presence of any fire retardants by characterising any polyurethane foam chars recovered from the fire and this concept could be extended to other polymer systems.

Whilst this research project has been a success, the work presented here is not without its limitations. The TVA technique is useful as it allows products of all natures to be studied, however, in its current set up it cannot provide quantitative information regarding the degradation products which are evolved. A future modification to the system would involve the use of alternative pressure gauges (such as those incorporating

ceramic diaphragms) which would allow for quantitative analysis. Furthermore, it was not possible in this research project to characterise the volatile degradation products which were evolved during the pyrolysis studies. The use of a pyrolysis/GC instrument would yield further information regarding the degradation products which are evolved under both inert and oxidative pyrolyses.

Finally, the technique of CPMAS solid-state ^{13}C NMR was used throughout this work in a qualitative manner to assess the structure of the charred residues which were generated during the pyrolysis studies. Solid-state NMR could, however, be employed in a quantitative manner to assess the chars. This could be achieved through use of single pulse excitation experiments which can provide information on the percentage of aliphatic and aromatic carbons in the char. This can then be combined with dipolar dephasing experiments which allow the determination of the percentage of protonated and unprotonated carbons within the sample, with a short dephasing delay generating the total carbon spectrum and a longer delay generating a spectrum containing the non-protonated aromatic carbons.

Appendix 1 – Standard Foam

1.1 Isothermal TVA Study

1.1.1 Non-condensable Volatiles

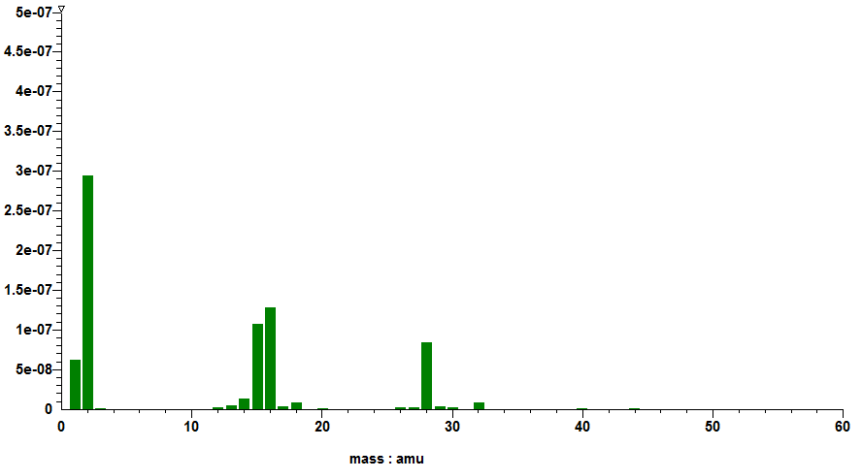

Figure 1.1: Mass spectrum of the non-condensable volatiles observed during the TVA at 350°C

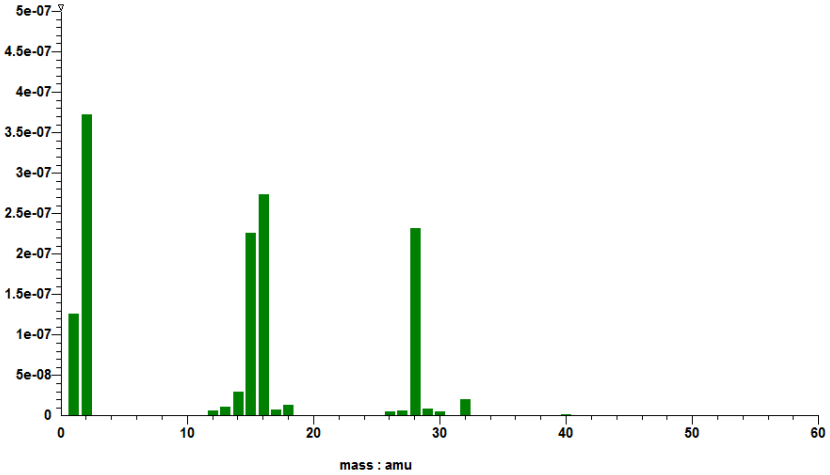

Figure 1.2: Mass spectrum of the non-condensable volatiles observed during the TVA at 400°C

1.1.2 Cold-ring Fractions

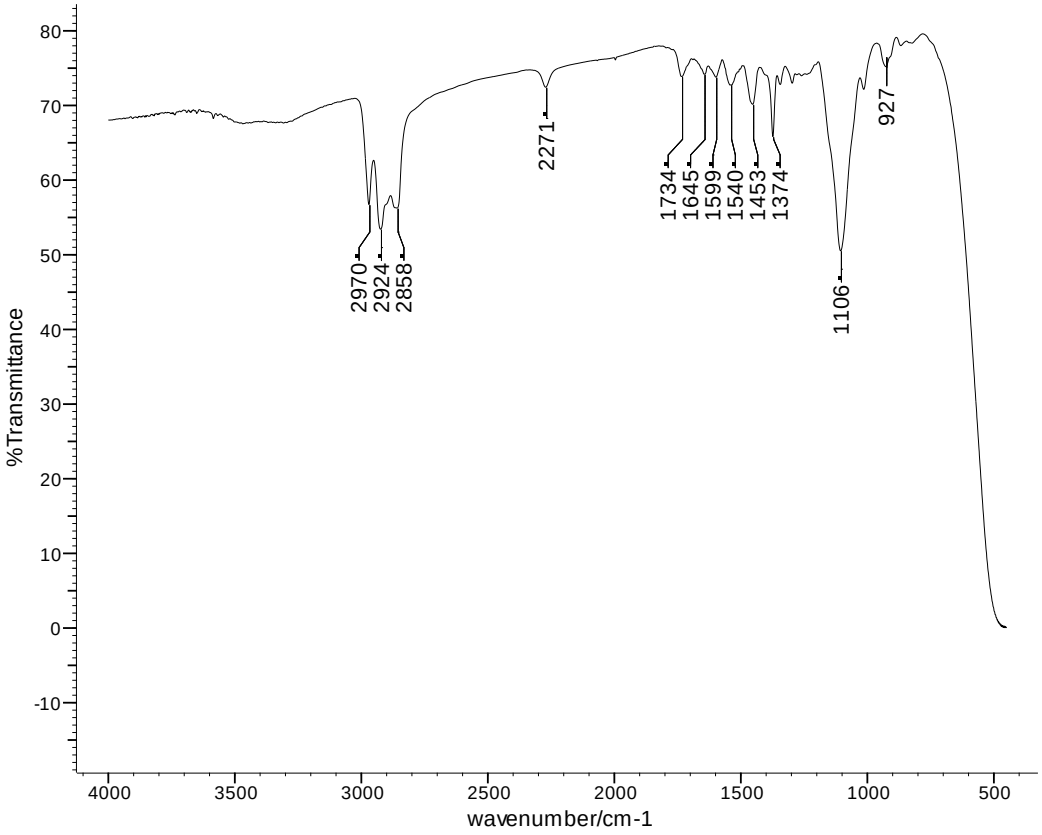

Figure 1.3: FTIR spectrum of the cold-ring fraction collected at 300°C

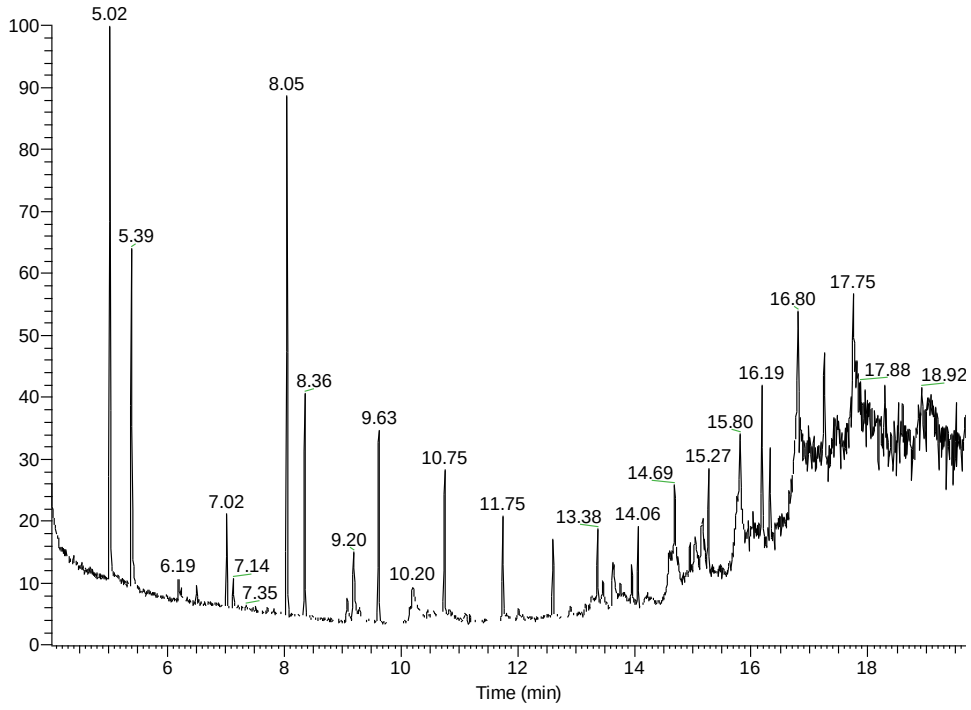

Figure 2: GC-MS chromatogram of the cold-ring fraction collected at 300°C

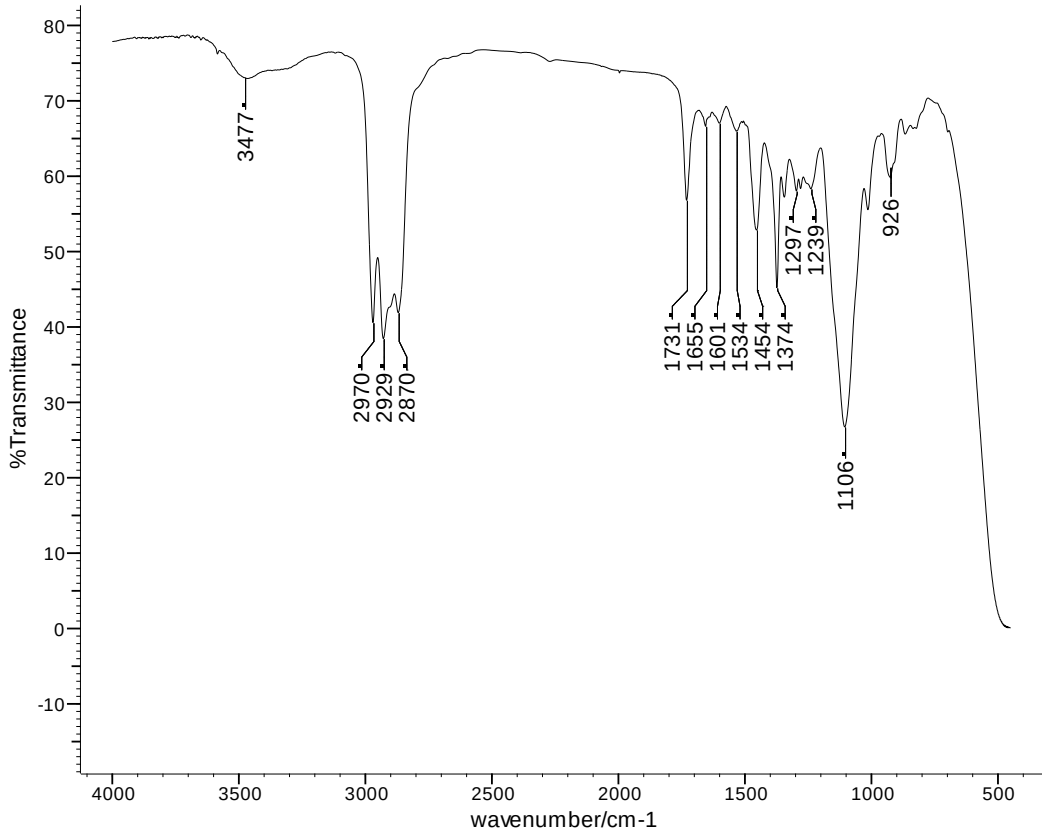

Figure 1.3: FTIR spectrum of the cold-ring fraction collected at 350°C

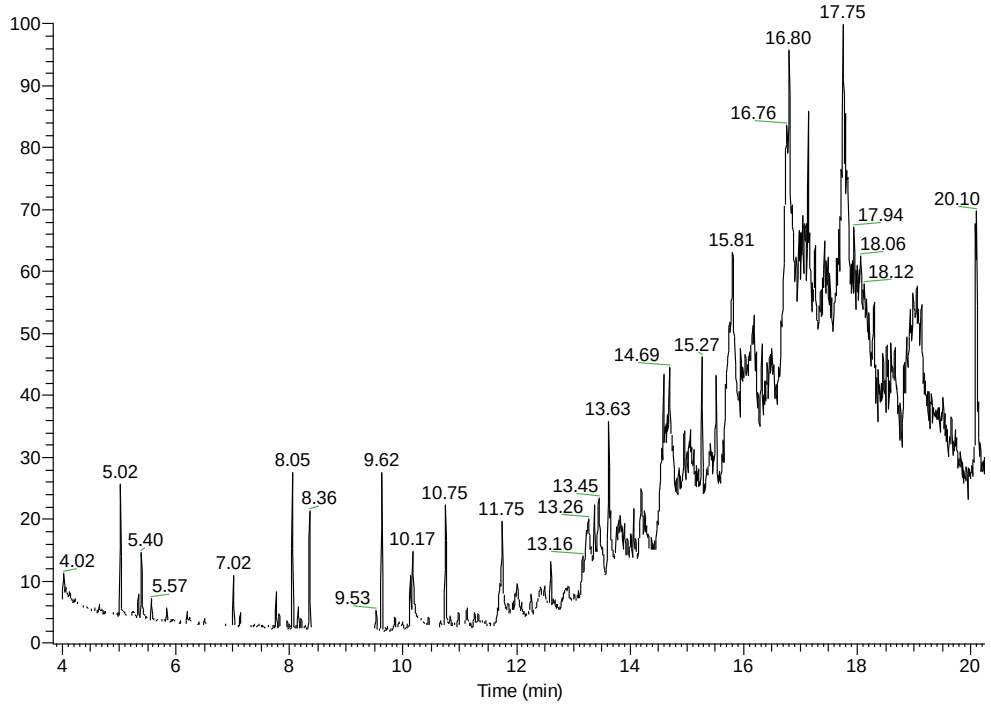

Figure 1.4: GC-MS chromatogram of the cold-ring fraction collected at 350°C

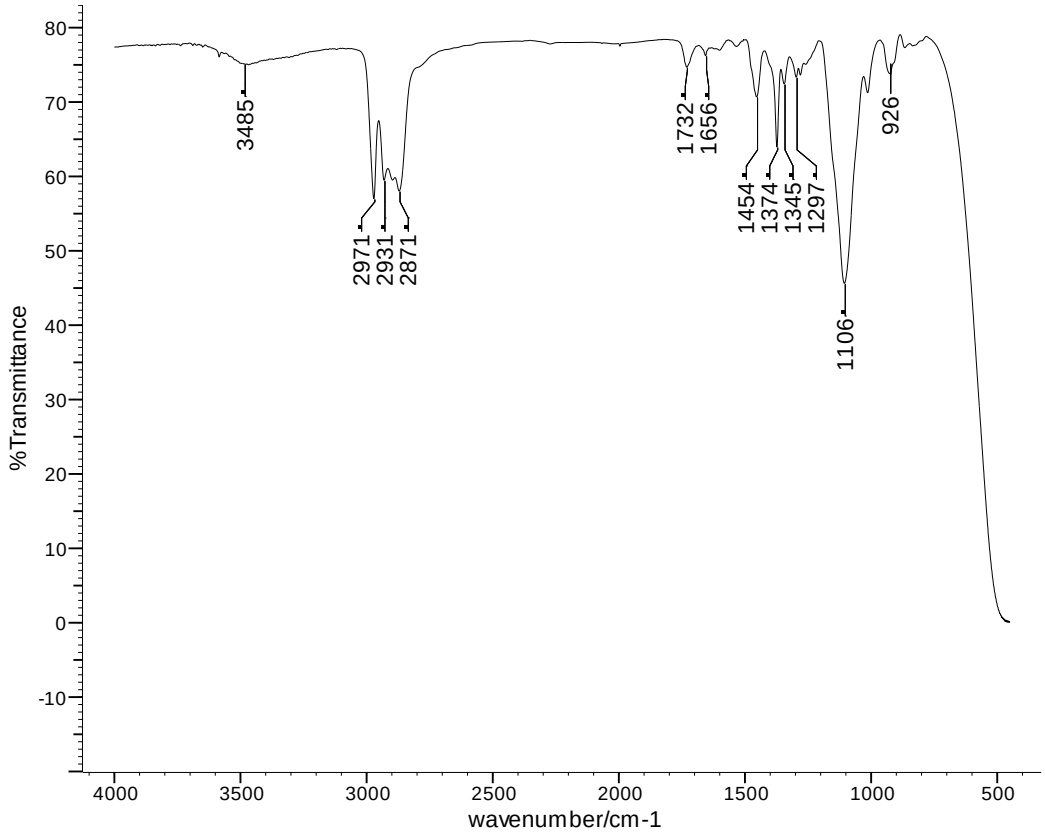

Figure1.5: FTIR spectrum of the cold-ring fraction collected at 400°C

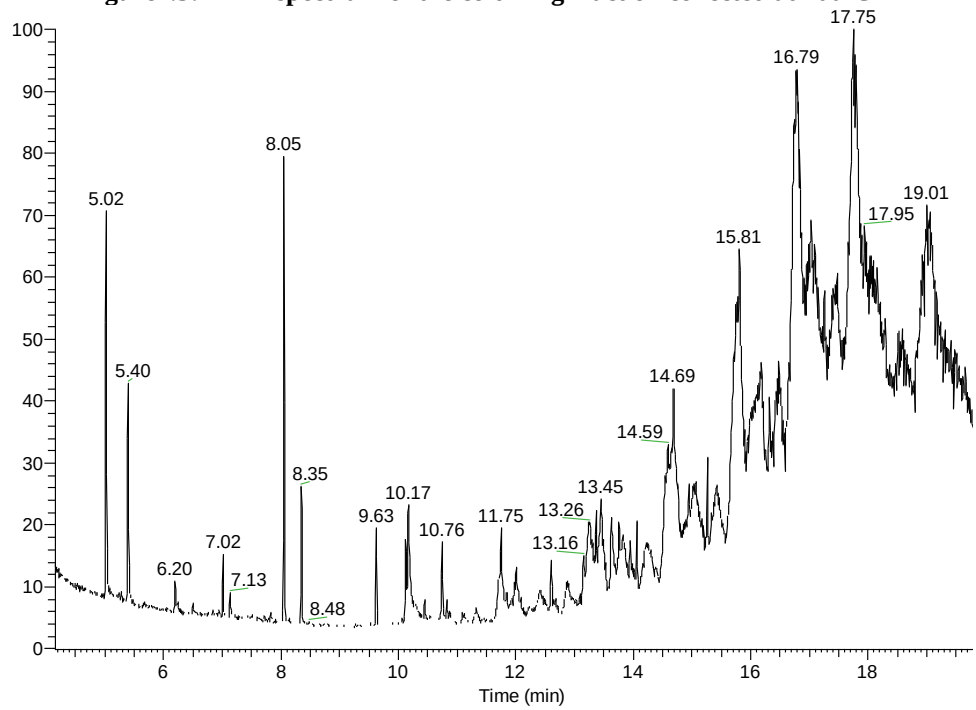

Figure 6: GC-MS chromatogram of the cold-ring fraction collected at 400°C

1.1.3 Residues

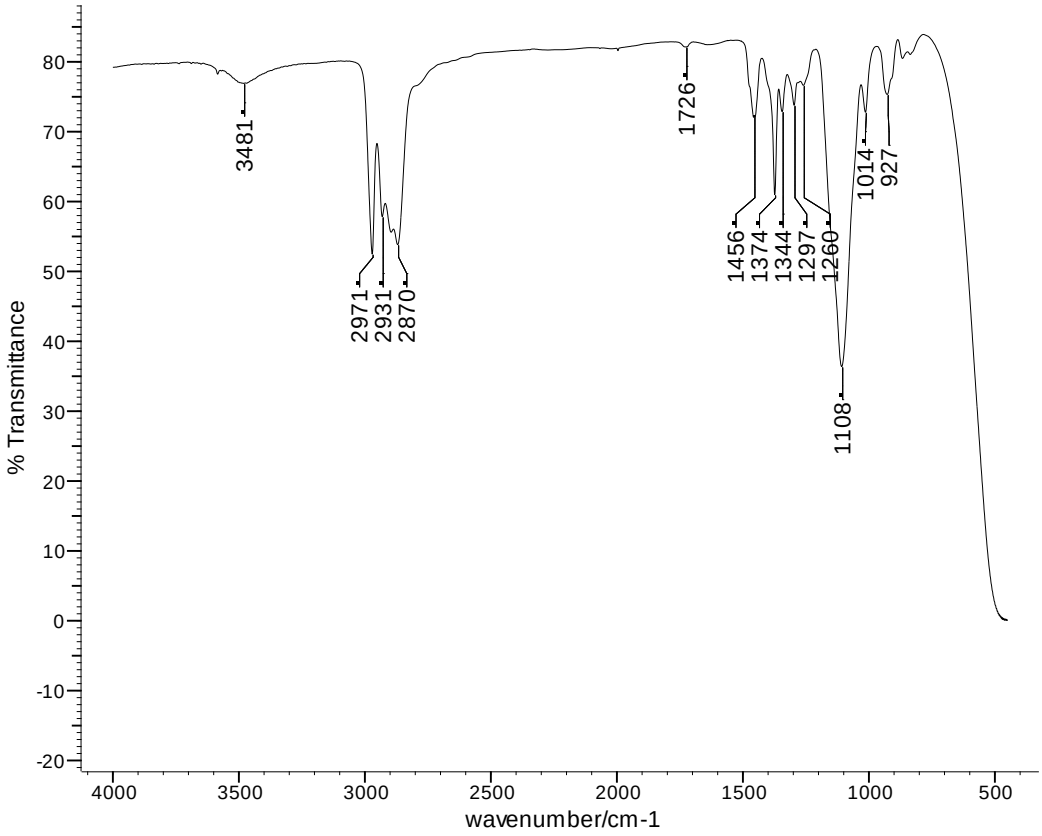

Figure 1.7: FTIR spectrum of the residue collected at 300°C

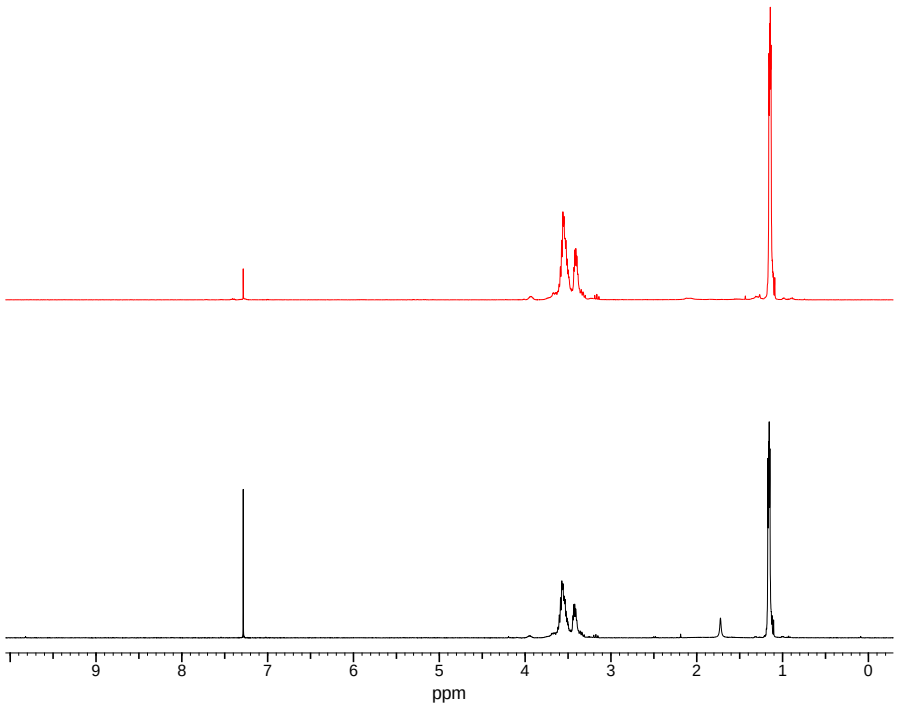

Figure 1.8: ^{1}H NMR spectrum of the residue at 300°C (black) and the polyol (red)

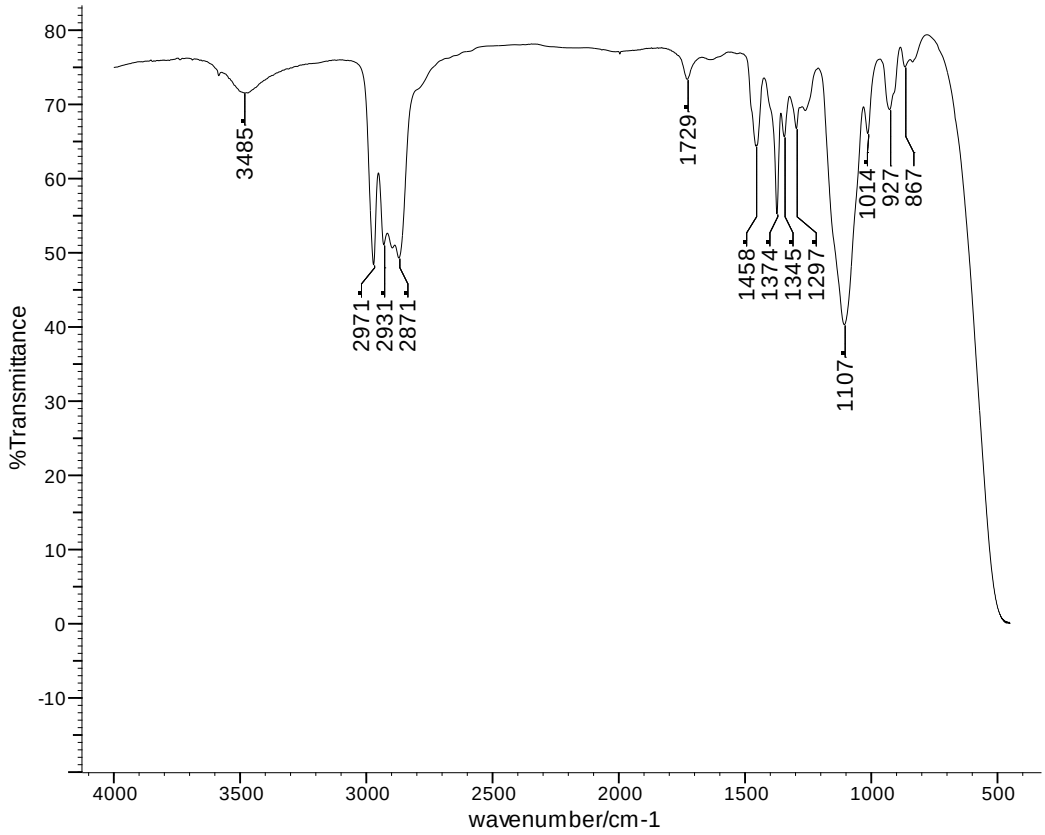

Figure 1.9: FTIR spectrum of the residue at 350°C

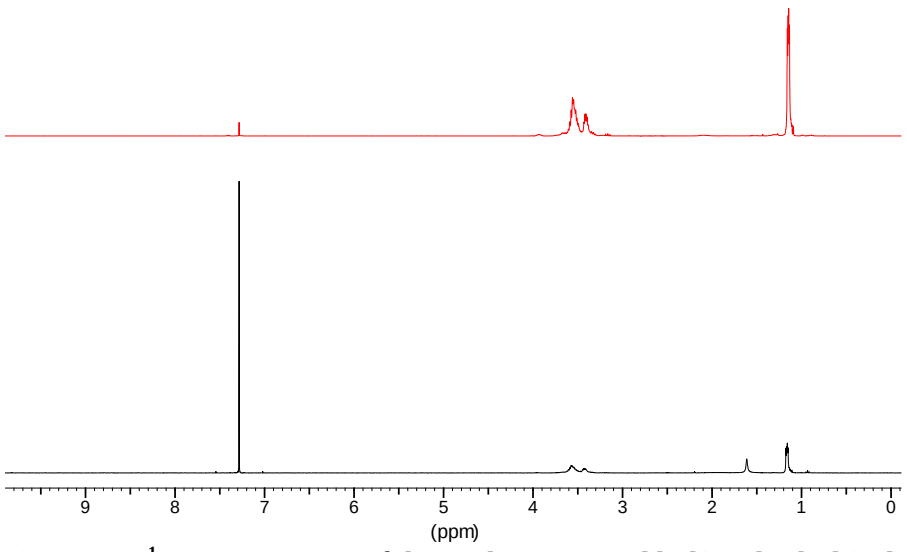

Figure 1.10: ^{1}H NMR spectrum of the residue at 350°C (black) and polyol (red)

1.1.4 Condensable Fraction

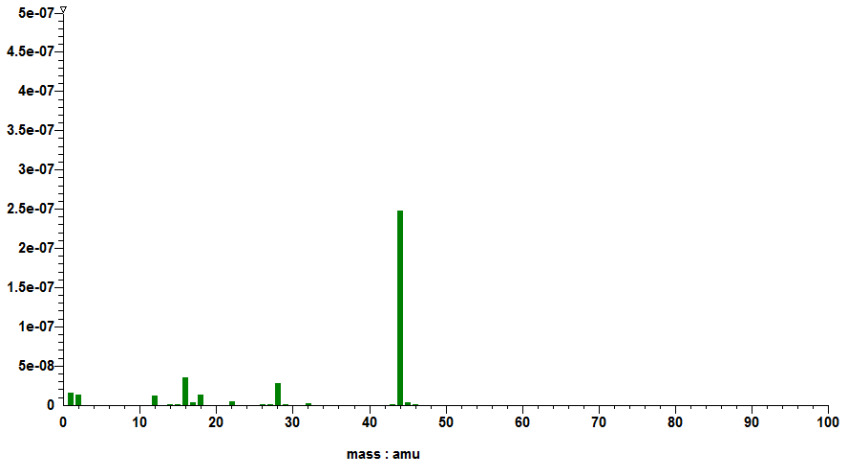

Figure 1.11: MS of CO_2 collected at 250°C

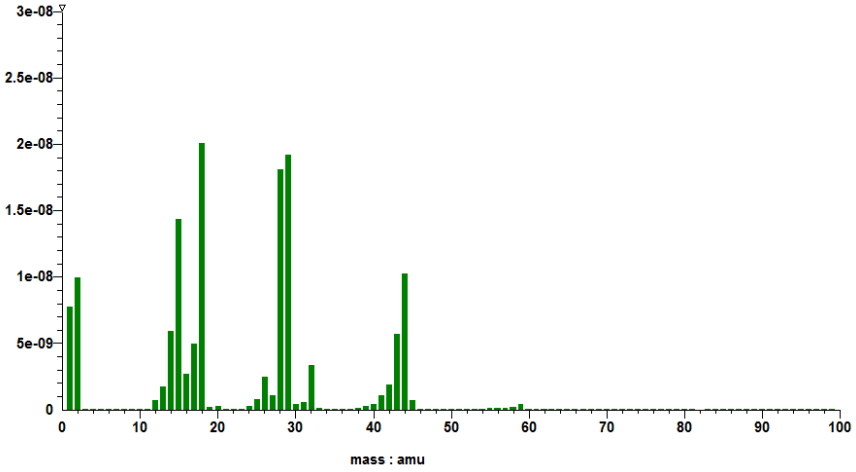

Figure 12: MS of acetaldehyde collected at 250°C

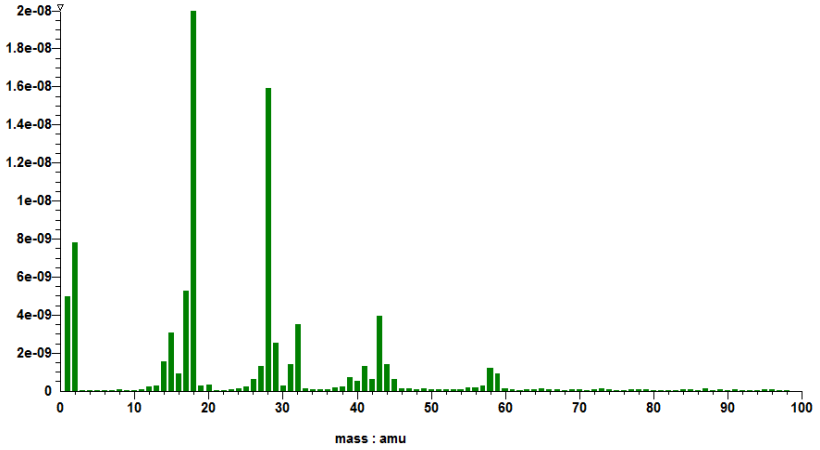

Figure 13: MS of C_3H_6O isomers collected at 250°C

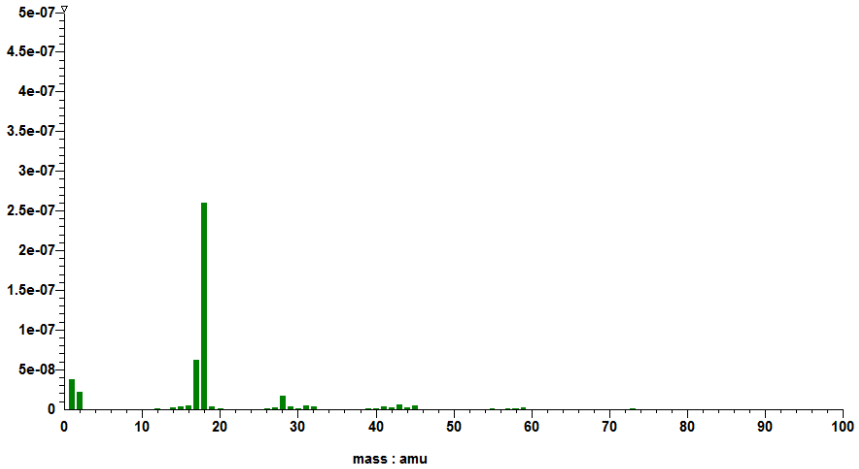

Figure 14: MS of water collected at 250°C

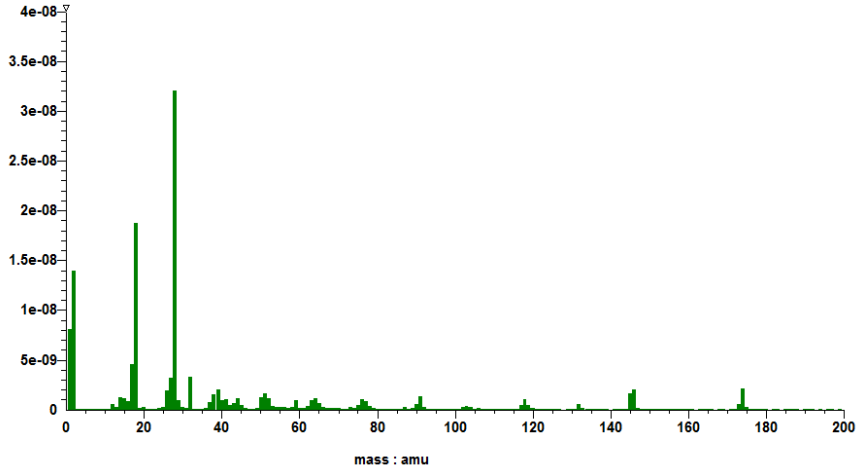

Figure 15: MS of high molar mass material collected at 250°C

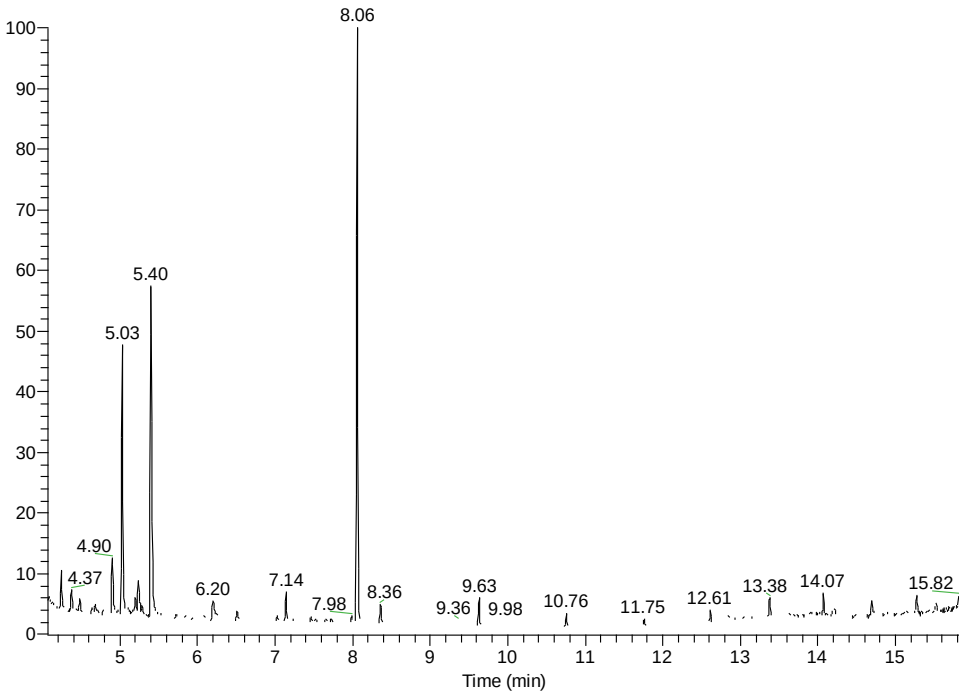

Figure 16: GC-MS chromatogram of fraction 4 at 250°C

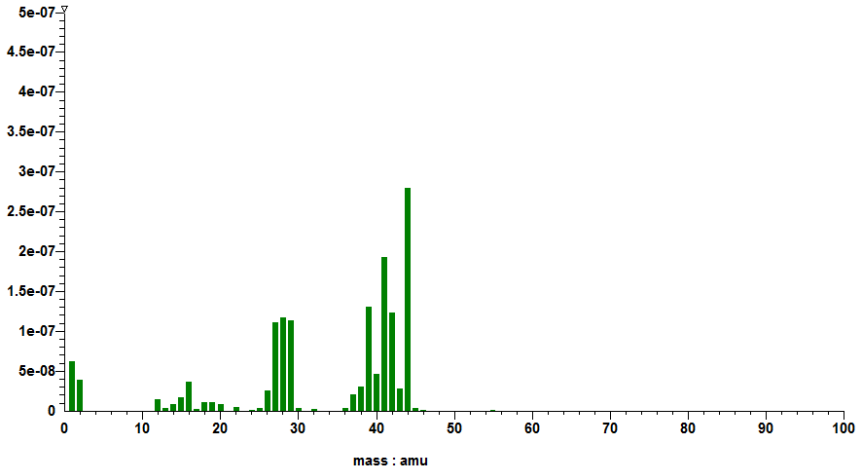

Figure 17: MS of propene and CO_2 collected at 300°C

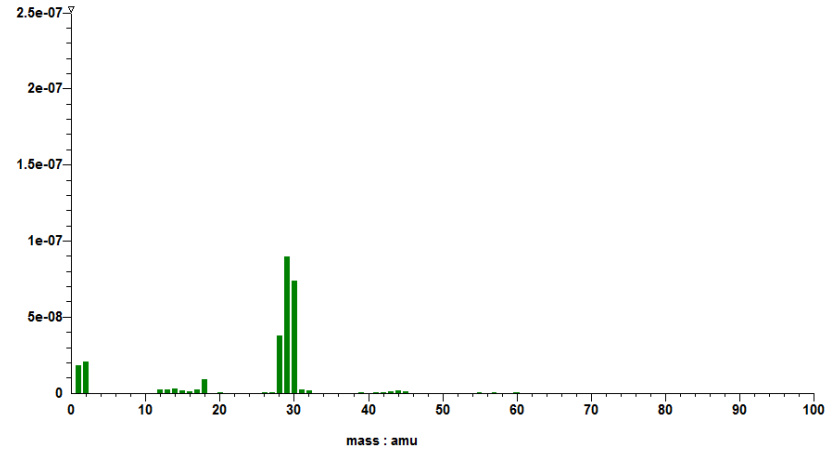

Figure 18: MS of formaldehyde collected at 300°C

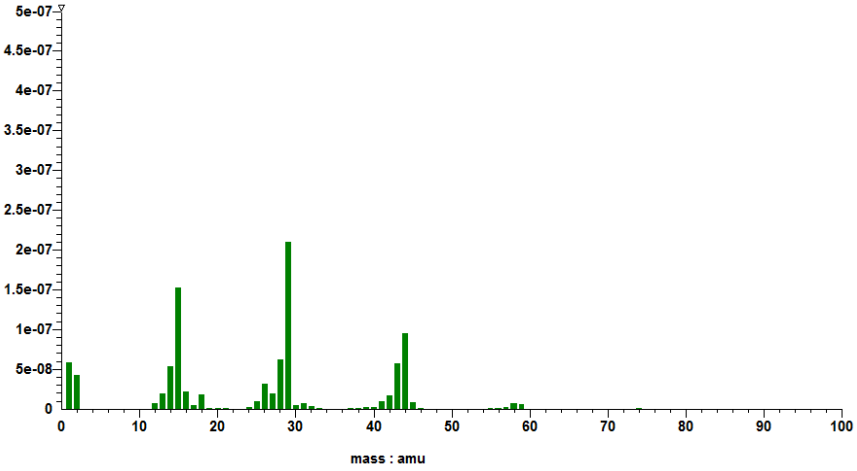

Figure 19: MS of acetaldehyde collected at 300°C

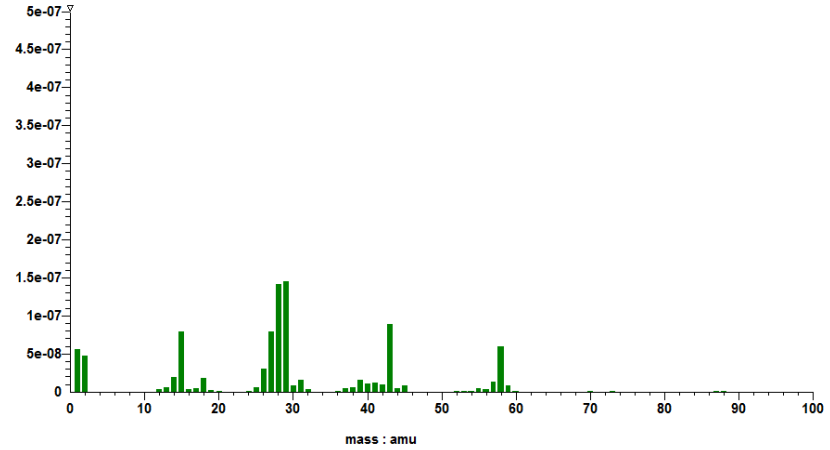

Figure 20: MS of C_3H_6O isomers collected at 300°C

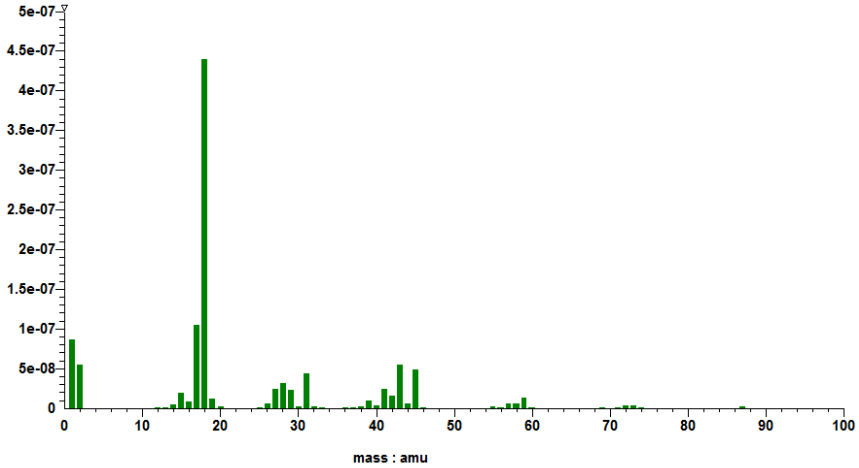

Figure 21: MS of water and high molar mass material collected at 300°C

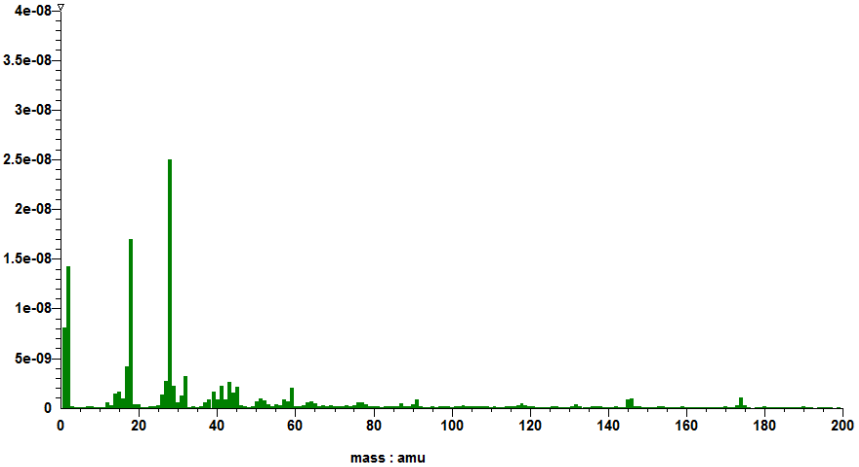

Figure 22: MS of high molar mass material collected at 300°C

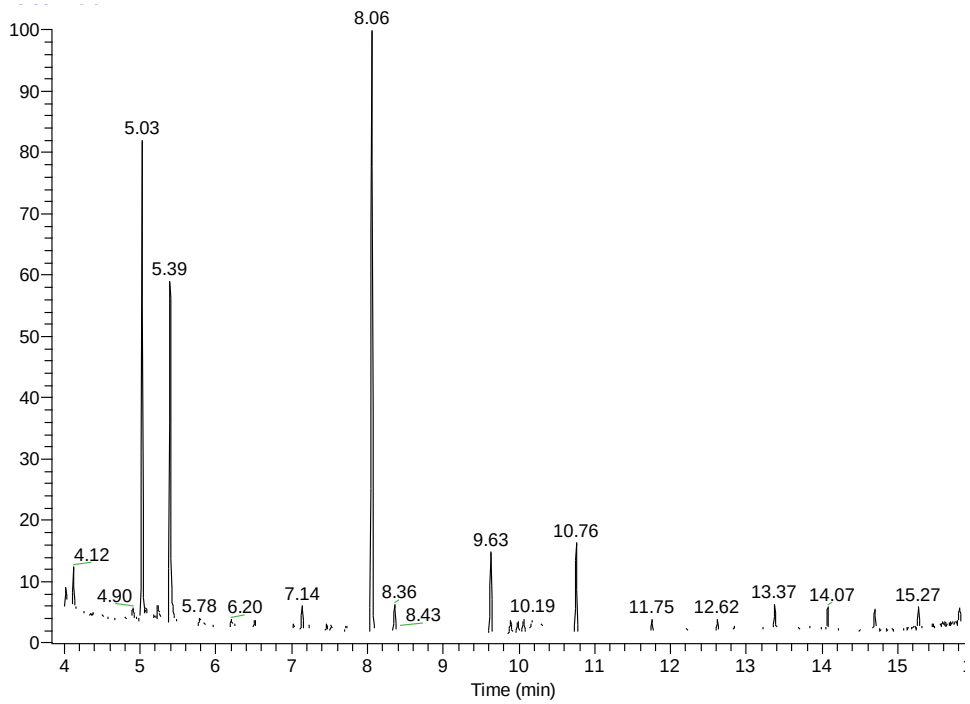

Figure 23: GC-MS chromatogram of fraction 4 at 300°C

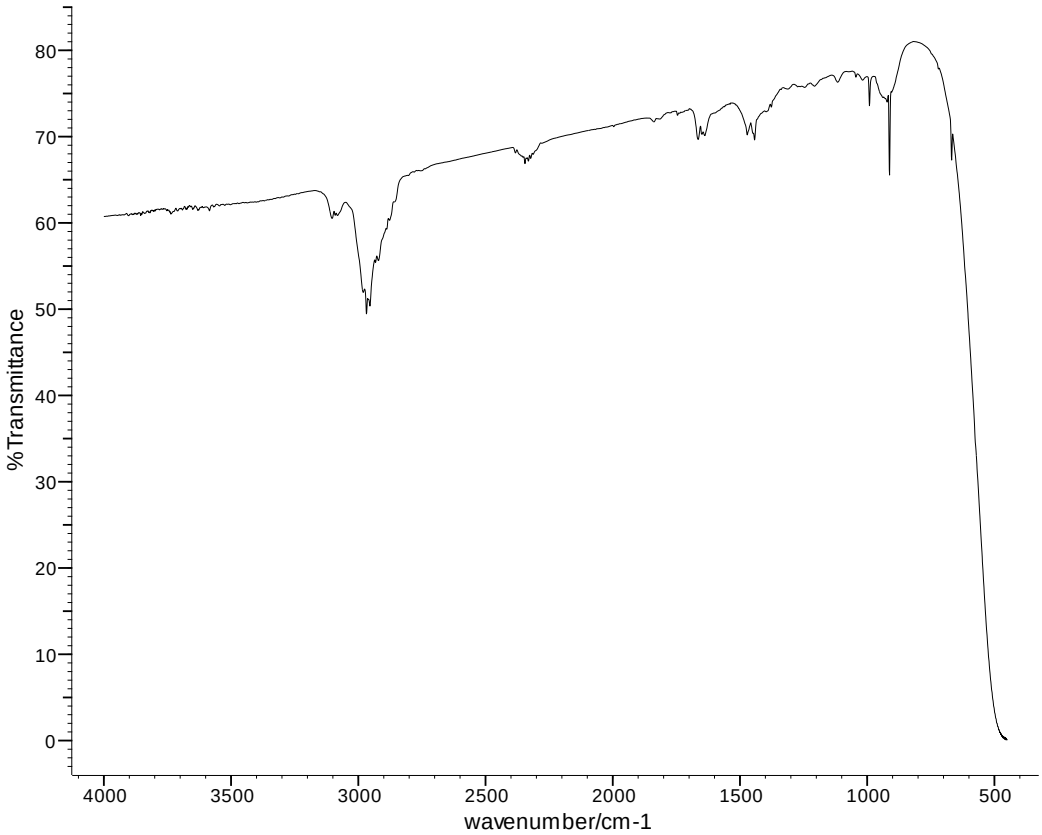

Figure 24: FTIR spectrum of fraction 1 at 350°C

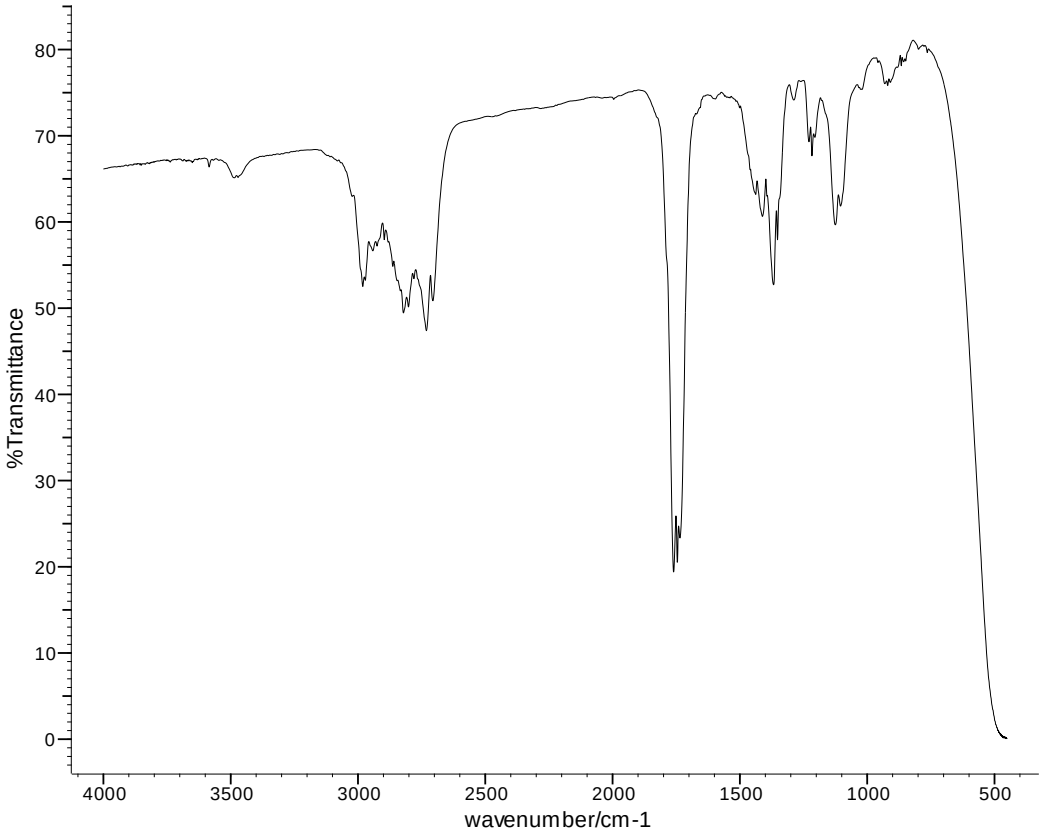

Figure 25: FTIR spectrum of fraction 2 at 350°C

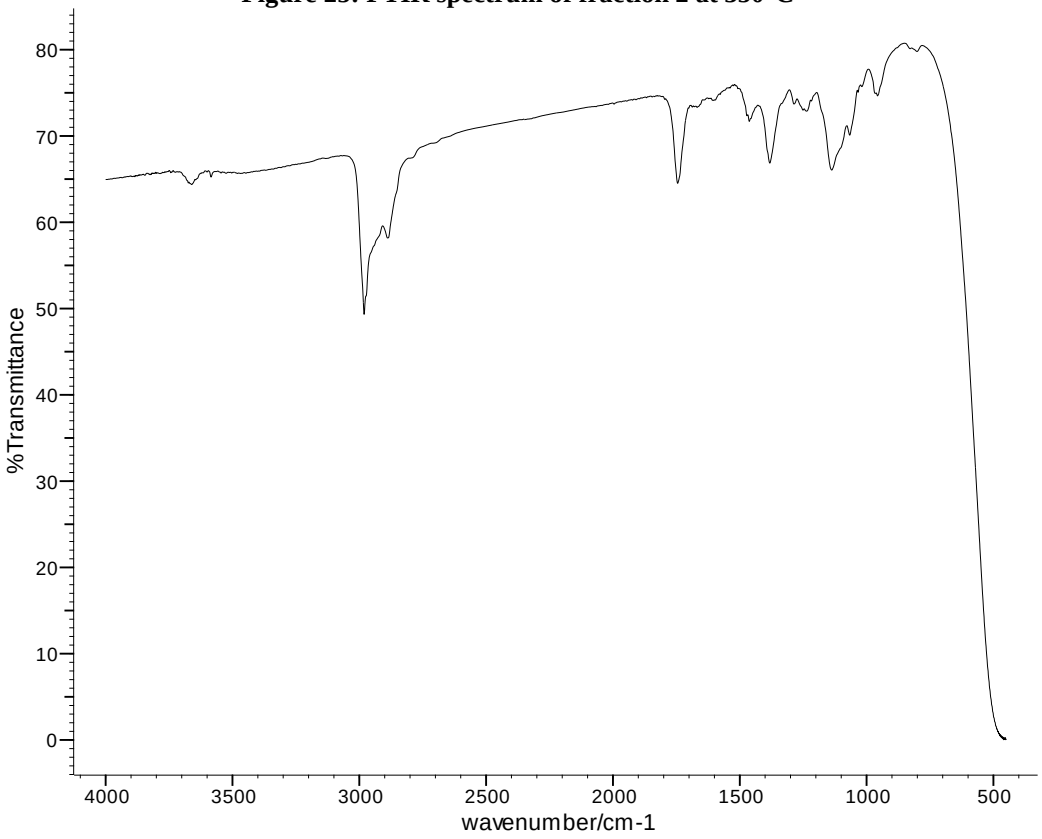

Figure 26: FTIR spectrum of fraction 3 at 350°C

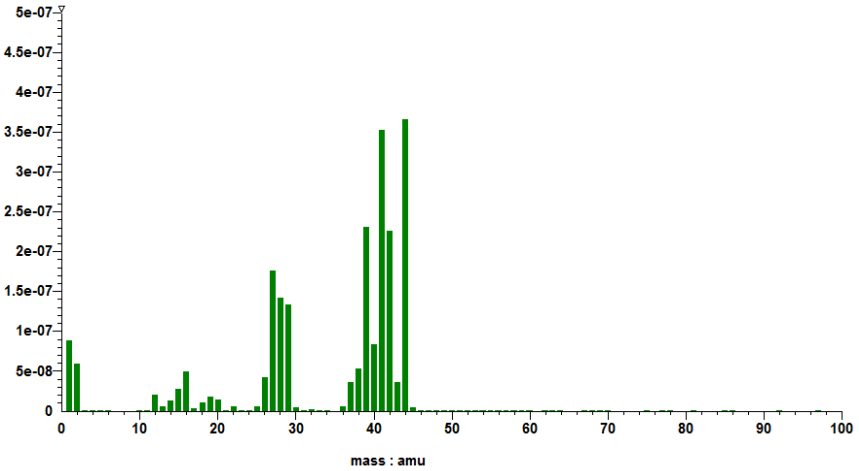

Figure 27: MS of propene and CO_2 collected at 350°C

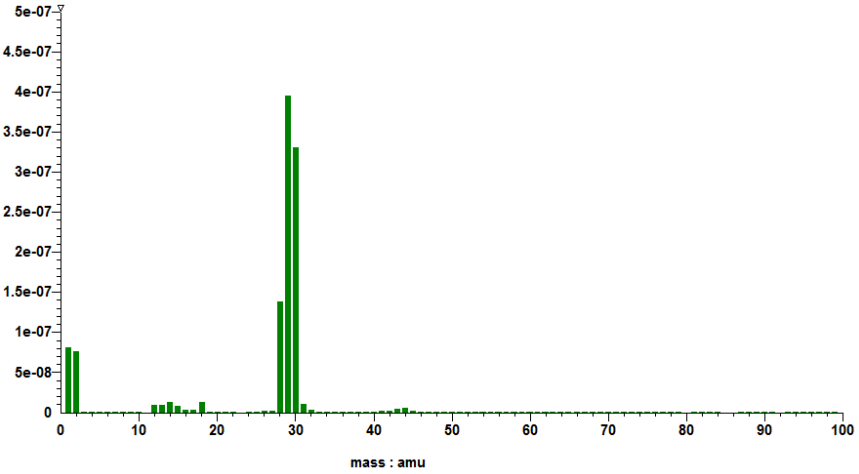

Figure 28: MS of formaldehyde collected at 350°C

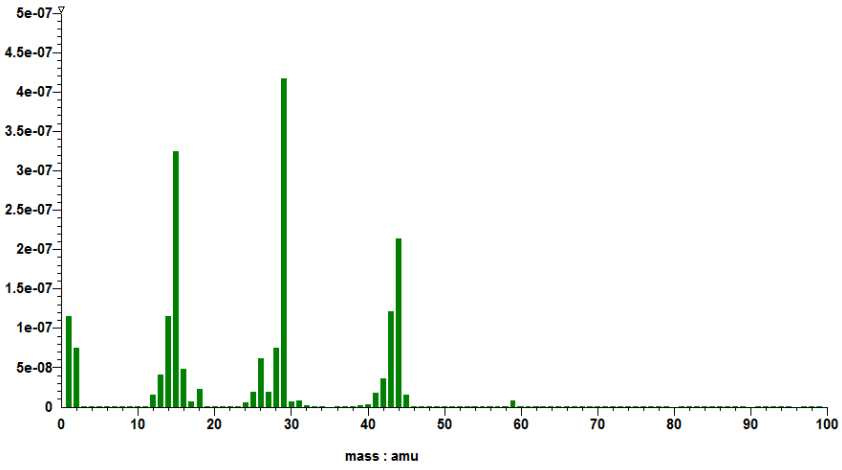

Figure 29: MS of acetaldehyde collected at 350°C

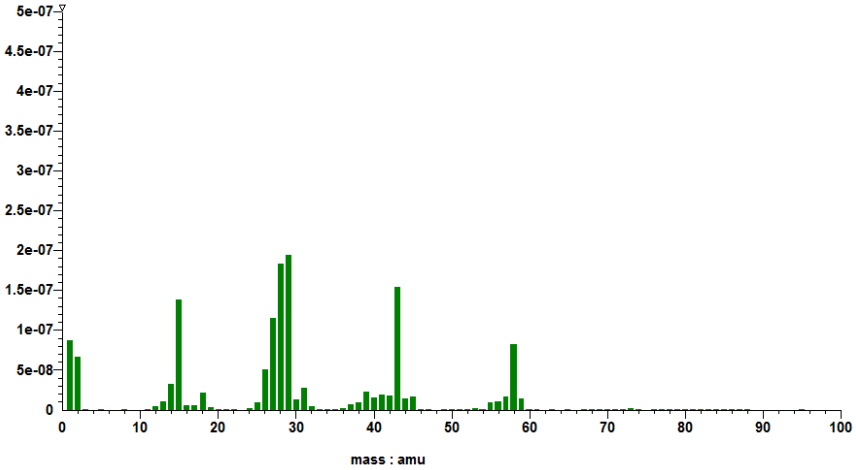

Figure 30: MS of C_3H_6O isomers collected at 350°C

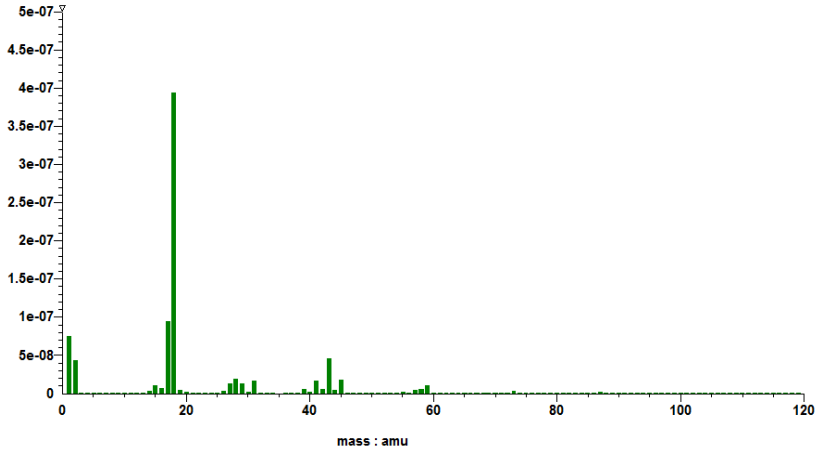

Figure 31: MS of water and higher molar mass material collected at 350°C

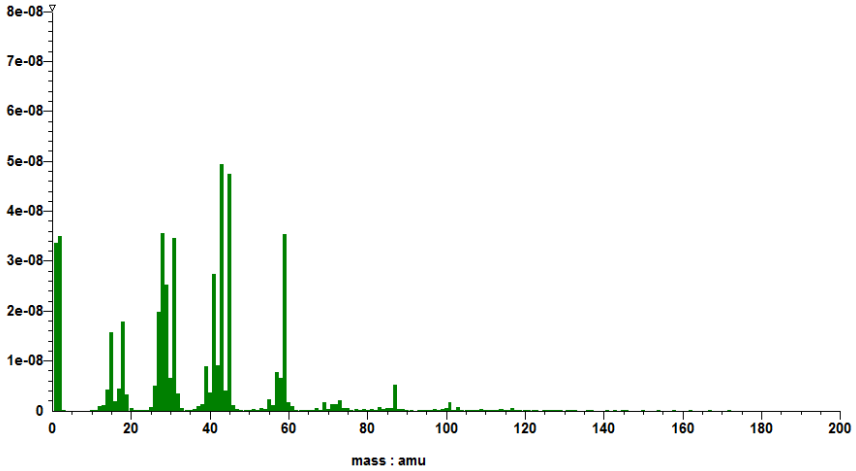

Figure 32:MS of high molar mass material collected at 350°C

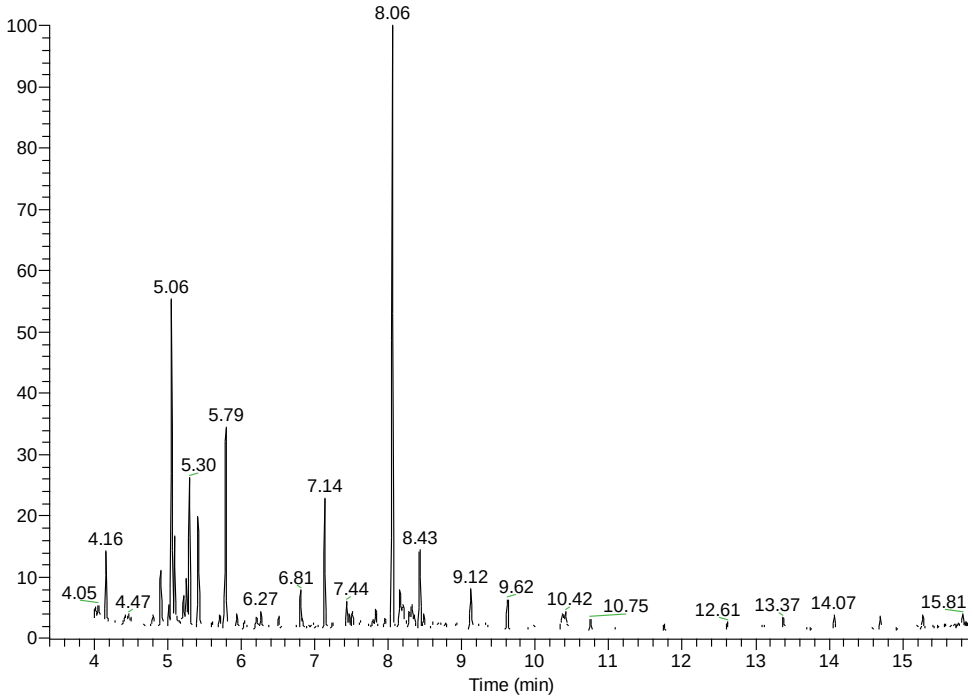

Figure 33: GC-MS chromatogram of fraction 4 at 350°C

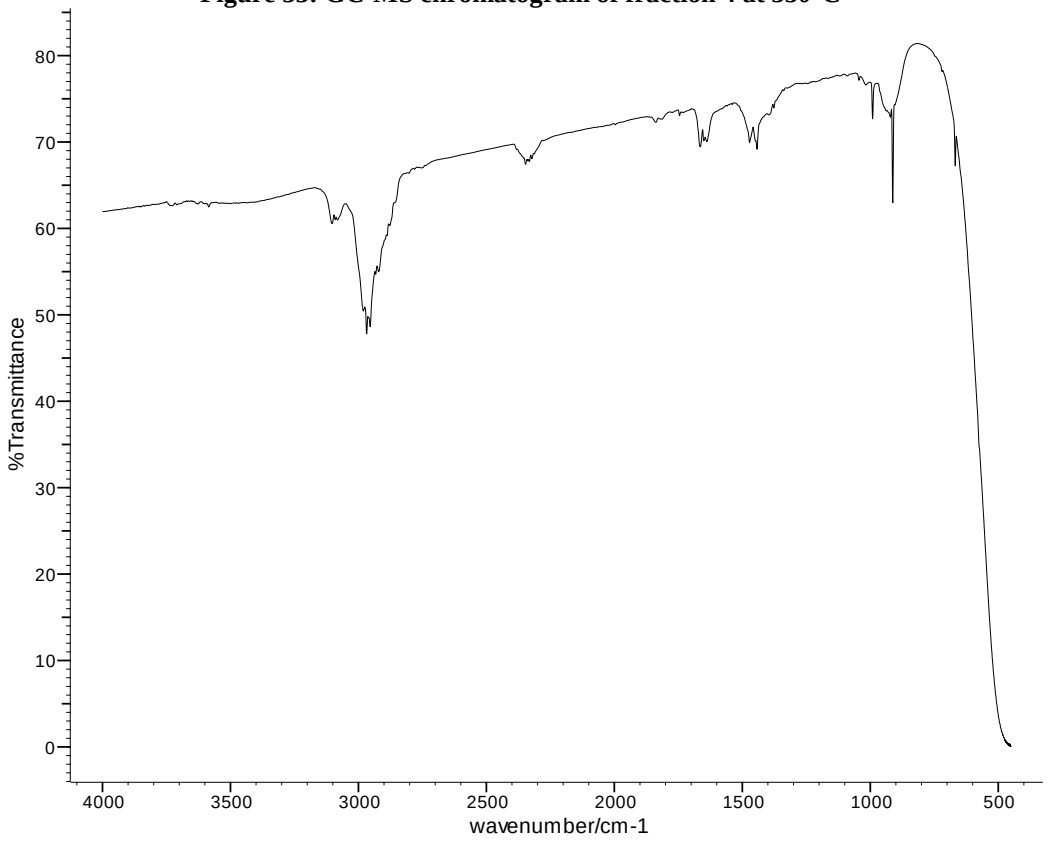

Figure 34: FTIR spectrum of fraction 1 at 400°C

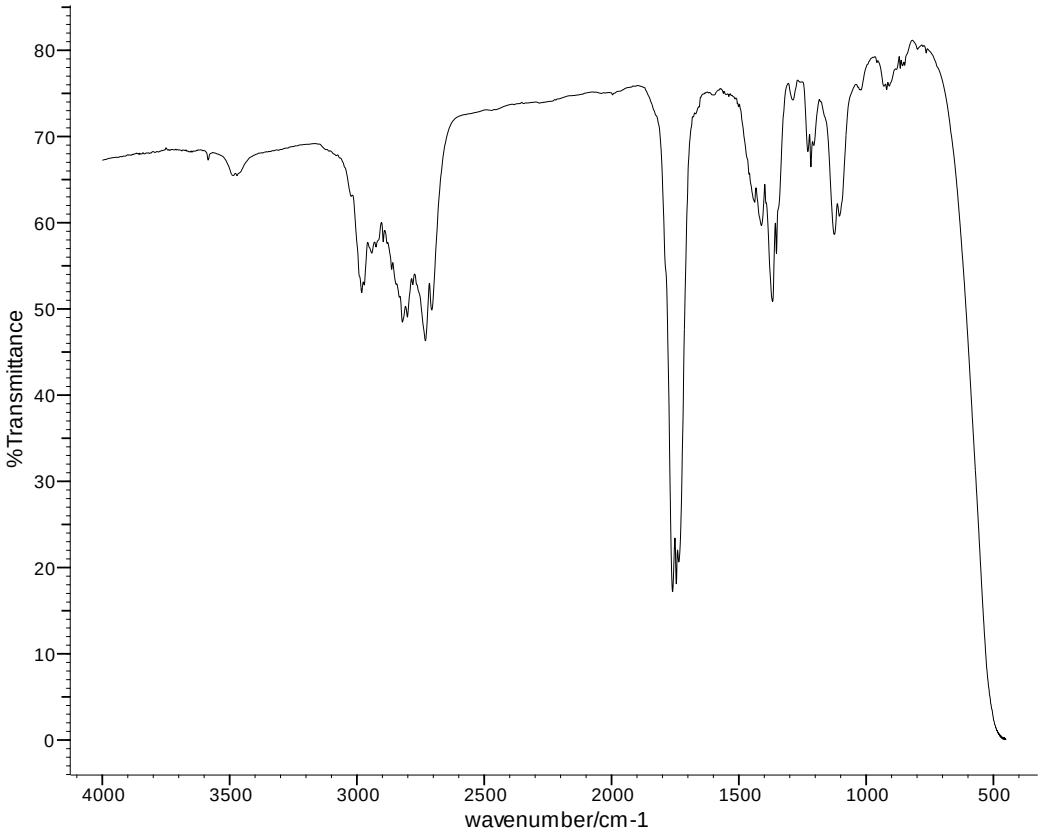

Figure 35: FTIR spectrum of fraction 2 at 400°C

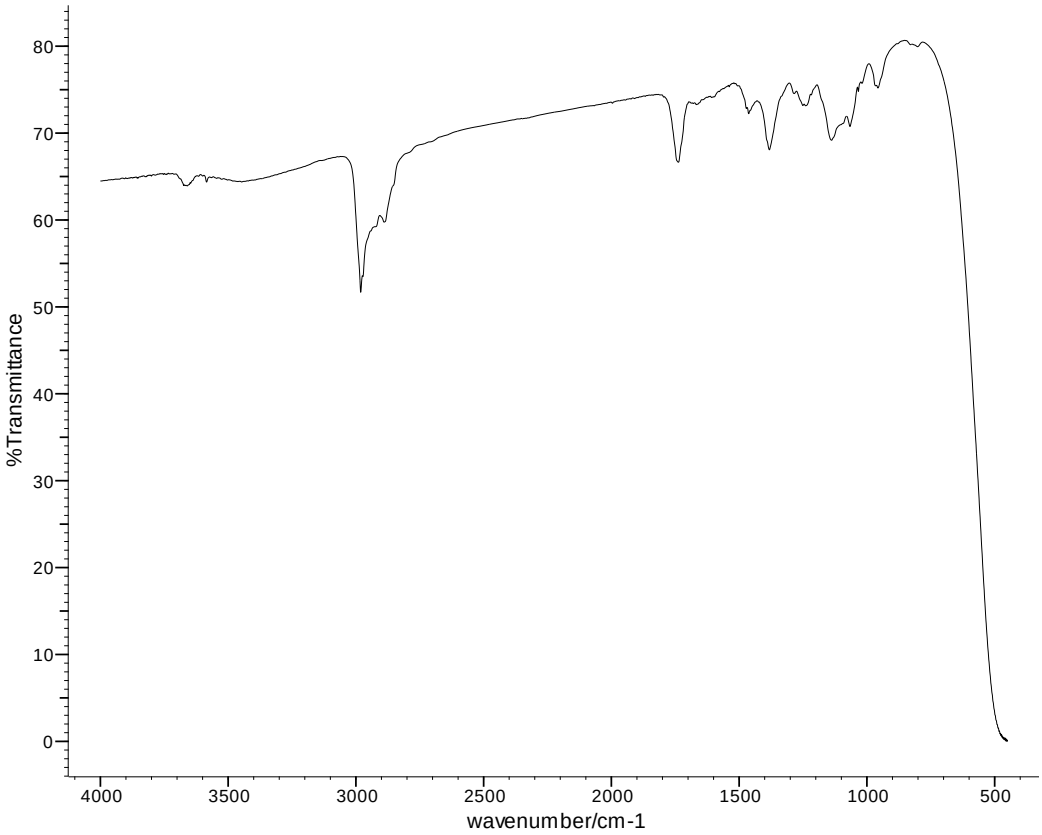

Figure 36: FTIR spectrum of fraction 3 at 400°C

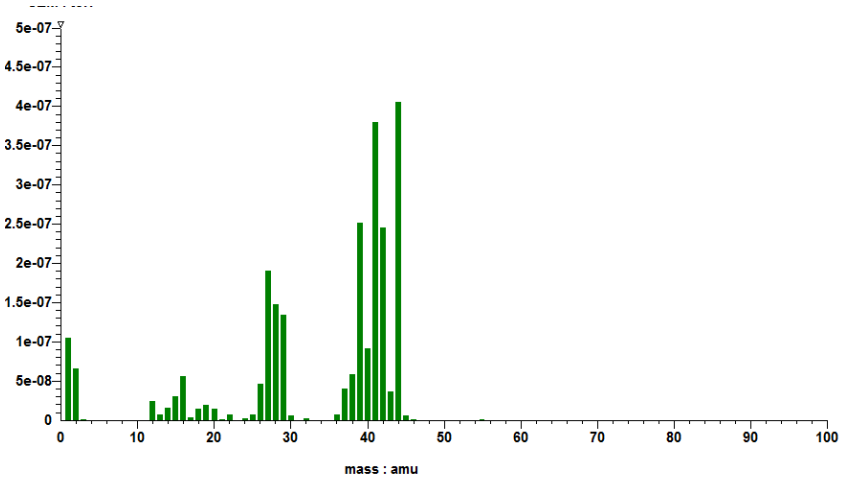

Figure 37: MS of propene and CO_2 collected at 400°C

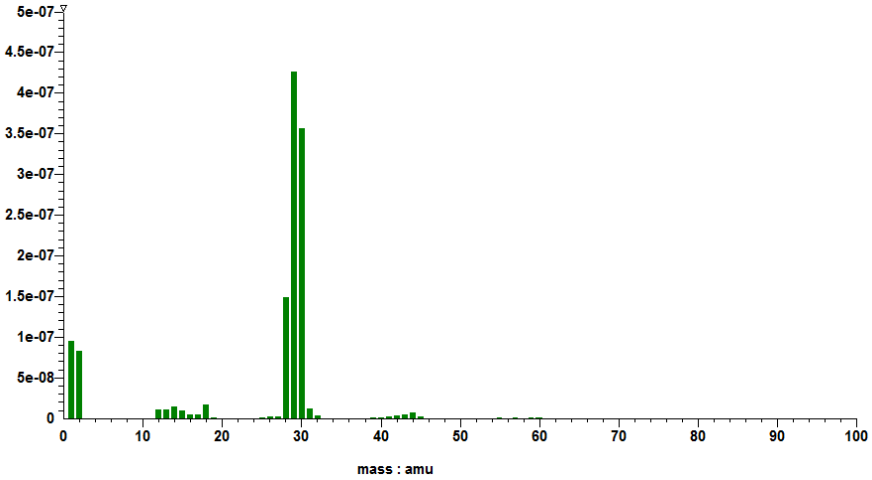

Figure 38:MS of formaldehyde collected at 400°C

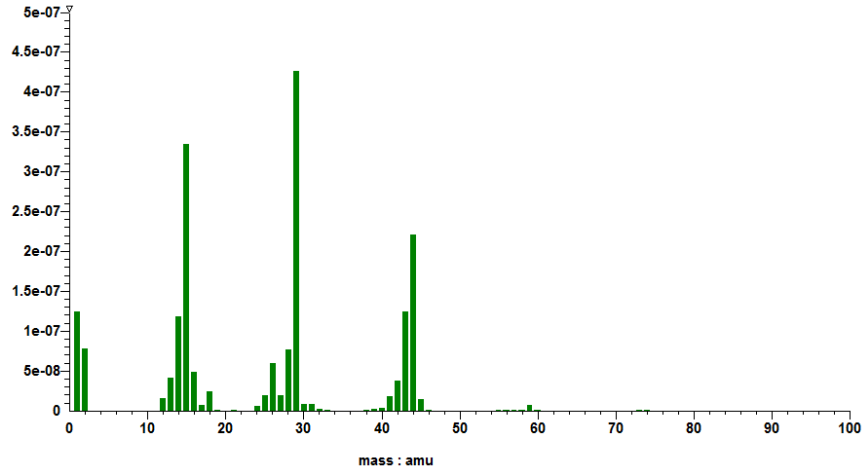

Figure 39: MS of acetaldehyde collected at 400°C

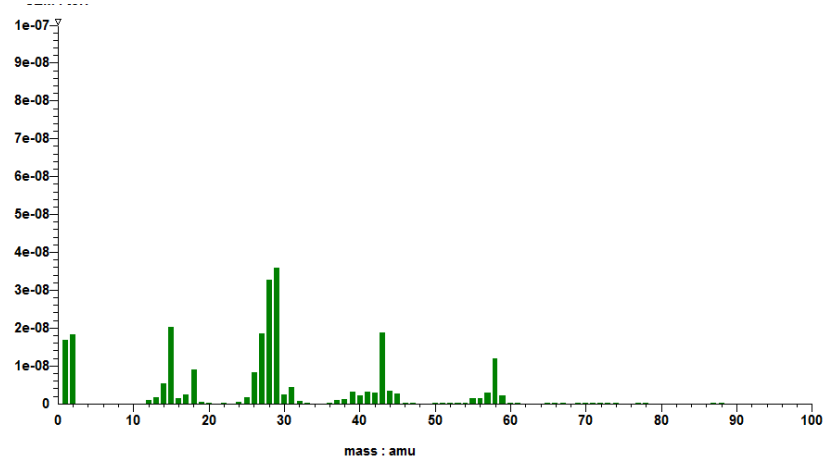

Figure 40: MS of C_3H_6O isomers collected at 400°C

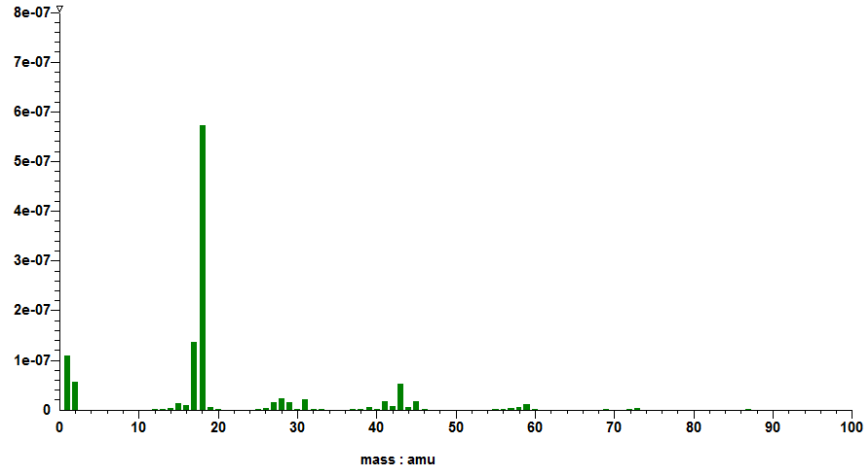

Figure 41: MS of water and high molar mass material at 400°C

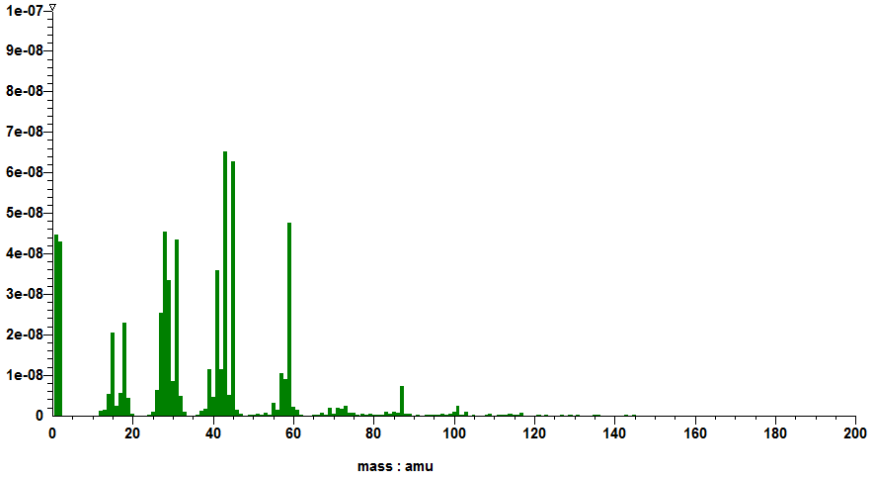

Figure 42: MS of high molar mass material at 400°C

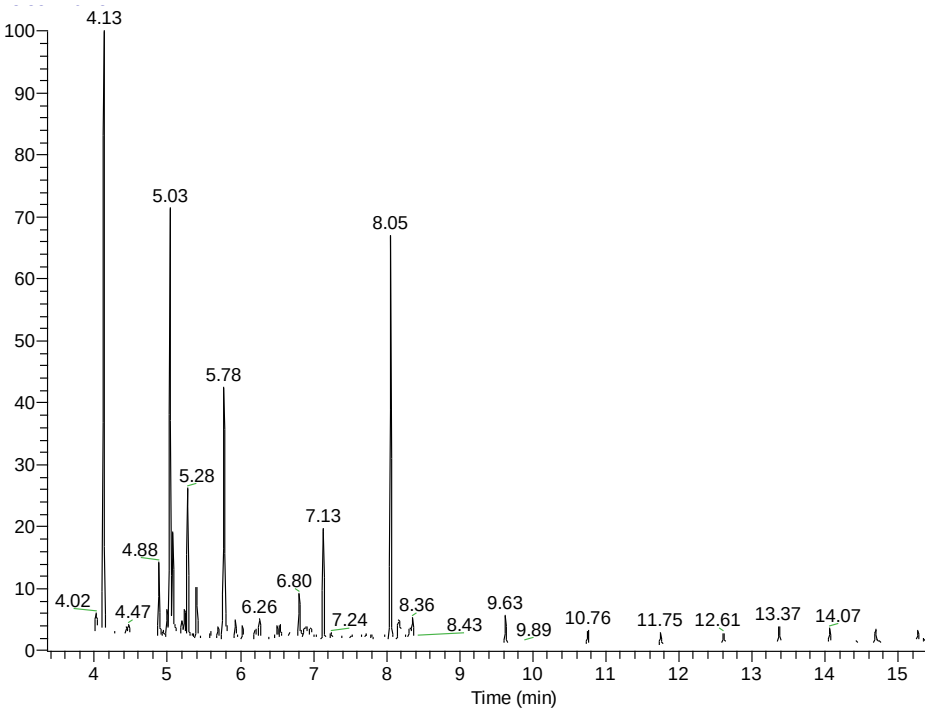

Figure 43: GC-MS chromatogram of fraction 4 at 400°C

1.1.5 TVA of Polyol

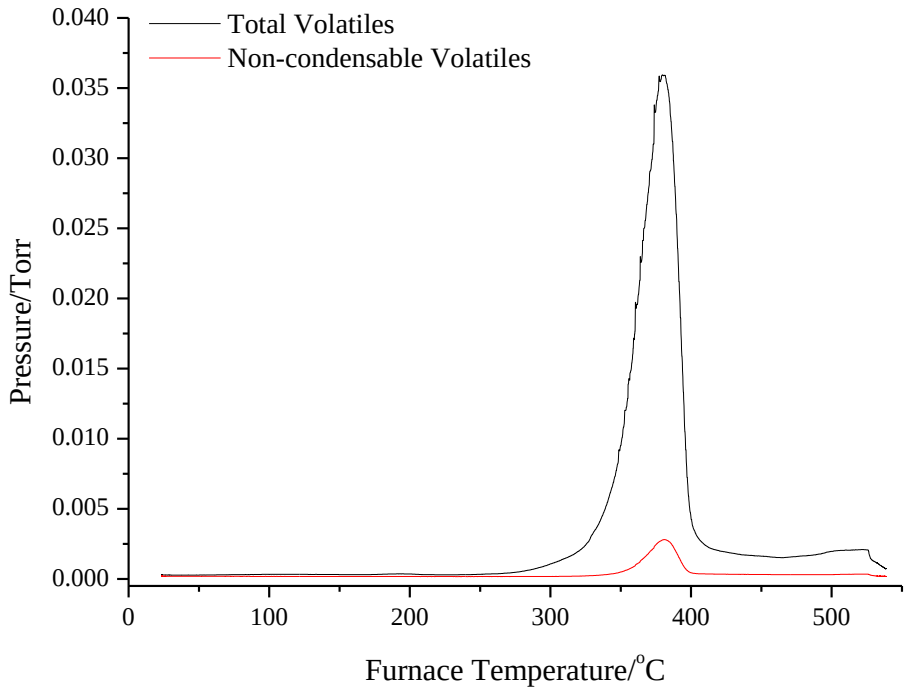

Figure 44: TVA degradation profile of neat polyol

1.2 Pyrolysis under nitrogen

1.2.1 Cold-ring fractions

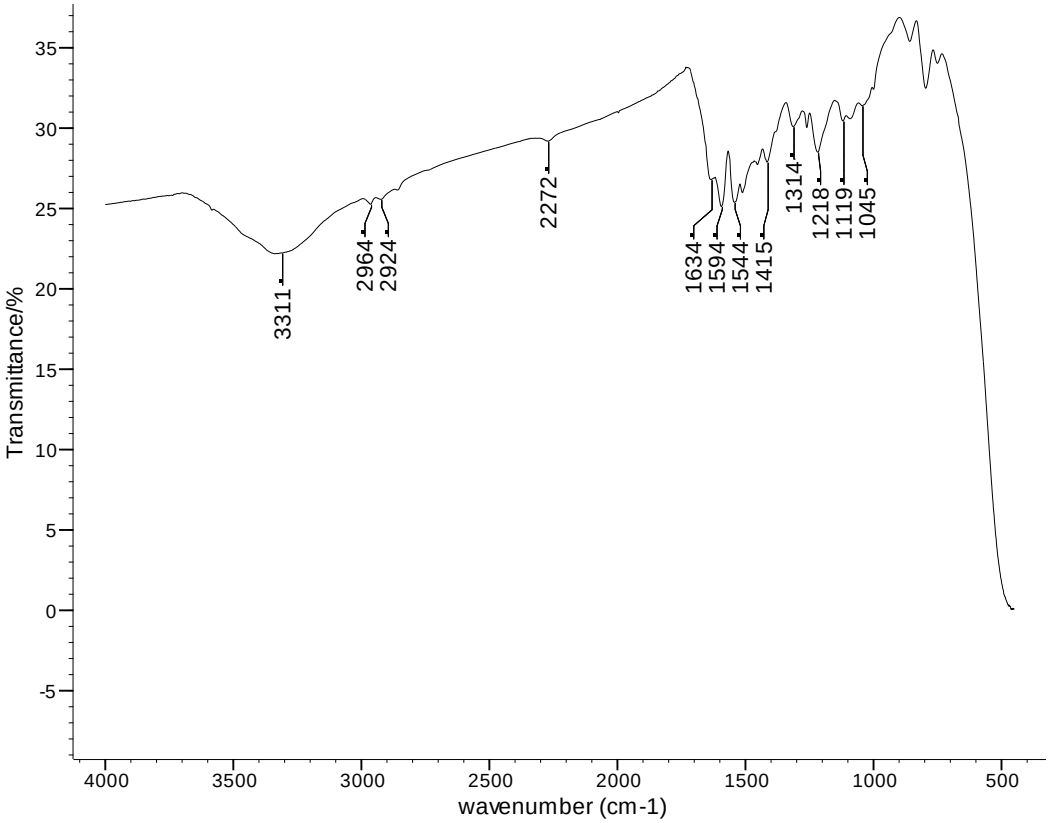

Figure 45: FTIR spectrum of the white insoluble cold-ring fraction collected from the standard foam under nitrogen

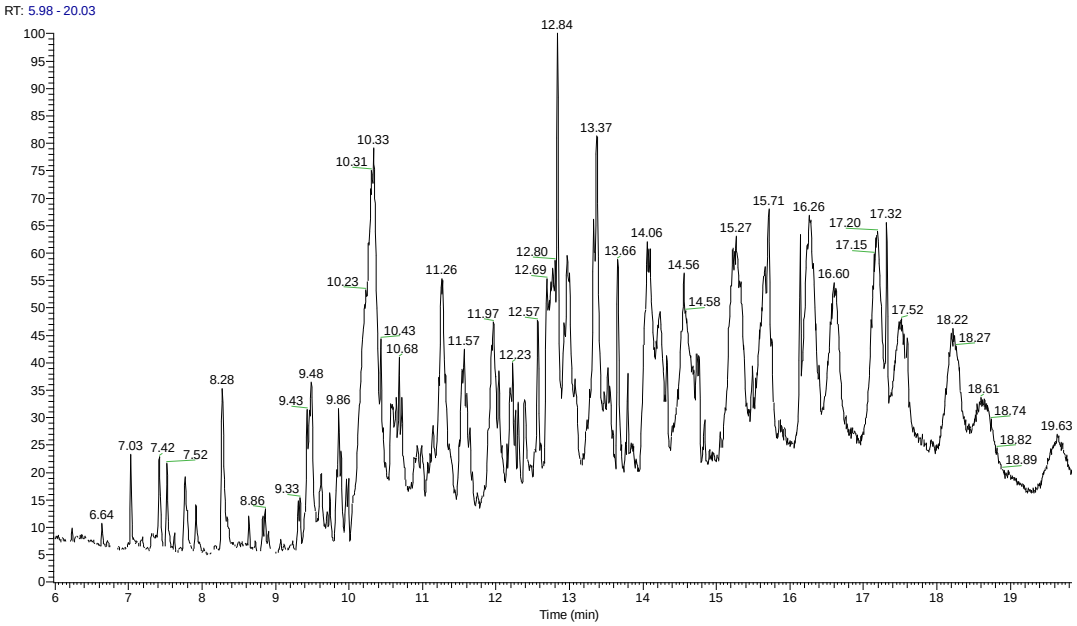

Figure 46: GC-MS chromatogram of the cold-ring fraction collected under nitrogen at 300°C

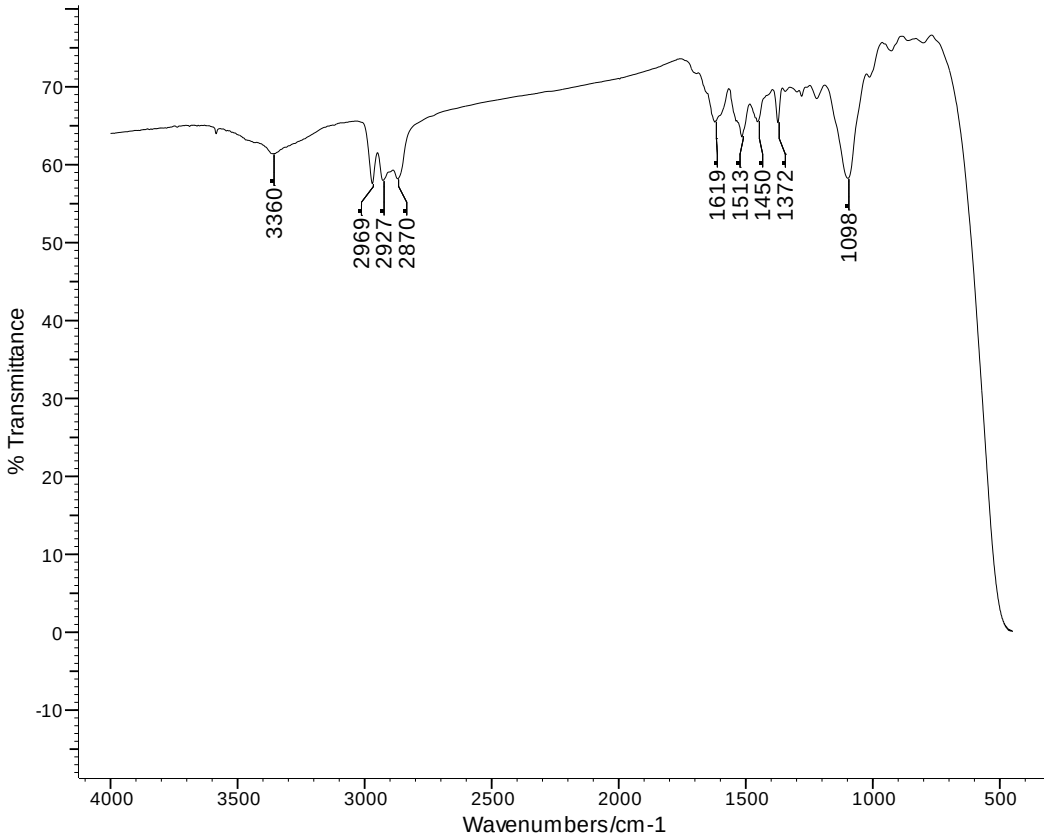

Figure 47: FTIR spectrum of the cold-ring fraction collected under nitrogen at 350°C

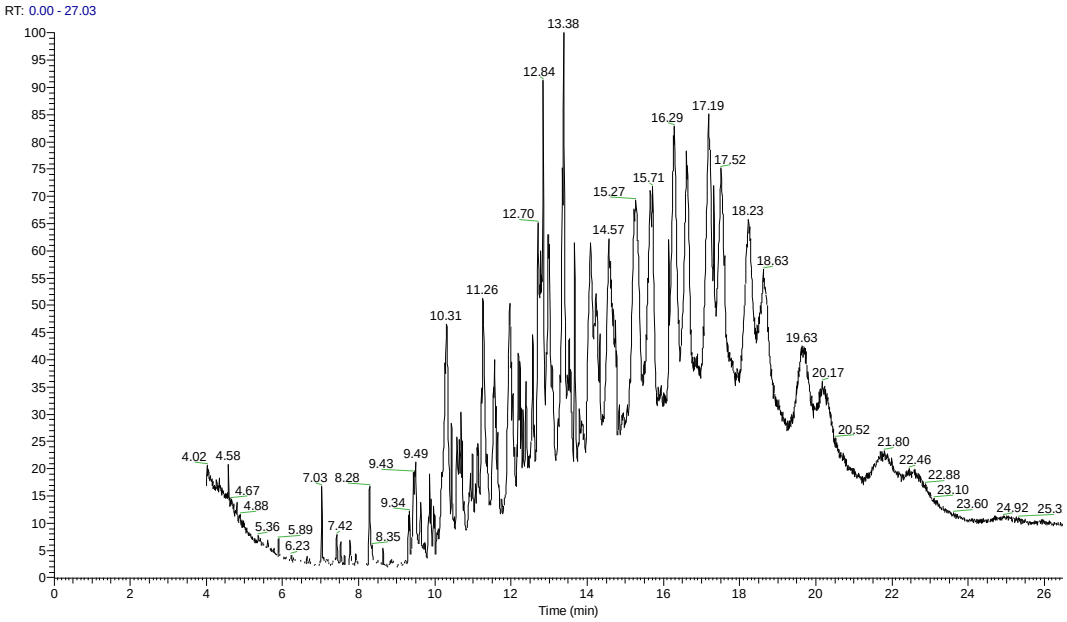

Figure 48: GC-MS chromatogram of the cold-ring fraction collected under nitrogen at 400°C

1.2.2 Tars

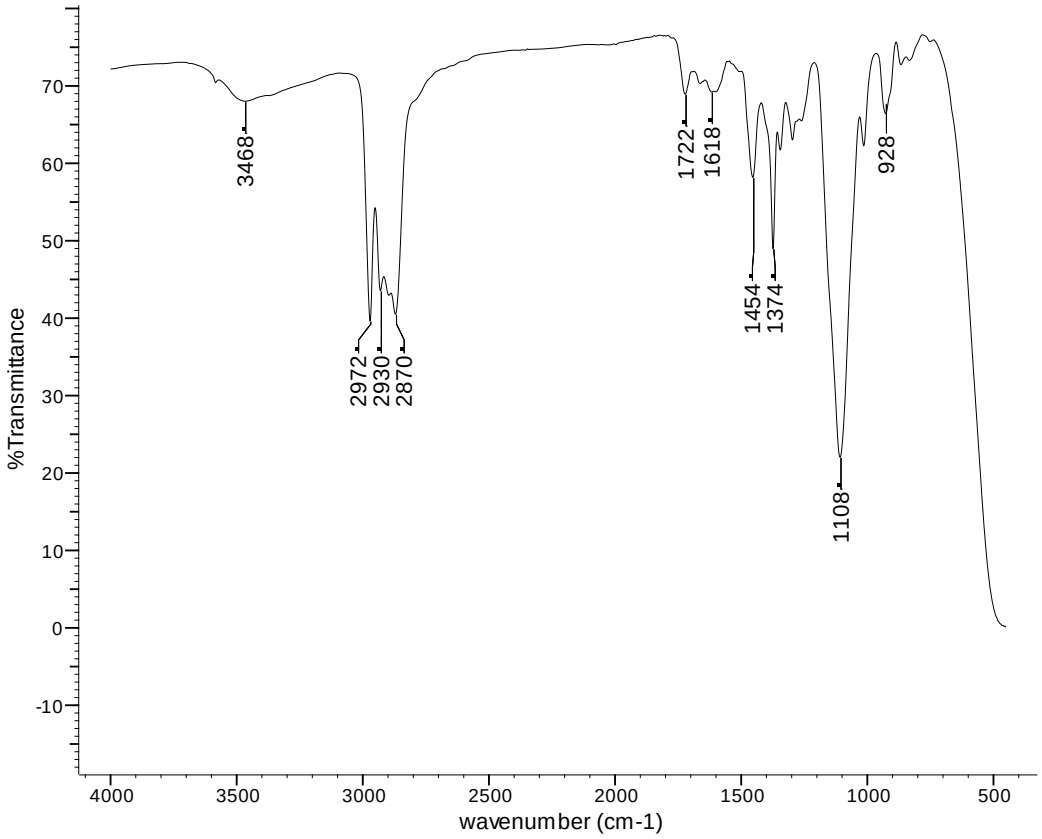

Figure 49: FTIR spectrum of the tar extracted at 350°C under nitrogen

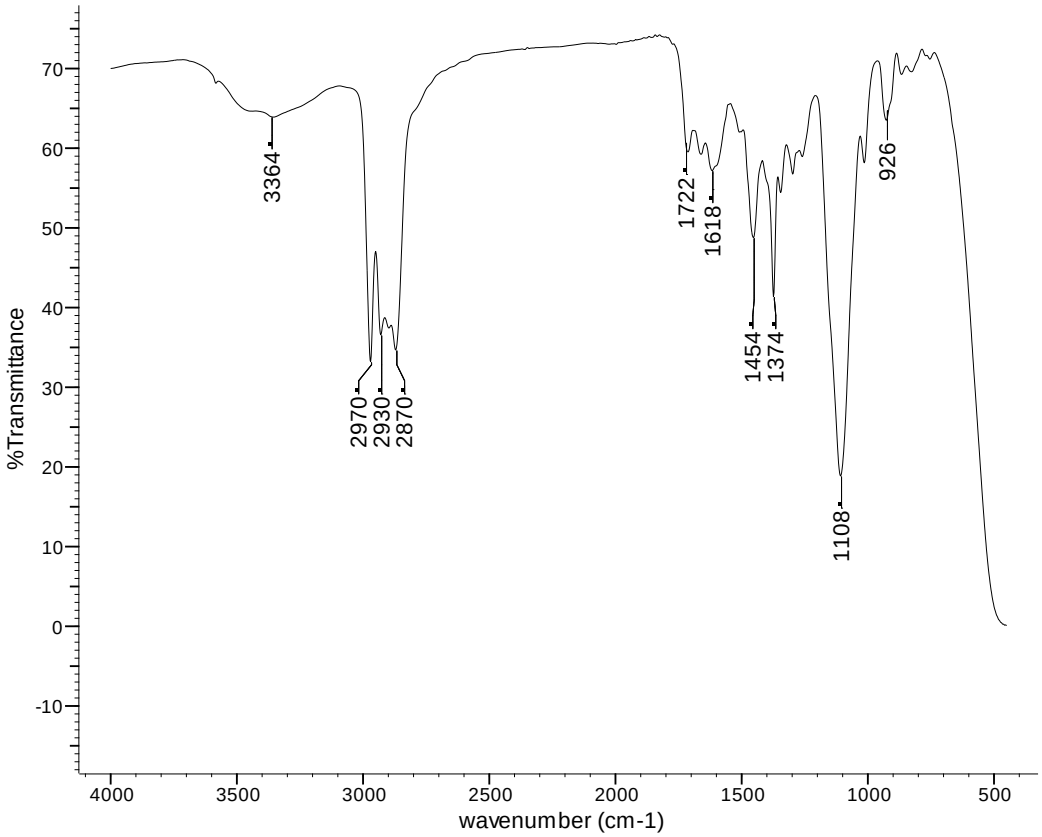

Figure 50: FTIR spectrum of the tar extracted at 400°C under nitrogen

1.3 Pyrolysis under air

1.3.1 Cold-ring Fractions

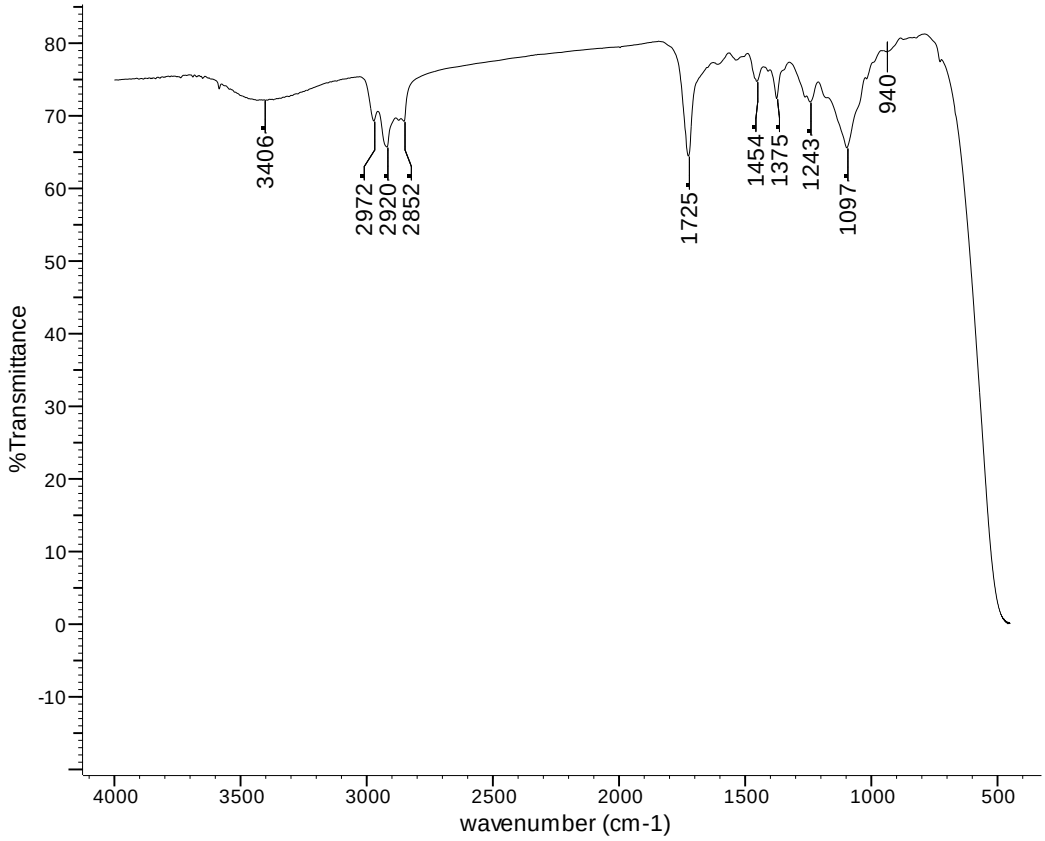

Figure 51: FTIR spectrum of the cold-ring fraction collected under air at 300°C

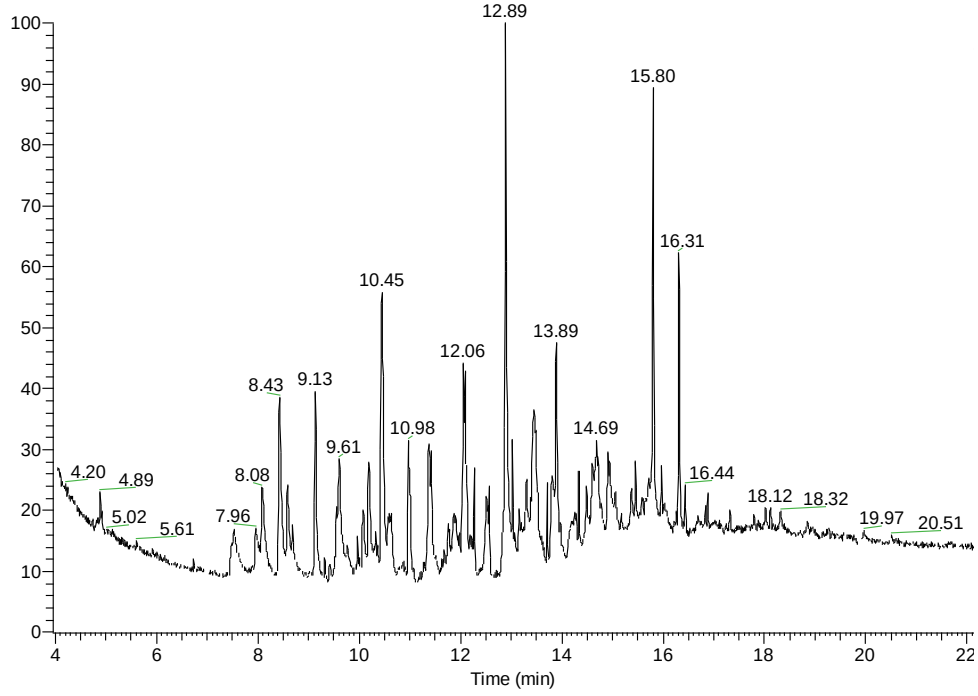

Figure 52:GC-MS total-ion chromatogram for the cold-ring fraction collected under air at 300°C

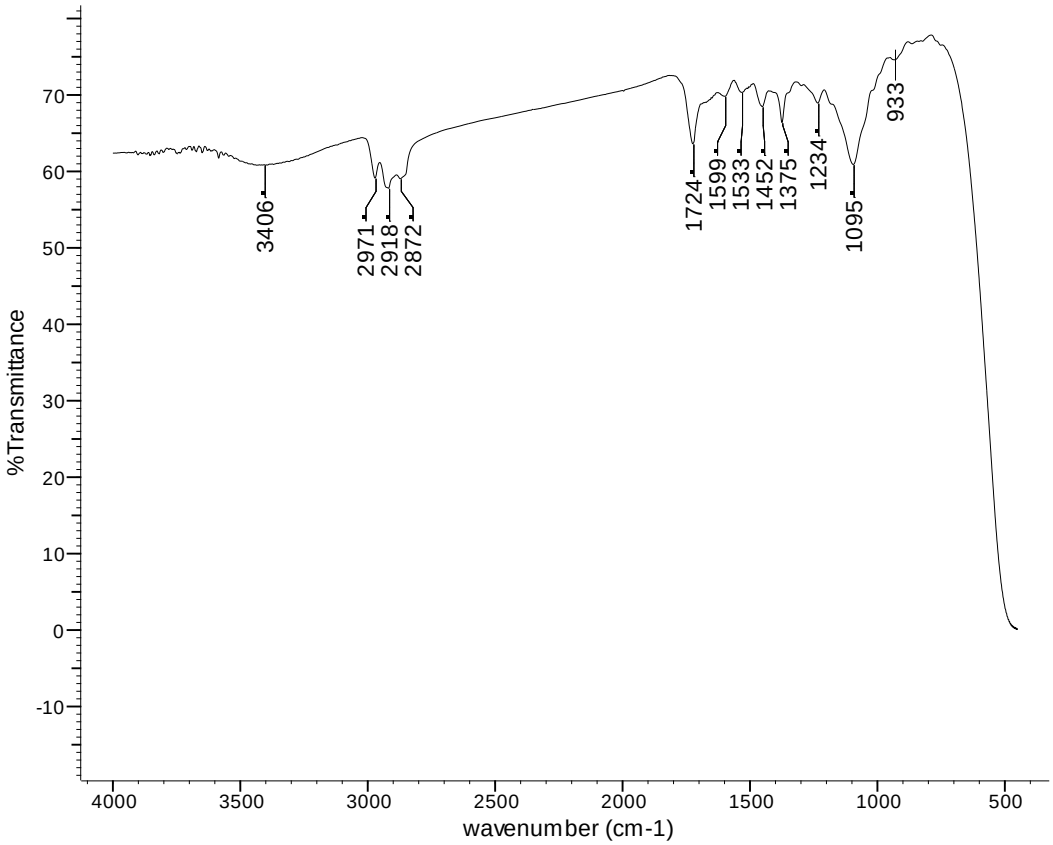

Figure 53: FTIR spectrum of the cold-ring fraction collected under air at 350°C

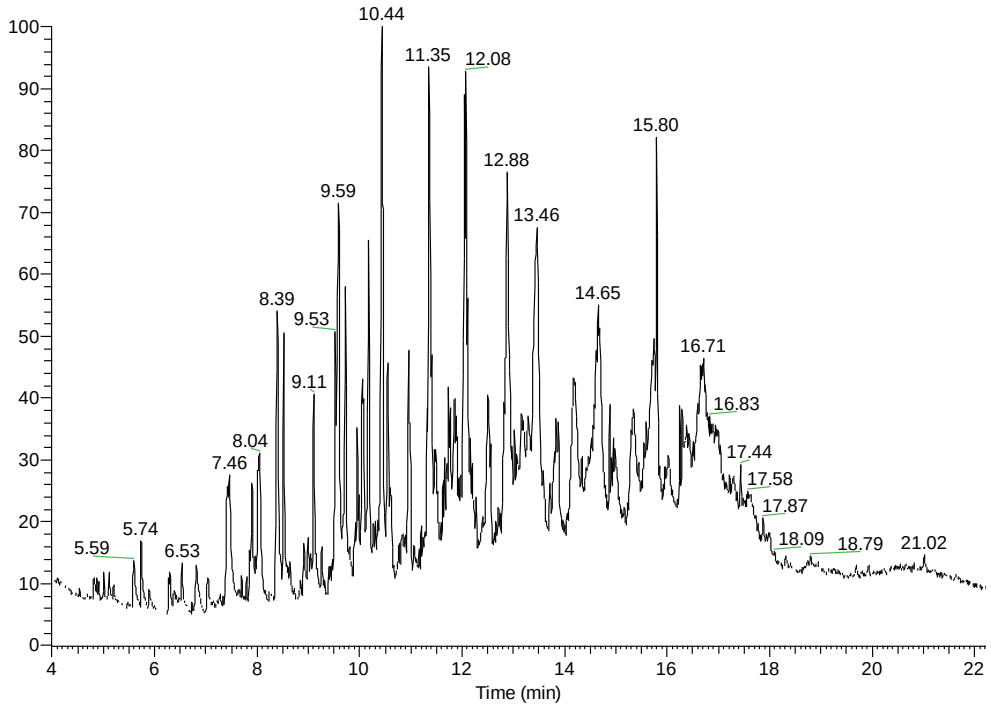

Figure 54:GC-MS total-ion chromatogram for the cold-ring fraction collected under air at 350°C

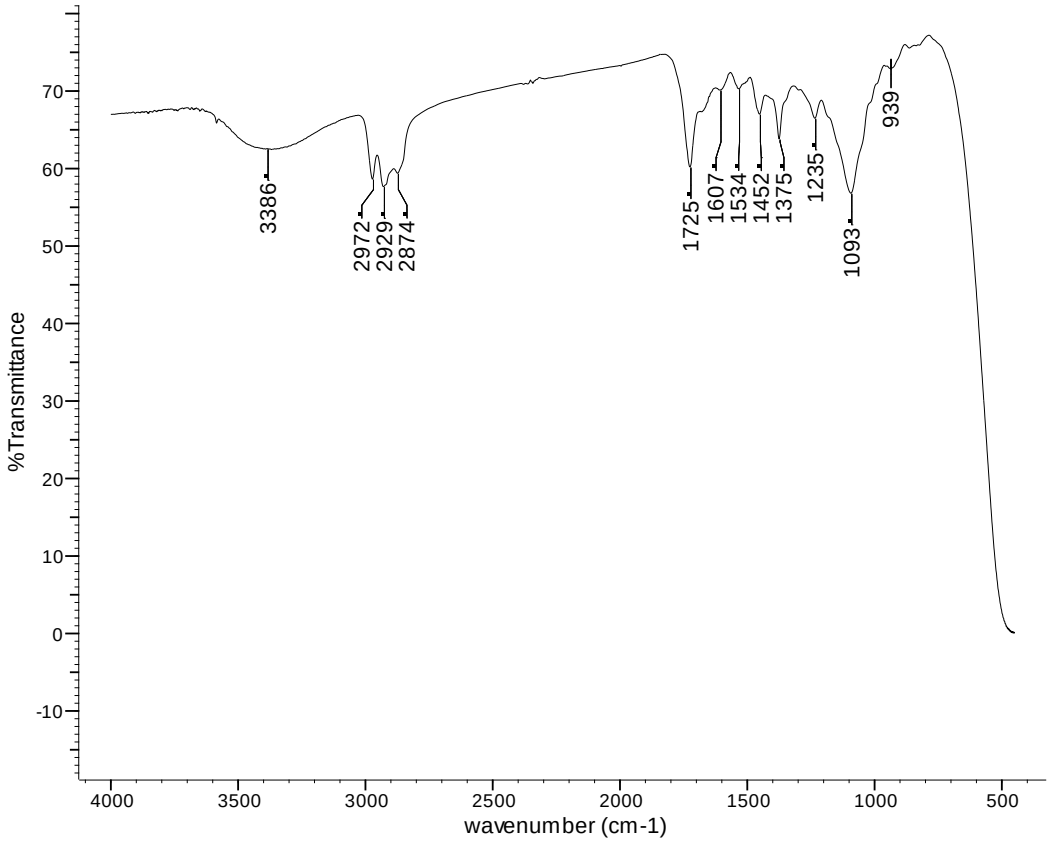

Figure 55:FTIR spectrum of the cold-ring fraction collected under air at 400°C

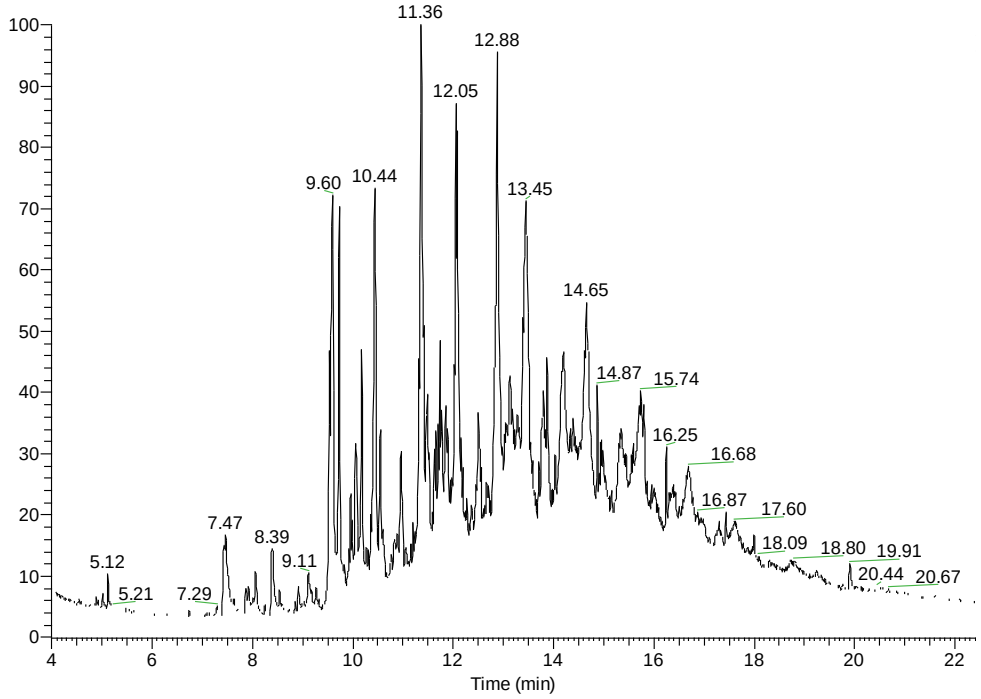

Figure 56: GC-MS total-ion chromatogram for the cold-ring fraction collected under air at 400°C

1.3.2 Tars

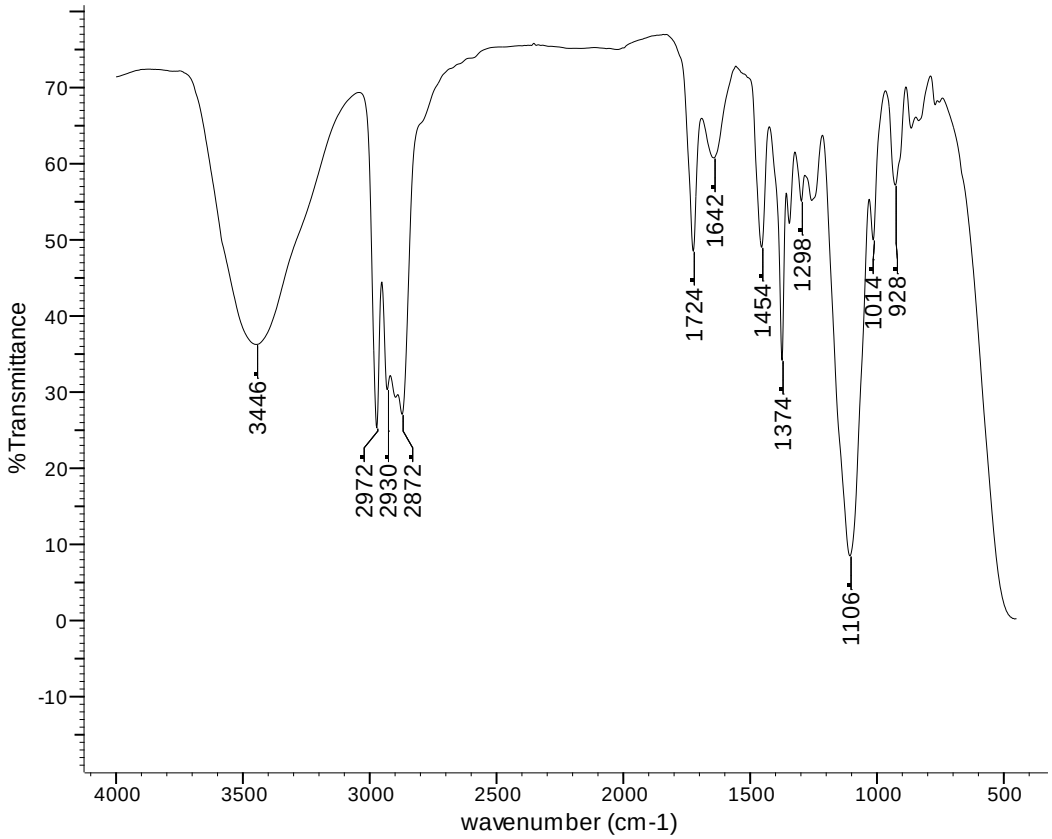

Figure 57: FTIR spectrum of the tar extracted at 300°C under air

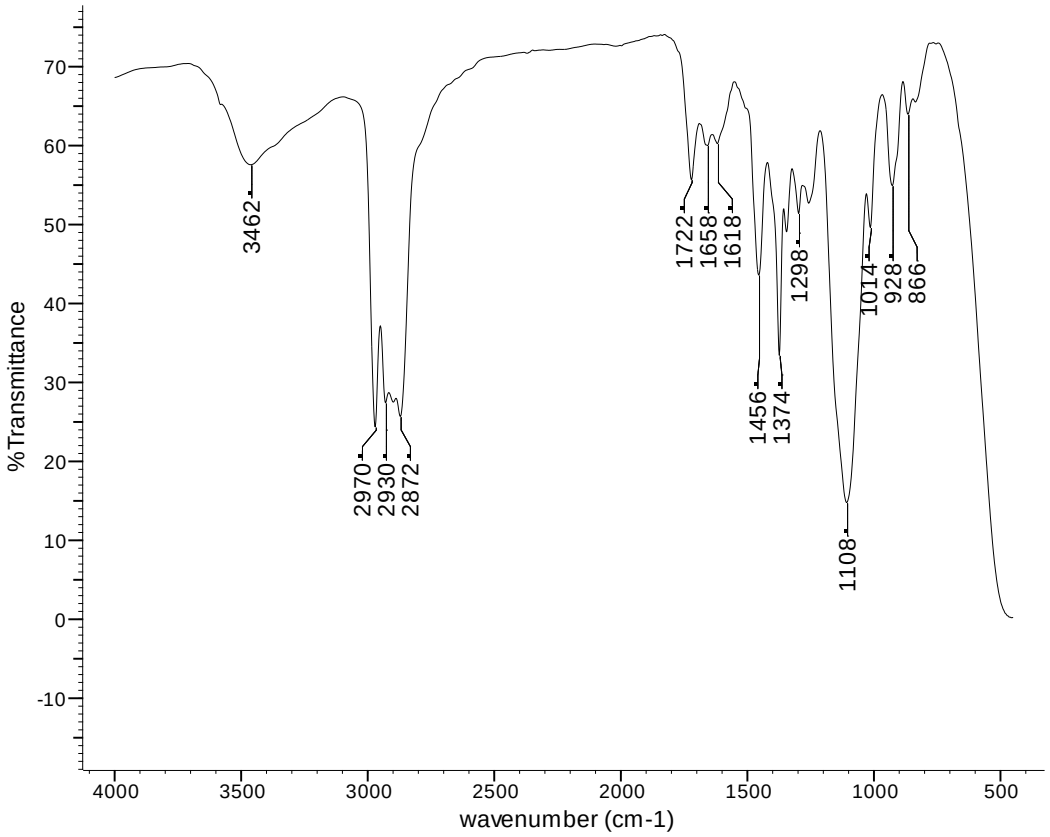

Figure 58: FTIR spectrum of the tar extracted at 350°C under air

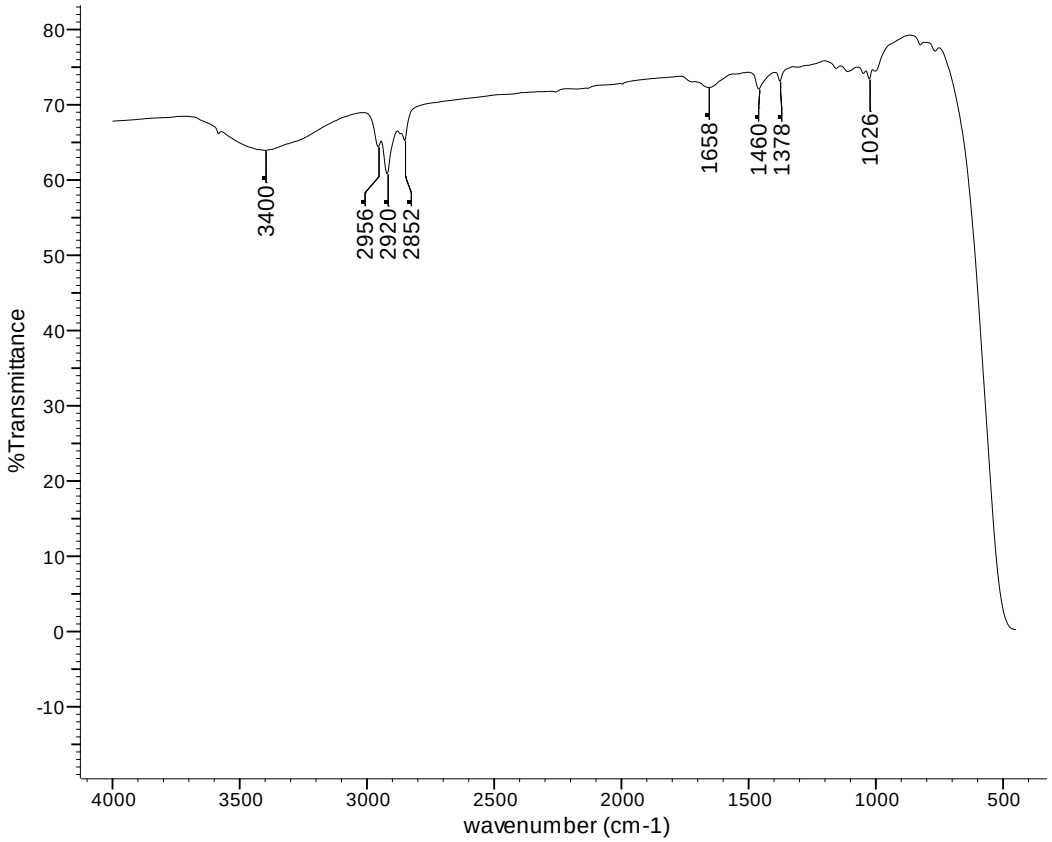

Figure 59: FTIR spectrum of the tar extracted at 400°C under air

1.4 Pyrolysis under 3% Oxygen in Nitrogen

1.4.1 Cold-ring fractions

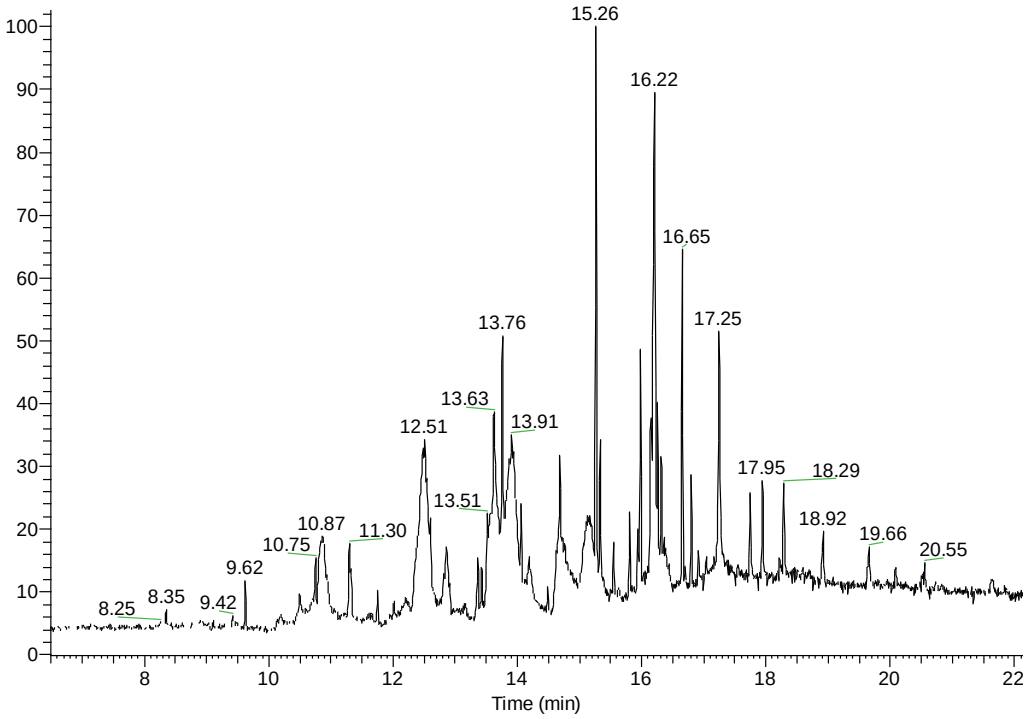

Figure 60: GC-MS chromatogram of the cold-ring fraction collected at 250°C under 3% O_2 in nitrogen

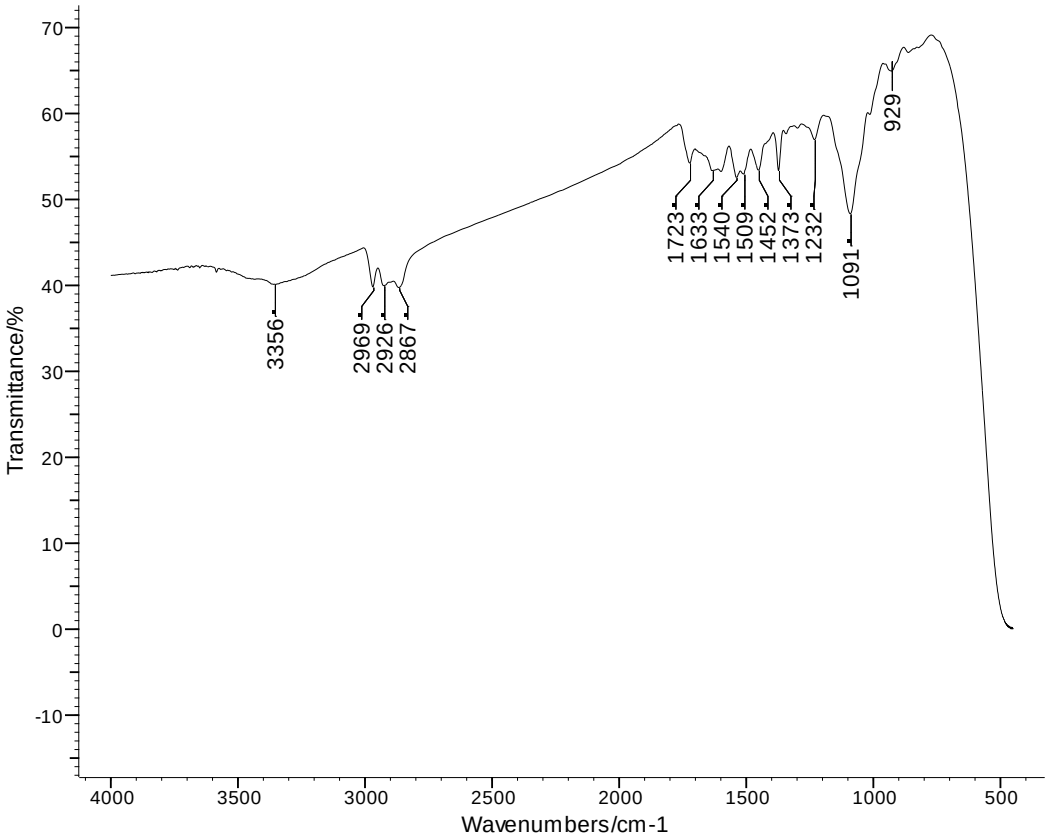

Figure 61: FTIR spectrum of the cold-ring fraction collected at 300°C under 3%O2 in nitrogen

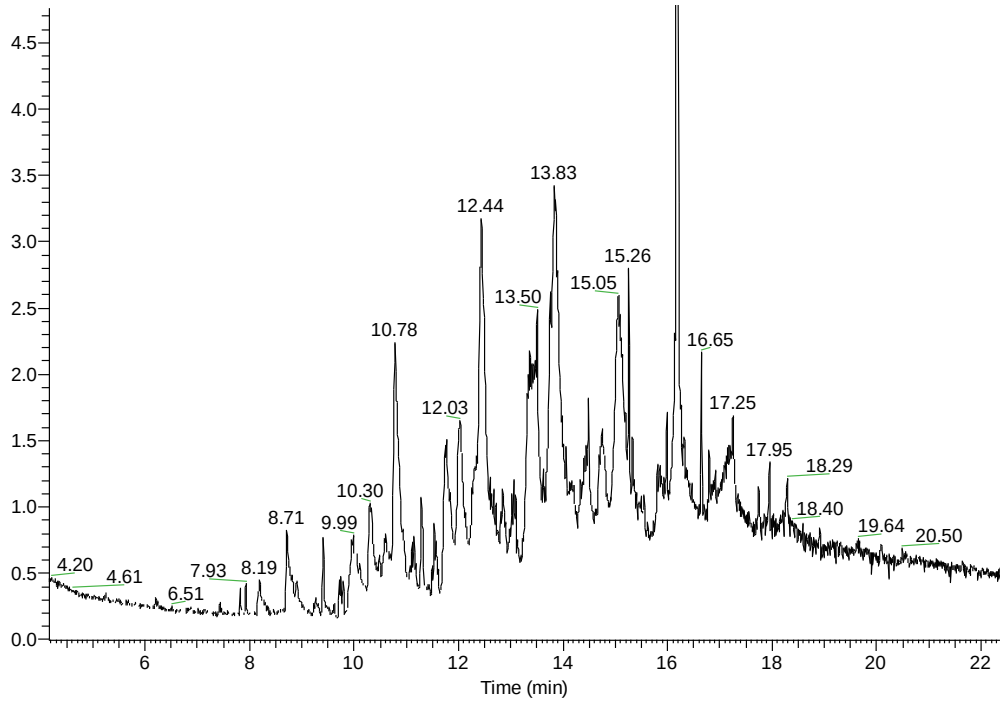

Figure 62: GC-MS chromatogram of the cold-ring fraction collected at 300°C under 3%O_2 in nitrogen

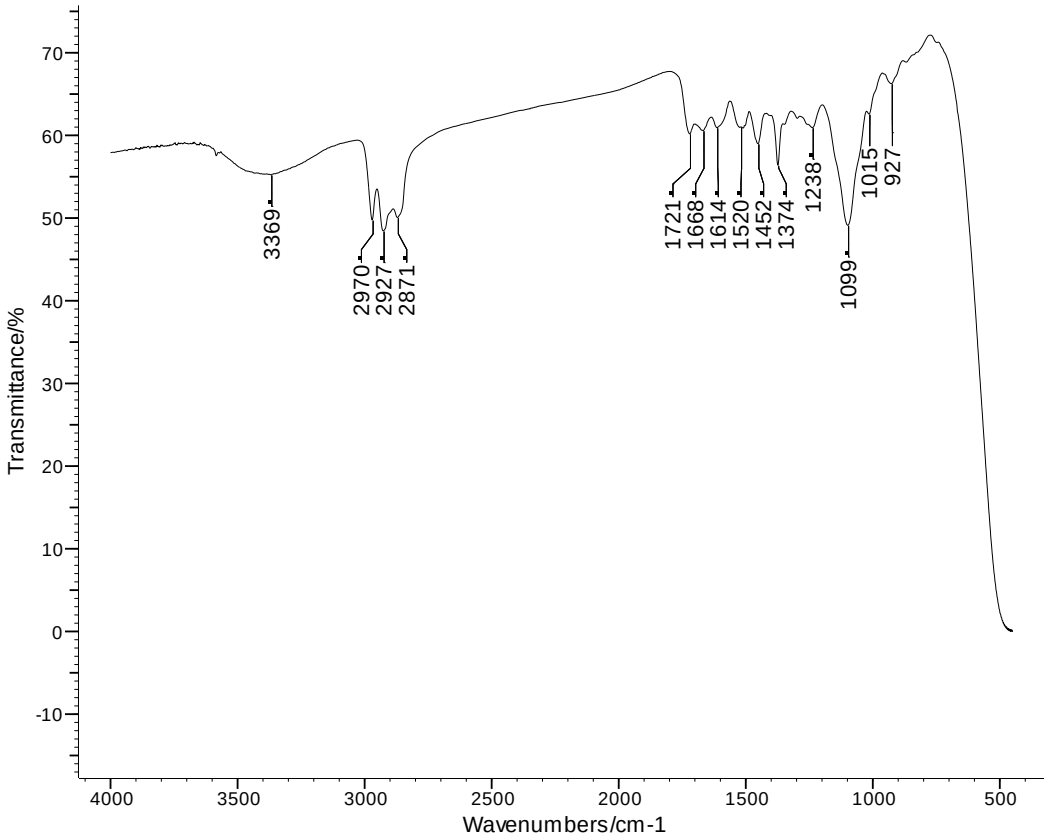

Figure 63: FTIR spectrum of the cold-ring fraction collected at 350°C under 3%O_2 in nitrogen

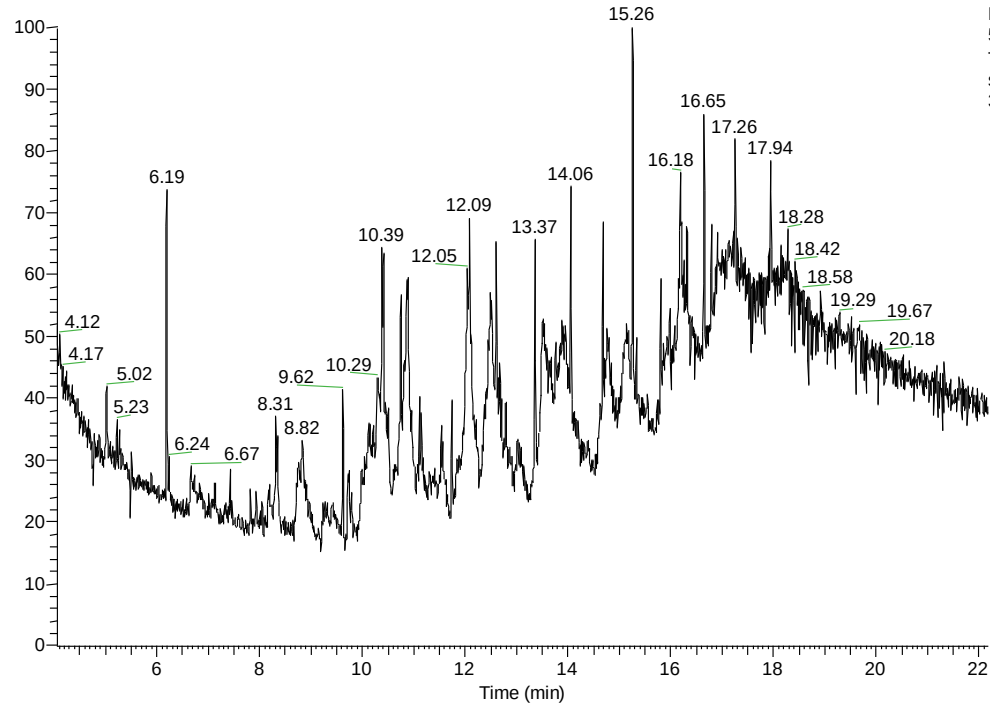

Figure 64: GC-MS chromatogram of the cold-ring fraction collected at 350°C under 3%O_2 in nitrogen

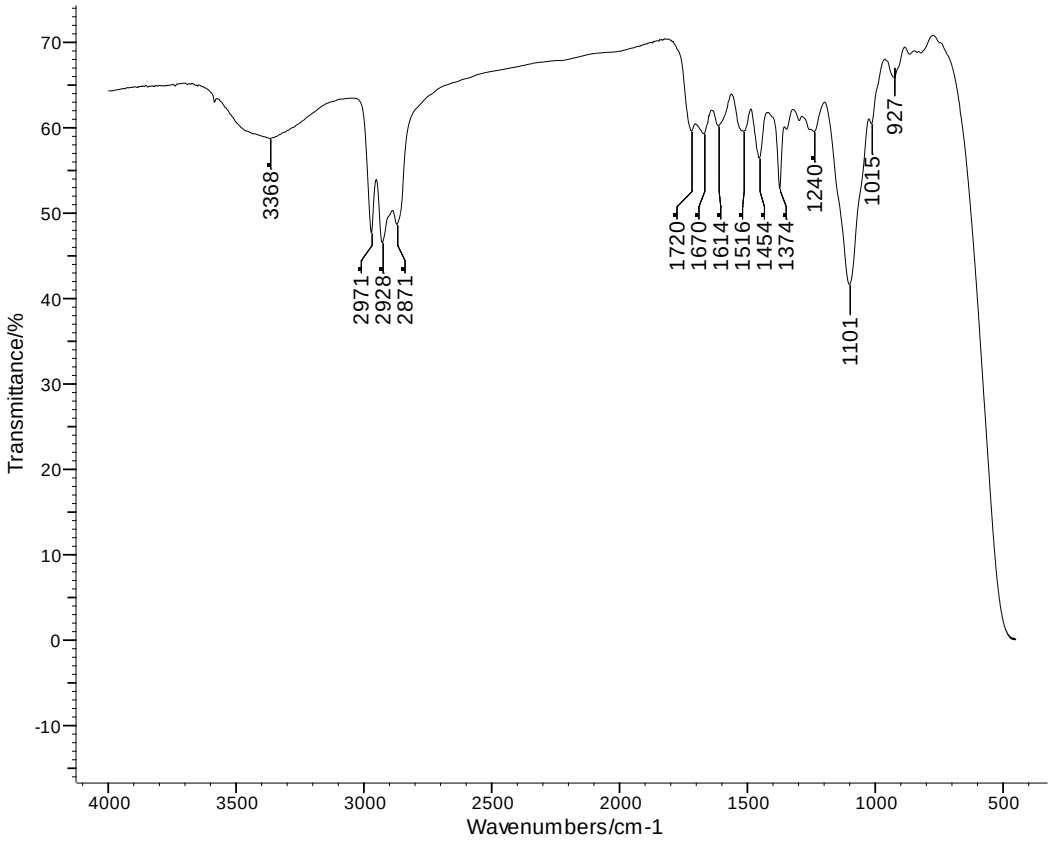

Figure 65:FTIR spectrum of the cold-ring fraction collected at 400°C under 3%O_2 under nitrogen

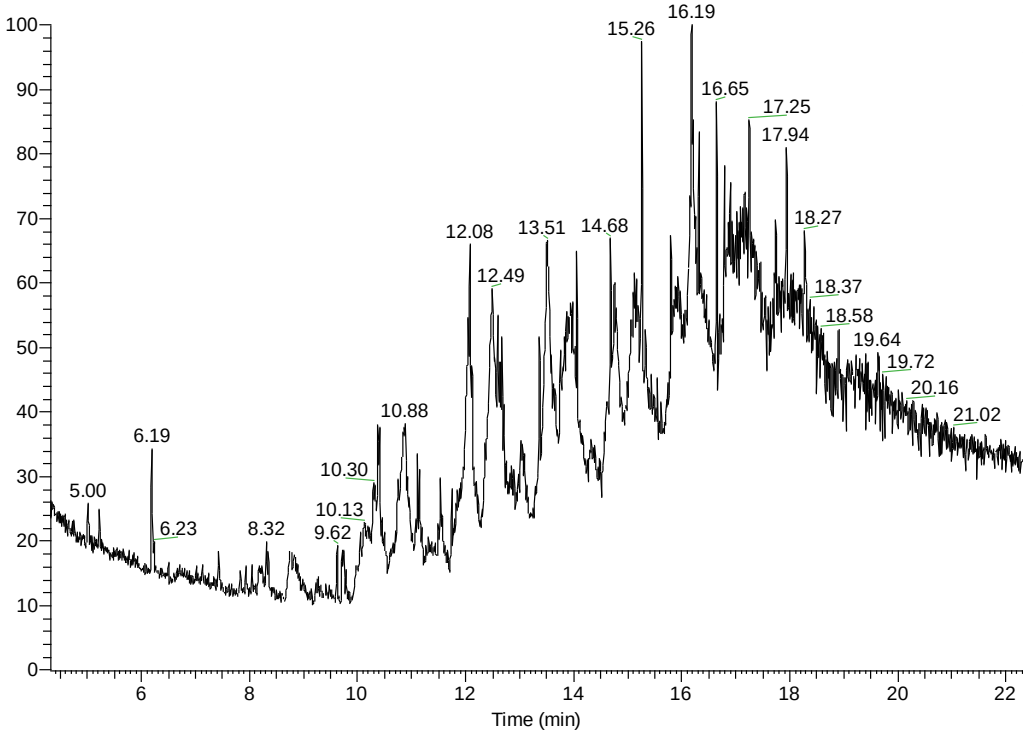

Figure 66: GC-MS chromatogram of the cold-ring fraction collected at 400°C under 3 %O_2 in nitrogen

1.4.2 Tars

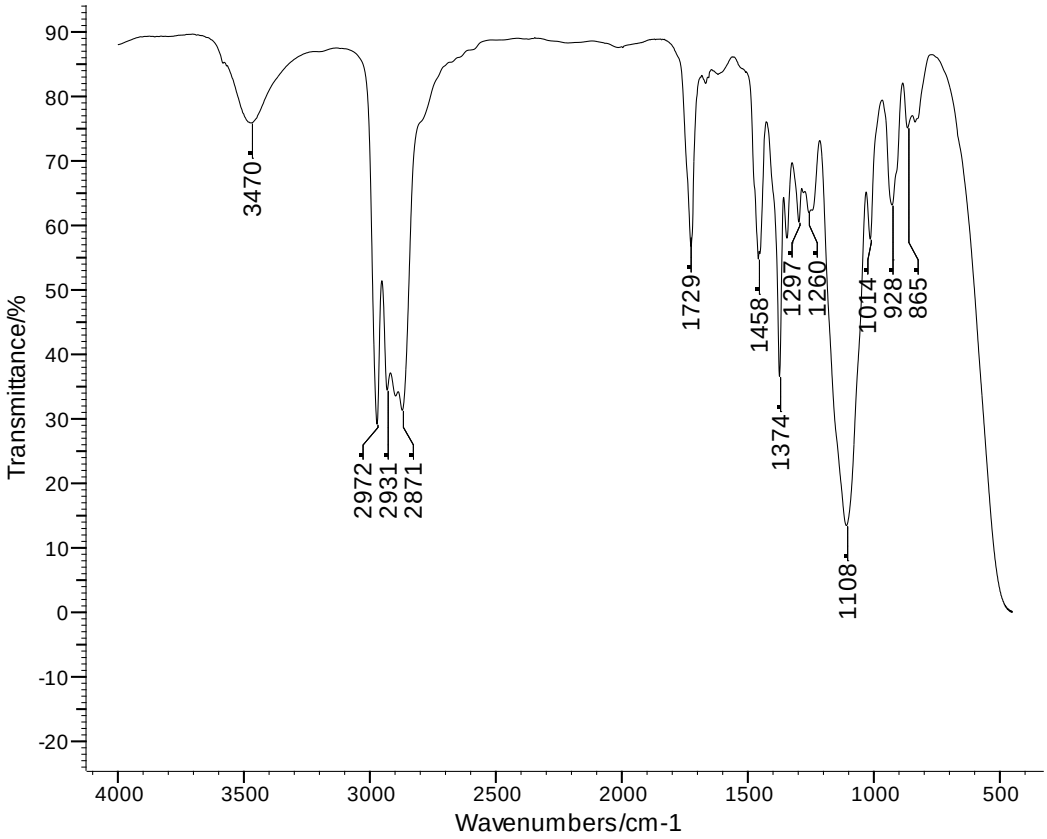

Figure 67: FTIR spectrum of the tar extracted at 300°C under 3%O_2 in nitrogen

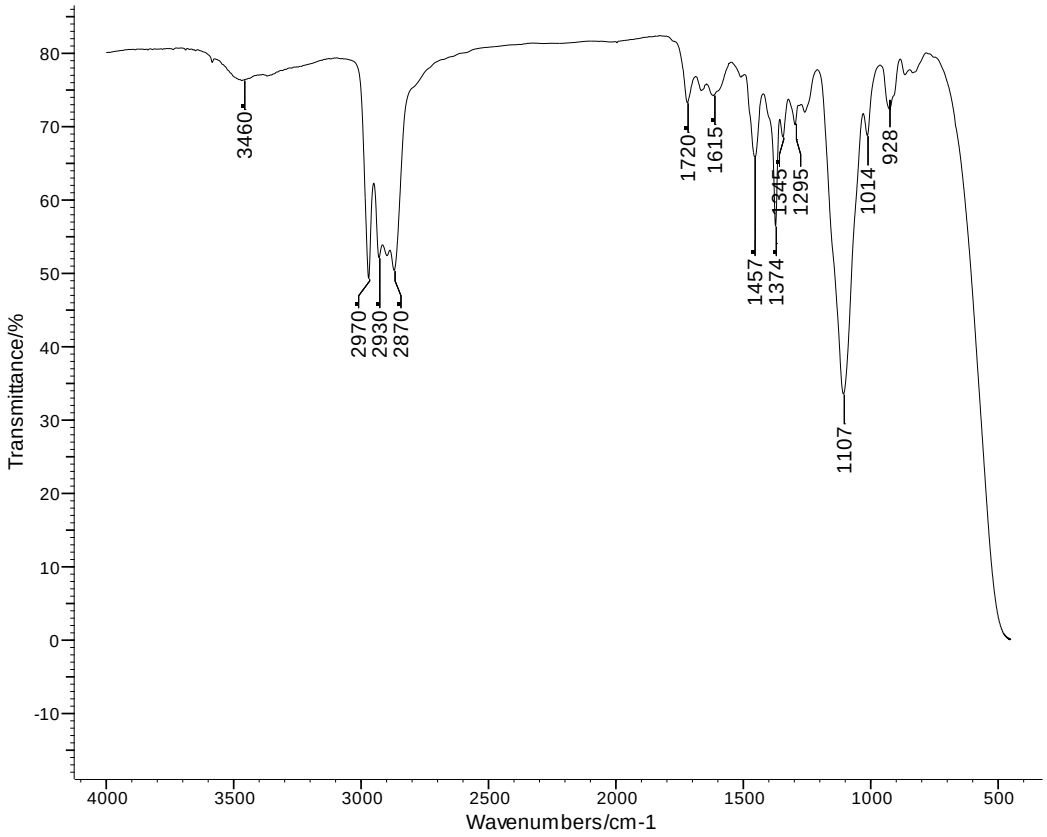

Figure 68: FTIR spectrum of the tar extracted at 350°C under 3%O_2 in nitrogen

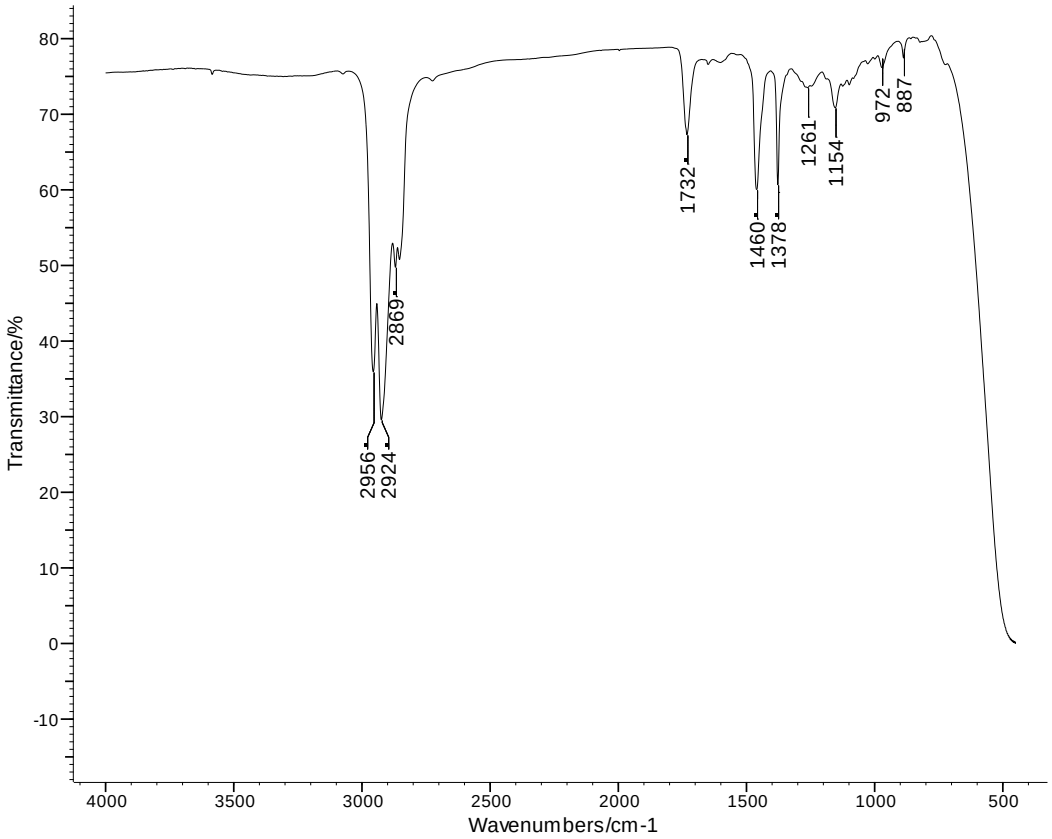

Figure 69: FTIR spectrum of the tar extracted at 400°C under 3%O_2 in nitrogen

1.4.3 ^{13}C Solid state NMR

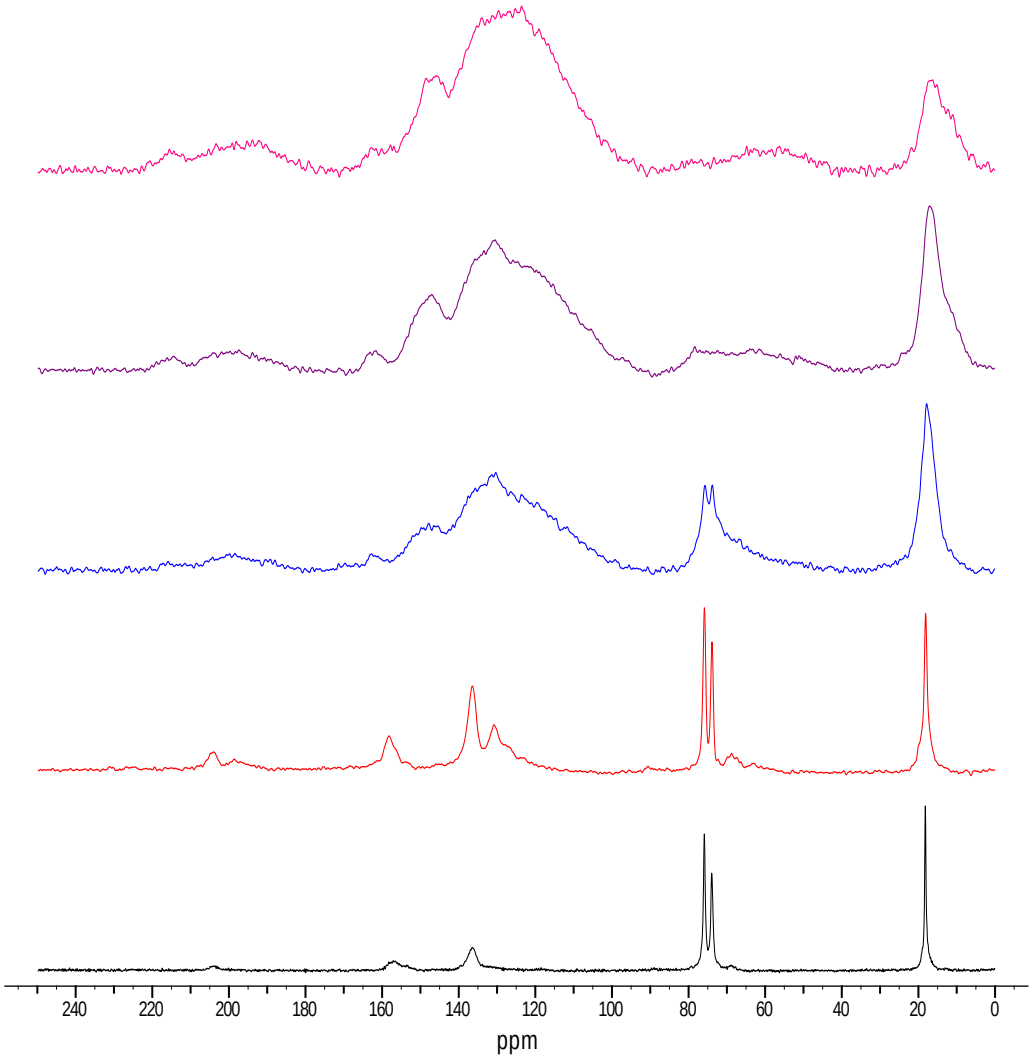

Figure 70: Comparison of the ^{13}C CPMAS dipolar dephased spectra of the virgin foam (black) with the chars obtained after pyrolysis under 3% oxygen in nitrogen at 250°C (red), 300°C (blue), 350°C (purple) and 400°C (pink)

Appendix 2 –APP Foam

2.1. DSC Repeat Analyses

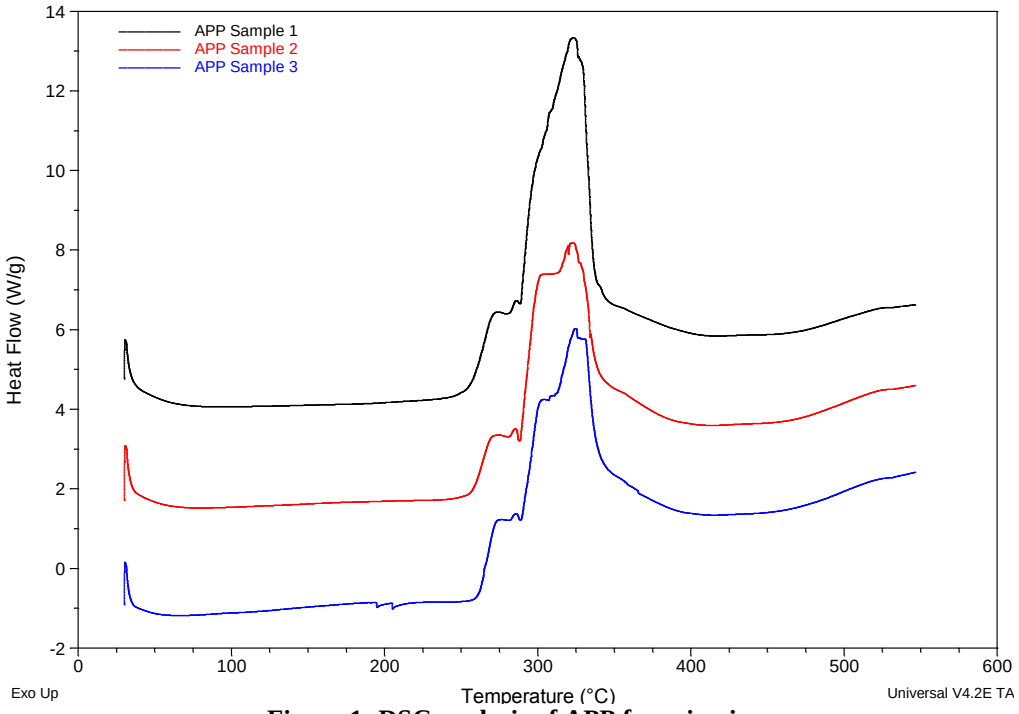

Figure 1: DSC analysis of APP foam in air

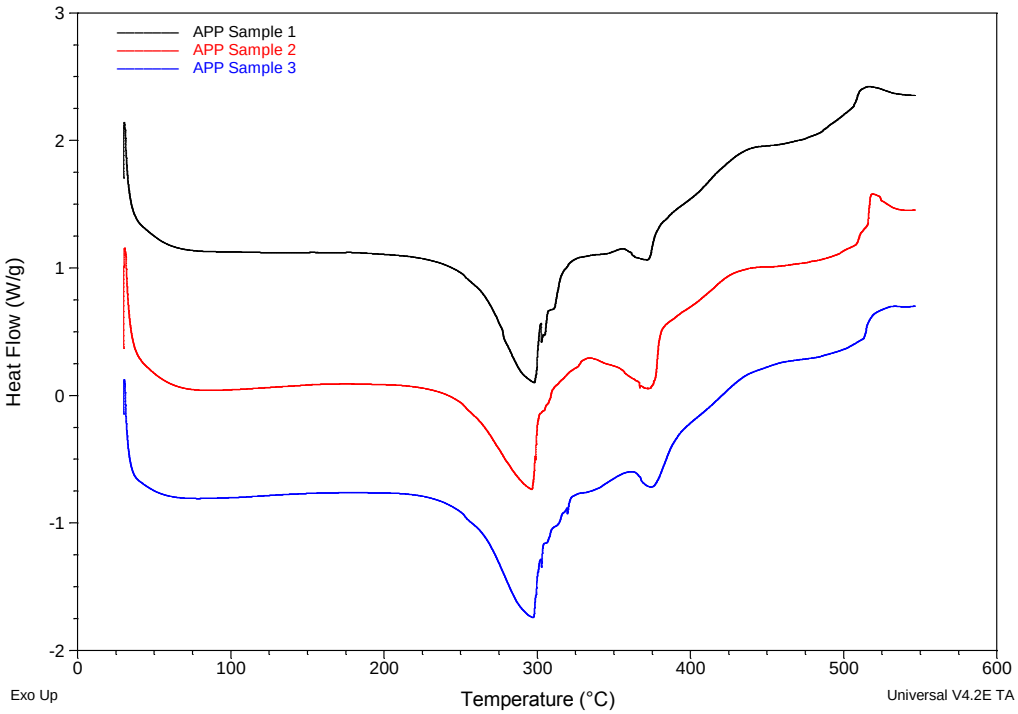

Figure 2: DSC analysis of APP foam in N_2

2.2 Dynamic TVA Study

2.2.1 Non-condensables

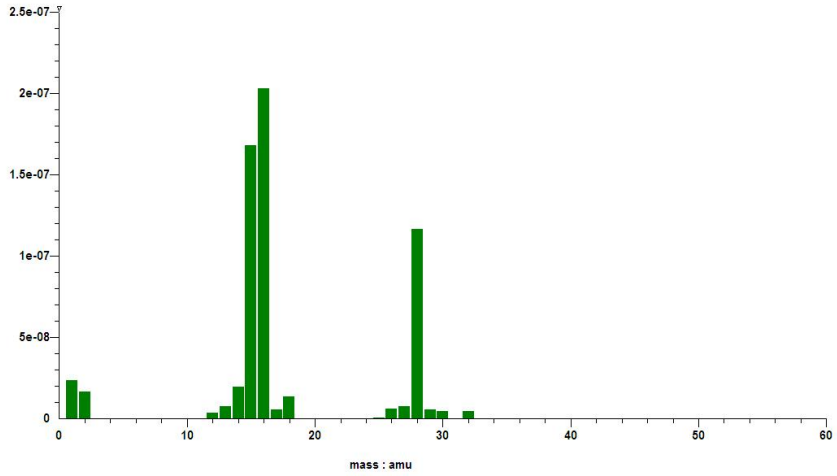

Figure 3: MS of the non-condensable volatiles from the APP foam

2.2.2 Cold-ring Fraction

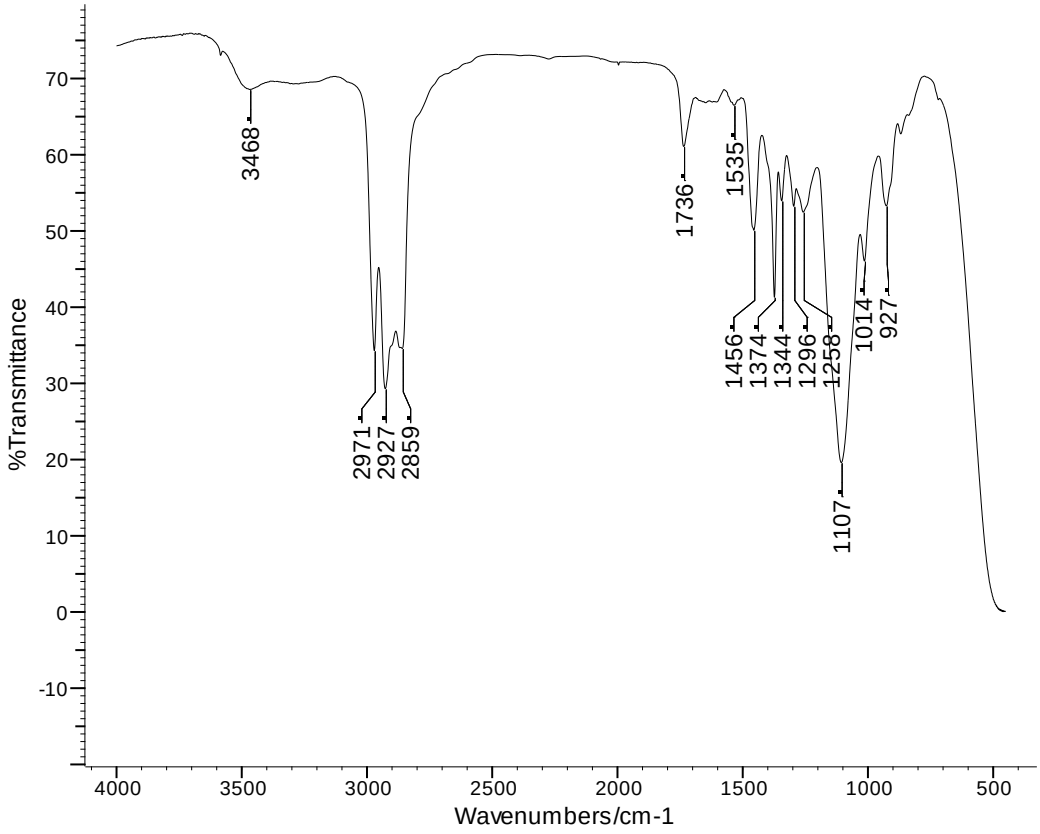

Figure 4: FTIR spectrum of the cold-ring fraction collected from the APP foam

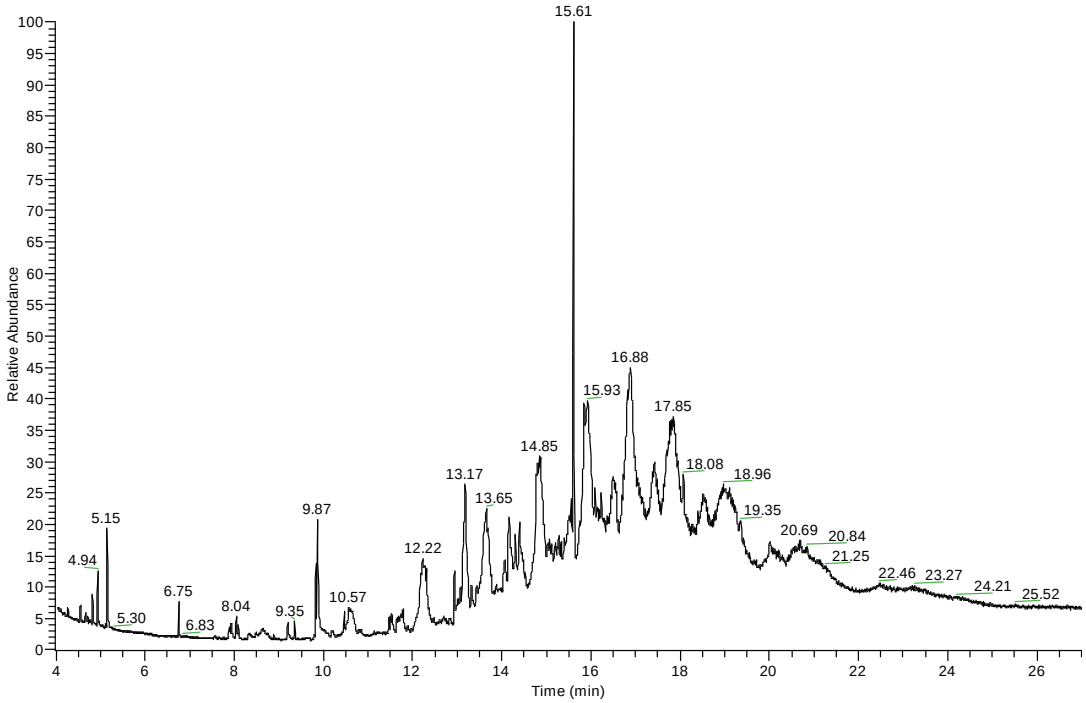

Figure 5: GC-MS total-ion chromatogram for the cold-ring fraction collected from the APP foam

2.2.3 Condensable Fraction

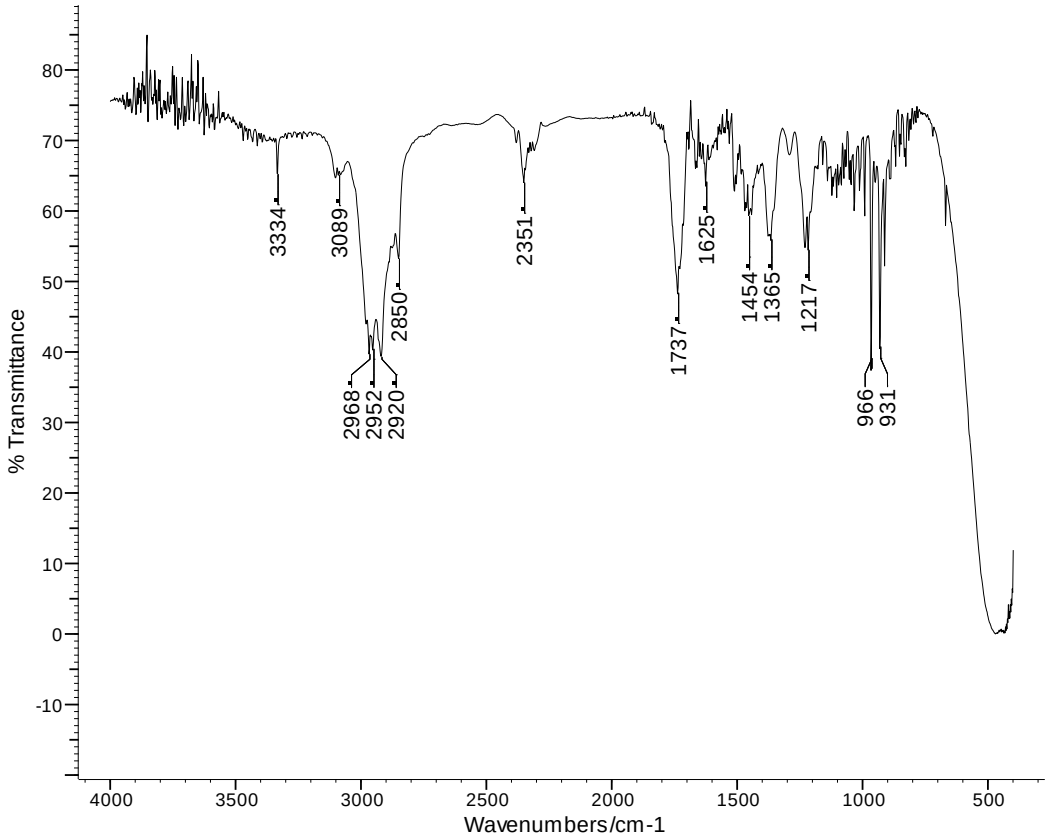

Figure 6: FTIR spectrum of fraction 1 from the APP foam

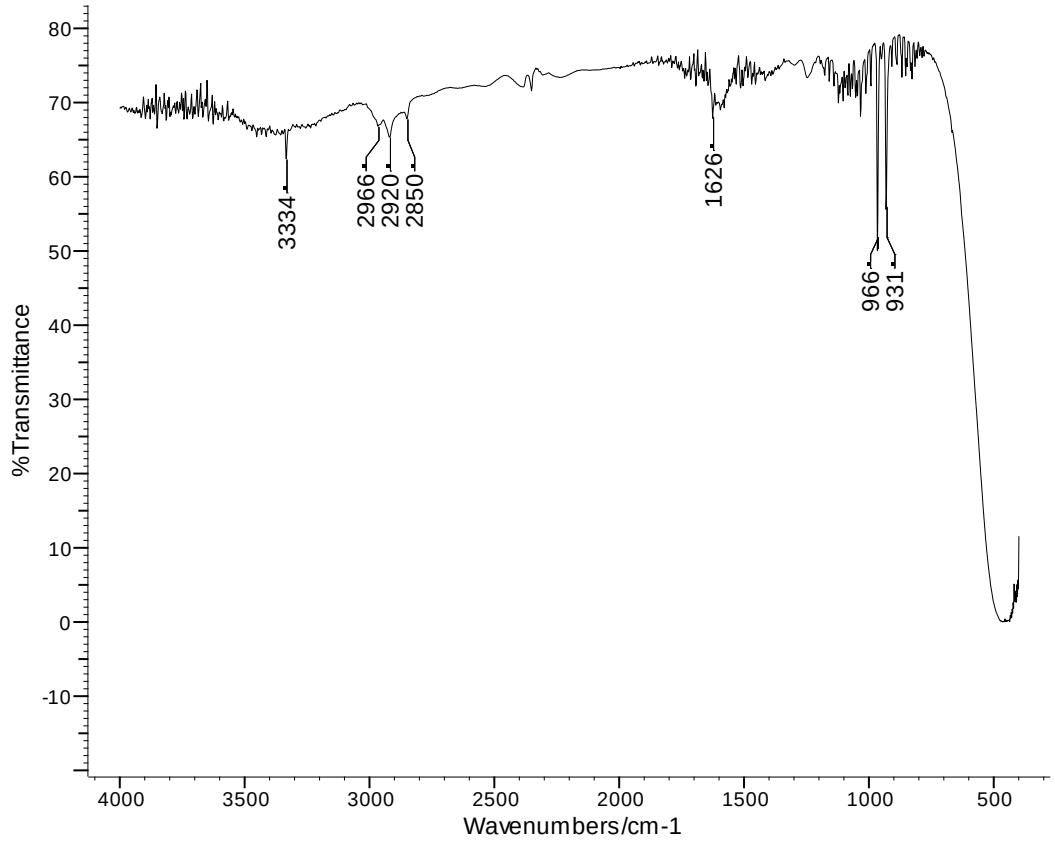

Figure 7: FTIR spectrum for fraction 2 collected from the APP foam

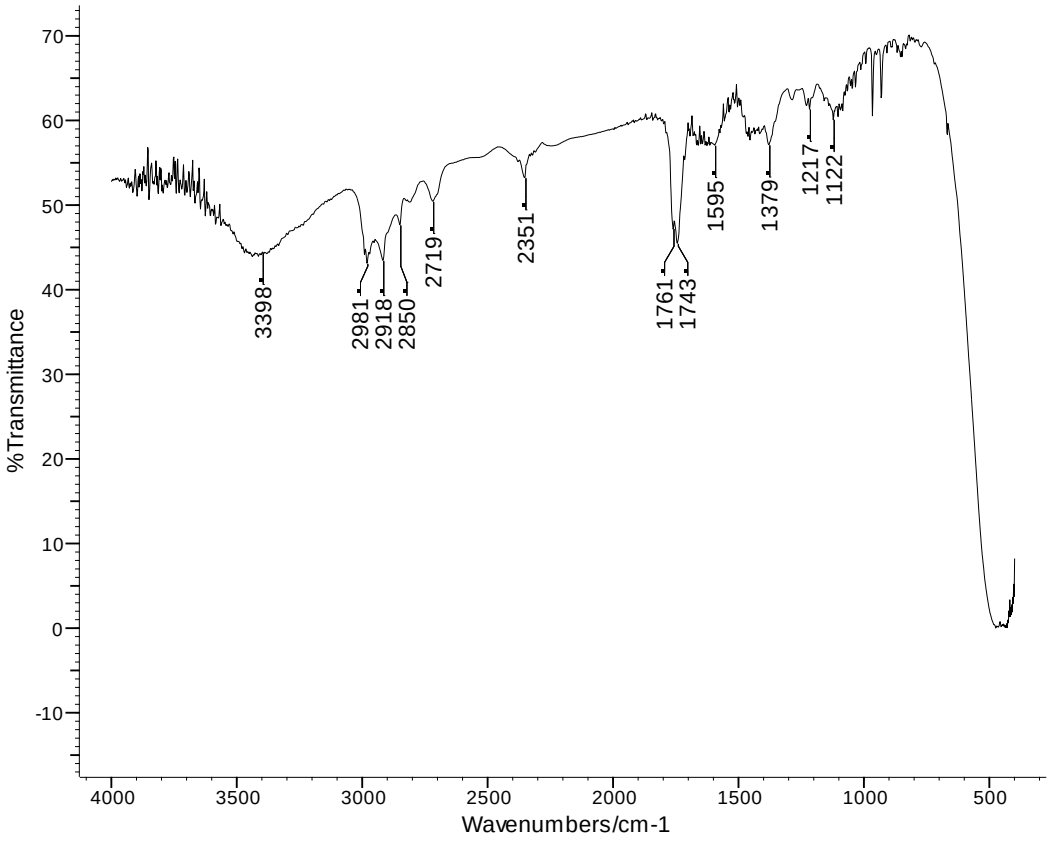

Figure 8: FTIR spectrum for fraction 3 collected from the APP foam

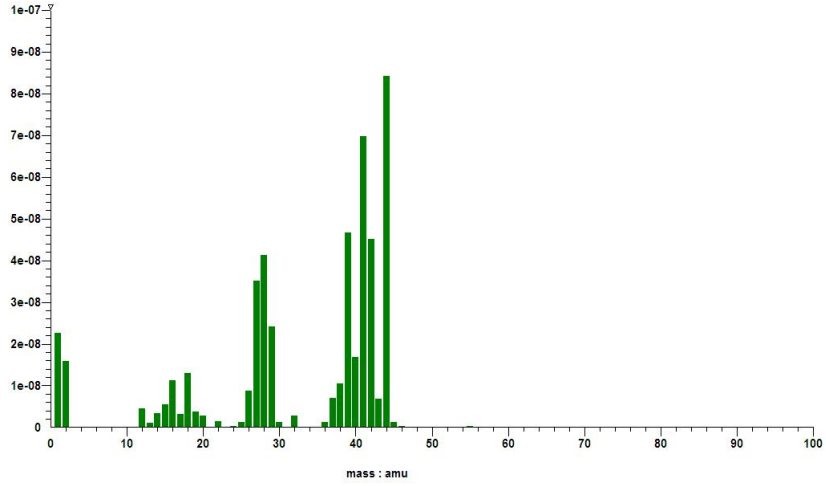

Figure 9: MS of propene and CO_2 collected from the APP foam

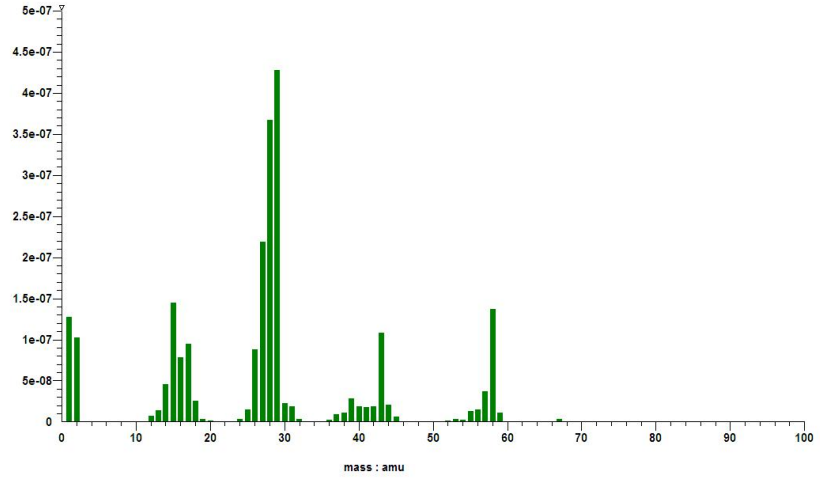

Figure 10:MS of propanal collected from the APP foam

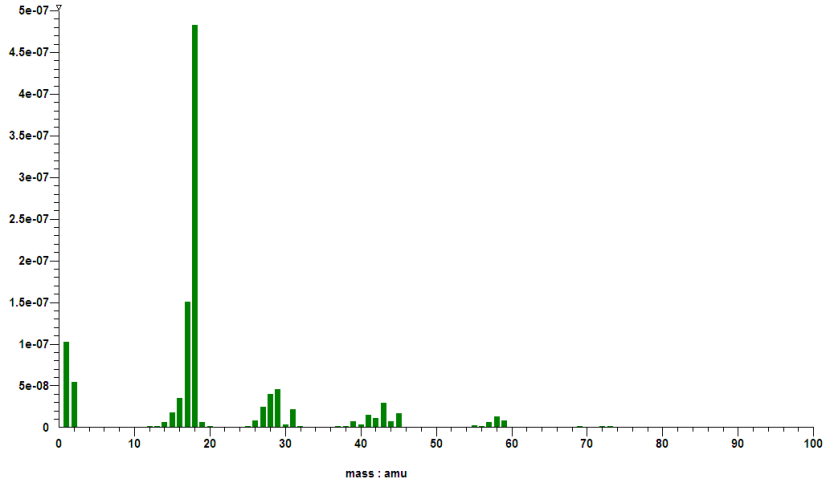

Figure 11: MS of water and high molar mass collected from the APP foam

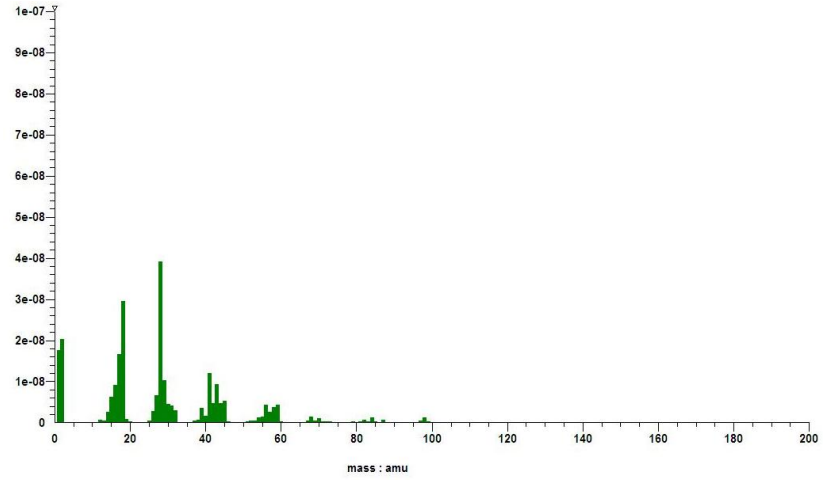

Figure 12: MS of high molar mass material collected from the APP foam

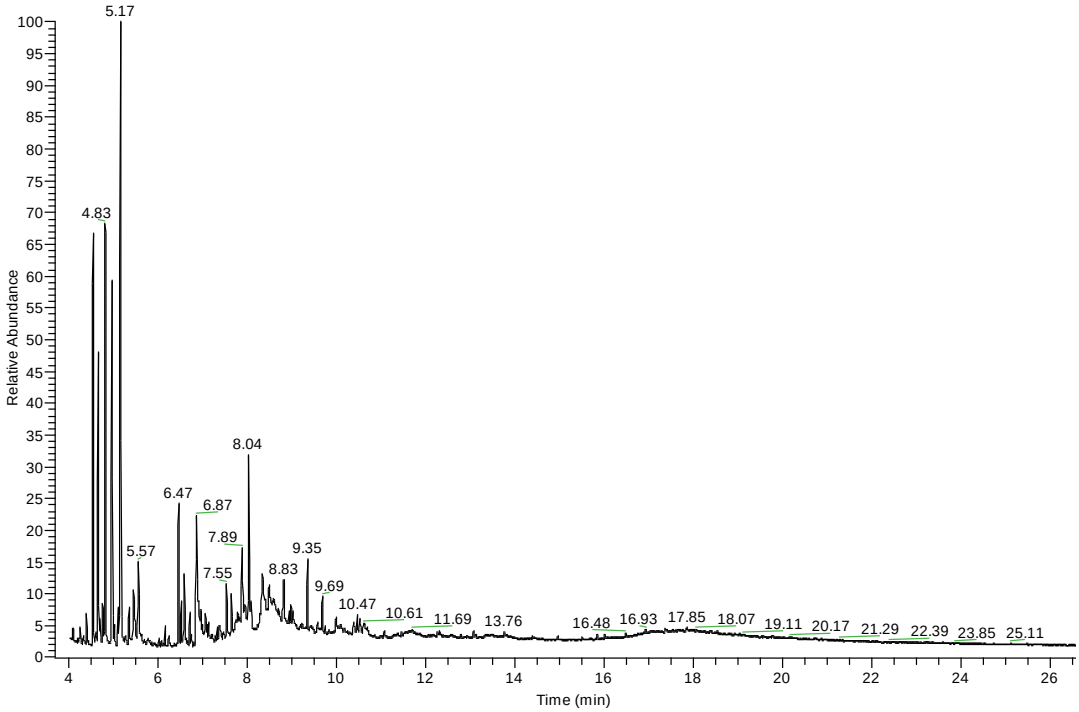

Figure 13: GC-MS chromatogram for fraction 3 from the APP foam

2.3 Isothermal TVA Study

2.3.1 Non-condensables

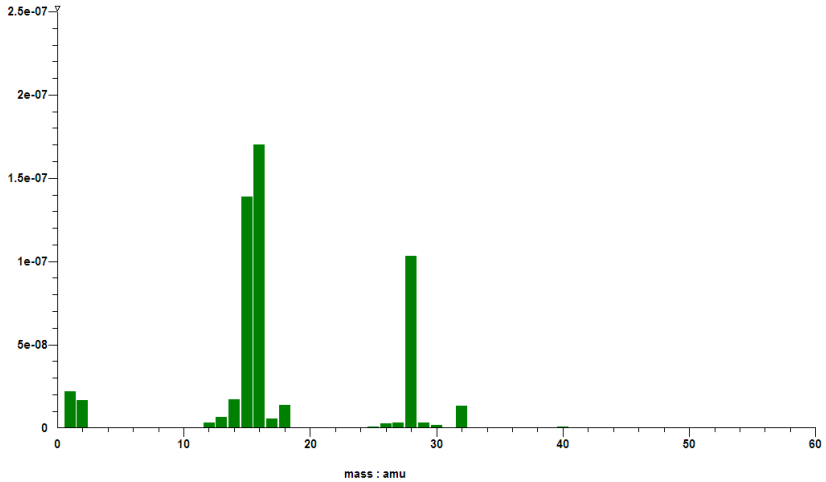

Figure 14:MS of the non-condensable volatiles from the APP foam at 350°C

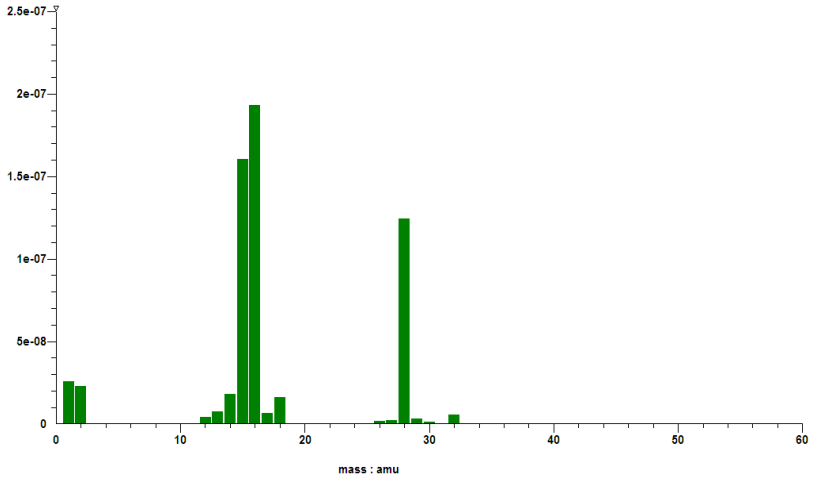

Figure 15: MS of the non-condensable volatiles from the APP foam at 400°C

2.3.2 Cold-ring Fractions

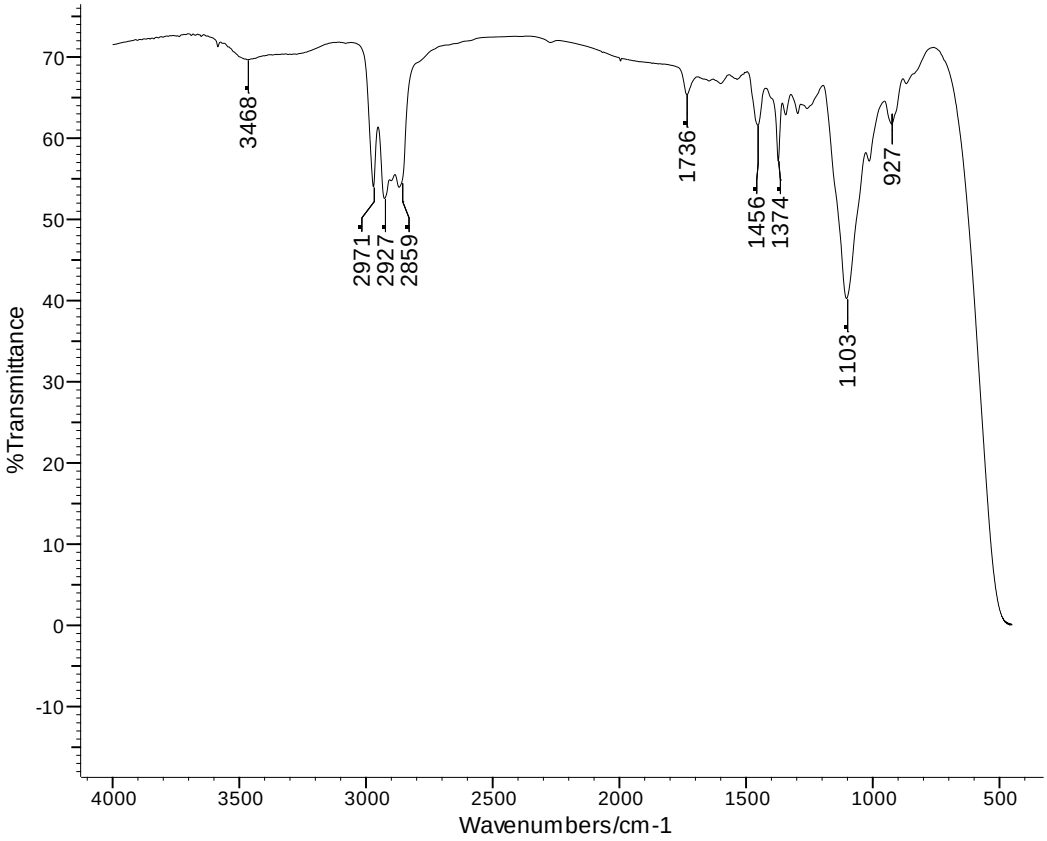

Figure 16: FTIR spectrum of the cold-ring fraction collected at 300°C

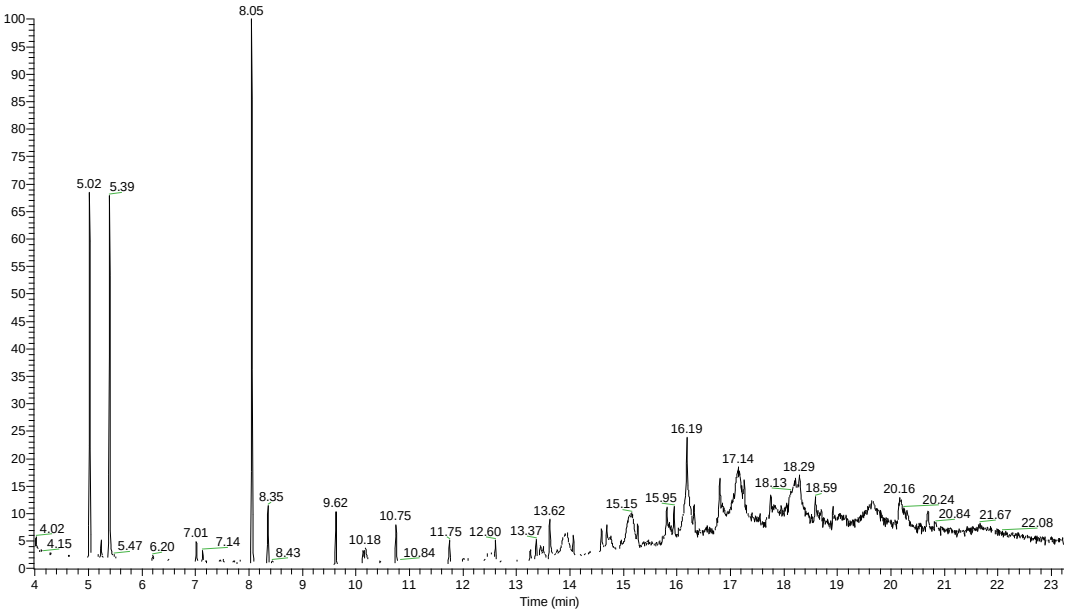

Figure 17: GC-MS chromatogram of the cold-ring fraction collected at 300°C

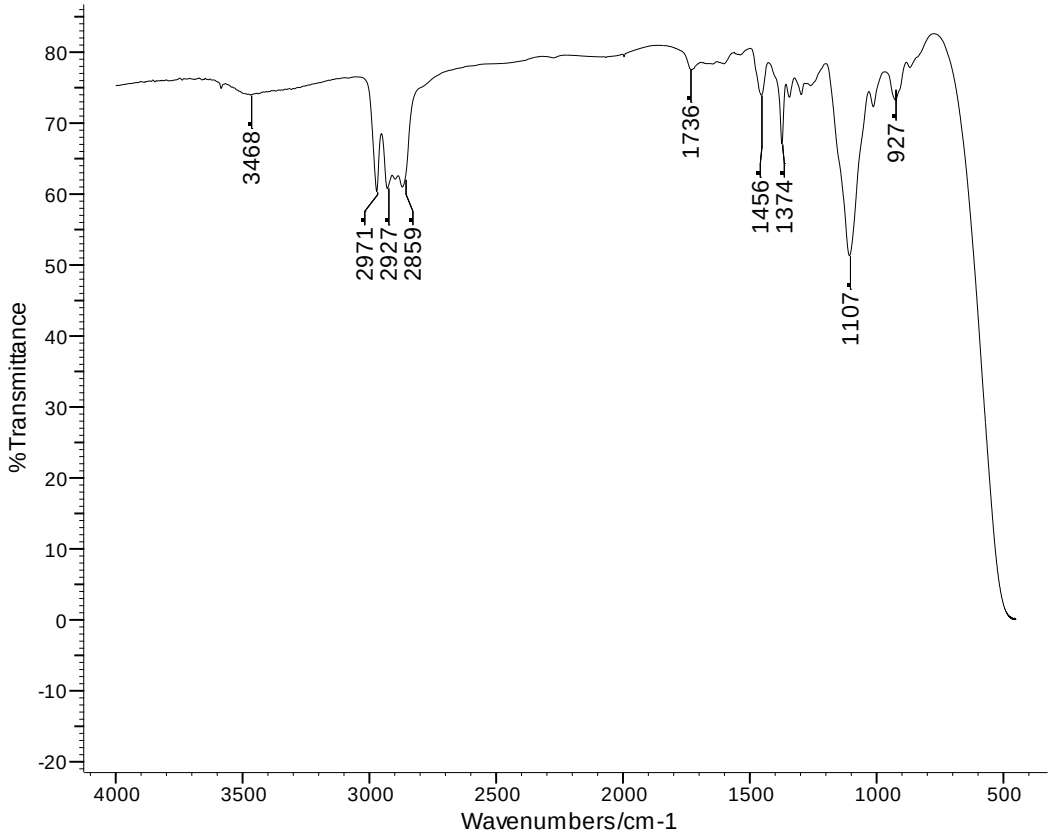

Figure 18: FTIR spectrum of the cold-ring fraction at 350°C

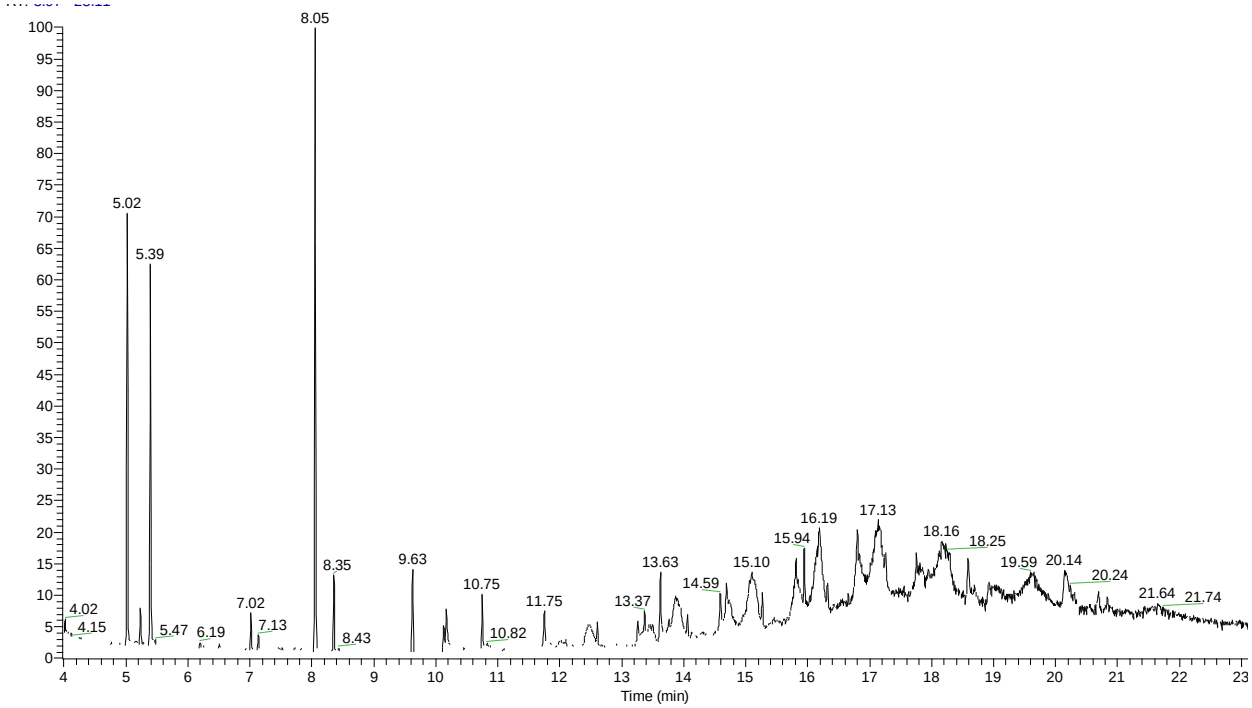

Figure 19: GC-MS chromatogram of the cold-ring fraction collected at 350°C

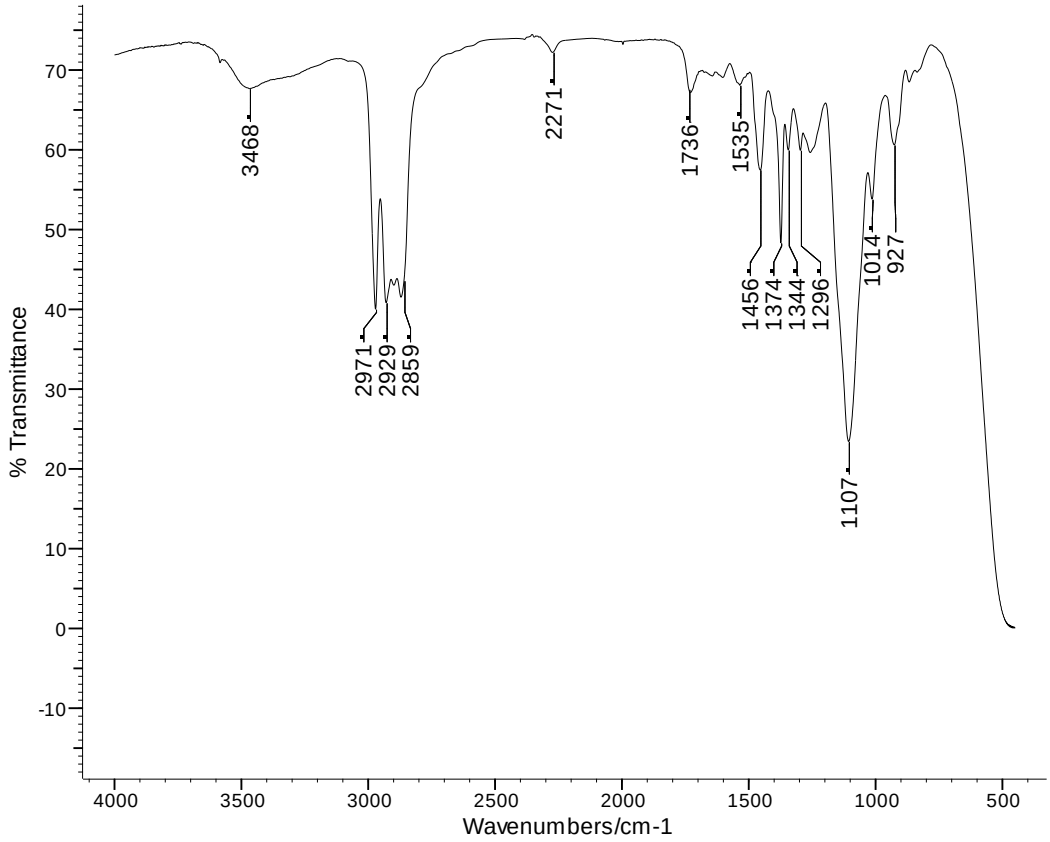

Figure 20: FTIR spectrum of the cold-ring fraction collected at 400°C

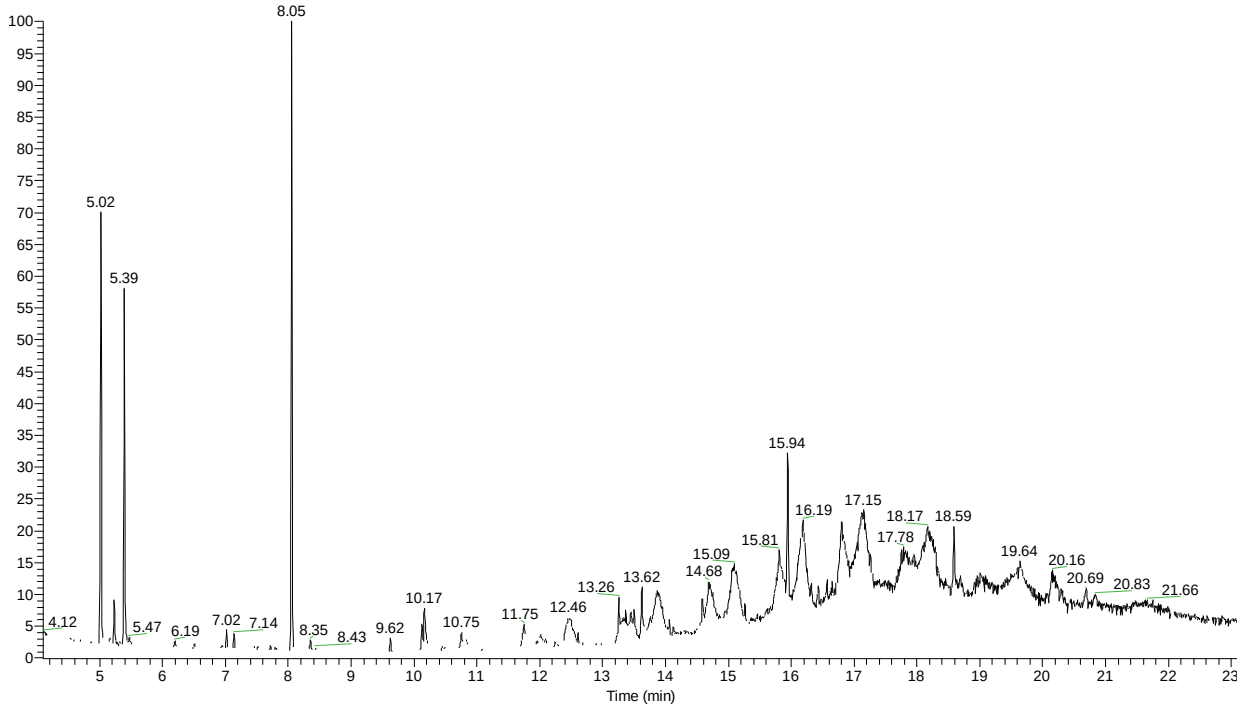

Figure 21: GC-MS chromatogram of the cold-ring fraction collected at 400°C

2.3.3 Residue

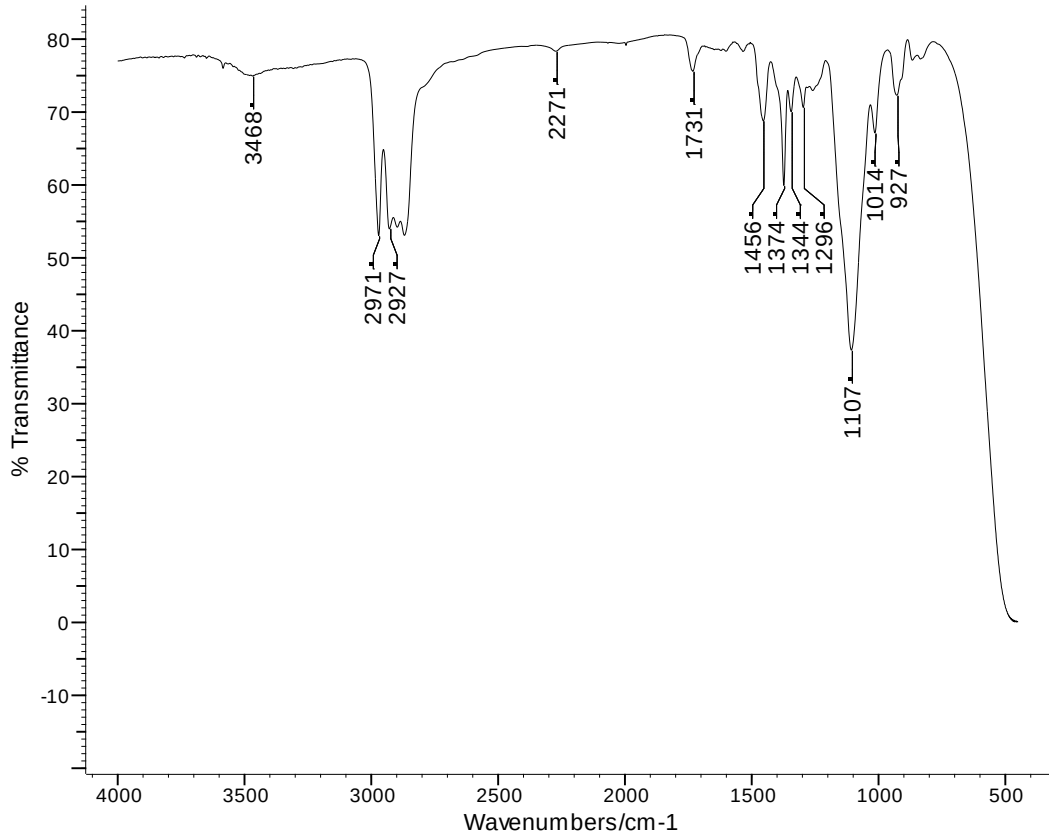

Figure 22: FTIR spectrum of the residue at 250°C

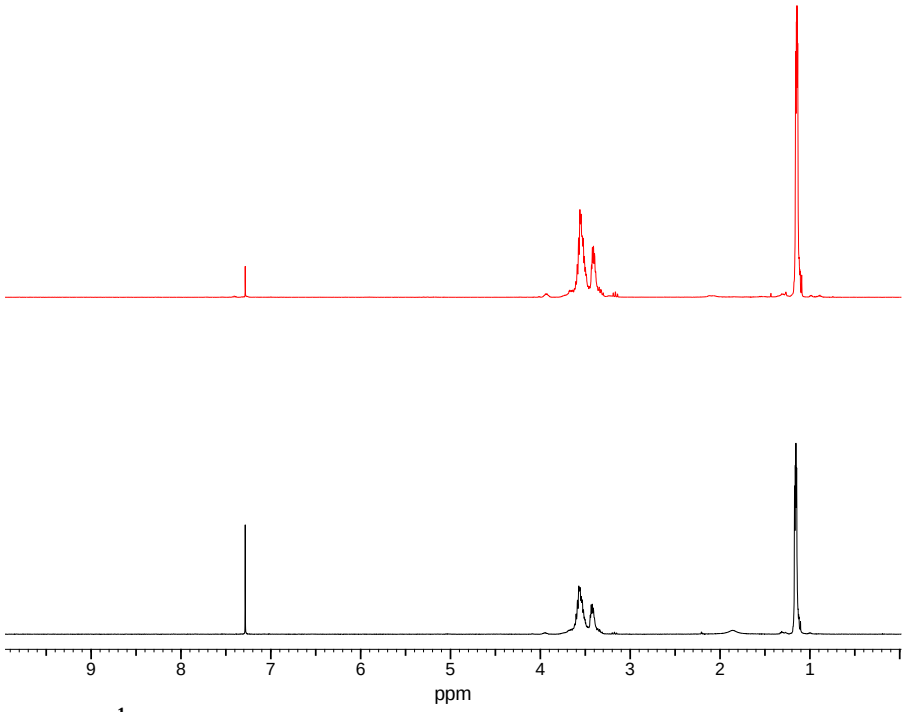

Figure 23: ^{1}H NMR spectrum of the residue at 250°C (black) and the polyol (red)

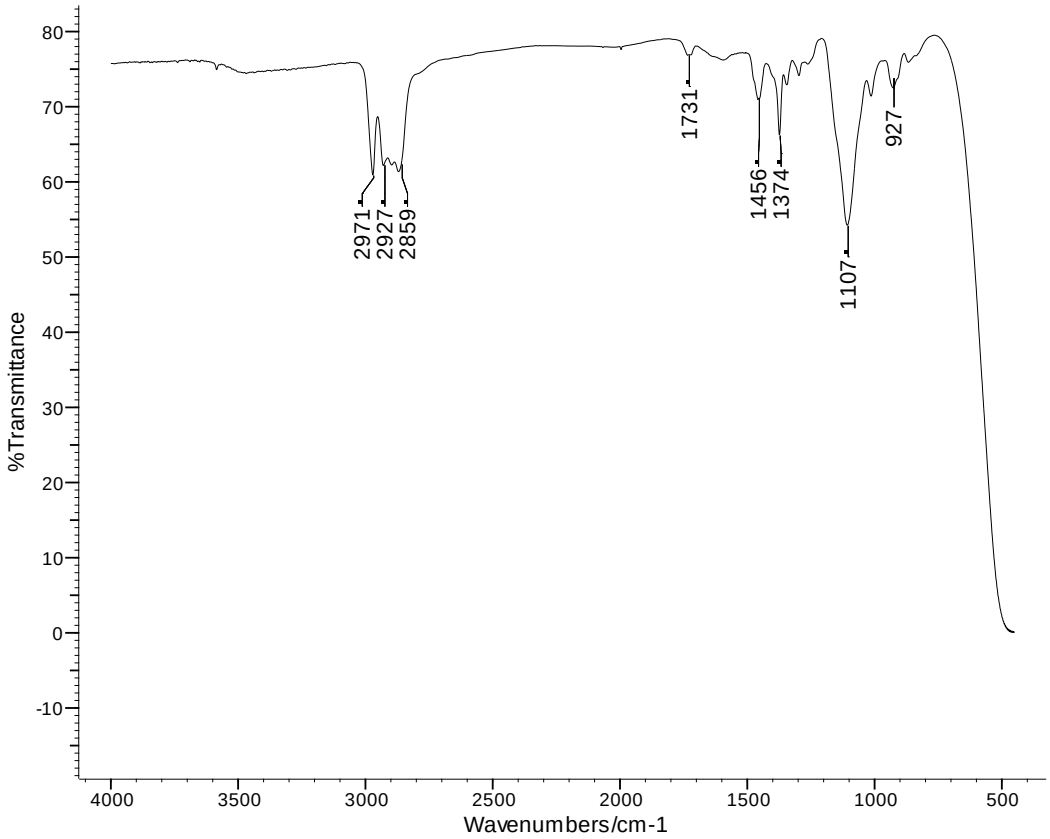

Figure 24: FTIR spectrum of the reside at 300°C

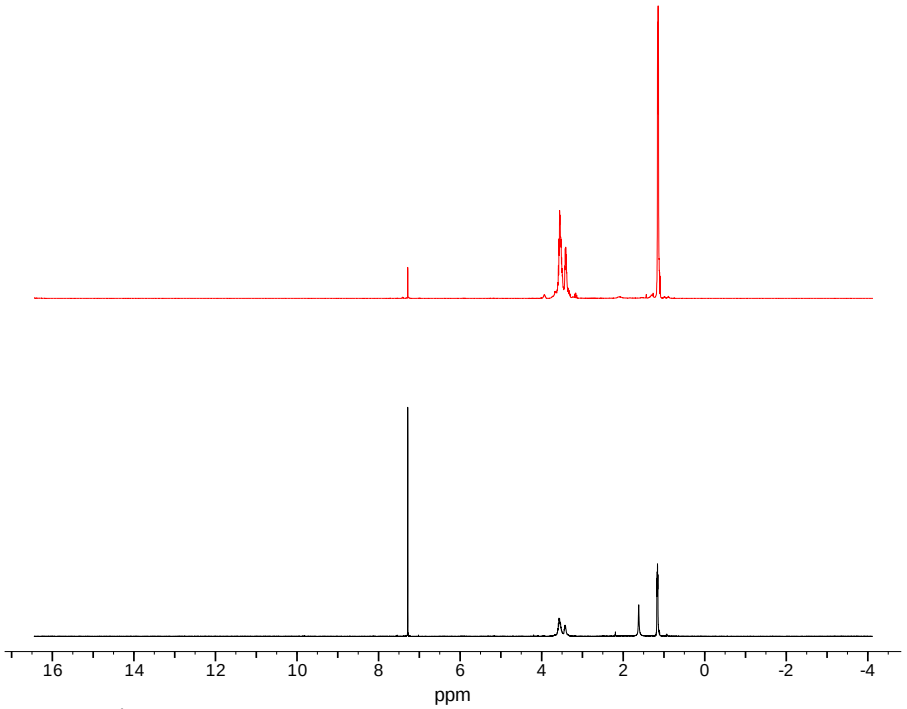

Figure 25: ^{1}H NMR spectrum of the residue at 300°C (black) and the polyol (red)

2.3.4 Condensable fraction

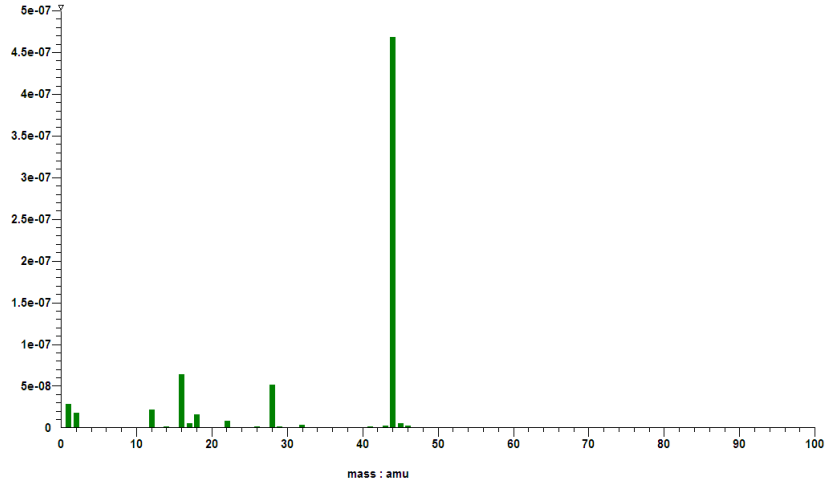

Figure 26: MS of CO_2 collected at 250°C

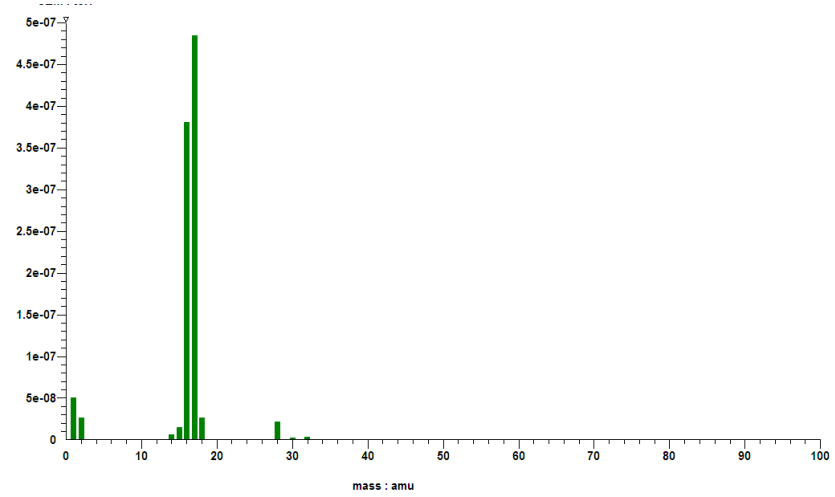

Figure 27: MS of ammonia collected at 250°C

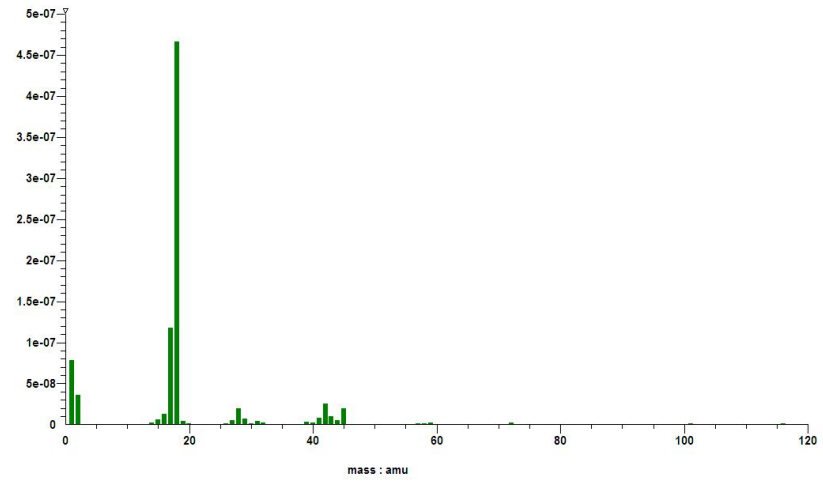

Figure 28: MS of water and higher molar mass collected at 250°C

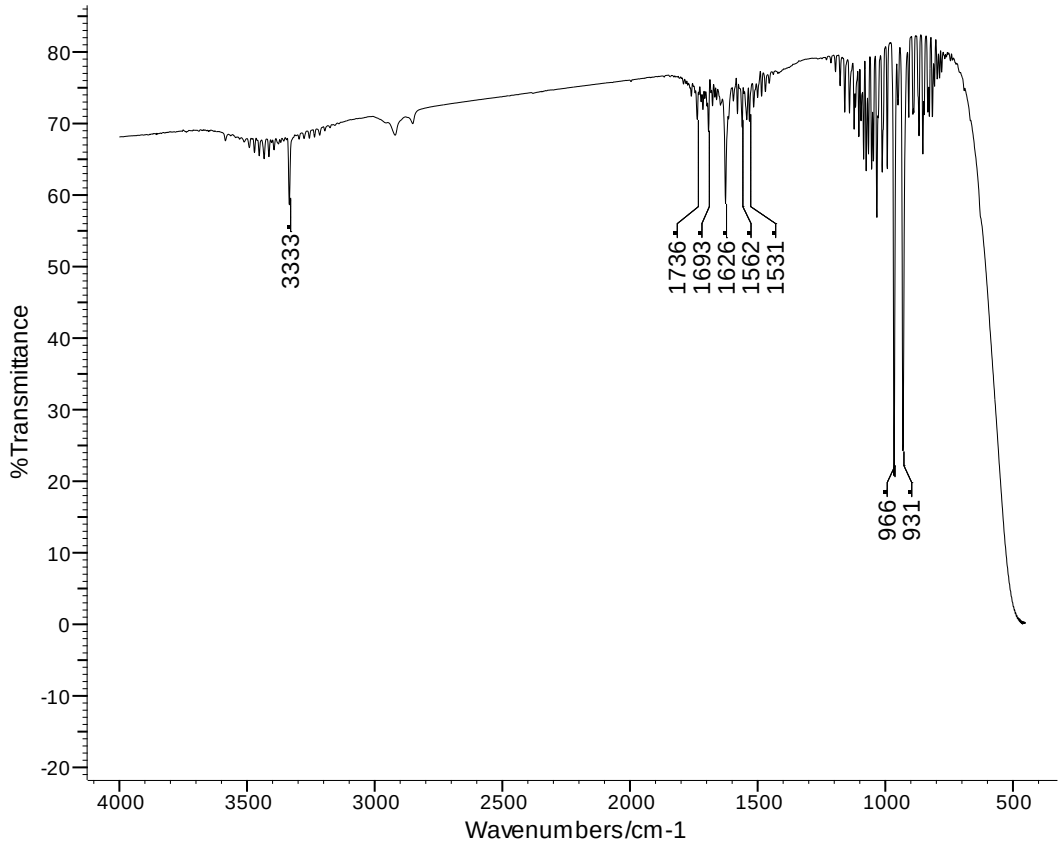

Figure 29: FTIR spectrum of fraction 2 at 250°C

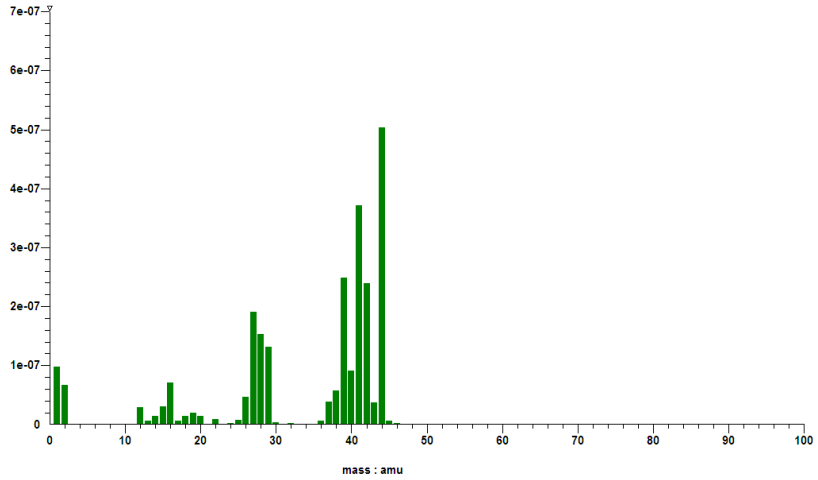

Figure 30: MS of propene and CO_2 collected at 300°C

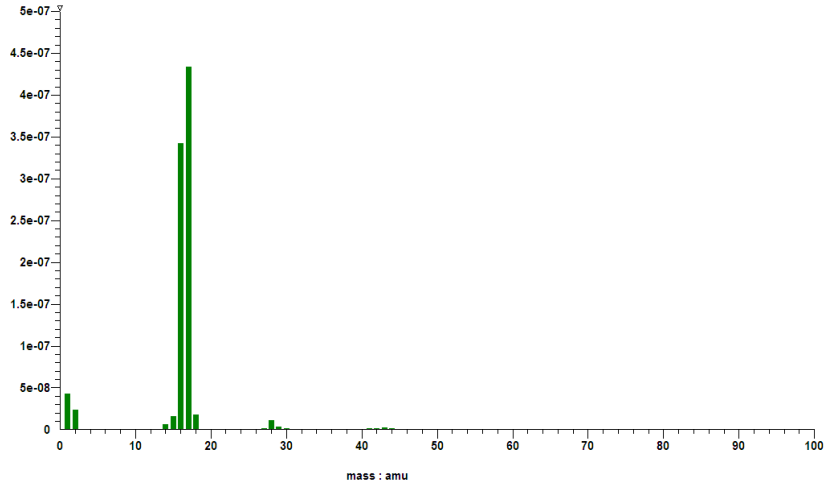

Figure 31: MS of ammonia collected at 300°C

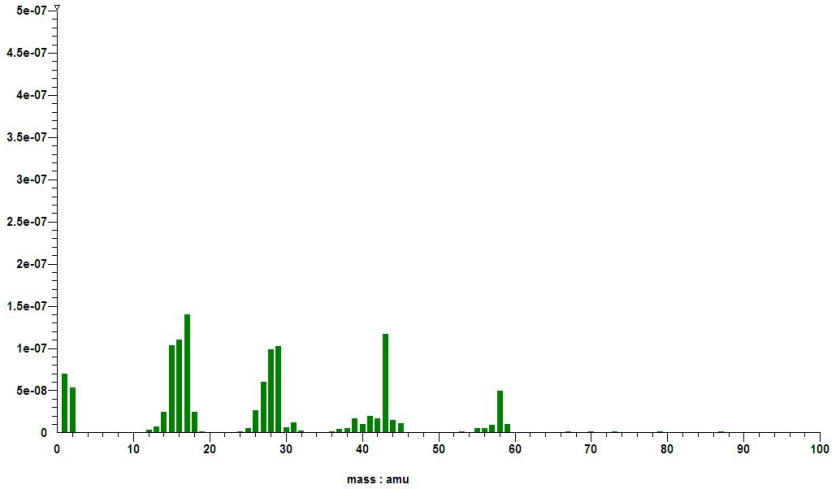

Figure 32: MS of propanal collected at 300°C

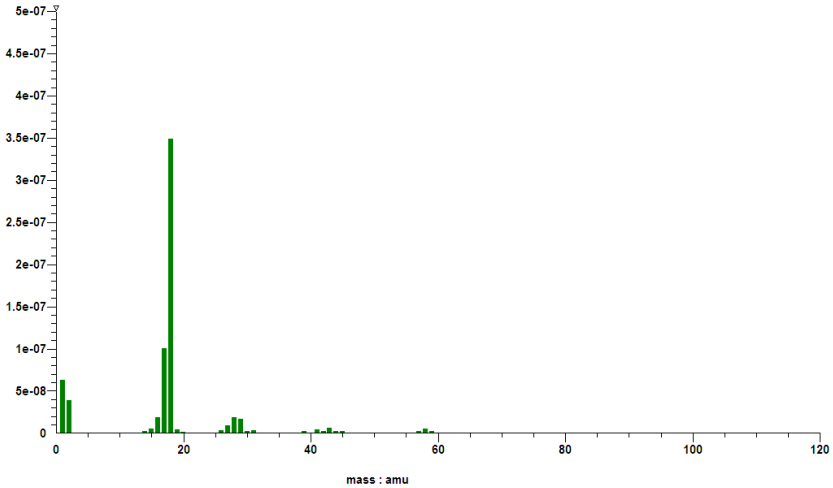

Figure 33: MS of water and higher molar mass material collected at 300°C

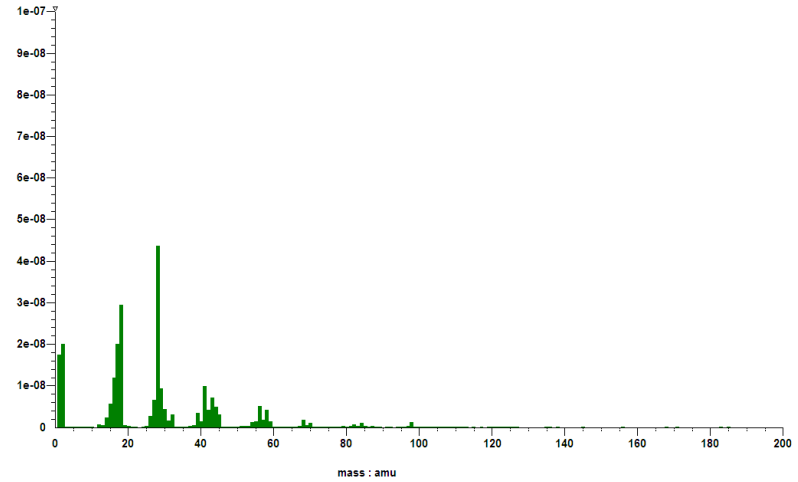

Figure 34: MS of high molar mass material collected at 300°C

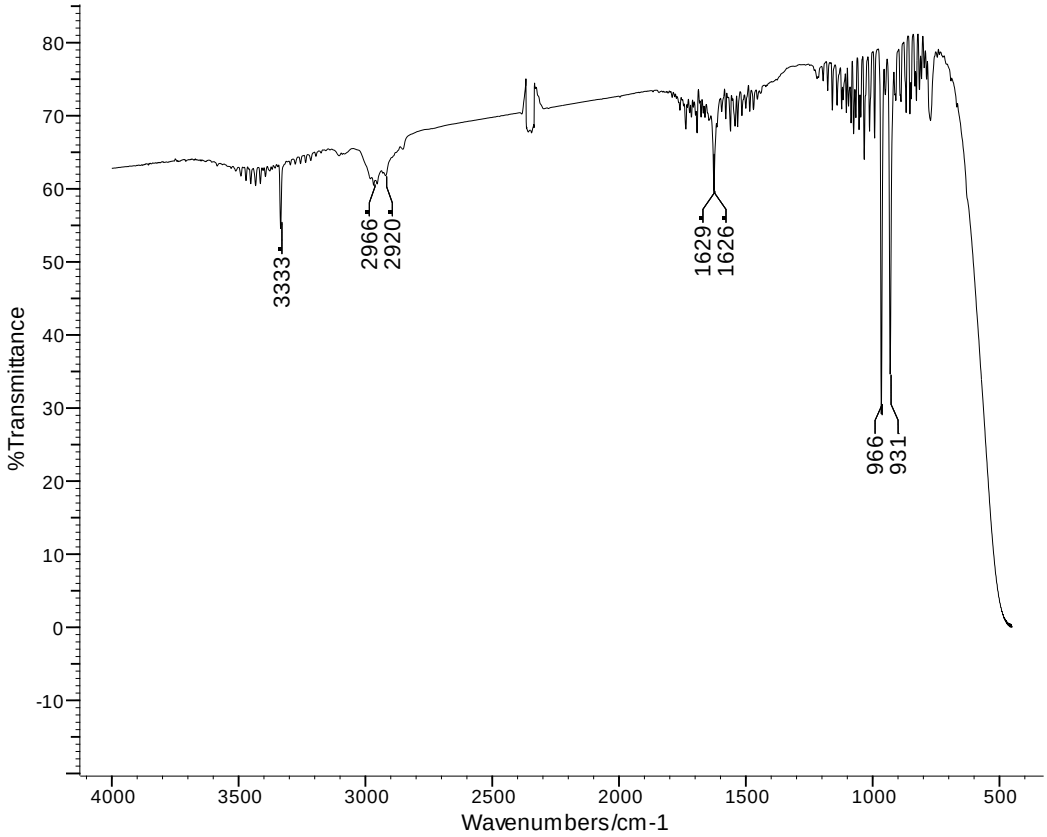

Figure 35: FTIR spectrum of fraction 1 at 300°C

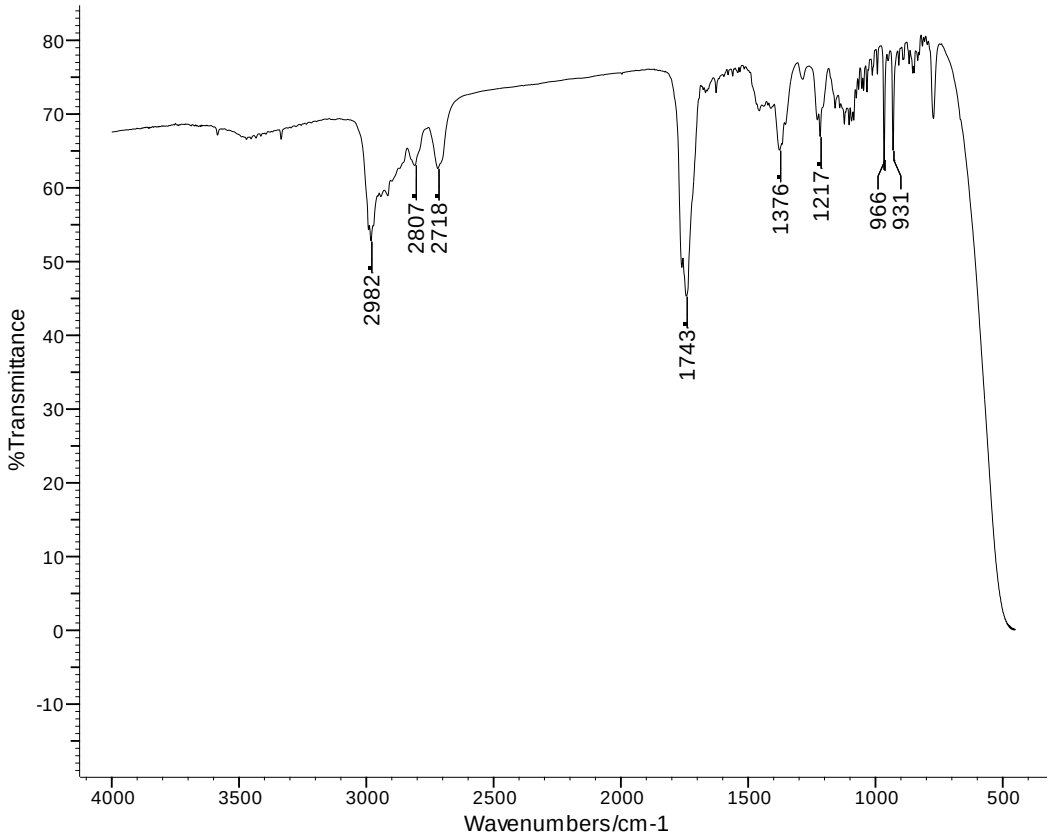

Figure 36: FTIR spectrum of fraction 2 at 300°C

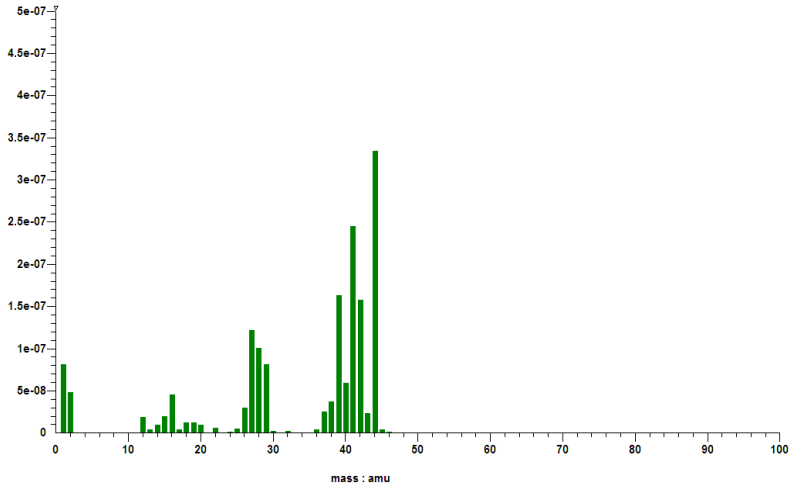

Figure 37: MS of propene and CO_2 collected at 350°C

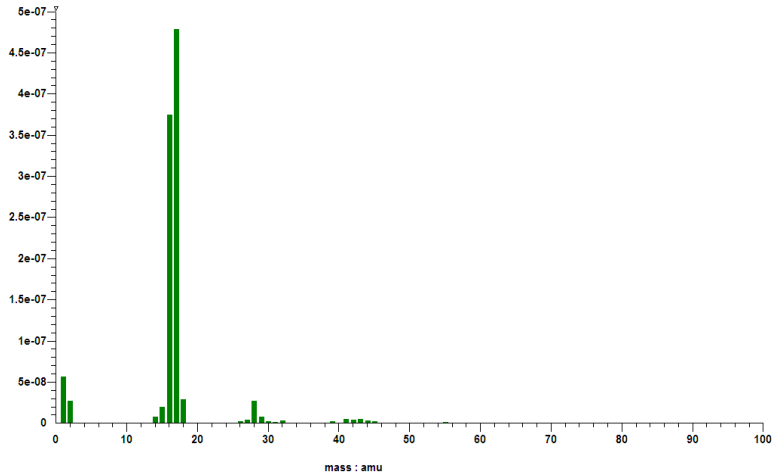

Figure 38: MS of ammonia collected at 350°C

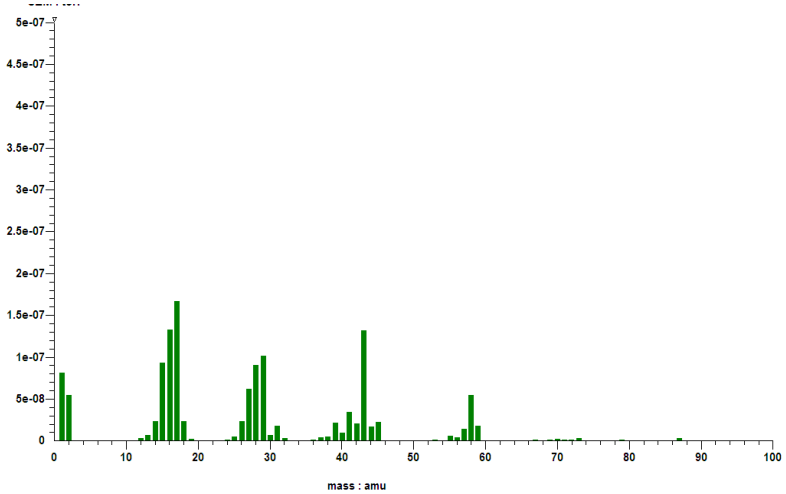

Figure 39: MS of propanal at 350°C

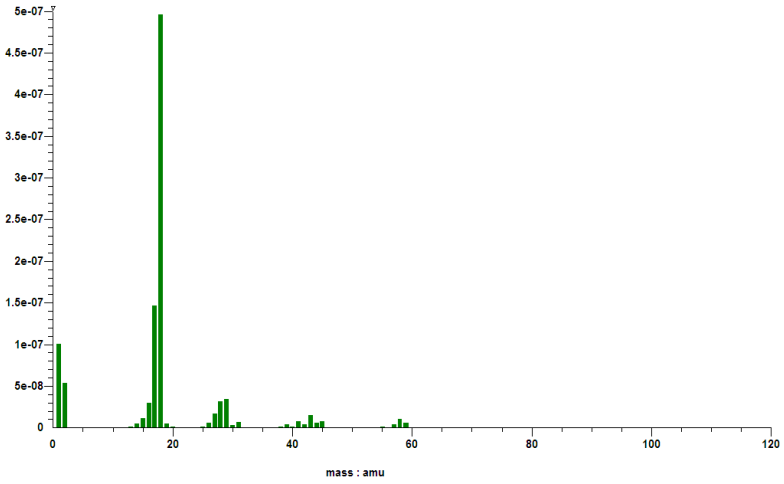

Figure 40: MS of water and higher molar mass material collected at 350°C

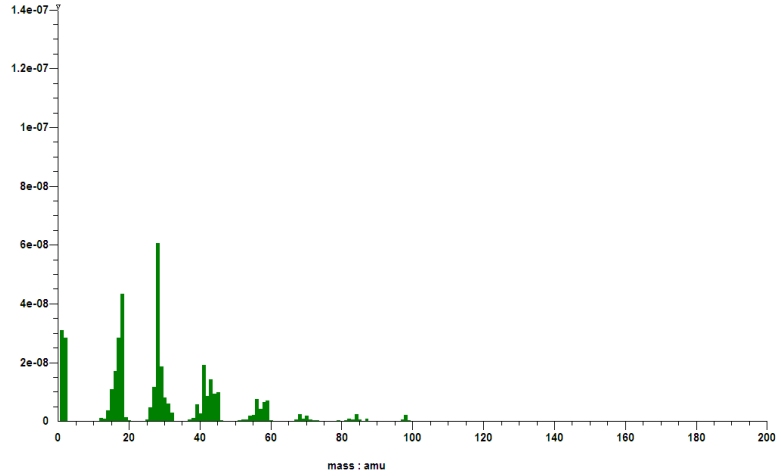

Figure 41: MS of high molar mass material collected at 350°C

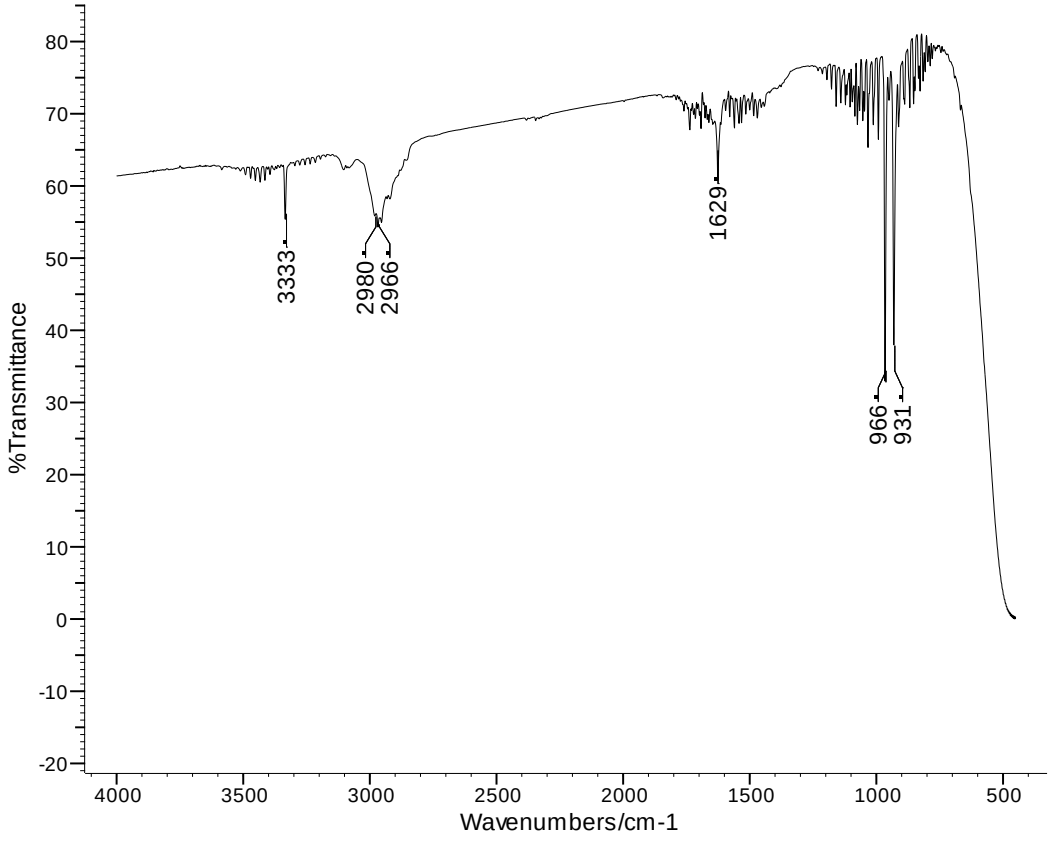

Figure 42: FTIR spectrum of fraction 1 at 350°C

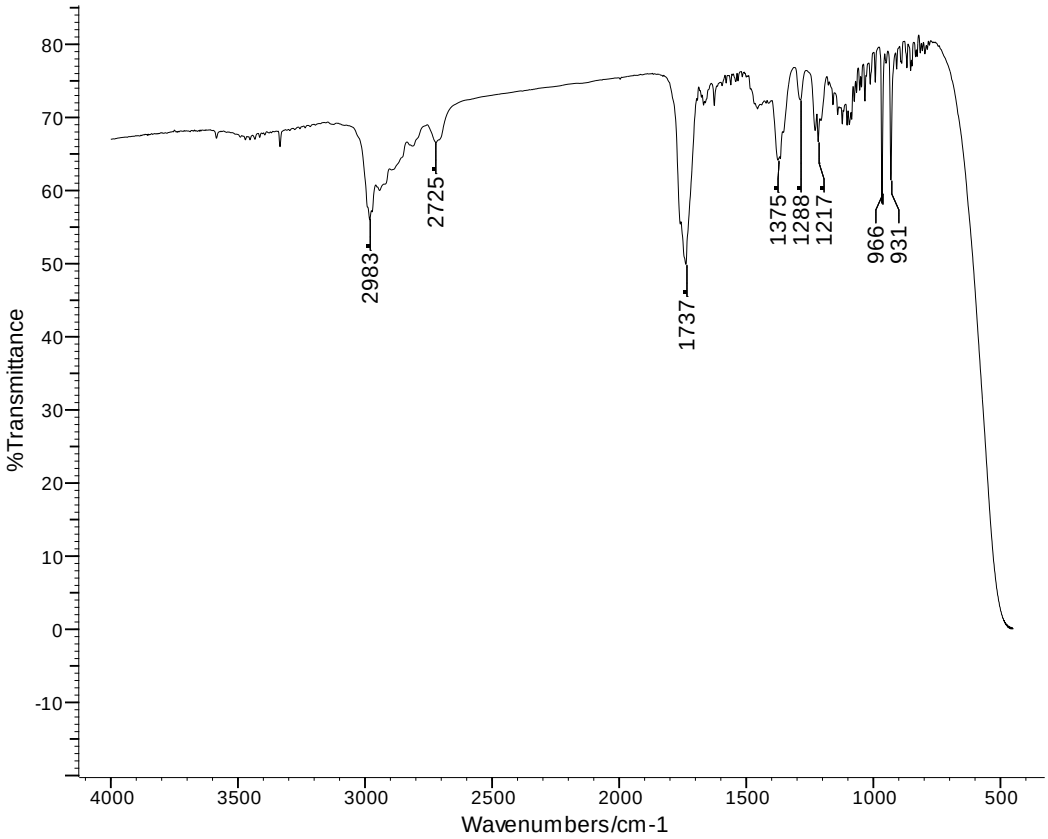

Figure 43: FTIR spectrum of fraction 2 at 350°C

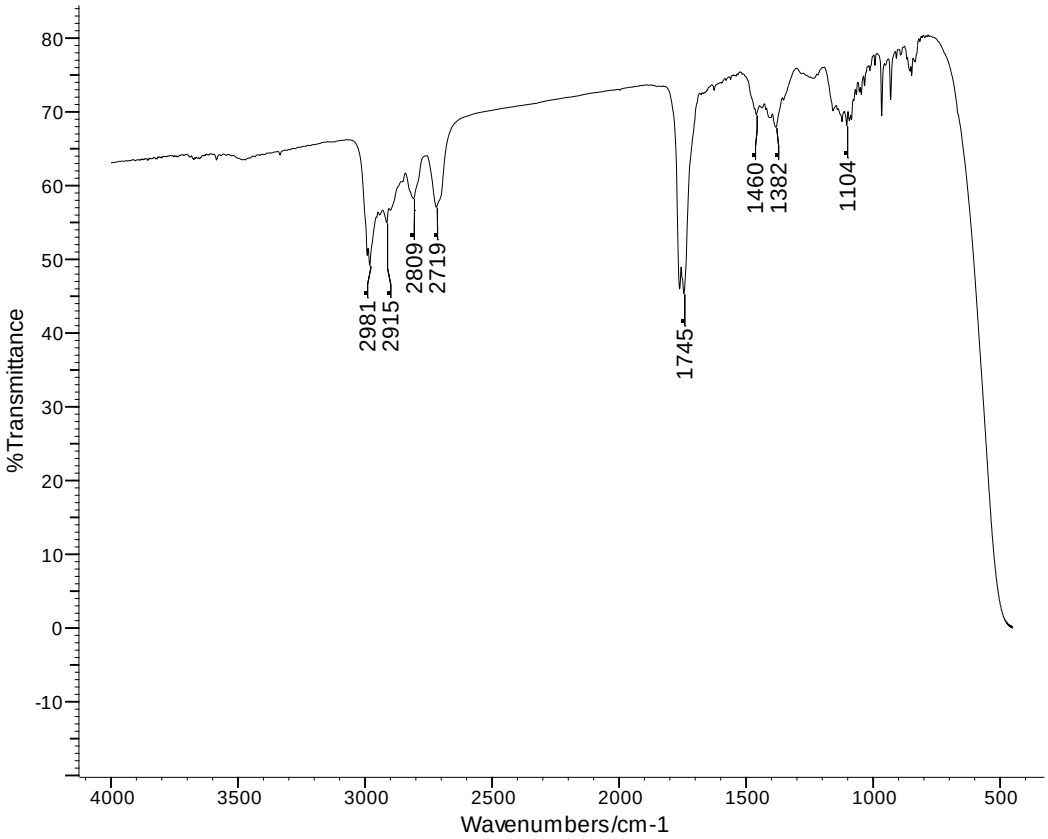

Figure 44: FTIR spectrum of fraction 3 at 350°C

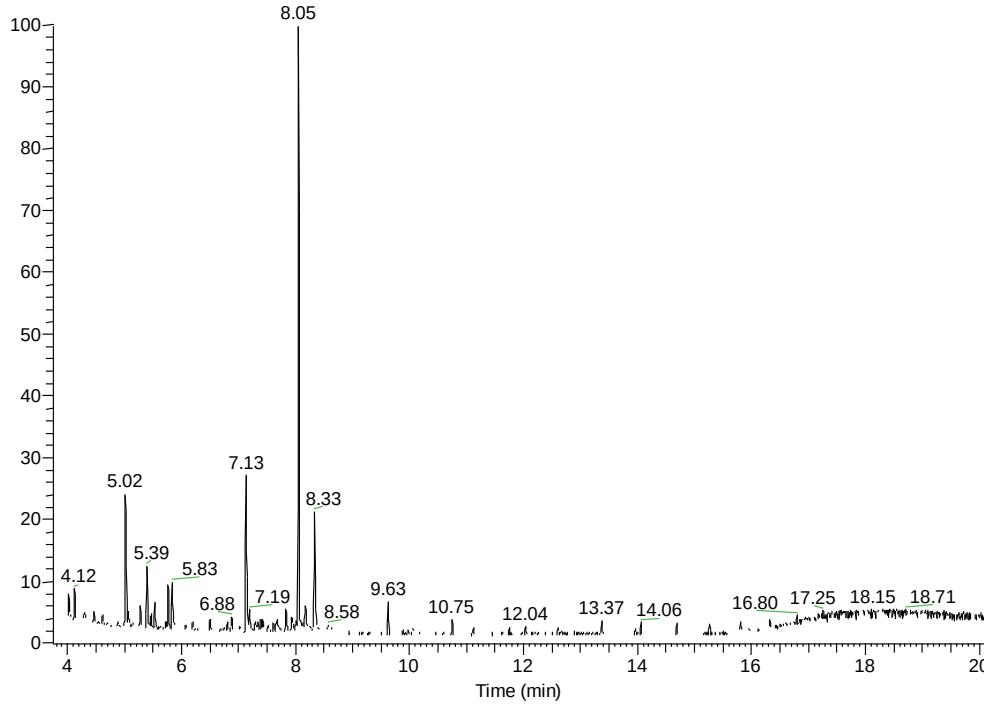

Figure 45: GC-MS chromatogram of fraction 4 at 350°C

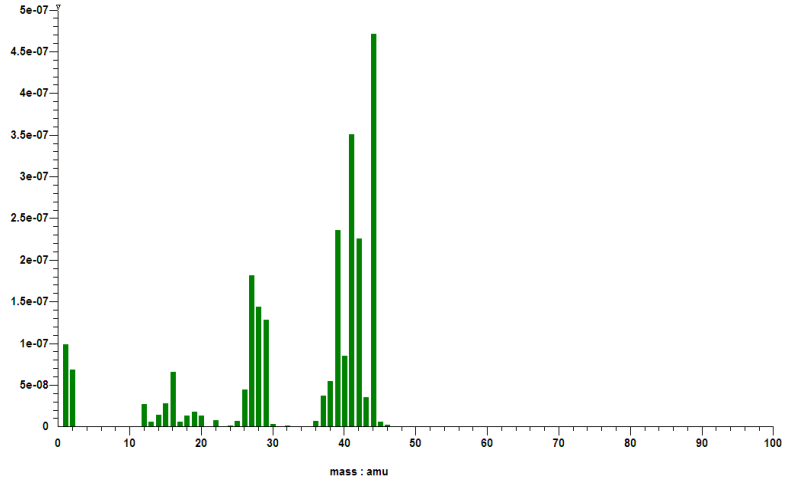

Figure 46: MS of propene and CO_2 collected at 400°C

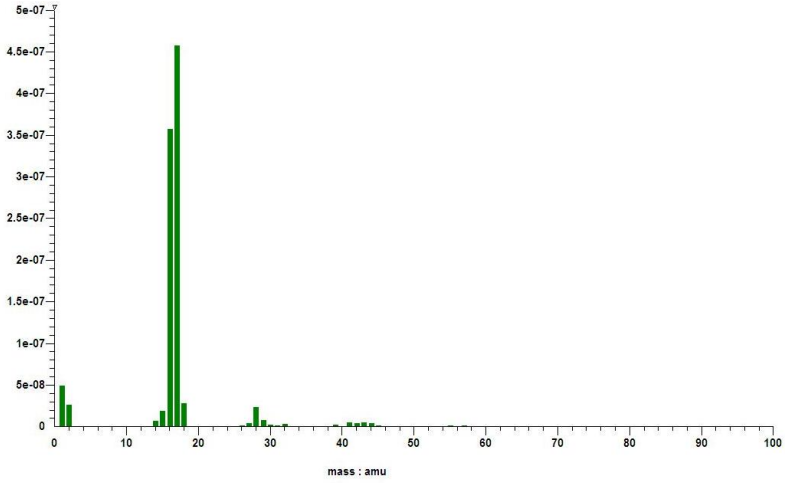

Figure 47: MS of ammonia collected at 400°C

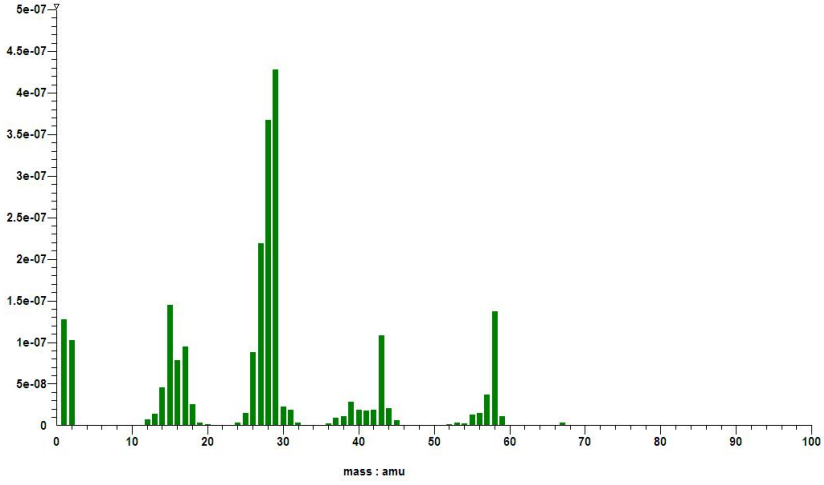

Figure 48: MS of propanal collected at 400°C

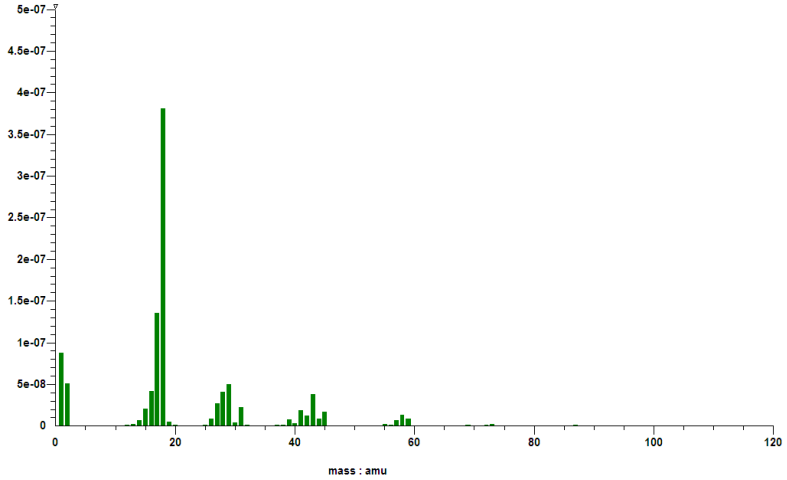

Figure 49: MS of water and higher molar mass material collected at 400°C

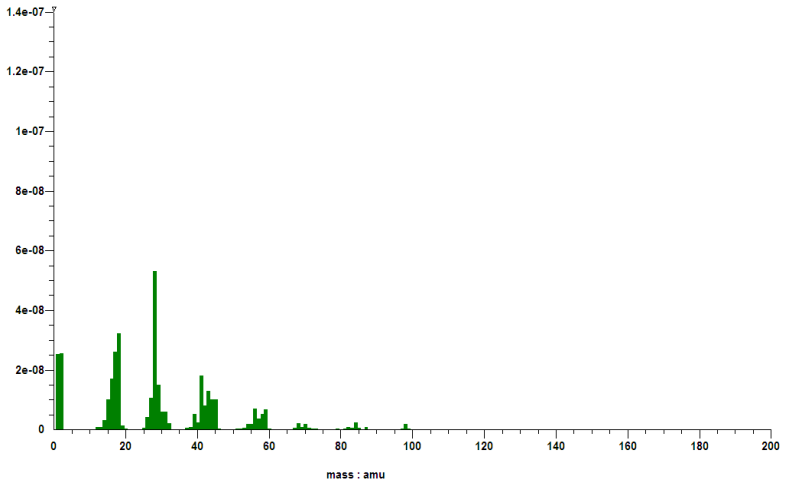

Figure 50: MS of high molar mass material at 400°C

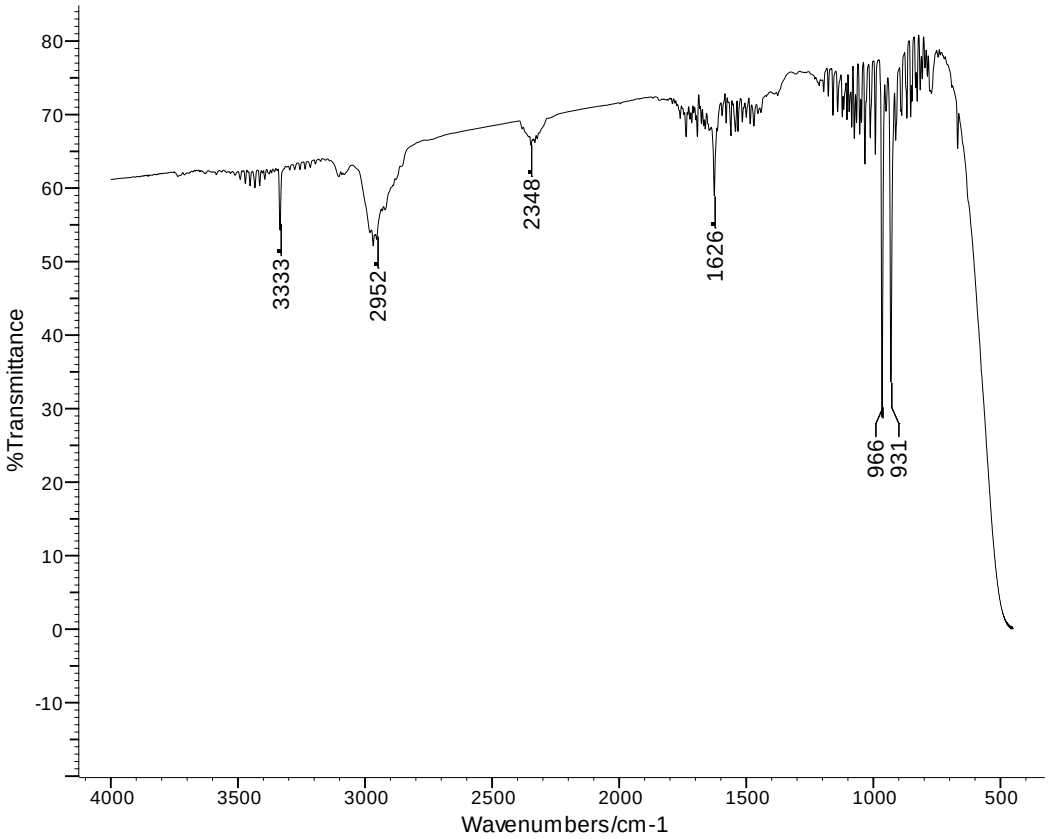

Figure 51: FTIR spectrum of fraction 1 at 400°C

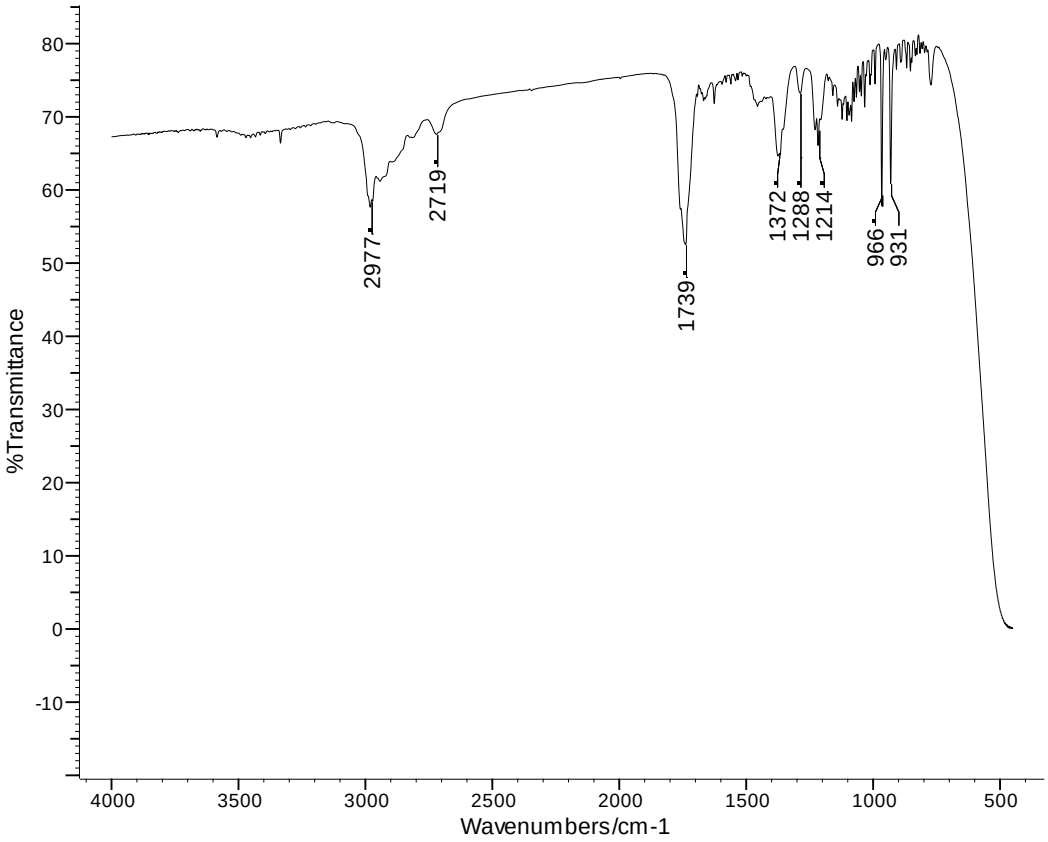

Figure 52: FTIR spectrum of fraction 2 at 400°C

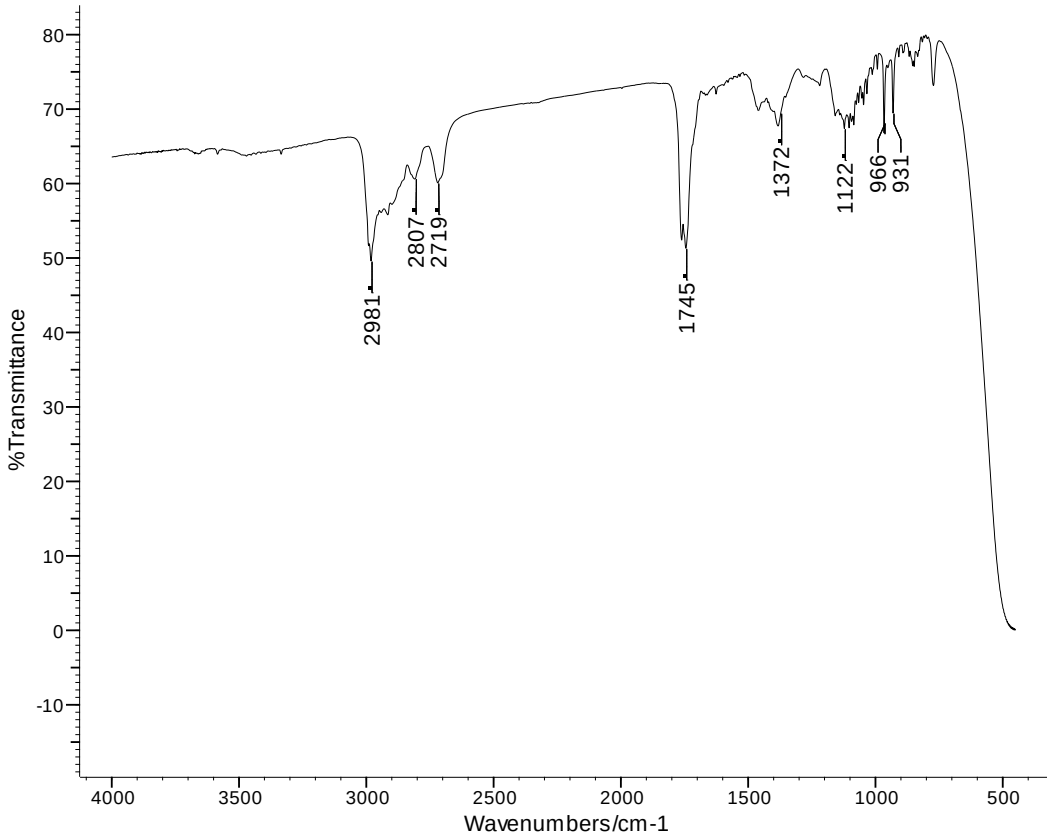

Figure 53: FTIR spectrum of fraction 3 at 400°C

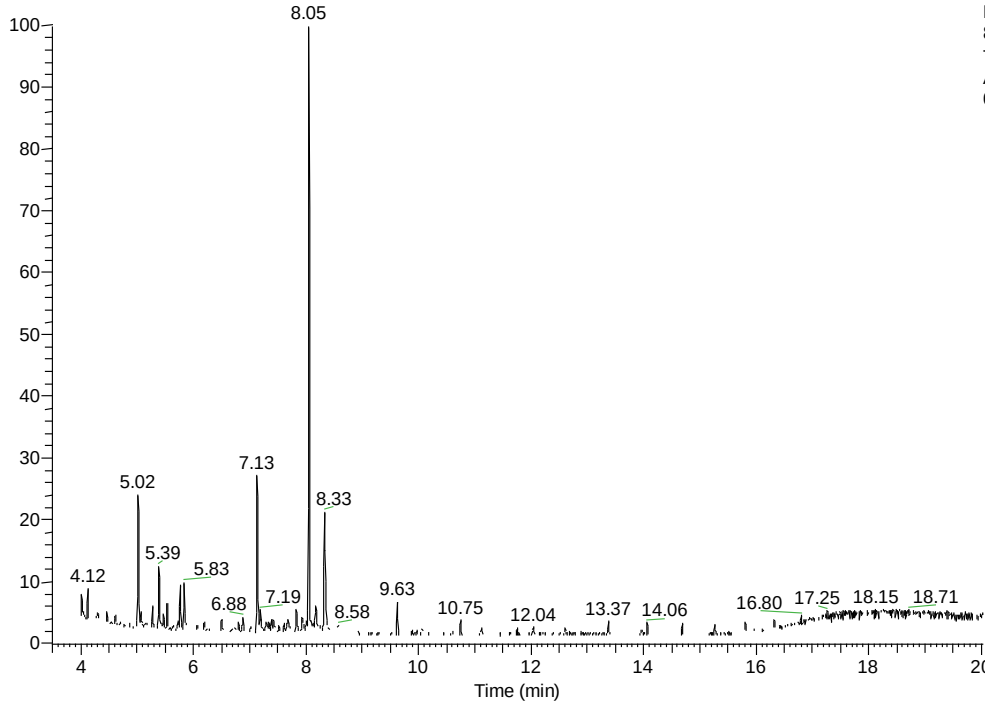

Figure 54: GC-MS chromatogram of fraction 4 at 400°C

2.4 Pyrolysis under Nitrogen

2.4.1 Cold-Ring Fractions

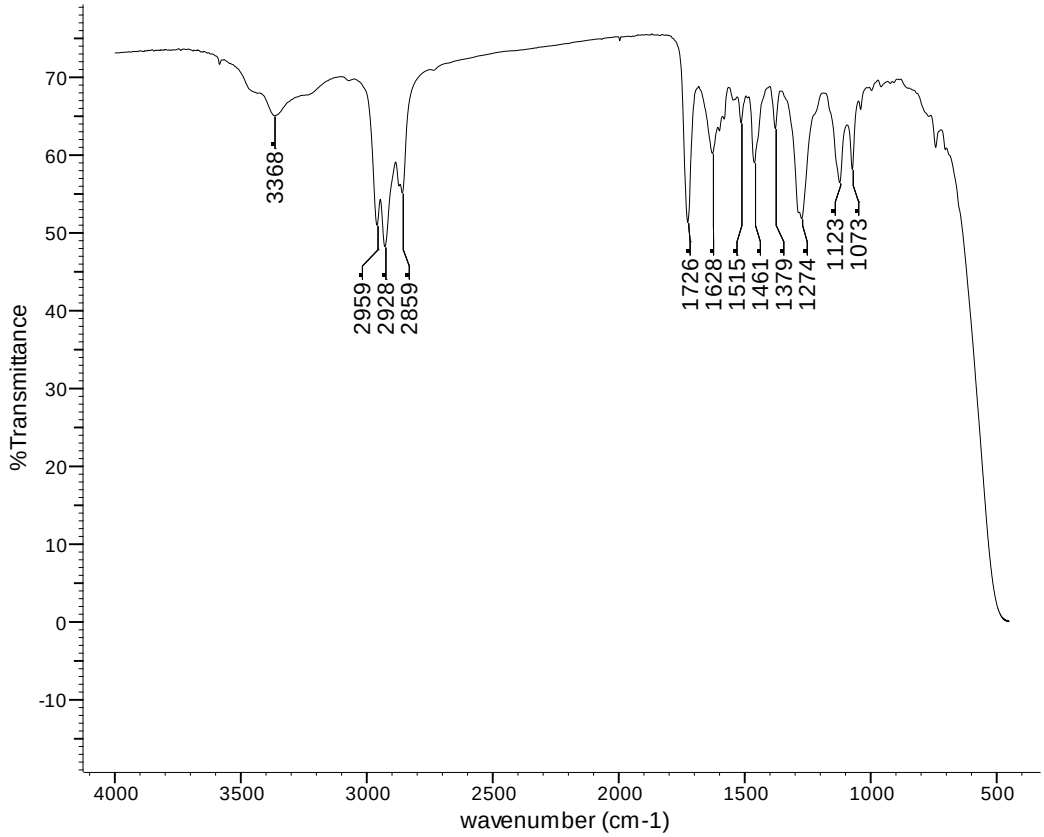

Figure 55:FTIR spectrum of the cold-ring obtained at 300°C under nitrogen

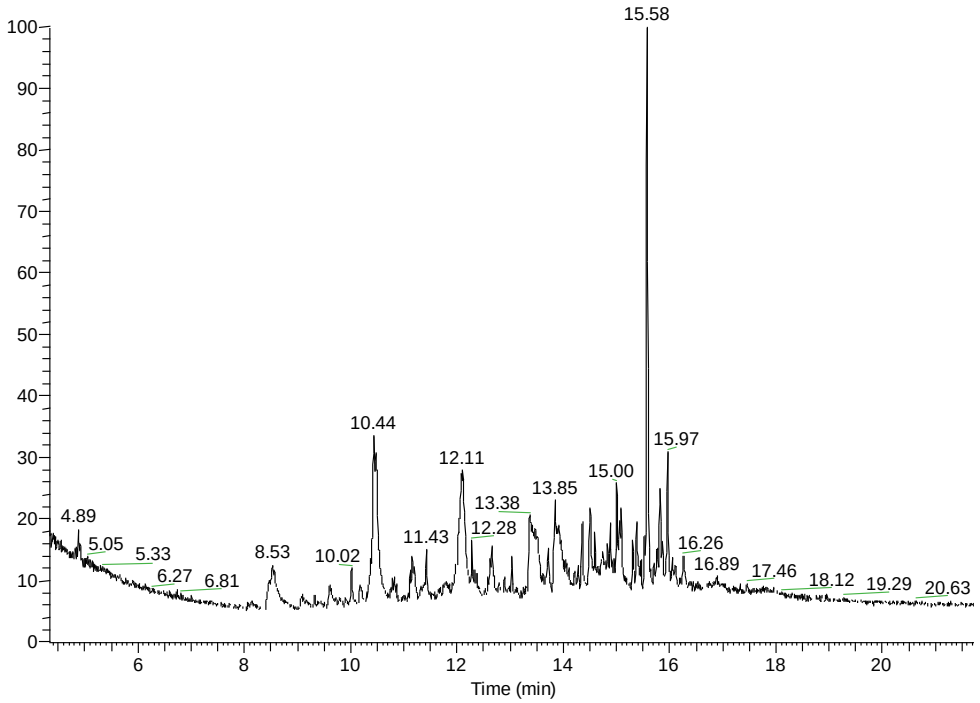

Figure 56: GC-MS chromatogram of the cold-ring fraction obtained at 300°C under nitrogen

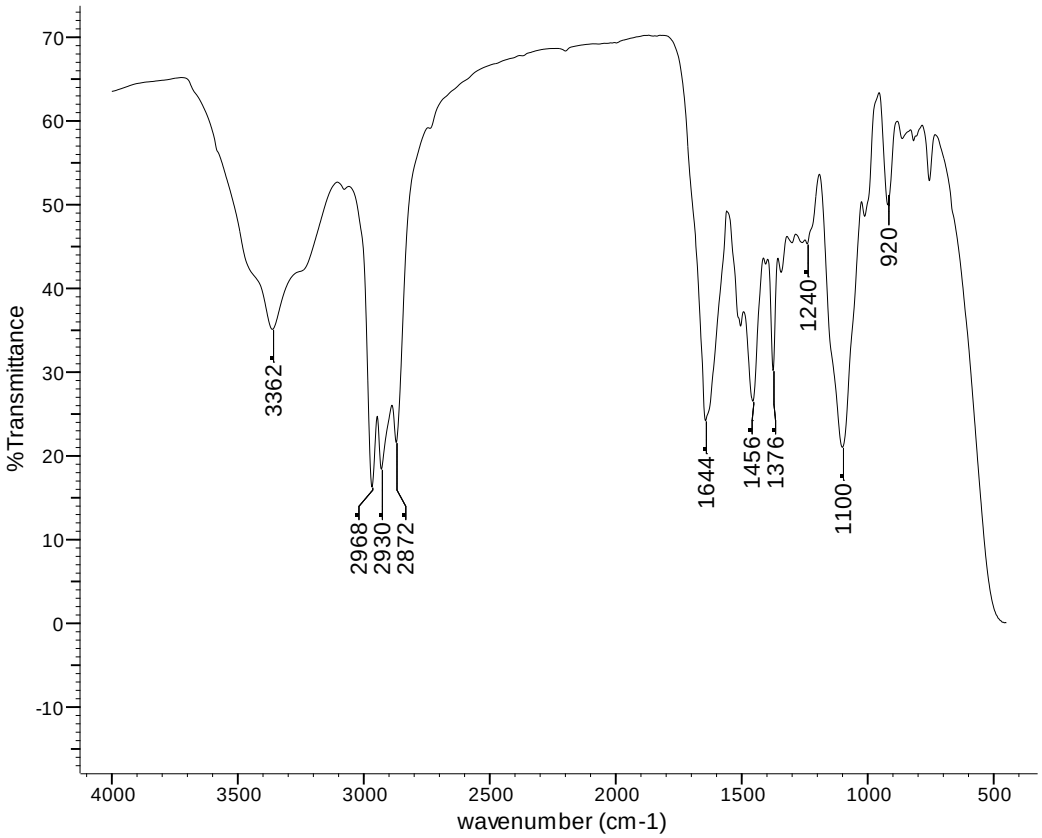

Figure 57: FTIR spectrum of the cold-ring fraction obtained at 350°C under nitrogen

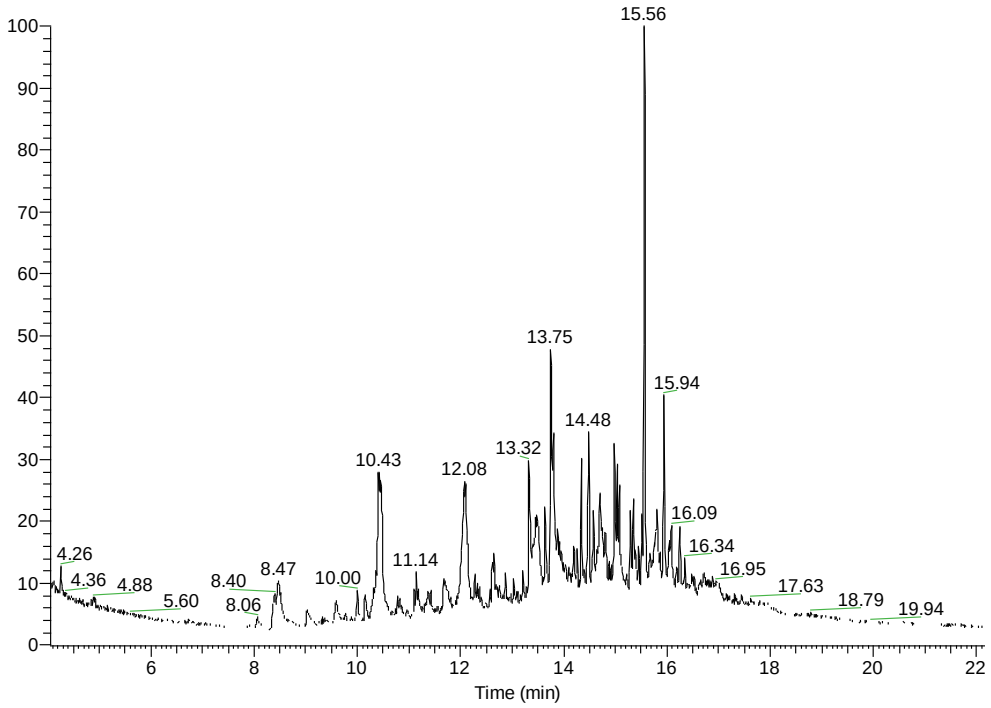

Figure 58: GC-MS chromatogram of the cold-ring fraction obtained at 350°C under nitrogen

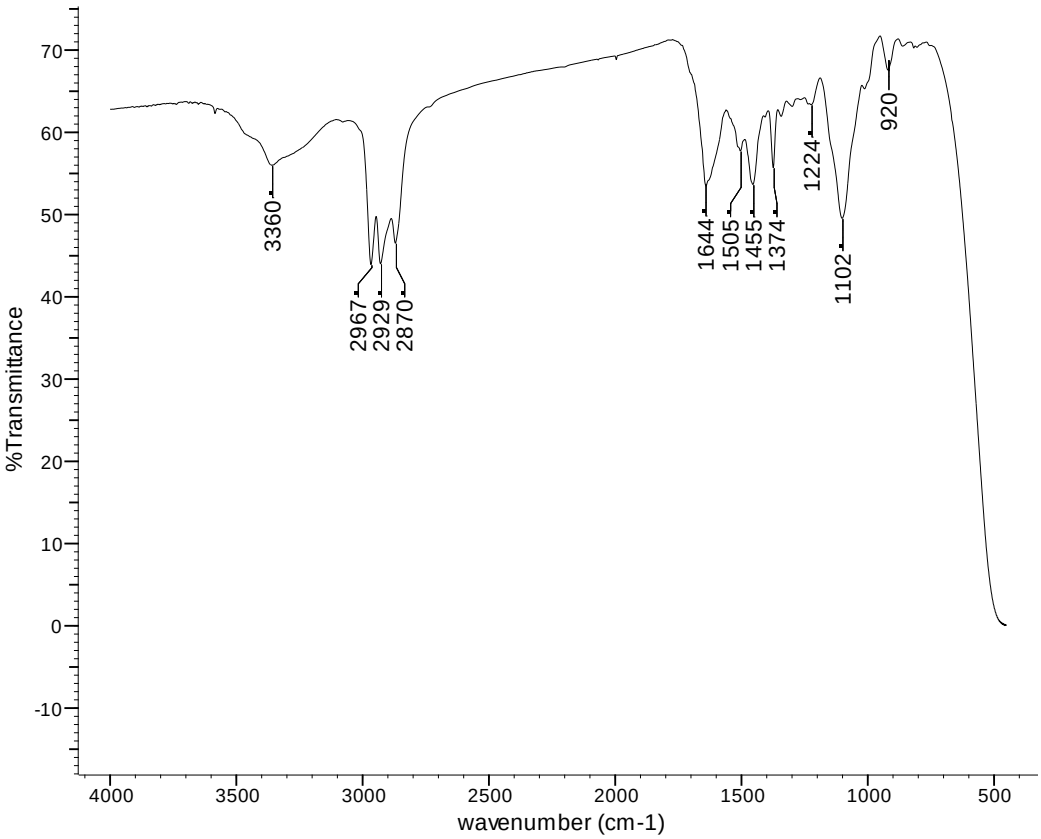

Figure 59: FTIR spectrum of the cold-ring fraction obtained at 400°C under nitrogen

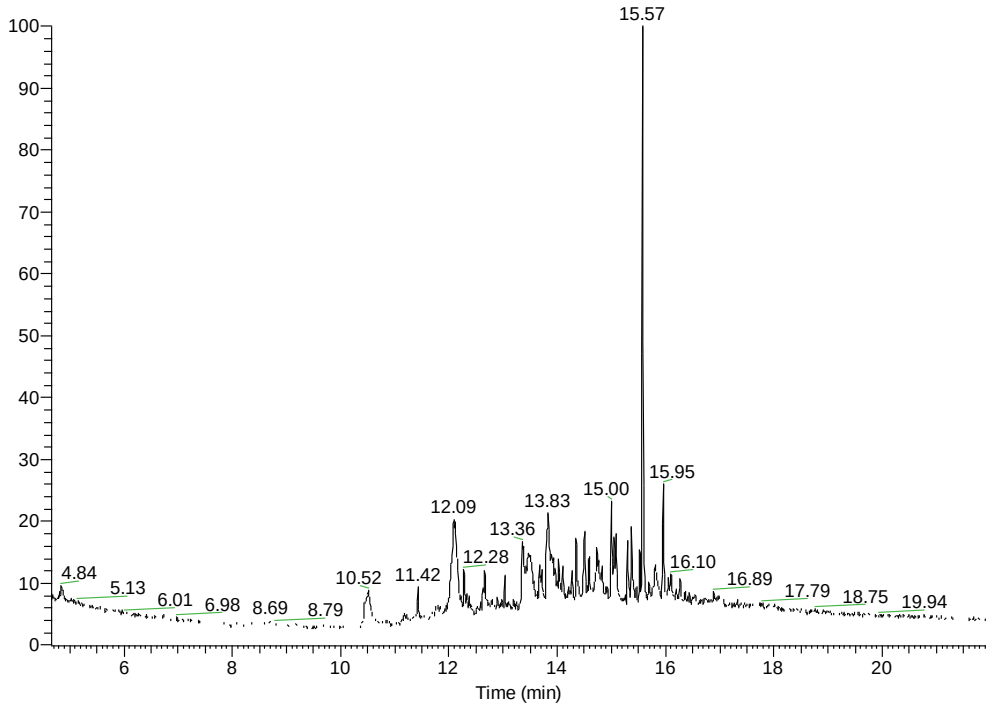

Figure 60: GC-MS chromatogram of the cold-ring fraction obtained at 400°C under nitrogen

2.4.2 Tars

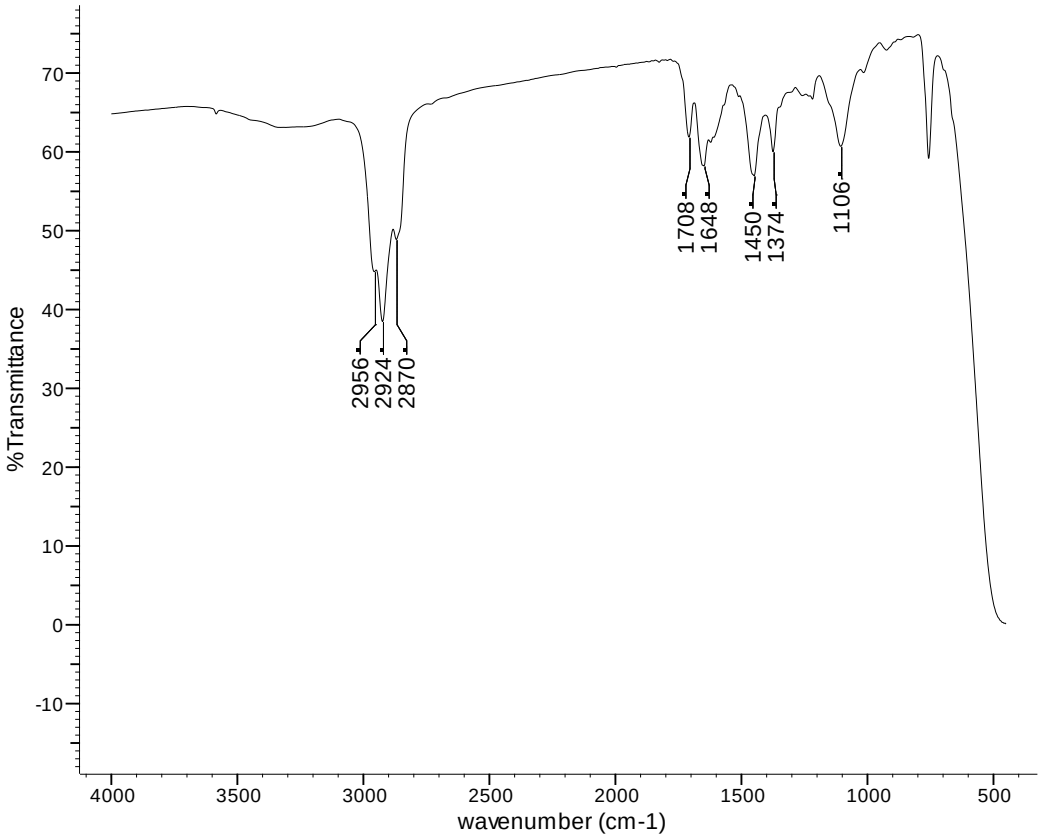

Figure 61: FTIR spectrum of the tar extracted at 350°C under nitrogen

2.5 Pyrolysis under Air

2.5.1 Cold-Ring Fractions

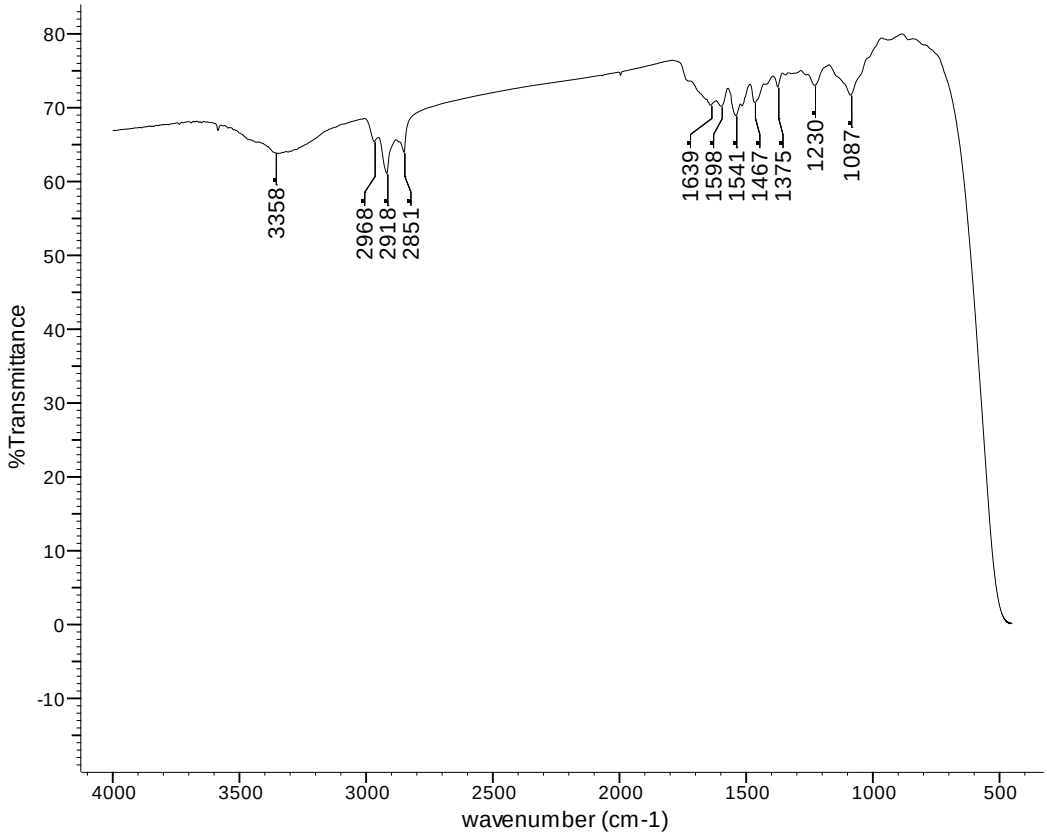

Figure 62: FTIR spectrum of the cold-ring fraction obtained at 250°C under air

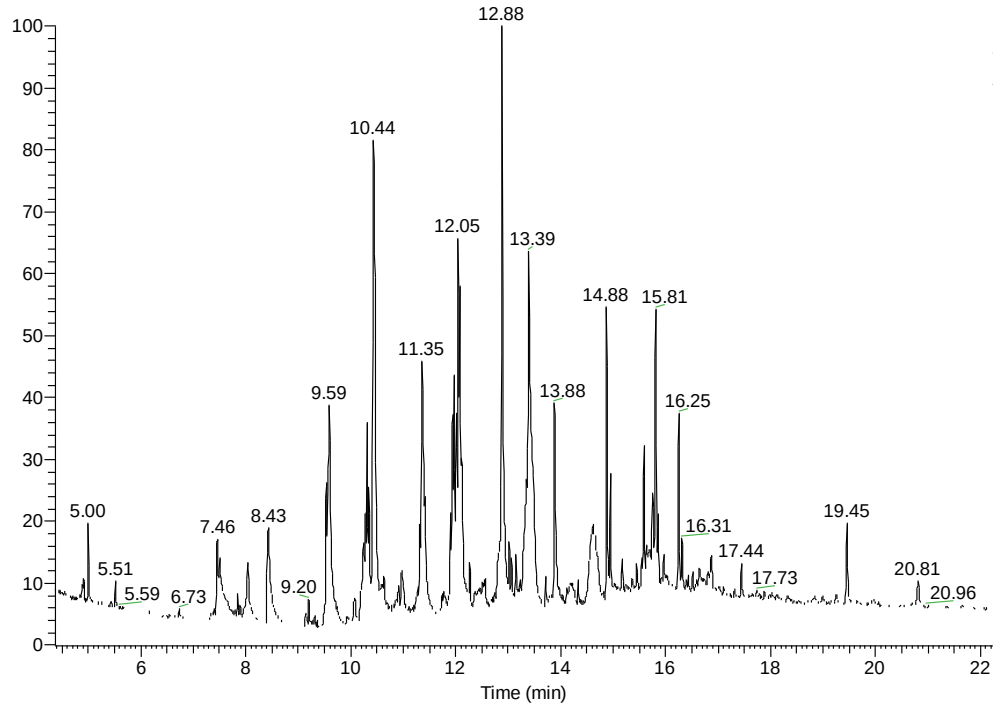

Figure 63: GC-MS chromatogram of the cold-ring fraction obtained at 250°C under air

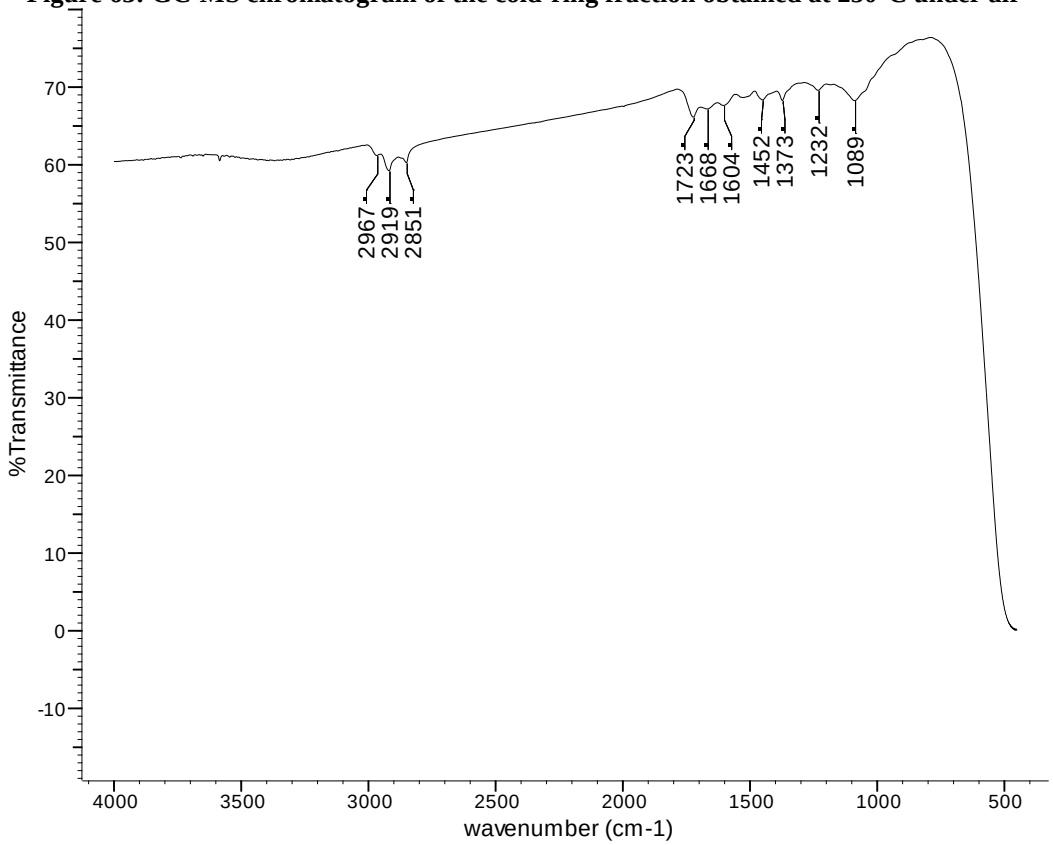

Figure 64:FTIR spectrum of the cold-ring fraction obtained at 300°C under air

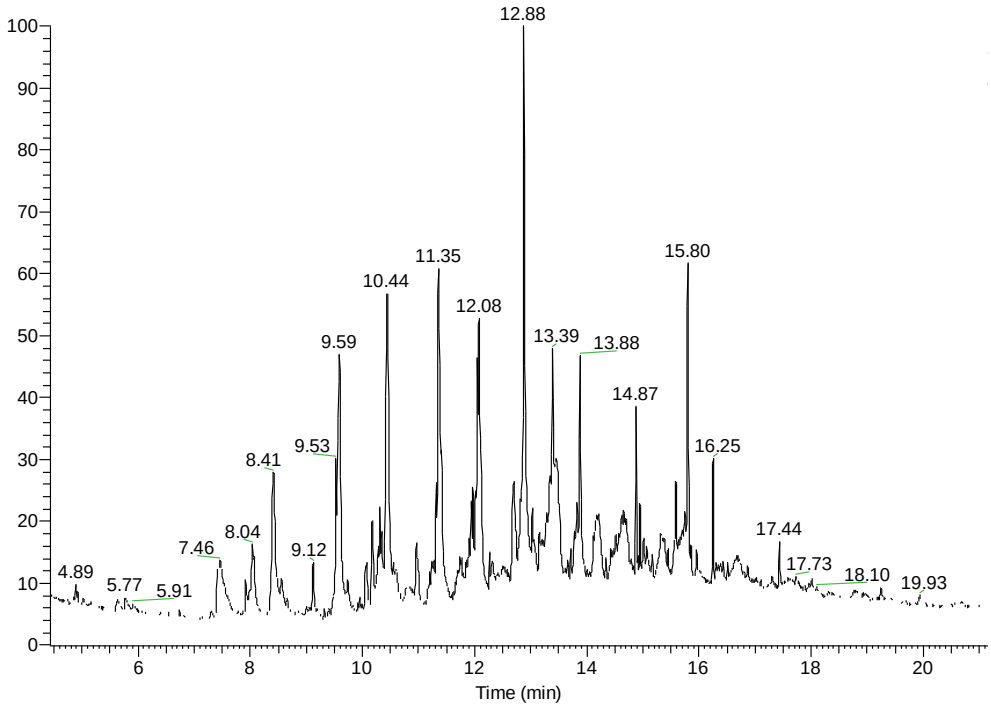

Figure 65:GC-MS chromatogram of the cold-ring fraction obtained at 300°C under air

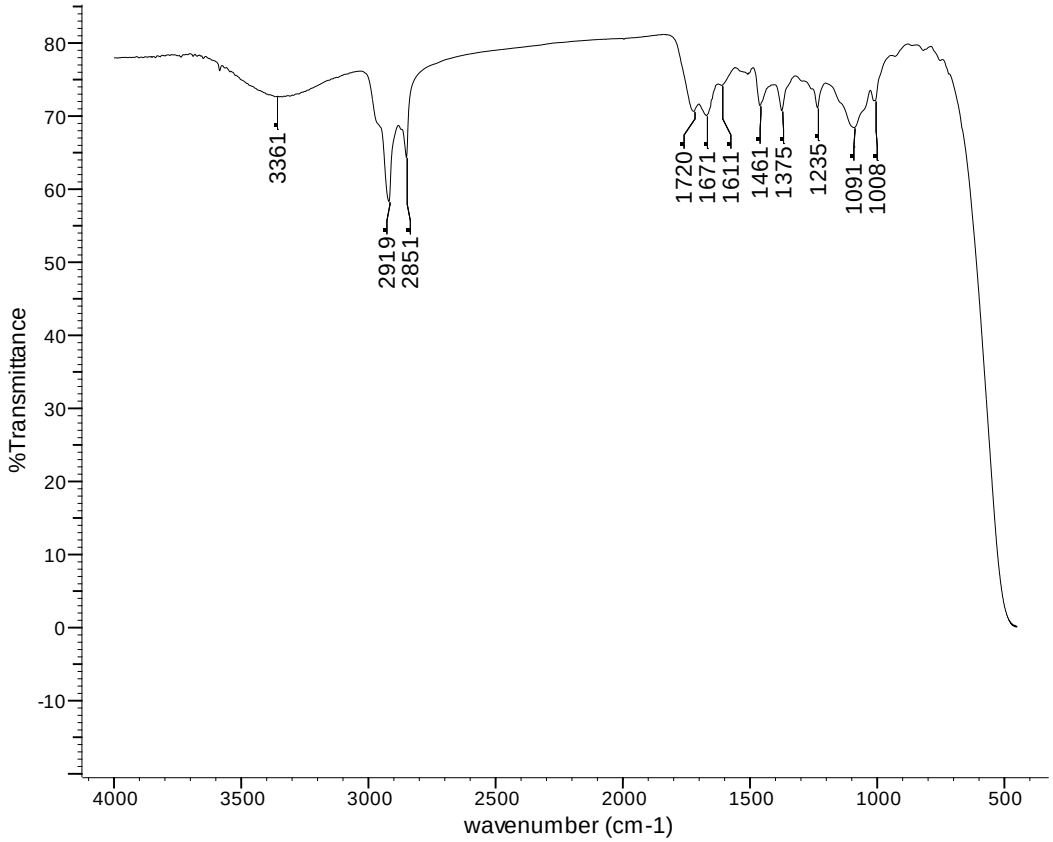

Figure 66: FTIR spectrum of the cold-ring fraction obtained at 350°C under air

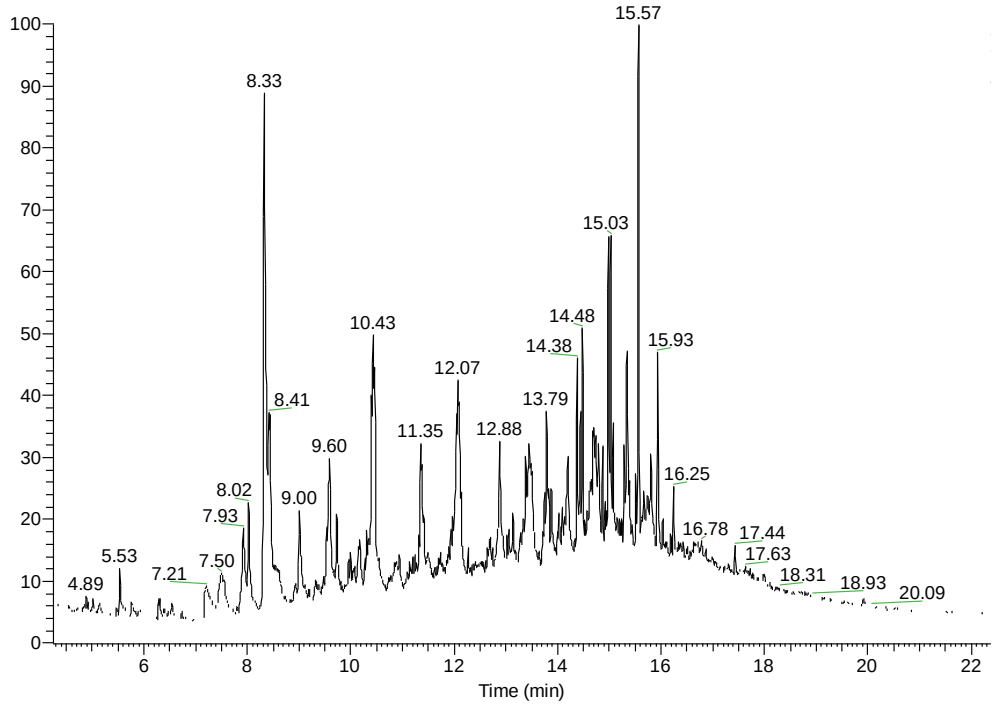

Figure 67:GC-MS chromatogram of the cold-ring fraction obtained at 350°C under air

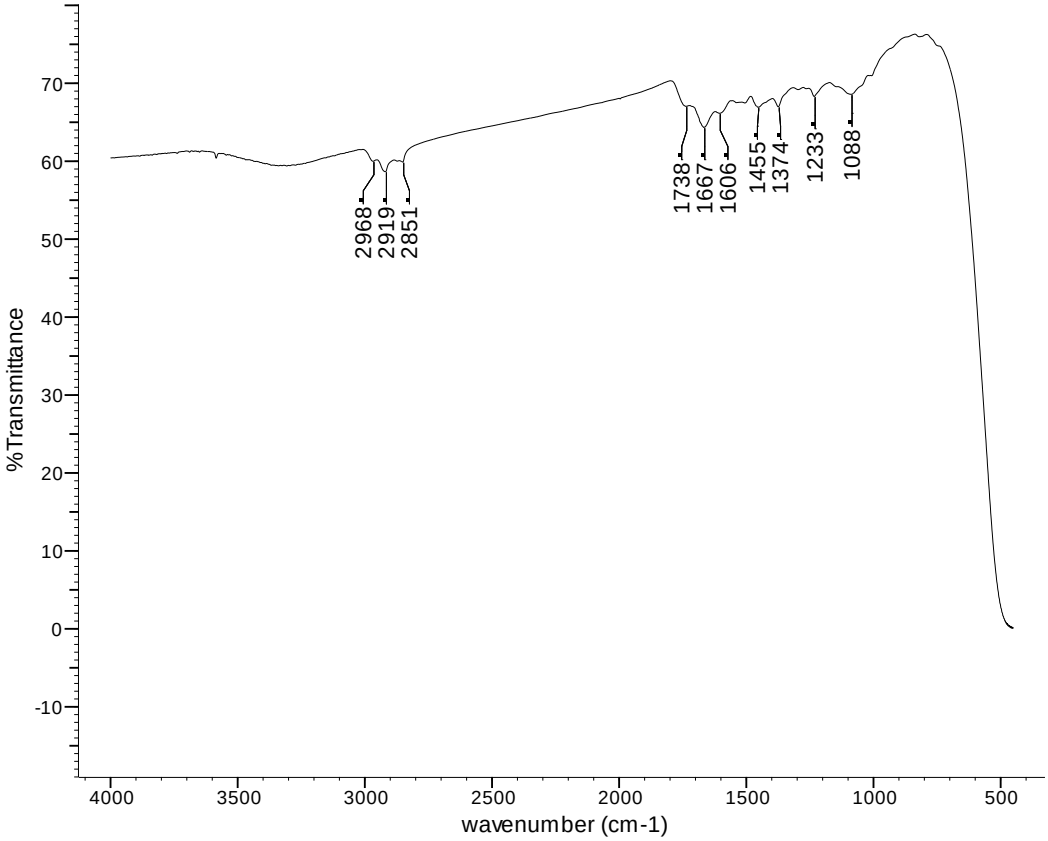

Figure 68:FTIR spectrum of the cold-ring fraction obtained at 400°C under air

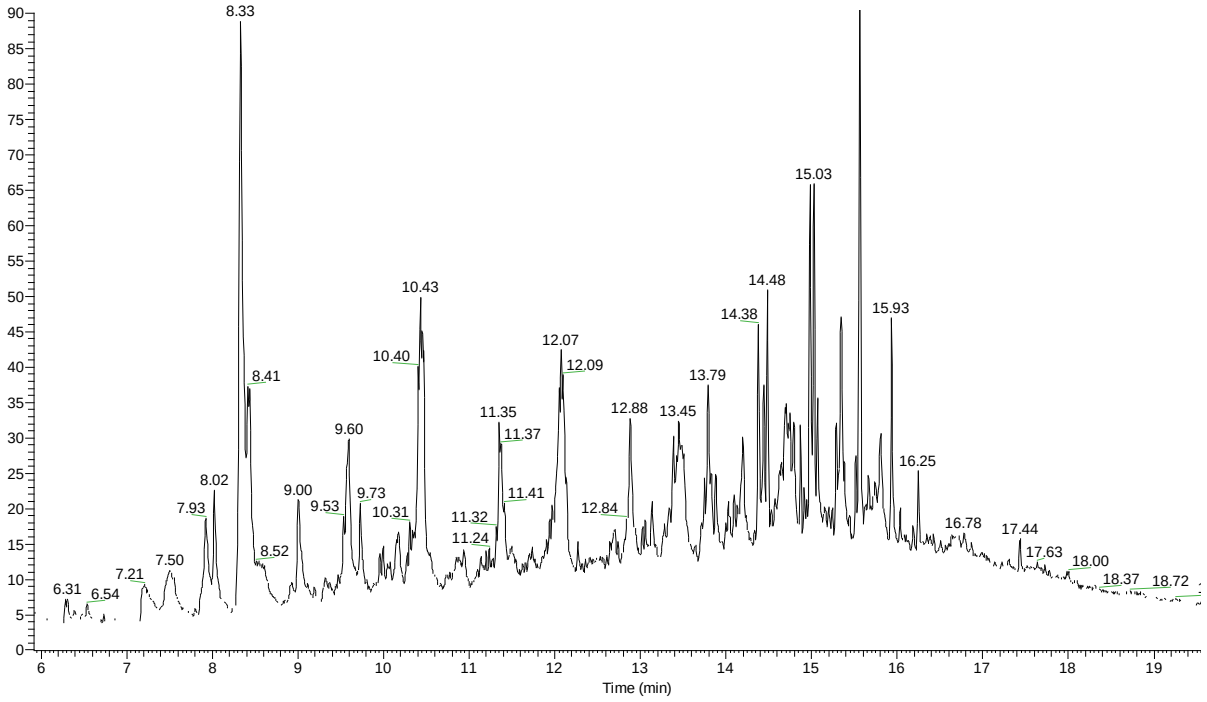

Figure 69:GC-MS chromatogram of the cold-ring fraction obtained at 400°C under air

2.5.2 Tars

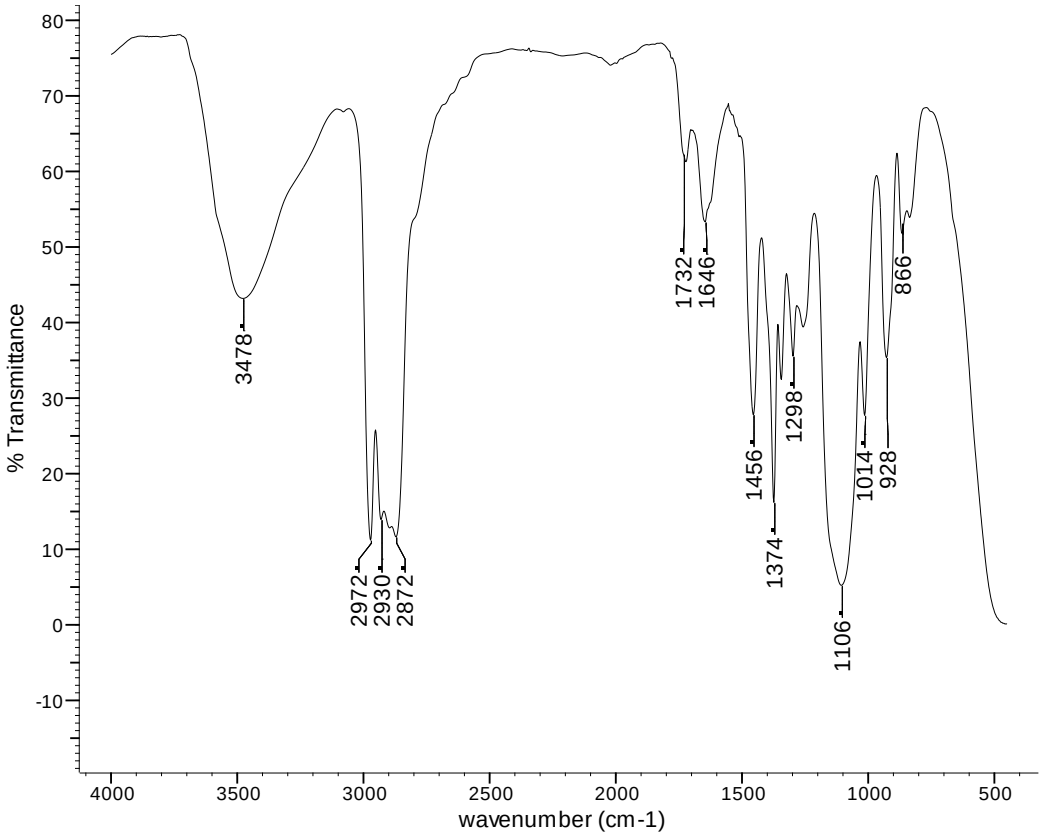

Figure 70: FTIR spectrum of the tar extracted at 300°C under air

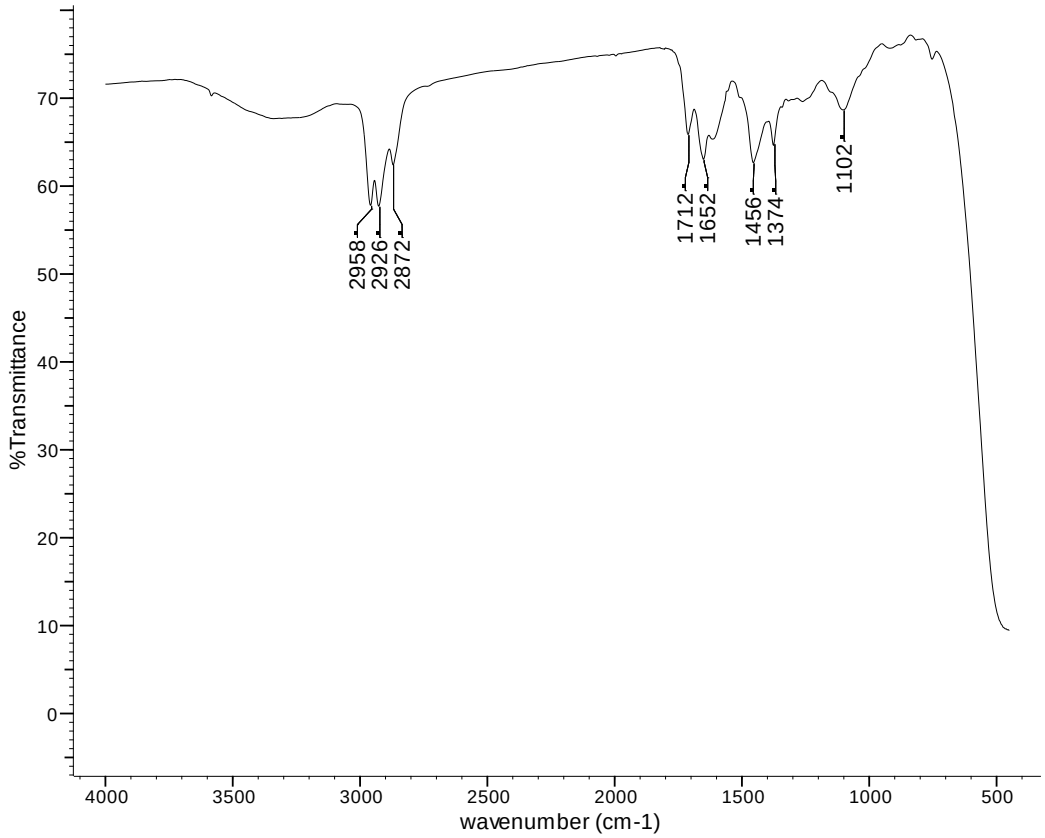

Figure 71: FTIR spectrum of the tar extracted at 350°C under air

2.6 Pyrolysis under 3% oxygen in nitrogen

2.6.1 Cold-Ring Fractions

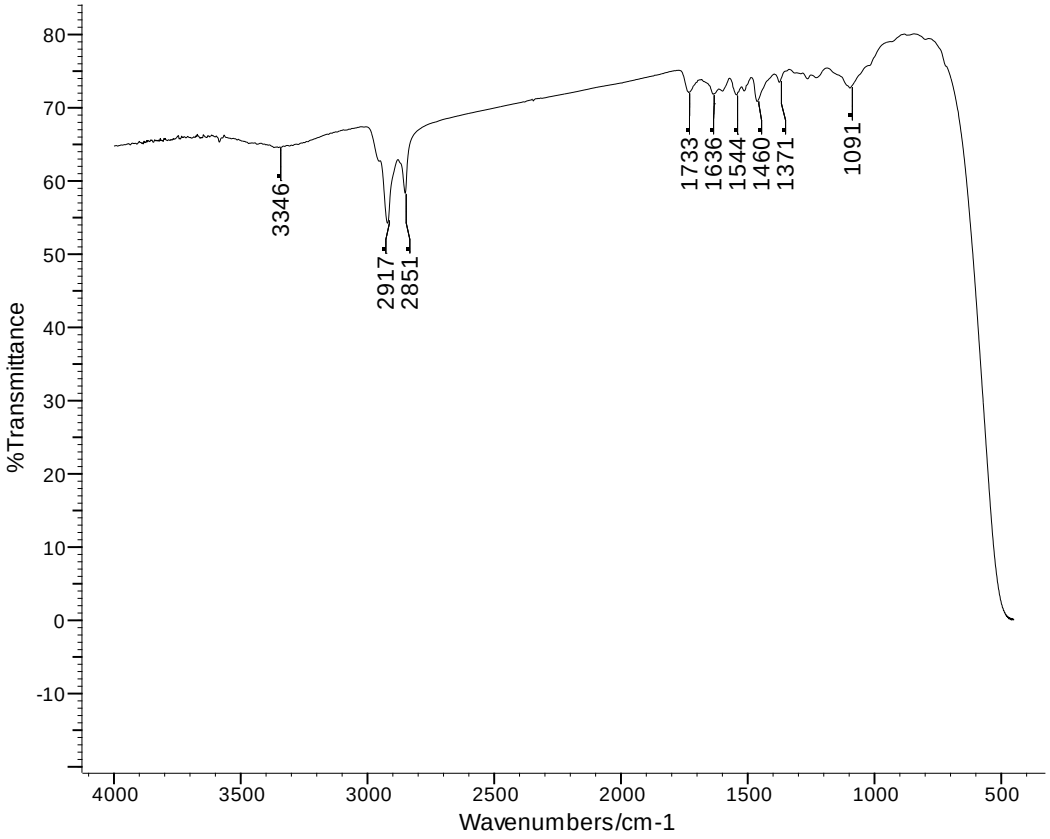

Figure 72: FTIR spectrum of the cold-ring fraction obtained at 250°C under3% O_2 in nitrogen

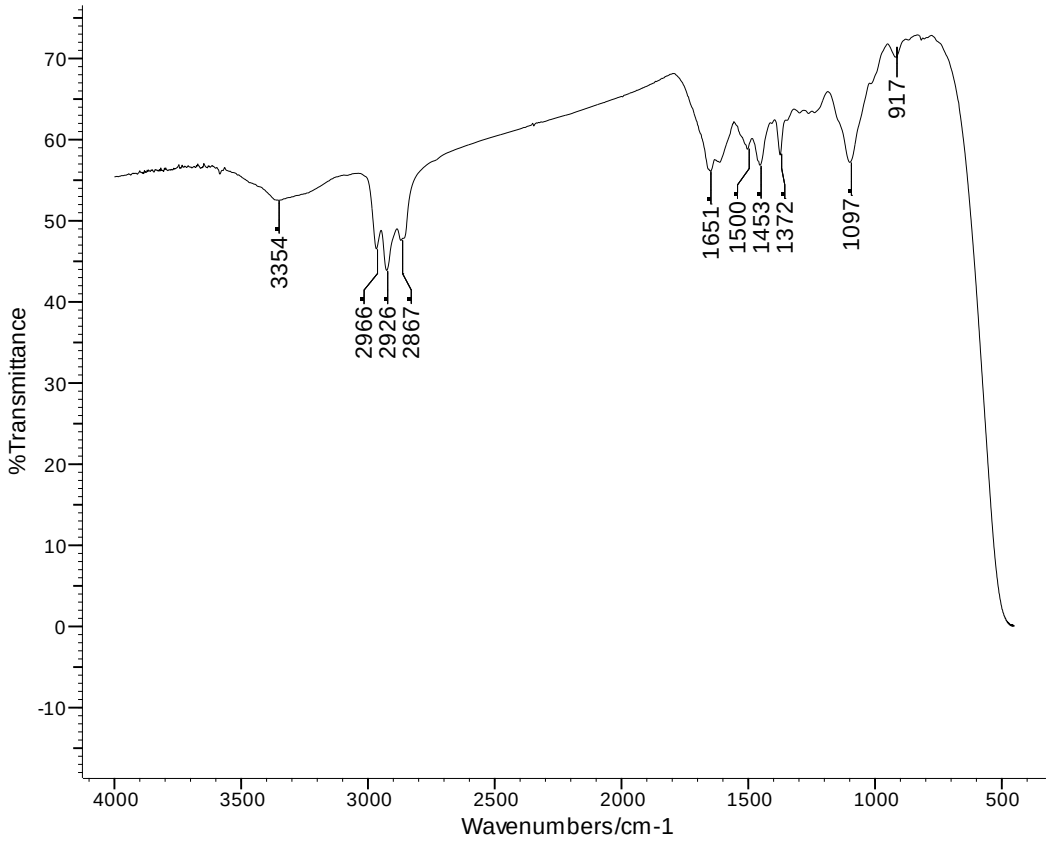

Figure 73: FTIR spectrum of the cold-ring fraction obtained at 300°C under3% O_2 in nitrogen

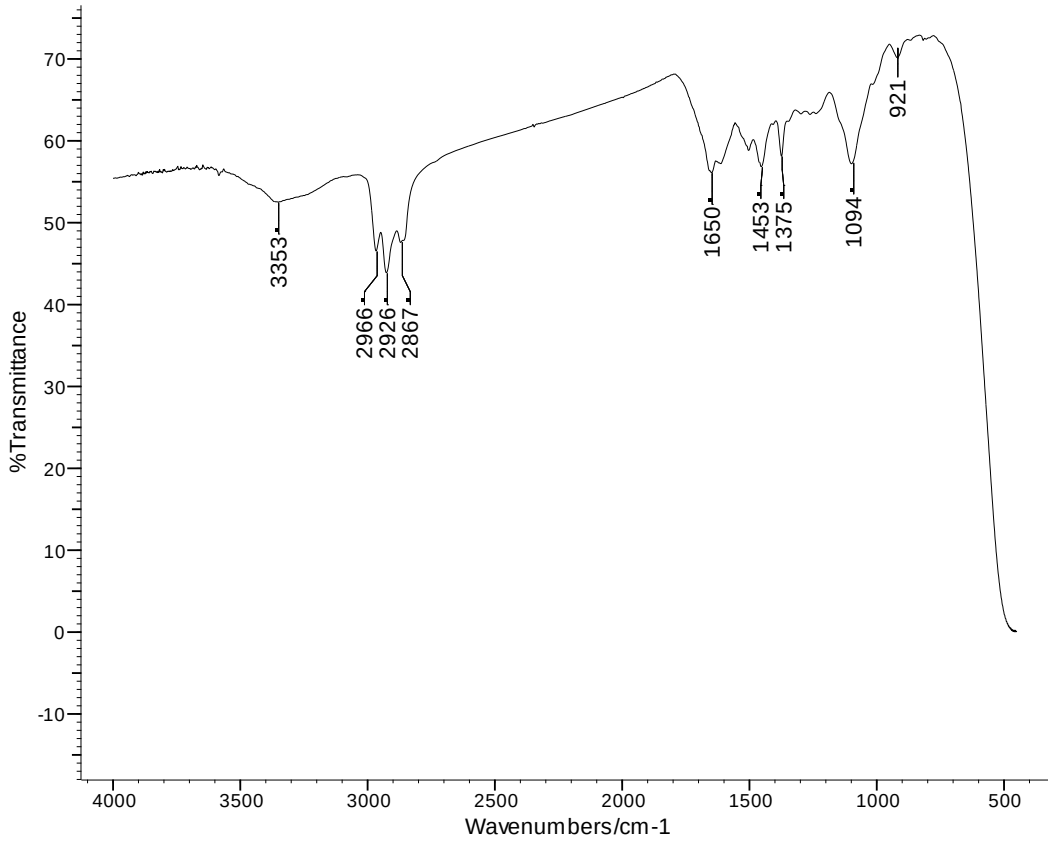

Figure 74: FTIR spectrum of the cold-ring fraction obtained at 350°C under3% O_2 in nitrogen

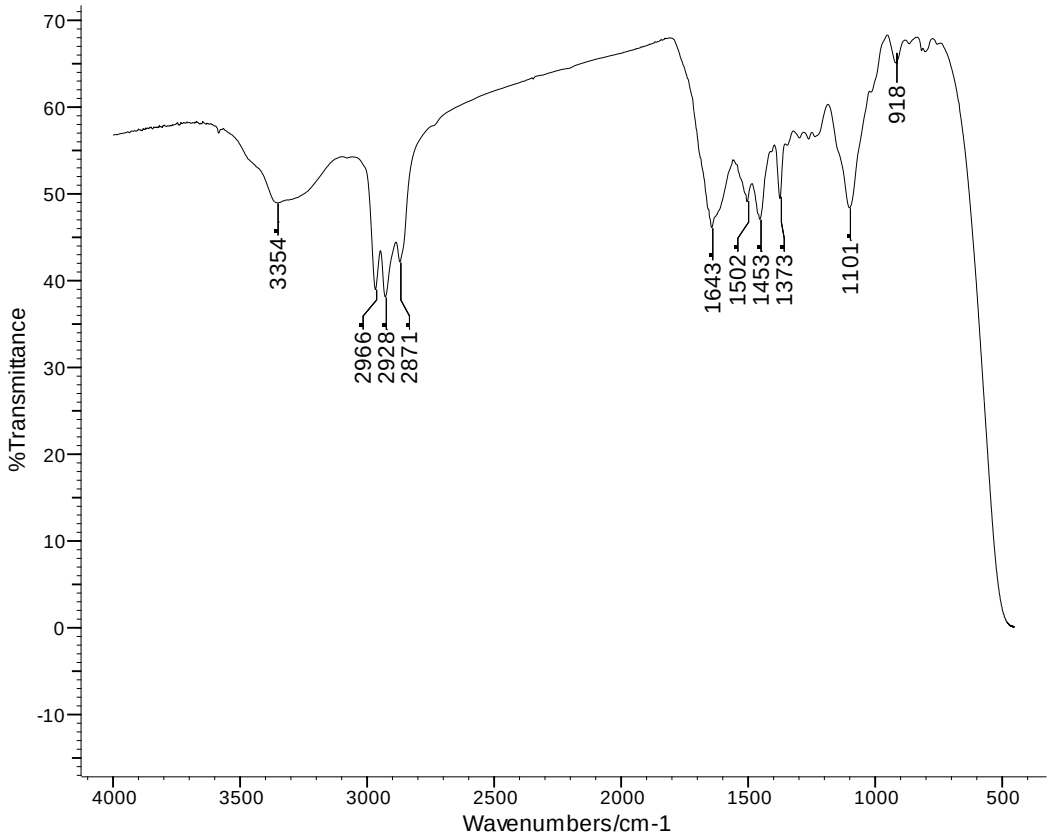

Figure 75: FTIR spectrum of the cold-ring fraction obtained at 400°C under3% O_2 in nitrogen

2.6.2 Tars

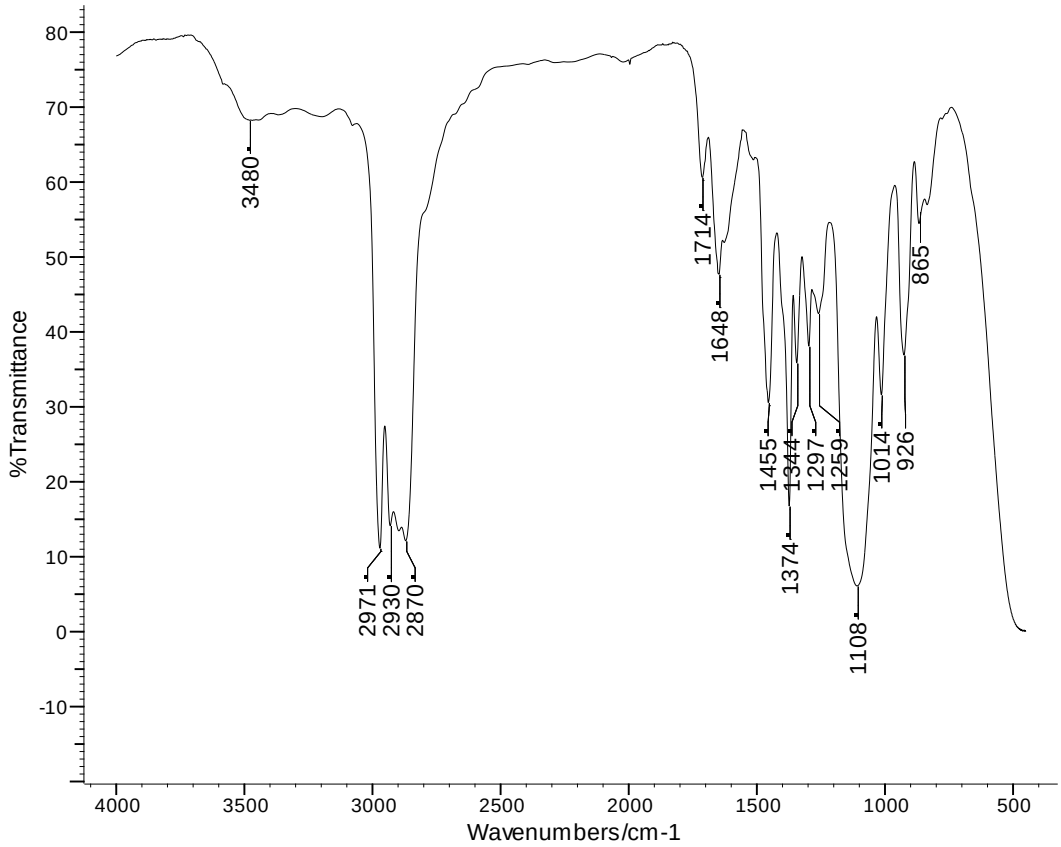

Figure 76: FTIR spectrum of the tar extracted at 300°C under 3% O_2 in nitrogen

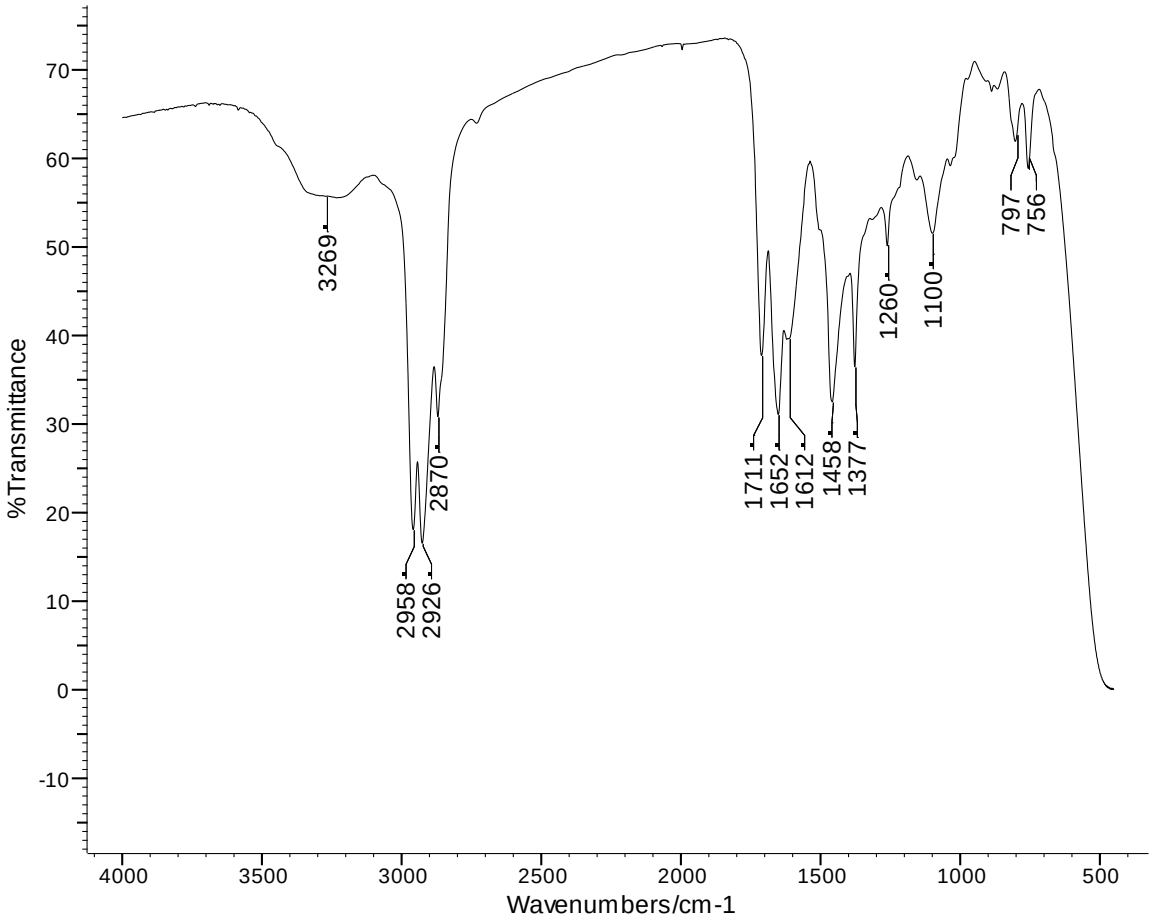

Figure 77: FTIR spectrum of the tar extracted at 350°C under 3% O_2 in nitrogen

2.6.3 Solid state NMR

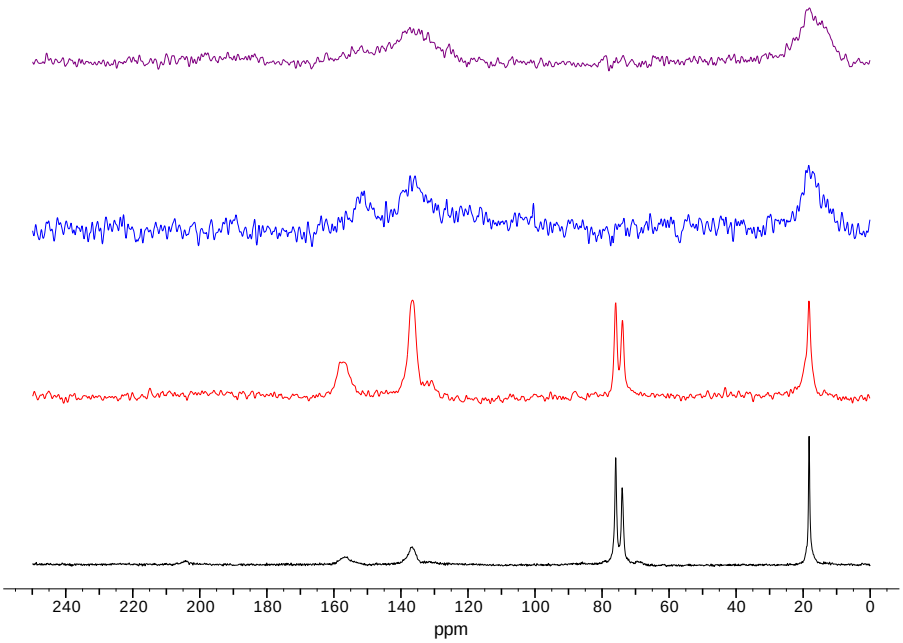

Figure 78: Comparison of the ^{13}C CPMAS dipolar dephased spectra of the virgin foam (black) with the chars obtained after pyrolysis under 3% oxygen in nitrogen at 250°C (red), 300°C (blue), 350°C (purple) and 400°C (pink)

Appendix 3: Nanocomposite Foams

2.7 DSC Repeat Analyses

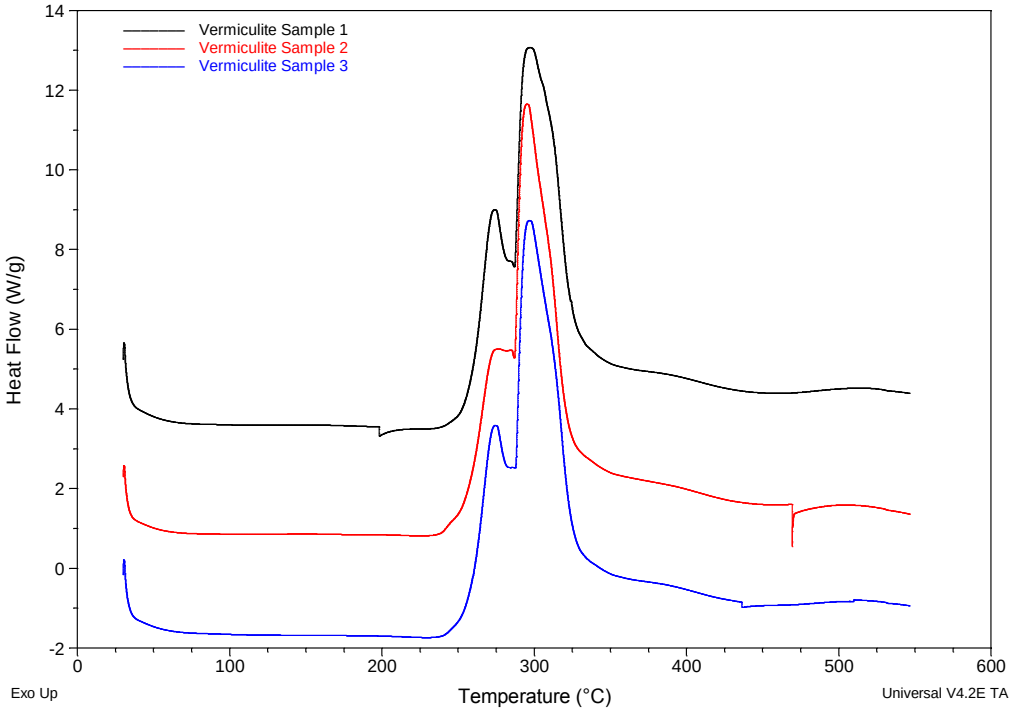

Figure 79: Vermiculite foam in air

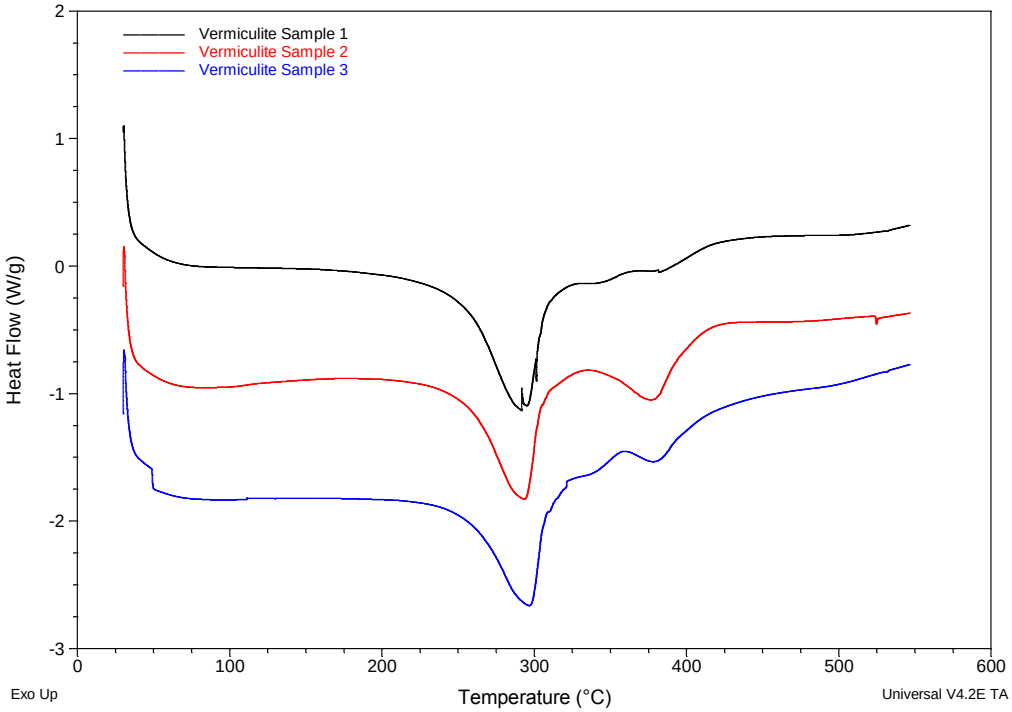

Figure 80: Vermiculite foam in N_2

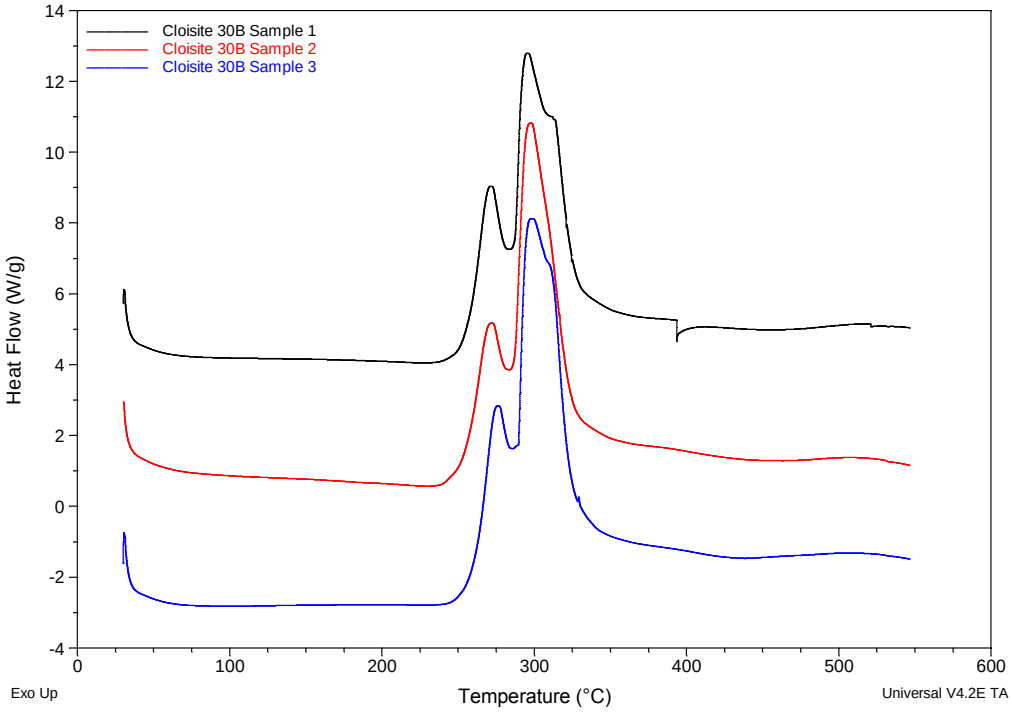

Figure 81: Cloisite 30B foam in air

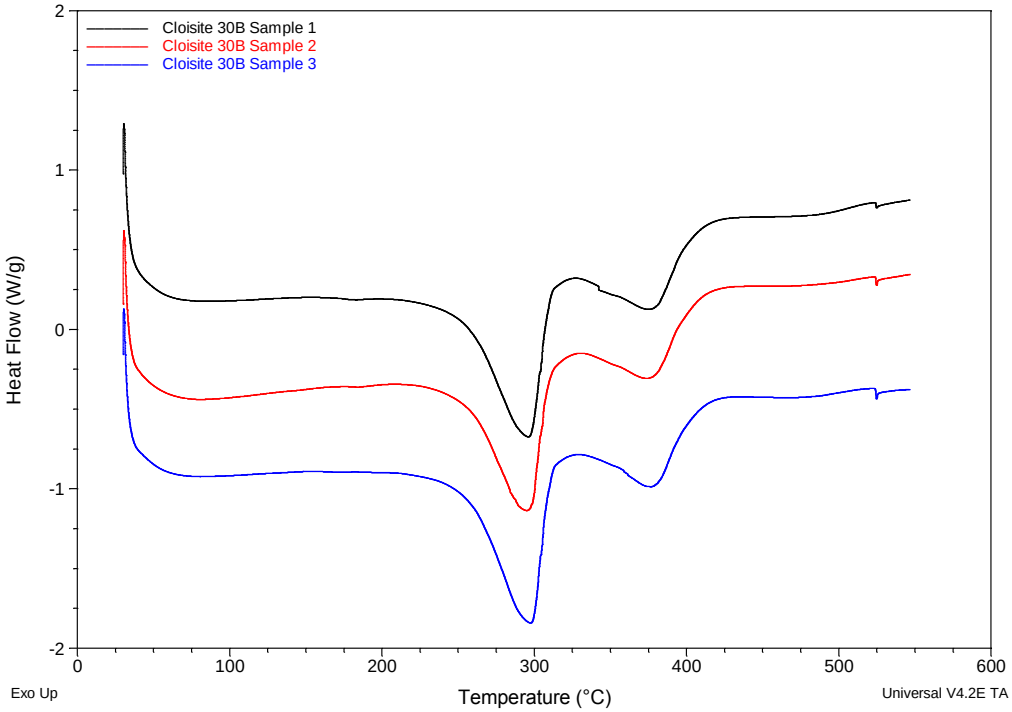

Figure 82: Cloisite 30B foam in N_2

2.8 TVA Studies

2.8.1 Non-condensables

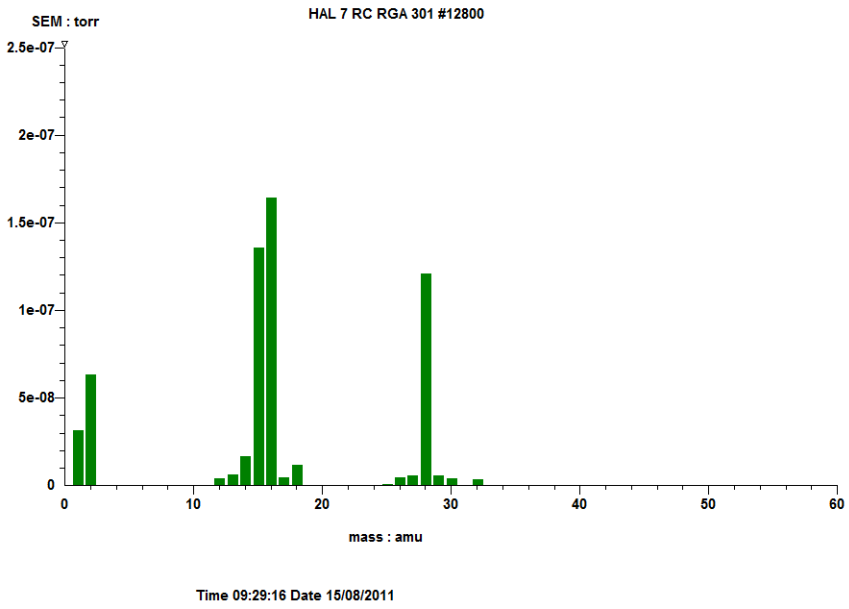

83: **vermiculite**

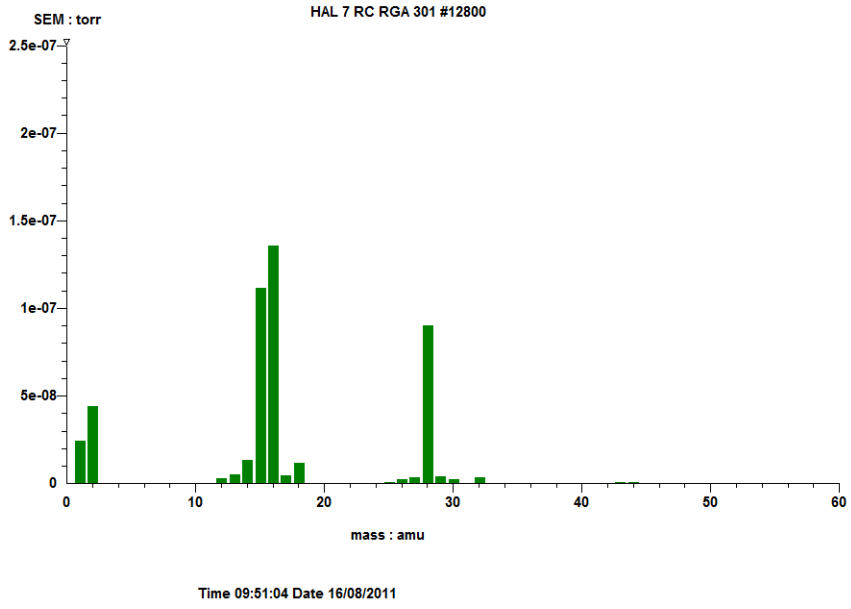

84: Clositie

2.9 TVA- cold ring fractions

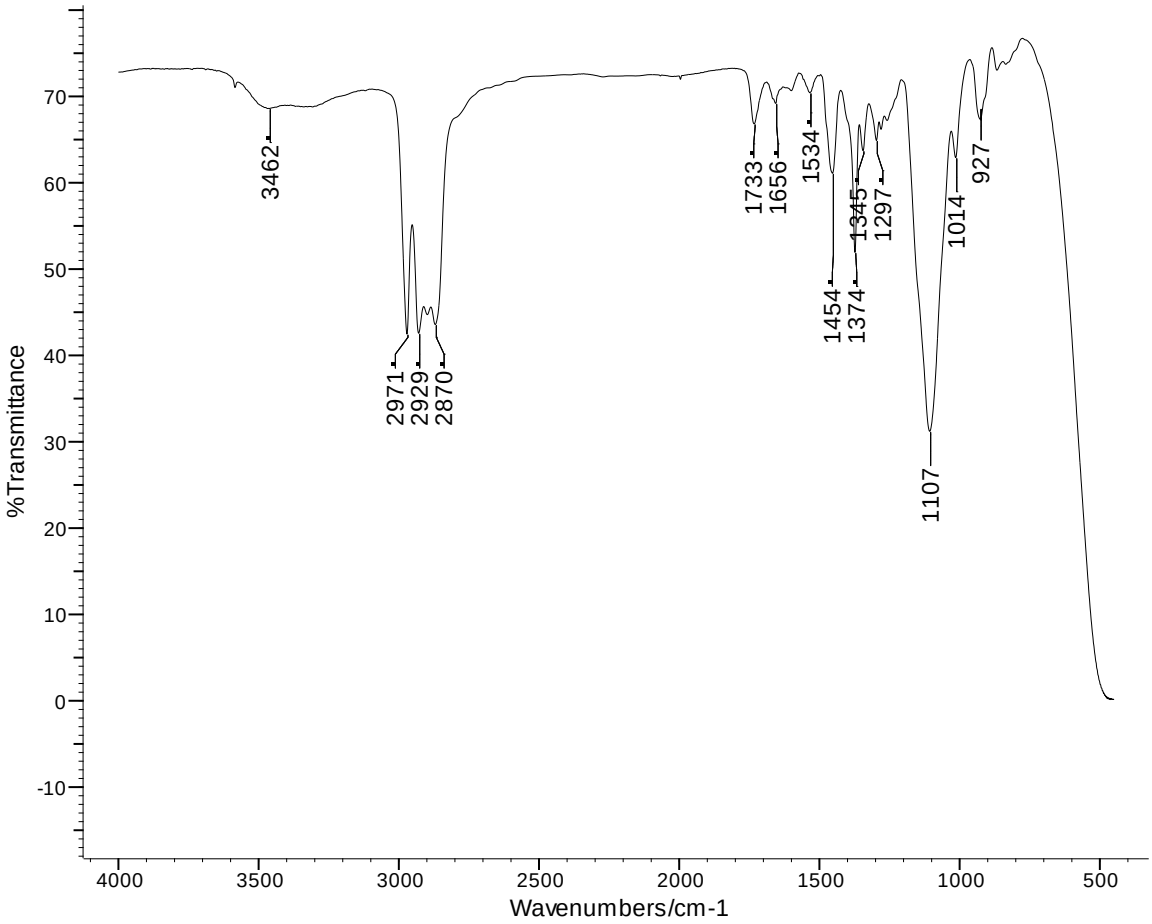

Figure 85: FTIR spectrum of the cold-ring fraction collected from the vermiculite foam

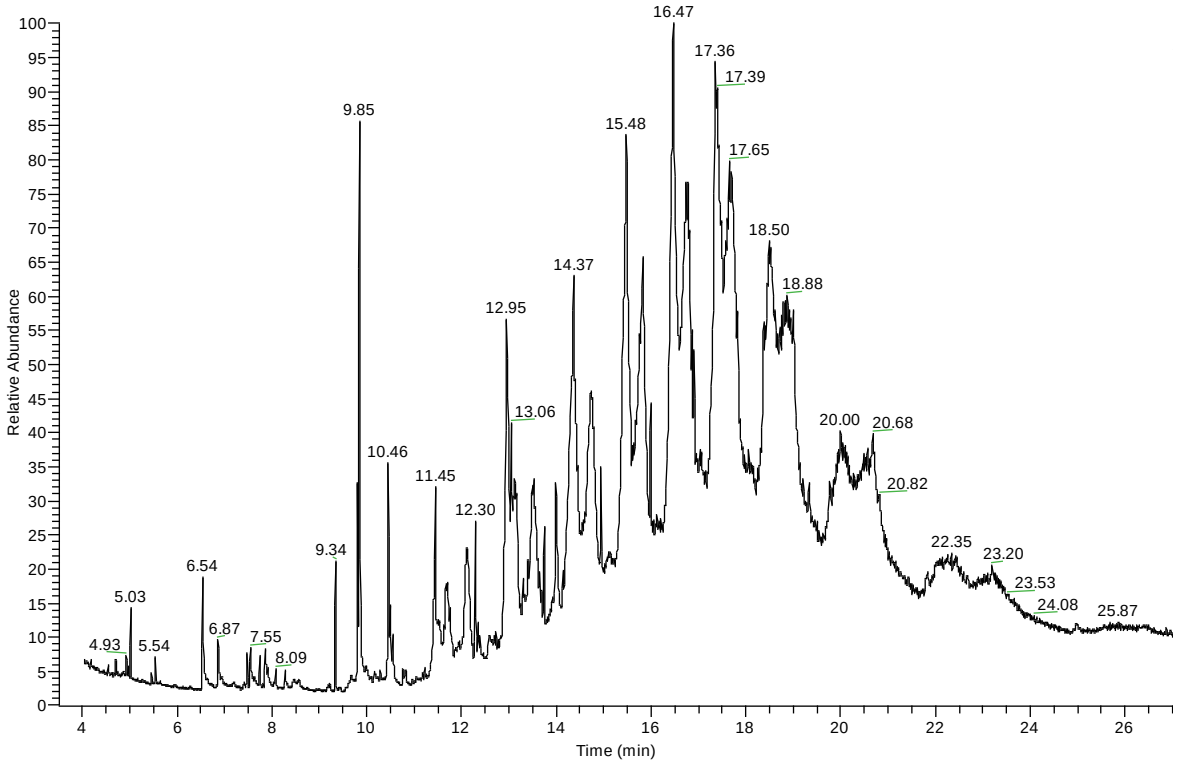

Figure 86: GC-MS total-ion chromatogram for the cold-ring fraction collected from the vermiculite foam

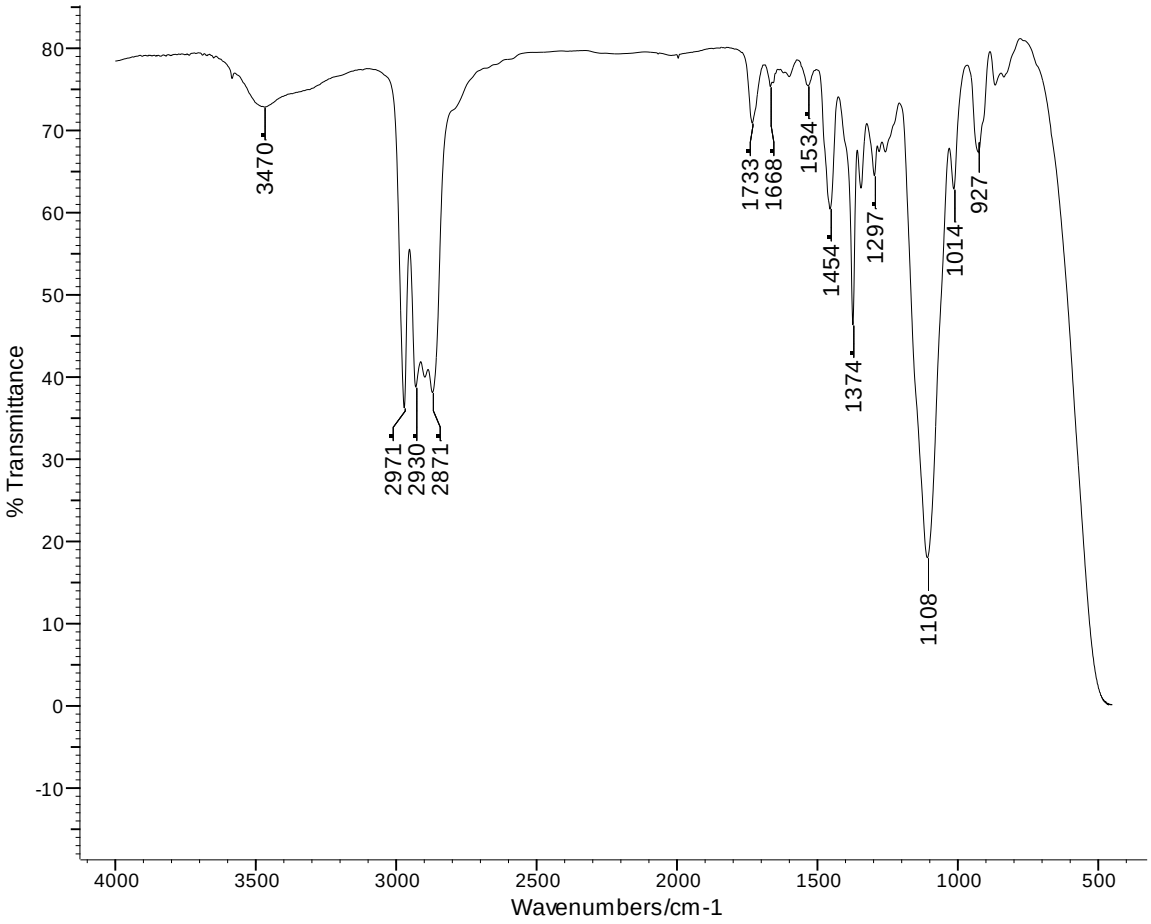

Figure 87: FTIR spectrum of the cold-ring fraction collected from the Cloisite® 30B foam

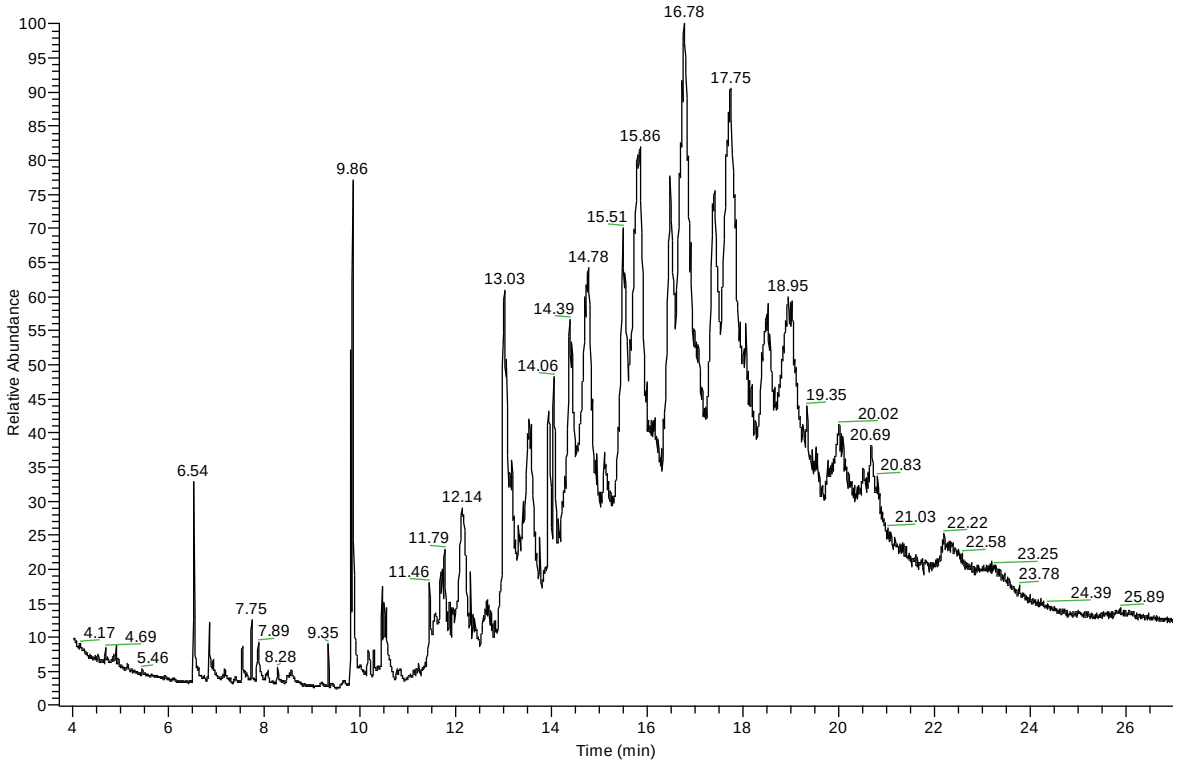

Figure 88: GC-MS total-ion chromatogram for the cold-ring fraction collected from the Cloisite 30B foam

2.10 TVA- condensables

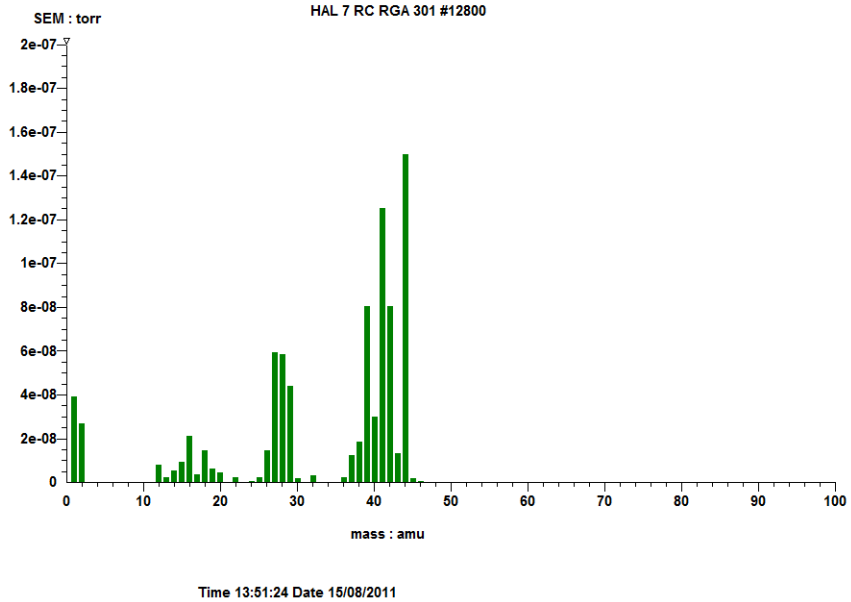

89: verm propene co2

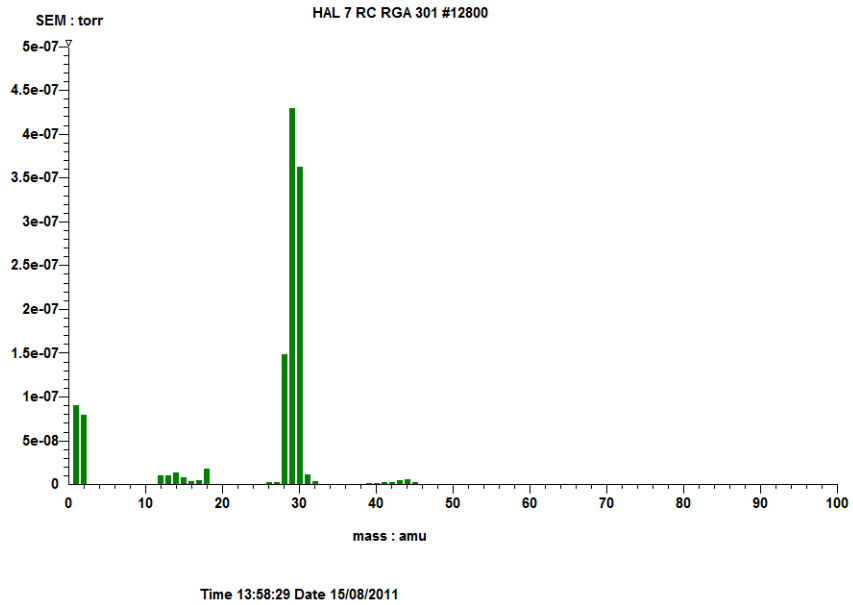

90: verm form

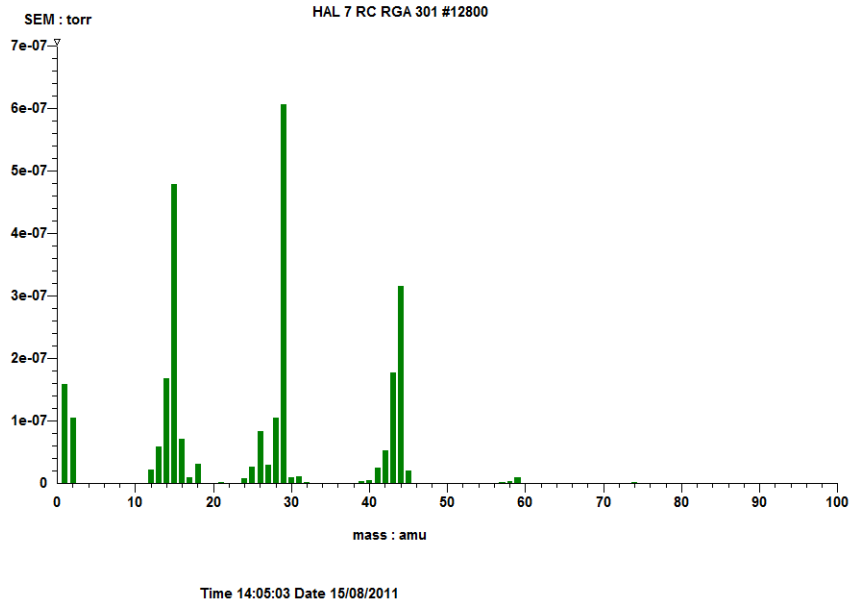

91: verm acetaldehyde

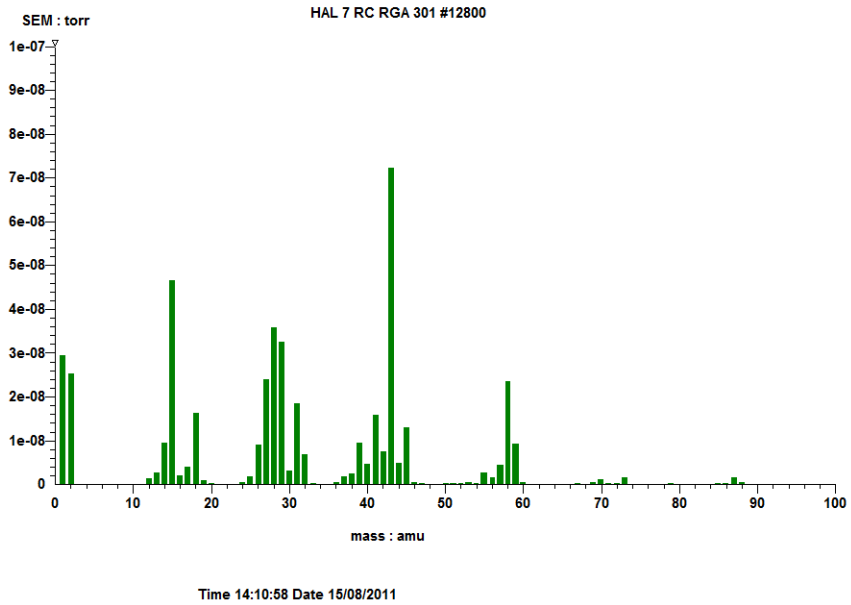

92: verm isomers

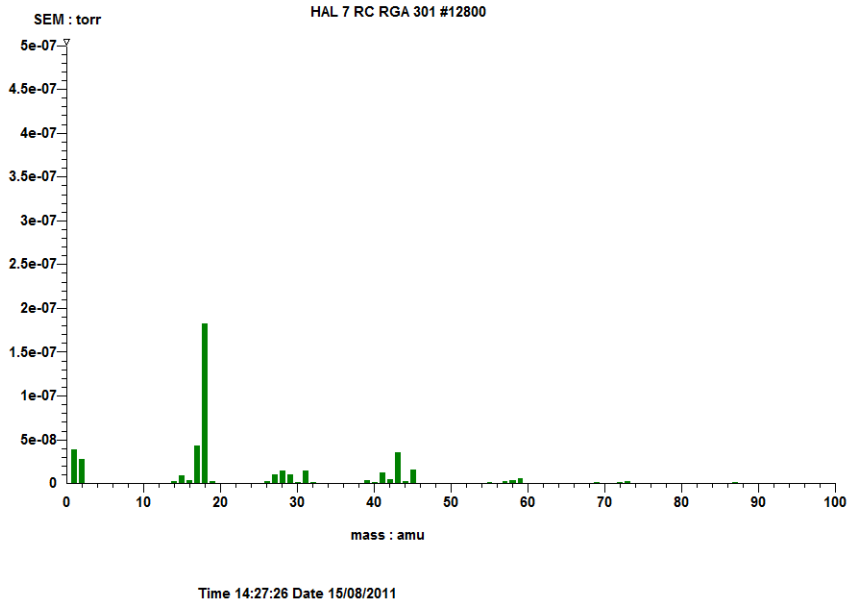

93: verm higher molar mass and water

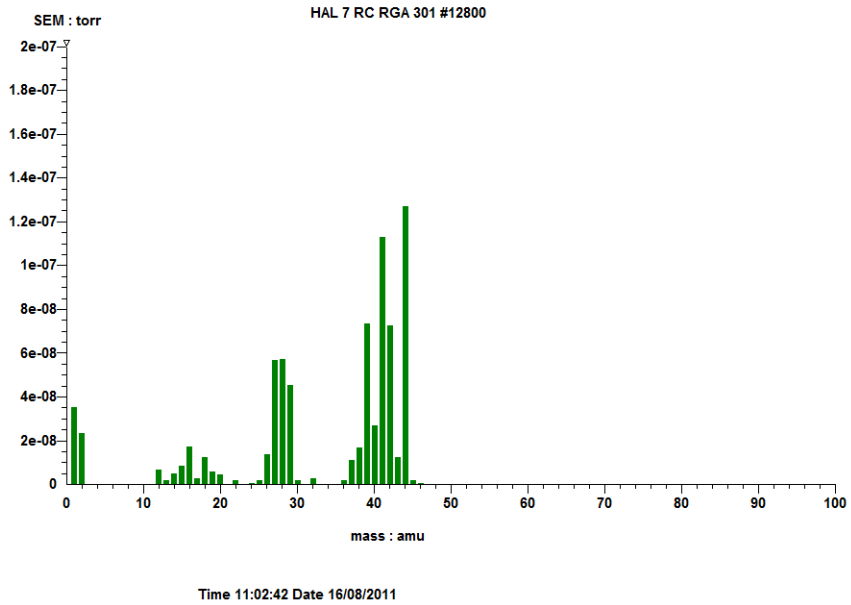

94: cloisite propene co2

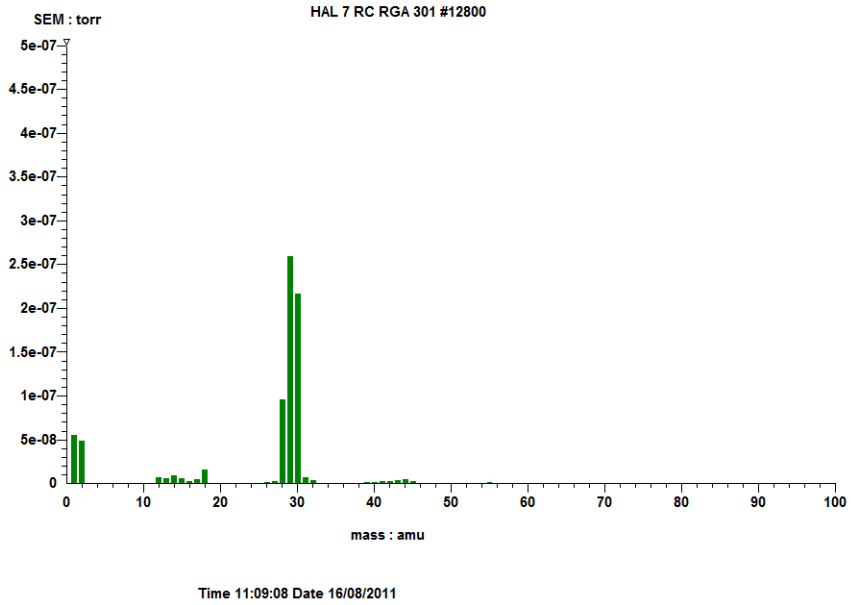

95: clositie formaldehyde

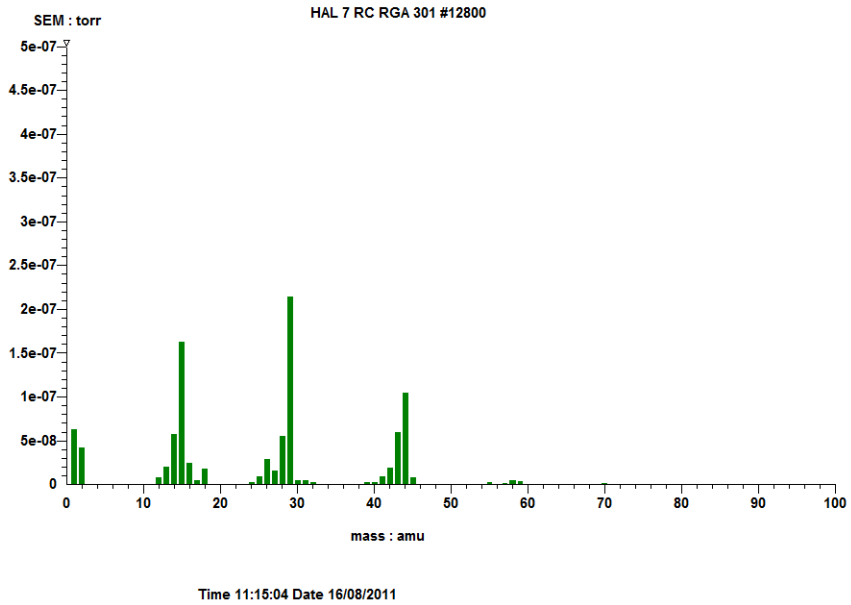

96: clositie acetaldehyde

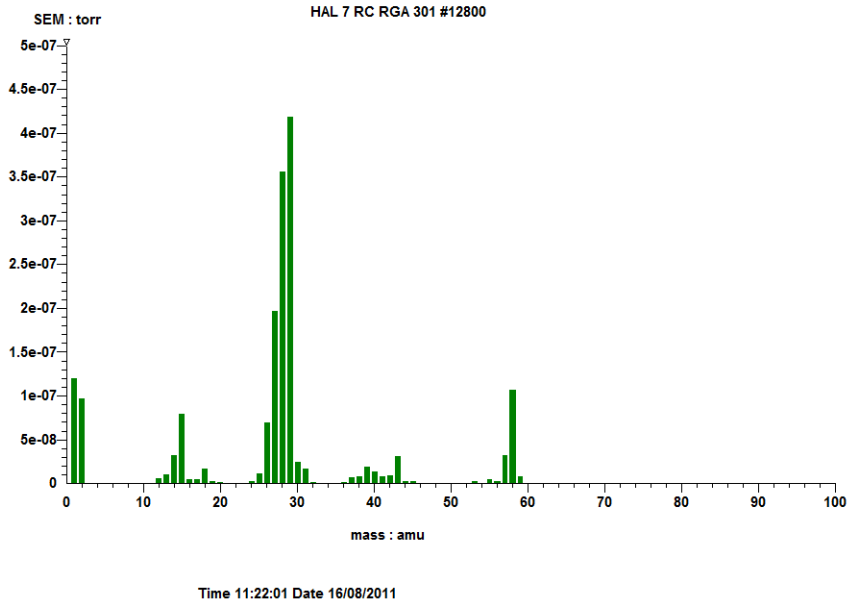

97: clositie propanal

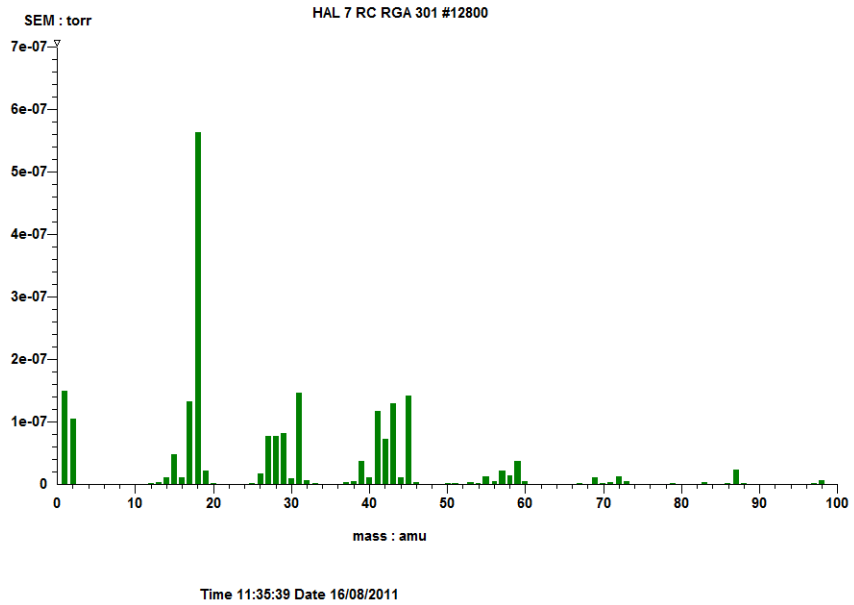

98cloisite water and high molar amss

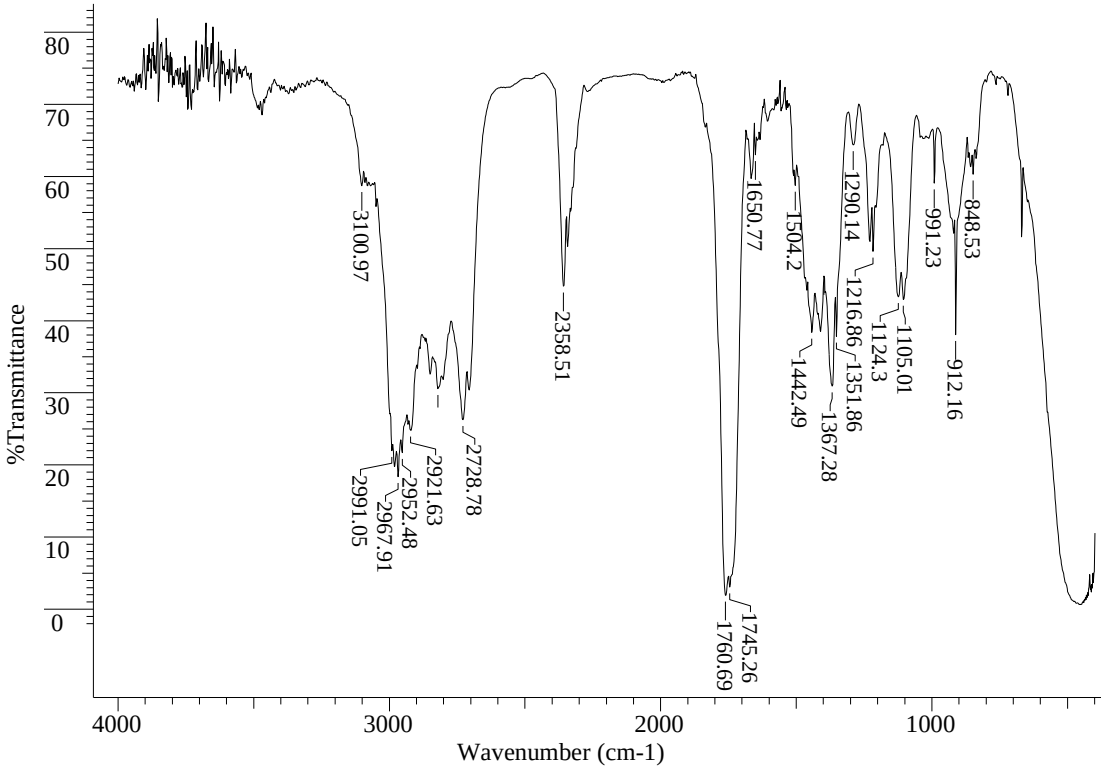

Figure 99: FTIR spectrum for fraction 1 collected from the vermiculite foam

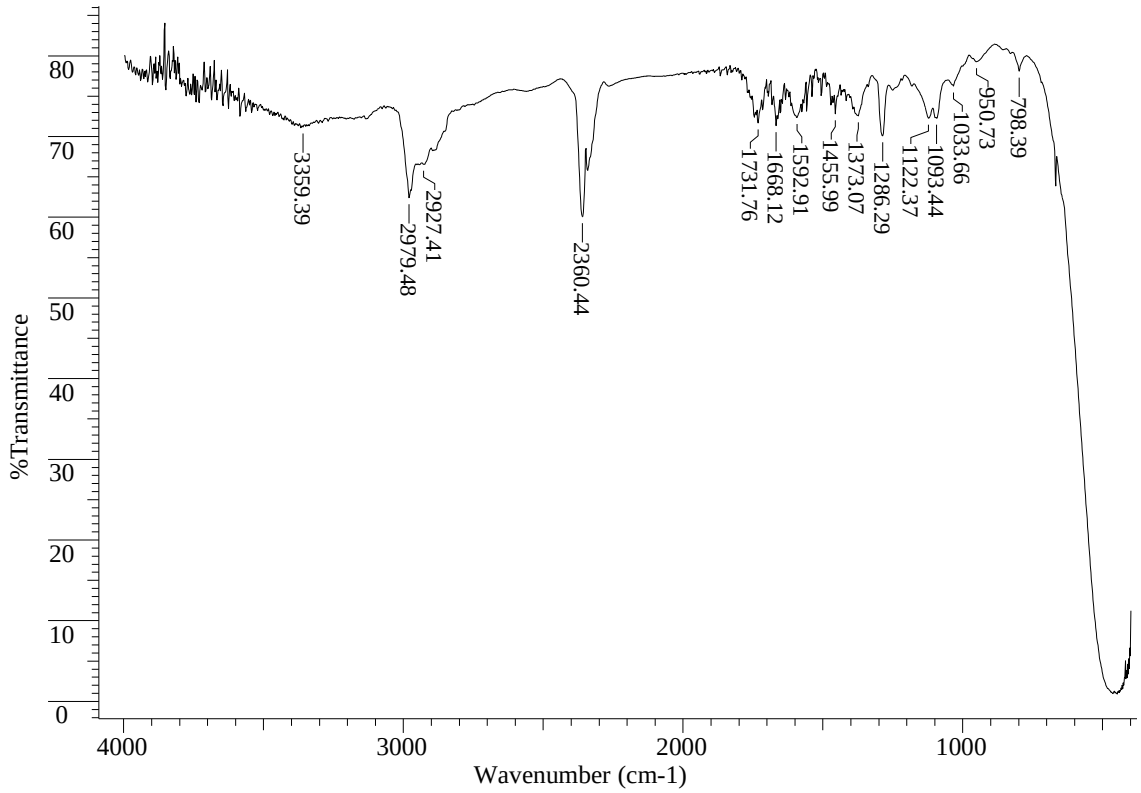

Figure 100: FTIR spectrum for fraction 2 collected from the vermiculite foam

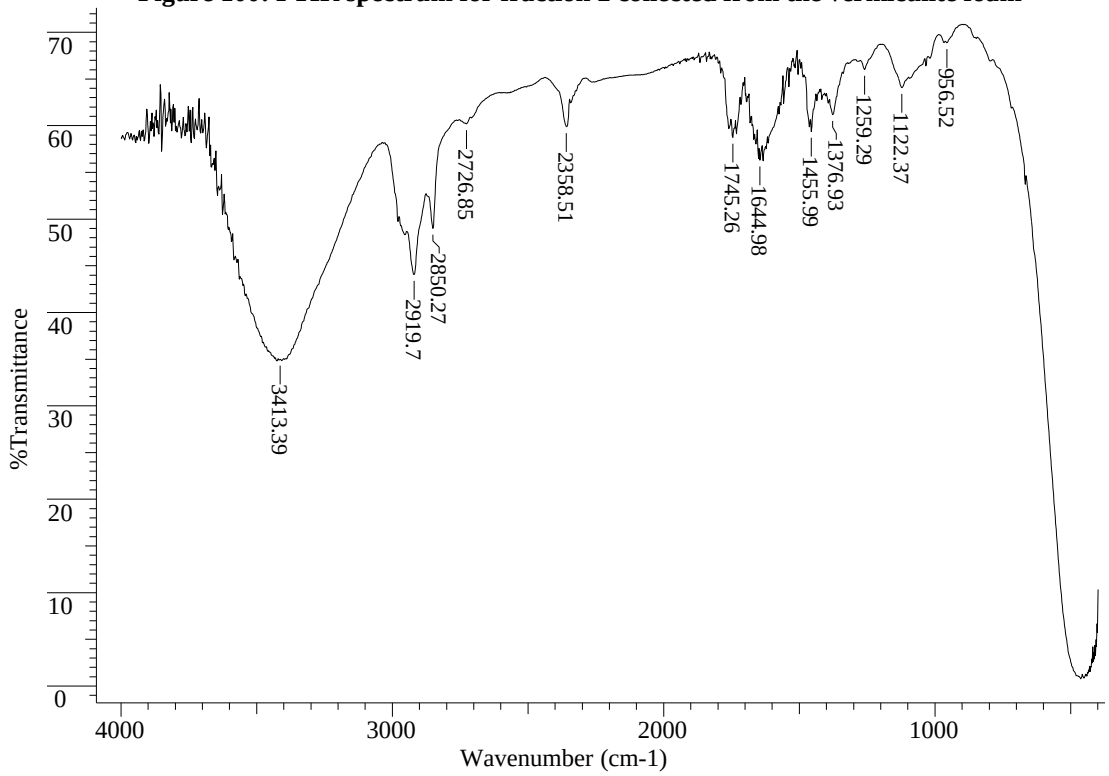

Figure 101: FTIR spectrum for fraction 3 collected from the vermiculite foam

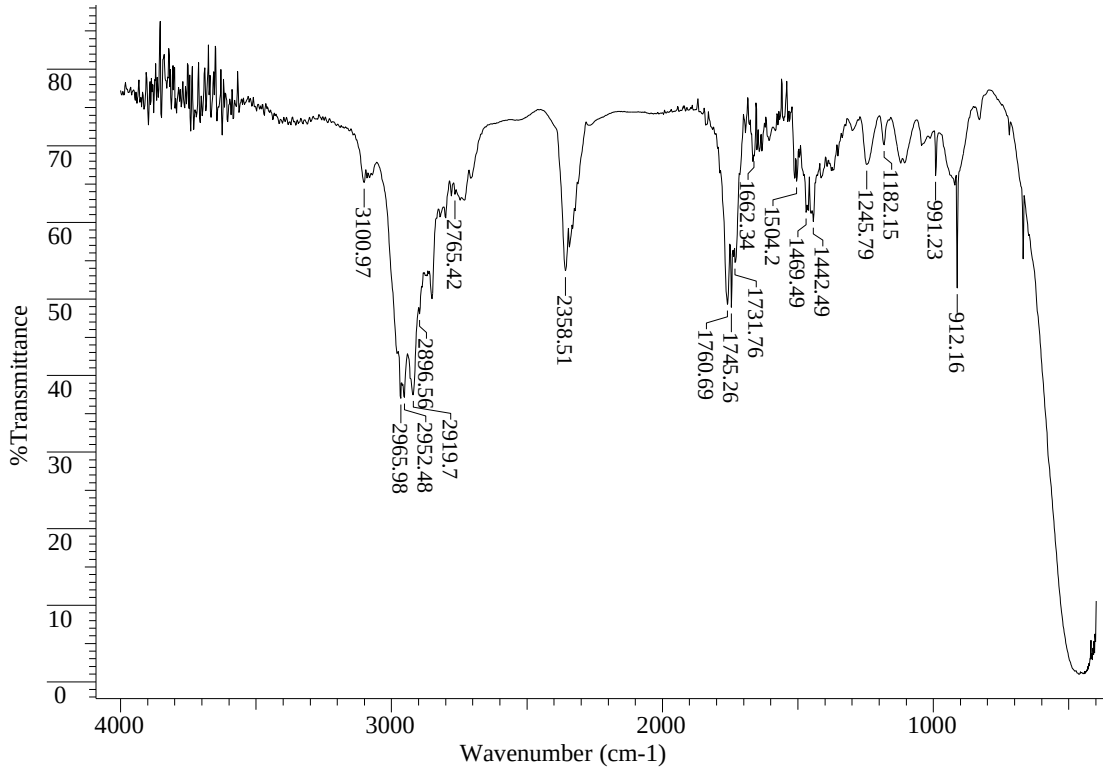

Figure 102: FTIR spectrum for fraction 1 collected from the Cloisite® 30B

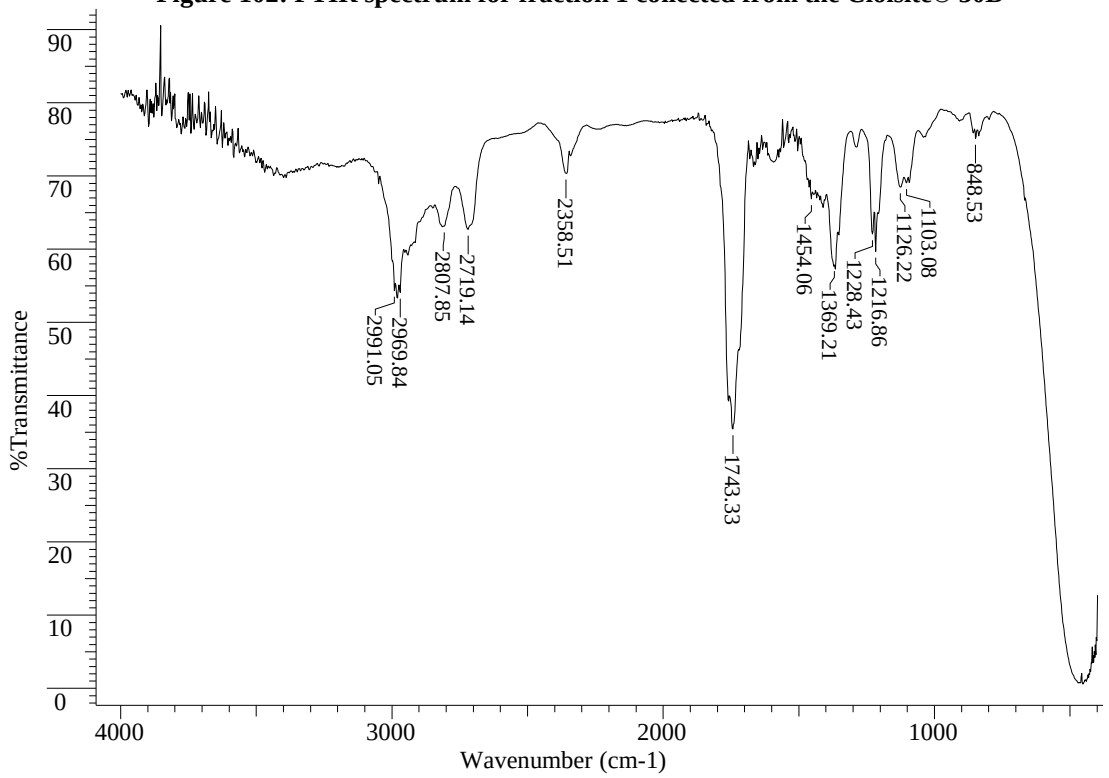

Figure 103: FTIR spectrum for fraction 2 collected from the Cloisite® 30B foam

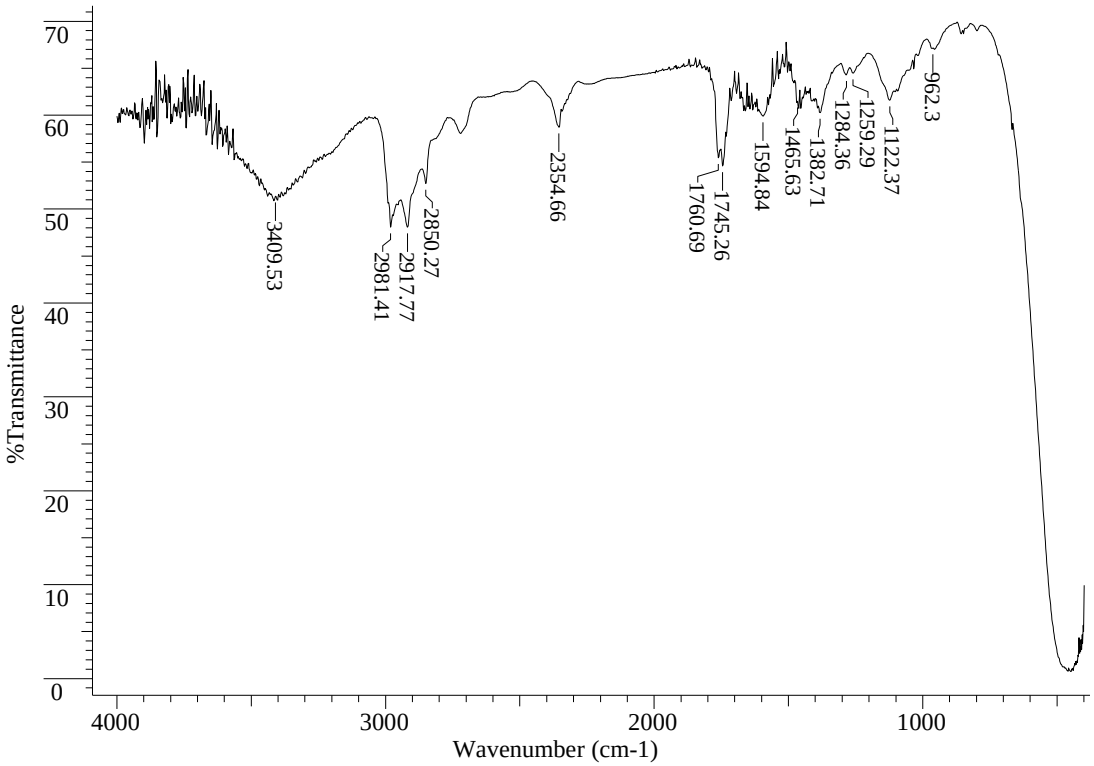

Figure 104: FTIR spectrum for fraction 3 collected from the Cloisite® 30B foam

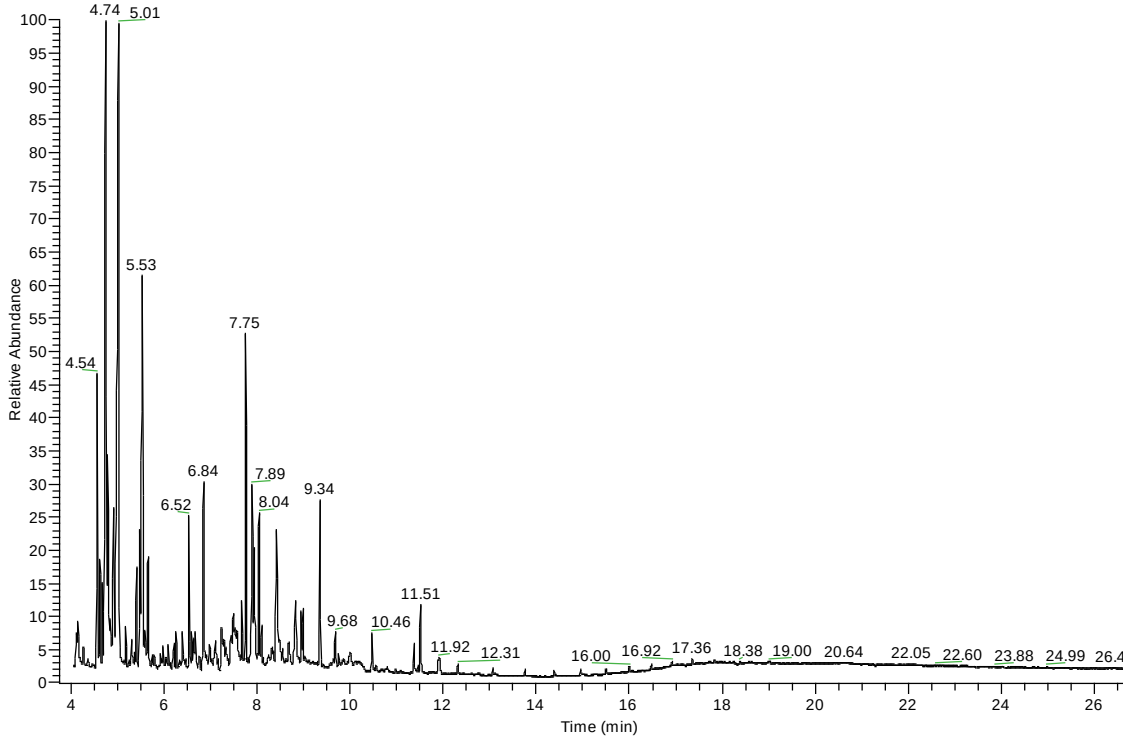

Figure 105: GC-MS total-ion chromatogram for fraction 3 from the vermiculite foam

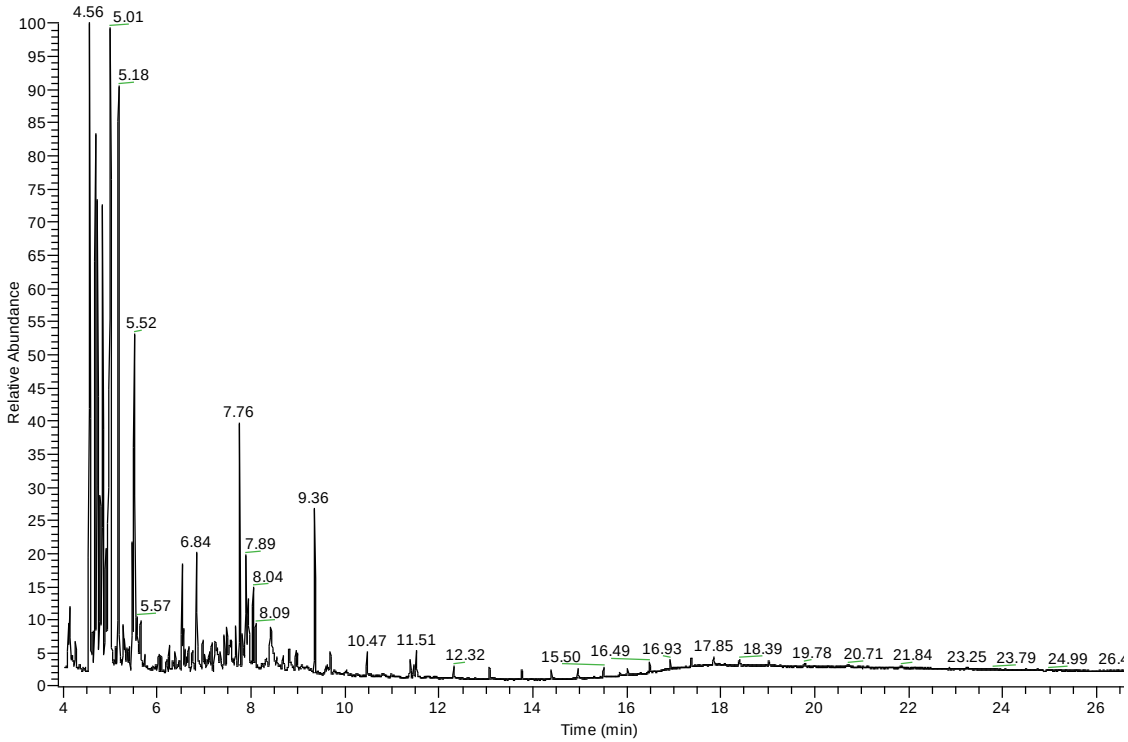

Figure 106: GC-MS total-ion chromatogram for fraction 3 from the Cloisite 30B foam

Appendix 3 –Nanocomposite Foams

3.1 DSC Repeat Analyses

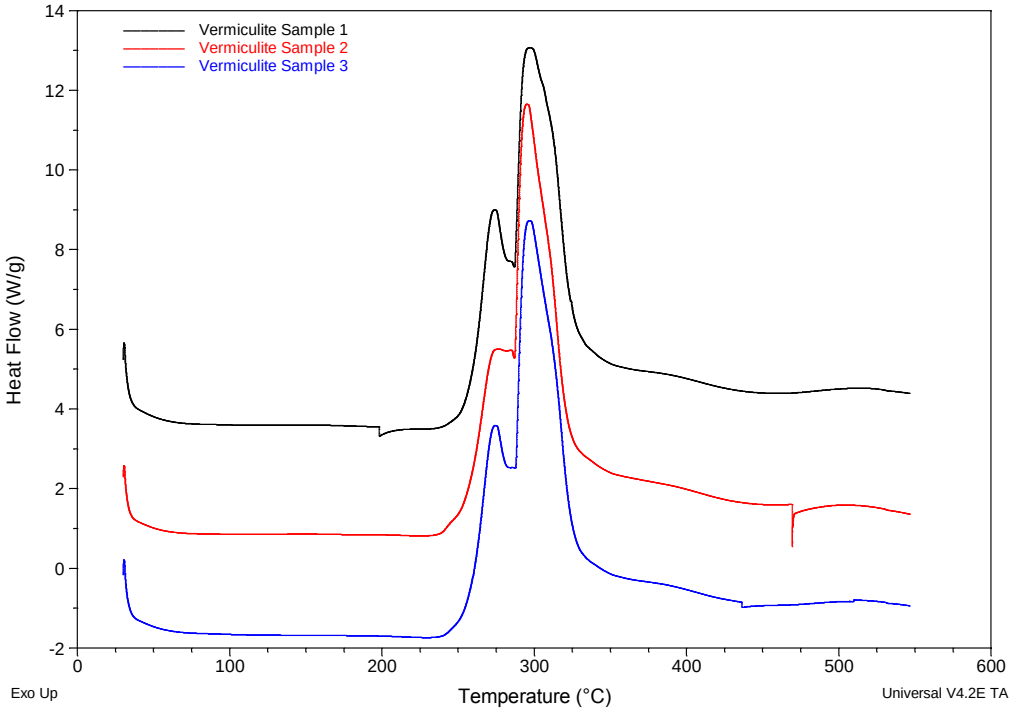

Figure 1:DSC analysis of vermiculite foam in air

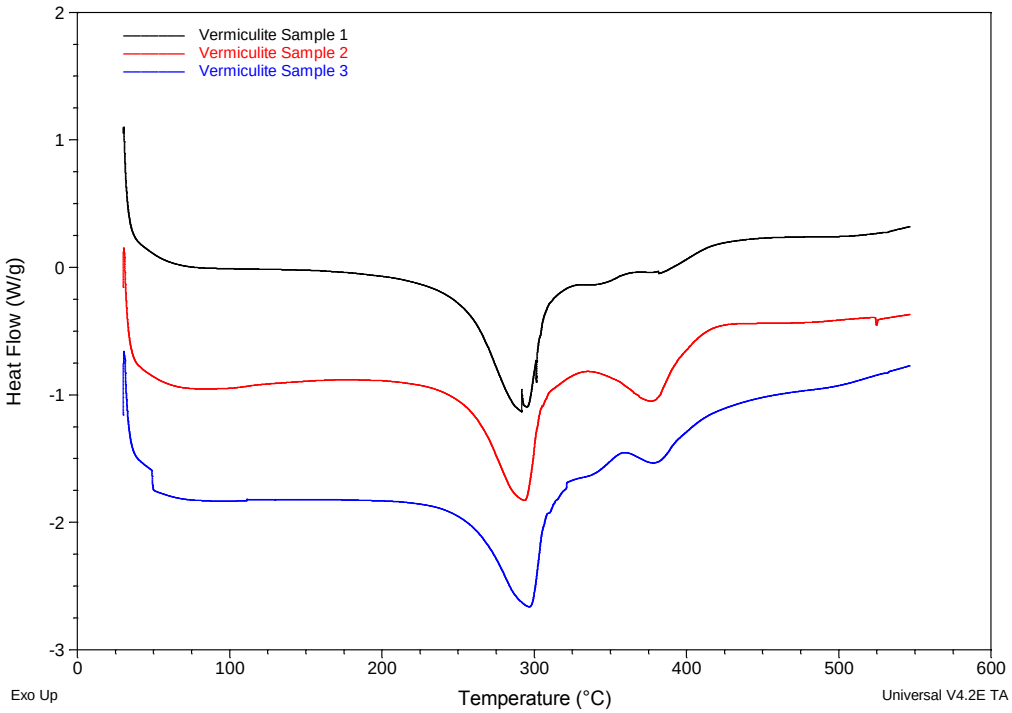

Figure 2: DSC analysis of vermiculite foam in N_2

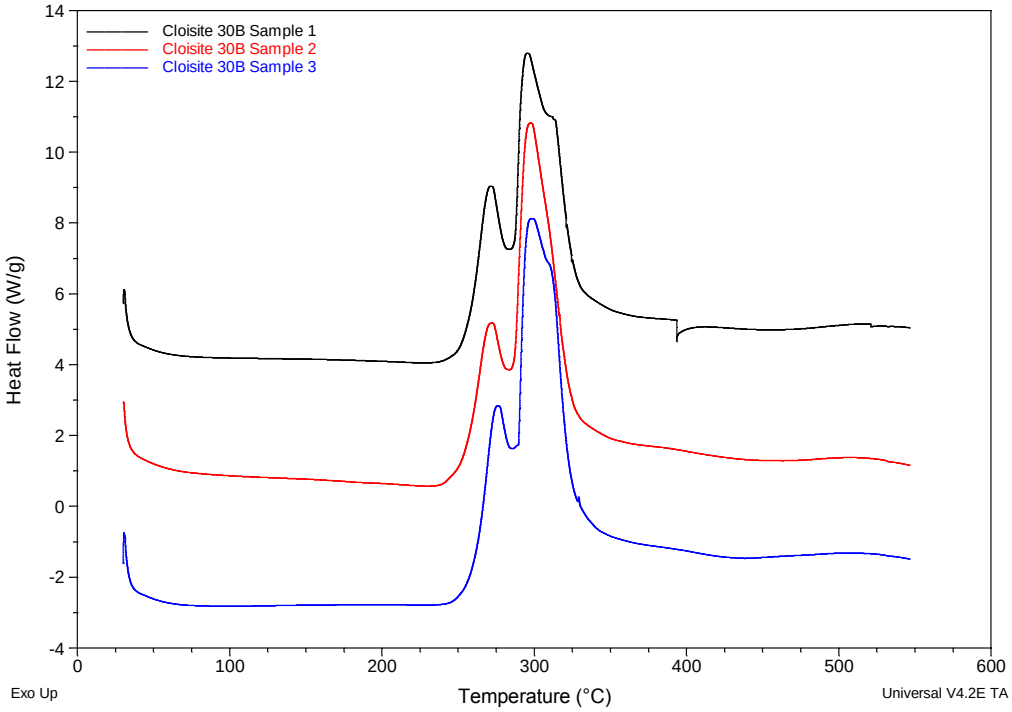

Figure 3: DSC analysis of Cloisite® 30B foam in air

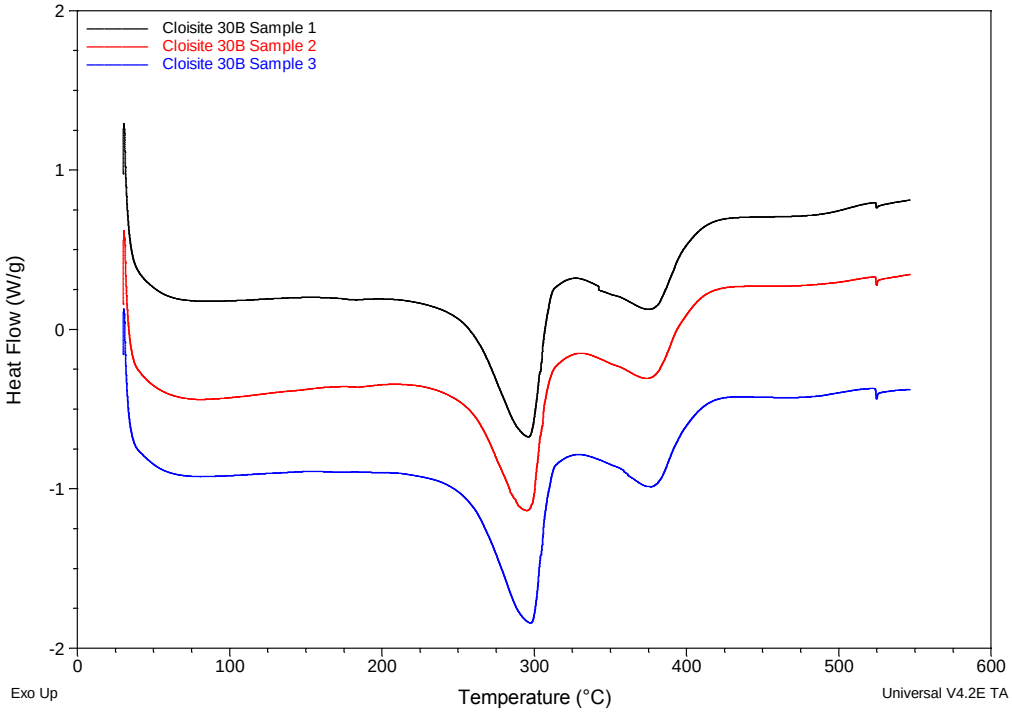

Figure 4: DSC analysis of Cloisite® 30B foam in N_2

2.2 TVA Study

2.2.1 Non-condensables

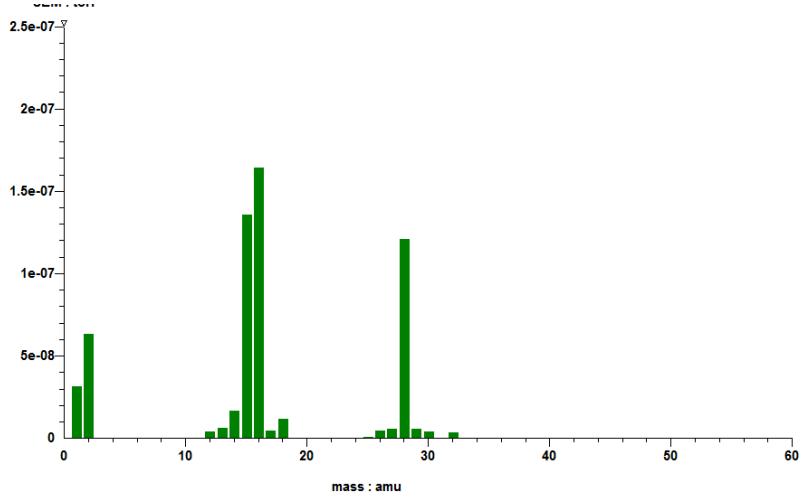

Figure 5: MS of the non-condensable volatiles from the vermiculite foam

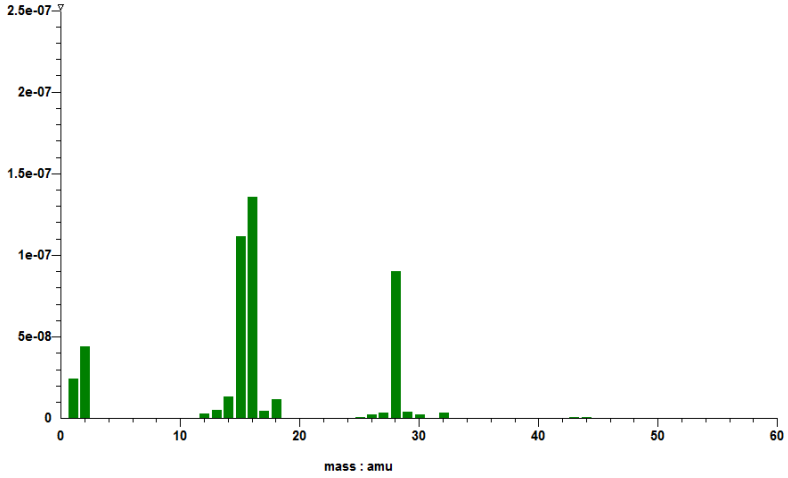

6: MS of the non-condensable volatiles from the Cloisite® 30B foam

2.2.2 Cold-ring Fractions

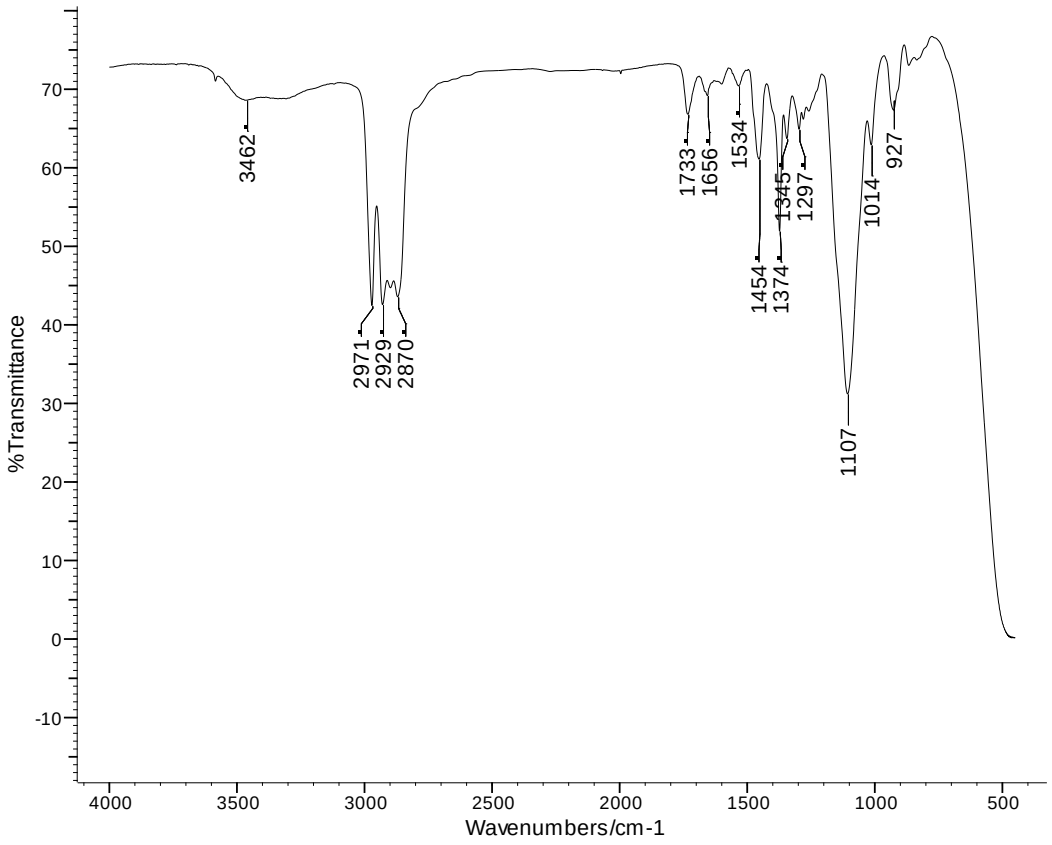

Figure 7: FTIR spectrum of the cold-ring fraction collected from the vermiculite foam

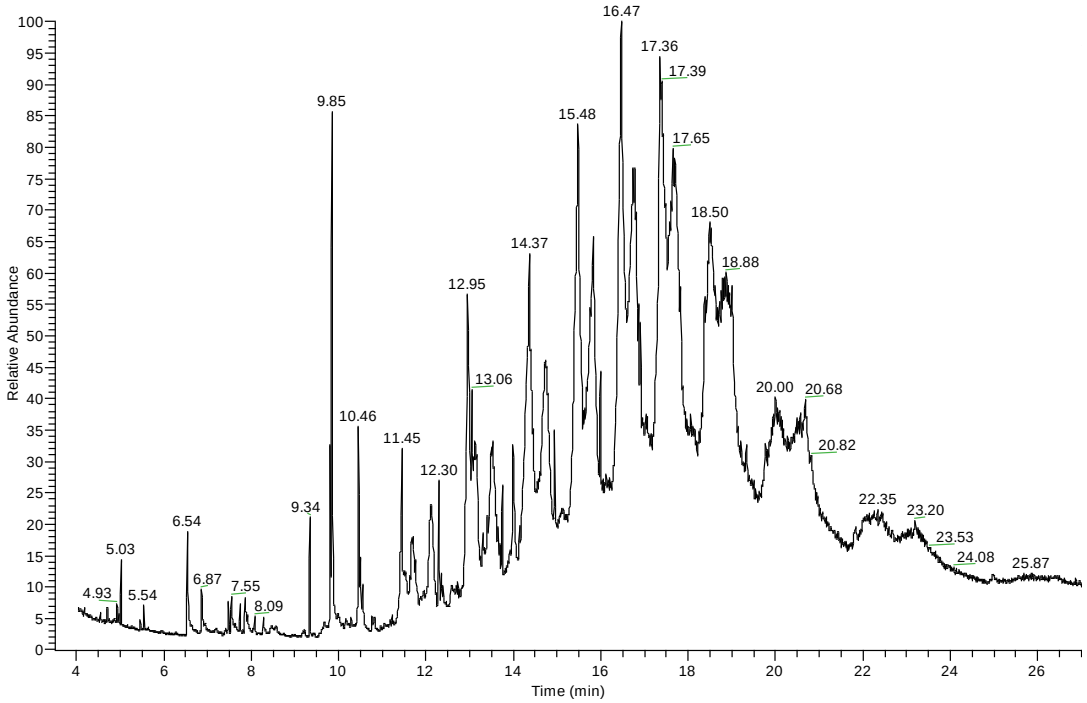

Figure 8: GC-MS chromatogram for the cold-ring fraction collected from the vermiculite foam

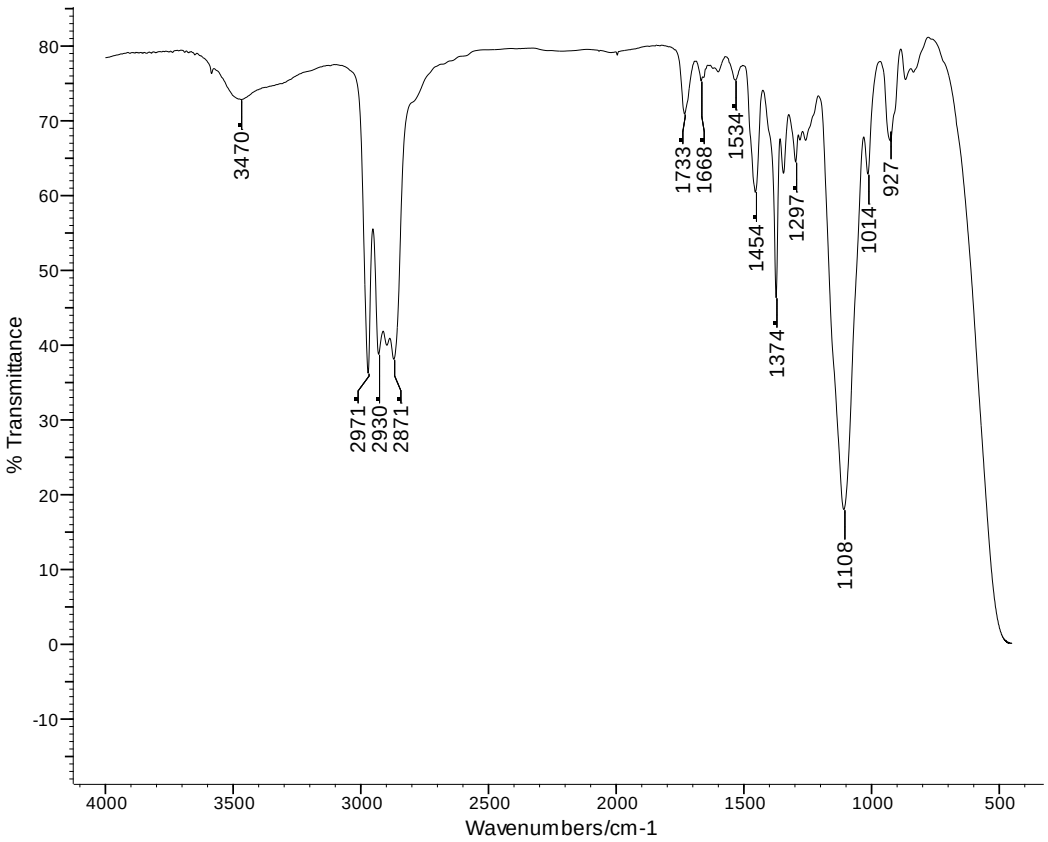

Figure 9: FTIR spectrum of the cold-ring fraction collected from the Cloisite® 30B foam

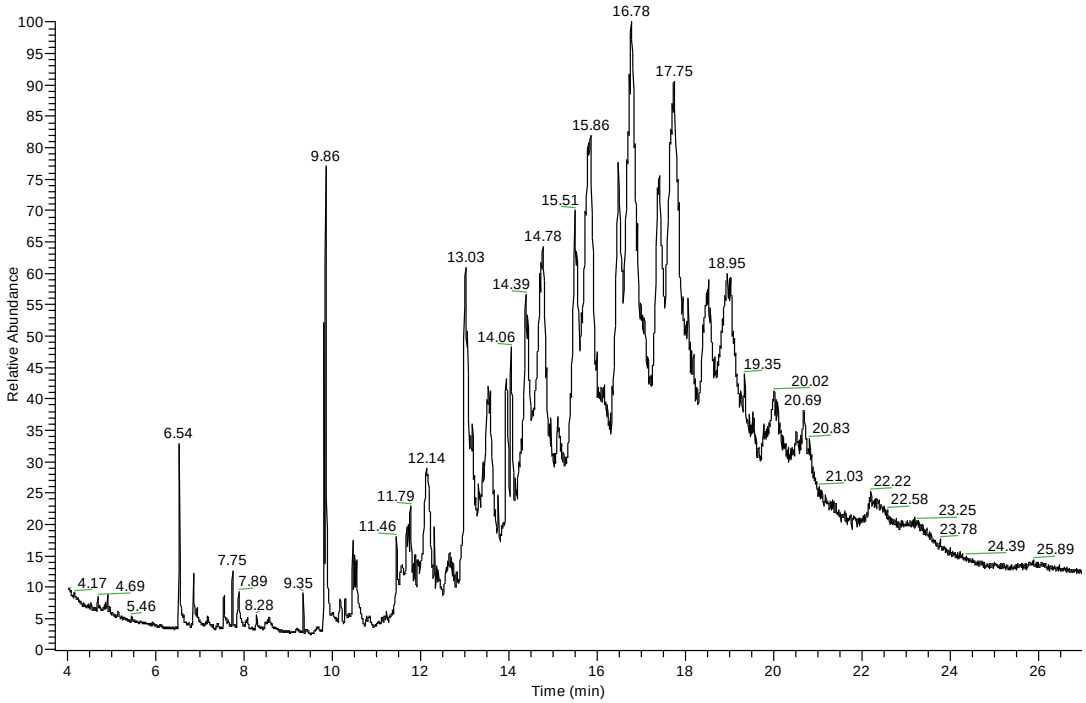

Figure 10: GC-MS chromatogram for the cold-ring fraction collected from the Cloisite 30B foam

2.2.3 Condensable Fractions

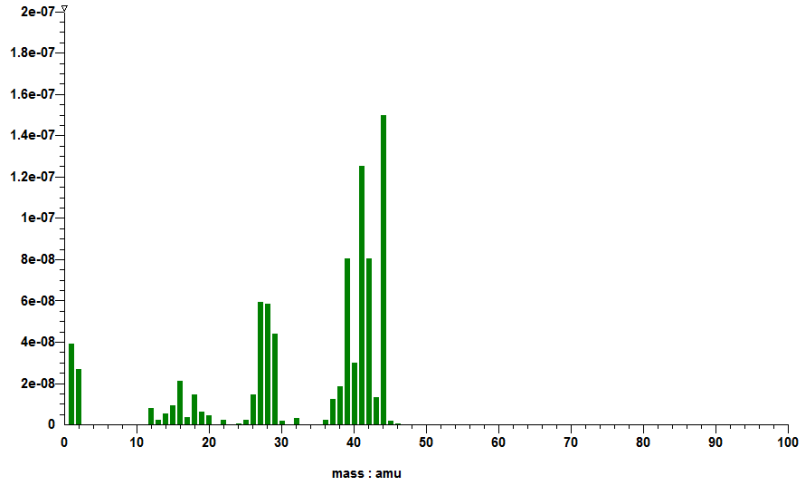

Figure 11: MS of propene and CO_2 collected from the vermiculite foam

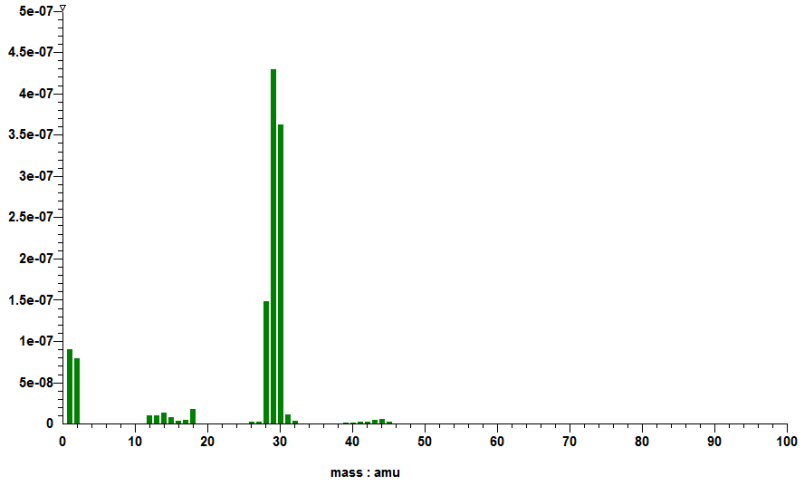

Figure 12: MS of formaldehyde collected from the vermiculite foam

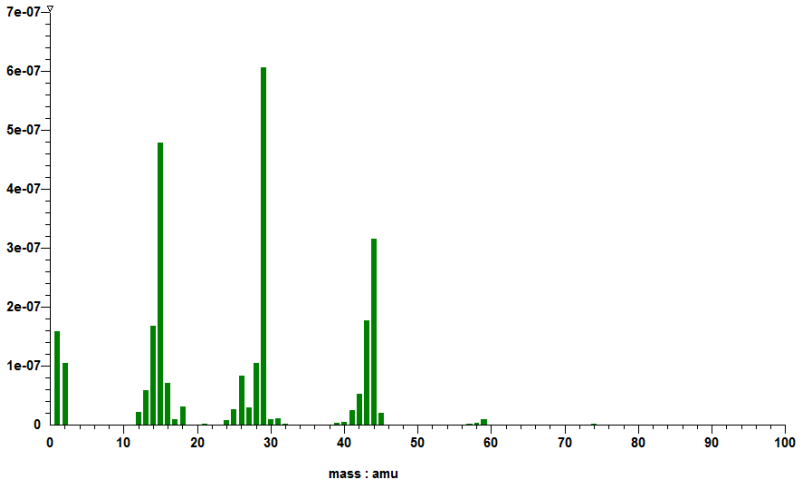

Figure 13: MS of acetaldehyde collected from the vermiculite foam

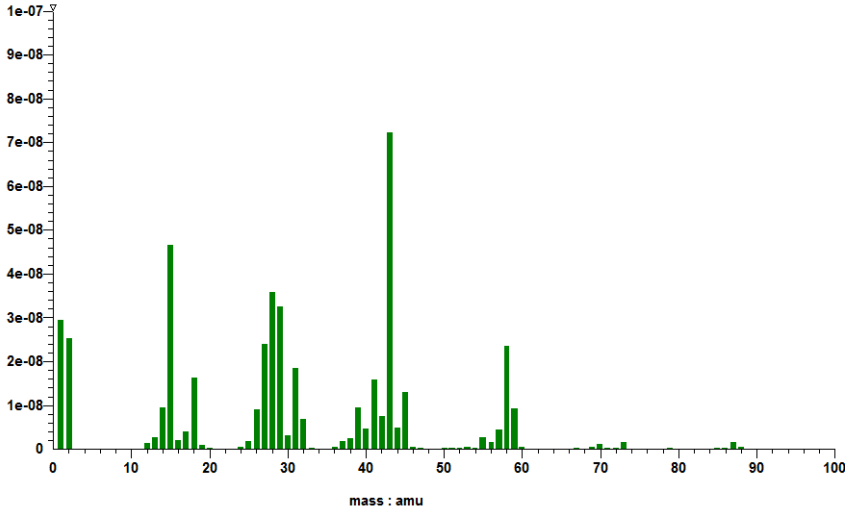

Figure 14: MS of C_3H_6O isomers collected from the vermiculite foam

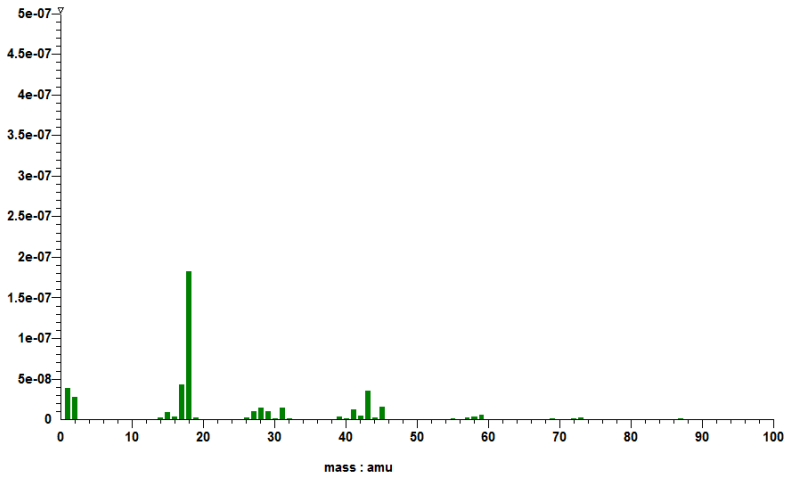

Figure 15: MS of water and higher molar mass material collected from the vermiculite foam

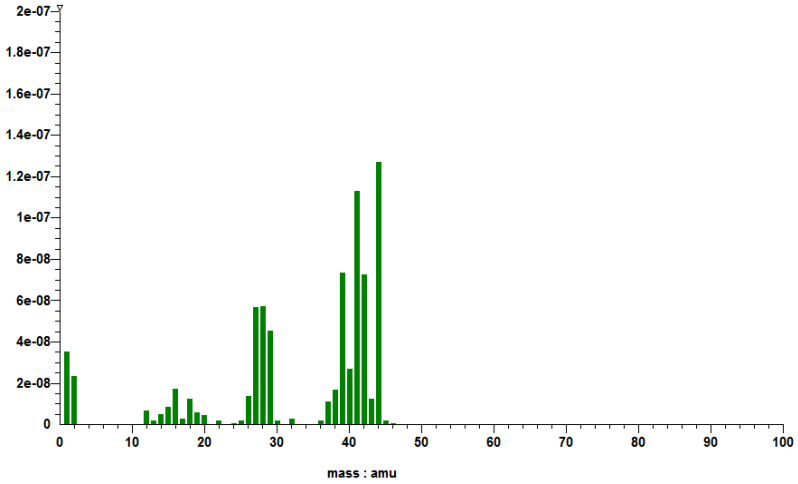

Figure 16: MS of propene and CO_2 collected from the Cloisite® 30B foam

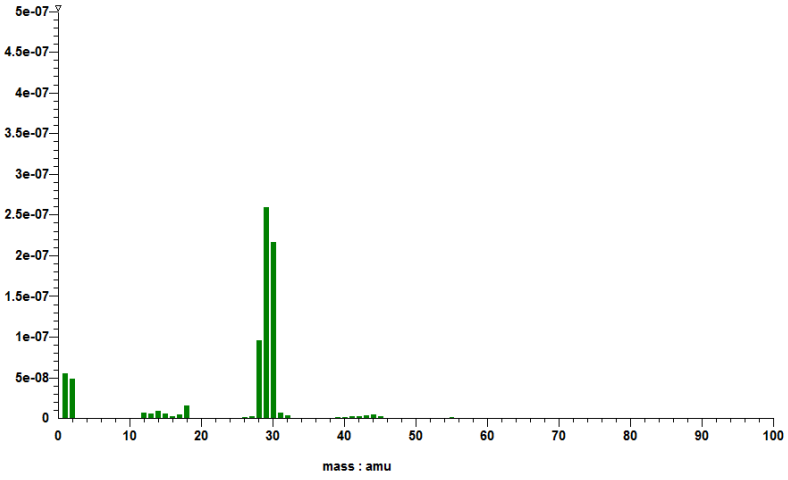

Figure 17: MS of formaldehyde collected from the Cloisite® 30B foam

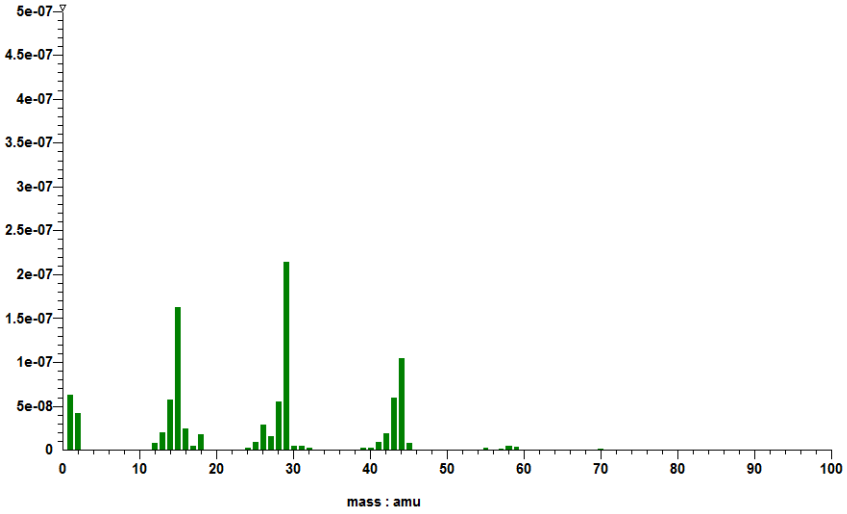

Figure 18: MS of acetaldehyde collected from the Cloisite® 30B foam

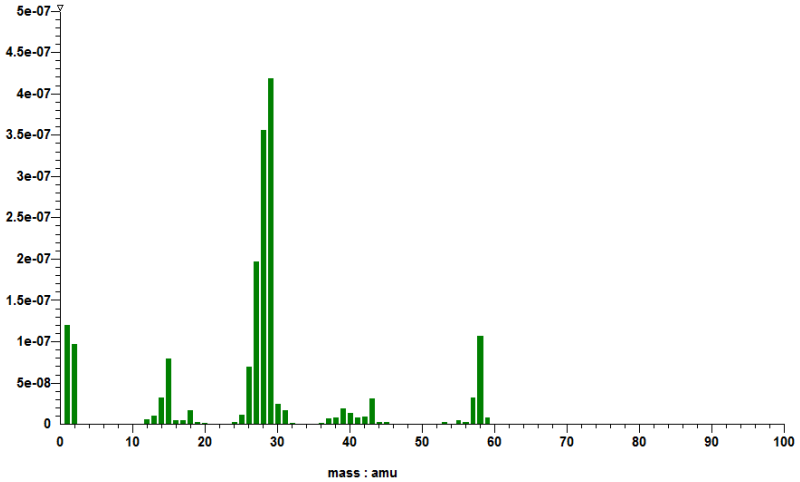

Figure 19: MS of propanal collected from the Cloisite® 30B foam

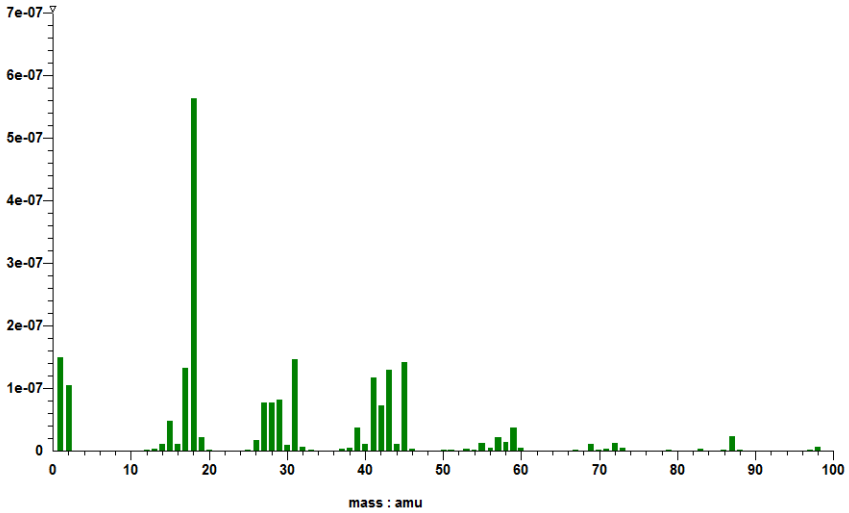

Figure 20: MS of water and high molar mass material collected from the Cloisite® 30B foam

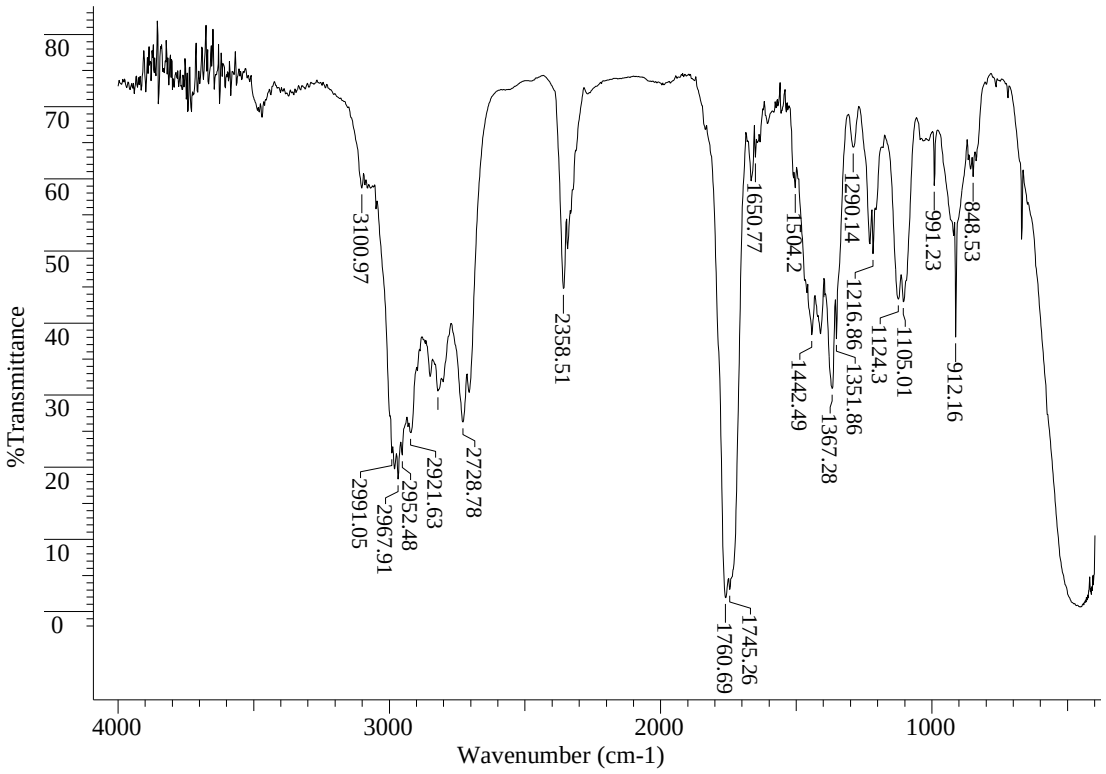

Figure 21: FTIR spectrum for fraction 1 collected from the vermiculite foam

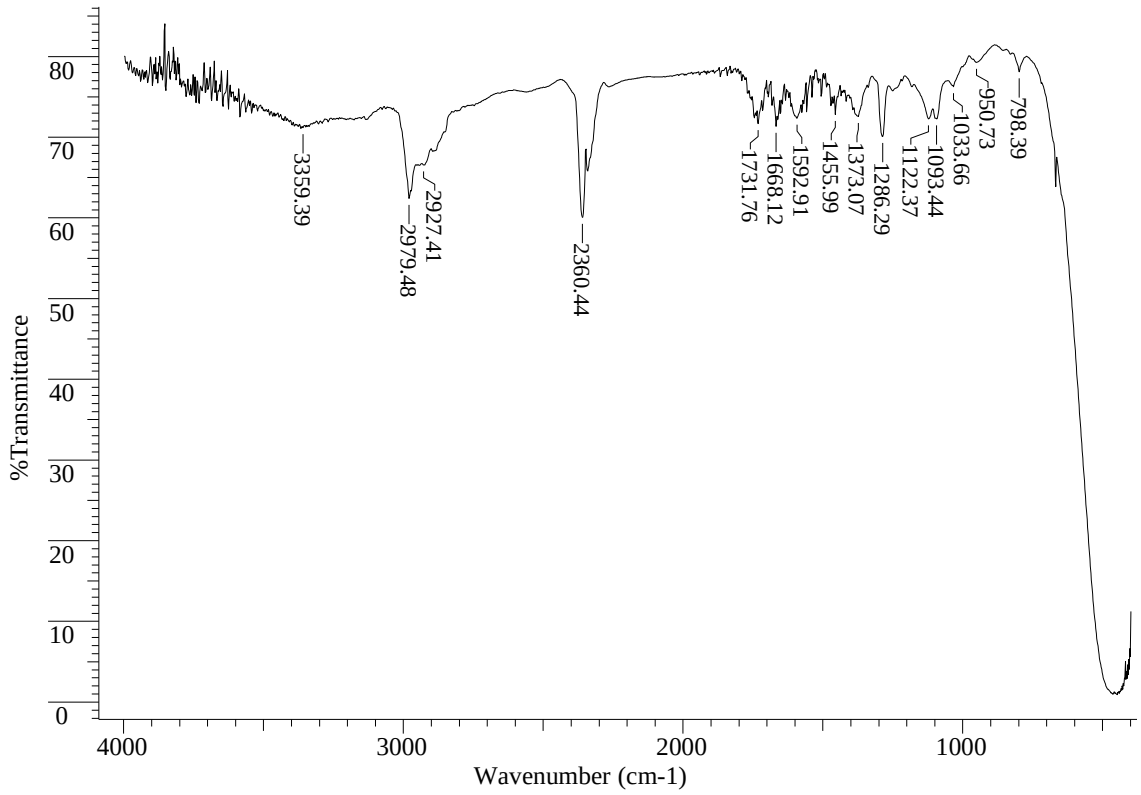

Figure 22: FTIR spectrum for fraction 2 collected from the vermiculite foam

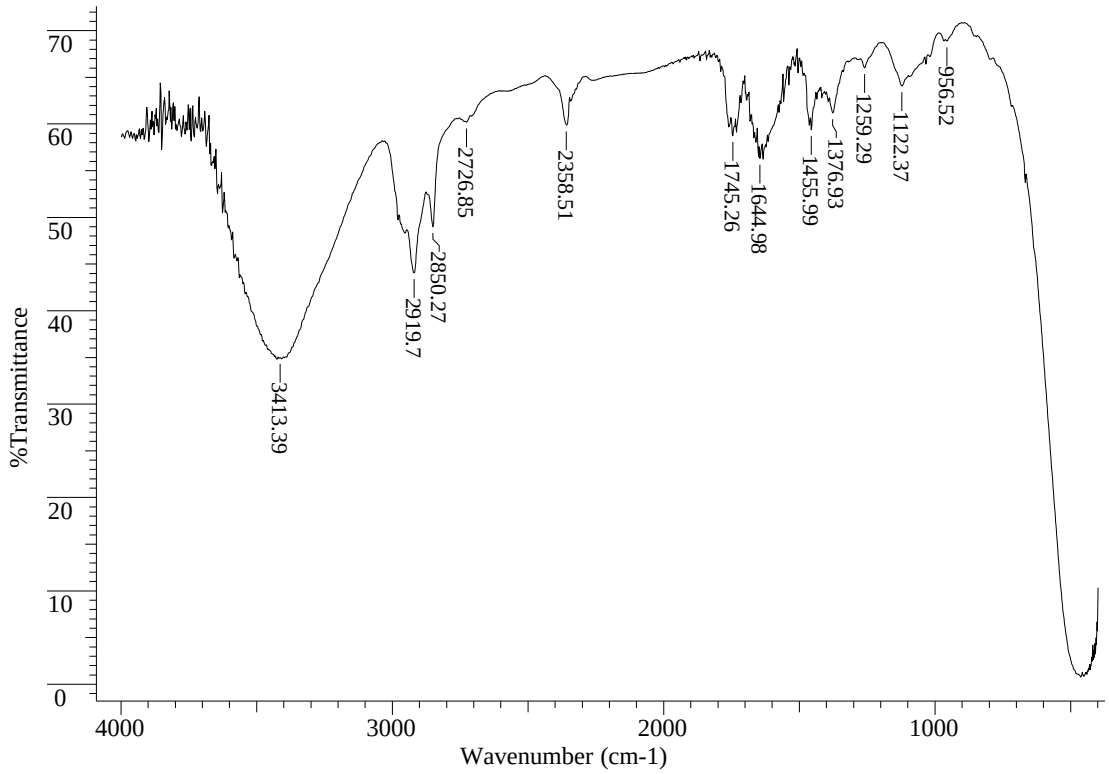

Figure 23: FTIR spectrum for fraction 3 collected from the vermiculite foam

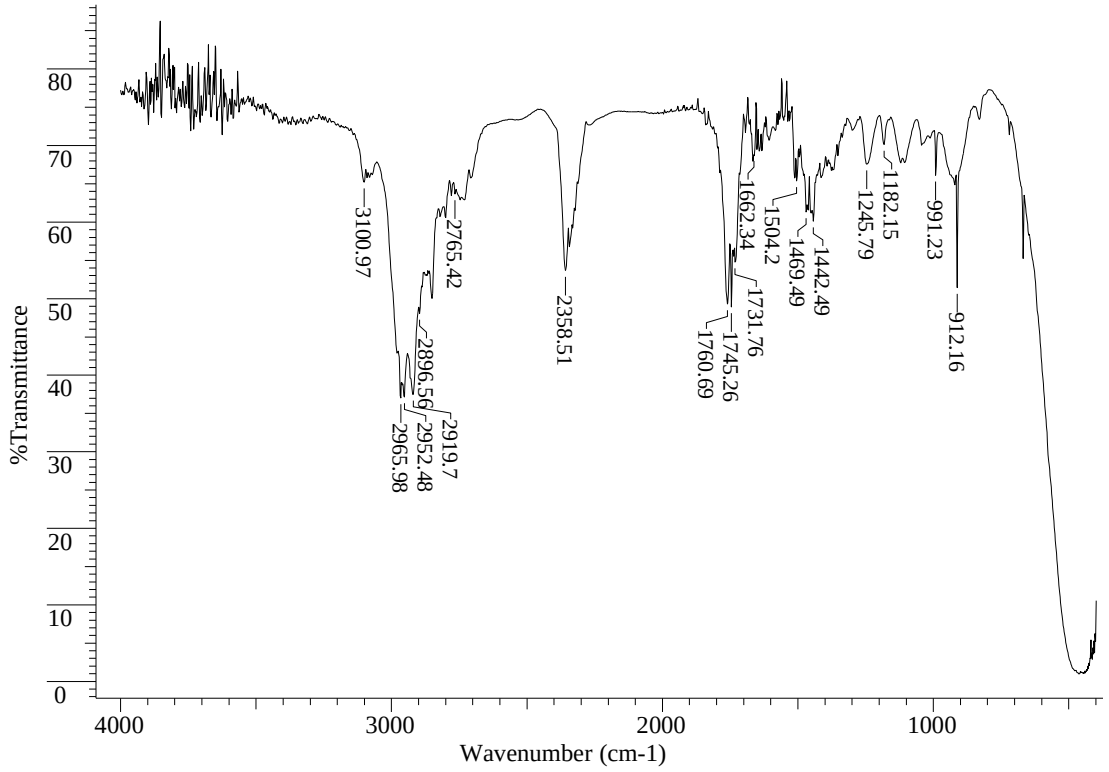

Figure 24: FTIR spectrum for fraction 1 collected from the Cloisite® 30B

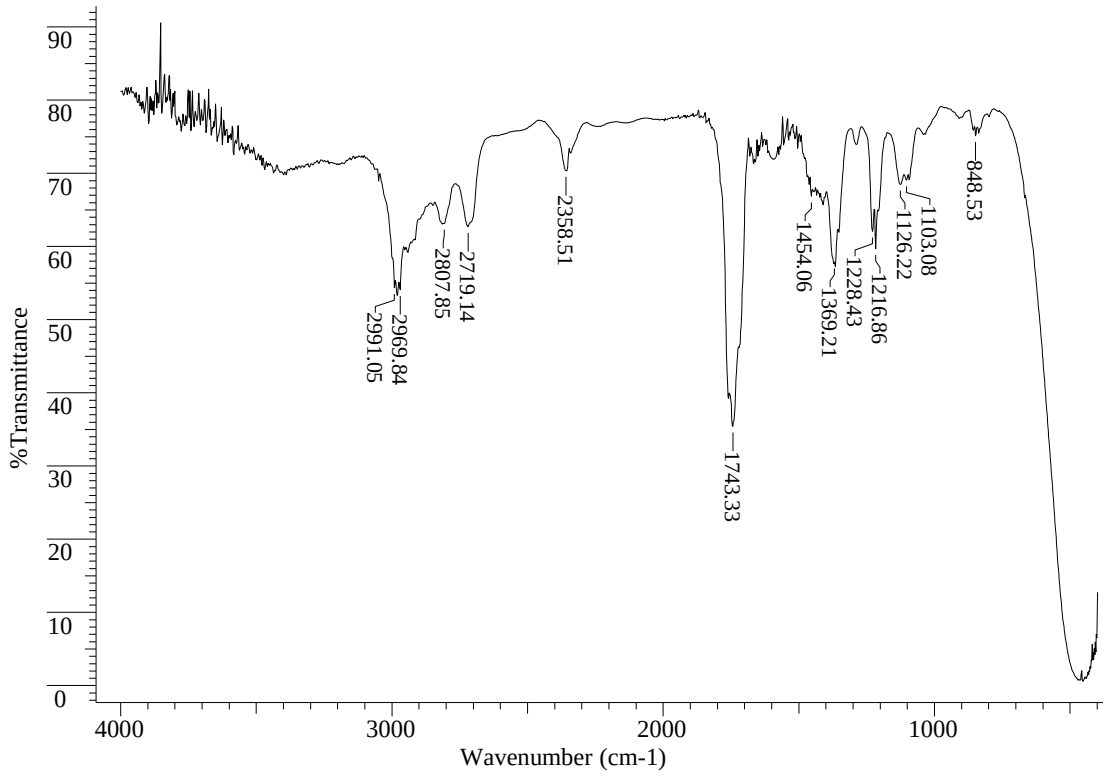

Figure 25: FTIR spectrum for fraction 2 collected from the Cloisite® 30B foam

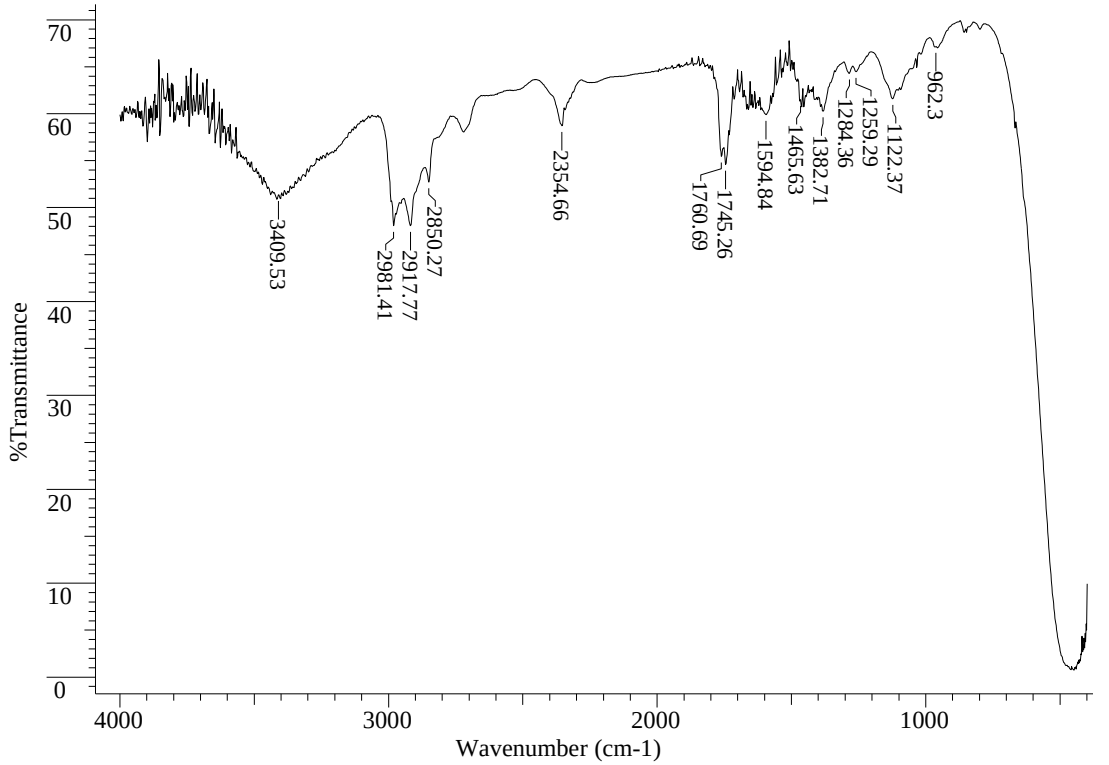

Figure 26: FTIR spectrum for fraction 3 collected from the Cloisite® 30B foam

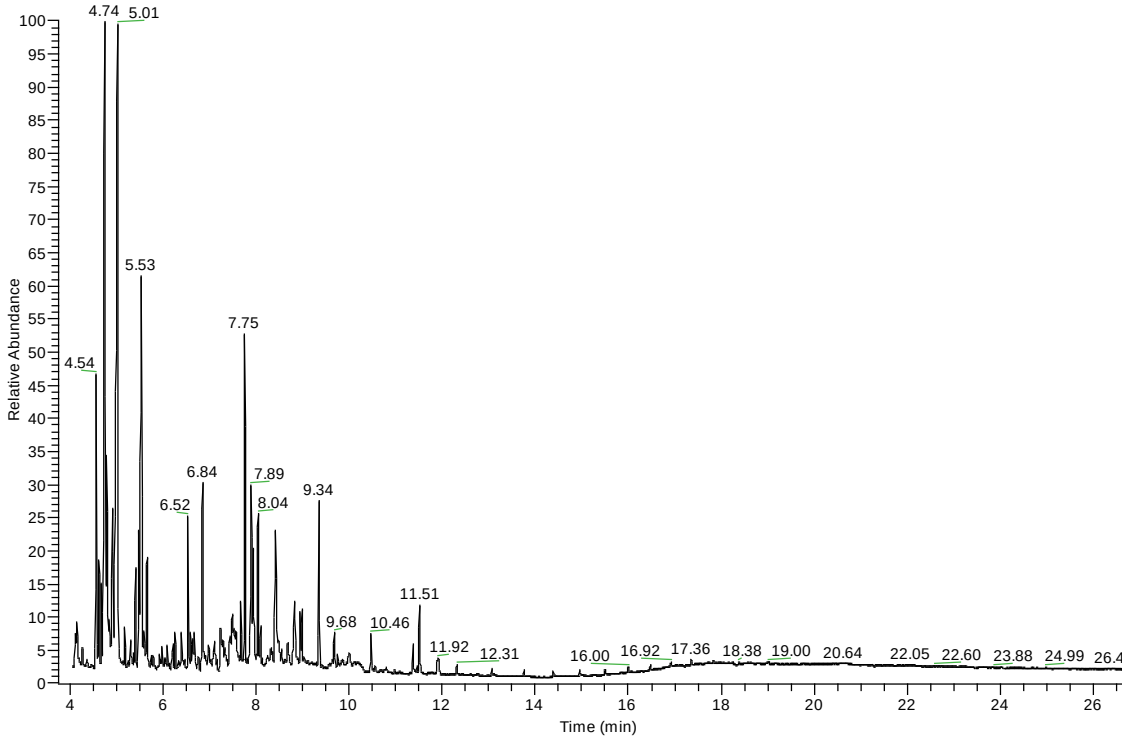

Figure 27: GC-MS total-ion chromatogram for fraction 3 from the vermiculite foam

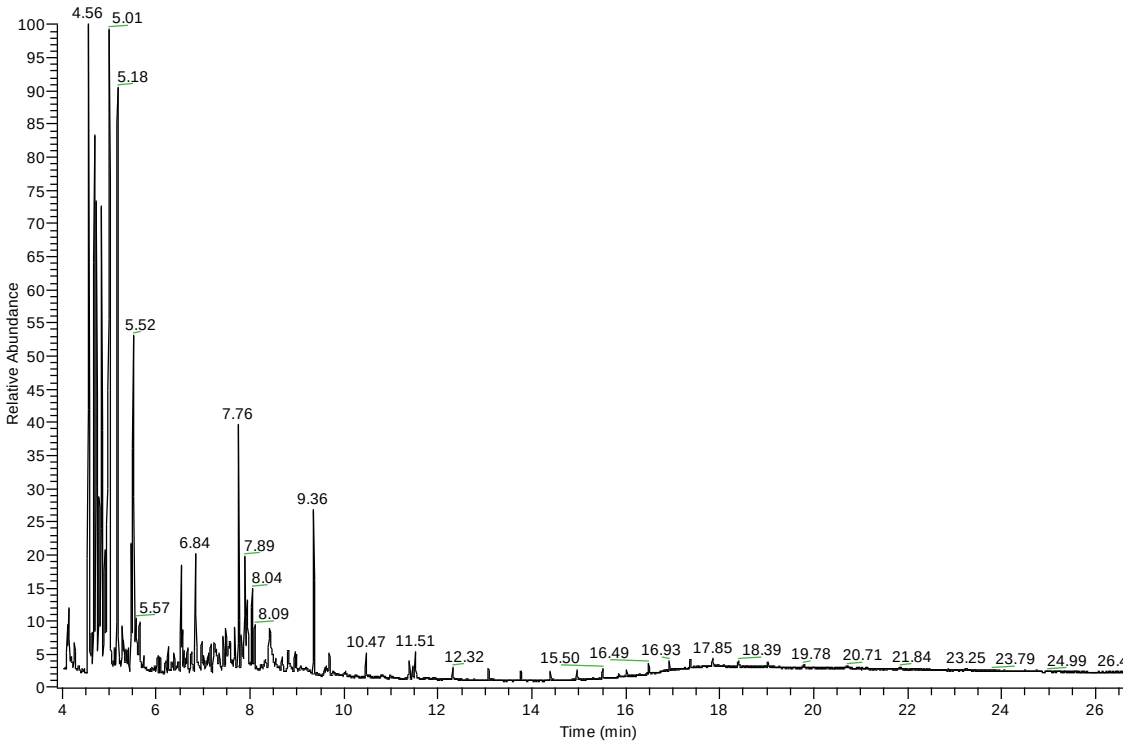

Figure 28: GC-MS total-ion chromatogram for fraction 3 from the Cloisite 30B foam